ISCHEMIC MYOCARDIAL INJURY AND PROTECTION: FROM BENCH TO BEDSIDE

EDITED BY: Hui Gong, Hongmei Tan and Yaoliang Tang
PUBLISHED IN: Frontiers in Cardiovascular Medicine

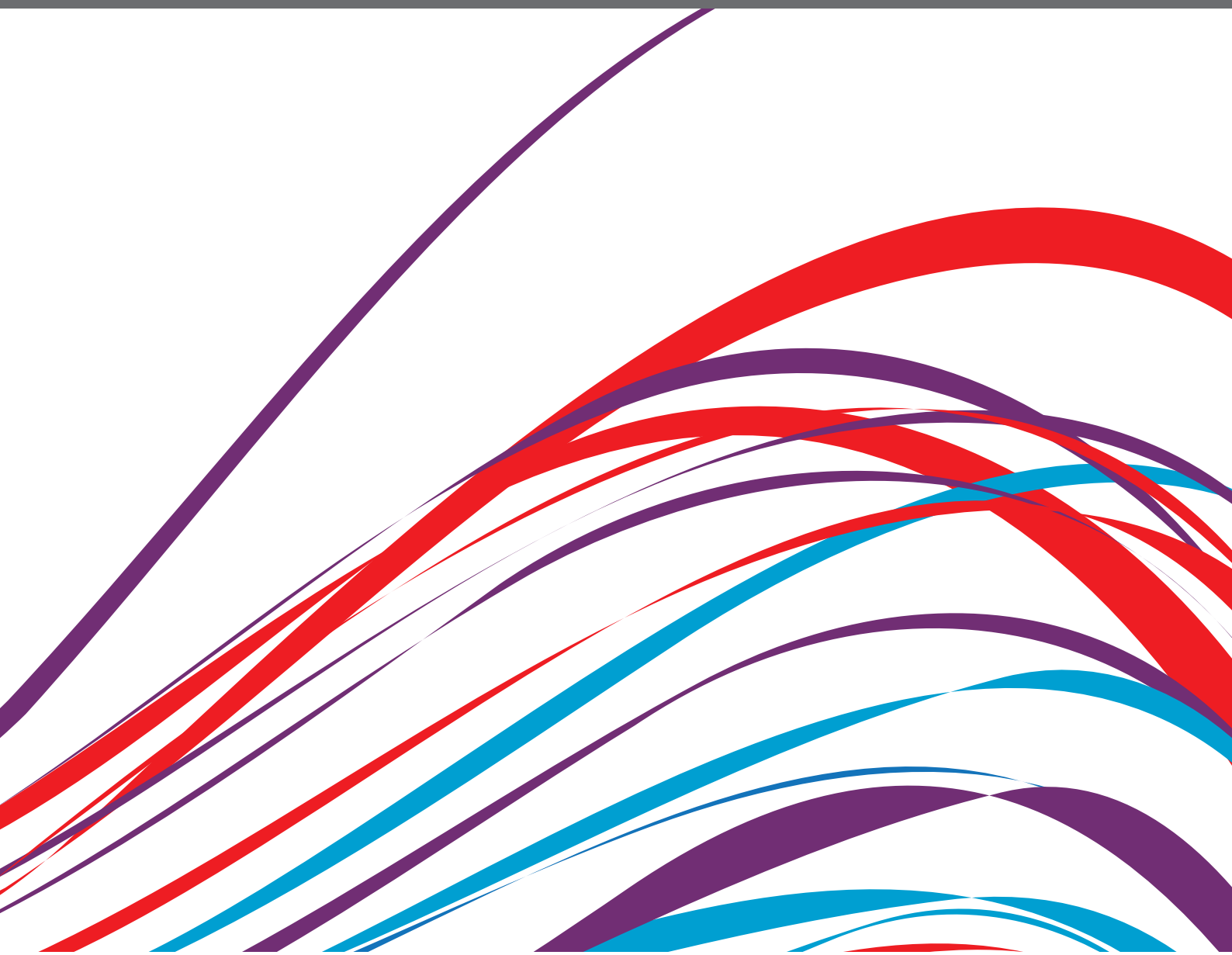

frontiers Research Topics

Frontiers eBook Copyright Statement

The copyright in the text of individual articles in this eBook is the property of their respective authors or their respective institutions or funders. The copyright in graphics and images within each article may be subject to copyright of other parties. In both cases this is subject to a license granted to Frontiers.

The compilation of articles constituting this eBook is the property of Frontiers.

Each article within this eBook, and the eBook itself, are published under the most recent version of the Creative Commons CC-BY licence. The version current at the date of publication of this eBook is CC-BY 4.0. If the CC-BY licence is updated, the licence granted by Frontiers is automatically updated to the new version.

When exercising any right under the CC-BY licence, Frontiers must be attributed as the original publisher of the article or eBook, as applicable.

Authors have the responsibility of ensuring that any graphics or other materials which are the property of others may be included in the CC-BY licence, but this should be checked before relying on the CC-BY licence to reproduce those materials. Any copyright notices relating to those materials must be complied with.

Copyright and source acknowledgement notices may not be removed and must be displayed in any copy, derivative work or partial copy which includes the elements in question.

All copyright, and all rights therein, are protected by national and international copyright laws. The above represents a summary only. For further information please read Frontiers' Conditions for Website Use and Copyright Statement, and the applicable CC-BY licence.

ISSN 1664-8714
ISBN 978-2-88976-358-0
DOI 10.3389/978-2-88976-358-0

About Frontiers

Frontiers is more than just an open-access publisher of scholarly articles: it is a pioneering approach to the world of academia, radically improving the way scholarly research is managed. The grand vision of Frontiers is a world where all people have an equal opportunity to seek, share and generate knowledge. Frontiers provides immediate and permanent online open access to all its publications, but this alone is not enough to realize our grand goals.

Frontiers Journal Series

The Frontiers Journal Series is a multi-tier and interdisciplinary set of open-access, online journals, promising a paradigm shift from the current review, selection and dissemination processes in academic publishing. All Frontiers journals are driven by researchers for researchers; therefore, they constitute a service to the scholarly community. At the same time, the Frontiers Journal Series operates on a revolutionary invention, the tiered publishing system, initially addressing specific communities of scholars, and gradually climbing up to broader public understanding, thus serving the interests of the lay society, too.

Dedication to Quality

Each Frontiers article is a landmark of the highest quality, thanks to genuinely collaborative interactions between authors and review editors, who include some of the world's best academicians. Research must be certified by peers before entering a stream of knowledge that may eventually reach the public - and shape society; therefore, Frontiers only applies the most rigorous and unbiased reviews.
Frontiers revolutionizes research publishing by freely delivering the most outstanding research, evaluated with no bias from both the academic and social point of view. By applying the most advanced information technologies, Frontiers is catapulting scholarly publishing into a new generation.

What are Frontiers Research Topics?

Frontiers Research Topics are very popular trademarks of the Frontiers Journals Series: they are collections of at least ten articles, all centered on a particular subject. With their unique mix of varied contributions from Original Research to Review Articles, Frontiers Research Topics unify the most influential researchers, the latest key findings and historical advances in a hot research area! Find out more on how to host your own Frontiers Research Topic or contribute to one as an author by contacting the Frontiers Editorial Office: frontiersin.org/about/contact

ISCHEMIC MYOCARDIAL INJURY AND PROTECTION: FROM BENCH TO BEDSIDE

Topic Editors:
Hui Gong, Fudan University, China
Hongmei Tan, Sun Yat-sen University, China
Yaoliang Tang, Augusta University, United States

Citation: Gong, H., Tan, H., Tang, Y., eds. (2022). Ischemic Myocardial Injury and Protection: From Bench to Bedside. Lausanne: Frontiers Media SA.
doi: 10.3389/978-2-88976-358-0

Table of Contents

frontiers | Frontiers in Cardiovascular Medicine

EDITORIAL
published: 24 May 2022
doi: 10.3389/fcvm.2022.940298

Editorial: Ischemic Myocardial Injury and Protection: From Bench to Bedside

Hui Gong[1]*, *Hongmei Tan*[2] *and Yaoliang Tang*[3]

[1] *Shanghai Institute of Cardiovascular Diseases, Zhongshan Hospital, Fudan University, Shanghai, China,* [2] *Department of Pathophysiology, Zhongshan School of Medicine, Sun Yat-sen University, Guangzhou, China,* [3] *Department of Medicine, Medical College of Georgia at Augusta University, Augusta, GA, United States*

Keywords: ischemic heart disease (IHD), myocardial injury, protection, metabolic syndrome (MS), heart failure

Editorial on the Research Topic

Ischemic Myocardial Injury and Protection: From Bench to Bedside

Ischemic heart disease (IHD) remains the primary cause of global mortality (about 17% of all death), and has been considered as a life-threatening problem (1). Myocardial ischemia is usually caused by atherosclerotic plaque complication or microvascular dysfunction, which induces cardiomyocytes loss, apoptosis, autophagy, inflammation or fibrosis, resulting in cardiac dysfunction or heart failure (2–4). Although currently basic, translational, and clinical findings have provided a massive amount of information about ischemic myocardial injury and protection, acumulating evidence suggests a complex pathophysiology of IHD. To better understand this complicated disease and provide future perspectives, we have the pleasure of bringing together the Research Topic "*Ischemic Myocardial Injury and Protection: From Bench to Bedside*" for the readers of *Frontiers in Cardiovascular Medicine*. This Research Topic includes twelves article and one review gathering an interdisciplinary overview of molecular mechanism, high risk factor, prognosis, complication, and novel treatment of ischemic myocardial injury.

The high mortality of IHD is attributed to sudden cardiac death (SCD), which results from lethal ventricular arrhythmias of ventricular tachycardia (VT) (5). Qi et al. found blockade of $Na_V1.8$ in cardiac ganglionated plexi (GP) increased the incidence of ventricular arrhythmias in acute myocardial infarction (AMI) hearts. Present results indicated suppression of GP activity might enhance the genesis of ventricular arrhythmia; $Na_V1.8$ plays an important role in cardiac conduction *via* regulation of action potential firing in intracardiac neurons. Qi et al. observed that $Na_V1.8$ was expressed in canine GPs, blockade of $Na_V1.8$ with A-803467 shortened ventricular effective refractory period (VERP), ventricular 90% of action potential duration (APD_{90}), and decreased ventricular fibrillation threshold (VFT) during AMI, and also reduced heart rate in response to GP stimulation. Although the detailed mechanisms are needed to further study to clarify, the study suggests $Na_V1.8$ may be as a potential novel therapeutic target for anti-arrhythmic intervention and prevention of SCD of patients with IHD.

Exosomes derived from a variety of cardiac cells have been reported to regulate intercellular communication and crosstalk in ischemic heart by the transfer of miRNA or other proteins (6). Li, Zhao et al. demonstrated plasma exosomes at the late phase of remote ischemic pre-conditioning (RIPC) alleviated myocardial ischemia-reperfusion injury *via* exosomal miR-126a-3p. On the basis

OPEN ACCESS

Edited and reviewed by:
Junjie Xiao,
Shanghai University, China

***Correspondence:**
Hui Gong
gonghui2005@fudan.edu.cn

Specialty section:
This article was submitted to General Cardiovascular Medicine, a section of the journal Frontiers in Cardiovascular Medicine

Received: *10 May 2022*
Accepted: *10 May 2022*
Published: *24 May 2022*

Citation:
Gong H, Tan H and Tang Y (2022) Editorial: Ischemic Myocardial Injury and Protection: From Bench to Bedside. Front. Cardiovasc. Med. 9:940298. doi: 10.3389/fcvm.2022.940298

of cardiac-protection of exosomes at the late phase of RIPC, they found the significant enrichment of miR-126a-3p in RIPC-exosome by miRNA array. Mechanistically, RIPC-exosomal miR-126a-3p, activated reperfusion injury salvage kinase (RISK) through Akt and Erk1/2 to inhibit apoptosis. This study is interesting, and presents a critical mechanism underlying the exosomal miR-126a-3p might be a novel cardioprotective molecule in the prevention and rehabilitation of ischemic myocardial injury. However, Tu et al. showed that sepsis-exosomes promoted the pyroptosis of cardiomyocytes and worsened cardiac dysfunction through miR-885-5p *via* HMBOX1. These findings suggest the different mechanisms or functions of exosomes in ischemic myocardial injury may dependent on exosomal source of pathophysiological process or cell-types.

Circular RNAs (circRNAs), function as a sponge and bind specific miRNAs to exert critical effects in ischemic heart diseases and vascular diseases. Liu et al. verified that downregulation of rno_circRNA_0009197, and upregulation of rno_circRNA_0005304, rno_circRNA_0005506, rno_circRNA_0005818, and rno_circRNA_0009301 in hypertensive aorta. Three promising circRNA-miRNA-mRNA regulatory axes, including rno_circRNA_0005818/miR-615/NOTCH1, rno_circRNA_0005818/miR-10b-5p/STAT3, and rrno_circRNA_0009197/miR-509-5p/FOXO3, may play potential roles in hypertensive vascular remodeling and dysfunction. The findings indicate that circRNAs are the vital therapeutic targets for ischemic heart diseases and vascular diseases.

Hydrogen sulfide (H_2S), an endogenously generated gaseous transmitter, has been shown to be cardiac protective in ischemic myocardial injury or heart failure (7, 8). Li, Xie et al. explored the cardiac protection and potential mechanism of S-propargyl-cysteine (SPRC), a novel modulator of endogenous H_2S. SPRC has been identified to be protective in myocardial infarction *via* a H2S-related pathway (9). In Li, Xie et al. study, SPRC treatment alleviated cardiac systolic dysfunction and myocardial hypertrophy or fibrosis, accompanied by a reduction in myocardial lipid accumulation in *db/db* diabetic mice. The functional improvement by SPRC was associated with activation of insulin receptor signaling and subsequent enhancement of glucose uptake in cardiomyocyte. These data suggest that SPRC might be a promising medication for patients with IHD and/or diabetic cardiomyopathy.

Clinical studies has revealed more risk factors including metabolic syndrome or metabolism disorder for coronary artery disease (CAD) or IHD. Metabolic syndrome (MS) is characterized by a cluster of risk factors including central obesity hypertension, hyperglycemia, and dyslipidemia, significantly increases the risk for cardiovascular disease (CVD), or the morbidity and mortality of CVD patients (10). Zhao F. et al. conducted this cross-sectional study with 1,958 participants from the Northern Shanghai Study aged over 65 years without a history of CVD. The authors' data revealed that a positive association between MS and various asymptomatic cardiovascular injury in an elderly Chinese population. Importantly, MS was significantly associated with left ventricular hypertrophy (LVH), LV diastolic dysfunction, arteriosclerosis, and microalbuminuria. Yu et al. performed a single-center, observational cohort study enrolled 183 acute heart failure (AHF) patients and evaluate the association between the serum circulating free fatty acids (FFAs) level and all-cause mortality or HF rehospitalization. Serum FFAs levels were positively correlated to the risk of death or HF rehospitalization, which was not related to the status of insulin resistance. In this retrospective cross-sectional study, patients who underwent elective percutaneous coronary intervention (PCI). Li, Li et al. found elevated HbA1c increased the atherosclerotic plaque vulnerability as evidenced by the thinner minimal fibrous cap thickness (FCT), higher lipid index, and greater macrophage index. Moreover, elevated average follow-up HbA1c level was positively associated with higher visit-to-visit variability of lipids levels, including LDL-C, HDL-C, non-HDL-C, TC, and TG. Our basic research showed deficiency of cardiac LRP6 induced lipid accumulation and heart failure, and overexpression of low-density lipoprotein receptor-related protein 6 (LRP6) protects heart from ischemic-reperfusion injury in mice (11–13). These data suggested that interventions for metabolic disorders may be critical for improvement of prognosis of CVD.

In treatment of CAD or IHD, PCI has become one of most effective treatments for patients with AMI. But it also induces some complications in patients such as contrast induced nephropathy (CIN), caused by intravascular contrast media. Mo et al. identified three novel predictors for CIN, baseline uric acid level, creatine kinase-MB level, and log (N-terminal pro-brain natriuretic peptide) level, in patients with CAD and relatively normal renal function (NRF). The authors developed the simplified risk score for contrast induced acute kidney injury (CI-AKI) model on the basis of the new criteria. It exhibits accurate predictive performance to identify high-risk patients with CIN. For drug treatment, β-blockers predominantly increase sympathetic nerve activity, and become the first-line agent for cardiovascular diseases. However, Dai et al. found β-blockers adversely affected erectile dysfunction (ED) improvement conferred by coronary revascularization in patients with early onset of coronary artery disease (EOCAD). This study calls for re-considering β-blockers as the first-line option for the EOCAD patients with ED.

Some researchers explored novel intervention for ischemic myocardial injury. Electrical stimulation (ES), a non-invasive and safe physiotherapy, is considered to be a promising clinical application in the treatment of IHD, which attracts more and more attention. Zhao Y. et al. systemically reviewed the types, the beneficial effects and molecular mechanisms of ES in the treatment of IHD. ES promotes angiogenesis by stimulating VEGF or FGF2 secretion, reduces cardiomyocytes apoptosis by inhibiting the production of TNF-α and intercellular adhesion factor-1 (ICAM-1), inhibits cardiac hypertrophy by suppression of ERK1/2 signaling, in the ischemic myocardium. ES also protects heart from ischemic injury by regulation of autophagy, inflammatory response and the production of ROS. This exhaustive review prompts to investigate in depth the molecular mechanisms underlying ES to develop new therapeutic opportunities. The authors suggest that appropriate parameters

and implementation methods and locations of ES are needed further study to provide better scientific data for clinical application in IHD. Moreover, cardiac shock wave therapy (CSWT), has been reported to be an effective and non-invasive therapy, which is mainly applied to ameliorate left ventricular remodeling after (AMI). Wang et al. found the application of CSWT significantly improved cardiac function and myocardial fibrosis by activation of PI3k /AKT signaling in experimental AMI model. Moreover, renal denervation (RDN) reduces the activation of the sympathetic nervous system (SNS) and renin-angiotensin-aldosterone system (RAAS) for hypertension treatment. Chen et al. investigated the cardioprotective effects of immediate renal denervation (RDN) after AMI and explored the underlying mechanism. They found immediate RDN could improve cardiac remodeling and function after AMI *via* regulation of IL-33/ST2 and downstream signaling. The study suggests RDN may become another viable application in emergency PCI beyond hypertension.

In conclusion, the articles collected for this Research Topic present current progress and perspectives on the pre-clinical, clinical and epidemiological studies on the ischemic myocardial injury and protection. We believe that these articles advance our understanding and perspectives on cardiovascular diseases fields. We are grateful for all contributors for sharing their interesting work for the Research Topic.

AUTHOR CONTRIBUTIONS

HG wrote the manuscript. HT and YT revised the manuscript. All authors listed have made a substantial, direct, and intellectual contribution to the work and approved it for publication.

FUNDING

This work was supported by grants from National Natural Science Foundation of China (NSFC) (No. 82070232 for HG, Nos. 82170357 and 81873514 for HT) and Science and Technology Commission of Shanghai Municipality (21XD1403300 for HG).

REFERENCES

1. Nowbar AN, Gitto M, Howard JP, Francis DP, Al-Lamee R. Mortality from ischemic heart disease. *Circ Cardiovasc Qual Outcomes.* (2019) 12:e005375. doi: 10.1161/CIRCOUTCOMES.118.005375
2. Pagliaro BR, Cannata F, Stefanini GG, Bolognese L. Myocardial ischemia and coronary disease in heart failure. *Heart Fail Rev.* (2020) 25:53–65. doi: 10.1007/s10741-019-09831-z
3. Bass-Stringer S, Tai CMK, McMullen JR. IGF1-PI3K-induced physiological cardiac hypertrophy: implications for new heart failure therapies, biomarkers, and predicting cardiotoxicity. *J Sport Health Sci.* (2021) 10:637–47. doi: 10.1016/j.jshs.2020.11.009
4. Xiao J, Rosenzweig A. Exercise and cardiovascular protection: update and future. *J Sport Health Sci.* (2021) 10:607–8. doi: 10.1016/j.jshs.2021.11.001
5. Amoni M, Dries E, Ingelaere S, Vermoortele D, Roderick HL, Claus P, et al. Ventricular arrhythmias in ischemic cardiomyopathy-new avenues for mechanism-guided treatment. *Cells.* (2021) 10:2629. doi: 10.3390/cells10102629
6. Valadi H, Ekstrom K, Bossios A, Sjostrand M, Lee JJ, Lotvall JO. Exosome-mediated transfer of mRNAs and microRNAs is a novel mechanism of genetic exchange between cells. *Nat Cell Biol.* (2007) 9:654–9. doi: 10.1038/ncb1596
7. Donnarumma E, Trivedi RK, Lefer DJ. Protective actions of H2S in acute myocardial infarction and heart failure. *Compr Physiol.* (2017) 7:583–602. doi: 10.1002/cphy.c160023
8. Yao LL, Huang XW, Wang YG, Cao YX, Zhang CC, Zhu YC. Hydrogen sulfide protects cardiomyocytes from hypoxia/reoxygenation-induced apoptosis by preventing GSK-3beta-dependent opening of mPTP. *Am J Physiol Heart Circ Physiol.* (2010) 298:H1310–9. doi: 10.1152/ajpheart.00339.2009
9. Wang Q, Liu HR, Mu Q, Rose P, Zhu YZ. S-propargyl-cysteine protects both adult rat hearts and neonatal cardiomyocytes from ischemia/hypoxia injury: the contribution of the hydrogen sulfide-mediated pathway. *J Cardiovasc Pharmacol.* (2009) 54:139–46. doi: 10.1097/FJC.0b013e3181ac8e12
10. Jing Z, Liu L, Shi Y, Du Q, Zhang D, Zuo L, et al. Association of coronary artery disease and metabolic syndrome: usefulness of serum metabolomics approach. *Front Endocrinol.* (2021) 12:692893. doi: 10.3389/fendo.2021.692893
11. Chen Z, Li Y, Wang Y, Qian J, Ma H, Wang X, et al. Cardiomyocyte-restricted low density lipoprotein receptor-related protein 6 (LRP6) deletion leads to lethal dilated cardiomyopathy partly through Drp1 signaling. *Theranostics.* (2018) 8:627–43. doi: 10.7150/thno.22177
12. Wang Y, Chen Z, Li Y, Ma L, Zou Y, Wang X, et al. Low density lipoprotein receptor related protein 6 (LRP6) protects heart against oxidative stress by the crosstalk of HSF1 and GSK3β. *Redox Biol.* (2020) 37:101699. doi: 10.1016/j.redox.2020.101699
13. Wang Y, Yin C, Chen Z, Li Y, Zou Y, Wang X, et al. Cardiac-specific LRP6 knockout induces lipid accumulation through Drp1/CPT1b pathway in adult mice. *Cell Tissue Res.* (2020) 380:143–53. doi: 10.1007/s00441-019-03126-3

Conflict of Interest: The authors declare that the research was conducted in the absence of any commercial or financial relationships that could be construed as a potential conflict of interest.

Publisher's Note: All claims expressed in this article are solely those of the authors and do not necessarily represent those of their affiliated organizations, or those of the publisher, the editors and the reviewers. Any product that may be evaluated in this article, or claim that may be made by its manufacturer, is not guaranteed or endorsed by the publisher.

Copyright © 2022 Gong, Tan and Tang. This is an open-access article distributed under the terms of the Creative Commons Attribution License (CC BY). The use, distribution or reproduction in other forums is permitted, provided the original author(s) and the copyright owner(s) are credited and that the original publication in this journal is cited, in accordance with accepted academic practice. No use, distribution or reproduction is permitted which does not comply with these terms.

frontiers in Cardiovascular Medicine

ORIGINAL RESEARCH
published: 16 June 2021
doi: 10.3389/fcvm.2021.693875

Cardiac Shock Wave Therapy Improves Ventricular Function by Relieving Fibrosis Through PI3K/Akt Signaling Pathway: Evidence From a Rat Model of Post-infarction Heart Failure

Luqiao Wang[1†], Xin Tian[1†], Yuting Cao[1], Xuejuan Ma[1], Leilei Shang[2], Hao Li[1], Xueting Zhang[1], Furong Deng[1], Shumin Li[1], Tao Guo[3] and Ping Yang[1]*

[1] Department of Cardiology, The First Affiliated Hospital of Kunming Medical University, Kunming, China, [2] Department of Cardiology, Suizhou Central Hospital, Suizhou, China, [3] Department of Cardiology, Yunnan Fuwai Cardiovascular Hospital, Kunming, China

OPEN ACCESS

Edited by:
Hongmei Tan,
Sun Yat-Sen University, China

Reviewed by:
Ying Shao,
Temple University, United States
Nahid Aboutaleb,
Iran University of Medical Sciences, Iran

***Correspondence:**
Ping Yang
15877990331@163.com

[†] These authors have contributed equally to this work and share first authorship

Specialty section:
This article was submitted to General Cardiovascular Medicine, a section of the journal Frontiers in Cardiovascular Medicine

Received: 12 April 2021
Accepted: 14 May 2021
Published: 16 June 2021

Citation:
Wang L, Tian X, Cao Y, Ma X, Shang L, Li H, Zhang X, Deng F, Li S, Guo T and Yang P (2021) Cardiac Shock Wave Therapy Improves Ventricular Function by Relieving Fibrosis Through PI3K/Akt Signaling Pathway: Evidence From a Rat Model of Post-infarction Heart Failure. Front. Cardiovasc. Med. 8:693875. doi: 10.3389/fcvm.2021.693875

Objection: Cumulative studies have identified the effectiveness of cardiac shock wave therapy (CSWT) in treating heart failure after acute myocardial infarction (AMI), but little have been discussed with regard to the beneficial effects of CSWT on anti-fibrosis along with the underlying mechanism. In this study, we investigated whether CSWT could reduce post-AMI fibrosis and further explored the molecular mechanism.

Methods: Rat heart failure (HF) models induced by ligating the left anterior descending coronary artery were established and validated by echocardiography. Eligible animals were randomly categorized into five groups: the sham group, the HF group, the HF + CSWT group, the HF + LY294002 group, and the HF + CSWT + LY294002 group. The cardiac weight, serum level of BNP, NT-pro BNP and echocardiography parameters were measured to assess cardiac function in different groups. Masson's trichrome staining was used to assess the proportions of the fibrotic area. The expression level of CD34, αSMA was measured by RT-PCR, Immunohistochemistry and Immunofluorescent analyses and the level of PI3K/Akt was quantified by Immunohistochemistry and Western blotting.

Results: The application of CSWT significantly improved cardiac function and reduced myocardial fibrosis and level of CD34 and αSMA, compared to the HF group. CSWT led to significant elevations of p-PI3K and p-Akt expression levels compared to that of the HF group and the inhibition of the PI3K/Akt pathway abolished the observed beneficial effects of CSWT.

Conclusion: CSWT can facilitate the alleviation of cardiac fibrosis induced by AMI through the activation of PI3K/Akt signaling pathway.

Keywords: cardiac shock wave therapy, heart failure, cardiac fibrosis, CD34/αSMA, PI3K/Akt signaling pathway

INTRODUCTION

Accounting for a staggering 30% of all deaths, ischemia heart disease (IHD) is the primary cause of global mortality and has long been considered as a life-threatening problem (1). The loss of normal cardiomyocytes initiated by myocardium infarction can eventually triggers the replacement of necrotic zone by fibrous scar tissue, which generally has invalid systolic function. This is known as ventricular remodeling and can finally result in post-infarction heart failure (HF). A greater increase in morbidity, mortality, and a poorer prognosis were observed among patients with HF following myocardial ischemia, due to the inextricable association of IHD and HF (2, 3). That existing therapies focused more on symptom improvement than ventricular remodeling avoidance has driven the desire for more curative strategies to reverse remodeled hearts in this aging society.

Serving as a dominating factor of the occurrence and development of post-infarction HF, cardiac fibrosis can be constantly seen in infarcted regions and border areas. The inhibition of fibrosis is gaining increasing attention for the reason that if effective anti-fibrosis can be achieved in infarcted myocardium and the border region, the pathophysiologic process of ventricular remodeling leading to HF may be restrained, and the prognosis of HF patients could be substantially improved. Therefore, novel therapies that focused on fibrosis antagonization should be considered as a therapeutic target for the management of IHD and related HF.

An emerging body of research has reported cardiac shock wave therapy (CSWT), an effective and non-invasive therapy mainly applied to ameliorate left ventricular remodeling after acute myocardial infarction (AMI) (4, 5). Our preceding work has demonstrated that hearts of rats with AMI treated by CSWT exhibited reductions of cardiomyocyte apoptosis index, shrinking fibrotic areas and satisfactory cardiac function parameters (6, 7). Involved mechanisms include the coronary micrangium arteriogenesis inducement, anti-apoptosis and anti-inflammation. Identically being one of the indispensable chains to post-infarction HF, however, AMI-induced cardiac fibrosis is surprisingly scanty in the field of CSWT. Two studies reported suppressed fibrotic extent by anti-inflammatory and decreasing the amount of fibrocytes in CSWT-treated hearts in animals (8, 9), nevertheless, it remains poorly-understood regarding the molecular mechanisms underlying these results.

In this study, we aimed to investigate the anti-fibrosis effect conferred by CSWT and further elucidate the mechanism of such benefit by building rat models of post-infarction HF.

Abbreviations: CSWT, cardiac shock wave therapy; AMI, acute myocardial infarction; HF, heart failure; IHD, ischemia heart disease; IACUC, The Institutional Animal Care and Use Committee; SD, Sprague-Dawley; LAD, left anterior descending; LVESD, left ventricular end-systolic diameter; LVEDD, left ventricular end-diastolic diameter; LVEF, left ventricular ejection fraction; FS, fractional shortening; OD, optical density; LV, left ventricular; DAB, diaminobenzidine; S.E.M, standard error of means; VEGF, vascular endothelial growth factor.

MATERIALS AND METHODS

The animal protocol of this study was approved by the Institutional Animal Care and Use Committee (IACUC) of the Institutional Ethics Committee at the First Affiliated Hospital of Kunming Medical University (Yunnan, China) (Animal Ethics NO.Kmmu2021050). Operations and animal care performed in this study conformed to "Guide for the care and use of laboratory animals" (National Institutes of Health, volume 25, no. 28, revised 1996).

Animal Models

Fifty adult male Sprague-Dawley (SD) rats with initial weight from 250 to 300 g were purchased from the Animal Laboratory of Kunming Medical University [Animal certification number: SYSK(Dian) 2005-0004]. All rats were inbred under a temperature-controlled environment with regular 12/12 light/dark cycles in cages and fed on commercial rat chow and water *ad libitum*. The rat model of heart failure was established as previously reported (10). Briefly, with chloral hydrate injected intra-peritoneally, animals were treated with left thoracotomy after endotracheal incubation and ventilator-assisted breathing (frequency: 75 breaths/min; inspiration/expiration: 1:1; tidal volume: 13 cc). An incision with pericardium exposure was inflicted on the fourth intercostal space and the chest was opened carefully. Followed by unfolding pericardium, the left anterior descending (LAD) occlusion was performed with 6-0 silk suture to induce acute myocardial infarction (AMI) model, which was identified by myocardium pathological change from reddish to blanching and AMI-specific ECG manifestations. Erythromycin ointment was then applied to local surgery wound post-operatively after the immediate close of the thoracic cavity by suturing, to avoid infections for 3 days.

Echocardiography

Heart function assessment by Vivid E9 Color Doppler ultrasound system equipped with a 10.0-MHz 9L-D transducer (GE Inc., Vivid E9 system, Wingmed, Milwaukee, USA) was performed prior to and 4, 8 weeks after the surgery, as previously reported (11). Left ventricular end-systolic diameter (LVESD), left ventricular end-diastolic diameter (LVEDD), and left ventricular ejection fraction (LVEF) were directly measured via the long axial section of the left ventricular and averaged from 3 consecutive cardiac cycles, while fractional shortening (FS) was calculated by the equation as follows: FS = [(LVEDD – LVESD)/LVEDD] × 100%. The evaluation was conducted by an independent experimenter in an observer-blinded way.

Animal Grouping and Treatment

Four weeks after the surgery, the surviving rats with heart failure proven by echocardiography (LVEF ranging from 35 to 50%) were randomly categorized into the following groups: the heart failure (HF) group ($n = 9$), the HF + cardiac shock wave therapy (CSWT) group ($n = 9$), the HF + LY294002 group ($n = 9$), and the HF + CSWT + LY294002 group ($n = 9$). Besides, nine rats underwent chest wall open surgery without LAD ligation were included as the sham group.

The procedure of CSWT treatment was depicted in detail in our previous works (6, 7). In short, inhaled isoflurane-anesthetized rats in the HF + CSWT and the HF + CSWT + LY294002 groups received a myocardium-focused shock wave, which was generated from the MODULITH SLC therapy device (Storz Medical, Lohstampfestr, Taegerwilen, Switzerland) with 200 impulses, 0.24 mJ/mm^2 energy flux density and the frequency of 1 Hz. Initiated 4 weeks after AMI model establishment, the CSWT treatment was administrated three times a week lasting for 4 weeks. An identical anesthesia process was given in non-CSWT group animals.

As the special inhibitor of the PI3K/Akt signal pathway, LY294002 was used to investigate the role PI3K/Akt played in CSWT. Animals in HF + LY294002 and HF + CSWT + LY294002 groups were treated with an intraperitoneal injection of LY294002 with a dose of 100 mg/kg. The same volume of saline was given in groups without the inhibition of PI3K/Akt.

Sample Collection

Whole blood was collected from rats' eye socket veins under peritoneal injection of 0.3 ml/100 g 10% chloral hydrate preoperatively, 4 weeks after the surgery and 4 weeks after the intervention. Experiment animals were executed 4 weeks after the intervention to obtain heart tissues. Before removing the hearts from the thoracic captivity, saline-based irrigation into LV was performed to purge the red blood cells. After that, the heart tissues were cut into cardiac apex and base, which were then fixed by 4% paraformaldehyde and preserved at the temperature of 4 and −80°C, respectively.

BNP and NT-pro BNP Detection

Serum BNP and NT-pro BNP levels were quantified by Rat BNP and NT-pro BNP ELISA Kit (Yinghua Institute of Biotechnology, Beijing, China; Sabbiotech Inc., Shanghai, China) as instructed by the manufacturer. Serum samples were added to the wells and then incubated for 2 h, followed by 1-h incubation of responding antibody and 30-min incubation of streptavidin–peroxidase conjugate at room temperature. Afterward, the reaction was terminated by adding 50 μl stop solution after incubating chromogen substrate solution for 15 min. The concentration was confirmed by detecting the optical density (OD) of each well at 450 nm using a micro reader.

Reverse Transcription Polymerase Chain Reaction

Rats left ventricular (LV) tissues were homogenized to obtain total RNA extractions by using TRIzol reagent (MRC Inc., Darmstadt, Germany), according to the producer's protocol. Following the directions of All-in-OneTM First-Strand-cDNA Synthesis Kit (GeneCopoeia Inc., Maryland, USA), 1 μl of RNA was used as a template for creating cDNA and real-time PCR was carried out on a type 2720 PCR instrument (Thermo Inc., Waltham, USA) in a final volume of 20 μl of reaction system that contained 10 μl SYBR Green/ROX qPCR Master Mix (GeneCopoeia Inc., Maryland, USA), 100 μg of cDNA, 0.16 μl of primer of each target RNA, and the corresponding volume of nuclease-free water with thermocycling conditions of 95°C for 10 min, 95°C for 15 s, 60°C for 20 s, and 72°C for 30 s, 40 cycles. The primer sequences were: GAPDH (forward) 5′-CAAGTTCAACGGCACAGTCAAGG-3′ and (reverse) 5′-ACATACTCAGCACCAGCATCACC-3′; CD34 (forward) 5′-TTCACAACCACAGACTTACCCAAC-3′ and (reverse) 5′-CCCTTTCCTTCTTAAACTCCTCAC-3′; αSMA (forward) 5′-ATCTGGAATCCCGAGTGACAAG-3′ ands (reverse) 5′-CGTGAAGAGGACCTGGGAGTAG-3′. The mRNA expression levels of CD34 and αSMA were determined by comparing that of the GAPDH, which was chosen as internal controls.

Masson's Trichrome Staining

The Masson Staining Kit (Solarbio Inc., Beijing, China) was employed to observe the extent of myocardial fibrosis in five microscopic fields (×200) per 5-μm section of LV myocardium. The fibrosis percentage was defined as the ratio of fibrosis area and myocardial area, which was quantified via Image-pro Plus 6.0 (Media Cybernetics Inc., Bethesda, Maryland, USA).

Immunohistochemical and Immunofluorescent Analyses

After de-waxing and hydrating, the prepared LV sections were initially incubated with 0.01 mmol/L citric acid solutions and then deionization water for 15 and 10 min, respectively, to inactivate endogenous peroxidase. For immunohistochemical analyses, serial sections were immunostained with primary antibodies against CD34, αSMA, and p-Akt (1:50, 1:100, 1:100, 1:200 rabbit polyclonal, respectively, both from Abcam Inc., Cambridge, Massachusetts, USA) at 4°C overnight and then incubated with the secondary biotinylated antibody for 20 min at 37°C. After diaminobenzidine (DAB) staining and hematoxylin counterstaining, tissue slices were subjected to regular dehydration, clearance, and cover. The proportion of positive cells for each slice were quantified by observing 10 randomly chosen microscopic fields (×400) and the averaged positive rates of five slices were identified as the final positive proportion for each target protein.

LV tissue sections were prepared as aforementioned. For endogenous peroxidase inactivation and membrane breaking, 0.01 mmol/L citric acid solutions and immunostaining permeate were used for 15 and 10 min, respectively. Thereafter, diluted primary antibodies against αSMA/CD34 (1:50/1:100, Abcam Inc., Cambridge, MA, USA) and Procollage-I/CD34 (1:100/1:100, Abcam Inc., Cambridge, MA, USA) were added to tissue sections for 4°C overnight incubation, followed by combined secondary antibodies for 40 min at 37°C (Beijing Ximeijie Technology Co., Ltd, Beijing, China). After PBS washing, Nuclei were stained with 1 mg/ml of DAPI (Boster Biotechnology Co. Ltd, Wuhan, China) for 7 min. The fluorescence analyses were performed with a confocal microscope (Olympus Tokyo, Japan).

Statistical Analysis

All data were expressed as mean ± standard error of means (S.E.M) and analyzed by SPSS 19.0 (SPSS Inc., Chicago, IL, USA). Normal distribution and homogeneity test for a variance were conducted prior to One-way ANOVA analyses, which were used to compare differences between multiple groups. *P*-values

<0.05, two-tailed, were deemed statistically significant. Statistical charts were produced by using GraphPad Prism 6.0 (San Diego, CA, USA).

RESULTS

Ischemic Heart Failure Model Establishment

The validity of the HF model is tested by transthoracic echocardiography and BNP, NT-pro BNP examination. Four weeks after the surgery, the ultrasound indexes revealed a considerable deterioration of cardiac function, when compared with baseline values (Baseline values: LVEDV 6.64 ± 0.44; LVESV 3.20 ± 0.45; FS% 51.70 ± 4.4; LVEF% 70.18 ± 2.30; 4 weeks later: LVEDV 7.95 ± 0.28; LVESV 5.76 ± 0.20; FS% 31.21 ± 3.21; LVEF% 30.42 ± 4.22). Meanwhile, heart weight, serum BNP, NT-pro BNP, the most wildly used HF indicators, were markedly elevated 4 weeks after the LAD ligation, suggesting a successful establishment of the HF model.

Rats Heart Failure and Fibrosis Alleviation Effects of CSWT

CSWT Improved Cardiac Function of Rats With HF

Rats' heart tissues were removed 8 weeks after AMI establishment. The general structure of hearts was shown in **Figure 1A**. Compared to the control, a less thickening regional wall of ventricular can be observed in the HF group while the CSWT group presented a thicker ventricular wall when comparing with that of the HF group. Quantitative analysis of heart weight suggested that hearts in the control group were heavier than that of in the HF group (1.16 ± 0.01 vs. 1.06 ± 0.01, $p < 0.05$) and heart weight in the HF + CSWT group were higher than that of in the HF group (1.11 ± 0.03 vs. 1.06 ± 0.01, $p < 0.05$). Besides, both the preoperative and post-operative serum levels of BNP, NT-pro BNP in 4 and 8 weeks were detected. As illustrated in **Figure 1A**, the results showed that BNP and NT-pro BNP had a lower level before the treatment than 4-week post-operative detection. Eight weeks following the surgery, in the HF group, the level of BNP and NT-pro BNP was markedly elevated compared to that of in the sham group. While it was decreased in rats receiving CSWT compared to the HF group.

Cardiac function was evaluated via transthoracic echocardiography, as presented in **Figure 1B**. Baseline cardiac function assessed before the treatment showed a relatively low tendency in LVESV and LVEDV and a high tendency in FS% and LVEF%, compared with the results obtained 4 weeks after LAD ligation. Furthermore, echocardiography parameters measured 8 weeks post-operatively exhibited significant deterioration of heart function in HF animals, as suggested by the disparity with the sham group (LVESV: 7.85 ± 0.35 vs. 2.94 ± 0.28, $p < 0.05$; LVEDV: 10.12 ± 0.33 vs. 5.39 ± 0.21, $p < 0.05$; FS%: 24.31 ± 2.39 vs. 55.12 ± 3.56, $p < 0.05$; LVEF%: 30.42 ± 4.22 vs. 70.18 ± 2.30, $p < 0.05$), whereas conspicuously improved in the CSWT + HF mouse, which yields markable discrepancies from HF mouse (LVESV: 5.97 ± 0.34 vs. 7.85 ± 0.35, $p < 0.05$; LVEDV: 8.05 ± 0.46 vs. 10.12 ± 0.33, $p < 0.05$; FS%: 35.36 ± 2.38 vs. 24.31 ± 2.39, $p < 0.05$; LVEF%: 52.13 ± 2.65 vs. 30.42 ± 4.22, $p < 0.05$).

CSWT Reduced Cardiac Fibrosis of Rats With HF

As **Figure 1C** showed, animal hearts were analyzed for CD34 and αSMA, which are two major fibrosis markers 4 weeks after CSWT via RT-PCR. As was revealed in **Figure 1C**, both CD34 and αSMA expression level increased in the condition of HF, compared with that of normal conditions (the HF group: CD34: 1.71 ± 0.06, $p < 0.05$; αSMA: 2.59 ± 0.16, $p < 0.05$), and the application of CSWT exhibited reversed tendency in comparison with that of the HF group (CD34: 1.24 ± 0.08 vs. 1.71 ± 0.06, $p < 0.05$; αSMA: 1.19 ± 0.01 vs. 2.59 ± 0.16, $p < 0.05$).

In addition, immunohistochemistry was used to assess the positive rate of CD34 and αSMA and the results showed that the positive expression rate of CD34 in myocardium tissues of the control and the HF group were 6.76 ± 0.58 and 17.13 ± 1.47% ($p < 0.05$), respectively (**Figure 1D**). However, the rate reached 10.25 ± 0.48% after applying CSWT, which was significantly heightened ($p < 0.05$). A similar trend was found in αSMA levels, which was strongly expressed in hearts from the HF group relative to the sham group (13.90 ± 0.85 vs. 5.07 ± 0.30%, $p < 0.05$), whereas was weakly expressed in the HF group with CSWT treatment, comparing to those in the HF group without CSWT administration (5.78 ± 0.51 vs. 5.07 ± 0.30%, $p < 0.05$).

Figure 1E presented the Masson's trichrome staining of rats LV myocardial sections from the sham, HF and HF + CSWT groups, in which the fibrosis region is blue-colored. It is suggested that, compared to the HF group, the collagen area proportion was obviously lower in the HF + CSWT group (the HF group: 53.89 ± 1.01, $p < 0.05$; the HF + CSWT group: 23.63 ± 0.54, $p < 0.05$).

Furthermore, the intensity of combinations of αSMA/CD34 and Procollage-I/CD34, two fibrotic indicators, were visualized by immunofluorescence staining (**Figure 1F**). The images showed higher levels of fibrosis in HF-suffered rats compared with those in untreated controls. Both two combinations were lightly-stained in CSWT-treated rats compared with that of the HF group.

PI3K/Akt Signaling Pathway May Be Involved in the Effect of Anti-fibrosis

Based on previous results that CSWT benefited cardiac function and alleviated myocardium fibrosis, we next examined whether PI3K/Akt signaling pathway, a key factor that has been shown to be responsible for withholding fibrotic progression after AMI, involved in the process of anti-fibrosis. **Figure 2A** presented specimens immunostained for p-PI3K and p-Akt. According to the analytic results from immunohistochemistry, the administration of CSWT led to a significant increase in the positive rates of p-PI3K and p-Akt, compared with that of the HF group. Meanwhile, as **Figure 2B** suggested, based on outcomes from western blotting analyses, the level of p-PI3K(Tyr508)/PI3K and p-Akt(ser473)/Akt were decreased in the HF group while CSWT treatment resulted in remarkable increase of p-PI3K(Tyr508) and p-Akt(ser473) levels.

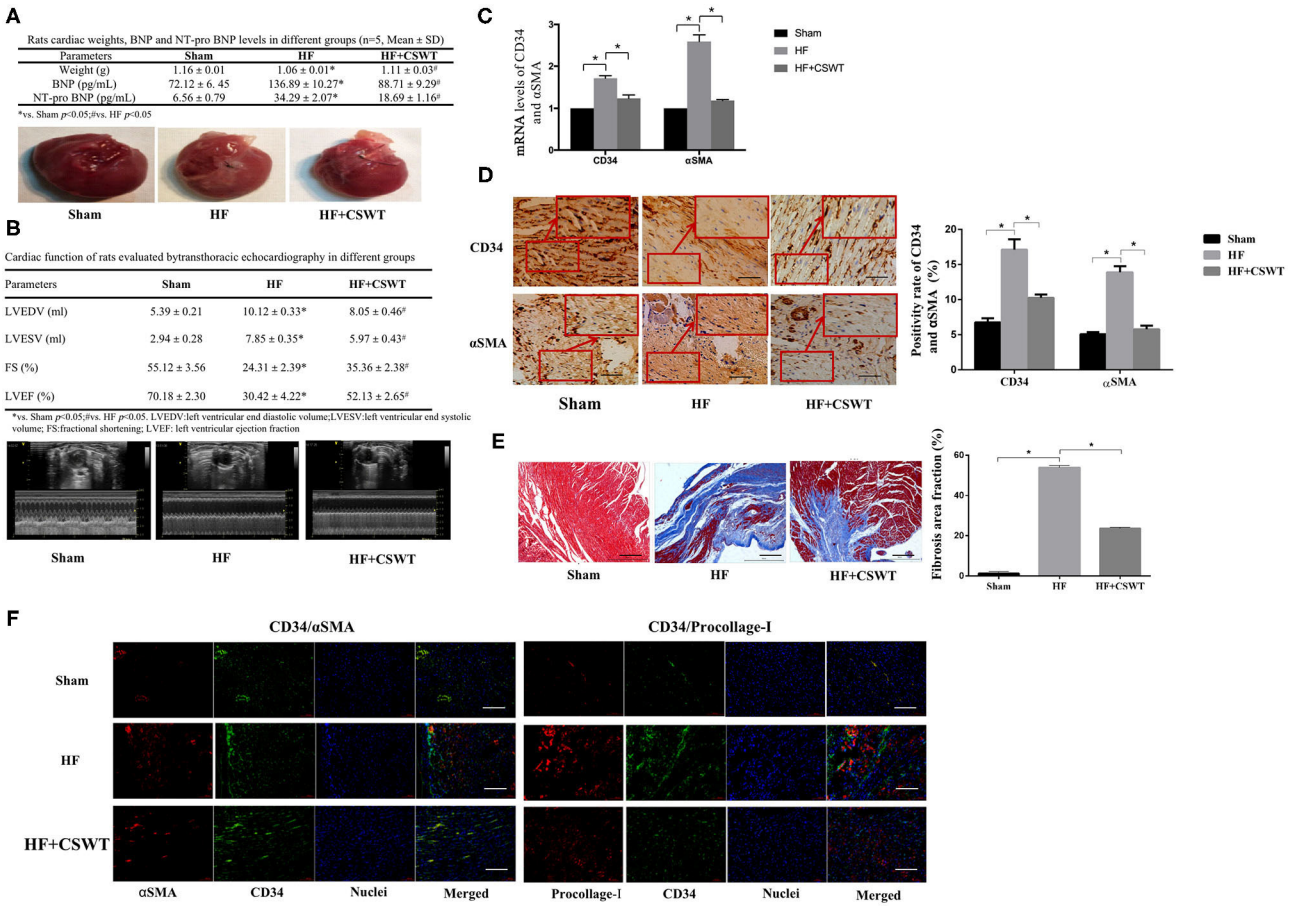

FIGURE 1 | CSWT improves cardiac functions and reduced fibrosis in rats with post-AMI HF. **(A)** The cardiac weight, serum levels of BNP and NT-pro BNP and gross view of whole hearts in study groups; **(B)** Representative M-mode images by echocardiography of rats in study group; **(C)** Fold changes in CD34 and αSMA mRNA levels determined by RT-PCR in study groups; **(D)** The positive rates of CD34 and αSMA in study groups using Immunochemistry analyses; scale bar, 100 μm; **(E)** Representative images of Masson's trichrome staining and quantification for fibrosis of rat hearts from each group; scale bar, 100 μm; **(F)** Representative photomicrographs of immnunofluorescence for the detection of CD34/αSMA and CD34/Procollage-I. Red fluorescence shows αSMA or Procollage-I expression. Green fluorescence shows CD34 expression. Blue fluorescence shows nuclei of total cardiomyocytes; scale bar, 50 μm. Values are expressed as mean ± S.E.M (n = 5). One-way ANOVA test was applied for determining the significance of data. *$p < 0.05$. CSWT, cardiac shock wave therapy; AMI, acute myocardial infarction; HF, heart failure; S.E.M, standard error of means.

PI3K/Akt Pathway Mediated CSWT Effects of Anti-fibrosis

LY294002 Abolished the Cardiac Function Improvement Effects of CSWT

Next, groups pretreated with LY294002 were set to inspect CSWT effects after PI3K/Akt pathway abolishment. Summarized cardiac weight of rats, level of BNP, NT-pro BNP along with the cardiac exteriors were listed in **Figure 3A**. Similarly, CSWT resulted in significantly higher cardiac weight, lower BNP, NT-pro BNP level. Nevertheless, P13K/Akt pathway inhibition eliminated such protective effects upon CSWT.

Post-AMI LV remodeling was assessed by LV dilatation, indicated by LVEDV and LVESV, and LV function, indicated by LVEF and FS. The representative images of echocardiography of animals in each group were exhibited in **Figure 3B**. In the HF + CSWT group, FS and LVEF were significantly improved compared with that of the HF group (FS: 37.07 ± 3.21 vs. 23.23 ± 2.76, $p < 0.05$; LVEF: 54.17 ± 2.17 vs. 31.87 ± 2.00, $p < 0.05$), while which were reduced in the HF + CSWT + LY294002 group (FS: 37.07 ± 3.21 vs. 33.55 ± 1.65, $p < 0.05$; LVEF: 54.17 ± 2.17 vs. 45.30 ± 2.21, $p < 0.05$). Similarly, LVEDV and LVESV were significantly enhanced in the HF group, which was significantly decreased in the HF + CSWT group (LVEDV: 9.94 ± 0.20 vs. 8.34 ± 0.41, $p < 0.05$; LVDSV: 7.72 ± 0.21 vs. 5.04 ± 0.27, $p < 0.05$). CSWT did not benefit FS, LVEF, LVEDV nor LVESV after inhibiting the PI3K/Akt signaling pathway, compared with animals in the HF + CSWT group.

LY294002 Abolished the Cardiac Anti-fibrosis Effects of CSWT

Lower mRNA level of CD34 and αSMA were noted in CSWT treatment group, however, which were again elevated after

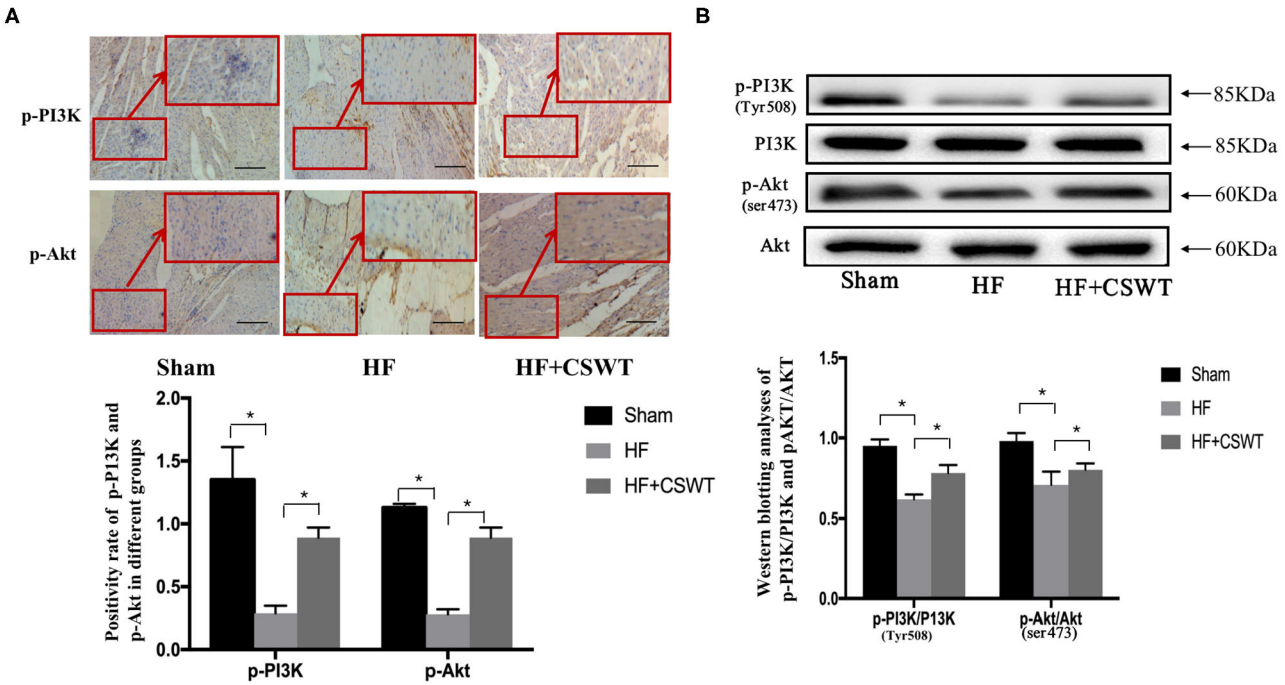

FIGURE 2 | CSWT led to increased PI3K/AKT expression levels. **(A)** The positive rates of p-P13K and p-Akt in cardiocytes of rats in study group using Immunochemistry analyses; scale bar, 100 μm; **(B)** Relative protein expressions of PI3K, Akt, p-PI3K and p-Akt in cardiocytes of rats in study group using Western blot analyses. Values are expressed as mean ± S.E.M ($n = 5$). One-way ANOVA test was applied for determining the significance of data. *$p < 0.05$. CSWT, cardiac shock wave therapy; AMI, acute myocardial infarction; HF, heart failure; S.E.M, standard error of means.

inactivating PI3K/Akt pathway, as shown in **Figure 3C** (CD34: the HF group:1.90 ± 0.14; the HF + CSWT group: 1.24 ± 0.08; the HF + CSWT + LY294002 group: 1.53 ± 0.12, HF + LY294002 2.79 ± 0.10, *p*-values <0.05; αSMA: the HF group: 2.85 ± 0.16; the HF + CSWT group: 1.22 ± 0.01; the HF + CSWT + LY294002 group: 1.75 ± 0.10; the HF + LY294002 group: 3.67 ± 0.14, *p*-values <0.05).

Meanwhile, the positive rates of CD34 and αSMA evaluated by immunohistochemistry showed the same pattern as mRNA levels among the four groups (**Figure 3D**). That is, the administration of CSWT led to fewer fibrosis-related molecular expressions and that the inhibition of PI3K/Akt caused variable increases in the positivity of CD34 and αSMA.

Myocardial sections subjected to Masson's trichrome staining were displayed in **Figure 3E**. As the results revealed, a significant reduction in the fibrotic area proportion was observed in the HF + CSWT group relative to the HF group, but this fraction was again elevated after adding LY294002 (the HF group: 53.89 ± 1.01%; the HF + CSWT group: 29.18 ± 1.73%; the HF + CSWT + LY294002 group: 32.25 ± 3.03%, the HF + LY294002 group: 57.63 ± 3.19, *p*-values <0.05).

Immunohistochemical analyses of phosphorylated PI3K and Akt were shown in **Figure 3F**. The positive expression rates of both p-PI3K and p-Akt showed the lowest number in the HF + LY294002 group, indicating a successful establishment of the PI3K/Akt-inhibition model (p-PI3K: 0.29 ± 0.04; p-Akt: 0.13 ± 0.02). Moreover, the positivities of these two molecules showed a significant trend for elevation after CSWT administration, and then a trend for reduction after LY294002 pretreatment.

Figure 3G represented immunofluorescence examples of αSMA/CD34 and Procollage-I/CD34 combinations identified in heart tissues. The lowest fluorescence intensity of αSMA/CD34 and procollagen-I/CD34 were found in specimens from CSWT-treated rats. By comparison, both tissues from groups of the HF and the HF + LY294002 showed significantly increased levels of fibrosis markers, with the latter one being the highest.

Altogether, the before-mentioned outcomes convergingly supported our assumption that CSWT improved cardiac function in post-AMI HF by exerting anti-fibrosis effects through PI3K/Akt signaling pathway in rats.

DISCUSSION

When attacked by pathophysiological insults, two forms of cardiac fibrosis—replacement and reactive fibrosis would manifest as a response, and the former one plays a dominating role in the development of cardiac remodeling (12). It triggers the displacement of the myocardium with fibrous tissue, which delivers detrimental effects on the structure, excitation-contraction coupling, and the systolic and diastolic function of hearts. Therefore, cardiac fibrosis is recognized as a prerequisite for almost all forms of HF, predisposing patients with heart diseases to the outcome of HF (13). Also, it has been shown

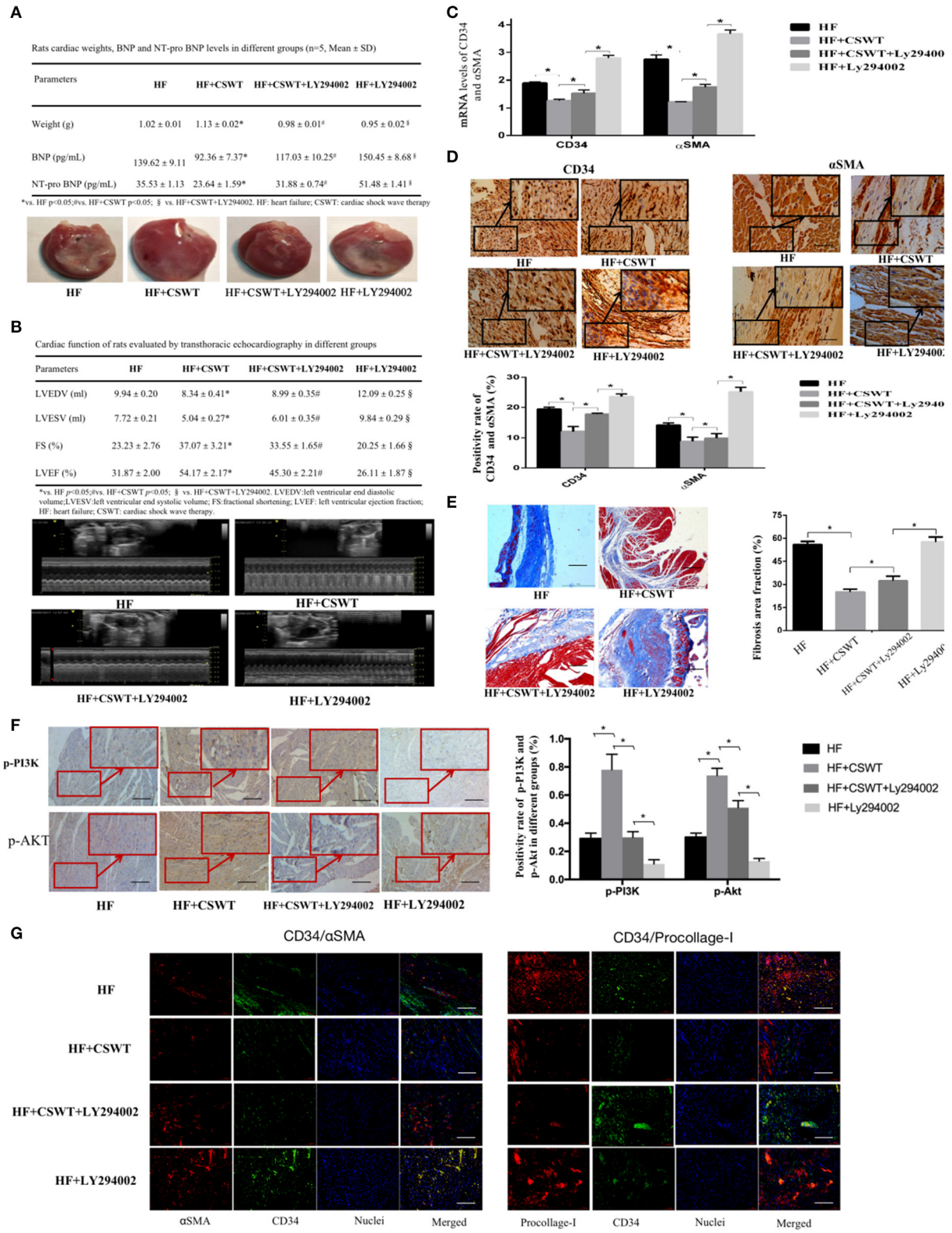

FIGURE 3 | The inhibition of PI3K/Akt pathway abolished the cardiac function improvement and anti-fibrosis effects of CSWT. **(A)** The cardiac weight, serum levels of BNP and NT-pro BNP and gross view of whole hearts in study groups; **(B)** Representative M-mode images by echocardiography of rats in study group; **(C)** Fold

(Continued)

FIGURE 3 | changes in CD34 and αSMA mRNA levels determined by RT-PCR in study groups; **(D)** The positive rates of CD34 and αSMA in study groups using Immunochemistry analyses; scale bar, 100 μm; **(E)** Representative images of Masson's trichrome staining and quantification for fibrosis in cardiomyocytes of rats in study group; scale bar, 100 μm; **(F)** The positive rates of p-P13K and p-Akt in cardiomyocytes of rats in study group using Immunochemistry analyses; scale bar, 100 μm; **(G)** Representative photomicrographs of immnunofluorescence for the detection of CD34/αSMA and CD34/Procollage-I. Red fluorescence shows αSMA or Procollage-I expression. Green fluorescence shows CD34 expression. Blue fluorescence shows nuclei of total cardiomyocytes; scale bar, 50 μm. Values are expressed as mean ± S.E.M ($n = 5$). One-way ANOVA test was applied for determining the significance of data. $^*p < 0.05$. CSWT, cardiac shock wave therapy; AMI, acute myocardial infarction; HF, heart failure; S.E.M, standard error of means.

that fibrotic severity is directly and positively associated with the long-term mortality of HF patients (14). Based on our earlier work, CSWT has been found to result in satisfactory improvement of cardiomyocyte apoptosis both *in vitro* and *in vivo* (6). And our published paper showed that CSWT promoted arteriogenesis of coronary micrangium and alleviated fibrosis after AMI by integrin linked kinase (ILK)-induced inhibition of myocardial apoptosis (7). Another evidence was from Hiroaki's study (8). They found that extracorporeal low-energy shock-wave therapy significantly ameliorated LV remodeling and fibrosis in rat after acute AMI. The mechanisms may involved in suppressing the infiltration of neutrophils and macrophages and enhancing the expression of endothelial nitric oxide synthase. However, both our previous study and Hiroaki's study failed to fully observe the anti-fibrosis effect of CSWT, nor to explore its molecular mechanism and signaling pathways. Furthermore, the proven clinical benefits, together with the well-documented anti-fibrosis of CSWT hinted us that CSWT may take effect through suppressing the occurrence and development of fibrosis and thus serving as a promising procedure to improve the prognosis of patients living with HF. Nevertheless, what mediates the CSWT effect is scarcely discussed. To our best knowledge, the current study is among the first to fully evaluate the anti-fibrosis effect and further delve into the potential signal pathways underlying such effects of CSWT through multiple measurements from Echocardiography and Masson's trichrome staining to Immunohistochemical and immunofluorescent analyses.

Establishing a robust as well as stable HF model is the precondition for subsequent experiments. In this study, the measurements of LVEDV, LVESV, LVEF, and FS by echocardiography, the evaluations of the architecture, weight of hearts, and the detection of serum BNP, NT-pro BNP were conducted simultaneously 4 weeks after the surgery and CSWT application, which lend support to the reliability of our model. It is observed that, the cardiac volume of rats is enlarged 4 weeks after the LAD ligation, as indicated by the significantly heightened LVEDV and LVESV. The expanded LV volume stimulated the release of BNP, a cardiac function criterion that is directly proportional to the volume enlargement. Followed by the decrease of LVEF and FS, stemmed from the impaired myocardium function due to the injurious stimulus of ischemia and necrosis. In all, the above-mentioned data consistently suggested the fact that the current model meets our anticipation and was able to pave the way for our further experiments.

The fact that we investigated reduced CD34 and αSMA mRNA expression levels and positive rates, smaller fibrous areas, and lower density of fibrocytes in the HF + CSWT group than in the control group suggested that CSWT suppressed fibrosis-related molecules, such as CD34 and αSMA, leading to the improvement of cardiac fibrosis. Consistent with our findings, Lei et al. demonstrated that the role CSWT played in myocardial anti-fibrosis may be related to the repression of fibrocytes amounts in pigs (9). Similarly, the study of Abe et al., using a model of AMI rats, clarified that CSWT therapy attenuated cardiac fibrosis by reducing the number of TGF-β1-positive cells, an important signal that is well-acknowledged to be closely associated with the formation of fibrosis (8). The anti-fibrosis effect of CSWT is not limited to cardiac tissues, as a newly-published study has introduced this therapy in a model of liver fibrosis, which also obtained satisfactory outcomes (15). The potentials of CSWT were also supported by fibroblast originated from human hypertrophic scar (16). As a general process characterized by the accumulation of fibroblasts and abnormal deposition of the extracellular matrix, the development of cardiac fibrosis and liver or human hypertrophic scar had many similarities. Therefore, the current finding of the anti-fibrosis effect of CSWT is well-founded, however, it still needs to be further elucidated what types of collagen or procollagen were exactly the targets.

The PI3K/Akt signaling pathway is known as a regulator mainly responsible for cellular survival and functions (17). It has already been shown in our previous publication and unpublished data that this pathway was associated with the anti-apoptosis effect of CSWT both *in vivo* and *in vitro* (6). This finding concorded with the research of Yu et al., in which they reported that the PI3K/Akt pathway involved in suppressing apoptosis-related protein expressions and thus the apoptosis of cardiomyocytes by CSWT therapy in H9c2 cells (18). For a long time, apoptosis has been considered serving as an initiator or perpetrator in fibrotic response, and the activation of apoptosis can be observed in nearly all kinds of fibrosis. The potential mechanism involves immune modulation and paracrine signaling, which potentially and substantially contribute to the presence and persistence of fibrosis (19). The closely-bonded relation between apoptosis and fibrosis, together with the demonstrated mechanism of PI3K/Akt pathway underlying the cardiac apoptosis alleviation conferred by CSWT gave us a strong hint that this pathway may also explain the protective effect of CSWT in post-infarction fibrosis. Current findings are encouraging and supported our anticipation. By immunohistochemistry and western blot, it is found that phosphorylation of PI3K and Akt presented enhancive changes after undergoing CSWT while untreated ones showed opposite outcomes, indicating the potential involvement of PI3K/Akt in the beneficial effects of CSWT and also laying the ground for further experiments.

In the next step, we inhibited the PI3K/Akt pathway to find out whether the cardioprotective effects of CSWT were impaired or abolished. As we expected, blocking the PI3K/Akt pathway resulted in a reversed pattern, wherein the originally improved cardiac function, reduced fibrous areas and expressive amounts of CD34, αSMA, and Procollagen I showed opposite trends, compared with a single application of CSWT. These results implied that the cardioprotection of CSWT is achieved partially by ameliorating fibrosis after AMI and such effect may be mediated via a PI3K/Akt-dependent pathway. In recent years, there is growing evidence that the activation of the PI3K/Akt path facilitates the improvement of cardiac fibrosis in models from ischemia/reperfusion to AMI and diabetic cardiomyopathy (20–22). It's speculated that the phosphorylation of PI3K/Akt may help enhance the proliferation and suppress apoptosis and inflammatory responses via working with a series of related proteins. The proteins that have been discovered by now included vascular endothelial growth factor (VEGF) and nuclear factor-κB (23, 24). Additionally, in this study, despite the fact that LY294002 weakened the effects of CSWT on fibrosis, the CSWT-induced anti-fibrosis effect was not fully eliminated. It hinted us that there existed more pathways being functional in recovering AMI-induced cardiac fibrosis after applying CSWT. Therefore, future studies focusing on the synergy or antagonism with PI3K/Akt by other proteins or signaling pathways have to be discussed to gain a greater understanding of the working mode of CSWT.

This investigation offered novel insights into the molecular mechanism with regard to the anti-fibrosis benefits of CSWT. Nevertheless, it should be noted that the chemical inhibition of PI3K/Akt pathway rather than the PI3K/Akt genes knockout limits the strengths of current conclusion to determine the clinical application of CSWT. Despite of the preliminary character, this study proposed a new mechanism for the first time that the anti-fibrosis effect of CSWT may involved this signal pathway. To tremendously consolidate the current findings, future investigations with the PI3K/Akt genes knockout models is constantly needed.

CONCLUSIONS

Taken together, CSWT is proved to promote the cardiac function indexes in rats with ischemic HF and deliver positive impacts on moderating cardiac fibrosis. Furthermore, we illuminated that the activation of the PI3K/Akt signal transduction pathway partially explained the biological effects that CSWT posed. These findings help expand the current understanding of CSWT-based HF therapy and it is certainly instigated that CSWT as an effective as well as non-invasive approach, is promised to protect hearts against fibrosis following ischemic HF.

DATA AVAILABILITY STATEMENT

The raw data supporting the conclusions of this article will be made available by the authors, without undue reservation.

ETHICS STATEMENT

The animal study was reviewed and approved by the Institutional Animal Care and Use Committee (IACUC) of the Institutional Ethics Committee at the First Affiliated Hospital of Kunming Medical University (Yunnan, China).

AUTHOR CONTRIBUTIONS

PY designed and supervised the study. LW supervised the study and critically revised the draft. XT performed the statistical analyses and drafted the manuscript. XT, YC, XM, LS, HL, XZ, FD, SL, and TG performed the experiments. All authors contributed to the article and approved the submitted version.

FUNDING

This research was supported by: the National Natural Science Foundation of China (Nos. 81760074 and 81860073); Special Foundation Projects of Joint Applied Basic Research of Yunnan Provincial Department of Science and Technology with Kunming Medical University [Nos. 2017FE468 (-034) and 2019FE001 (-138)]; Yunnan Provincial Department of Science and Technology (No. 202001AT070039); Projects of 2017 Yunnan Provincial Health Research Institute (No. 2017NS016); Yunnan Health Training Project of High Level Talents (Nos. D-2018020 an H-2018032); Foundation Projects of Yunnan Provincial Department of Education (No. 2018JS206); 100 Young and Middle-aged Academic and Technical Backbones of Kunming Medical University (No. 60118260106); Young Talents of Yunnan Thousand Talents Plan (No. YNQR-QNRC-2019-006); Clinical Medcial Center for Cardiovascular and Cerebrovascular Disease of Yunnan Province (No. ZX2019-03-01). The sponsor provided financial support in experimental materials and the decision to submit the article for publication.

REFERENCES

1. World Health Organization. *Global Health Estimates 2016: Deaths by Cause, Age, Sex, by Country and by Region, 2000–2016.* (2018). Available online at: http://www.who.int/healthinfo/global_burden_disease/estimates/en/ (accessed November 16, 2018).
2. Jessup M, Brozena S. Heart failure. *N Engl J Med.* (2003) 348:2007–18. doi: 10.1385/159259347X
3. Poustchi F, Amani H, Ahmadian Z, Niknezhad SV, Mehrabi S, Santos HA, et al. Combination therapy of killing diseases by injectable hydrogels: from concept to medical applications. *Adv Healthc Mater.* (2021) 10:e2001571 doi: 10.1002/adhm.202001571
4. Gollmann-Tepeköylü C, Pölzl L, Graber M, Hirsch J, Nägele F, Lobenwein D, et al. miR-19a-3p containing exosomes improve function of ischaemic myocardium upon shock wave

therapy. *Cardiovasc Res.* (2020) 116:1226–36. doi: 10.1093/cvr/cvz209
5. Ceccon CL, Duque AS, Gowdak LH, Mathias W Jr, Chiang HP, Sbano JCN, et al. Shock-wave therapy improves myocardial blood flow reserve in patients with refractory angina: evaluation by real-time myocardial perfusion echocardiography. *J Am Soc Echocardiogr.* (2019) 32:1075–85. doi: 10.1016/j.echo.2019.04.420
6. Shang LL, Su Z, Ma XJ, Wang YQ, Wang Y, Wang QX, et al. Role of PI3K/Akt signaling pathway in ischemic rats underwent cardiac shock waves therapy. *Zhonghua Xin Xue Guan Bing Za Zhi.* (2019) 47:457–64. doi: 10.3760/cma.j.issn.0253-3758.2019.06.007
7. Yang W, He Y, Gan L, Zhang F, Hua B, Yang P, et al. Cardiac shock wave therapy promotes arteriogenesis of coronary micrangium, and ILK is involved in the biomechanical effects by proteomic analysis. *Sci Rep.* (2018) 8:1814. doi: 10.1038/s41598-018-19393-z
8. Abe Y, Ito K, Hao K, Shindo T, Ogata T, Kagaya Y, et al. Extracorporeal low-energy shock-wave therapy exerts anti-infammatory effects in a rat model of acute myocardial infarction. *Circ J.* (2014) 78:2915–25. doi: 10.1253/circj.CJ-14-0230
9. Lei PP, Tao SM, Shuai Q, Bao YX, Wang SW, Qu YQ, et al. Extracorporeal cardiac shock wave therapy ameliorates myocardial fibrosis by decreasing the amount of fibrocytes after acute myocardial infarction in pigs. *Coron Artery Dis.* (2013) 24:509–15. doi: 10.1097/MCA.0b013e3283640ec7
10. Fu YH, Lin QX, Li XH, Fei HW, Shan ZX, Huang XZ, et al. A novel rat model of chronic heart failure following myocardial infarction. *Methods Find Exp Clin Pharmacol.* (2009) 31:367–73. doi: 10.1358/mf.2009.31.6.1393631
11. Primessnig U, Schonleitner P, Holl A, Pfeiffer S, Bracic T, Rau T, et al. Novel pathomechanisms of cardiomyocyte dysfunction in a model of heart failure with preserved ejection fraction. *Eur J Heart Fail.* (2016) 18:987–97. doi: 10.1002/ejhf.524
12. Krenning G, Zeisberg EM, Kalluri R. The origin of fibroblasts and mechanism of cardiac fibrosis. *J Cell Physiol.* (2010) 225:631–7. doi: 10.1002/jcp.22322
13. Diez F, Jaisser A, Pizard F. Myocardial fibrosis: biomedical research from bench to bedside. *Eur J Heart Fail.* (2017) 19:177–91. doi: 10.1002/ejhf.696
14. Aoki T, Fukumoto Y, Sugimura K, Oikawa M, Satoh K, Nakano M, et al. Prognostic impact of myocardial interstitial fibrosis in non-ischemic heart failure–comparison between preserved and reduced ejection fraction heart failure. *Circ J.* (2011) 75:2605–13. doi: 10.1253/circj.CJ-11-0568
15. Ujiie N, Nakano T, Yamada M, Sato C, Nakanishi C, Fujishima F, et al. Low-energy extracorporeal shock wave therapy for a model of liver cirrhosis ameliorates liver fibrosis and liver function. *Sci Rep.* (2020) 10:2405. doi: 10.1038/s41598-020-58369-w
16. Cui HS, Hong AR, Kim JB, Yu JH, Cho YS, Joo SY, et al. Extracorporeal shock wave therapy alters the expression of fibrosis-related molecules in fibroblast derived from human hypertrophic scar. *Int J Mol Sci.* (2018) 19:124. doi: 10.3390/ijms19010124
17. Berk BC, Fujiwara K, Lehoux S. ECM remodeling in hypertensive heart disease. *J. Clin Invest.* (2007) 117:568–75. doi: 10.1172/JCI31044
18. Yu WW, Shen T, Liu BY, Wang S, Li J, Dai D, et al. Cardiac shock wave therapy attenuates H9c2 myoblast apoptosis by activating the AKT signal pathway. *Cell Physiol Biochem.* (2014) 33:1293–303. doi: 10.1159/000358697
19. Yu P, Ma S, Dai X, Wang S, Li J, Dai D, et al. Elabela alleviates myocardial ischemia reperfusion-induced apoptosis, fibrosis and mitochondrial dysfunction through PI3K/AKT signaling. *Am J Transl Res.* (2020) 12:4467–77.
20. Hou N, Mai Y, Qiu X, Yuan W, Li Y, Luo C, et al. Carvacrol attenuates diabetic cardiomyopathy by modulating the PI3K/AKT/GLUT4 pathway in diabetic mice. *Front Pharmacol.* (2019) 10:998. doi: 10.3389/fphar.2019.00998
21. Wang X, Lu L, Tan Y, Yuan W, Li Y, Luo C, et al. GPR 30 reduces myocardial infarct area and fibrosis in.female ovariectomized mice by activating the PI3K/AKT pathway. *Life Sci.* (2019) 226:22–32. doi: 10.1016/j.lfs.2019.03.049
22. Zhang CJ, Huang Y, Lu JD, Lin J, Ge ZR, Huang H. Upregulated microRNA-132 rescues cardiac fibrosis and restores cardiocyte proliferation in dilated cardiomyopathy through the phosphatase and tensin homolog-mediated PI3K/Akt signal transduction pathway. *J Cell Biochem [preprint].* (2018) 1–13. doi: 10.1002/jcb.27081
23. Williams DL, Ozment-Skelton T, Li C. Modulation of the phosphoinositide 3-kinase signaling pathway alters host response to sepsis, inflammation, and ischemia/reperfusion injury. *Shock.* (2006) 25:432–9. doi: 10.1097/01.shk.0000209542.76305.55
24. Aneja R, Hake PW, Burroughs TJ, Denenberg AG, Wong HR, Zingarelli B. Epigallocatechin, a green tea polyphenol, attenuates myocardial ischemia reperfusion injury in rats. *Mol Med.* (2004) 10:55–62. doi: 10.2119/2004-00032.Aneja

Conflict of Interest: The authors declare that the research was conducted in the absence of any commercial or financial relationships that could be construed as a potential conflict of interest.

Copyright © 2021 Wang, Tian, Cao, Ma, Shang, Li, Zhang, Deng, Li, Guo and Yang. This is an open-access article distributed under the terms of the Creative Commons Attribution License (CC BY). The use, distribution or reproduction in other forums is permitted, provided the original author(s) and the copyright owner(s) are credited and that the original publication in this journal is cited, in accordance with accepted academic practice. No use, distribution or reproduction is permitted which does not comply with these terms.

frontiers in Cardiovascular Medicine

ORIGINAL RESEARCH
published: 09 July 2021
doi: 10.3389/fcvm.2021.690521

Cardiac, Macro-, and Micro-Circulatory Abnormalities in Association With Individual Metabolic Syndrome Component: The Northern Shanghai Study

Fang Zhao[1†], Rong Yang[1†], Rusitanmujiang Maimaitiaili[2], Jiamin Tang[2], Song Zhao[2], Jing Xiong[2], Jiadela Teliewubai[2], Chen Chi[2], Jacques Blacher[3], Jue Li[4], Yawei Xu[2], Yan Jiang[1], Yi Zhang[2] and Weiming Li[2*]*

[1] Department of Geriatrics, Shanghai Putuo People's Hospital, School of Medicine, Tongji University, Shanghai, China, [2] Department of Cardiology, Shanghai Tenth People's Hospital, School of Medicine, Tongji University, Shanghai, China, [3] Paris Descartes University, AP-HP, Diagnosis and Therapeutic Center, Hôtel-Dieu, Paris, France, [4] Institute of Clinical Epidemiology and Evidence-Based Medicine, Tongji University, Shanghai, China

OPEN ACCESS

Edited by:
Hui Gong,
Fudan University, China

Reviewed by:
Xuejuan Jin,
Fudan University, China
Rongchong Huang,
Capital Medical University, China

***Correspondence:**
Yi Zhang
yizshcn@gmail.com
Weiming Li
18917683469@189.cn

† These authors have contributed equally to this work and share first authorship

Specialty section:
This article was submitted to General Cardiovascular Medicine, a section of the journal Frontiers in Cardiovascular Medicine

Received: *03 April 2021*
Accepted: *04 June 2021*
Published: *09 July 2021*

Citation:
Zhao F, Yang R, Maimaitiaili R, Tang J, Zhao S, Xiong J, Teliewubai J, Chi C, Blacher J, Li J, Xu Y, Jiang Y, Zhang Y and Li W (2021) Cardiac, Macro-, and Micro-Circulatory Abnormalities in Association With Individual Metabolic Syndrome Component: The Northern Shanghai Study. Front. Cardiovasc. Med. 8:690521. doi: 10.3389/fcvm.2021.690521

Objective: This study investigated the association of metabolic syndrome (MS) and its components with cardiac, macro-, and micro-circulatory abnormalities in an elderly Chinese population.

Methods: This cross-sectional study was conducted using data for 1,958 participants from the Northern Shanghai Study aged over 65 years without a history of cardiovascular disease. MS was defined according to the National Cholesterol Education Program Adult Treatment Panel III in 2005 (NCEPIII 2005). Asymptomatic cardiovascular impairment parameters, including the left ventricle mass index (LVMI), peak transmitral pulsed Doppler velocity/early diastolic tissue Doppler velocity (E/Ea), carotid-femoral pulse wave velocity (cf-PWV), ankle-brachial index (ABI), carotid intima-media thickness (CIMT), arterial plaque, and urinary albumin–creatinine rate (UACR), were evaluated.

Results: LVMI, E/Ea, cf-PWV, and the proportion of UACR > 30 mg/g exhibited increasing trends while ABI exhibited a decreasing trend according to the number of MS components (all p for trend <0.01). Logistic regression analysis revealed that MS was significantly associated with LV hypertrophy (LVH), LV diastolic dysfunction, arteriosclerosis, and microalbuminuria (all $p < 0.001$). Central obesity and high blood pressure were associated with all cardiovascular abnormalities (all $p < 0.05$), whereas elevated plasma glucose was associated with arteriosclerosis and microalbuminuria (both $p < 0.001$). In addition, high triglyceride levels were associated with microalbuminuria ($p < 0.05$).

Conclusions: MS is significantly associated with cardiac, macro-, and micro-circulatory abnormalities in elderly Chinese. Moreover, the presence of individual MS components may have specific prognostic significance.

Keywords: elderly population, cardiac abnormality, macrocirculatory abnormality, microcirculatory abnormality, metabolic syndrome

INTRODUCTION

Metabolic syndrome (MS) is characterized by a cluster of risk factors that together significantly raise the risk for cardiovascular disease (CVD), stroke, diabetes, and other health issues (1). These risk factors include central obesity (i.e., excessive accumulation of abdominal fat around the waist), hypertension, hyperglycemia, and dyslipidemia (i.e., abnormal cholesterol and/or triglyceride levels), and MS is diagnosed when three or more of the abovementioned risk factors are present (2). MS has become a significant health burden worldwide, particularly with the expansion of the aging population, because MS not only is closely related to aging (3) but also promotes precocious aging (4). In addition, the presence of MS may significantly increase the morbidity and mortality of CVD patients. For example, in a study involving 4,483 participants, MS substantially increased the cardiovascular mortality rate by 12% compared with 2.2% in those without MS (5).

Asymptomatic cardiovascular impairments, which may be reflected by the presence of cardiac, macro-, and micro-circulatory abnormalities, are considered an intermediate state between risk factors and CVD, and can develop into CVD if not managed appropriately (6). Thus, it is imperative to identify the presence of cardiac, macro-, and micro-circulatory abnormalities as early as possible so that patients with a high risk of CVD may be managed in a timely and appropriately manner. The vast majority of cardiac, macro-, and micro-circulatory abnormalities can be screened by using simple and noninvasive methods as part of risk assessment, and several clinical studies have shown the relationship between MS and one or more asymptomatic cardiovascular impairments in select populations (7–9). However, few studies have systematically examined the correlation of MS and its individual components with various asymptomatic cardiovascular impairments in the same cohort of participants (10).

Abnormal macro-circulation is commonly characterized by two forms of arterial impairments, arteriosclerosis and atherosclerosis. It is recommended that arterial stiffness should be determined noninvasively by measuring the carotid-femoral pulse wave velocity (cf-PWV) as a gold standard, and PWV $>$ 10 m/s is defined as arteriosclerosis (11). An ankle-brachial index (ABI, the ratio of the ankle and systolic brachial pressure) $<$0.9 for low-limb arterial plaque and plaque in the carotid artery detected by ultrasonography are the most commonly used indexes for atherosclerosis in routine clinical practice (12). Due to the special structure of the kidney, renal micro-circulation is most susceptible to microvascular damage and the kidney is usually the site where the earliest microvascular injury occurs (13). Microalbuminuria reflects the functional status of renal micro-circulation and is commonly used to detect abnormal micro-circulation in daily clinical practice (14). In the present study, we used PWV, ABI, and the presence of carotid artery plaque as the indexes to represent abnormal macro-circulation, and microalbuminuria as the index to represent abnormal micro-circulation.

This study investigated the association between various asymptomatic cardiovascular impairments and MS as well as its components in a community-dwelling elderly Chinese population with no history of CVD. We found that MS is significantly associated with cardiac, macro-, and micro-circulatory abnormalities in elderly Chinese and that individual MS components exhibit associations with cardiac, macro-, and micro-circulatory abnormalities.

MATERIALS AND METHODS

Ethics Statement

This study was approved by the Ethics Committee of Shanghai Tenth People's Hospital, and written informed consent was obtained from all participants.

Study Participants

The present study is included in the Northern Shanghai Study (15). The Northern Shanghai Study (clinicaltrials.gov Identifier: NCT02368938) was a prospective study designed to establish a CV risk score based on a community dwelling Chinese elderly population, determining the profile of the associated CV risk factors and target organ damages, so as to guide the later intervention. According to *the Elderly population and cause of aging monitoring statistics of Shanghai in 2014*, the northern region has the largest population of elderly adults in Shanghai, with a total population of 1.57 million and an elderly proportion of over 19%. Thus, the northern Shanghai region, including Zhabei district and Putuo district, was selected. We used a computer-generated list of communities and randomly selected 10 communities for recruitment. The recruitment strategies included the following: (1) posting study recruitment posters in neighborhood committees and community hospitals; (2) according to the health files of the candidates, community hospitals recruited potential participants by telephone; and (3) distributing recruitment flyers directly to potential participants. When eligible individuals showed interest in participating in the study, they were sufficiently informed. Individuals who fulfilled all of the following criteria were included in the study: (1) age $\geq$ 65 years; (2) residents from urban communities in the northern region of Shanghai; and (3) availability for long-term follow-up. Candidates who met any of the following criteria were excluded from the study: (1) severe cardiac disease (New York Heart Association IV) or end-stage renal disease (chronic kidney disease $\geq$ stage 4); (2) history of stroke within 3 months; (3) a malignant tumor with a life expectancy $<$5 years. A total of 3,590 residents from communities in northern Shanghai were invited to participate in this study between June 2014 and 2019, and 3,363 (93.7%) participated in the initial screening process. A subsample of 2,200 participants [1,100 with MS according to the revised National Cholesterol Education Program Adult Treatment Panel III (NCEPIII) in 2005 (16) and 1,100 participants without MS], all of them without a history of CVD at baseline, were selected for the present study. This sample size was calculated based on a 1:1 exposed-to-non-exposed ratio, a cumulative incidence of 4.5–5% for cardiovascular event, an estimated hazard ratio of 2 for MS, a statistical power of 0.8, and an *a priori* defined alpha error of 0.05. Sample size was further overestimated for a possible 10% dropout rate. Finally, 968 participants with MS

and 1,090 participants without MS were contacted. Of these, 935 participants with MS and 1,065 participants without MS were recruited. Of the 2,000 participants, 42 were excluded due to incomplete data. Thus, the effective sample size for our analyses was 1,958 participants (908 with MS and 1,050 without MS).

All participants were instructed to complete a standardized questionnaire to obtain information on their history of present illnesses, smoking habits, medical therapy, and family history of premature CVD. Participants who smoked at least one cigarette per day for more than 6 months were defined as smokers and those who had quit smoking for more than 12 months were defined as former smokers (17). A family history of CVD was determined using the ASSIGN criteria for premature CVD or stroke before the age of 60 years in parents or siblings (18). MS was defined according to the revised NCEPIII (2005) as having at least three of the following metabolic disorders with central obesity modified for Asian populations (16): (1) waist circumference (WC) $\geq$ 90 cm for men and $\geq$ 80 cm for women; (2) blood pressure (BP) $\geq$ 130/85 mmHg and/or treatment of previously diagnosed hypertension; (3) fasting plasma glucose (FPG) $\geq$ 5.6 mmol/L and/or previously diagnosed type 2 diabetes; (4) serum triglyceride (TG) $\geq$ 1.7 mmol/L and/or specific treatment for lipid abnormality; and (5) high-density lipoprotein cholesterol (HDL-c) $<$ 1.03 mmol/L for men and $<$1.29 mmol/L for women and/or specific treatment for lipid abnormality. The revised NCEPIII (2005) criteria were used for the statistical analyses of the association between cardiovascular impairments and MS. The study also compared the differences in this association, according to the other three MS definitions: the International Diabetes Federation (IDF), the Chinese Diabetes Society (CDS), and the Chinese Joint Committee for Developing Chinese Guidelines on Prevention and Treatment of Dyslipidemia in Adults (JCDCG). According to the IDF definition (19), MS was defined as subjects with central obesity (men: WC $\geq$ 90 cm; women: WC $\geq$ 80 cm) together with two or more of the following metabolic disorders: (1) BP $\geq$ 130/85 mmHg and/or treatment of previously diagnosed hypertension; (2) FPG $\geq$ 5.6 mmol/L and/or previously diagnosed type 2 diabetes; (3) TG $\geq$ 1.7 mmol/L and/or specific treatment for lipid abnormality; (4) HDL-c $<$ 1.03 mmol/L for men and $<$1.29 mmol/L for women and/or specific treatment for lipid abnormality. According to the CDS definition (20), MS was defined as $\geq$3 of the following metabolic disorders: (1) body mass index (BMI) $\geq$ 25 kg/m^2; (2) BP $\geq$ 140/90 mmHg and/or treatment of previously diagnosed hypertension; (3) FPG $\geq$ 6.1 mmol/L and/or 2 h PG $\geq$ 7.8 mmol/L and/or treatment of previously diagnosed type 2 diabetes; (4) TG $\geq$ 1.7 mmol/L; and/or (5) HDL-c $<$0.9 mmol/L for men and $<$1.0 mmol/L for women. According to the 2016 JCDCG definition (21), MS was defined as $\geq$3 of the following metabolic disorders: (1) WC $\geq$ 90 cm for men and $\geq$85 cm for women; (2) BP $\geq$ 130/85 mmHg and/or treatment of previously diagnosed hypertension; (3) FPG $\geq$ 6.1 mmol/L and/or 2 h PG $\geq$ 7.8 mmol/L and/or treatment of previously diagnosed type 2 diabetes; (4) TG $\geq$ 1.7 mmol/L; and (5) HDL-c $<$ 1.0 mmol/L.

Anthropometric Measurements

General physical examination was conducted on all participants, and the following data were collected: body height, WC, and BP. BMI was calculated as weight in kilograms divided by the square of height in meters. Waist and hip circumferences were measured while standing with reference to external landmarks at the narrowest section of the waist, and at the level of the largest circumference between the iliac crest to the crotch, respectively. BP was measured three times after 10 min of rest in the sitting position with a semi-automatic oscillometric device (Omron Healthcare, Kyoto, Japan) by specialized physicians based on the recommendations of the European Society of Hypertension (22), and an average of three readings was used as the final BP for data analysis.

Biochemical Measurements

Blood and urine samples were collected after 10 h of overnight fasting to measure the FPG, total cholesterol (TC), TG, low-density lipoprotein cholesterol (LDL-c), HDL-c, alanine aminotransferase (ALT), aspartate aminotransferase (AST), serum creatinine, serum uric acid, urinary creatinine, and urinary albumin levels. Standard techniques were used to determine all of these parameters at the laboratory of Shanghai Tenth People's Hospital.

Definitions and Measurements of Cardiovascular Impairments

Cardiac Assessment

Echocardiography was performed on all participants by an experienced cardiologist who was blinded to the patients' data using a MyLab 30 Gold CV machine (ESAOTE SpA, Genoa, Italy) according to the American Society of Echocardiography recommendations (23, 24). Left ventricular internal diameter at end-diastole (LVIDd) and septal (SWTd) and posterior wall thickness at end-diastole (PWTd) were measured in the parasternal long-axis view. The left ventricle mass (LVM) was calculated based on the following formula: LVM (g) $= 0.8 \times \{1.04 \times [(\text{LVIDd} + \text{PWTd} + \text{SWTd})^3 - (\text{LVIDd})^3]\} + 0.6$ (25). The LVM index (LVMI) was assessed by dividing LVM by the body surface area (BSA) (26). Left atrial parameters including the M-mode left atrial dimension (SA1) in the parasternal short-axis view and measurements of short (SA2) and long axes (LA) in the apical four-chamber view at ventricular end-systole were measured. The left atrial volume (LAV) was determined using the ellipse model formula: LAV $= [\pi \times (\text{SA1} \times \text{SA2} \times \text{LA})/6]$ (27) and divided by BSA to determine the LAV index (LAVI). The peak transmitral pulsed Doppler velocity/early diastolic tissue Doppler velocity (E/Ea) was determined with continual wave Doppler in the four-chamber view and computed to evaluate the LV diastolic dysfunction.

LV hypertrophy (LVH) was defined as an LVMI $\geq$ 115 g/m^2 (men) or $\geq$95 g/m^2 (women). LV diastolic dysfunction was evaluated using E/Ea and other parameters of abnormal LV relaxing and filling, such as increased LVM and enlarged LAV. LV diastolic dysfunction was defined as an E/Ea $\geq$ 15 or 15 $>$ E/Ea $>$ 8 with the following: (1) LAVI $>$ 40 ml/m^2 and (2) LVMI $>$ 149 g/m^2 (men) or $\geq$122 g/m^2 (women) (28, 29).

Macro-Circulatory Assessment

Carotid ultrasonography was performed on the common carotid arteries on both sides using a 7.5-MHz transducer to record the carotid intima-media thickness (CIMT) and the presence or absence of plaques. Ankle BPs and bilateral brachial were automatically and simultaneously determined to calculate the ABI using the VP-1000 system (Omron Healthcare, Kyoto, Japan). PWV was determined with an applanation tonometer (SphygmoCor, AtCor Medical, Sydney, Australia) by a physician who was not involved with the ultrasound examination, in accordance with the European Expert Consensus on Arterial Stiffness (11) as previously detailed (15).

Macro-circulatory abnormalities were defined as arteriosclerosis with a PWV $>$ 10 m/s, and atherosclerosis with an ABI $<$ 0.9 or the presence of plaques (11, 12).

Micro-Circulatory Assessment

The urinary albumin–creatinine ratio (UACR) was determined as the ratio of urinary albumin divided by urinary creatinine. Microalbuminuria (UACR $>$ 30 mg/g) represented a micro-circulatory abnormality.

Statistical Analyses

The revised NCEPIII (2005) criteria were used for the statistical analyses of the association between cardiovascular impairments and MS. The normality of variables was examined with the Kolmogorov–Smirnov test. Normally distributed variables are presented as mean ± standard deviation (SD), whereas skewed variables are presented as median (interquartile range 25–75%). Categorical variables are expressed as a number with a percentage. Participants were categorized into four groups according to the number of metabolic disorders ($\leq$1, 2, 3, and $\geq$4). One-way analysis of variance (ANOVA) was used to compare the differences in data among multiple groups, followed by the Student-Newman-Keuls (SNK) test to compare the differences in data between two groups. The Kruskal–Wallis test was used to compare skewed variables among the groups. The chi-square test was used to compare the differences in the frequency between the groups. A UACR $>$ 30 mg/g was used as the cutoff point for trend analysis because UACR had a skewed distribution. Trends for the mean or frequency among the groups were estimated using the ANOVA test or a linear-by-linear association. The odds ratios (ORs) and 95% confidence interval (CI) were calculated to estimate the associations of various cardiovascular impairments with MS or its individual components using binary logistic regression models. All reported p-values were two tailed, and $p < 0.05$ were considered statistically significant. All statistical analyses were performed with the Statistical Package for Social Sciences version 13.0 (SPSS, IL, USA).

RESULTS

Demographic and Baseline Clinical Characteristics of Participants

After application of the inclusion and exclusion criteria, a total of 1,958 participants (879 men and 1,079 women) were finally included in this study. The median (interquartile range) age of the participants was 68.9 (66.5–73.1) years. According to the NCEPIII (2005) criteria for MS, the prevalence of MS was 46.4% (40.8% for men and 50.9% for women, $p < 0.001$). According to the IDF criteria for MS, the prevalence of MS was 37.1% (29.9% for men and 42.9% for women, $p < 0.001$). According to the CDS criteria for MS, the prevalence of MS was 21.6% (22.8% for men and 20.6% for women, $p = 0.244$). According to the JCDCG criteria for MS, the prevalence of MS was 28.7% (30.9% for men and 26.8% for women, $p < 0.05$). According to the NCEPIII (2005) criteria for individual MS components, the number and prevalence of high BP, central obesity, elevated PG, high TG, and low HDL-c were 1,433 (73.2%), 1,097 (56.0%), 714 (36.5%), 796 (40.7%), and 694 (35.4%), respectively. The number of participants with 0, 1, 2, 3, 4, and 5 components of MS according to the NCEPIII (2005) criteria was 161 (8.2%), 379 (19.4%), 510 (26.0%), 437 (22.3%), 331 (16.9%), and 140 (7.2%), respectively. Participants were categorized into four groups according to the number of metabolic disorders: group 1, participants with $\leq$1 metabolic disorders ($n = 540$); group 2, participants with 2 metabolic disorders ($n = 510$); group 3, participants with 3 metabolic disorders ($n = 437$); and group 4, participants with $\geq$4 metabolic disorders ($n = 471$). The demographic and baseline clinical characteristics of the participants in each group are presented in **Table 1**. No differences in age, AST, TC, LDL-c, urinary creatinine, family history of premature CVD, anti-hypertensive treatment, and anti-diabetic treatment were found among the groups. However, BMI, WC, hip circumference, systolic BP (SBP), diastolic BP (DBP), ALT, serum creatinine, serum uric acid, FPG, TG, HDL-c, urinary albumin, and the proportion of male, current smokers, and lipid-lowering treatment showed differences among the four groups (all $p < 0.05$).

The characteristics of cardiovascular assessment according to the number of metabolic disorders are shown in **Table 2**. No differences were observed in CIMT and the frequency of plaques in the carotid artery among the groups. However, LVMI, E/Ea, cf-PWV, ABI, and UACR showed significant differences among the four groups (all $p < 0.01$). Intergroup comparisons revealed that (i) groups 2, 3, and 4 had higher LVMI, E/Ea, cf-PWV, and UACR than group 1; (ii) groups 3 and 4 had higher cf-PWV than group 2; and (iii) group 4 had higher UACR than group 2, but lower ABI than groups 1 and 2. In addition, trend analyses revealed that LVMI, E/Ea, cf-PWV, and the proportion of UACR $>$ 30 mg/g presented an increasing trend, while ABI presented a decreasing trend according to the number of MS components (all p for trend $<$0.01; **Figure 1**).

Associations of Asymptomatic Cardiovascular Impairments With MS and Its Components

According to the definitions of cardiovascular impairment in this study, the number and prevalence of LVH, LV diastolic dysfunction, arteriosclerosis, atherosclerosis, and microalbuminuria were 404 (20.6%), 198 (10.1%),

TABLE 1 | Characteristics of the participants according to the number of metabolic disorders.

Parameters	All participants (n = 1,958)	Number of metabolic disorders				p-value
		≤1 (n = 540)	2 (n = 510)	3 (n = 437)	≥4 (n = 471)	
Age (years)	68.9 (66.5–73.1)	68.6 (66.4–72.7)	69.0 (66.5–73.4)	69.1 (66.6–73.6)	69.0 (66.6–72.8)	0.550
Male, *N* (%)	879 (44.9%)	289 (53.5%)	231 (45.3%)*	202 (46.2%)	157 (33.3%)*†‡	<0.001
BMI (kg/m^2)	24.4 ± 3.5	22.0 ± 2.6	24.5 ± 3.2*	25.1 ± 3.2*†	26.2 ± 3.2*†‡	<0.001
WC (cm)	85.9 ± 9.8	78.8 ± 7.4	86.3 ± 9.2*	88.1 ± 8.9*†	91.6 ± 8.6*†‡	<0.001
Hip circumference (cm)	96.2 ± 7.1	92.0 ± 5.7	96.8 ± 6.9*	97.7 ± 6.9*	99.1 ± 6.9*†‡	<0.001
SBP (mm Hg)	134.8 ± 16.7	125.7 ± 16.0	137.4 ± 16.8*	137.2 ±15.4*	140.1 ± 14.5*†‡	<0.001
DBP (mm Hg)	80.1 ± 9.6	76.6 ± 8.7	80.9 ± 9.7*	81.2 ± 9.4*	82.1 ± 9.5*	<0.001
ALT (U/L)	15.4 (12.3–20.9)	13.9 (11.1–17.8)	15.1(12.4–21.0)*	15.9 (12.8–20.8)*	17.5 (13.1–24.2)*†‡	<0.001
AST (U/L)	19.4 (16.8–22.8)	19.6 (16.8–22.8)	19.4 (17.2–22.8)	19.1 (16.8–22.7)	19.2 (16.4–23.2)	0.759
Serum creatinine (μmol/L)	73.6 ± 17.8	74.6 ± 16.2	73.8 ± 18.4	74.8 ± 19.4	71.3 ± 17.2*‡	<0.05
Serum uric acid (μmol/L)	328.3 ± 78.2	314.2 ± 75.5	328.1 ± 80.2*	331.2 ± 74.6*	342.1 ± 79.5*†	<0.001
FPG (mmol/L)	5.20 (4.80–5.90)	4.90 (4.70–5.30)	5.10 (4.80–5.50)*	5.40 (4.90–6.30)*†	6.00 (5.30–7.20)*†‡	<0.001
TC (mmol/L)	5.17 ± 0.98	5.13 ± 0.94	5.21 ± 0.94	5.15 ± 1.00	5.19 ± 1.06	0.556
TG (mmol/L)	1.36 (1.04–1.88)	1.08 (0.85-1.33)	1.26 (1.02–1.57)*	1.59 (1.17–2.07)*†	1.98 (1.54–2.62)*†‡	<0.001
HDL-c (mmol/L)	1.40 ± 0.36	1.59 ± 0.36	1.46 ± 0.33*	1.32 ± 0.31*†	1.19 ± 0.30*†‡	<0.001
LDL-c (mmol/L)	3.20 ± 0.86	3.15 ± 0.81	3.26 ± 0.79	3.22 ± 0.90	3.17 ± 0.93	0.160
Urinary creatinine (mmol/L)	5,884.2 ± 3,345.5	6,157.3 ± 3,467.6	5,878.7 ± 3,323.3	5,843.4 ± 3,188.6	5,612.7 ± 3,355.0	0.083
Urinary albumin (mg/L)	18.6 (8.4–27.5)	16.0 (7.2–24.7)	18.5 (8.0–26.7)*	19.5 (9.0–31.0)*	20.7 (9.5–34.5)*†	<0.001
Current smoker, *N* (%)	328 (16.8%)	109 (20.2%)	84 (16.5%)	70 (16.0%)	65 (13.8%)*†‡	0.003
Family history of premature CVD, *N* (%)	358 (18.3%)	91 (16.9%)	99 (19.4%)	76 (17.4%)	92 (19.5%)	0.593
Anti-hypertensive treatment, *N* (%)	814 (93.3%)	100 (95.2%)	218 (92.4%)	214 (91.5%)	282 (94.9%)	0.315
Anti-diabetic treatment, *N* (%)	268 (87.0%)	23 (88.5%)	53 (89.8%)	74 (87.1%)	118 (85.5%)	0.864
Lipid-lowering treatment, *N* (%)	239 (12.2%)	0 (0.0%)	21 (4.1%)*	61 (14.0%)*†	157 (33.3%)*†‡	<0.001

*Data were presented as mean ± standard deviation, median (interquartile range 25%−75%), or number with a percentage. *vs. group 1, †vs. group 2, and ‡vs. group 3. One-way analysis of variance, Kruskal–Wallis test, and chi-square test were used for comparisons among the four groups.*

ALT, alanine aminotransferase; AST, aspartate aminotransferase; BMI, body mass index; CVD, cardiovascular disease; DBP, diastolic blood pressure; FPG, fasting plasma glucose; HDL-c, high-density lipoprotein cholesterol; LDL-c, low-density lipoprotein cholesterol; systolic blood pressure; TC, total cholesterol; TG, triglyceride; WC, waist circumference.

184 (9.4%), 1,279 (65.3%), and 942 (48.1%). We next performed binary logistic regression analyses to examine the associations of various asymptomatic cardiovascular impairments with MS (**Table 3**). After adjustment for age (continuous variable), sex (categorical variable), smoking status (categorical variable), and family history of premature CVD (categorical variable), MS was significantly associated with LVH, LV diastolic dysfunction, arteriosclerosis, and microalbuminuria (all $p < 0.001$).

We also examined the associations of asymptomatic cardiovascular impairments with individual components of MS (**Table 4**). In model 1, MS components were separately identified as independent variables after adjustment for age (continuous variable), sex (categorical variable), serum creatinine (continuous variable), serum uric acid (continuous variable), smoking status (categorical variable), and family history of premature CVD (categorical variable). In this model, some individual MS components were associated with LVH, LV diastolic dysfunction, arteriosclerosis, and microalbuminuria. In model 2 (**Figure 2**), further adjustments were made for the other four MS components simultaneously (categorical variable). The results showed that (i) central obesity and high BP were associated with LVH (both $p < 0.01$); (ii) central obesity and high BP were associated with LV diastolic dysfunction (all $p < 0.05$); (iii) central obesity, high BP, and elevated PG were associated with arteriosclerosis (all $p < 0.05$); and (iv) central obesity, high BP, elevated PG, and high TG were associated with microalbuminuria (all $p < 0.05$).

Associations of Asymptomatic Cardiovascular Impairments With MS Defined by Four Criteria

We next compared the differences in this association between various asymptomatic cardiovascular impairments and MS, which was defined using the following four criteria: NCEPIII (2005), IDF, CDS, and JCDCG criteria. Logistic regression analysis with no adjustment showed that MS defined according to all four definitions was significantly associated with LVH, LV diastolic dysfunction, arteriosclerosis, and microalbuminuria (all $p < 0.01$). After adjustment for age (continuous variable), sex (categorical variable), smoking status (categorical variable), and family history of premature CVD (categorical variable), the association of MS with the

TABLE 2 | Characteristics of cardiovascular assessment according to the number of metabolic disorders.

Parameters	All participants	Number of metabolic disorders				P
		≤1 (*n* = 540)	2 (*n* = 510)	3 (*n* = 437)	≥4 (*n* = 471)	
Cardiac assessment						
LVMI (g/m^2)	85.58 ± 27.41	78.91 ± 23.81	87.27 ± 27.74*	89.35 ± 27.26*	87.94 ± 29.73*	<0.001
E/Ea	9.09 ± 3.58	8.36 ± 3.17	9.30 ± 3.73*	9.36 ± 3.71*	9.46 ± 3.63*	<0.001
Macrocirculatory assessment						
cf-PWV (m/s)	9.10 ± 2.18	8.29 ± 1.86	9.14 ± 2.09*	9.51 ± 2.20*†	9.62 ± 2.34*†	<0.001
ABI	1.07 ± 0.12	1.07 ± 0.11	1.07 ± 0.12	1.06 ± 0.12	1.05 ± 0.12*†	0.006
C-IMT (mm)	0.67 ± 0.17	0.65 ± 0.16	0.67 ± 0.18	0.67 ± 0.18	0.68 ± 0.18	0.056
Plaque in carotid artery, *N* (%)	1,254 (64.2%)	355 (65.9%)	316 (62.5%)	279 (63.8%)	302 (64.7%)	0.708
Microcirculatory assessment						
UACR (mg/g)	28.96 (13.40–55.86)	22.86 (11.16–41.24)	28.81 (12.95–55.34)*	31.65 (14.56–62.43)*	37.55 (16.34–70.83)*†	<0.001

*Data were presented as mean ± standard deviation, median (interquartile range 25–75%), or number with a percentage. The characteristics of asymptomatic cardiovascular impairment according to the number of MS components were evaluated with one-way analysis of variance, Kruskal–Wallis test, and chi-square test. *vs. group 1, †vs. group 2.*
ABI, ankle-brachial index; cf-PWV, carotid-femoral pulse wave velocity; C-IMT, carotid intima-media thickness; E/Ea, peak transmitral pulsed Doppler velocity/early diastolic tissue Doppler velocity; LVMI, left ventricle mass index; PP, pulse pressure; UACR, urinary albumin–creatinine rate.

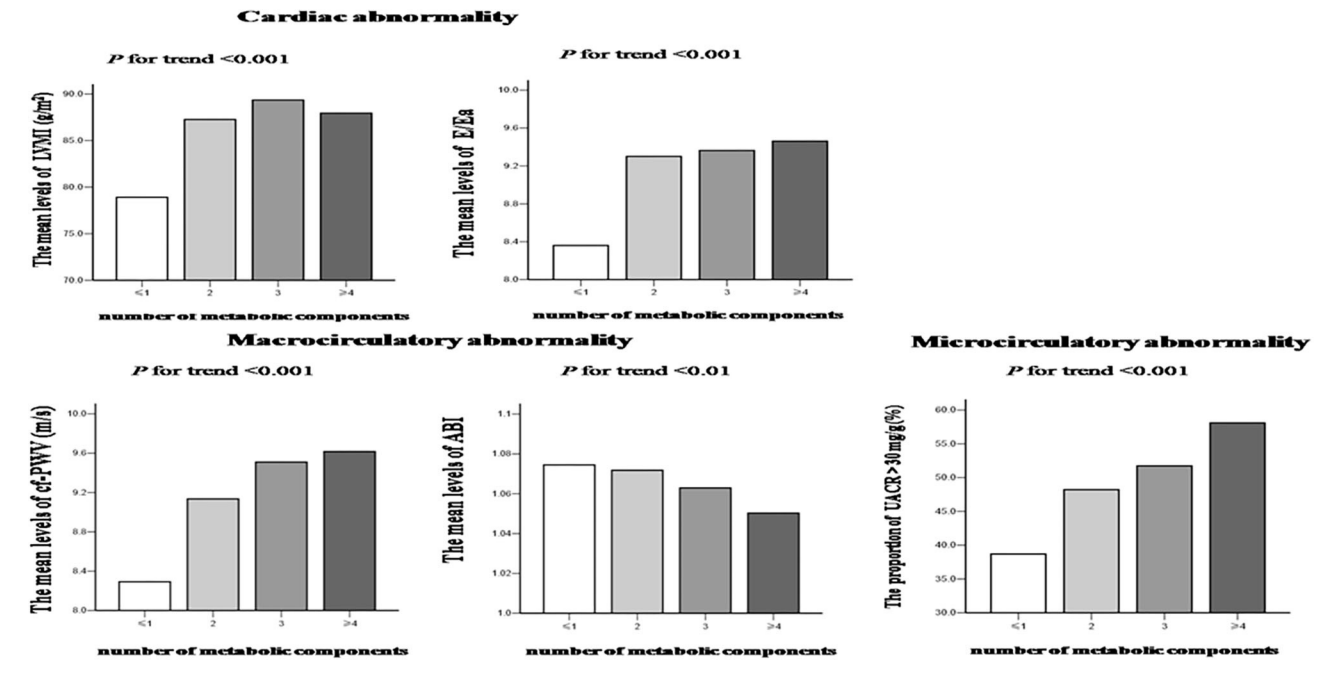

FIGURE 1 | Distributions of asymptomatic cardiovascular impairments according to the number of metabolic syndrome components. A UACR > 30 mg/g was used as the cutoff point for trend analysis because UACR had a skewed distribution. Trends for the mean or frequency among the groups were estimated using the ANOVA test or a linear-by-linear association.

aforementioned four asymptomatic cardiovascular impairments persisted (all $p < 0.01$).

DISCUSSION

In the present study, we examined the associations of MS and its components with various asymptomatic cardiovascular impairments in an elderly Chinese population without a history of CVD. We simultaneously assessed cardiac, macro-, and micro-circulatory abnormalities in the same population. We found that (1) these structural and functional abnormalities presented increasing or decreasing trends according to the number of metabolic disorders present; (2) MS was associated with LVH, LV diastolic dysfunction, arteriosclerosis, and microalbuminuria after adjustment for age, sex, smoking status, and family history of premature CVD; and (3) individual MS components were correlated with asymptomatic cardiovascular impairments to varying degrees.

TABLE 3 | Association of various asymptomatic cardiovascular impairments with MS.

Asymptomatic cardiovascular impairment	Unadjusted		Adjusted*	
	OR (95% CI)	*p*-value	OR (95% CI)	*p*-value
Cardiac abnormality				
LVH	1.664 (1.334–2.075)	<0.001	1.521 (1.213–1.909)	<0.001
LV diastolic dysfunction	1.904 (1.410–2.571)	<0.001	1.736 (1.279–2.356)	<0.001
Macrocirculatory abnormality				
Arteriosclerosis	2.278 (1.660–3.127)	<0.001	2.360 (1.699–3.279)	<0.001
Atherosclerosis	1.031 (0.855–1.243)	0.752	1.040 (0.860–1.258)	0.685
Microcirculatory abnormality				
Microalbuminuria	1.602 (1.338–1.918)	<0.001	1.566 (1.304–1.879)	<0.001

*The ORs and 95% CI were calculated to estimate the associations of various cardiovascular impairments with MS by using binary logistic regression models. *Adjusted for age, sex, smoking status, and family history of premature CVD.*

CI, confidence interval; CVD, cardiovascular disease; LV, left ventricle; LVH, left ventricle hypertrophy; MS, metabolic syndrome; OR, odds ratio.

Previously, the Strong Heart Study, a longitudinal investigation conducted in American Indian communities, analyzed the impact of NCEP III-defined MS on cardiac structure and function in 1,436 nondiabetic participants without a history of CVD, and revealed a higher prevalence of LVH in participants with MS than in those without MS (30). After adjustment for age and sex, high BP and central obesity were identified as the only two MS components associated with changes in LV mass (30). Similarly, a population survey performed in Italy showed that participants with IDF-defined MS had a higher prevalence of LVH, reduced early-to-late diastolic function, and early impairment of diastolic function compared to those without MS (31). Among the five components of MS, WC and BP were more significantly associated with LV mass (31). In line with the above findings, in the present study, we found that high BP and central obesity were strongly linked to cardiac abnormality. It is well-known that a chronic increase in LV workload in hypertensive patients can result in LVH and LV diastolic dysfunction. On the other hand, according to collective mechanistic investigations, the heart of an obese individual is chronically overloaded with an elevation in cardiac output, even in the absence of hypertension (32, 33). Therefore, it is conceivable that central obesity is significantly linked to cardiac abnormality.

PWV has been shown to reflect arterial stiffness and is a useful marker of both the severity of macro-circulatory abnormality and the prognosis of CVD in elderly individuals (34, 35). Previous studies have also shown an association between increased PWV in individuals with MS (8, 36, 37). Although studies on both animals and humans have resulted in the position of several mechanisms underlying the relationship between metabolic disorders and arterial stiffness, it was unclear which metabolic disorders were associated with PWV. In the present study, we found that high BP and central obesity were associated with PWV. It is highly likely that elevated BP accelerates arterial stiffening because it forces endothelial and arterial smooth muscle cells to be chronically exposed to increased arterial wall distensibility (38). Nevertheless, the findings regarding the association between obesity and arterial stiffness were inconsistent, and the pathophysiological processes linking abdominal adiposity to arterial stiffness were still incompletely defined (39, 40).

In the present study, we found that high BP and central obesity were also associated with microalbuminuria, which is regarded as a marker of micro-circulatory abnormality (14). Previously, Lee et al. (41) conducted a population-based cross-sectional study in Korean adults to evaluate the association between MS and microalbuminuria and found that all of the MS components were associated with an increased risk of microalbuminuria after adjustment for covariates, with high BP having the strongest and low HDL-c having the weakest association in both sexes. The mechanism underpinning the association between high BP and microalbuminuria might be related to high BP-induced renal hemodynamic changes, resulting in increased glomerular filtration, reduced tubular reabsorption of albumin, and finally structural damage to glomeruli and arterioles (42). In the present study, we also found a correlation between central obesity and microalbuminuria, which was inconsistent with the findings from a study performed in Japan (9) and the NHANES III study (43). The discrepancy in the association between central obesity and microalbuminuria between these studies was probably due to the different populations selected for the respective studies.

We showed that hyperglycemia and high BP exhibited the strongest association with PWV, which was consistent with the findings of Chen et al. in southern China (8) and a population-based study performed in Korea (41). Hyperglycemia induces pathological alterations in vascular tissues at the cellular level, which potentially accelerates the atherosclerotic process (44). We also found that hyperglycemia was the strongest determinant of microalbuminuria, which was in agreement with previous findings (9, 43).

The present study identified relatively weaker associations of high TG with microalbuminuria, whereas low HDL-c was not associated with any cardiovascular impairment. Some studies have shown that lipid-lowering treatments such as statins failed to consistently and significantly reduce the risk of major

TABLE 4 | Association of asymptomatic cardiovascular impairments with individual components of MS.

Variables	LVH				LV diastolic dysfunction				Arteriosclerosis				Microalbuminuria			
	Model 1		Model 2		Model 1		Model 2		Model 1		Model 2		Model 1		Model 2	
	OR (95% CI)	*p*-value	OR (95% CI)	*p*-value	OR (95% CI)	*p*-value	OR (95% CI)	*p*-value	OR (95% CI)	*p*-value	OR (95% CI)	*p*-value	OR (95% CI)	*p*-value	OR (95% CI)	*p*-value
Central obesity	1.866 (1.451–2.400)	<0.001	1.750 (1.354–2.262)	<0.001	1.730 (1.230–2.433)	0.002	1.543 (1.091–2.182)	0.014	1.751 (1.234–2.483)	0.002	1.468 (1.025–2.102)	0.036	1.393 (1.151–1.687)	0.001	1.257 (1.032–1.532)	0.031
High BP	1.734 (1.310–2.294)	<0.001	1.577 (1.185–2.099)	0.002	1.968 (1.320–2.935)	0.001	1.744 (1.162–2.617)	0.007	3.241 (1.953–5.379)	<0.001	2.853 (1.702–4.783)	<0.001	1.490 (1.210-−1.835)	<0.001	1.340 (1.082–1.661)	0.007
Elevated PG	1.158 (0.917–1.462)	0.217	1.055 (0.830–1.340)	0.661	1.453 (1.073–1.969)	0.016	1.306 (0.957–1.783)	0.092	2.711 (1.965–3.741)	<0.001	2.561 (1.838–3.569)	<0.001	1.524 (1.261–1.842)	<0.001	1.419 (1.169–1.722)	<0.001
High TG	1.096 (0.869–1.383)	0.4401	1.023 (0.781–1.340)	0.867	1.463 (1.078–1.987)	0.015	1.414 (0.994–2.012)	0.054	1.345 (0.974–1.855)	0.072	1.289 (0.892–1.863)	0.177	1.351 (1.120–1.630)	0.002	1.293 (1.040–1.608)	0.021
Low HDL-c	1.048 (0.828–1.327)	0.697	0.949 (0.722–1.248)	0.710	1.115 (0.818–1.520)	0.490	0.853 (0.597–1.219)	0.382	0.909 (0.649–1.274)	0.579	0.685 (0.467–1.018)	0.063	1.130 (0.933–1.368)	0.212	0.913 (0.731–1.141)	0.425

The ORs and 95% CI were calculated to estimate the associations of various cardiovascular impairments with individual components of MS by using binary logistic regression models. Model 1 was adjusted for age, sex, serum creatinine, serum uric acid, smoking status, and family history of premature CVD. Model 2 was further adjusted for the other four MS components simultaneously.

BP, blood pressure; CI, confidence interval; CVD, cardiovascular diseases; HDL-c, high-density lipoprotein cholesterol; LV, left ventricle; LVH, left ventricle hypertrophy; MS, metabolic syndrome; OR, odds ratio; PG, plasma glucose; TG, triglyceride.

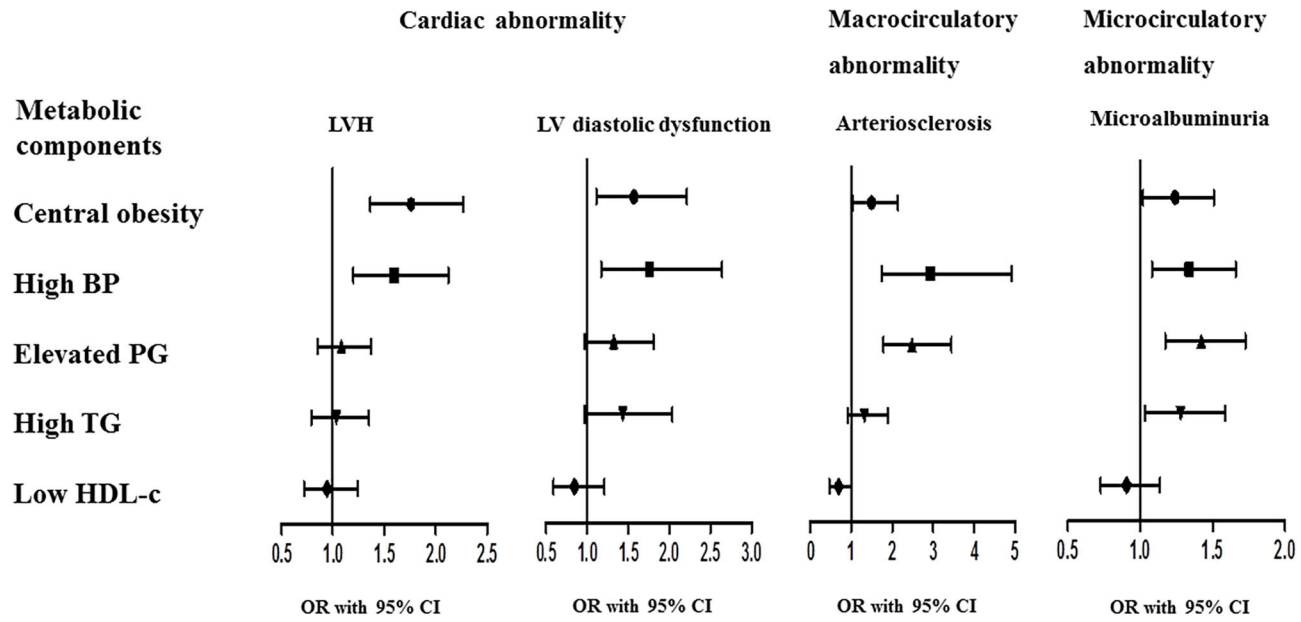

FIGURE 2 | Association of asymptomatic cardiovascular impairments with individual components of metabolic syndrome. The ORs and 95% CI were calculated to estimate the associations of various cardiovascular impairments with individual components of MS using binary logistic regression models, adjusted for age, sex, smoking status, family history of premature CVD, and the other four MS components.

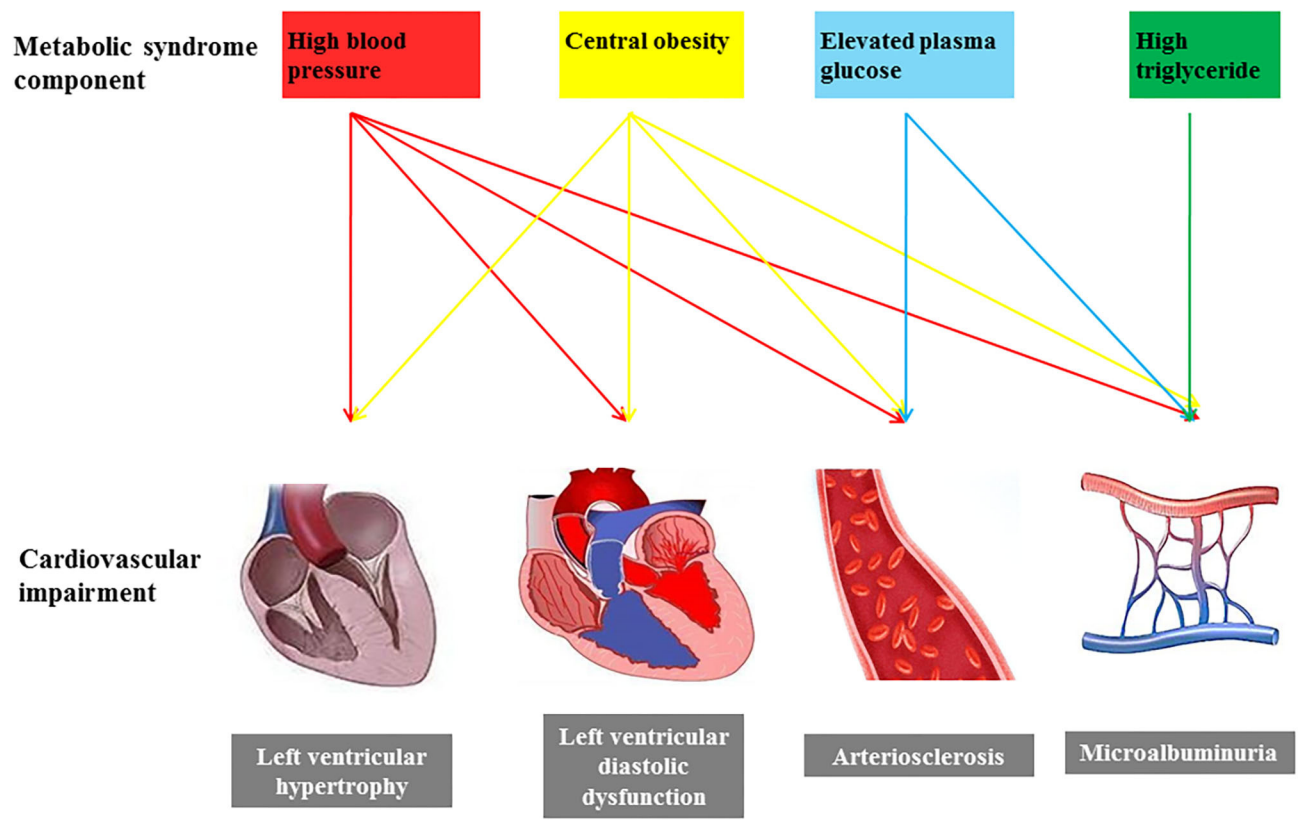

FIGURE 3 | The possible effect of individual components of metabolic syndrome on asymptomatic cardiovascular impairments.

cardiovascular events (45, 46). On the other hand, HDLs have been shown to form a heterogeneous class of lipoproteins that differ in protein and lipid composition, shape, size, and density (47, 48). Therefore, there is a possibility that the association of HDL with CVD may depend on the subclasses of HDLs. Unfortunately, in the present study, we did not analyze various HDL subclasses. This might explain why low HDL-c had no correlation with any cardiovascular impairment in the present study. Our previous study showed that in an elderly community sample, non-HDL-c and TC/HDL-c had a stronger association with macro- and micro-circulatory abnormalities compared with other lipid parameters (49). However, other studies reported that HDL-c was inversely associated with the LV structure and diastolic function (50, 51). These discrepant findings merit further clarification in the future.

In our study, atherosclerosis was defined as ABI < 0.9 or the presence of plaques. We found no significant association between atherosclerosis and MS, which was inconsistent with the conclusions of other studies (52, 53). Pathologically, atherosclerosis is a chronic inflammatory response to the accumulation of lipid in the artery wall and causes intimal plaques in the arteries. Although its prevalence is also age-related, the major risk factor that promotes the development of atherosclerosis is a high level of cholesterol (54). According to the definition of MS, dyslipidemia was diagnosed in participants receiving statin treatment for lipid abnormality. When participants were categorized into four groups according to the number of metabolic disorders, we found that the proportion of lipid-lowering treatment showed significant differences among the four groups [0 (0.0%), 21 (4.1%), 61 (14.0), and 157 (33.3%), $p < 0.01$], but no differences in the proportion of plaque in the carotid artery were found among the four groups. We speculated that lipid-lowering treatments such as statins significantly reduce the risk of plaques in the arteries.

Asymptomatic cardiovascular impairment is currently regarded as an intermediate stage in the continuum of CVD and a strong determinant of total cardiovascular risk. The components of MS are related to each other and frequently appear as cluster features. A recent study in Korea showed that only high BP was significantly associated with asymptomatic cardiovascular impairment when the individual components of MS were considered (10). However, in the present study, we found that individual components of MS had different degrees of associations with asymptomatic cardiovascular impairments (**Figure 3**). Both high BP and central obesity were associated with all cardiovascular abnormalities, while hyperglycemia had a significant correlation with arterial stiffness and micro-circulatory abnormality. In addition, high TG was associated with micro-circulatory abnormality. We believe that identifying the association of individual MS components with cardiac, macro-, and micro- circulatory abnormalities is more important than the association of MS as a whole with cardiac, macro-, and micro-circulatory abnormalities for clinical practice. This information can help with screening and interventions for different levels of cardiovascular risk in participants with different metabolic disorders.

Although the definitions of major components of MS according to different criteria are similar, individual components of MS and their diagnostic threshold values are defined differently based on different criteria. For instance, BMI or WC is used for obesity definition and the cutoff values for FPG and HDL-c are different with different criteria. To eliminate the impacts of different definitions on MS, in the present study, we examined the associations between cardiovascular impairments and MS in our study population based on four criteria: NCEPIII 2005, IDF, CDS, and JCDCG. Interestingly, we found that MS was consistently significantly correlated with LVH, LV diastolic dysfunction, arteriosclerosis, and microalbuminuria with all four definitions we examined.

The limitations of this study should be acknowledged. First, this study was cross-sectional and hence a causal relationship between MS and cardiovascular impairments could not be identified. Second, the study population only represented a subset of the Chinese elderly population, and therefore, whether the findings obtained from this study can be generalized to other ethnicities and age groups need to be further interrogated. Third, this study did not examine the levels of 2 h post-load plasma glucose, which might affect the assessment of hyperglycemia for the definition of MS according to the CDS and JCDCG criteria. Fourth, unfortunately we did not assess retinopathy in participants using fundoscopy in the present study; thus, we were not able to evaluate the association between retinal micro-circulation and MS.

CONCLUSION

In the present study, we demonstrated an association between MS and various asymptomatic cardiovascular impairments in an elderly Chinese population. Moreover, individual MS components were associated with LVH, LV diastolic dysfunction, arteriosclerosis, and microalbuminuria to varying degrees. Given the limitations of this study, prospective studies with large cohorts are warranted in the future to further clarify the role of these metabolic disorders in the development of asymptomatic cardiovascular impairments.

DATA AVAILABILITY STATEMENT

The raw data supporting the conclusions of this article will be made available by the authors, without undue reservation.

ETHICS STATEMENT

The studies involving human participants were reviewed and approved by the ethics committee of Shanghai Tenth People's Hospital. The patients/participants provided their written informed consent to participate in this study.

AUTHOR CONTRIBUTIONS

YZ and WL formulated the methods and designed the protocol. FZ and RY drafted the manuscript. RY and YZ contributed toward data analysis. YZ, WL, and FZ revised the article. All authors read the article and agree to be accountable for all aspects of the work.

FUNDING

This study was financially supported by the National Key Research and Development Program (2016YFC1301202), and Clinical Research Plan of SHDC (No. SHDC2020CR1040B, SHDC2020CR5009, SHDC2020CR5015-002).

REFERENCES

1. Ford ES. Risks for all-cause mortality, cardiovascular disease, and diabetes associated with the metabolic syndrome: a summary of the evidence. *Diabetes Care.* (2005) 28:1769–78. doi: 10.2337/diacare.28.7.1769
2. Rochlani Y, Pothineni NV, Kovelamudi S, Mehta JL. Metabolic syndrome: pathophysiology, management, and modulation by natural compounds. *Ther Adv Cardiovasc Dis.* (2017) 11:215–25. doi: 10.1177/1753944717711379
3. Guarner-Lans V, Rubio-Ruiz ME, Pérez-Torres I, Baños de MacCarthy G. Relation of aging and sex hormones to metabolic syndrome and cardiovascular disease. *Exp Gerontol.* (2011) 46:517–23. doi: 10.1016/j.exger.2011.02.007
4. Bonomini F, Rodella LF, Rezzani R. Metabolic syndrome, aging and involvement of oxidative stress. *Aging Dis.* (2015) 6:109–20. doi: 10.14336/AD.2014.0305
5. Isomaa B, Almgren P, Tuomi T, Forsén B, Lahti K, Nissén M, et al. Cardiovascular morbidity and mortality associated with the metabolic syndrome. *Diabetes Care.* (2001) 24:683–9. doi: 10.2337/diacare.24.4.683
6. Mancia G, Fagard R, Narkiewicz K, Redon J, Zanchetti A, Böhm M, et al. 2013 ESC/ESH Guidelines for the management of arterial hypertension: the Task Force for the Management of Arterial Hypertension of the European Society of Hypertension (ESH) and of the European Society of Cardiology (ESC). *Eur Heart J.* (2013) 34:2159–219. doi: 10.1093/eurheartj/eht151
7. Mulè G, Cerasola G. The metabolic syndrome and its relationship to hypertensive target organ damage. *J Clin Hypertens.* (2006) 8:195–201. doi: 10.1111/j.1524-6175.2006.04716.x
8. Chen L, Zhu W, Mai L, Fang L, Ying K. The association of metabolic syndrome and its components with brachial-ankle pulse wave velocity in south China. *Atherosclerosis.* (2015) 240:345–50. doi: 10.1016/j.atherosclerosis.2015.03.031
9. Hao Z, Konta T, Takasaki S, Abiko H, Ishikawa M, Takahashi T, et al. The association between microalbuminuria and metabolic syndrome in the general population in Japan: the Takahata study. *Intern Med.* (2007) 46:341–6. doi: 10.2169/internalmedicine.46.6056
10. Kim HL, Joo HJ, Lim WH, Seo JB, Kim SH, Zo JH, et al. Association between metabolic syndrome and parameters of subclinical target organ damage in urban subjects without documented cardiovascular disease. *Metab Syndr Relat Disord.* (2020) 18:373–80. doi: 10.1089/met.2020.0026
11. Van Bortel LM, Laurent S, Boutouyrie P, Chowienczyk P, Cruickshank JK, De Backer T, et al. Expert consensus document on the measurement of aortic stiffness in daily practice using carotid-femoral pulse wave velocity. *J Hypertens.* (2012) 30:445–8. doi: 10.1097/HJH.0b013e32834fa8b0
12. Aboyans V, Ricco JB, Bartelink MEL, Björck M, Brodmann M, Cohnert T, et al. 2017 ESC Guidelines on the Diagnosis and Treatment of Peripheral Arterial Diseases, in collaboration with the European Society for Vascular Surgery (ESVS): Document covering atherosclerotic disease of extracranial carotid and vertebral, mesenteric, renal, upper and lower extremity arteries Endorsed by: the European Stroke Organization (ESO) The Task Force for the Diagnosis and Treatment of Peripheral Arterial Diseases of the European Society of Cardiology (ESC) and of the European Society for Vascular Surgery (ESVS). *Eur Heart J.* (2018) 39:763–816. doi: 10.1093/eurheartj/ehx095
13. Heagerty AM, Aalkjaer C, Bund SJ, Korsgaard N, Mulvany MJ. Small artery structure in hypertension. Dual processes of remodeling and growth. *Hypertension.* (1993) 21:391–7. doi: 10.1161/01.HYP.21.4.391
14. Gowda S, Desai PB, Kulkarni SS, Hull VV, Math AA, Vernekar SN. Markers of renal function tests. *N Am J Med Sci.* (2010) 2:170–3.
15. Ji H, Xiong J, Yu S, Chi C, Fan X, Bai B, et al. Northern Shanghai Study: cardiovascular risk and its associated factors in the Chinese elderly-a study protocol of a prospective study design. *BMJ open.* (2017) 7:e013880. doi: 10.1136/bmjopen-2016-013880
16. Grundy SM, Cleeman JI, Daniels SR, Donato KA, Eckel RH, Franklin BA, et al. Diagnosis and management of the metabolic syndrome: an American Heart Association/National Heart, lung, and Blood Institute Scientific Statement. *Circulation.* (2005) 112:2735–52. doi: 10.1161/CIRCULATIONAHA.105.169404
17. Yang G, Fan L, Tan J, Qi G, Zhang Y, Samet JM, et al. Smoking in China: Findings of the 1996 National Prevalence Survey. *JAMA.* (1999) 282:1247–53. doi: 10.1001/jama.282.13.1247
18. Williamson C, Jeemon P, Hastie CE, McCallum L, Muir S, Dawson J, et al. Family history of premature cardiovascular disease: blood pressure control and long-term mortality outcomes in hypertensive patients. *Eur Heart J.* (2014) 35:563–70. doi: 10.1093/eurheartj/eht539
19. Alberti KG, Zimmet P, Shaw J. The metabolic syndrome-a new worldwide definition. *Lancet.* (2005) 366:1059–62. doi: 10.1016/S0140-6736(05)67402-8
20. Metabolic syndrome study cooperation group of Chinese Diabetes Society. Recommendations of the Chinese diabetes society on metabolic syndrome. *Chin J Diabetes.* (2004) 12:156–61.
21. Joint committee issued Chinese guideline for the management of dyslipidemia in adults. 2016 Chinese guideline for the management of dyslipidemia in adults. *Zhonghua Xin Xue Guan Bing Za Zhi.* (2016) 44:833–53. doi: 10.3760/cma.j.issn.0253-3758.2016.10.005
22. O'Brien E, Asmar R, Beilin L, Imai Y, Mancia G, Mengden T, et al. Practice guidelines of the European Society of Hypertension for clinic, ambulatory and self blood pressure measurement. *J Hypertens.* (2005) 23:697–701. doi: 10.1097/01.hjh.0000163132.84890.c4
23. Lang RM, Bierig M, Devereux RB, Flachskampf FA, Foster E, Pellikka PA, et al. Recommendations for chamber quantification: a report from the American Society of Echocardiography's Guidelines and Standards Committee and the Chamber Quantification Writing Group, developed in conjunction with the European Association of Echocardiography, a branch of the European Society of Cardiology. *J Am Soc Echocardiogr.* (2005) 18:1440–63. doi: 10.1016/j.echo.2005.10.005
24. Lang RM, Bierig M, Devereux RB, Flachskampf FA, Foster E, Pellikka PA, et al. Recommendations for chamber quantification. *Eur J Echocardiogr.* (2006) 7:79–108. doi: 10.1016/j.euje.2005.12.014
25. Devereux RB, Alonso DR, Lutas EM, Gottlieb GJ, Campo E, Sachs I, et al. Echocardiographic assessment of left ventricular hypertrophy: comparison to necropsy findings. *Am J Cardiol.* (1986) 57:450–8. doi: 10.1016/0002-9149(86)90771-X
26. Brilla CG. What is the value of the left ventricular muscle mass index (LVMI) in echocardiographic diagnosis of left heart hypertrophy?. *Internist (Berl).* (1993) 34:986.
27. Lang RM, Badano LP, Mor-Avi V, Afilalo J, Armstrong A, Ernande L, et al. Recommendations for cardiac chamber quantification by echocardiography in adults: an update from the American Society of Echocardiography and the European Association of Cardiovascular Imaging. *J Am Soc Echocardiogr.* (2015) 28:1–39.e14. doi: 10.1016/j.echo.2014.10.003
28. Kane GC, Karon BL, Mahoney DW, Redfield MM, Roger VL, Burnett JC Jr, et al. Progression of left ventricular diastolic dysfunction and risk of heart failure. *JAMA.* (2011) 306:856–63. doi: 10.1001/jama.2011.1201
29. Zhang Y, Kollias G, Argyris AA, Papaioannou TG, Tountas C, Konstantonis GD, et al. Association of left ventricular diastolic dysfunction with 24-h aortic ambulatory blood pressure: the SAFAR study. *J Hum Hypertens.* (2015) 29:442–8. doi: 10.1038/jhh.2014.101

30. Chinali M, Devereux RB, Howard BV, Roman MJ, Bella JN, Liu JE, et al. Comparison of cardiac structure and function in American Indians with and without the metabolic syndrome (The Strong Heart Study). *Am J Cardiol.* (2004) 93:40–4. doi: 10.1016/j.amjcard.2003.09.009
31. Ferrara LA, Cardoni O, Mancini M, Zanchetti A. Metabolic syndrome and left ventricular hypertrophy in a general population. *Results from the Gubbio Study*. *J Hum Hypertens.* (2007) 21:795–801. doi: 10.1038/sj.jhh.1002232
32. Lauer MS, Evans JC, Levy D. Prognostic implications of subclinical left ventricular dilatation and systolic dysfunction in men free of overt cardiovascular disease (the Framingham Heart Study). *Am J Cardiol.* (1992) 70:1180–4. doi: 10.1016/0002-9149(92)90052-Z
33. Kuch B, Muscholl M, Luchner A, Döring A, Riegger GA, Schunkert H, et al. Gender specific differences in left ventricular adaptation to obesity and hypertension. *J Hum Hypertens.* (1998) 12:685–91. doi: 10.1038/sj.jhh.1000689
34. Laurent S, Cockcroft J, Van Bortel L, Boutouyrie P, Giannattasio C, Hayoz D, et al. Expert consensus document on arterial stiffness: methodological issues and clinical applications. *Eur Heart J.* (2006) 27:2588–605. doi: 10.1093/eurheartj/ehl254
35. Doba N, Tokuda Y, Tomiyama H, Goldstein NE, Kushiro T, Hinohara S. Changes in ankle brachial pulse wave velocity during a five-year follow-up period in older Japanese adults: sub-analysis results of the health research volunteer study in Japan. *Intern Med.* (2013) 52:21–7. doi: 10.2169/internalmedicine.52.8671
36. Tsubakimoto A, Saito I, Mannami T, Naito Y, Nakamura S, Dohi Y, et al. Impact of metabolic syndrome on brachial-ankle pulse wave velocity in Japanese. *Hypertens Res.* (2006) 29:29–37. doi: 10.1291/hypres.29.29
37. Hwang IC, Suh SY, Seo AR, Ahn HY, Yim E. Association between metabolic components and subclinical atherosclerosis in Korean adults. *Korean J Fam Med.* (2012) 33:229–36. doi: 10.4082/kjfm.2012.33.4.229
38. Kass DA. Ventricular arterial stiffening: integrating the pathophysiology. *Hypertension.* (2005) 46:185–93. doi: 10.1161/01.HYP.0000168053.34306.d4
39. Hall JE. The kidney, hypertension, and obesity. *Hypertension.* (2003) 41:625–33. doi: 10.1161/01.HYP.0000052314.95497.78
40. Ferreira I, Snijder MB, Twisk JW, van Mechelen W, Kemper HC, Seidell JC, et al. Central fat mass versus peripheral fat and lean mass: opposite (adverse versus favorable) associations with arterial stiffness? The Amsterdam Growth and Health Longitudinal Study. *J Clin Endocrinol Metab.* (2004) 89:2632–9. doi: 10.1210/jc.2003-031619
41. Lee HO, Bak HJ, Shin JY, Song YM. Association between metabolic syndrome and microalbuminuria in Korean adults. *Korean J Fam Med.* (2015) 36:60–71. doi: 10.4082/kjfm.2015.36.2.60
42. Rodicio JL, Campo C, Ruilope LM. Microalbuminuria in essential hypertension. *Kidney Int Suppl.* (1998) 68:S51–4. doi: 10.1046/j.1523-1755.1998.06813.x
43. Palaniappan L, Carnethon M, Fortmann SP. Association between microalbuminuria and the metabolic syndrome: NHANES III. *Am J Hypertens.* (2003) 16:952–8. doi: 10.1016/S0895-7061(03)01009-4
44. Aronson D. Hyperglycemia and the pathobiology of diabetic complications. *Adv Cardiol.* (2008) 45:1–16. doi: 10.1159/000115118
45. Ginsberg HN, Elam MB, Lovato LC, Crouse JR 3rd, Leiter LA, Linz P, et al. Effects of combination lipid therapy in type 2 diabetes mellitus. *N Engl J Med.* (2010) 362:1563–74. doi: 10.1056/NEJMoa1001282
46. Boden WE, Probstfield JL, Anderson T, Chaitman BR, Desvignes-Nickens P, Koprowicz K, et al. Niacin in patients with low HDL cholesterol levels receiving intensive statin therapy. *N Engl J Med.* (2011) 365:2255–67. doi: 10.1056/NEJMoa1107579
47. Rosenson RS, Brewer HB Jr., Chapman MJ, Fazio S, Hussain MM, Kontush A, et al. HDL measures, particle heterogeneity, proposed nomenclature, and relation to atherosclerotic cardiovascular events. *Clin Chem.* (2011) 57:392–410. doi: 10.1373/clinchem.2010.155333
48. Superko HR, Pendyala L, Williams PT, Momary KM, King SB 3rd, Garrett BC. High-density lipoprotein subclasses and their relationship to cardiovascular disease. *J Clin Lipidol.* (2012) 6:496–523. doi: 10.1016/j.jacl.2012.03.001
49. Chi C, Teliewubai J, Lu YY, Fan XM, Yu SK, Xiong J, et al. Comparison of various lipid parameters in association of target organ damage: a cohort study. *Lipids Health Dis.* (2018) 17:199. doi: 10.1186/s12944-018-0800-y
50. Horio T, Miyazato J, Kamide K, Takiuchi S, Kawano Y. Influence of low high-density lipoprotein cholesterol on left ventricular hypertrophy and diastolic function in essential hypertension. *Am J Hypertens.* (2003) 16:938–44. doi: 10.1016/S0895-7061(03)01015-X
51. Cuspidi C, Meani S, Fusi V, Severgnini B, Valerio C, Catini E, et al. Metabolic syndrome and target organ damage in untreated essential hypertensives. *J Hypertens.* (2004) 22:1991–8. doi: 10.1097/00004872-200410000-00023
52. Mitu F, Mitu O, Leon MM, Jitaru A. The correlation between the ankle-brachial index and the metabolic syndrome. *Rev Med Chir Soc Med Nat Iasi.* (2014) 118:965–70.
53. Zhou PA, Zhang CH, Chen YR, Li D, Song DY, Liu HM, et al. Association between metabolic syndrome and carotid atherosclerosis: a cross-sectional study in Northern China. *Biomed Environ Sci.* (2019) 32:914–21. doi: 10.3967/bes2019.114
54. Otsuka F, Kramer MC, Woudstra P, Yahagi K, Ladich E, Finn AV, et al. Natural progression of atherosclerosis from pathologic intimal thickening to late fibroatheroma in human coronary arteries: A pathology study. *Atherosclerosis.* (2015) 241:772–82. doi: 10.1016/j.atherosclerosis.2015.05.011

Conflict of Interest: The authors declare that the research was conducted in the absence of any commercial or financial relationships that could be construed as a potential conflict of interest.

Copyright © 2021 Zhao, Yang, Maimaitiaili, Tang, Zhao, Xiong, Teliewubai, Chi, Blacher, Li, Xu, Jiang, Zhang and Li. This is an open-access article distributed under the terms of the Creative Commons Attribution License (CC BY). The use, distribution or reproduction in other forums is permitted, provided the original author(s) and the copyright owner(s) are credited and that the original publication in this journal is cited, in accordance with accepted academic practice. No use, distribution or reproduction is permitted which does not comply with these terms.

frontiers in Cardiovascular Medicine

ORIGINAL RESEARCH
published: 21 July 2021
doi: 10.3389/fcvm.2021.708200

Sexual Dysfunction and the Impact of Beta-Blockers in Young Males With Coronary Artery Disease

Yuxiang Dai[1†], Zhendong Mei[2†], Shuning Zhang[1†], Shalaimaiti Shali[1], Daoyuan Ren[1], Lili Xu[1], Wei Gao[1], Shufu Chang[1], Yan Zheng[2,3], Juying Qian[1], Kang Yao[1] and Junbo Ge[1*]*

[1] Department of Cardiology, Zhongshan Hospital, Shanghai Institute of Cardiovascular Disease, National Clinical Research Center for Interventional Medicine, Shanghai, China, [2] State Key Laboratory of Genetic Engineering, School of Life Sciences, Human Phenome Institute, Fudan University, Shanghai, China, [3] Ministry of Education Key Laboratory of Public Health Safety, School of Public Health, Fudan University, Shanghai, China

Objective: We aimed to assess the association of erectile dysfunction (ED) with the extent of coronary atherosclerosis, and to examine whether revascularization and medication use have an impact on ED status in patients with early onset of coronary artery disease (EOCAD).

Methods: International Index of Erectile Function (IIEF-5) was used to evaluate sexual function in 296 male patients with EOCAD (age, 39.9 ± 4.8 years), and 354 male controls (age, 40.6 ± 4.4 years). The extent of coronary atherosclerosis was measured by Gensini score. Endothelial function was evaluated by two vasomotor indexes including endothelin-1 (ET-1) and nitric oxide (NO) by ELISA.

Results: ED was more frequent (57.8 vs. 31.1%, $P < 0.001$) and serious (IIEF-5 score:17.7 ± 6.0 vs. 21.6 ± 5.0, $P < 0.001$) among EOCAD patients than that among controls. IIEF-5 score was negatively correlated with Gensini score ($r = -0.383$, $P < 0.001$). The adjusted odds ratio (OR) for the presence of ED (EOCAD vs. controls) was 1.88 [95% confidential interval (CI), 1.12-3.18]. However, ET-1 and NO attenuated the association between ED and EOCAD (adjusted OR: 1.54, 95% CI: 0.84-2.80). IIEF-5 score increased after coronary revascularization in patients not on beta-blockers (18.71 ± 4.84 vs. 17.59 ± 6.05, $P < 0.001$) as compared with baseline, while stayed unchanged in the subgroup using beta-blockers (17.82 ± 5.12 vs. 17.70 ± 5.98, $P = 0.09$).

Conclusions: ED was common in patients with EOCAD, and associated with the severity of coronary atherosclerosis. Endothelial dysfunction may be a pathophysiologic mechanism underlying both ED and EOCAD. Coronary revascularization confers a benefit in ED amelioration, while this effect did not appear in patients using beta-blocker.

Keywords: early onset of coronary artery disease, erectile dysfunction, revascularization, beta-blockers, Chinese males

OPEN ACCESS

Edited by:
Hongmei Tan,
Sun Yat-sen University, China

Reviewed by:
Xiaodong Zhuang,
The First Affiliated Hospital of Sun Yat-sen University, China
Shujie Guo,
Shanghai Institute of Hypertension, China

***Correspondence:**
Kang Yao
yao.kang@zs-hospital.sh.cn
Junbo Ge
jbge@zs-hospital.sh.cn

[†]These authors have contributed equally to this work

Specialty section:
This article was submitted to General Cardiovascular Medicine, a section of the journal Frontiers in Cardiovascular Medicine

Received: *11 May 2021*
Accepted: *29 June 2021*
Published: *21 July 2021*

Citation:
Dai Y, Mei Z, Zhang S, Shali S, Ren D, Xu L, Gao W, Chang S, Zheng Y, Qian J, Yao K and Ge J (2021) Sexual Dysfunction and the Impact of Beta-Blockers in Young Males With Coronary Artery Disease. Front. Cardiovasc. Med. 8:708200. doi: 10.3389/fcvm.2021.708200

INTRODUCTION

Coronary artery disease (CAD) is the most commonly diagnosed heart disease and the leading cause of death in adults, predominantly the elderly (1). The growing number of cases of early onset of coronary artery disease (EOCAD) over the past decades has raised major concern, especially in developing countries such as China, where CAD-related morbidity and mortality continue to rise

despite notable advances in diagnostic and treatment capabilities (2). Depression and unhealthy lifestyles possibly play crucial roles in EOCAD, which is associated with increased risk of heart failure, cardiac death, impaired quality of life, and reduced work capacity with their socioeconomic consequences (3). Although adults aged $\leq$ 45years tend to be more sexually active, erectile dysfunction (ED), defined as persistent inability to achieve and maintain an erection sufficient to provide adequate sexual activity (4), is now increasingly common and an important cause of poor quality of life and psychosocial morbidity in this population (5, 6). Nonetheless, little is known about the prevalence of ED in patients with EOCAD, and coronary atherosclerotic burden has not been previously linked to ED severity. The present study therefore tested the hypotheses that the prevalence of ED is higher in patients with EOCAD as compared with the age-matched control group and the severity of ED is associated with the extent of coronary atherosclerosis. We further examined whether revascularization and beta-blockers have an impact on ED symptoms in EOCAD patients.

METHODS

Study subjects consisted of individuals enrolled in the prospective, multicenter, observational GRAND (Genetics and clinical characteristics in coRonary Artery disease in ChiNese young aDults) study. A total of 296 male cases with CAD aged 18-45 years, and 354 age-matched male controls were enrolled in the present study. Patients with EOCAD had a minimum of one major epicardial coronary artery (left anterior descending artery, left circumflex artery, or right coronary artery) with $\geq$50% stenosis documented by coronary angiography (CAG), and underwent coronary revascularization. Controls did not meet the latter CAG criteria. Patients and controls unwilling to answer the International Index of Erectile Function (IIEF-5) questionnaire (7, 8) were excluded. The investigation conformed to the principles outlined in the Declaration of Helsinki. All subjects provided informed consent, and the study protocol was approved by the ethical committee of the Zhongshan Hospital.

Clinical data were derived from the electronic medical records (EMR) of hospitalized patients. Each patient completed a detailed questionnaire on lifestyle and medical history before CAG. Risk factors analyzed included age, sex, body mass index (BMI), obesity, smoking, drinking, hypertension, hyperlipidemia, atrial fibrillation, and diabetes mellitus. Laboratory data were collected upon admission to the hospital, including hemoglobin, neutrophil to lymphocyte ratio (NLR), red cell distribution width (RDW), platelet distribution width (PDW), alanine transaminase (ALT), serum creatinine (Crea), estimated glomerular filtration rate (eGFR) calculated by the abbreviated MDRD equation, uric acid (UA), C reative protein (CRP), glycosylated hemoglobin (HbA1c), total cholesterol (TC), triglycerides (TG), low-density lipoprotein cholesterol (LDL-C), high-density lipoprotein cholesterol (HDL-C), apolipoprotein A1 (Apo A1), apolipoprotein B (Apo B), apolipoprotein E (Apo E). Left ventricular end-systolic dimension (LVESD), left ventricular end-diastolic dimension (LVEDD), and left ventricular ejection fraction (LVEF), and other parameters, were assessed by transthoracic echocardiography using the Teichholz method prior to CAG.

Peripheral venous blood (2 ml) was collected from all enrolled subjects before angiography. The serum samples were stored at -80°C until analysis. Serum levels of endothelin-1 (ET-1) and nitric oxide (NO) was detected by the ELISA method using endothelin-1 quantikine ELISA kit (R&D Systems Inc., Minneapolis, USA) and total nitric oxide and nitrate/nitrite parameter assay kit (R&D Systems Inc., Minneapolis, USA) respectively.

Medications, including beta-blockers, aspirin, clopidogrel, statins, diuretics, angiotensin-converting enzyme inhibitors (ACEI), angiotensin receptor blocker (ARB), calcium channel blockers (CCB), nitrates, oral hypoglycemic, and insulin, were evaluated through reviewing EMRs and by personal interviews before CAG and after discharge.

CAG analysis was performed by the cardiologist who was unaware of the patient's condition of ED. The lesions were analyzed in multiple projections. Gensini score was calculated to assess the coronary atherosclerotic severity. Each coronary stenosis was assigned a score according to the degree of luminal narrowing (stenosis of 25, 50, 75, 90, 99%, and complete occlusion were assigned a Gensini score of 1, 2, 4, 8, 16, and 32, respectively). The score was then multiplied by the coefficient according to the functional importance of the myocardial area supplied by that segment (9).

Erectile function was evaluated by using IIEF-5, which is an internationally validated self-administered assessment designed to quantitatively evaluate the patient's erectile function through a five-item short-form questionnaire (7, 8). The sum score ranges from 5 to 25 points with lower values corresponding to decreased erectile function. The severity of ED was classified into five levels based on the scores: severe (5–7), moderate (8–11), mild to moderate (12–16), mild (17–21), and no ED (22–25) (7, 8). Each subject was followed by telephone interview and the IIEF-5 questionnaire was reassessed at the 1-year follow-up timepoint.

Data are presented as mean $\pm$ standard deviation (SD) for continuous variables and percentage (%) for categorical variables. Continuous variables were compared between cases and controls using *t*-test. Categorical variables were compared using the chi-square test. The Pearson correlation coefficient was used to indicate correlations between quantitative variables. The independent association between ED status and the occurrence of EOCAD was determined by using a multivariable logistic regression model. The odds ratio (OR) and 95% confidence interval (CI) were calculated. Covariates were identified if the *P*-value was <0.1 in univariate analyses. Changes in IIEF-5 score after coronary revascularization were analyzed by linear mixed-effects models after adjustment for the identified covariates. Hypothesis testing was two-tailed and a P-value < 0.05 was considered statistically significant. All the statistical analyses were performed using R version 3.5.1 (https://www.r-project.org/).

RESULTS

Baseline Characteristics

The baseline characteristics of the 296 patients with EOCAD and 354 control subjects are provided in **Table 1**. Patients

TABLE 1 | Baseline clinical characteristics of EOCAD patients and controls.

	EOCAD group (*N* = 296)	Control (*N* = 354)	*P*-value
Demographic data			
Age (years)	39.9 (±4.8)	40.6 (±4.4)	0.065
BMI (kg/m^2)	29.2 (±9.1)	26.3 (±4.8)	<0.001
Obesity			0.128
Normal	81 (27.4%)	108 (30.5%)	
Overweight	94 (31.8%)	115 (32.5%)	
Obese	116 (39.2%)	106 (29.9%)	
Lifestyle			
Smoking			<0.001
Never	80 (27.0%)	187 (52.8%)	
Ever	111 (37.5%)	91 (25.7%)	
Current	104 (35.1%)	76 (21.5%)	
Drinking			<0.001
No	117 (39.5%)	264 (74.6%)	
Mild	138 (46.6%)	38 (10.7%)	
Severe	31 (10.5%)	51 (14.4%)	
Coronary angiographic evaluation			
Gensini score	82.4 (±54.8)	1.7 (±2.6)	<0.001
Medical history			
Hypertension	114 (38.5%)	136 (38.4%)	0.563
Hyperlipidemia	49 (16.6%)	33 (9.3%)	0.003
Atrial fibrillation	7 (2.4%)	8 (2.3%)	1.000
Diabetes mellitus	37 (12.5%)	39 (11.0%)	0.449
Echocardiography parameters			
LVEF (%)	59.9 (±9.0)	61.3 (±10.1)	0.058
LVSED (mm)	33.0 (±6.4)	33.6 (±7.3)	0.252
LVDED (mm)	50.6 (±5.6)	50.6 (±6.9)	0.983
Biochemical measurements			
HgB (g/L)	146.0 (±15.1)	146.6 (±17.8)	0.688
Neutrophil to lymphocyte ratio (NLR)	2.6 (±2.2)	2.2 (±1.9)	0.024
RDW (%)	12.4 (±1.3)	12.5 (±2.2)	0.975
PDW (%)	13.4 (±3.2)	13.2 (±3.3)	0.505
ALT (U/L)	38.3 (±25.4)	39.8 (±63.5)	0.691
Crea (μmol/L)	85.6 (±19.1)	84.4 (±25.0)	0.483
eGFR (ml/min/1.73m^2)	100.1 (±17.1)	99.8 (±16.2)	0.849
UA (μmol/L)	427.6 (±93.1)	387.0 (±87.2)	<0.001
CRP (mg/L)	10.5 (±31.0)	7.4 (±24.5)	0.199
HbA1c (%)	6.1 (±1.4)	5.8 (±1.0)	0.018
TC (mmol/L)	4.45 (±1.46)	4.22 (±1.00)	0.028
TG (mmol/L)	2.70 (±1.64)	2.31 (±1.97)	0.007
HDL-C (mmol/L)	0.92 (±0.28)	1.01 (±0.26)	<0.001
LDL-C (mmol/L)	2.55 (±1.34)	2.3 (±0.9)	0.019
Apo A1 (g/L)	1.15 (±0.20)	1.22 (±0.23)	<0.001
Apo B (g/L)	0.92 (±0.31)	0.87 (±0.25)	0.034
Apo E (mg/L)	46.2 (±25.4)	41.9 (±17.4)	0.016
NHDL-C (mmol/L)	3.53 (±1.51)	3.21 (±1.02)	0.002
TG/HDL-C	3.31 (±2.5)	2.7 (±3.4)	0.014
ET-1 (pg/mL)	3.0 (±1.6)	2.2 (±1.0)	<0.001
NO (μmol/L)	35.7 (±15.2)	40.0 (±14.3)	<0.001
Previous use of drugs			
Aspirin	34 (11.5%)	28 (7.9%)	0.122
Beta-blockers	22 (7.4%)	27 (7.6%)	0.925
Statins	35 (11.8%)	34 (9.6%)	0.360
Diuretics	6 (2.3%)	8 (2.3%)	0.839
ACEI	36 (12.2%)	35 (9.9%)	0.354
ARB	33 (11.1%)	39 (11.0%)	0.958
CCB	45 (15.2%)	51 (14.4%)	0.776
Nitrates	13 (4.4%)	14 (4.0%)	0.781
Oral hypoglycemic	32 (10.8%)	34 (9.6%)	0.592
Insulin	5 (1.7%)	4 (1.1%)	0.787

P-values were estimated from t-test for continuous variables and chi-square test for categorical variables.

LVSED, left ventricular end-systolic dimension; LVDED, left ventricular end-diastolic dimension; LVEF, left ventricular ejection fraction; HgB, hemoglobin; NLR, neutrophil to lymphocyte ratio; RDW, red cell distribution width; PDW, platelet distribution width; ALT, alanine transaminase; Crea, serum creatinine; eGFR, estimated glomerular filtration rate calculated by the abbreviated MDRD equation; UA, uric acid; CPR, C reative protein; HbA1c, glycosylated hemoglobin; TC, total cholesterol; TG, triglycerides; LDL-C, low-density lipoprotein cholesterol; HDL-C, high-density lipoprotein; Apo A1, apolipoprotein A1; Apo B, apolipoprotein B; Apo E, apolipoprotein E.

TABLE 2 | Baseline erectile function evaluated by IIEF5 in EOCAD patients and controls.

	EOCAD group	Control	*P*-value
IIEF5 Score	17.7 (±6.0)	21.6 (±5.0)	<0.001
No ED (22–25)	125 (42.2%)	244 (68.9%)	<0.001
Mild (17–21)	45 (15.2%)	42 (11.9%)	
Mild to moderate (12–16)	56 (18.9%)	48 (13.6%)	
Moderate (8–11)	54 (18.2%)	17 (4.8%)	
Severe (5–7)	16 (5.4%)	3 (0.8%)	

P-values were estimated from t-test for continuous variables and Chi-square test for categorical variables.

and controls were well-matched for age (mean of ∼40 years for both) and had similar distributions of history of hypertension, diabetes mellitus, atrial fibrillation, values of echocardiographic parameters (including LVEF, LVESD, and LVEDD), and hemoglobin level, RDW, PDW, ALT, Creatine, eGFR, and CRP. However, the proportions of individuals with smoking and (or) drinking habits or hyperlipidemia, and the levels of BMI, NLR, UA, HbA1c, TC, TG, LDL-C, ApoB, non-HDLC, and the ratio of TG/HDL-C were considerably higher in the EOCAD group, while the levels of HDL-C and ApoA1 were lower as compared with controls (**Table 1**).

In addition, current and cumulative use of medications (aspirin, beta-blockers, statins, diuretics, ACEI, ARB, CCB, nitrates, oral hypoglycemic, and insulin) were similarly distributed between groups ($P > 0.05$, **Table 1**).

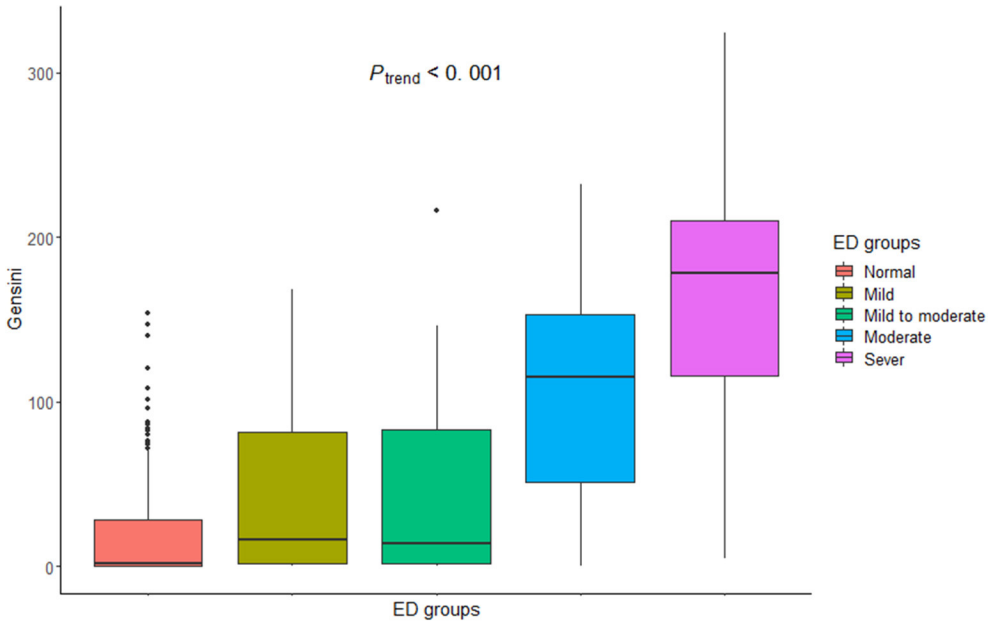

FIGURE 1 | Gensini score among different groups of varying ED severity.

Prevalence of ED

ED was more common among patients with EOCAD than controls (57.8 vs. 31.1%, $P < 0.001$) (**Table 2**). Besides, the prevalence of ED of different degrees was higher in EOCAD subjects than controls (**Table 2**). The average IIEF-5 score was significantly lower in patients with EOCAD vs. controls (17.7 ± 6.0 vs. 21.6 ± 5.0, $P < 0.001$), suggesting more serious ED conditions in the EOCAD group comparing with controls (**Table 2**).

Relationship Between Severity of Coronary Artery Atherosclerosis and ED

The mean of Gensini score, indicative of coronary artery atherosclerosis of varying severity, was higher in the EOCAD group vs. controls (82.4 ± 54.8 vs. 1.7 ± 2.6, $P < 0.001$). The Gensini score increased from the normal erectile function group to the severe ED group with means ± SDs of 48.87 ± 30.19 in the normal erectile function group, 81.18 ± 38.06 in the mild ED group, 79.80 ± 41.79 in the mild to moderate ED group, 135.20 ± 43.11 in the moderate ED group, and 179.00 ± 69.84 in the severe ED group ($P_{trend} < 0.001$, **Figure 1**).

Logistic Regression Models for Prediction of ED

In univariate analysis, BMI, smoking, alcohol use, levels of UA, HbA1c, TG, HDL, ApoA, ApoE, non-HDL-C and TG/HDL, presence of EOCAD, and Gensini score were significantly associated with ED. In logistic regression analysis, adjusted OR for the presence of ED (EOCADs vs. controls) was 1.88 [95% confidence interval (CI), 1.12-3.18]. Other independent predictors for ED were BMI (OR: 1.17, 95%CI: 1.08-1.28), UA level (OR: 1.97, 95%CI: 1.64-2.39, per 58.94 umol/L increment), current smoking (OR: 10.48, 95%CI: 5.45-20.91), and ever smoking (OR: 2.11, 95%CI: 1.20-3.73) (**Table 3**). Interestingly, we further introduced vasoconstrictor index (ET-1) and vasodilator index (NO) into the multiple logistic regression model, and found that they attenuated the association between ED and EOCAD (OR: 1.54, 95% CI: 0.84-2.80), but did not materially affect the relationships of ED with other risk factors (**Table 3**). To understand this mediation effect, we next assessed the associations of ET-1 and NO with IIEF-5 and Gensini score, and expectedly found that these two vasomotor indexes were significantly correlated with IIEF-5 ($r = -0.55$ for ET-1, and $r = 0.46$ for NO, both $P < 0.001$) and Gensini score ($r = -0.53$ for ET-1, and $r = 0.42$ for NO, both $P < 0.001$) (**Supplementary Figure 1**).

Improvement of ED After Coronary Revascularization and the Impact of Beta-Blockers

Among EOCAD patients, IIEF-5 score significantly elevated 1 year after coronary revascularization relative to baseline (18.24 ± 5.00 vs. 17.65 ± 6.00, $P < 0.001$; **Figure 2**). Patients were further divided into subgroups according to the use of beta-blockers, with 157 patients (53.0%) receiving beta-blockers after coronary revascularization. Use of other medications (aspirin, clopidogrel, statins, diuretics, ACEI, ARB, CCB, nitrates, oral hypoglycemic and insulin) was similarly distributed between groups on or not on beta-blockers after discharge (**Supplementary Table 1**). In this subgroup analysis, the IIEF-5 scores after revascularization significantly increased in patients not on beta-blockers (18.71 ± 4.84 vs. 17.59 ± 6.05, $P < 0.001$), while stayed unchanged in

TABLE 3 | Associations between ED and risk factors by univariable analysis and multivariable logistic regression.

	Univariable		Multivariable model 1		Multivariable model 2	
Variables	**OR (95% CI)**	***P*-value**	**OR (95% CI)**	***P*-value**	**OR (95% CI)**	***P*-value**
Age (years)	0.98 (0.94-1.01)	0.154	–	–	–	–
BMI (kg/m^2)	1.23 (1.16-1.30)	<0.001	1.17 (1.08-1.28)	<0.001	1.19 (1.09-1.32)	<0.001
Smoking						
No	1.00		1.00		1.00	
Ever	2.37 (1.58-3.57)	<0.001	2.11 (1.20-3.73)	0.010	2.19 (1.17-4.18)	0.016
Current	15.26 (9.63-24.75)	<0.001	10.48 (5.45-20.91)	<0.001	11.1 (5.06-25.55)	<0.001
Drinking						
No	1.00		1.00		1.00	
Mild	2.54 (1.77-3.67)	<0.001	0.96 (0.53-1.73)	0.892	0.83 (0.42-1.64)	0.602
Severe	1.72 (1.06-2.78)	0.028	0.89 (0.45-1.76)	0.743	0.64 (0.28-1.41)	0.277
History of hypertension	1.27 (0.92-1.76)	0.139	–	–	–	–
History of diabetes mellitus	1.54 (0.95-2.50)	0.078	0.66 (0.29-1.48)	0.319	0.78 (0.32-1.87)	0.589
History of dyslipidemia	0.92 (0.57-1.47)	0.734	–	–	–	–
History of atrial fibrillation	2.67 (0.94-8.65)	0.077	2.41 (0.45-13.05)	0.298	1.98 (0.34-11.75)	0.444
LVEF (%)	0.99 (0.98-1.01)	0.468	–	–	–	–
LVEDD (mm)	1.01 (0.99-1.04)	0.355	–	–	–	–
LVSED (mm)	1.01 (0.98-1.03)	0.614	–	–	–	–
HgB (g/L)	1.00 (0.99-1.01)	0.358	–	–	–	–
NLR	0.94 (0.85-1.02)	0.185	–	–	–	–
RDW (%)	1.06 (0.96-1.18)	0.273	–	–	–	–
PDW (%)	0.97 (0.92-1.02)	0.222	–	–	–	–
ALT (U/L)	1.00 (1.00-1.01)	0.313	–	–	–	–
Crea (μmol/L)	1.00 (0.99-1.00)	0.565	–	–	–	–
eGFR (ml/min/1.73m^2)	1.00 (1.00-1.01)	0.345	–	–	–	–
UA (Per 58.94 umol/L increment)	2.18 (1.89-2.53)	0.000	1.97 (1.64-2.39)	<0.001	1.80 (1.46-2.26)	<0.001
CRP (mg/L)	1.01 (1.00-1.01)	0.080	1.00 (0.99-1.01)	0.427	1.00 (0.99-1.02)	0.694
HbA1c (%)	1.25 (1.09-1.44)	0.002	1.13 (0.88-1.44)	0.326	1.05 (0.79-1.39)	0.721
TC (mmol/L)	1.10 (0.96-1.25)	0.166	–	–	–	–
TG (mmol/L)	1.14 (1.04-1.26)	0.005	–	–	–	–
HDL (mmol/L)	0.38 (0.21-0.70)	0.002	–	–	–	–
LDL (mmol/L)	1.05 (0.91-1.21)	0.474	–	–	–	–
ApoA (g/L)	0.33 (0.15-0.68)	0.003	0.63 (0.21-1.92)	0.421	0.63 (0.18-2.22)	0.472
ApoB (g/L)	1.49 (0.84-2.64)	0.174	–	–	–	–
ApoE (g/L)	1.01 (1.01-1.02)	0.003	1.01 (0.99-1.03)	0.570	1.02 (1.00-1.05)	0.144
NHDL-C (mmol/L)	1.14 (1.01-1.30)	0.041	0.93 (0.73-1.17)	0.536	0.87 (0.65-1.15)	0.323
TG/HDL	1.09 (1.03-1.17)	0.005	0.97 (0.85-1.09)	0.585	0.94 (0.82-1.09)	0.422
ET-1 (pg/ml)	2.50 (2.11-3.00)	<0.001	–	–	1.97 (1.49-2.64)	<0.001
NO (μmol/L)	0.92 (0.91-0.94)	<0.001	–	–	0.93 (0.90-0.95)	<0.001
EOCAD	3.03 (2.20-4.20)	<0.001	1.88 (1.12-3.18)	0.017	1.54 (0.84-2.80)	0.159
Gensini score	1.02 (1.02-1.03)	<0.001	–	–	–	–

Factors with P < 0.1 in univariable analysis were included for multivariable logistic regression. TG/HDL-C was included in multivariable logistic regression instead of TG or HDL-C separately because of obvious interaction. Gensini score was excluded in multivariable logistic regression because of obvious colinearity with EOCAD.

patients on beta-blockers (17.82 ± 5.12 vs. 17.70 ± 5.98, $P = 0.09$) as compared with those at baseline (**Figure 2**).

DISCUSSION

In the present study, we found ED was more prevalent in EOCAD patients than that in controls. While two vasomotor indexes (i.e., ET-1 and NO) attenuated the association between ED and EOCAD. Among EOCAD patients, we found the IIEF-5 score elevated 1 year after coronary revascularization. Of note, this beneficial effect of revascularization did not appear in patients using beta-blockers.

ED is considered to affect a large number of men (10). However, the accurate incidence and prevalence of ED are

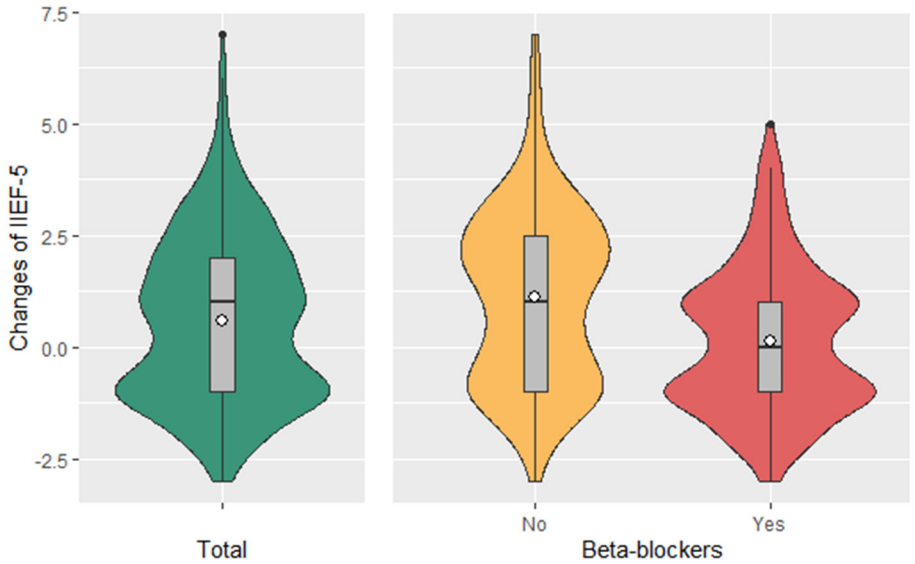

FIGURE 2 | Changes in IIEF-5 Score in patients with or without beta blocker use. Mean change in IIEF-5 in patients on beta blockers (157, 53.0%) was 0.12, $P = 0.09$; mean change in IIEF-5 in patients not on beta blockers (139, 47.0%) was 1.11, $P < 0.001$. *P*-values were estimated from the linear mixed-effects models after adjustment for BMI, smoking, alcohol use, UA, CRP, HbA1c, Apo-A, Apo-E, the TG and HDL-C ratio, and the history of diabetes mellitus and atrial fibrillation. ANOVA $P < 0.001$ for the comparison between patients with or without beta blocker use, adjusted for BMI, smoking, alcohol use, UA, CRP, HbA1c, Apo-A, Apo-E, the TG and HDL-C ratio, and the history of diabetes mellitus and atrial fibrillation.

uncertain because of considerable limitations when conducting epidemiological studies of sexual function. The diagnosis of ED is mainly based on a questionnaire and therefore subjective, and because it is not life-threatening, individuals who suffer it tend not to seek treatment. Studies have estimated that ED incidence ranges from 31.7 to 80% in different age groups (11, 12), and ED prevalence ranges from 12.9 to 52% in different populations (13–16). The Massachusetts male aging study (MMAS) was the first population study to show that the prevalence of ED was 52% in men aged 40–70 years (13). In young males, ED is a particularly important issue because they are sexually active. The National Health of Social Life Survey (NHSLS) showed an ED prevalence of 50% in men aged 18-59 years (14). The incidence of ED in young males is underestimated, and ED has become increasingly common because of the increased stress, anxiety, depression, and sympathetic tone in modern society (6). In this study, the prevalence of ED in young controls aged $\leq$ 45 years without CAD was 31.1%, which was similar to that reported previously in the general population for that age group.

During the last two decades, somatic factors, especially atherosclerotic lesions, have been recognized to play a major role in the development of ED. The landmark MMAS (13) and other recent studies (17–19) have raised awareness of the significant association between cardiovascular disease and the occurrence of ED and its severity in a general population of men. Secondary to systemic atherosclerosis and concomitant endothelial dysfunction, which can restrict blood flow to the corpus cavernosum during erection, the prevalence of sexual dysfunction is higher in patients with cardiovascular disease as compared with the general population. Likewise, the prevalence of sexual dysfunction in this study is higher in EOCAD patients compared with controls. Furthermore, the severity of ED is significantly related to the extent of coronary lesion severity and atherosclerotic burden revealed by the Gensini score.

Both cardiovascular disease and ED share common causal factors, such as older age, cigarette smoking, lack of exercise, hypertension, obesity, diabetes mellitus, dyslipidemia, hyperuricemia, and metabolic syndrome (20), all of which might lead to systemic atherosclerosis and concomitant impairment of the endothelial function (21). In response to humoral, neural, and mechanical stimuli, the vascular endothelium releases a variety of factors including NO and ET-1 to regulate the contractile and relaxatory homeostasis. Imbalance in the production of vasodilator and vasoconstrictor agents may contribute to the onset of endothelial dysfunction (22). Endothelial-derived NO plays a crucial role in the physiology of erection, including initiating and maintaining intracavernous pressure increase, penile vasodilatation, and penile erection that are dependent on activation of guanylate cyclase and the subsequent production of cGMP by NO in smooth muscle cells (23, 24). Therefore, incidence and severity of the endothelial dysfunction, which is also one of the earliest landmarks in the development of atherosclerotic lesions and a predictor of cardiovascular outcome, maybe a pathophysiologic mechanism underlying both ED and CVD, forming a unifying link between these two conditions (25). In clinical practice, ED might even be considered as an early clinical manifestation of endothelial dysfunction and a harbinger of undesirable cardiovascular events, especially in the young male (26). In our current study,

the association of EOCAD with ED is dependent on endothelial dysfunction. EOCAD was an independent predictor of ED only in the multivariate model without the adjustment of endothelial dysfunction, while not when parameters of ED were included. It indicated that endothelial dysfunction may be an underlying common cause of EOCAD and ED.

Of note, a few studies have suggested that low levels of testosterone were associated with the development and severity of EOCAD in males (27). Such an association could not be explored in the present cohort because of the lack of data on testosterone levels and warrants further investigation.

Another possible explanation for ED in EOCAD patients may be the fear or anxiety of developing coital angina during sexual activity, particularly at orgasm, during which the maximal energy expenditure occurs, and oxygen uptake reaches its peak. Hence, sexual activity can trigger coital angina *via* dynamic and transient increased myocardial oxygen demand secondary to an increase in heart rate, blood pressure, and the effects of arousal (28). Because revascularization helps to improve myocardial blood flow and the tolerance for maximal energy expenditure, it may eliminate coital angina and thereby improve erectile function. In this study, IIEF-5 score was significantly increased after coronary revascularization, indicating the amelioration of ED symptoms.

Previous studies indicated that beta-blockers may cause ED (29). The potential mechanisms underlying the impact of beta-blockers on sexual function may include inhibition of the sympathetic nervous system, which is involved in the integration of erection, emission and ejaculation, impairment of vasodilation of the corpora cavernosa, effects on luteinizing hormone and testosterone secretion and a tendency to produce sedation or depression (30). However, beta-blockers are the first-line agent for angina pectoris and also preferably used in young patients with hypertension due to the predominant increase in sympathetic nerve activity in this population. In the present study, beta-blockers adversely affected ED improvement conferred by coronary revascularization. Their apparent disadvantageous effects on erectile function and quality of life for the young, calls for into question considering beta-blockers as the first-line option after coronary revascularization in the EOCAD patients with ED.

LIMITATIONS

Interpretation and generalizability of the findings presented are limited by the observational, single-center design of this study in a Chinese population of men. Larger, multicenter studies with greater ethnic diversity are warranted to validate the findings presented. In addition, we did not measure the testosterone level, which may be a confounder for the association between ED and EOCAD.

CONCLUSIONS

In our study, we revealed that ED cannot be neglected in young men with active sexual desire, with an especially higher prevalence in EOCAD patients. Endothelial dysfunction may be a pathophysiologic mechanism underlying both ED and EOCAD. Coronary revascularization appeared beneficial to the improvement of ED, while this improvement did not appear in patients using beta-blockers. Beta-blockers for antianginal therapy after revascularization should be used with extra caution after fully informing the patients who have EOCAD and ED.

DATA AVAILABILITY STATEMENT

The original contributions presented in the study are included in the article/**Supplementary Material**, further inquiries can be directed to the corresponding author/s.

ETHICS STATEMENT

The studies involving human participants were reviewed and approved by the ethical committee of the Zhongshan Hospital. The patients/participants provided their written informed consent to participate in this study.

AUTHOR CONTRIBUTIONS

YD, KY, and JG conceived and designed the study. YD, ZM, and SZ conducted the statistical analysis and drafted the manuscript. KY and JG had full access to all of the data and took responsibility for the integrity of the data and the accuracy of the data analysis. All authors participated in the interpretation of the results and revision of the manuscript and read and approved the final manuscript.

FUNDING

This work was supported by the National Key Research and Development Program of China (2016YFC1301200), Clinical Research Plan of SHDC (No. SHDC2020CR1007A), and Exploratory Clinical Research Projects of National Clinical Research Center for Interventional Medicine (No. 2021-002). The funding agencies had no role in the design and conduct of the study, in the collection, management, analysis, and interpretation of the data, or in the preparation, review, or approval of the manuscript, or decision to submit for publication.

ACKNOWLEDGMENTS

The authors thank all the participants of the study.

SUPPLEMENTARY MATERIAL

The Supplementary Material for this article can be found online at: https://www.frontiersin.org/articles/10.3389/fcvm.2021.708200/full#supplementary-material

REFERENCES

1. Benjamin EJ, Blaha MJ, Chiuve SE, Cushman M, Das SR, Deo R, et al. Heart disease and stroke statistics-2017 update: a report from the American Heart Association. *Circulation.* (2017) 135:e146-603. doi: 10.1161/CIR.0000000000000491
2. He J, Gu D, Wu X, Reynolds K, Duan X, Yao C, et al. Major causes of death among men and women in China. *N Engl J Med.* (2005) 353:1124-34. doi: 10.1056/NEJMsa050467
3. Aggarwal A, Srivastava S, Velmurugan M. Newer perspectives of coronary artery disease in young. *World J Cardiol.* (2016) 8:728-34. doi: 10.4330/wjc.v8.i12.728
4. McCabe MP, Sharlip ID, Atalla E, Balon R, Fisher AD, Laumann E, et al. Definitions of sexual dysfunctions in women and men: a consensus statement from the Fourth International Consultation on Sexual Medicine 2015. *J Sex Med.* (2016) 13:135-43. doi: 10.1016/j.jsxm.2015.12.019
5. Rastrelli G, Maggi M. Erectile dysfunction in fit and healthy young men: psychological or pathological? *Transl Androl Urol.* (2017) 6:79-90. doi: 10.21037/tau.2016.09.06
6. Nguyen HMT, Gabrielson AT, Hellstrom WJG. Erectile dysfunction in young men-a review of the prevalence and risk factors. *Sex Med Rev.* (2017) 5:508-20. doi: 10.1016/j.sxmr.2017.05.004
7. Rosen RC, Cappelleri JC, Smith MD, Lipsky J, Peña BM. Development and evaluation of an abridged, 5-item version of the International Index of Erectile Function (IIEF-5) as a diagnostic tool for erectile dysfunction. *Int J Impot Res.* (1999) 11:319-26. doi: 10.1038/sj.ijir.3900472
8. Rhoden EL, Telöken C, Sogari PR, Vargas Souto CA. The use of the simplified International Index of Erectile Function (IIEF-5) as a diagnostic tool to study the prevalence of erectile dysfunction. *Int J Impot Res.* (2002) 14:245-50. doi: 10.1038/sj.ijir.3900859
9. Gensini GG. A more meaningful scoring system for determining the severity of coronary heart disease. *Am J Cardiol.* (1983) 51:606. doi: 10.1016/S0002-9149(83)80105-2
10. Shamloul R, Ghanem H. Erectile dysfunction. *Lancet.* (2013) 381:153-65. doi: 10.1016/S0140-6736(12)60520-0
11. Hsu B, Hirani V, Naganathan V, Blyth FM, Le Couteur DG, Seibel MJ, et al. Sexual function and mortality in older men: the concord health and ageing in men project. *J Gerontol A Biol Sci Med Sci.* (2017) 72:520-7. doi: 10.1093/gerona/glw101
12. Martin SA, Atlantis E, Lange K, Taylor AW, O'Loughlin P, Wittert GA. Predictors of sexual dysfunction incidence and remission in men. *J Sex Med.* (2014) 11:1136-47. doi: 10.1111/jsm.12483
13. Feldman HA, Goldstein I, Hatzichristou DG, Krane RJ, McKinlay JB. Impotence and its medical and psychosocial correlates: results of the Massachusetts Male Aging Study. *J Urol.* (1994) 151:54-61. doi: 10.1016/S0022-5347(17)34871-1
14. Laumann EO, Paik A, Rosen RC. Sexual dysfunction in the United States: prevalence and predictors. *JAMA.* (1999) 281:537-44. doi: 10.1001/jama.281.6.537
15. Rosen RC, Fisher WA, Eardley I, Niederberger C, Nadel A, Sand M. The multinational Men's Attitudes to Life Events and Sexuality (MALES) study: I. Prevalence of erectile dysfunction and related health concerns in the general population. *Curr Med Res Opin.* (2004) 20:607-17. doi: 10.1185/030079904125003467
16. Laumann EO, Nicolosi A, Glasser DB, Paik A, Gingell C, Moreira E, et al. Sexual problems among women and men aged 40-80 y: prevalence and correlates identified in the Global Study of Sexual Attitudes and Behaviors. *Int J Impot Res.* (2005) 17:39-57. doi: 10.1038/sj.ijir.3901250
17. Montorsi P, Ravagnani PM, Galli S, Rotatori F, Veglia F, Briganti A, et al. Association between erectile dysfunction and coronary artery disease. Role of coronary clinical presentation and extent of coronary vessels involvement: the COBRA trial. *Eur Heart J.* (2006) 27:2632-9. doi: 10.1093/eurheartj/ehl142
18. Inman BA, Sauver JL, Jacobson DJ, McGree ME, Nehra A, Lieber MM, et al. A population-based, longitudinal study of erectile dysfunction and future coronary artery disease. *Mayo Clin Proc.* (2009) 84:108-13. doi: 10.4065/84.2.108
19. Banks E, Joshy G, Abhayaratna WP, Kritharides L, Macdonald PS, Korda RJ, et al. Erectile dysfunction severity as a risk marker for cardiovascular disease hospitalisation and all-cause mortality: a prospective cohort study. *PLoS Med.* (2013) 10:e1001372. doi: 10.1371/journal.pmed.1001372
20. Ibrahim A, Ali M, Kiernan TJ, Stack AG. Erectile dysfunction and ischaemic heart disease. *Eur Cardiol.* (2018) 13:98-103. doi: 10.15420/ecr.2017.21.3
21. Giuliano F. New horizons in erectile and endothelial dysfunction research and therapies. *Int J Impot Res.* (2008) 20(Suppl 2):S2-8. doi: 10.1038/ijir.2008.46
22. Deanfield JE, Halcox JP, Rabelink TJ. Endothelial function and dysfunction: testing and clinical relevance. *Circulation.* (2007) 115:1285-95. doi: 10.1161/CIRCULATIONAHA.106.652859
23. Traish AM, Galoosian A. Androgens modulate endothelial function and endothelial progenitor cells in erectile physiology. *Korean J Urol.* (2013) 54:721-31. doi: 10.4111/kju.2013.54.11.721
24. Bivalacqua TJ, Usta MF, Champion HC, Kadowitz PJ, Hellstrom WJ. Endothelial dysfunction in erectile dysfunction: role of the endothelium in erectile physiology and disease. *J Androl.* (2003) 24(6 Suppl):S17-37. doi: 10.1002/j.1939-4640.2003.tb02743.x
25. Solomon H, Man JW, Jackson G. Erectile dysfunction and the cardiovascular patient: endothelial dysfunction is the common denominator. *Heart.* (2003) 89:251-3. doi: 10.1136/heart.89.3.251
26. Katsiki N, Wierzbicki AS, Mikhailidis DP. Erectile dysfunction and coronary heart disease. *Curr Opin Cardiol.* (2015) 30:416-21. doi: 10.1097/HCO.0000000000000174
27. Turhan S, Tulunay C, Güleç S, Ozdöl C, Kilickap M, Altin T, et al. The association between androgen levels and premature coronary artery disease in men. *Coron Artery Dis.* (2007) 18:159-62. doi: 10.1097/MCA.0b013e328012a928
28. Levine GN, Steinke EE, Bakaeen FG, Bozkurt B, Cheitlin MD, Conti JB, et al. Sexual activity and cardiovascular disease: a scientific statement from the American Heart Association. *Circulation.* (2012) 125:1058-72. doi: 10.1161/CIR.0b013e3182447787
29. Rasmussen L, Hallas J, Madsen KG, Pottegård A. Cardiovascular drugs and erectile dysfunction - a symmetry analysis. *Br J Clin Pharmacol.* (2015) 80:1219-23. doi: 10.1111/bcp.12696
30. Nicolai MP, Liem SS, Both S, Pelger RC, Putter H, Schalij MJ, et al. A review of the positive and negative effects of cardiovascular drugs on sexual function: a proposed table for use in clinical practice. *Neth Heart J.* (2014) 22:11-9. doi: 10.1007/s12471-013-0482-z

Conflict of Interest: The authors declare that the research was conducted in the absence of any commercial or financial relationships that could be construed as a potential conflict of interest.

Copyright © 2021 Dai, Mei, Zhang, Shali, Ren, Xu, Gao, Chang, Zheng, Qian, Yao and Ge. This is an open-access article distributed under the terms of the Creative Commons Attribution License (CC BY). The use, distribution or reproduction in other forums is permitted, provided the original author(s) and the copyright owner(s) are credited and that the original publication in this journal is cited, in accordance with accepted academic practice. No use, distribution or reproduction is permitted which does not comply with these terms.

frontiers in Cardiovascular Medicine

ORIGINAL RESEARCH
published: 02 August 2021
doi: 10.3389/fcvm.2021.708279

Blockade of $Na_V1.8$ Increases the Susceptibility to Ventricular Arrhythmias During Acute Myocardial Infarction

Baozhen Qi[1†], Shimo Dai[1†], Yu Song[1†], Dongli Shen[1], Fuhai Li[1], Lanfang Wei[1], Chunyu Zhang[1], Zhenning Nie[1], Jiaxiong Lin[1], Lidong Cai[2] and Junbo Ge[1*]*

[1] Department of Cardiology, Zhongshan Hospital, Shanghai Institute of Cardiovascular Disease, Fudan University, Shanghai, China, [2] Department of Cardiology, Shanghai General Hospital, School of Medicine, Shanghai Jiao Tong University, Shanghai, China

SCN10A/$Na_V1.8$ may be associated with a lower risk of ventricular fibrillation in the setting of acute myocardial infarction (AMI), but if and by which mechanism $Na_V1.8$ impacts on ventricular electrophysiology is still a matter of debate. The purpose of this study was to elucidate the contribution of $Na_V1.8$ in ganglionated plexi (GP) to ventricular arrhythmias in the AMI model. Twenty beagles were randomized to either the A-803467 group ($n = 10$) or the control group ($n = 10$). $Na_V1.8$ blocker (A-803467, 1 μmol/0.5 mL per GP) or DMSO (0.5 mL per GP) was injected into four major GPs. Ventricular effective refractory period, APD_{90}, ventricular fibrillation threshold, and the incidence of ventricular arrhythmias were measured 1 h after left anterior descending coronary artery occlusion. A-803467 significantly shortened ventricular effective refractory period, APD_{90}, and ventricular fibrillation threshold compared to control. In the A-803467 group, the incidence of ventricular arrhythmias was significantly higher compared to control. A-803467 suppressed the slowing of heart rate response to high-frequency electrical stimulation of the anterior right GP, suggesting that A-803467 could inhibit GP activity. *SCN10A*/$Na_V1.8$ was readily detected in GPs, but was not validated in ventricles by quantitative RT-PCR, western blot and immunohistochemistry. While *SCN10A*/$Na_V1.8$ is detectible in canine GPs but not in ventricles, blockade of $Na_V1.8$ in GP increases the incidence of ventricular arrhythmias in AMI hearts. Our study shows for the first time an influence of *SCN10A*/$Na_V1.8$ on the regulation of ventricular arrhythmogenesis via modulating GP activity in the AMI model.

Keywords: SCN10A, cardiac ganglionated plexi, ventricular arrhythmia, acute myocardial infarction, sodium channel

OPEN ACCESS

Edited by:
Hongmei Tan,
Sun Yat-sen University, China

Reviewed by:
Yi Zhang,
Tongji University, China
Ning Zhou,
Huazhong University of Science and Technology, China

***Correspondence:**
Junbo Ge
jbge@zs-hospital.sh.cn
Lidong Cai
1015651169@qq.com

† These authors have contributed equally to this work

Specialty section:
This article was submitted to General Cardiovascular Medicine, a section of the journal Frontiers in Cardiovascular Medicine

Received: *11 May 2021*
Accepted: *12 July 2021*
Published: *02 August 2021*

Citation:
Qi B, Dai S, Song Y, Shen D, Li F, Wei L, Zhang C, Nie Z, Lin J, Cai L and Ge J (2021) Blockade of $Na_V1.8$ Increases the Susceptibility to Ventricular Arrhythmias During Acute Myocardial Infarction. Front. Cardiovasc. Med. 8:708279. doi: 10.3389/fcvm.2021.708279

INTRODUCTION

Acute myocardial infarction (AMI) always results in electrical instability and fatal ventricular arrhythmias which leads to sudden cardiac death. Ventricular fibrillation (VF) is one of the most common acute ventricular arrhythmias during AMI, which is associated with autonomic imbalance (1). The cardiac autonomic nervous system involves of both the intrinsic and extrinsic components. The intrinsic cardiac autonomic nervous system (ICANS) is a complex neural network formed by interconnecting nerves and ganglionated plexi (GP) concentrated in epicardial fat pads (2).

SCN10A encodes the alpha subunit of $Na_V1.8$. $Na_V1.8$ is a tetrodotoxin-resistant sodium channel and most highly expressed in dorsal root ganglia, which is reported to function in the transmission of pain signals (3). Recently, $Na_V1.8$ has been identified in intrinsic cardiac nerve fibers and the cardiac GP (4–6). Several studies have shown that *SCN10A*/$Na_V1.8$ is associated with myocardial repolarization and cardiac conduction, as well as atrial fibrillation (AF) and VF (7, 8). Data from Chambers et al. indicated that a common variant in *SCN10A* is associated with a lower risk of VF during AMI (7). However, if and by which mechanism *SCN10A*/$Na_V1.8$ impacts on cardiac electrophysiology is still a matter of debate.

Inhibition of $Na_V1.8$ by the blocker A-803467 has been reported to decrease late I_{Na} and shorten APD in mouse and rabbit cardiomyocytes (9), whereas the absence of functional $Na_V1.8$ has been described in non-diseased atrial and ventricular cardiomyocytes (6, 10). We and others have shown that $Na_V1.8$ plays a critical role in cardiac conduction via modulation of AP firing in intracardiac neurons (4, 6, 11). In the present study, we investigated the functional relevance of $Na_V1.8$ in cardiac GP, focusing on the contribution of $Na_V1.8$ to ventricular electrophysiology and ventricular arrhythmias in the AMI model.

MATERIALS AND METHODS

Surgical Preparation and Experimental Design

The animal protocol used for this study was reviewed and approved by the Institutional Animal Care and Use Committee of Zhongshan Hospital, Fudan University, and conformed to the Guide for the Care and Use of Laboratory Animals by the US National Institutes of Health (Publication No. 85-23, revised 1996). Twenty male beagles weighting 12 to 15 kg were anesthetized by administrating an intramuscular injection of xylazine (2.2 mg/kg) and ketamine (30 mg/kg), and maintained by 1–2% isoflurane/O_2. All measures were taken to minimize suffering. All animals were euthanized with a lethal dose of pentobarbital at the end of the experiments (100 mg/Kg, IV).

Twenty beagles were randomized to either the A-803467 group ($n = 10$) or the control group ($n = 10$). A-803467 (TargetMol, T2024) was dissolved in DMSO. The study protocol is shown in **Figure 1A**. Both right and left thoracotomies were performed at the fourth intercostal space, and the pericardium was opened. A-803467 (1 μmol/0.5 mL at each GP) or DMSO (0.5 mL at each GP, control) was injected into four major GPs within four epicardial fat pads: the superior left GP, the anterior right GP (ARGP), the inferior left GP, and the inferior right GP (**Figures 1B,C**). High frequency electrical stimulation (HFS, 0.1 ms duration, 20 Hz, square waves) was applied by a bipolar electrode probe (AtriCure, West Chester, Ohio, USA) to identify the cardiac GP. And the response was a progressive slowing of heart rate (HR) or atrioventricular conduction.

Electrophysiological Study Protocol

Two multi-electrode catheters (Capsure Epi, Medtronic, Minneapolis, MN, USA) were sutured on the left and right ventricular free walls to perform ventricular pacing with twice the diastolic pacing threshold (**Figures 1B,C**). Electrocardiographic and intracardiac electrograms were recorded on a Bard Computerized Electrophysiology system (**Figure 1D**, CR Bard Inc., Bard, Billerica, Massachusetts, USA) and were filtered and amplified from 0.05 to 500 Hz.

Ventricular pacing was performed at a cycle length of 300 ms (S1-S1). Ventricular effective refractory period (VERP) was started at 250 ms and repeated with progressively shorter S1-S2 intervals until the ventricular capture failed (S1:S2 = 8:1). VERP was defined as the longest coupling interval that did not capture the ventricle.

The monophasic action potential (MAP) was recorded by a catheter (Foehr Medical Instruments GMBH, Seeheim, Germany) at the left ventricle during atrial pacing with a custom-made Ag-AgCl electrode sutured on the right atrial appendage (BCL = 340 ms). The 90% of action potential duration (APD_{90}) was defined as MAP measured at 90% repolarization.

In order to verify whether the action of A-803467 was mediated by regulating GP function, we examined GP activity at 10 min after A-803467 or DMSO injection into the ARGP. HFS (square waves, 0.1 ms duration, 20 Hz) was applied to the ARGP with increasing voltages, and voltage-HR response curves were constructed. Changes of HR response to ARGP stimulation at different voltages were used as the surrogate marker for GP activity (12).

AMI Protocol and Ventricular Arrhythmias

As the largest action of A-803467 was observed at 35 min after local injection (13), which lasted at least 90 min, we occluded left anterior descending coronary artery (LAD) at 35 min after drug injection. LAD was occluded by using 3.0 silk suture positioned at approximately half of the distance from the apex. Then the incidence of ventricular arrhythmias including ventricular tachycardia (VT), ventricular premature contraction (VPC), and VF were recorded during 1 h after LAD occlusion.

Ventricular fibrillation threshold (VFT) was determined with right ventricular pacing at 1 h after LAD occlusion. S1-S1 (100 ms) was applied at the end of a 20-beat drive train with a pacing cycle length of 300ms. VFT was determined by progressively increase of pacing current in 2V steps. The minimum voltage required producing sustained VF was defined as VFT. Hearts were defibrillated with direct-current cardioversion.

Quantitative Real-time Polymerase Chain Reaction

Cardiac GPs, atria and ventricles were snap frozen in liquid N_2, and stored at −80°C until ready for quantitative real-time polymerase chain reaction (qPCR) and western blot analysis. Total RNA was isolated with RNeasy Mini Kit (74104, Qiagen) and was digested with DNase I (79254, Qiagen) according to manufacturer's instructions. cDNA was synthesized using the iScript cDNA Synthesis Kit (170-8891, Bio-Rad). Sequences of the primers are as follows: *SCN10A*, forward, 5′- CACCAGCTTTGATTCCTTTGC-3′

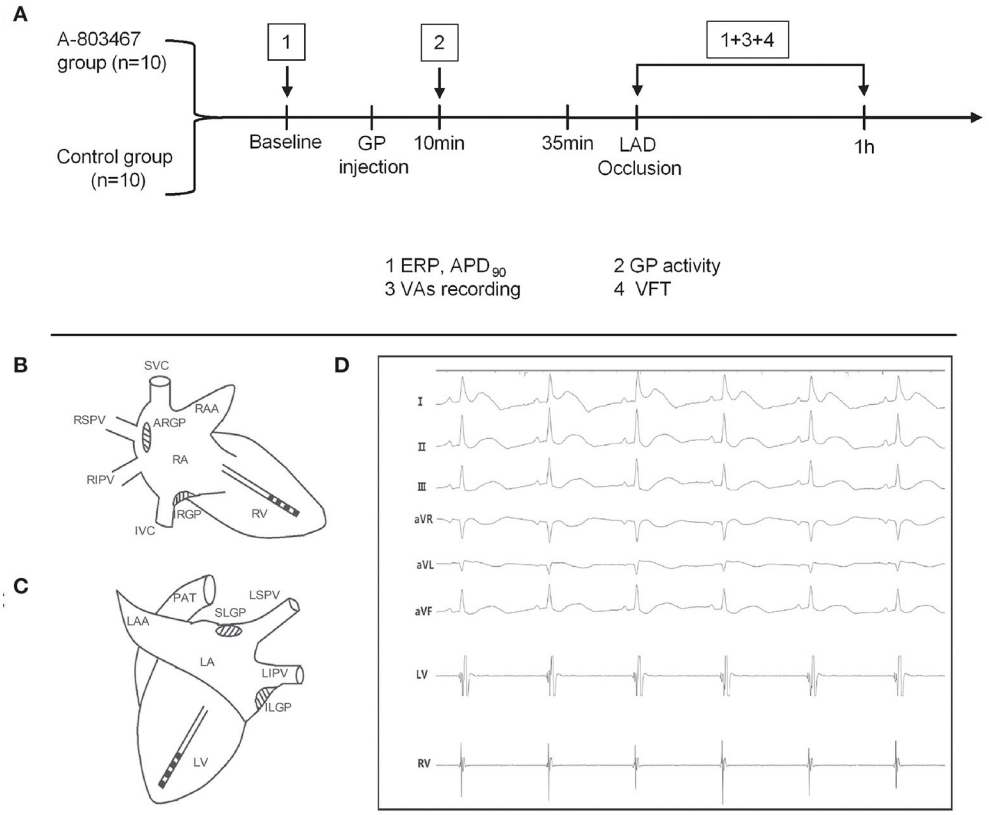

FIGURE 1 | Schematic representation of the study protocol **(A)** and catheter positions in the right **(B)** and left **(C)** ventricular free walls. **(D)** Surface electrocardiograms and local cardiac electrograms recording after left anterior descending coronary artery occlusion.

and reverse: 5′-ATTTTCCCAGATGCCCTCAG-3′ and *β-actin*, forward, 5′-TCCACGAGACCACTTTCAAC-3′ and reverse: 5′-TTTCCTTCTGCATCCTGTCG-3′. qPCR was performed on a 7500 Fast Real-Time PCR system (ABI, UK) with the SYBR Green PCR kit (Takara), and β-actin was used as an internal control. Each sample was analyzed in triplicate.

Western Blot Analysis

Samples were lysed with RIPA buffer (Beyotime, China) and the concentration of protein was assayed using a BCA Protein Assay Kit (Sigma-Aldrich, St. Louis, MO, USA). A total of 10 μg of protein was separated on SDS-PAGE (10 %) at 80 V for 1.5 h, and transferred onto PVDF membranes (Bio-Rad, USA) at 300 mA for 1.5 h. The following primary antibodies: $Na_V1.8$ (1:500, ab114110, Abcam) and β-actin (1:5000, ab8227, Abcam, Cambridge, UK) were used to incubate the blots at 37 °C for 2 h with gentle shaking. Afterwards, the secondary antibody Goat Anti-Rabbit IgG H&L (HRP) (1:5000; ab205718, Abcam, Cambridge, UK) was used to incubate the blots for 1 h at room temperature. The band density was analyzed using a gel imaging system and compared with an internal control.

Immunohistochemistry

Cardiac GPs, atria and ventricles were fixed with 10% formalin and embedded in paraffin. Then, 5-μm-thick tissues were serially cut from paraffin blocks and mounted onto glass slides coated with 1% (W/V) gelatin solution. After antigen retrieval, the tissue sections were incubated with primary antibodies against $Na_V1.8$ α subunit (1:20, ab114110, Abcam, Cambridge, UK) at 4°C overnight. After washing three times with PBS, the sections were then incubated with the secondary antibody (HRP labeled goat anti rabbit, 1:200, ab205718, Abcam, Cambridge, UK) expression were detected using DAB (brown) staining.

Ischemic Size Determination

The left auricular appendage was cannulated. Evans blue solution (200 mL, 2% in physiological saline) was infused into the left atrium, left ventricle, aorta and coronary artery, which resulted in a dark blue staining of the non-ischemic area. The heart was rapidly excised, and the atria and right ventricular free wall was removed. Both the non-trained ischemic areas and the blue-stained normal areas of the left ventricular free wall and of the septum were weighed separately. The mass of the ischemic tissue

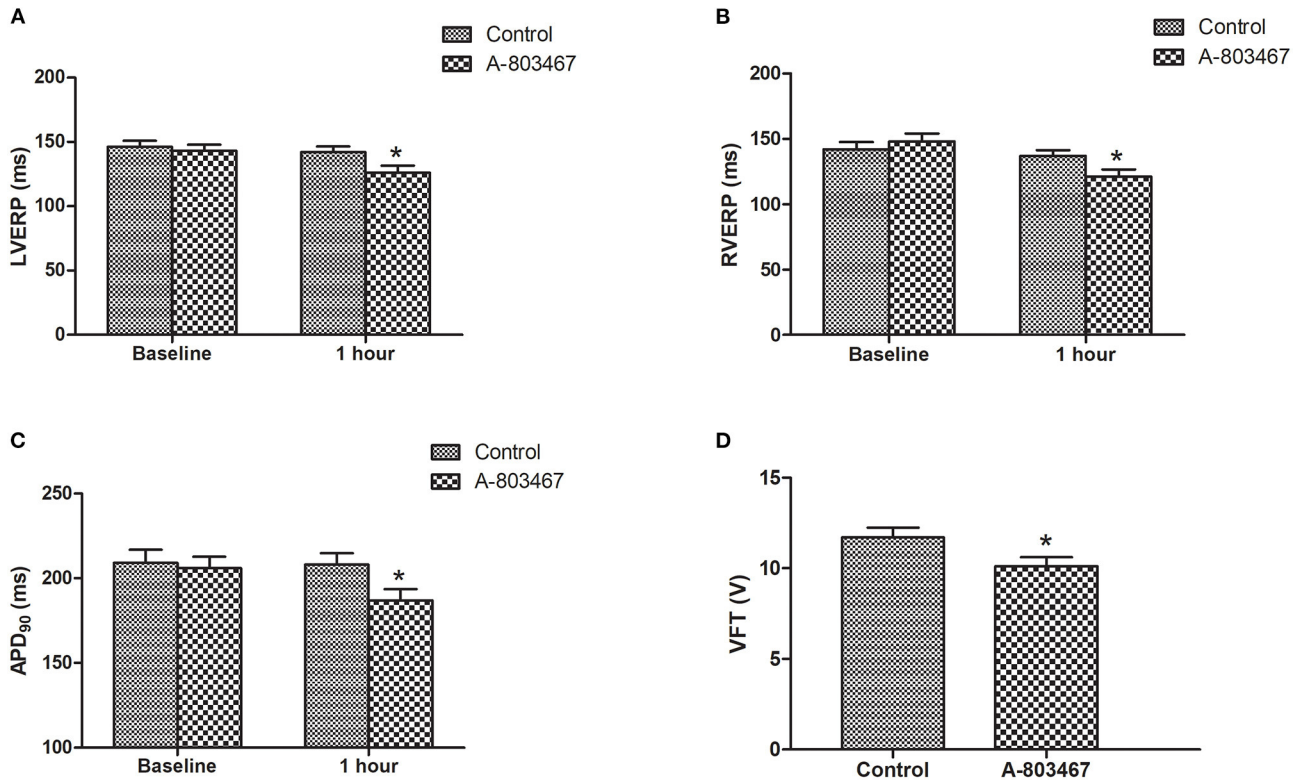

FIGURE 2 | Effects of A-803467 on Ventricular electrophysiology in the both two groups. **(A)** The left ventricular effective refractory period (LVERP) was decreased in the A-803467 group compared to control. **(B)** The right ventricular effective refractory period (RVERP) was decreased in the A-803467 group compared to control. **(C)** A-803467 significantly shortened 90% of action potential duration (APD_{90}) at 1 h after LAD occlusion. **(D)** The ventricular fibrillation threshold (VFT) was significantly shorter in the A-80467 group compared to control. *$P < 0.05$ vs. Control group.

was expressed as fraction of the left, or septal ventricular tissue mass.

Statistical Analysis

Data are shown as mean ± SEM. The repeated measures analysis of variance (ANOVA) was used to compare the mean of VERP, APD_{90}, and the slowing of HR with increasing voltage between the A-803467 group and the control group. The Mann-Whitney U test was used to compare the maximal percent change of HR. The independent-samples *t*-test was used to compare the mean of VPC, the duration of VT, VFT, and infarct size between two groups. Incidence of VF was compared between the A-803467 group and the control group using Fisher's exact test. GraphPad Prism software version 6.0 (GraphPad Software, La Jolla, California) was used for statistical analysis, and $P < 0.05$ was considered statistically significant.

RESULTS

Effect of Blocking $Na_V1.8$ on Ventricular Electrophysiology

Change of repolarization and refractoriness contributes greatly to proarrhythmic substrate. Both left ventricular effective refractory period (LVERP) and right ventricular effective refractory period (RVERP) were significantly shorter in the A-803467 group compared to control at 1 h after LAD occlusion (**Figures 2A,B**). A-803467 injection in cardiac GP significantly shortened ventricular APD_{90} at 1 h after LAD occlusion compared to control ($P < 0.05$, **Figure 2C**). For comparison between groups, VFTs were significantly shorter in the A-803467 group compared to control ($P < 0.05$, **Figure 2D**). A-803467 injection in cardiac GP shortened VERP, ventricular APD_{90}, and decreased VFT in AMI hearts, demonstrating that blocking $Na_V1.8$ in GP distant from the ventricles can influence ventricular electrophysiological properties.

Effect of Blocking $Na_V1.8$ on Ventricular Arrhythmias

An increase in susceptibility to ventricular arrhythmia was observed during 1 h after LAD occlusion in the A-803467 group compared to control. Examples of VF, VT, and VPCs ECG tracings (lead II) were shown in **Figures 3A,B**. As shown in **Figure 3C**, the number of VPC was significantly increased in the A-803467 group compared to control ($P < 0.05$). The mean duration of VT in the A-803467 group was longer compared to control ($P < 0.05$, **Figure 3D**). VF occurred in only 30%

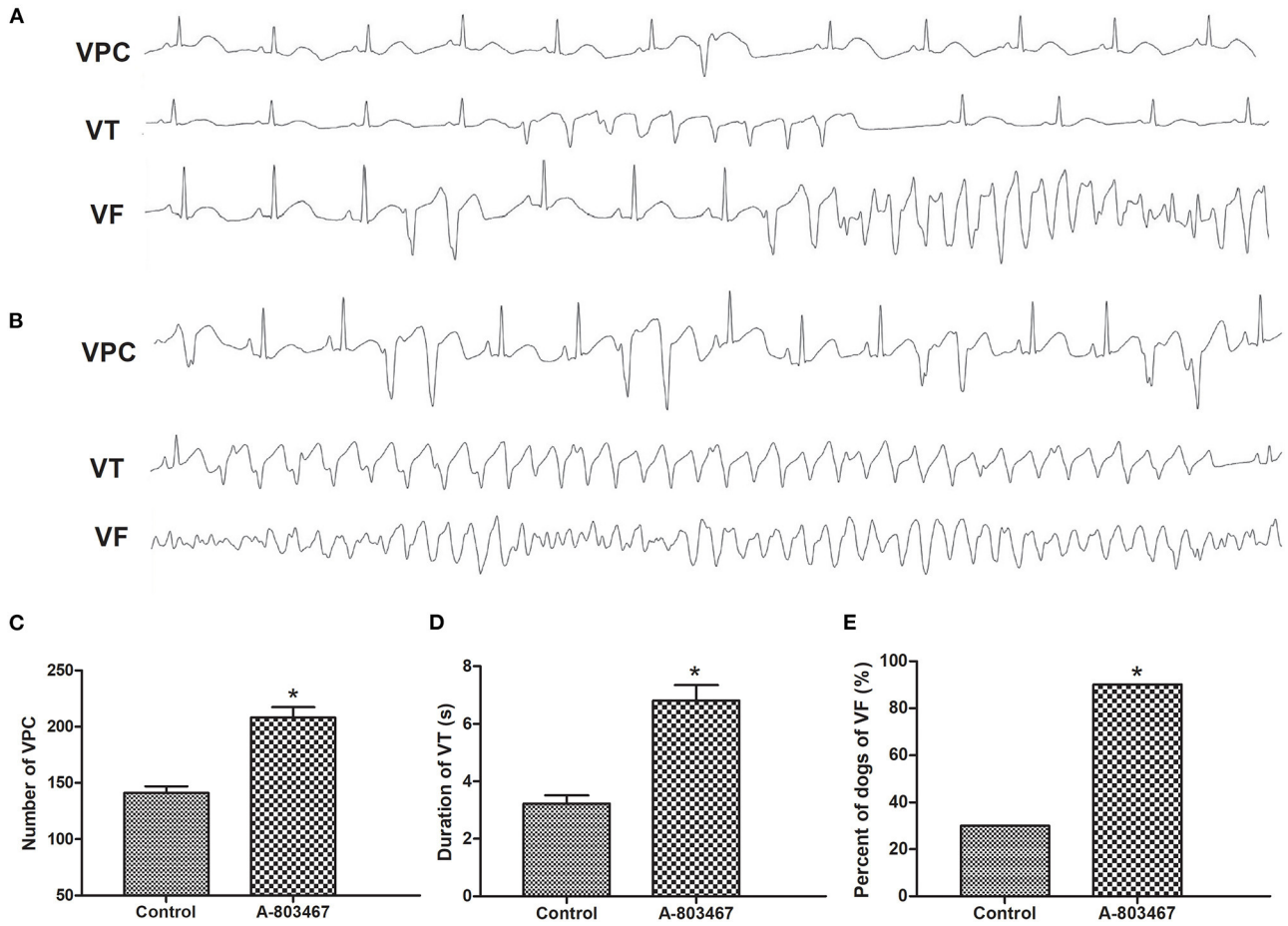

FIGURE 3 | The occurrence of ventricular arrhythmias during 1 h after LAD occlusion. Representative examples of the ventricular premature contraction (VPC), ventricular tachycardia (VT), and ventricular fibrillation (VF) ECG tracings (lead II) in the Control group **(A)** and the A-803467 group **(B)**. **(C)** VPCs were markedly increased in the A-803467 group after LAD occlusion compared to Control. **(D)** The mean duration of VT was longer in the A-803467 group after LAD occlusion compared to Control. **(E)** Percentage of dogs with VF was apparently increased in the A-803467 group after LAD occlusion compared to Control. *$P < 0.05$ vs. Control group.

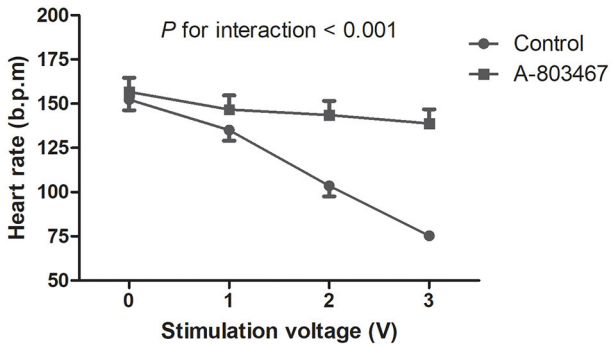

FIGURE 4 | Effects of A-803467 on the ganglionated plexi activity at 10 min after local injection into the anterior right ganglionated plexi. The trend in the heart rate change with increasing stimulation voltage was significantly different between the A-803467 group and the control group.

(3/10) of dogs in the control group, but 90% (9/10) of dogs in the A-803467 group experienced VF during AMI ($P < 0.05$, **Figure 3E**).

Effect of Blocking $Na_V1.8$ on GP Activity

A progressive slowing of HR was induced by HFS to the ARGP under incremental voltage levels. The maximal percent change in HR was decreased by 50.1 ± 1.3% compared to baseline in the control group, which was significantly higher compared with the A-803467 group ($P < 0.05$). HR decreased linearly with incremental stimulation voltage in the control group, whereas HR remained relatively flat after A-803467 injection. The treatment group by voltage interaction was significant, demonstrating that HR change with incremental voltage is different between the A-803467 and control group ($P < 0.001$, **Figure 4**). The results suggested that A-803467 could inhibit the activation of the neural elements within the GP.

Presence of scn10a/$Na_V1.8$ in Cardiac GPs and the Myocardium

$Na_V1.8$ protein expression in canine GPs and the myocardium was detected by western blot analysis and immunohistochemistry staining (**Figures 5A,B**). The results confirmed the presence of $Na_V1.8$ proteins in canine GPs but rarely expression in atria and ventricles. We also examined the relative abundance of *scn10a* transcripts in canine GPs and the myocardium by qPCR (**Figure 5C**). *Scn10a* transcripts were readily detected in both SLGP and ARGP but were not detected in atria and ventricles.

Size of the Ischemic Area

A well-defined borderline was present between the ischemic zone and the non-ischemic cardiac tissue. **Table 1** summarized the left ventricle and septum myocardial mass of the ischemic area in the two groups. There was no significant difference between the two groups.

DISCUSSION

The present study demonstrated for the first time that blocking $Na_V1.8$ in cardiac GPs promotes occurrences of ventricular arrhythmias including VPCs, VT and spontaneous VF in the AMI model. Blockade of $Na_V1.8$ shortened VERP, ventricular APD_{90}, and decreased VFT during AMI. These effects may be mediated by inhibiting cardiac GP activity, as evidenced by the attenuation of the slowing of HR response to GP stimulation.

Of note, *SCN10A*/$Na_V1.8$ was readily detected in canine GPs, but was not validated in canine ventricles by qPCR and western blot. Immunohistochemistry on canine tissue sections showed $Na_V1.8$ labeling in cardiac GP (4), and A-803467 significantly

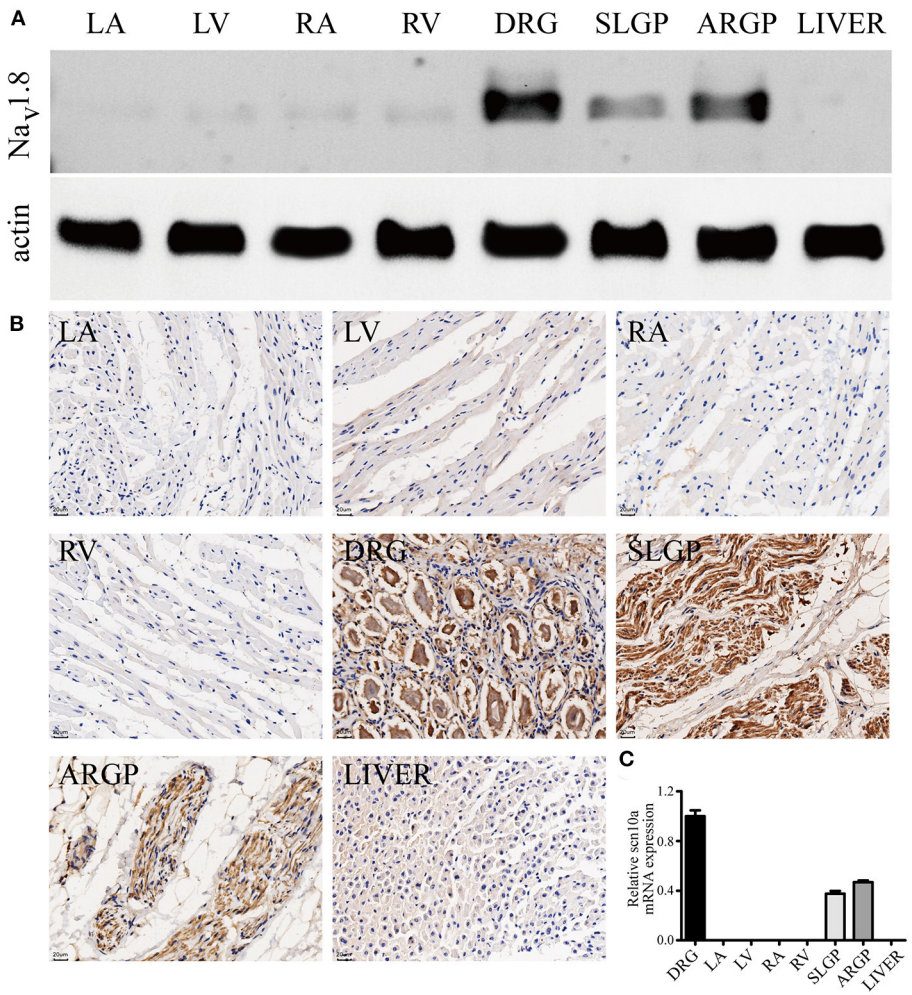

FIGURE 5 | *Scn10a*/$Na_V1.8$ expression in canine GPs and the myocardium. **(A)** Typical western blots for $Na_V1.8$, $n = 4$. **(B)** Typical immunohistochemistry-stained sections for $Na_V1.8$, scale bar = 20 μm, $n = 4$. The results confirmed the presence of $Na_V1.8$ proteins in canine GPs but rarely expression in atria and ventricles. **(C)** *Scn10a* transcripts were readily detected in both superior left ganglionated plexi (SLGP) and anterior right ganglionated plexi (ARGP) but were not detected in right atrium (RA), left atrium (LA), left ventricle (LV), and right ventricle (RV) by qPCR. $n = 4$. Dorsal root ganglia (DRG) was used as the positive control and the liver was used as the negative control.

TABLE 1 | Percentage of ischemic myocardial mass (%).

	Septum	Left ventricle
Control group ($n = 10$)	27.4 ± 2.5	30.3 ± 2.4
A-803467 group ($n = 10$)	25.7 ± 1.9	28.5 ± 2.2
P	>0.05	>0.05

reduced action potential firing frequency in GP neurons but did not affect cardio-myocyte action potential upstroke velocity (6). Low to absent expression levels of *scn10a* were observed in rabbit ventricular tissue, human atrial tissue and hiPSC-CMs (10). It has been reported that $Na_V1.8$ is up-regulated in the human hypertrophied myocardium and the failing human myocardium, suggesting that inhibition of $Na_V1.8$ could be an antiarrhythmic therapeutic target (14, 15). However, they made no attempt to identify the presence of $Na_V1.8$ in intracardiac neurons or study their effects. We previously reported that blockade of $Na_V1.8$ by A-803467 suppresses AF inducibility and cardiac conduction during vagus nerve stimulation, most likely through inhibiting GP activity (11). In order to localize the effects on cardiac GPs and minimize its systemic action on the myocardium, we intentionally injected A-803467 into cardiac GPs. In the present study, A-803467 can shorten APD_{90} and VERP, which accompanied by increasing incidences of VF and VT during myocardial ischemia. We have shown that inhibition of $Na_V1.8$ channels increase the incidence of ventricular arrhythmias in AMI hearts through modulating GP activity.

The cardiac GP exerts a significant role in the initiation and maintenance of AF, and radiofrequency GP ablation is demonstrated to improve the success rate of AF ablation (16). The cardiac cholinergic neurons could also modulate ventricular electrophysiology. Pharmacological blockade or mechanical disruption of parasympathetic innervation decreased ventricular cAMP levels, shortened VERP, and increased the incidence of ventricular arrhythmias (17). He et al. reported that VF was significantly facilitated and ventricular arrhythmia incidence was significantly increased after GP ablation in AMI dogs (18). The present study also showed that suppression of GP activity may result in an imbalanced modulation of the heart, which may promote the genesis of ventricular arrhythmias during myocardial ischemia.

A study by Yu et al. showed that inhibition of $Na_V1.8$ attenuated ischemia-induced ventricular arrhythmia by suppressing left stellate ganglion activity (19). At first glance, our finding may appear inconsistent with Yu's study; it is not. The cardiac GP contains entities representing both parasympathetic and sympathetic neurons, while a majority of GP neurons has been found to be parasympathetic (20). GP activation by HFS can evoke negative chronotropic effects and affect ventricular repolarization properties (18), and GP ablation can significantly decrease the ERP of the ventricular myocardium (21). Blocking $Na_V1.8$ in left stellate ganglion could decrease sympathetic activity and attenuate ischemia-induced ventricular arrhythmia, however, blocking $Na_V1.8$ in GP could inhibit parasympathetic activity and increase ischemia-induced ventricular arrhythmia.

The GP neurons could synthesize many different neurotransmitters. Acetylcholine is one of the principal excitatory neurotransmitters in the cardiac GP. Blasius et al. found that mice carrying the hypermorphic mutation of *SCN10A*, with enhanced $Na_V1.8$ sodium currents, exhibited marked R-R variability and sinus bradycardia upon "scruffing," which could be abrogated by atropine infusion (22). Brack et al. reported that nitric oxide can play a vagal protective role of suppressing VF, possibly through modulating APD restitution in rabbit hearts (23). We hypothesize that $Na_V1.8$ could possibly modulate release of neurotransmitters in the cardiac GP, and nitric oxide or acetylcholine may represent potential candidates.

Our study has some limitations. First, we did not record neural activity directly within the GP. However, we have provided the evidence of altered GP function which could correlate well with GP neural activity based on prior studies (12). Second, other potentially important GPs were not studied, such as the GP near the ligament of Marshall. However, a complete GP blockade might be difficult to achieve. Third, the signaling pathway mediating the protective role of $Na_V1.8$ remains to be determined. Our further study will be performed to clarify the exact mechanism and the downstream pathways involved in the antiarrhythmic actions of $Na_V1.8$.

In view of the present results, as suppression of GP activity may promote the genesis of ventricular arrhythmias, GP ablation should be avoided in patients with ischemia diseases. Our results may identify $Na_V1.8$ as a potential novel therapeutic target for antiarrhythmic intervention aiming at modulating the neural control of the ischemic heart to treat patients with refractory ventricular arrhythmias or electrical storm. Our study may lead to the development of a novel oral $Na_V1.8$ stimulator with more specific action and less adverse effects.

In conclusion, *SCN10A*/$Na_V1.8$ is detectible in canine GPs but not in ventricles, and blockade of $Na_V1.8$ in cardiac GPs increases the incidence of ventricular arrhythmias in AMI hearts. Our study shows for the first time an influence of *SCN10A*/$Na_V1.8$ on the regulation of ventricular arrhythmogenesis via modulating cardiac GP activity in the AMI model.

DATA AVAILABILITY STATEMENT

The original contributions presented in the study are included in the article/supplementary material, further inquiries can be directed to the corresponding author/s.

ETHICS STATEMENT

The animal study was reviewed and approved by Institutional Animal Care and Use Committee of Zhongshan Hospital, Fudan University.

AUTHOR CONTRIBUTIONS

BQ, SD, YS, LC, and JG: conception, design, data analysis, and interpretation. BQ, LC, YS, DS, FL, and LW: administrative

support. BQ, SD, CZ, ZN, and JL: collection and assembly of data. BQ: manuscript writing. All authors wrote first draft, read, amended the draft, and final approval of manuscript.

FUNDING

This work was supported by the National Natural Science Foundation of China (81500248).

REFERENCES

1. Zipes DP, Rubart M. Neural modulation of cardiac arrhythmias and sudden cardiac death. *Heart Rhythm.* (2006) 3:108–13. doi: 10.1016/j.hrthm.2005.09.021
2. Chang HY, Lo LW, Chou YH, Lin WL, Lin YJ, Yamada S, et al. Effect of vagotomy on the activity of cardiac autonomic ganglia: insight from left atrial high density frequency mapping. *Int J Cardiol.* (2016) 220:435–9. doi: 10.1016/j.ijcard.2016.06.183
3. Abrahamsen B, Zhao J, Asante CO, Cendan CM, Marsh S, Martinez-Barbera JP, et al. The cell and molecular basis of mechanical, cold and inflammatory pain. *Science.* (2008) 321:702–5. doi: 10.1126/science.1156916
4. Chen X, Yu L, Shi S, Jiang H, Huang C, Desai M, et al. Neuronal $Na_V1.8$ Channels as a novel therapeutic target of acute atrial fibrillation prevention. *J Am Heart Assoc.* (2016) 5:e004050. doi: 10.1161/JAHA.116.004050
5. Facer P, Punjabi PP, Abrari A, Kaba RA, Severs NJ, Chambers J, et al. Localisation of SCN10A gene product Na(v)1.8 and novel pain-related ion channels in human heart. *Int Heart J.* (2011) 52:146–52. doi: 10.1536/ihj.52.146
6. Verkerk AO, Remme CA, Schumacher CA, Scicluna BP, Wolswinkel R, de Jonge B, et al. Functional $Na_V1.8$ channels in intracardiac neurons: the link between SCN10A and cardiac Electrophysiology. *Circ Res.* (2012) 111:333–43. doi: 10.1161/CIRCRESAHA.112.274035
7. Chambers JC, Zhao J, Terracciano CM, Bezzina CR, Zhang W, Kaba R, et al. Genetic variation in SCN10A influences cardiac conduction. *Nat Genet.* (2010) 42:149–52. doi: 10.1038/ng.516
8. Delaney JT, Muhammad R, Shi Y, Schildcrout JS, Blair M, Short L, et al. Common SCN10A variants modulate PR interval and heart rate response during atrial fibrillation. *Europace.* (2014) 16:485–90. doi: 10.1093/europace/eut278
9. Yang T, Atack TC, Stroud DM, Zhang W, Hall L, Roden DM. Blocking Scn10a channels in heart reduces late sodium current and is antiarrhythmic. *Circ Res.* (2012) 111:322–32. doi: 10.1161/CIRCRESAHA.112.265173
10. Casini S, Marchal GA, Kawasaki M, Nariswari FA, Portero V, van den Berg NWE, et al. Absence of functional $Na_V1.8$ channels in non-diseased atrial and ventricular cardiomyocytes. *Cardiovasc Drugs Ther.* (2019) 33:649–60. doi: 10.1007/s10557-019-06925-6
11. Qi B, Wei Y, Chen S, Zhou G, Li H, Xu J, et al. $Na_V1.8$ channels in ganglionated plexi modulate atrial fibrillation inducibility. *Cardiovas Res.* (2014) 102:480–6. doi: 10.1093/cvr/cvu005
12. Yu L, Scherlag BJ, Li S, Sheng X, Lu Z, Nakagawa H, et al. Low-level vagosympathetic nerve stimulation inhibits atrial fibrillation inducibility: direct evidence by neural recordings from intrinsic cardiac Ganglia. *J Cardiovasc Electrophysiol.* (2011) 22:455–63. doi: 10.1111/j.1540-8167.2010.01908.x
13. McGaraughty S, Chu KL, Scanio MJ, Kort ME, Faltynek CR, Jarvis MF. A Selective $Na_V1.8$ Sodium channel blocker, A-803467 [5-(4-Chlorophenyl-N-(3,5- dimethoxyphenyl) furan-2- carboxamide], attenuates spinal neuronal activity in neuropathic rats. *J Pharmacol Exp Ther.* (2008) 324:1204–11. doi: 10.1124/jpet.107.134148
14. Dybkova N, Ahmad S, Pabel S, Tirilomis P, Hartmann N, Fischer TH, et al. Differential regulation of sodium channels as a novel proarrhythmic mechanism in the human failing heart. *Cardiovasc Res.* (2018) 114:1728–37. doi: 10.1093/cvr/cvy152
15. Ahmad S, Tirilomis P, Pabel S, Dybkova N, Hartmann N, Molina CE, et al. The functional consequences of sodium channel Na_V 1.8 in human left ventricular hypertrophy. *ESC Heart Fail.* (2019) 6:154–63. doi: 10.1002/ehf2.12378
16. Katritsis DG, Pokushalov E, Romanov A, Giazitzoglou E, Siontis GC, Po SS, et al. Autonomic denervation added to pulmonary vein isolation for paroxysmal atrial fibrillation: a randomized clinical trial. *J Am Coll Cardiol.* (2013) 62:2318–25. doi: 10.1016/j.jacc.2013.06.053
17. Jungen C, Scherschel K, Eickholt C, Kuklik P, Klatt N, Bork N, et al. Disruption of cardiac cholinergic neurons enhances susceptibility to ventricular arrhythmias. *Nat Commun.* (2017) 8:14155. doi: 10.1038/ncomms14155
18. He B, Lu Z, He W, Wu L, Cui B, Hu X, et al. Effects of ganglionated plexi ablation on ventricular electrophysiological properties in normal hearts and after acute myocardial ischemia. *Int J Cardiol.* (2013) 168:86–93. doi: 10.1016/j.ijcard.2012.09.067
19. Yu L, Wang M, Hu D, Huang B, Zhou L, Zhou H, et al. Blocking the $Na_V1.8$ channel in the left stellate ganglion suppresses ventricular arrhythmia induced by acute ischemia in a canine model. *Sci Rep.* (2017) 7:534. doi: 10.1038/s41598-017-00642-6
20. Hoover DB, Isaacs ER, Jacques F, Hoard JL, Pagé P, Armour JA. Localization of multiple neurotransmitters in surgically derived specimens of human atrial ganglia. *Neuroscience.* (2009) 164:1170–9. doi: 10.1016/j.neuroscience.2009.09.001
21. Mao J, Yin X, Zhang Y, Yan Q, Dong J, Ma C, et al. Ablation of epicardial ganglionated plexi increases atrial vulnerability to arrhythmias in dogs. *Circ Arrhythm Electrophysiol.* (2014) 7:711–7. doi: 10.1161/CIRCEP.113.000799
22. Blasiusa AL, Dubinb AE, Petrusc MJ, Lim BK, Narezkina A, Criado JR, et al. Hypermorphic mutation of the voltage-gated sodium channel encoding gene Scn10a causes a dramatic stimulus-dependent neurobehavioral phenotype. *Proc Natl Acad Sci USA.* (2011) 108:19413–18. doi: 10.1073/pnas.1117020108
23. Brack KE, Patel VH, Coote JH, Ng GA. Nitric oxide mediates the vagal protective effect on ventricular fibrillation via effects on action potential duration restitution in the rabbit heart. *J Physiol.* (2007) 583:695–704. doi: 10.1113/jphysiol.2007.138461

Conflict of Interest: The authors declare that the research was conducted in the absence of any commercial or financial relationships that could be construed as a potential conflict of interest.

Publisher's Note: All claims expressed in this article are solely those of the authors and do not necessarily represent those of their affiliated organizations, or those of the publisher, the editors and the reviewers. Any product that may be evaluated in this article, or claim that may be made by its manufacturer, is not guaranteed or endorsed by the publisher.

Copyright © 2021 Qi, Dai, Song, Shen, Li, Wei, Zhang, Nie, Lin, Cai and Ge. This is an open-access article distributed under the terms of the Creative Commons Attribution License (CC BY). The use, distribution or reproduction in other forums is permitted, provided the original author(s) and the copyright owner(s) are credited and that the original publication in this journal is cited, in accordance with accepted academic practice. No use, distribution or reproduction is permitted which does not comply with these terms.

frontiers in Cardiovascular Medicine

ORIGINAL RESEARCH
published: 17 September 2021
doi: 10.3389/fcvm.2021.737191

S-Propargyl-Cysteine Attenuates Diabetic Cardiomyopathy in *db/db* Mice Through Activation of Cardiac Insulin Receptor Signaling

Ye Li[1†], *Kui-Fang Xie*[1†], *Ya-Hong Chang*[1], *Cheng Wang*[2], *Ying Chen*[1], *Ming-Jie Wang*[1*] *and Yi-Chun Zhu*[1*]

[1] *Shanghai Key Laboratory of Bioactive Small Molecules and Shanghai Key Laboratory of Clinical Geriatric Medicine, Innovative Research Team of High-Level Local Universities in Shanghai, Department of Physiology and Pathophysiology, School of Basic Medical Sciences, Fudan University, Shanghai, China,* [2] *Laboratory Animal Technical Platform, Shanghai Institute of Nutrition and Health, University of Chinese Academy of Sciences, Chinese Academy of Sciences, Shanghai, China*

OPEN ACCESS

Edited by:
Hongmei Tan,
Sun Yat-sen University, China

Reviewed by:
Fenghua Yang,
Guangdong Laboratory Animals Monitoring Institute, China
Ying Shao,
Temple University, United States

***Correspondence:**
Ming-Jie Wang
mjwang@shmu.edu.cn
Yi-Chun Zhu
yczhu@shmu.edu.cn

[†] *These authors have contributed equally to this work*

Specialty section:
This article was submitted to General Cardiovascular Medicine, a section of the journal Frontiers in Cardiovascular Medicine

Received: *06 July 2021*
Accepted: *24 August 2021*
Published: *17 September 2021*

Citation:
Li Y, Xie K-F, Chang Y-H, Wang C, Chen Y, Wang M-J and Zhu Y-C (2021) S-Propargyl-Cysteine Attenuates Diabetic Cardiomyopathy in db/db Mice Through Activation of Cardiac Insulin Receptor Signaling. Front. Cardiovasc. Med. 8:737191. doi: 10.3389/fcvm.2021.737191

Background: Endogenous hydrogen sulfide (H_2S) is emerging as a key signal molecule in the development of diabetic cardiomyopathy. The aim of this study was to explore the effect and underlying mechanism of S-propargyl-cysteine (SPRC), a novel modulator of endogenous H_2S, on diabetic cardiomyopathy in *db/db* diabetic mice.

Methods and Results: Vehicle or SPRC were orally administered to 8-month-old male *db/db* mice and their wild type littermate for 12 weeks. SPRC treatment ameliorated myocardial hypertrophy, fibrosis, and cardiac systolic dysfunction assessed by histopathological examinations and echocardiography. The functional improvement by SPRC was accompanied by a reduction in myocardial lipid accumulation and ameliorated plasma lipid profiles. SPRC treatment improved glucose tolerance in *db/db* mice, with fasting blood glucose and peripheral insulin resistance remaining unchanged. Furthermore, insulin receptor signaling involving the phosphorylation of protein kinase B (Akt/PKB) and glycogen synthase kinase 3β (GSK3β) were elevated and activated by SPRC treatment. Primary neonatal mice cardiomyocytes were cultured to explore the mechanisms of SPRC on diabetic cardiomyopathy *in vitro*. Consistent with the results *in vivo*, SPRC not only up-regulated insulin receptor signaling pathway in cardiomyocytes in dose-dependent manner in the basal state, but also relieved the suppression of insulin receptor signaling induced by high concentrations of glucose and insulin. Furthermore, SPRC also enhanced the expression of glucose transporter 4 (GLUT4) and ^3H glucose uptake in cardiomyocytes.

Conclusions: In this study, we found a novel beneficial effect of SPRC on diabetic cardiomyopathy, which was associated with activation of insulin receptor signaling. SPRC may be a promising medication for diabetic cardiomyopathy in type 2 diabetes mellitus patients.

Keywords: S-propargyl-cysteine, hydrogen sulfide, diabetic cardiomyopathy, insulin receptor signaling, glucose uptake

INTRODUCTION

Among adults in China, the number of diabetic patients have explosively increased. The estimated overall prevalence of diabetes was 10.9%, and that for prediabetes was 35.7% (1). Cardiovascular disease, is a leading cause of mortality in the development of diabetic complications (2). After adjusting for other risk factors including age, hypertension, obesity, dyslipidemia, the incidence of heart failure increases 2.4–5 fold in diabetic patients than non-diabetic patients (3). Diabetic cardiomyopathy (DCM) is defined as structural and functional abnormalities in the myocardium of diabetic patients independent of underlying coronary artery disease and hypertension (4). At present, treatment strategy for DCM mainly rely on conventional therapies that focus on optimizing glycemic control (5). However, meta-analysis of large clinical trials revealed that strict glycemic control had no impact on the incidence of heart failure in diabetic patients (6, 7). Therefore, it is particularly important to explore the pathogenesis mechanism and novel therapeutic drugs of DCM.

Hydrogen sulfide (H_2S) has been considered toxic and odorous for a long time. However, it has been recognized as the third gasotransmitter following nitric oxide and carbon monoxide to play an important role in many physiological and pathological processes since the 1990s. Accumulating studies have shown that H_2S is involved in improving DCM by multiple mechanisms (8), such as supplementation of exogenous H_2S reduced endoplasmic reticulum pressure in cardiomyocytes (9, 10) and inhibited myocardial oxidative Stress, inflammation, and apoptosis (11). Endogenous H_2S production by cystathionine-γ-lyase (CTH, also named CSE, the main producing enzyme of endogenous H_2S in cardiovascular system) is inhibited in myocardium of DCM rats (12). Consistently, H_2S levels in serum of DCM patients were significant decreased and the supplement of H_2S could rescue the cardiomyopathy dysfunction induced by hyperglycemia (10, 13). However, H_2S cannot be used for clinical therapy because of its instability and gaseous characteristics. S-Propargyl-Cysteine (SPRC, also named as ZYZ-802), a novel water-soluble modulator of endogenous H_2S, promotes the activity of CSE and then increases H_2S levels in plasma or tissue (14–16). In this study, we evaluated the effect of SPRC on DCM in *db/db* mice and further explored the underlying mechanism, both *in vivo and in vitro*.

Abbreviations: Akt/PKB, protein kinase B; AUC, area under the curve; CSE (CTH), cystathionine-γ-lyase; DCM, diabetic cardiomyopathy; DM, diabetes mellitus; DT, deceleration time; ECL, enhanced chemiluminescence; EF, ejection fraction; FBG, fasting blood glucose; FINS, fasting plasma insulin; FS, fraction shortening; H_2S, hydrogen sulfide; GLUT4, glucose transporter 4; GSK3β, glycogen synthase kinase 3β; HE, hematoxylin-eosin; HDL-C, high-density lipoprotein cholesterol; HOMA-IR, homeostasis model assessment-insulin resistance index; IPGTT, Intraperitoneal glucose tolerance test; IPITT, Intraperitoneal Insulin Tolerance Test; LDL-C, low-density lipoprotein cholesterol; SPRC, S-propargyl-cysteine; TEM, transmission electron microscope; TC, total cholesterol; TG, triglycerides.

MATERIALS AND METHODS

Chemicals

S-Propargyl-Cysteine (SPRC, purity > 99%) was synthesized as described previously (17) and provided by Professor Zhu Yi-Zhun (State Key Laboratory of Quality Research in Chinese Medicine and School of Pharmacy, Macau University of Science and Technology, Macau, China). Chemical formula of SPRC is shown in **Supplementary Figure 1A.**

Animals and Treatments

All experimental procedures were performed in accordance with Guide for the Care and Use of Laboratory Animals of the National Institutes of Health (NIH) of the United States and approved by the Ethics Committee of Experimental Research, Fudan University Shanghai Medical College. Male C57BLKS/J *db/db* mice and their wild type littermates (7-week-old) were purchased from Nanjing Biomedical Research Institute of Nanjing University and were housed in a climate-controlled environment (22 ± 2°C, 45–75% relative humidity) with a 12 h light-dark cycle and unrestricted access to food and water. After acclimatization for 1 weeks, wild-type (WT) mice were used as a normal control group and *db/db* mice were randomly divided into four different groups (n = 15–16 per group): diabetic model group, low-dose SPRC treatment group (20 mg/kg per day), medium-dose SPRC treatment group (40 mg/kg per day), and high-dose SPRC treatment group (80 mg/kg per day). Both WT control group and diabetic model group were orally administered an equal volume of vehicle (ddH_2O). After 12 weeks of administration, mice were anesthetized by intraperitoneal injection of 1% sodium pentobarbital and blood samples were collected. Heart weights (HW) and tibia lengths (TL) were measured and heart tissue specimens were obtained.

Transthoracic Echocardiography

At the first and last week of SPRC treatment, the hair was removed from the chest of mice using depilatory cream. The mice were then anesthetized with 1.5% isoflurane and placed in a supine position on the test bench, with ultrasound gel applied onto the chest. Mouse two-dimensional echocardiography was performed using a Vevo3100 ultrasound device (VisualSonics Inc., Canada), as previously described (18). B-mode, M-mode, and Power Doppler Mode ultrasound images of the left ventricle were recorded. All measurements were averaged for five consecutive cardiac cycles.

Fasting Blood Glucose, Body Weight, and Fasting Plasma Insulin Levels

The FBG levels and BW of mice were monitored every 2 weeks after food was removed for 12 h. Glucose measurements were performed with venous blood collected from mice tails by glucose monitors (ONETOUCH, Johnson and Johnson, USA). After food was removed overnight for 16 h, FINS were detected by enzyme-linked immunosorbent assay (ELISA) kit (Mercodia, Sweden). The formula of homeostasis model assessment for insulin resistance index (HOMA-IR) is [(HOMA-IR) = (FBG × FINS)/22.5] (19).

IPGTTs and IPITTs

Intraperitoneal glucose tolerance test (IPGTT) and intraperitoneal insulin tolerance test (IPITT) were performed in the morning on nonfasted mice that had their food removed 1 h prior to intraperitoneal injection (IPGTT 1 g glucose per kg body weight and IPITT 1unit recombinant human insulin (Humulin 70/30, Lilly, USA) per kg body weight), Blood glucose levels were measured before the injection (time 0) and 15, 30, 60, and 120 min after the injection. Areas under the curve (AUC) were determined using the trapezoidal rule.

Biochemical Analyses

The total cholesterol (TC), triglycerides (TG), high-density lipoprotein cholesterol (HDL-C), low-density lipoprotein cholesterol (LDL-C), non-esterified fatty acid (NEFA) in plasma were determined using commercial kits (Nanjing Jiancheng, China) according to the manufacturer's instructions. Briefly, full-wavelength microplate reader (Infinite® 200 PRO, TECAN, Switzerland) was used to detect the absorbance of plasma samples at 510 nm for TC and TG or at 546 nm for HDL-C, LDL-C and NEFA.

Histological Analysis

Heart specimens were fixed in 4% paraformaldehyde solution. After being embedded in paraffin, the specimens were cut into 5-μm-thick sections and stained with wheat germ agglutinin (WGA) and Masson's trichrome. The other heart tissue specimens were frozen and stained with Oil Red O lipid stain. The size of myocardial cells, fiber area fraction, and myocardial lipid content were determined using Image J software (Bethesda, MA, USA).

Transmission Electron Microscopy

To observe myocardial ultrastructure, heart tissues were cut into 1 mm transverse sections and immersed in 2% glutaraldehyde overnight. The sections were then immersed in 1% osmium tetroxide for 2 h, dehydrated in graded ethanol, and embedded in epoxy resin. Ultrathin sections (60–70 nm) were obtained, stained with uranyl acetate and lead citrate, and examined using a Tecnai G20 Twin transmission electron microscope (FEI, USA).

Primary Culture of Neonatal Mice Cardiomyocytes

Primary cultures of cardiomyocytes were prepared from neonatal mice hearts. In brief, hearts were excised from 1- to 2-day-old mice pups. Ventricles were minced by small scissors and digested using 1 mg/ml collagenase type II (Worthington, USA). The digested solution was collected. The process was repeated 3–4 times until no chunks of tissue were visible. The final pooled solution was centrifuged and the cell pellet re-suspended in Dulbecco's Modified Eagle Medium (DMEM, Hyclone, USA), high Glucose containing 10% fetal bovine serum (FBS, Gibco, USA). The cells were pre-plated for 1 h to allow the attachment and removal of fibroblasts. The unattached cardiomyocytes remaining in suspension were then collected and plated in DMEM, high Glucose containing 10% FBS. After 48 h Cardiomyocytes cultures were used for subsequent experiments.

Cell Viability

Cell viability was determined by cell counting kit-8 assay according to manufacturer's instructions (DOJINDO, Japan). Cardiomyocytes were cultured in a 96-well-culture plate and treated with different concentrations of SPRC (0–1,000 μM) for 24 h. Cells were subsequently incubated with 10 ml CCK-8 solution at 37°C for 4 h. The absorbance at 450 nm was measured.

Real-Time PCR

Total RNA was extracted by Trizol reagent from heart tissue or cardiomyocytes. RNA was reverse-transcribed using a cDNA synthesis kit (Toyobo Life Science, Japan). Real-Time PCR was performed using a StepOnePlus Real-Time PCR Detection System (Applied Biosystems Inc., CA, USA). A total volume of 20 μL reaction mix containing 2 μL cDNA, 10 μL SYBR Green PCR Master Mix (Toyobo, Japan) and 1 μL each primer (10 μM). G*apdh* was used for normalization and the relative expression of mRNA was calculated according to the $^{\Delta\Delta}$Ct method. The specific primers were as follows: *Myh7*: 5′-ATCAATGCAACCCTGGAG AC-3′, 5′-CGAACATGTGGTGGTTGAAG-3′; *InsR*: 5′-GCT TCTGCCAAGACCTTCAC-3′, 5′-CACTCGGGGATGCACTTA TT-3′; *Glut4*: 5′-ACCCTGGGCTCTGTATCCC-3′, 5′-CCCTGA CCACTGAGTGCAAA-3′; *Gapdh:* 5′-TTCACCACCATGGAG AAGGC-3′, 5′-GGCATGGACTGTGGTCATGA-3′; *β-actin:* 5′-GACAGGATGCAGAAGGAGATTACT-3′, TGATCCACATCT GCTGGAAGGT-3′.

Western Blotting

Left ventricular tissue and cell samples were lysed with Cell Lysis Buffer for Western (P0031; Beyotime Biotechnology, China) containing a protease inhibitor cocktail (049693132001; Roche, Basel, Switzerland). The crude cell lysate was centrifuged and the supernatant was harvested. The concentration of protein in the supernatant was quantified by standard bicinchoninic acid assay (BCA, P0012, Beyotime Biotechnology, China). For western blotting, equal amounts of proteins were resolved by sodium dodecyl sulfate polyacrylamide gel electrophoresis and transferred to polyvinylidene difluoride membranes. Membranes were then incubated with horseradish peroxidase-conjugated secondary antibodies (1:10,000; A0208; Beyotime Biotechnology, China) for 2 h, and immunoreactive bands were visualized by chemiluminescence. And the gray value of the captured bands was determined by ImageJ software. The primary antibodies used included: anti-Insulin Receptor β (#3025), anti-Phospho-Insulin Receptor β Tyr1150/1151(#3024), anti-Akt (#9272), anti-phospho-Akt Ser473 (#4060), anti-GSK-3β (#9315), anti-Phospho-GSK-3β Ser9 (#5558) were purchased from Cell Signaling Technology (Beverly, MA, USA); anti-GAPDH (60004-1), anti-β-Actin (66009-1), and anti-α-Tubulin (11224-1) purchased from Proteintech Group (Chicago, USA), and anti-CSE(sc-374249) were purchased from Santa Cruz Biotechnology (Texas, USA).

2-Deoxyglucose Uptake

Primary mice cardiomyocytes were incubated with 33.3 mM glucose (HG), 100 nM insulin (HI), or 33.3 mM glucose and

100 nM insulin (HG++HI) for 48 h. Among them, the HG+HI group treated with vehicle or different doses of SPRC (25–100 μM) for 24 h. then the uptake of 2-deoxyglucose by cardiomyocytes was measured as previously described (20). The cardiomyocytes were rinsed with pre-warmed KRP buffer (128 mM NaCl, 4.7 mM KCl, 1.25 mM $CaCl_2$, 1.25 mM $MgSO_4$, 5 mM NaH_2PO_4, 5 mM Na_2HPO_4, and 10 mM HEPES, pH 7.4) for three times and then treated with 100 nM insulin in KRP buffer without glucose for 30 min in 37°C. Subsequently, the cardiomyocytes were incubated with 2-deoxy-D[^{3}H]-glucose (1 μCi/ml) dissolved in KRP buffer with 100 nM insulin for 10 min in 37°C. After washing with pre-cold phosphate-buffered saline (PBS) containing 10 mM glucose for 3 times, the cells were lysed with 0.4 mM NaOH for 2 h. The radioactivity of ^{3}H was measured in a liquid scintillation counter (Beckman LS6500) and the concentration of protein were detected by BCA method for standardization.

Measurement of H_2S Levels

H_2S levels in heart tissues and plasma were measured as previously described (21). Briefly, heart tissues were homogenized in Tris-HCl (100 mmol/L, pH 8.5), then centrifuged at 12,000 g for 20 min at 4°C. The plasma sample were directly centrifuged at 3,500 rpm for 15 min at 4°C. And 30 μl of the supernatant from heart tissues and plasma were derivatized by MBB and detected by HPLC-MS. The concentration of protein from heart tissues were detected by BCA method for standardization.

Statistical Analysis

All data were expressed as the means ± SEM from at least three independent experiments. SPSS 13.0 software (SPSS, Inc., Chicago, USA) was used for statistical analysis. Student's unpaired *t*-test was performed to statistically analyze individual group data. Multiple-group comparisons were evaluated by one-way analysis of variance (ANOVA) followed by Fisher's Least Significant Difference (LSD) and the non-parametric test was used when the variance was not equal. Values of $P < 0.05$ were considered to be statistically significant.

RESULTS

SPRC Treatment Improves Cardiac Function, and Alleviates Myocardial Hypertrophy and Fibrosis on Diabetic Cardiomyopathy

To explore the effect of SPRC on cardiac function of *db/db* diabetic mice, echocardiograph images were recorded before and after 12 weeks of SPRC treatment (**Figure 1A**). Compared with WT littermates, *db/db* mice preserved cardiac function at 8-week-old, but developed diastolic and systolic dysfunction at 20-week-old characterized by elevated deceleration time (DT, **Figure 1B**), reduced left ventricular ejection fraction (EF, **Figure 1D**) and decreased fractional shortening (FS, **Figure 1E**, $P = 0.054$) with a consistent heart rate (HR, **Figure 1C**). All of three parameters examined were improved by SPRC treatment (**Supplementary Tables 1, 2**). The beneficial effect of SPRC treatment on cardiac hypertrophy was confirmed by histopathological examinations and RT-PCR **(Figure 2).** Heart weight to tibia length (HW/TL) ratio was significantly increased in *db/db* mice compared with WT mice **(Figure 2C)**. Consistently, cardiomyocyte cross-sectional area examined in *db/db* mice by wheat germ agglutinin (WGA) was markedly enlarged **(Figure 2D)**. Administration of SPRC to *db/db* mice decreased HW/TL ratios and cardiomyocyte cross-sectional area, reduced mRNA level of beta-myosin heavy chain (Myh7) gene, marker for cardiac hypertrophy **(Figure 2B)**. Masson staining revealed that obvious fibrosis in the interstitial of myocardium was observed in *db/db* mice, but significantly alleviated by SPRC treatment **(Figure 2E)**. These data suggest that SPRC treatment improves cardiac function, and alleviates cardiac hypertrophy and fibrosis in the *db/db* diabetic model.

SPRC Treatment Alleviated Abnormal Myocardial Ultrastructure on Diabetic Cardiomyopathy

SPRC treatment protected *db/db* mice from abnormalities in the ultrastructure of cardiomyocytes. The mitochondria in the cardiomyocytes of WT mice were regularly arranged and exerted integral cristae, and the myofilaments were arranged tightly, while a portion of mitochondria in the myocardium of *db/db* mice were swollen, disorderly arranged with broken cristae, and the myofilaments were loose. After SPRC treatment, fewer abnormal ultrastructure of mitochondria and myofilaments were observed in diabetic mice **(Figure 3)**.

SPRC Treatment Reduces Myocardial Lipid Accumulation and Dyslipidemia on Diabetic Cardiomyopathy

Oil red O staining showed a predictable and significantly increase in lipid droplets of *db/db* hearts, which was markedly decreased in response to SPRC **(Figures 4A,B)**. Meanwhile, systemic dyslipidemia was observed in *db/db* mice characterized by markedly increased TC, TG, LDL-C, and NEFA. SPRC treatment inhibited the increased plasma TC levels, indicating that SPRC has a certain lipid-lowering effect **(Figures 4C–G)**.

SPRC Treatment Improves Glucose Tolerance in *db/db* Mice, With Fasting Blood Glucose and Systemic Insulin Resistance Remaining Unchanged

Throughout the experiment, the body weight and fasting blood glucose of *db/db* mice were significantly increased compared to their WT littermates. However, SPRC treatment showed no significant impact on body weight and blood glucose **(Figures 5A,B)**. To investigate the effect of SPRC on systemic insulin resistance, IPGTT and IPITT were preformed and the results demonstrated SPRC treatment at a dosing of 80 $mg{\cdot}kg^{-1}{\cdot}day^{-1}$ improved glucose tolerance to a certain extent, but has no significant impact on IPITT and its area under curve **(Figures 5C–F)**. Furthermore, fasting plasma insulin levels and HOMA-IR index were remarkably elevated, with SPRC treatment failed to alleviate **(Figures 5G,H)**.

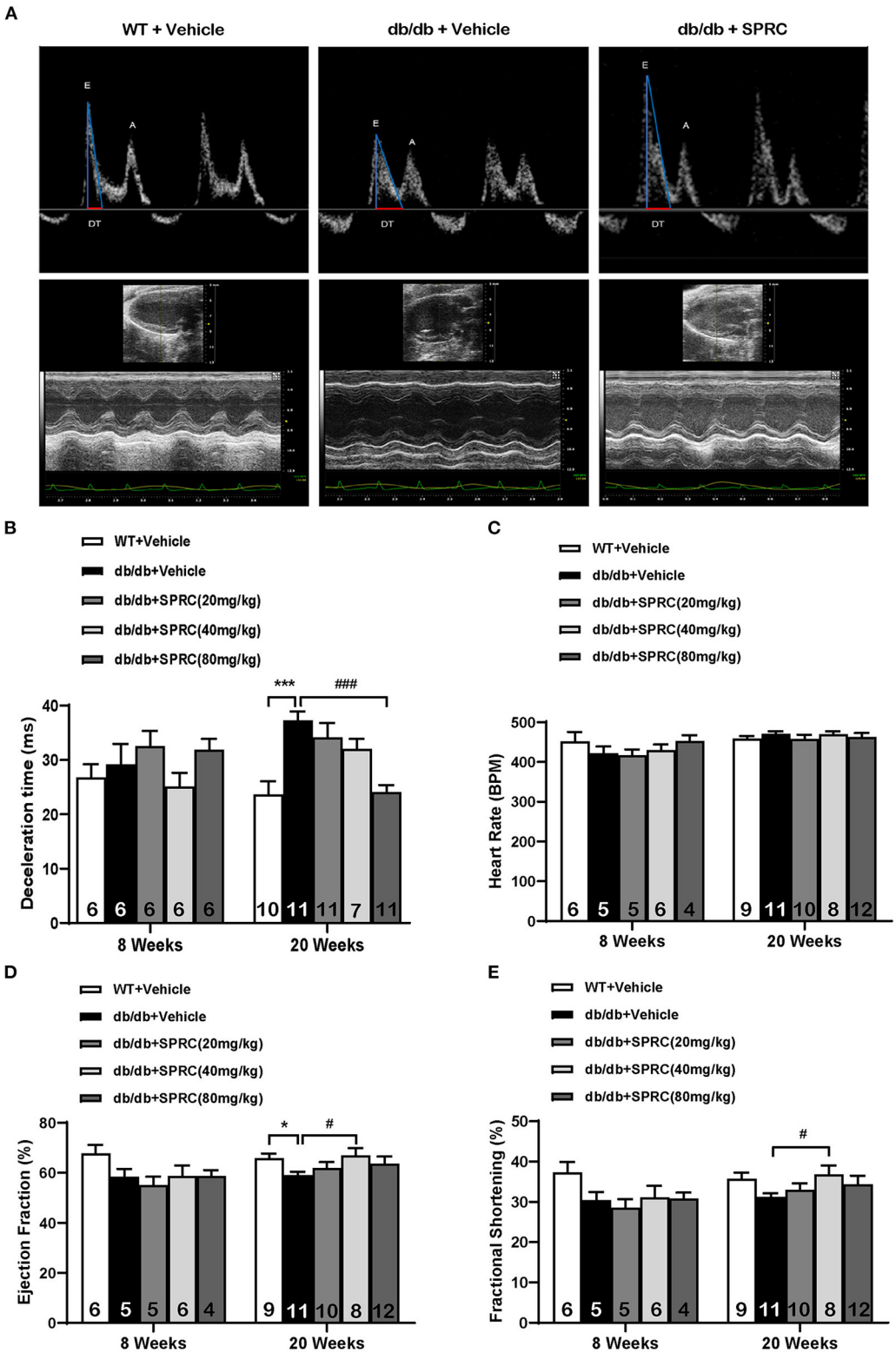

FIGURE 1 | SPRC treatment improves cardiac function in *db/db* mice. Vehicle or SPRC (20, 40, or 80 mg/kg/day) was orally administered to WT mice or *db/db* mice for 12 weeks. Echocardiograph images were recorded before and after 12 weeks of SPRC treatment. **(A)** Representative Power Doppler Mode (upper) and M-Mode (lower) echocardiograph images. **(B–E)** Echocardiographic assessment of deceleration time (DT), heart rate (HR), left ventricular ejection fraction (EF), and fractional shortening (FS). Values are presented as means ± SEM ($n = 4–12$). $^{*}P < 0.05$, $^{***}P < 0.001$ vs. WT + Vehicle group, $^{\#}P < 0.05$, $^{\#\#\#}P < 0.001$ vs. *db/db* + Vehicle mice.

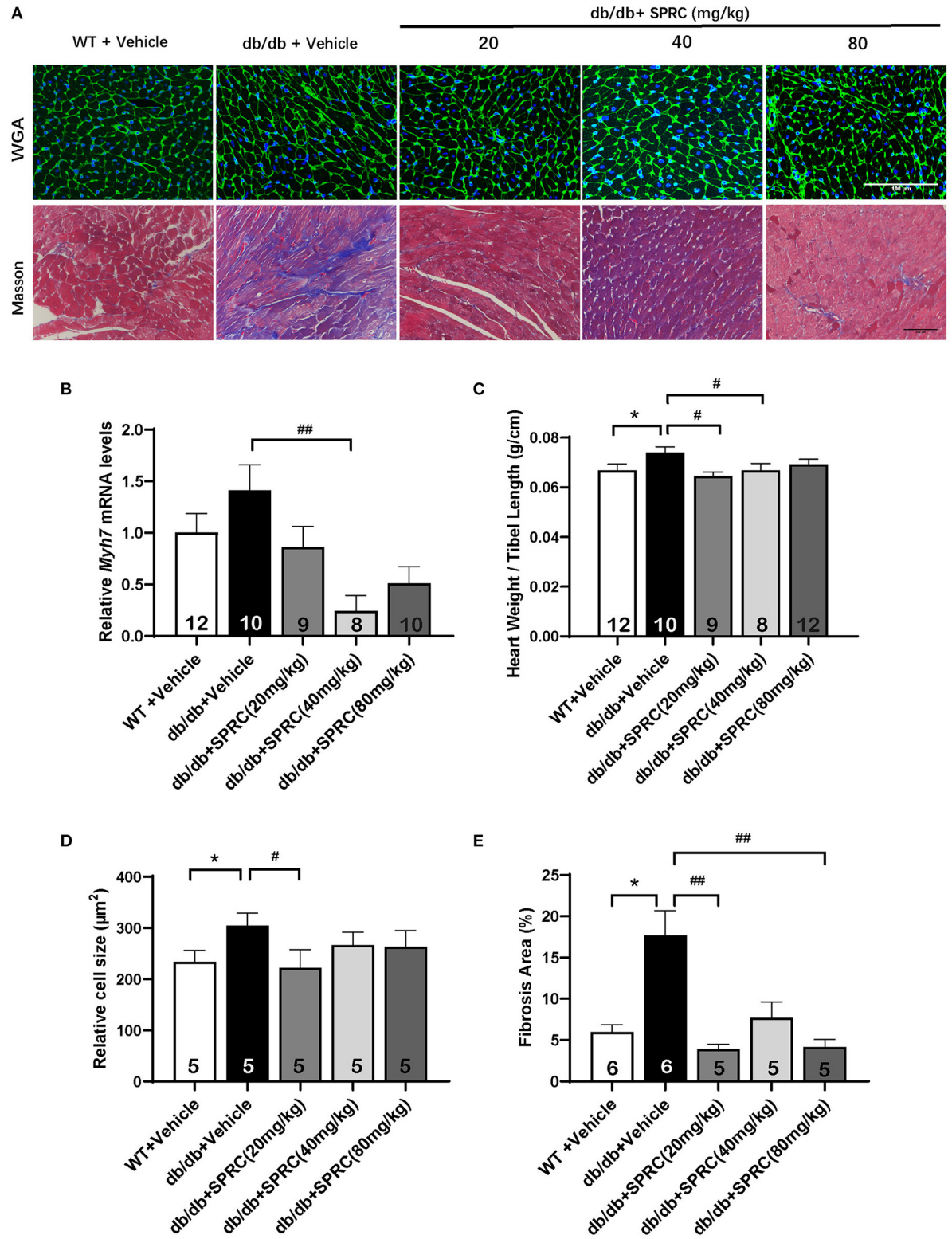

FIGURE 2 | SPRC treatment improves myocardial hypertrophy and fibrosis in *db/db* mice. Vehicle or SPRC (20, 40, or 80 mg/kg/day) was orally administered to WT mice or *db/db* mice for 12 weeks. Heart tissue specimens were collected. **(A)** Wheat germ agglutinin (WGA) and masson staining of myocardium were performed. **(B)** mRNA levels of *Myh7* in heart tissue were determined by real-time qPCR. mRNA levels of *Gapdh* was used as reference for normalization ($n = 8$–12). **(C)** The ratio of heart weights (HW) and tibia lengths (TL) was calculated ($n = 8$–12). Average cell area ($n = 5$) **(D)** and fibrosis area ($n = 5$–6) **(E)** were shown. Values are presented as means ± SEM. $^{*}P < 0.05$ vs. WT + Vehicle group, $^{\#}P < 0.05$, $^{\#\#}P < 0.01$ vs. *db/db* + Vehicle mice.

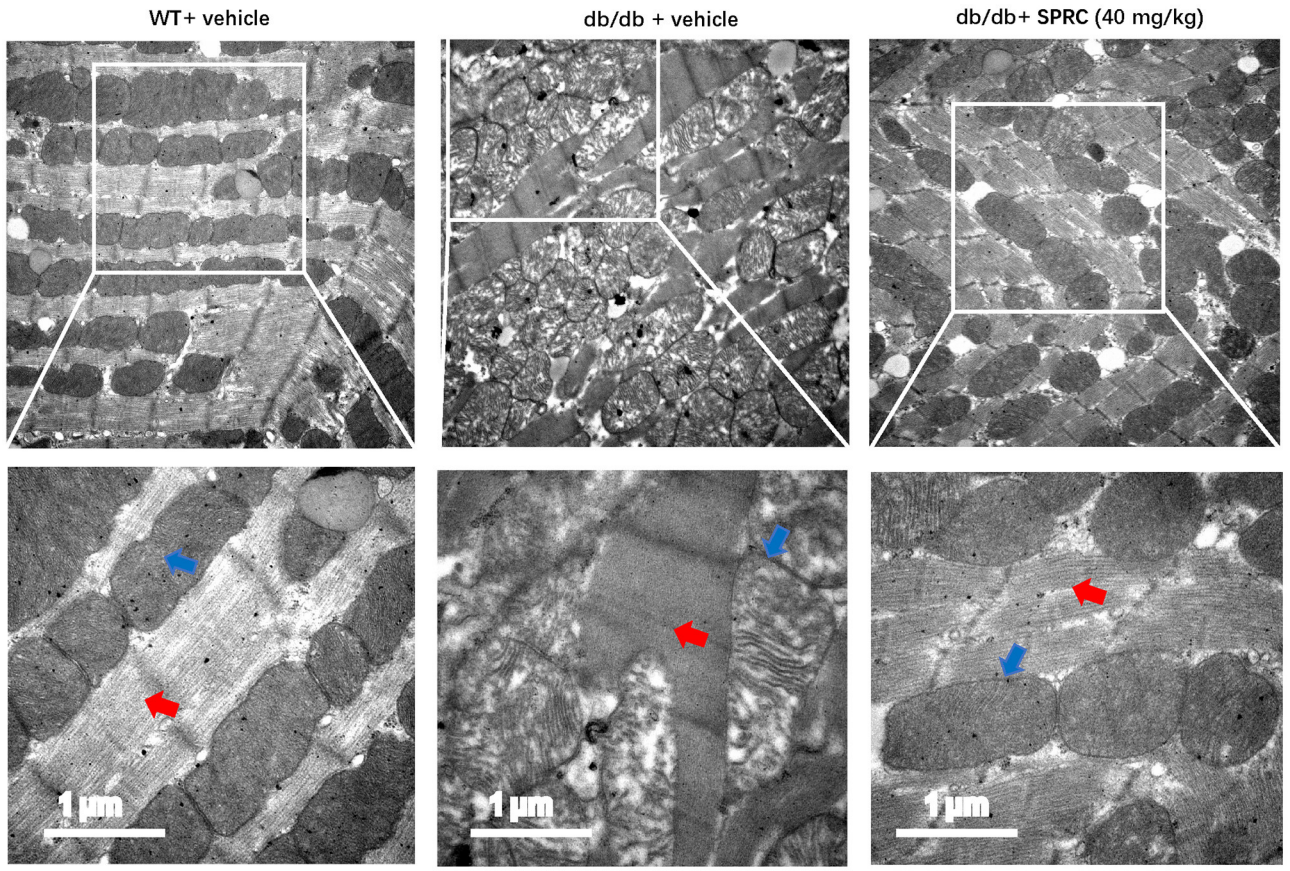

FIGURE 3 | SPRC treatment improves abnormal ultrastructure of cardiomyocytes in *db/db* mice. Vehicle or SPRC (20,40, or 80 mg/kg/day) was orally administered to WT mice or *db/db* mice for 12 weeks. Heart tissue specimens were collected and representative images of the ultrastructural morphology of cardiomyocytes were shown. The red arrow indicates myofilament and the blue arrow indicates mitochondria ($n = 2$).

SPRC Treatment Activated Insulin Receptor Signaling in Both Primary Mice Cardiomyocytes and Myocardium of *db/db* Mice

Primary neonatal mice cardiomyocytes were cultured and identified to explore the mechanisms of SPRC on diabetic cardiomyopathy *in vitro* **(Supplementary Figure 1B).** Incubation of cardiomyocytes with SPRC (0.1–1,000 μM) for 24 h had no detectable cytotoxicity. Moreover, the cell viability was significantly increased at doses of 0.1 and 10 μM of SPRC treatment **(Figure 6A)**. SPRC improved both mRNA and protein expression level of IR in cardiomyocytes, with the classical downstream pathway protein kinase B (Akt/PKB) and glycogen synthase kinase 3β (GSK3β) activated in the dose-dependently manner **(Figures 6B–F)**.

The cardiac inulin receptor signaling *in vivo* were also determined. As shown in **Figures 7A–D**, SPRC treatment increased the mRNA of IR in myocardium, and it also improved protein expression of IR to a certain extent ($P = 0.095$). It is noteworthy that IR in the myocardium of diabetic mice was significantly phosphorylated, which is exacerbated by SPRC treatment. The phosphorylation levels of Akt and GSK3β in myocardium of *db/db* mice were significantly decreased, SPRC (80 mg/kg) significantly increased the phosphorylation levels of Akt and GSK3β in myocardium of DCM mice **(Figures 7E,F)**.

We then exposed neonatal mice cardiomyocytes to 33.3 mM glucose and 100 nM insulin to mimic hyperglycemia and hyperinsulinemia in cardiomyocyte of diabetic heart. High concentrations of glucose and insulin stimulation significantly reduced the phosphorylation levels of Akt and GSK3β and the expression level of IR. However, after incubation with 50 μM SPRC for 24 h, the phosphorylation level of IR was preserved, and the expression level of IR was partly increased without statistical significance ($P = 0.077$). Consistently, the downstream of IR signaling including the phosphorylation levels of Akt and GSK3β were preserved **(Figures 7G–K)**.

SPRC Treatment Increased GLUT4 Expression in Myocardium and Enhanced ^{3}H Glucose Uptake in Cultured Primary Cardiomyocytes

GLUT4 transporter is the most abundant glucose transporter in the heart, which is also the major glucose transporter translocating to the plasma membrane in response to insulin

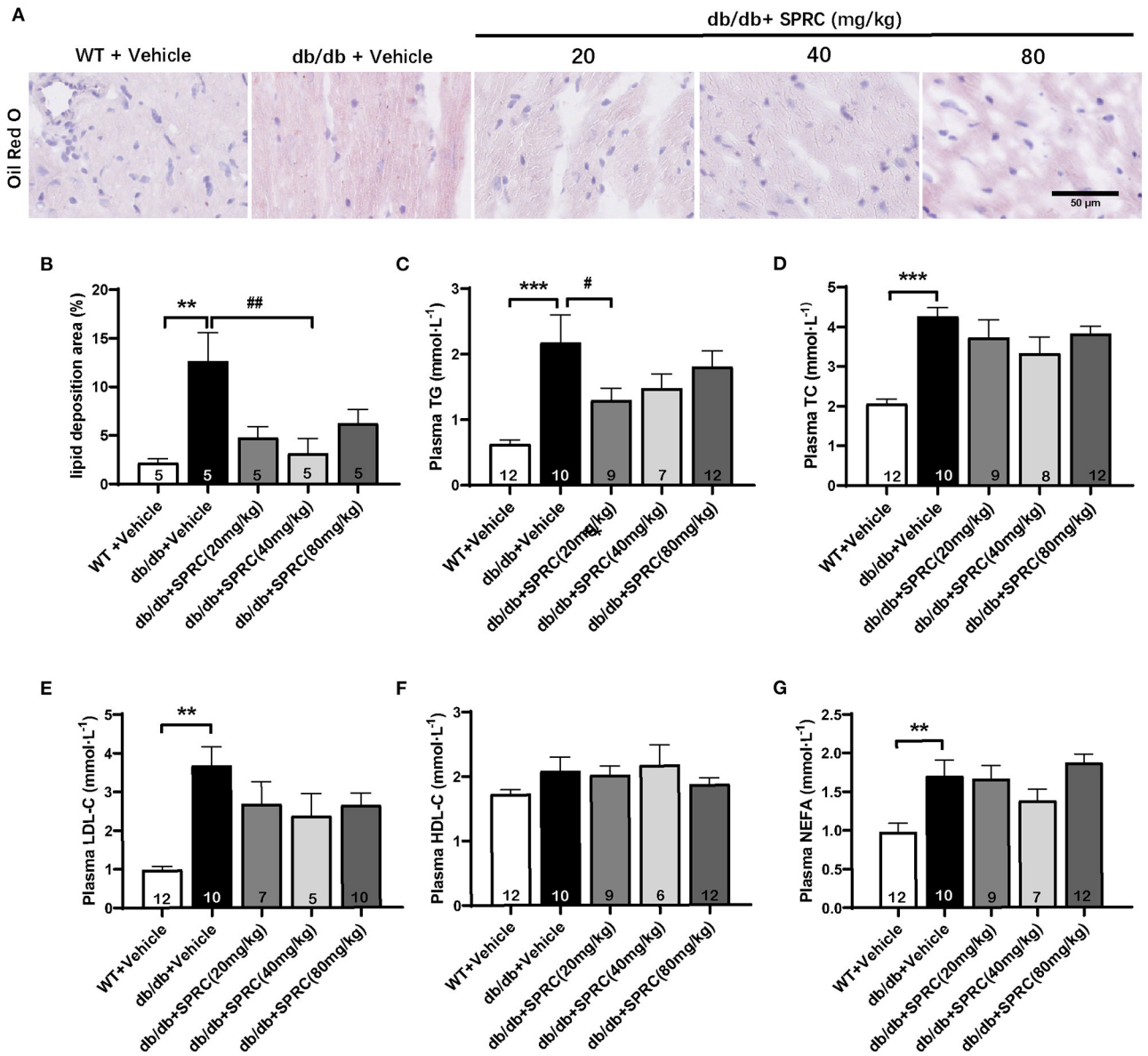

FIGURE 4 | SPRC treatment reduces myocardial lipid accumulation and dyslipidemia in *db/db* mice. Vehicle or SPRC (20, 40, or 80 mg/kg/day) was orally administered to WT mice or *db/db* mice for 12 weeks. Heart tissue specimens and plasma were collected. **(A)** Oil Red O staining of myocardium were performed (n = 5) lipid deposition area **(B)** was shown. The levels of TC **(C)**, TG **(D)**, LDL-C **(E)**, HDL-C **(F)**, NEFA **(G)** were measured (n = 5–12). Values are presented as means ± SEM. $^{**}P < 0.01$, and $^{***}P < 0.001$ vs. WT + Vehicle group, $^{\#}P < 0.05$, $^{\#\#}P < 0.01$ vs. *db/db* + Vehicle mice.

(22). As shown in **Figures 8A,B**, the protein expression level of GLUT4 were significantly decreased in diabetic heart, and SPRC treatment increased the mRNA and protein expression level of GLUT4. SPRC also enhanced the glucose uptake *in vitro* **(Figure 8C)**.

SPRC Treatment Increased CSE Expression and H_2S Content in the Myocardium

CSE is the primary H_2S-generating enzyme in the cardiovascular system, catalyzing the synthesis of endogenous H_2S from L-cysteine, and SPRC is an activator of CSE. We confirmed that SPRC increases the protein expression of CSE in primary cardiomyocytes **(Figure 9A)**. Moreover, SPRC enhanced CSE expression in the left ventricular tissues of *db/db* mice **(Figure 9B)**. Furthermore, H_2S concentration in plasma and myocardium were detected. SPRC treatment at the doses of 40 and 80 $mg{\cdot}kg^{-1}{\cdot}day^{-1}$ improved H_2S levels in the myocardium of *db/db* mice **(Figure 9C)**. And H_2S levels in plasma of *db/db* mice was significantly lower than that of WT mice, with SPRC treatment failed to rescue **(Figure 9D)**.

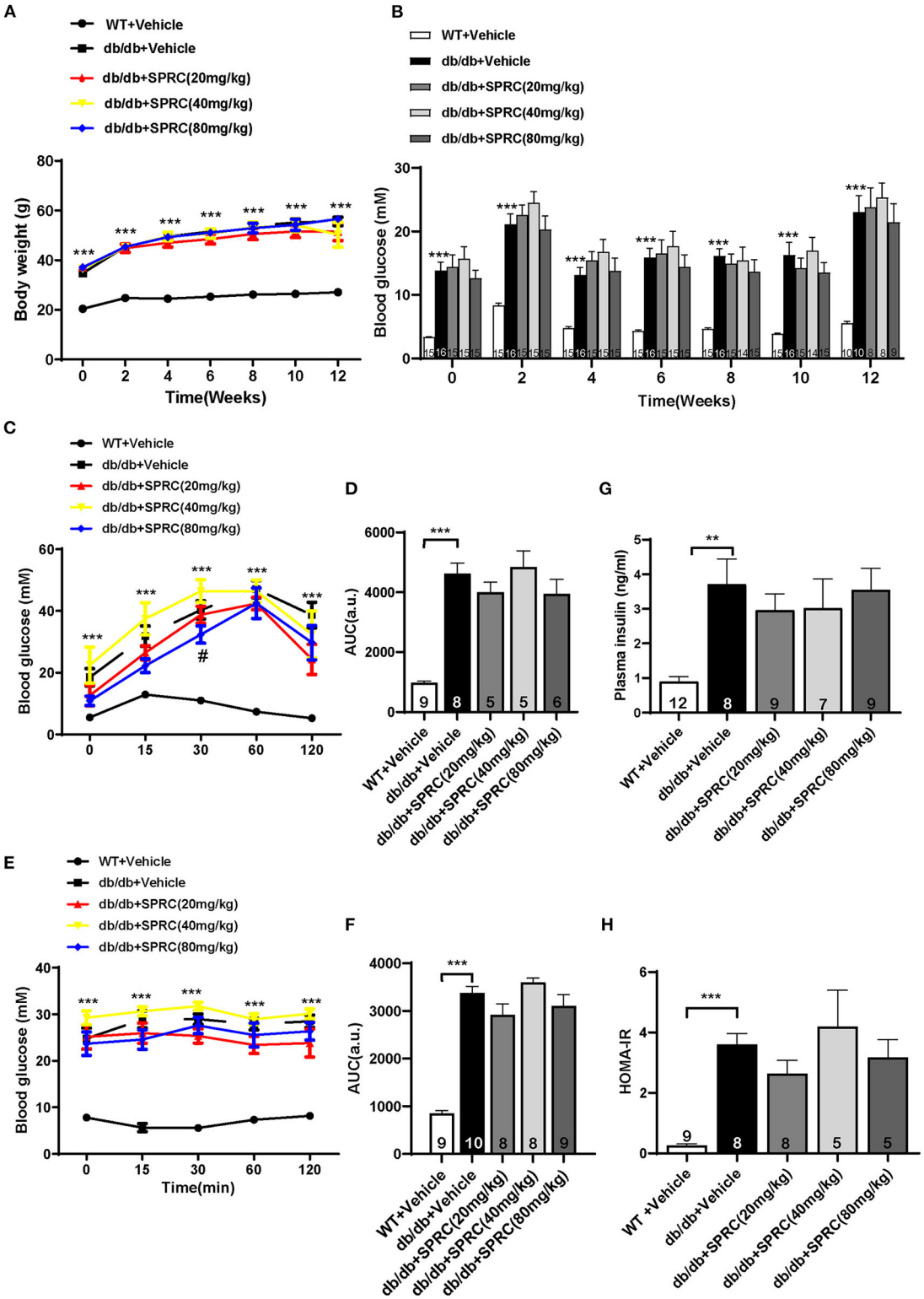

FIGURE 5 | SPRC treatment improves glucose tolerance in *db/db* mice, with fasting blood glucose and systemic insulin resistance remaining unchanged. Vehicle or SPRC (20, 40, or 80 mg/kg/day) was orally administered to WT mice or db/db mice for 12 weeks. **(A)** Body weight ($n = 8$–16), **(B)** fasting blood glucose ($n = 8$–16), **(C)** intraperitoneal glucose tolerance test (IPGTT) and **(D)** area under curve (AUC) of IPGTT ($n = 5$–9), **(E)** intraperitoneal insulin tolerance test (IPITT) and **(F)** area under curve (AUC) of IPITT ($n = 8$–10), **(G)** fasting plasma insulin ($n = 7$–12), and **(H)** HOMA-IR index were determined ($n = 5$–9). Values are presented as means ± SEM. $^{**}P < 0.01$, and $^{***}P < 0.001$ vs. WT + Vehicle group, $^{\#}P < 0.05$ vs. *db/db* + Vehicle mice.

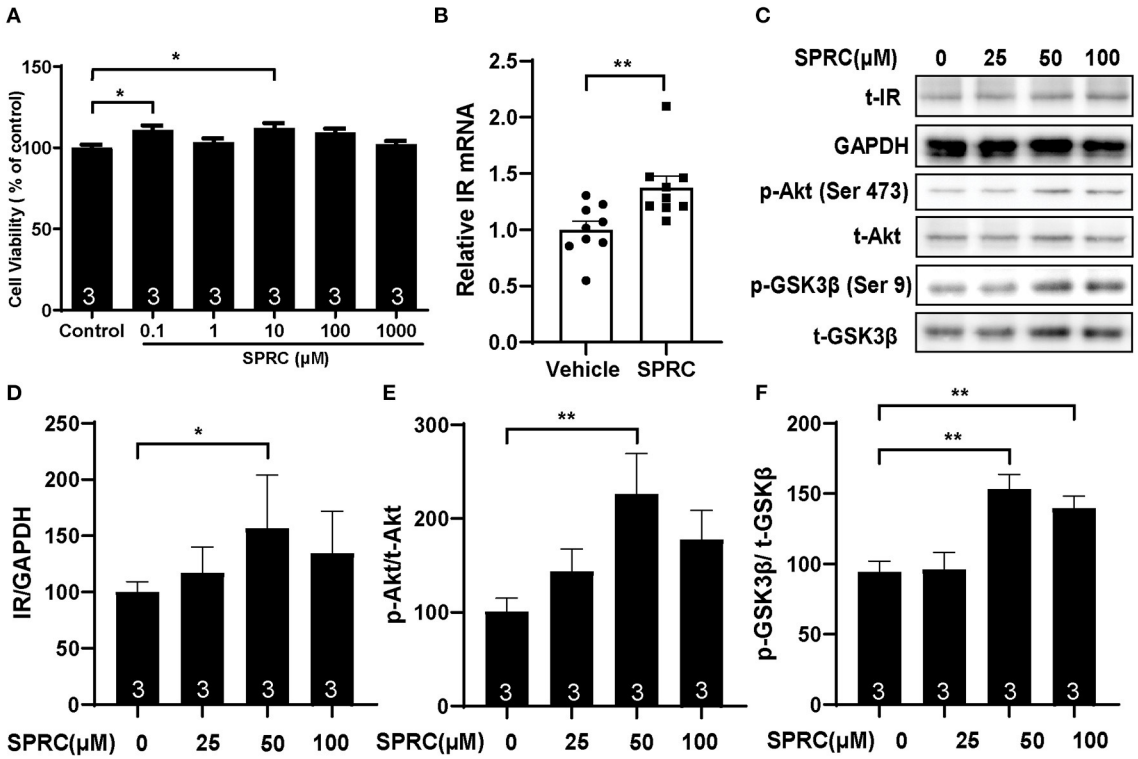

FIGURE 6 | SPRC treatment activated cardiac insulin receptor signaling in primary cardiomyocytes. **(A)** Primary mice cardiomyocytes were exposed to various concentrations of SPRC (0.1–1,000 μM) for 24 h. Cell viability was determined ($n = 3$). *$P < 0.05$ vs. control group. **(B)** Primary mice cardiomyocytes were treated with 50 μM SPRC for 24 h. mRNA levels of insulin receptor (*Insr*) were determined by real-time qPCR. mRNA levels of *Gapdh* was used as reference for normalization ($n = 3$). **$P < 0.01$ vs. Vehicle group. **(C–F)** Primary mice cardiomyocytes were treated with vehicle or SPRC (25, 50, and 100 μM) for 24 h. The expression level of protein in insulin receptor signaling were determined by western blotting ($n = 3$). *$P < 0.05$, **$P < 0.01$ vs. Vehicle. Values are presented as means ± SEM.

DISCUSSION

In this study, we investigated the effects of SPRC on diabetic cardiomyopathy. Our results suggested that SPRC treatment could improve the myocardial function in diabetic mice with diabetic cardiomyopathy by attenuating myocardial hypertrophy, myocardial fibrosis, myocardial lipid accumulation, abnormalities in the ultrastructure of cardiomyocytes. Importantly, we unveiled the molecular mechanism underlying SPRC protected myocardium, which involves the activation of cardiac insulin receptor signaling.

The global prevalence of type 2 diabetes mellitus has been gradually increasing over half a century especially in developing countries (23). The systemic metabolic disorder in diabetic patients exposes myocardium to hyperglycemia, hyperinsulinemia, hyperlipidemia, and insulin resistance, all of which trigger the development of myocardial dysfunction. It is widely accepted that morphological phenotypes of diabetic cardiomyopathy include cardiac hypertrophy, cardiac fibrosis, increased intramyocardial lipids, while the functional phenotypes include left ventricular diastolic dysfunction which usually precede systolic dysfunction (24–26). In this study, we used spontaneously diabetic *db/db* mice as type 2 diabetes model which basically reflects all the manifestation of diabetic cardiomyopathy (18, 27). Moreover, 12 weeks of SPRC treatment, especially in the medium-dose group (40 $mg{\cdot}kg^{-1}{\cdot}day^{-1}$), alleviated almost all the morphological and functional phenotype of diabetic cardiomyopathy in *db/db* mice, which indicated the protective effect of SPRC on diabetic cardiomyopathy. Consistently, only the medium-dose group (40 $mg{\cdot}kg^{-1}{\cdot}day^{-1}$) had a significant increase in H_2S levels in the myocardium (**Figure 9C**), while high-dose (80 $mg{\cdot}kg^{-1}{\cdot}day^{-1}$) SPRC only raised H_2S levels in the myocardium a little and has no statistical significance when compared with vehicle. It has been reported that the mechanisms of SPRC releasing H_2S include up-regulating CSE gene and protein expression (28, 29), as well as binding and activating CSE (16). Detailed mechanism of effective dose range of SPRC *in vivo* needs further study.

Next, we explored the mechanism of SPRC to protect diabetic cardiomyopathy. Abnormal mitochondrial morphology is common in the progression of diabetic cardiomyopathy, and suggests the possibility of impaired mitochondrial dynamics, metabolic substrate imbalance and increased oxidative stress (5, 30). Under transmission electron microscopy, we observed obvious damage of myocardial ultrastructure in *db/db* mice, especially alterations of mitochondria. SPRC treatment markedly restored mitochondrial and

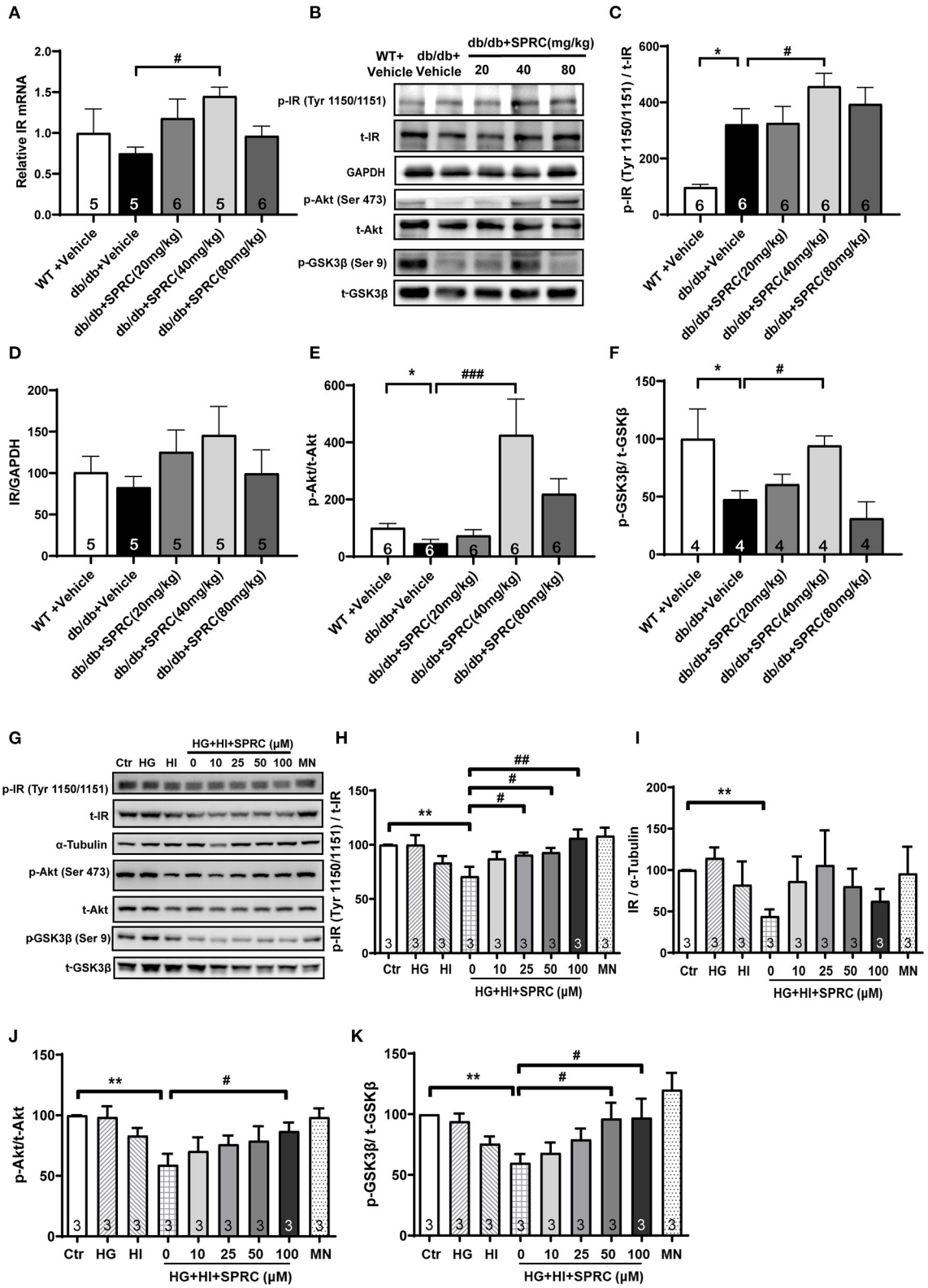

FIGURE 7 | SPRC treatment activated insulin receptor signaling in *db/db* mice. Vehicle or SPRC (20, 40, or 80 mg/kg/day) was orally administered to WT mice or *db/db* mice for 12 weeks. **(A)** The mRNA levels of insulin receptor (*Insr*) were determined by real-time qPCR. mRNA levels of *Gapdh* was used as reference for

(Continued)

FIGURE 7 | normalization ($n = 5$–6). $^{\#}P < 0.05$ vs. *db/db* + Vehicle mice. **(B–F)** the expression level of protein in insulin receptor signaling were determined by western blotting. $^{*}P < 0.05$, $^{**}P < 0.01$, and $^{***}P < 0.001$ vs. WT + Vehicle group, $^{\#}P < 0.05$, $^{\#\#}P < 0.01$, and $^{\#\#\#}P < 0.001$ vs. *db/db* + Vehicle mice. **(G–K)** Primary mice cardiomyocytes were incubated with 33.3 mM glucose (HG), 100 nM insulin (HI), or 33.3 mM glucose + 100 nM insulin (HG + HI) for 48 h. The cardiomyocytes were then incubation with SPRC (50 μM) for 24 h. Expression of insulin receptor signaling were determined ($n = 3$). $^{*}P < 0.05$, $^{**}P < 0.01 < 0.001$ vs. control group, $^{\#}P < 0.05$, $^{\#\#}P < 0.01$, and $^{\#\#\#}P < 0.001$ vs. HG + HI group. Values are presented as means ± SEM.

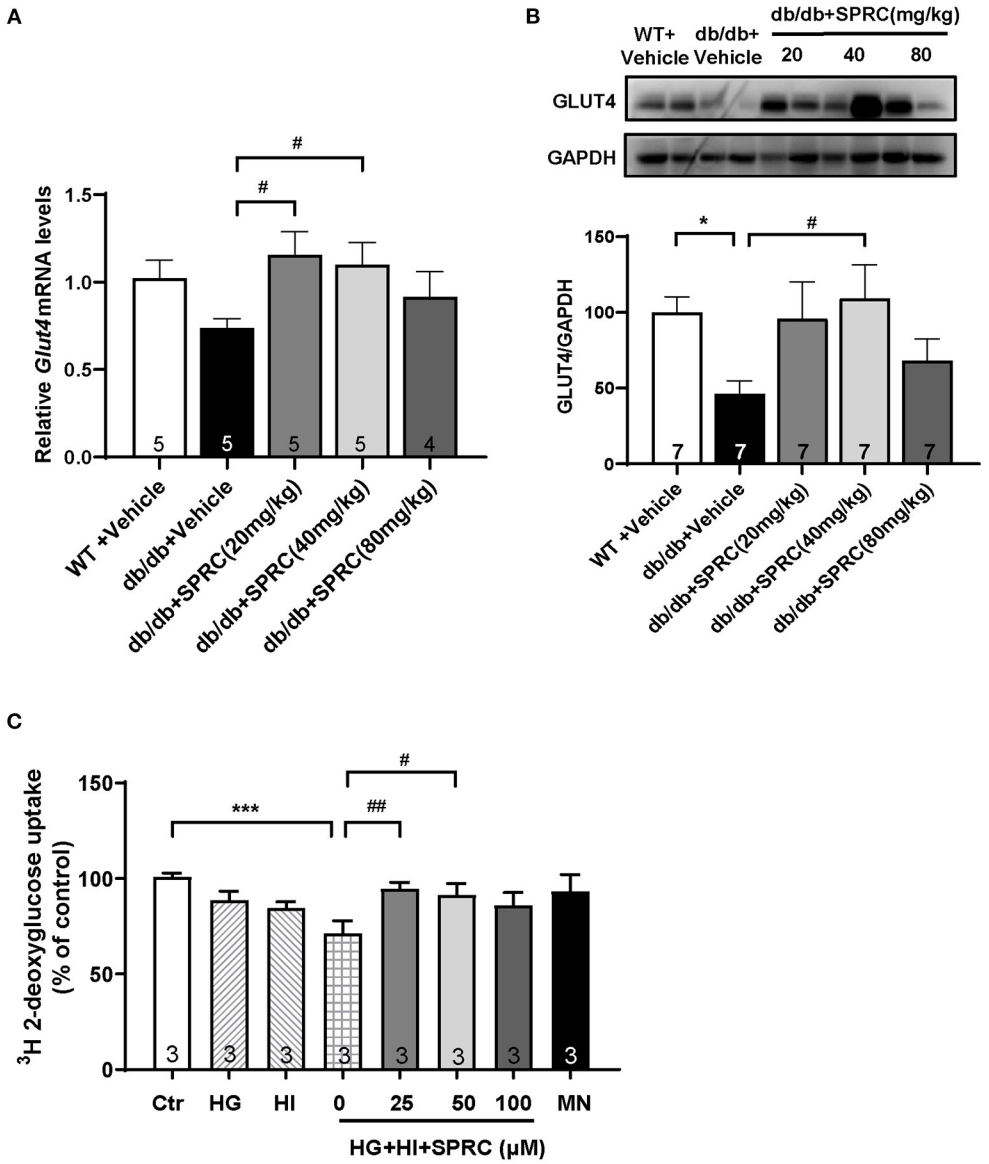

FIGURE 8 | SPRC treatment increased GLUT4 expression and enhanced ^{3}H glucose uptake. Vehicle or SPRC (20, 40, or 80 mg/kg/day) was orally administered to WT mice or *db/db* mice for 12 weeks. **(A)** The mRNA levels of *Glut4* were determined by real-time qPCR, and the mRNA levels of *Gapdh* was used as reference for normalization ($n = 4$–5). $^{\#}P < 0.05$ vs. *db/db* + Vehicle mice. **(B)** The expression level of *Glut4* in the myocardium were determined by western blotting ($n = 7$). $^{*}P < 0.05$, $^{**}P < 0.01$, and $^{***}P < 0.001$ vs. WT + Vehicle group, $^{\#}P < 0.05$, $^{\#\#}P < 0.01$, and $^{\#\#\#}P < 0.001$ vs. *db/db* + Vehicle mice. **(C)** Primary mice cardiomyocytes were incubated with 33.3 mM glucose (HG), 100 nM insulin (HI), or 33.3 mM glucose + 100 nM insulin (HG + HI) for 48 h. The cardiomyocytes were then incubation with SPRC (50 μM) for 24 h. ^{3}H glucose uptake was measured in a liquid scintillation counter and the concentration of protein were detected by BCA method for standardization ($n = 3$). $^{*}P < 0.05$ and $^{***}P < 0.001$ vs. control group, $^{\#}P < 0.05$, $^{\#\#}P < 0.01$ vs. HG+HI group. Values are presented as means ± SEM.

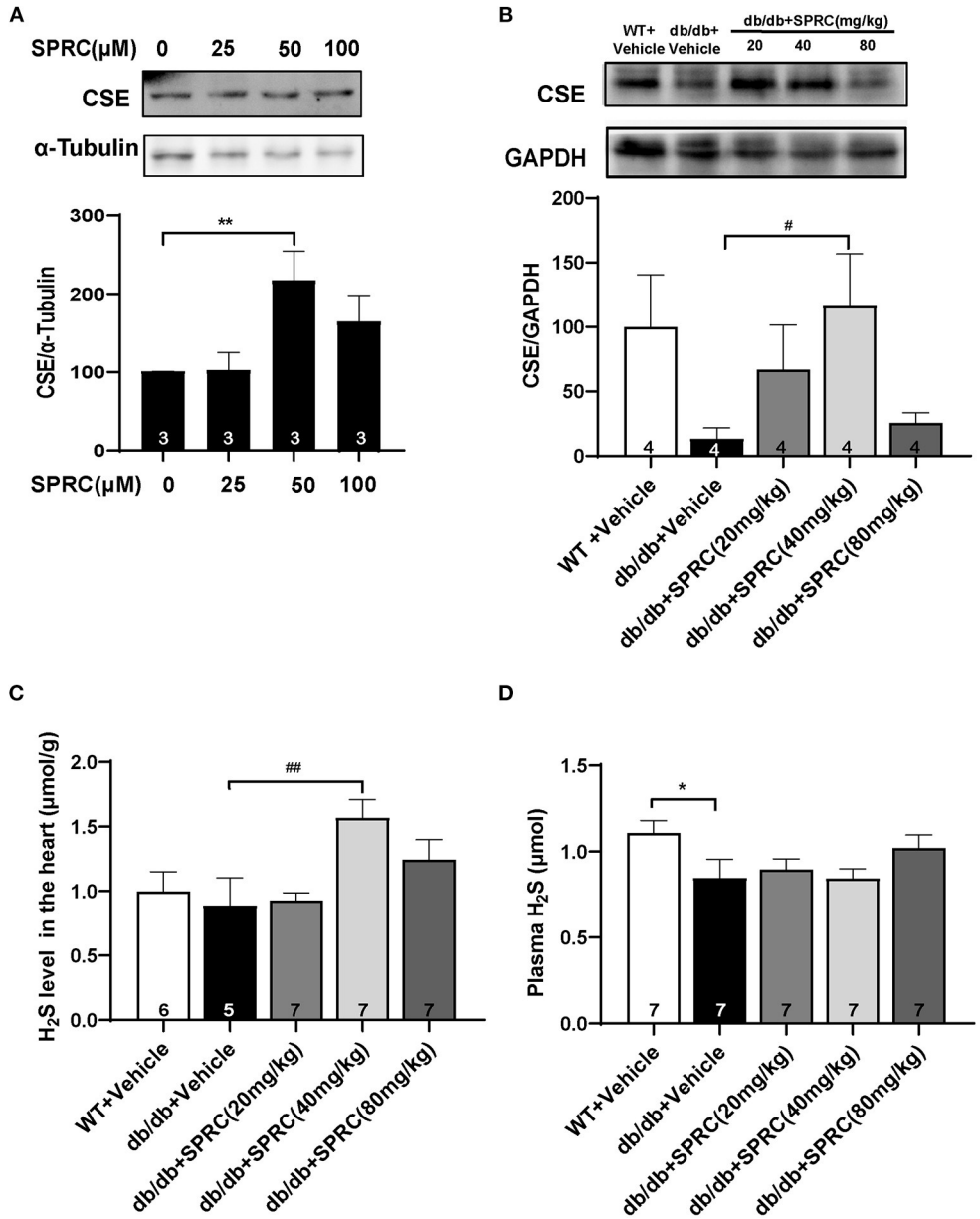

FIGURE 9 | SPRC treatment increased CSE expression and H_2S content in the myocardium. **(A)** Primary mice cardiomyocytes were treated with vehicle or SPRC (25, 50, and 100 μM) for 24 h. The expression level of CSE were determined by western blotting ($n = 3$). $^{**}P < 0.01$ vs. Vehicle group. **(B–D)** Vehicle or SPRC (20, 40, or 80 mg/kg/day) was orally administered to WT mice or *db/db* mice for 12 weeks. The expression level of CSE were determined by western blotting ($n = 4$), H_2S levels in the myocardium ($n = 5$–7), and plasma ($n = 7$) were detected. $^{*}P < 0.05$, $^{**}P < 0.01$ vs. WT + Vehicle group, $^{\#}P < 0.05$, $^{\#\#}P < 0.01$ vs. *db/db* + Vehicle mice. Values are presented as means ± SEM.

myocardial ultrastructure. This result suggests that the effect of SPRC on diabetic cardiomyopathy may associated with improvement of myocardial mitochondria. The effect of SPRC treatment on mitochondrial function, myocardial oxidative stress and underlying signaling pathway is worth of further study.

Under conventional conditions in heart, glucose and lactic acid only supply 30% of ATP generation, with the majority of ATP generated by fatty acid (FA) oxidation. Whereas, in the case of type 2 diabetes mellitus, hyperglycemia maintains cardiac glucose uptake, but the proportion of FA as a metabolic substrate further increases in consequence of plasma FA availability (31–35). Within the heart, lipid droplet accumulation generally only appears in patients with diabetes or metabolic syndrome, indicating an imbalance of FA uptake/synthesis and consumption (36, 37). In this study, both hyperlipidaemia and cardiac

lipid droplet accumulation were observed in *db/db* mice, and the effect of SPRC treatment on improving lipid content in myocardium seems superior to the improvement of lipid content in circulation. Similarly, SPRC treatment protected diabetic mice from cardiac insulin resistance by activating the AKT/GLUT4 signaling, with no obvious improvement on systemic insulin resistance, which were consistent with the improvement of H_2S levels in myocardium but not in plasma. This may be because *db/db* mice as transgenic rodent is completely resistant to leptin receptor, developed morbid obesity and severe systemic metabolic phenotype at 20 weeks of age which is irreversible by SPRC treatment (23). Besides, this also demonstrates that the protective effect of SPRC treatment is targeted to the myocardium, rather than the consequence of alleviating the metabolic phenotype of whole body. In addition, SPRC releases H_2S *via* the up-regulating of CSE, thus the organ distribution of CSE is critical to the effect of SPRC. Next, we focus on the effect of SPRC on cardiac molecular signaling pathway in the following experiments.

Insulin resistance is defined as impaired insulin signaling together with diminution in glucose transport, which promotes the development of diabetic cardiomyopathy (38). Myocardial insulin signaling plays an important role in myocardial metabolic remodeling in response to myocardial metabolic disorders by regulating glucose uptake, long-chain fatty acid uptake, and protein synthesis, wherein insulin receptor (IR) is a key protein for signal transduction (39–41). Cardiomyocyte-selective insulin receptor knockout mice revealed decreased insulin signaling in cardiomyocytes without systemic metabolic disturbances, and showed worsen cardiac remodeling in respond to stress (42) and accelerated cardiac mitochondrial dysfunction after myocardial infarction (43).

IR is a polymer transmembrane glycoprotein composed of $\alpha_2\beta_2$ heterotetramer and belongs to the receptor tyrosine kinases (RTK) family Type Ò subfamily activated by ligands such as insulin and insulin-like growth factor (IGF) (44). The binding of insulin triggers autophosphorylation in kinase activation region of IR at Tyr-1146 and either Tyr-1150 or Tyr-1151 (45). The activated IR recruits and phosphorylates scaffold proteins such as insulin receptor substrates (IRS) to activate the classical PI3K/AKT pathway, with other downstream pathway of insulin signaling (including Ras/MAPK-dependent pathways) unaffected. The activation of AKT subsequently promotes the translocation of GLUT4 to the membrane, and enhances glucose uptake. The phosphorylation of AKT also inactivates GSK-3β, an essential negative regulator of cardiac hypertrophy and cardiomyopathy (46, 47). Consistent with these studies, our results showed inhibited insulin signaling such as decreased phosphorylation levels of Akt and GSK-3β and reduced protein expression of GLUT4 in the cardiomyocyte of diabetic hearts, which was notably activated by SPRC treatment. Moreover, we speculate that SPRC enhanced the glucose uptake to regulate metabolic substrate proportion, thereby protecting the heart caused by metabolic disorders. Interestingly, although the effect of SPRC on IR downstream signaling *in vivo* and *in vitro* were consistent, the phosphorylation status of IR differs. The phosphorylation level of IR was reduced by acute high concentrations of glucose and insulin in *vitro*, but tends to increase in chronic diabetic myocardium which may due to compensation. This suggests that in the myocardium of type 2 diabetes, the inhibition of IR signaling is not due to the decrease of phosphorylation level of IR, but the decrease of IR expression and downstream signaling transduction.

In summary, we provided evidences that SPRC protects against cardiac fibrosis and improves myocardial function in diabetic mice. This mechanism involves increased expression and activity of IR and activated Akt/ GSK-3β signaling, which subsequently enhanced glucose uptake in cardiomyocyte, resulting in improved diabetic cardiomyopathy. Thereby, SPRC may be a promising medication for diabetic cardiomyopathy in type 2 diabetes mellitus patients.

DATA AVAILABILITY STATEMENT

The original contributions presented in the study are included in the article/**Supplementary Material**, further inquiries can be directed to the corresponding author/s.

ETHICS STATEMENT

The animal study was reviewed and approved by The Ethics Committee of Experimental Research, Fudan University, Shanghai Medical College.

AUTHOR CONTRIBUTIONS

Y-CZ and YL: designed experiments. YL, K-FX, Y-HC, and CW: performed experiments. YL and K-FX: analyzed data. Y-CZ, YC, and M-JW: provided laboratory space, reagents, and technical support. YL: wrote the manuscript. M-JW: revised the manuscript. Y-CZ: supervised the study. All authors contributed to the article and approved the submitted version.

FUNDING

This work was supported by the National Natural Science Foundation of China (NSFC) (31830042 and 81870212 to Y-CZ, 81970361 to M-JW), the National Key Science and Technology Project of China (2018YFC2000200/02), Macau Science and Technology Development fund (FDCT 0007/2019/AKP), and the funding of Innovative research team of high-level local universities in Shanghai and a key laboratory program of the Education Commission of Shanghai Municipality (ZDSYS14005 to Y-CZ).

SUPPLEMENTARY MATERIAL

The Supplementary Material for this article can be found online at: https://www.frontiersin.org/articles/10.3389/fcvm.2021.737191/full#supplementary-material

REFERENCES

1. Wang L, Gao P, Zhang M, Huang Z, Zhang D, Deng Q, et al. Prevalence and ethnic pattern of diabetes and prediabetes in China in 2013. *JAMA*. (2017) 317:2515–23. doi: 10.1001/jama.2017.7596
2. Dal Canto E, Ceriello A, Rydén L, Ferrini M, Hansen TB, Schnell O, et al. Diabetes as a cardiovascular risk factor: an overview of global trends of macro and micro vascular complications. *Eur J Prev Cardiol.* (2019) 26:25–32. doi: 10.1177/2047487319878371
3. Kannel WB, McGee DL. Diabetes and cardiovascular disease: the Framingham Study. *JAMA*. (1979) 241:2035–8. doi: 10.1001/jama.241.19.2035
4. Rubler S, Dlugash J, Yuceoglu YZ, Kumral T, Branwood AW, Grishman A. New type of cardiomyopathy associated with diabetic glomerulosclerosis. *Am J Cardiol.* (1972) 30:595–602. doi: 10.1016/0002-9149(72)90595-4
5. Tan Y, Zhang Z, Zheng C, Wintergerst KA, Keller BB, Cai L. Mechanisms of diabetic cardiomyopathy and potential therapeutic strategies: preclinical and clinical evidence. *Nat Rev Cardiol.* (2020) 17:585–607. doi: 10.1038/s41569-020-0339-2
6. Castagno D, Baird-Gunning J, Jhund PS, Biondi-Zoccai G, MacDonald MR, Petrie MC, et al. Intensive glycemic control has no impact on the risk of heart failure in type 2 diabetic patients: Evidence from a 37,229 patient meta-analysis. *Am Heart J.* (2011) 162:938–48.e2. doi: 10.1016/j.ahj.2011.07.030
7. Turnbull FM, Abraira C, Anderson RJ, Byington RP, Chalmers JP, Duckworth WC, et al. Intensive glucose control and macrovascular outcomes in type 2 diabetes. *Diabetologia.* (2009) 52:2288–98. doi: 10.1007/s00125-009-1470-0
8. Zhao S, Li X, Li X, Wei X, Wang H. Hydrogen sulfide plays an important role in diabetic cardiomyopathy. *Front Cell Dev Biol.* (2021) 9:627336. doi: 10.3389/fcell.2021.627336
9. Sun X, Zhao D, Lu F, Peng S, Yu M, Liu N, et al. Hydrogen sulfide regulates muscle RING finger-1 protein S-sulfhydration at Cys44 to prevent cardiac structural damage in diabetic cardiomyopathy. *Br J Pharmacol.* (2020) 177:836–56. doi: 10.1111/bph.14601
10. Guo R, Wu Z, Jiang J, Liu C, Wu B, Li X, et al. New mechanism of lipotoxicity in diabetic cardiomyopathy: deficiency of endogenous H2S production and ER stress. *Mech Ageing Dev.* (2017) 162:46–52. doi: 10.1016/j.mad.2016.11.005
11. Ansari M, Kurian GA. Mechanism of hydrogen sulfide preconditioning-associated protection against ischemia–reperfusion injury differs in diabetic heart that develops myopathy. *Cardiovasc Toxicol.* (2020) 20:155–67. doi: 10.1007/s12012-019-09542-9
12. Mard SA, Ahmadi I, Ahangarpour A, Gharib-Naseri MK, Badavi M. Delayed gastric emptying in diabetic rats caused by decreased expression of cystathionine gamma lyase and H2S synthesis: *in vitro* and *in vivo* studies. *Neurogastroenterol Motil.* (2016) 28:1677–89. doi: 10.1111/nmo.12867
13. Liang W, Chen J, Mo L, Ke X, Zhang W, Zheng D, et al. ATP-sensitive K+ channels contribute to the protective effects of exogenous hydrogen sulfide against high glucose-induced injury in H9c2 cardiac cells. *Int J Mol Med.* (2016) 37:763–72. doi: 10.3892/ijmm.2016.2467
14. Wang M, Tang W, Xin H, Zhu YZ. S-propargyl-cysteine, a novel hydrogen sulfide donor, inhibits inflammatory hepcidin and relieves anemia of inflammation by inhibiting IL-6/STAT3 pathway. *PLoS One.* (2016) 11:e0163289. doi: 10.1371/journal.pone.0163289
15. Yang H, Mao Y, Tan B, Luo S, Zhu Y. The protective effects of endogenous hydrogen sulfide modulator, S-propargyl-cysteine, on high glucose-induced apoptosis in cardiomyocytes: a novel mechanism mediated by the activation of Nrf2. *Eur J Pharmacol.* (2015) 761:135–43. doi: 10.1016/j.ejphar.2015.05.001
16. Kan J, Guo W, Huang C, Bao G, Zhu Y, Zhu YZ. S-propargyl-cysteine, a novel water-soluble modulator of endogenous hydrogen sulfide, promotes angiogenesis through activation of signal transducer and activator of transcription 3. *Antioxid Redox Signal.* (2014) 20:2303–16. doi: 10.1089/ars.2013.5449
17. Wang Q, Liu HR, Mu Q, Rose P, Zhu YZ. S-propargyl-cysteine protects both adult rat hearts and neonatal cardiomyocytes from ischemia/hypoxia injury: the contribution of the hydrogen sulfide-mediated pathway. *J Cardiovasc Pharmacol.* (2009) 54:139–46. doi: 10.1097/FJC.0b013e3181ac8e12
18. Mori J, Patel Vaibhav B, Abo Alrob O, Basu R, Altamimi T, DesAulniers J, et al. Angiotensin 1-7 ameliorates diabetic cardiomyopathy and diastolic dysfunction in *db/db* mice by reducing lipotoxicity and inflammation. *Circ. Heart Failure.* (2014) 7:327–39. doi: 10.1161/CIRCHEARTFAILURE.113.000672
19. Parks BW, Sallam T, Mehrabian M, Psychogios N, Hui ST, Norheim F, et al. Genetic architecture of insulin resistance in the mouse. *Cell Metab.* (2015) 21:334–47. doi: 10.1016/j.cmet.2015.01.002
20. Xue R, Hao DD, Sun JP, Li WW, Zhao MM, Li XH, et al. Hydrogen sulfide treatment promotes glucose uptake by increasing insulin receptor sensitivity and ameliorates kidney lesions in type 2 diabetes. *Antioxid Redox Signal.* (2013) 19:5–23. doi: 10.1089/ars.2012.5024
21. Shen X, Pattillo CB, Pardue S, Bir SC, Wang R, Kevil CG. Measurement of plasma hydrogen sulfide *in vivo* and *in vitro*. *Free Radic Biol Med.* (2011) 50:1021–31. doi: 10.1016/j.freeradbiomed.2011.01.025
22. Shao D, Tian R. Glucose transporters in cardiac metabolism and hypertrophy. *Compr Physiol.* (2015) 6:331–51. doi: 10.1002/cphy.c150016
23. Ritchie RH, Abel ED. Basic mechanisms of diabetic heart disease. *Circ Res.* (2020) 126:1501–25. doi: 10.1161/CIRCRESAHA.120.315913
24. Poornima IG, Parikh P, Shannon RP. Diabetic cardiomyopathy. *Circ Res.* (2006) 98:596–605. doi: 10.1161/01.RES.0000207406.94146.c2
25. Lewis GA, Schelbert EB, Williams SG, Cunnington C, Ahmed F, McDonagh TA, et al. Biological phenotypes of heart failure with preserved ejection fraction. *J Am Coll Cardiol.* (2017) 70:2186–200. doi: 10.1016/j.jacc.2017.09.006
26. SeferoviÄ‡ PM, Paulus WJ. Clinical diabetic cardiomyopathy: a two-faced disease with restrictive and dilated phenotypes. *Eur Heart J.* (2015) 36:1718–27. doi: 10.1093/eurheartj/ehv134
27. Waldman M, Cohen K, Yadin D, Nudelman V, Gorfil D, Laniado-Schwartzman M, et al. Regulation of diabetic cardiomyopathy by caloric restriction is mediated by intracellular signaling pathways involving 'SIRT1 and PGC-1α'. *Cardiovasc Diabetol.* (2018) 17:111. doi: 10.1186/s12933-018-0757-1
28. Li W, Ma F, Zhang L, Huang Y, Li X, Zhang A, et al. S-Propargyl-cysteine exerts a novel protective effect on methionine and choline deficient diet-induced fatty liver *via* Akt/Nrf2/HO-1 pathway. *Oxid Med Cell Longev.* (2016) 2016:4690857. doi: 10.1155/2016/4690857
29. Gong QH, Wang Q, Pan LL, Liu XH, Xin H, Zhu YZ. S-propargyl-cysteine, a novel hydrogen sulfide-modulated agent, attenuates lipopolysaccharide-induced spatial learning and memory impairment: involvement of TNF signaling and NF-κB pathway in rats. *Brain Behav Immun.* (2011) 25:110–9. doi: 10.1016/j.bbi.2010.09.001
30. Kubli DA, Gustafsson ÃB. Unbreak my heart: targeting mitochondrial autophagy in diabetic cardiomyopathy. *Antioxid Redox Signal.* (2015) 22:1527–544. doi: 10.1089/ars.2015.6322
31. Wan A, Rodrigues B. Endothelial cell and cardiomyocyte crosstalk in diabetic cardiomyopathy. *Cardiovasc Res.* (2016) 111:172–83. doi: 10.1093/cvr/cvw159
32. Larsen TS, Aasum E. Metabolic (In)flexibility of the diabetic heart. *Cardiovasc Drugs Ther.* (2008) 22:91–5. doi: 10.1007/s10557-008-6083-1
33. Lopaschuk GD, Ussher JR, Folmes CDL, Jaswal JS, Stanley WC. Myocardial fatty acid metabolism in health and disease. *Physiol Rev.* (2010) 90:207–58. doi: 10.1152/physrev.00015.2009
34. van den Brom CE, Huisman MC, Vlasblom R, Boontje NM, Duijst S, Lubberink M, et al. Altered myocardial substrate metabolism is associated with myocardial dysfunction in early diabetic cardiomyopathy in rats: studies using positron emission tomography. *Cardiovasc Diabetol.* (2009) 8:39. doi: 10.1186/1475-2840-8-39
35. van de Weijer T, Schrauwen-Hinderling VB, Schrauwen P. Lipotoxicity in type 2 diabetic cardiomyopathy. *Cardiovasc Res.* (2011) 92:10–18. doi: 10.1093/cvr/cvr212
36. Marfella R, Di Filippo C, Portoghese M, Barbieri M, Ferraraccio F, Siniscalchi M, et al. Myocardial lipid accumulation in patients with pressure-overloaded heart and metabolic syndrome[S]. *J Lipid Res.* (2009) 50:2314–23. doi: 10.1194/jlr.P900032-JLR200
37. Gao Y, Ren Y, Guo Y-K, Liu X, Xie L-J, Jiang L, et al. Metabolic syndrome and myocardium steatosis in subclinical type 2 diabetes mellitus: a (1)H-magnetic resonance spectroscopy study. *Cardiovasc Diabetol.* (2020) 19:70. doi: 10.1186/s12933-020-01044-1
38. Jia G, DeMarco VG, Sowers JR. Insulin resistance and hyperinsulinaemia in diabetic cardiomyopathy. *Nat Rev Endocrinol.* (2016) 12:144–53. doi: 10.1038/nrendo.2015.216

39. Riehle C, Abel ED. Insulin signaling and heart failure. *Circ Res.* (2016) 118:1151–69. doi: 10.1161/CIRCRESAHA.116.306206
40. Zamora Mn, Villena JA. Contribution of impaired insulin signaling to the pathogenesis of diabetic cardiomyopathy. *Int J Mol Sci.* (2019) 20:2833. doi: 10.3390/ijms20112833
41. Fu F, Zhao K, Li J, Xu J, Zhang Y, Liu C, et al. Direct evidence that myocardial insulin resistance following myocardial ischemia contributes to post-ischemic heart failure. *Sci Rep.* (2015) 5:17927. doi: 10.1038/srep 17927
42. McQueen AP, Zhang D, Hu P, Swenson L, Yang Y, Zaha VG, et al. Contractile dysfunction in hypertrophied hearts with deficient insulin receptor signaling: possible role of reduced capillary density. *J Mol Cell Cardiol.* (2005) 39:882–92. doi: 10.1016/j.yjmcc.2005.07.017
43. Sena S, Hu P, Zhang D, Wang X, Wayment B, Olsen C, et al. Impaired insulin signaling accelerates cardiac mitochondrial dysfunction after myocardial infarction. *J Mol Cell Cardiol.* (2009) 46:910–8. doi: 10.1016/j.yjmcc.2009.02.014
44. Escribano O, Beneit N, Rubio-Longás C, López-Pastor AR, Gómez-Hernández A. The role of insulin receptor isoforms in diabetes and its metabolic and vascular complications. *J Diabetes Res.* (2017) 2017:1403206. doi: 10.1155/2017/1403206
45. White MF, Shoelson SE, Keutmann H, Kahn CR. A cascade of tyrosine autophosphorylation in the beta-subunit activates the phosphotransferase of the insulin receptor. *J Biol Chem.* (1988) 263:2969–80. doi: 10.1016/S0021-9258(18)69163-X
46. Hardt Stefan E, Sadoshima J. Glycogen synthase kinase-3beta: a novel regulator of cardiac hypertrophy and development. *Circ Res.* (2002) 90:1055–63. doi: 10.1161/01.RES.0000018952.70505.F1
47. Sharma AK, Thanikachalam PV, Bhatia S. The signaling interplay of GSK-3β in myocardial disorders. *Drug Discov Today.* (2020) 25:633–41. doi: 10.1016/j.drudis.2020.01.017

Conflict of Interest: The authors declare that the research was conducted in the absence of any commercial or financial relationships that could be construed as a potential conflict of interest.

Publisher's Note: All claims expressed in this article are solely those of the authors and do not necessarily represent those of their affiliated organizations, or those of the publisher, the editors and the reviewers. Any product that may be evaluated in this article, or claim that may be made by its manufacturer, is not guaranteed or endorsed by the publisher.

Copyright © 2021 Li, Xie, Chang, Wang, Chen, Wang and Zhu. This is an open-access article distributed under the terms of the Creative Commons Attribution License (CC BY). The use, distribution or reproduction in other forums is permitted, provided the original author(s) and the copyright owner(s) are credited and that the original publication in this journal is cited, in accordance with accepted academic practice. No use, distribution or reproduction is permitted which does not comply with these terms.

frontiers in Cardiovascular Medicine

ORIGINAL RESEARCH
published: 01 October 2021
doi: 10.3389/fcvm.2021.746934

Immediate Renal Denervation After Acute Myocardial Infarction Mitigates the Progression of Heart Failure via the Modulation of IL-33/ST2 Signaling

Han Chen[1,2,3†], *Rui Wang*[1,2,3†], *Quan Li*[4†], *Jiasheng Yin*[1,2,3], *Zhenyi Ge*[4], *Fei Xu*[1,2,3], *Tongtong Zang*[1,2,3], *Zhiqiang Pei*[1,2,3], *Chaofu Li*[1,2,3], *Li Shen*[1,2,3*] *and Junbo Ge*[1,2,3*]

[1] *Department of Cardiology, Zhongshan Hospital, Fudan University, Research Unit of Cardiovascular Techniques and Devices, Chinese Academy of Medical Sciences, Shanghai, China,* [2] *National Clinical Research Center for Interventional Medicine, Shanghai, China,* [3] *Shanghai Institute of Cardiovascular Diseases, Shanghai, China,* [4] *Department of Echocardiography, Zhongshan Hospital, Fudan University, Shanghai, China*

OPEN ACCESS

Edited by:
Yaoliang Tang,
Augusta University, United States

Reviewed by:
Cheng-Chao Ruan,
Fudan University, China
Liming Yang,
Harbin Medical University, China

***Correspondence:**
Junbo Ge
ge.junbo2@zs-hospital.sh.cn
Li Shen
shen.li1@zs-hospital.sh.cn

† *These authors have contributed equally to this work*

Specialty section:
This article was submitted to General Cardiovascular Medicine, a section of the journal Frontiers in Cardiovascular Medicine

Received: *25 July 2021*
Accepted: *06 September 2021*
Published: *01 October 2021*

Citation:
Chen H, Wang R, Li Q, Yin J, Ge Z, Xu F, Zang T, Pei Z, Li C, Shen L and Ge J (2021) Immediate Renal Denervation After Acute Myocardial Infarction Mitigates the Progression of Heart Failure via the Modulation of IL-33/ST2 Signaling. Front. Cardiovasc. Med. 8:746934. doi: 10.3389/fcvm.2021.746934

Objective: Previous studies have demonstrated the protective effects of renal denervation (RDN) in pre-existing heart failure, but the effects of immediate RDN after acute myocardial infarction (AMI) on subsequent cardiac remodeling have not been reported. This study aimed to investigate the cardioprotective effects of immediate RDN after AMI and its underlying mechanism.

Methods: AMI was induced by intracoronary gelatin sponge embolization in 14 Shanghai white pigs that were randomized to undergo either renal angiography (AMI+sham group) or RDN (AMI+RDN group) after 1 h of hemodynamic monitoring. Cardiac function of the two groups was measured at baseline, 1 h post-AMI and at the 1 month follow-up (1M-FU) by transthoracic echocardiography (TTE). Plasma NT-proBNP, soluble ST2 (sST2), norepinephrine (NE), and renin-angiotensin-aldosterone system activity were detected simultaneously. The renal cortex was harvested for NE measurement after the 1M-FU, and the renal arteries were stained with tyrosine hydroxylase for the evaluation of sympathetic activity. Heart tissues in the non-ischemic areas were collected to assess histological and molecular left ventricular (LV) remodeling by pathological staining, RT-PCR, and western blotting.

Results: There was no difference in the hemodynamic stability or cardiac function between the two groups at baseline and 1 h post-AMI. Six pigs from each of the two groups completed the 1M-FU. TTE analysis revealed the improved cardiac function of immediate RDN in the AMI+RDN group and circulating NT-proBNP levels were lower than those in the AMI+sham group. Further analysis showed significantly less interstitial fibrosis in the remote non-ischemic myocardium after immediate RDN, together with decreased cardiomyocyte hypertrophy and inflammatory cell infiltration. sST2 levels in circulating and myocardial tissues of animals in the AMI+RDN group were significantly higher than those in the AMI+sham group, accompanied by corresponding alterations in IL-33/ST2 and downstream signaling.

Conclusions: Immediate RDN can improve cardiac function and myocardial remodeling after AMI via modulation of IL-33/ST2 and downstream signaling.

Keywords: renal denervation, acute myocardial infarction, heart failure, myocardial remodeling, fibrosis, soluble ST2 (sST2)

INTRODUCTION

Although percutaneous coronary intervention (PCI) have significantly reduced acute mortality rates of acute myocardial infarction (AMI) by timely revascularization and myocardial salvage, ventricular remodeling afterwards, which involves cardiomyocyte hypertrophy, chronic inflammatory response, and the progression of fibrosis, can cause deteriorating cardiac function and even death (1–5). Additionally, recent studies have reported that an overactivated neurohumoral system plays a deleterious role in ventricular remodeling and many targeted drugs have be developed (6–8). However, due to drug tolerance and compliance difficulties, heart failure (HF) after AMI is still poorly controlled in the population worldwide, which is a substantial concern for society and also a strain from economic and healthcare perspectives (9, 10).

Denervation of sympathetic nerves around renal arteries (renal denervation; RDN) results in reduced activation of the sympathetic nervous system (SNS) and renin-angiotensin-aldosterone system (RAAS) (11). Studies on animal models have reported that RDN is beneficial in the treatment of diseases associated with SNS and RAAS hyperactivation in addition to its use for hypertension treatment (12–16). Among these effects, the cardioprotective effect of RDN on pre-existing HF has been confirmed (17, 18).

Inspired by the idea that concomitant RDN with pulmonary vein isolation (PVI) can further reduce the recurrence rate of atrial fibrillation, we brought up the hypothesis of a "one-stop" treatment for HF after AMI by performing RDN with a cryoablation catheter immediately after the onset of AMI, rather than for chronic ischemic HF (19). Therefore, in this study, we evaluated the cardioprotective effect of immediate RDN after AMI in a swine model and the possible mechanism on adverse myocardial remodeling.

MATERIALS AND METHODS

Animals

A total of 14 Shanghai white pigs of either sex, with body weights ranging from 30 to 35 kg, were used in this study. All animals used in this study were cared for and handled according to the National Institutes of Health Guidelines. The study protocol was reviewed and approved by the Animal Care and Use Committee of Zhongshan Hospital, Fudan University.

Abbreviations: RDN, renal denervation; AMI, acute myocardial infarction; RAAS, renin-angiotensin-aldosterone system activity; TH, tyrosine hydroxylase; PCI, percutaneous coronary intervention; HF, heart failure; LAD, left anterior descending; LV, left ventricular; BUN, blood urea nitrogen; EF, ejection fraction.

Study Design

An AMI was induced by occlusion of the proximal left anterior descending coronary artery (LAD) with gelatin sponges and set as the baseline. One hour after AMI, the surviving pigs were randomized into two groups that underwent either RDN with a cryoablation balloon catheter (CryoFocus, Shanghai, China) (AMI+RDN group) or renal angiography (AMI+sham group). All animals were sacrificed at 1 month follow-up (1M-FU), and the cardiac tissue was collected for further molecular or histological analysis. Transthoracic echocardiography (TTE) was performed at baseline, 1 h post-AMI and at the 1M-FU. Furthermore, peripheral blood samples were obtained at the same time points to assess cardiac injury and function.

AMI Induction

The AMI was induced by intracoronary gelatin sponge embolization as described previously, and the total procedure lasted ∼10 min (20). The animals were fasted for 12 h with unrestricted access to water. Anesthesia was induced by intramuscular injection of 6.0 mg/kg Zoletil® (a mixture of tiletamine hydrochloride and zolazepam hydrochloride, Virbac Laboratory, Carros, France) followed by an intravenous injection of propofol (5 mg/kg). A volatile anesthetic with isoflurane (1.5–2%) was used to maintain general anesthesia. An unfractured heparin bolus of 200 U/kg was administered after sheath placement in the right femoral artery. Invasive monitoring of aortic pressure was obtained using a pressure sensor (Transpac, ICUMEDICAL, CA, USA) and recorded by Mac-lab hemodynamic recording system (GE healthcare, MA, USA). A 6F SAL catheter (Medtronic, MN, USA) was introduced through the arterial sheath to the left main coronary artery. After angiography, a 1.8F Finecross microcatheter (Terumo, Tokyo, Japan) was placed in the middle of the LAD (between the first and second diagonal branches) under the guidance of a 0.014" guidewire. A mixture of gelatin sponge particles (300–1,000 μm) and heparinized contrast media was slowly injected through the microcatheter under fluoroscopy. The injection was stopped after total occlusion of the middle LAD. The pigs were carefully monitored under volatile anesthesia for 60 min, and then randomized for further operation. After the 1M-FU, the pigs were sacrificed by rapid intravenous injection of 20 mL of 10 % potassium chloride, and samples were harvested for analysis.

Renal Denervation

RDN was performed using a cryoablation balloon catheter as previously described (21, 22). After randomization, pigs in the AMI+sham group underwent renal angiography with a 6F JR 4 guiding catheter (Medtronic). For pigs in the

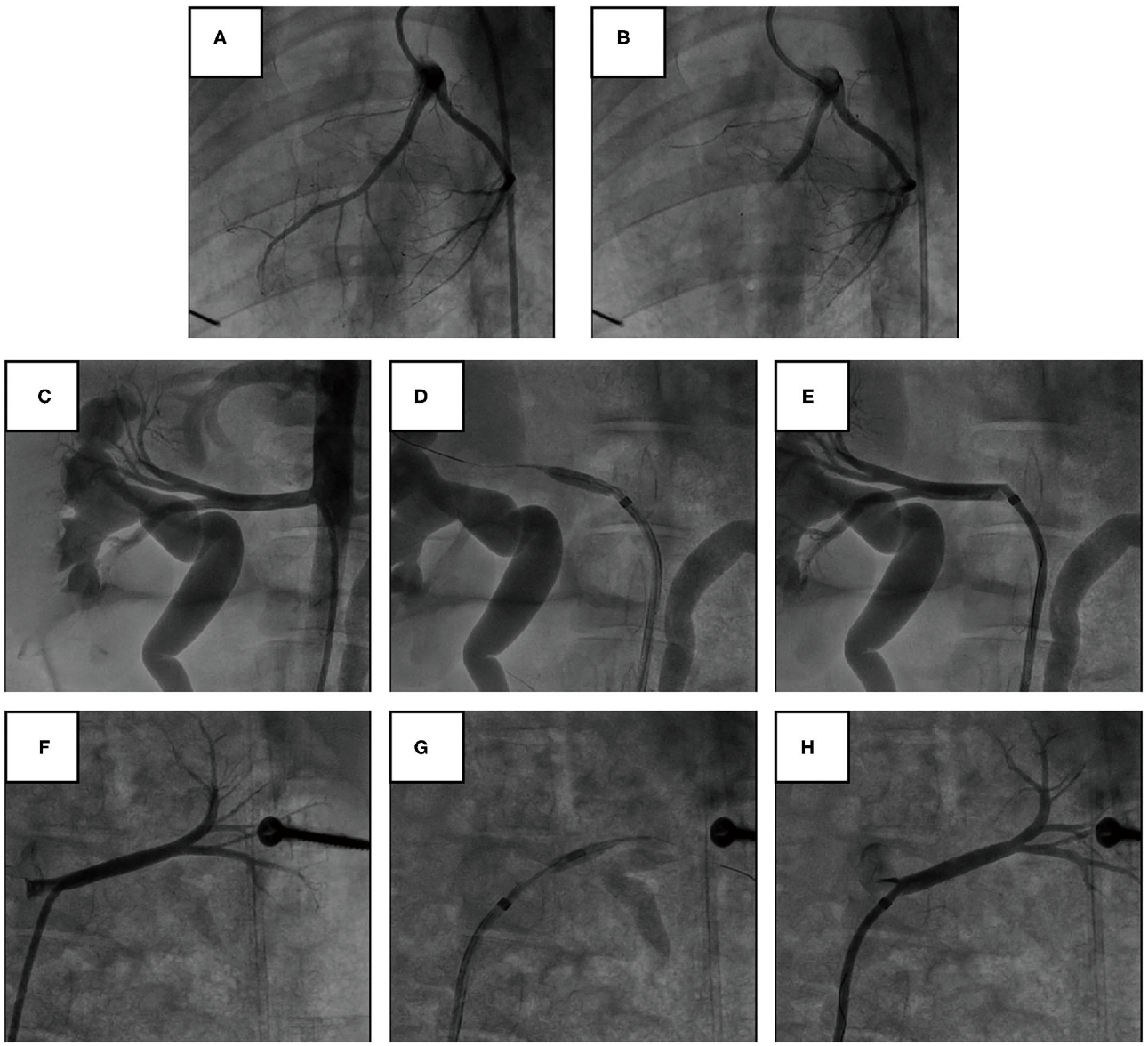

FIGURE 1 | Angiography of coronary and renal arteries in pig models. **(A,B)** Representative angiography of the LAD before and after gelatin sponge embolization. **(C–E)** Representative angiography of the right renal artery before, during, and immediately after cryoablation of RDN. **(F–H)** Representative angiography of the left renal artery before, during, and immediately after cryoablation of RDN.

AMI+RDN group, a 7F sizable cryoablation balloon catheter was selected based on the diameter of the middle to distal part of the main renal arteries and was introduced into the renal artery via the same percutaneous femoral access as in the AMI modeling. After confirming a complete attachment to the artery wall, the balloon was inflated with liquid nitrogen, and a complete RDN for one side of the renal artery took ∼5 min. Additional renal angiography was performed before catheter removal to confirm the absence of complications, such as severe vascular dissection, thrombosis, or spasm. The animals were then allowed to recover to a stable state.

TTE Analysis

Two-dimensional TTE was performed at baseline, 1 h and 1 month post-AMI in all pigs under anesthesia with isoflurane (1.5–2%). Transthoracic images were acquired from a right parasternal approach using a Vivid E9 ultrasound system (GE Vingmed Ultrasound AS, Horten, Norway) equipped with an M5S probe according to the recommendations of the American Society of Echocardiography (23). The images were stored in the DICOM format and analyzed offline using EchoPAC (Version 203). The end-diastolic and systolic volumes (EDV, ESV) were measured from the apical four-chamber view. The left ventricular (LV) ejection fraction (EF) was determined using Simpson's

TABLE 1 | Hemodynamic and biological parameters at baseline, end-procedure and during the 1M-FU.

	AMI	AMI+RDN	*p*
N	6	6	—
Baseline mean arterial pressure, mmHg	75.63 ± 3.96	77.00 ± 6.38	0.65
1 h post-AMI mean arterial pressure, mmHg	69.17 ± 4.66	69.80 ± 6.43	0.87
1M-FU mean arterial pressure, mmHg	74.56 ± 5.75	78.08 ± 6.75	0.35
Baseline heart rate, bpm	76.13 ± 5.69	78.50 ± 5.47	0.48
1 h post-AMI heart rate, bpm	91.50 ± 5.28	87.00 ± 7.90	0.34
1M-FU heart rate, bpm	79.13 ± 5.46	76.33 ± 5.09	0.38
Baseline plasma BUN, mg/dL	8.40 ± 1.77	8.19 ± 2.06	0.85
1M-FU plasma BUN, mg/dL	12.10 ± 1.36	9.58 ± 2.20	0.03
Baseline plasma creatinine, μmol/L	92.94 ± 15.93	89.25 ± 8.48	0.65
1M-FU plasma creatinine, μmol/L	136.87 ± 14.99	115.90 ± 16.11	0.04
Baseline plasma Na+, mmol/L	125.54 ± 5.15	126.62 ± 1.99	0.64
1M-FU plasma Na+, mmol/L	127.01 ± 4.28	126.74 ± 6.93	0.94
Baseline plasma K+, mmol/L	15.32 ± 1.72	14.61 ± 2.75	0.60
1M-FU plasma K+, mmol/L	15.99 ± 1.53	15.67 ± 3.62	0.85
Baseline plasma AST, U/L	28.39 ± 8.72	24.87 ± 5.23	0.44
1M-FU plasma AST, U/L	31.55 ± 10.65	27.92 ± 13.63	0.62
Baseline plasma ALT, U/L	35.31 ± 5.92	39.53 ± 7.84	0.31
1M-FU plasma ALT, U/L	48.04 ± 10.22	48.23 ± 21.45	0.98
Baseline plasma DBil, μmol/L	2.23 ± 0.37	2.23 ± 0.46	1.00
1M-FU plasma DBil, μmol/L	2.74 ± 0.47	2.25 ± 0.57	0.17
Baseline plasma TBil, μmol/L	4.15 ± 0.82	4.17 ± 0.91	0.97
1M-FU plasma TBil, μmol/L	5.64 ± 1.01	4.96 ± 0.97	0.26

method. A single researcher was blinded to the profile of all animals and analyzed the images.

Analysis of Plasma Biomarkers and Norepinephrine (NE) in the Renal Cortex

The plasma samples were obtained 15 min after insertion of the arterial sheath, when the animal was intubated under no pain and in a steady state regarding anesthesia at baseline, 1 h and 1 month after modeling. An automatic biochemistry analyzer (Chemray, Guangzhou, China) and the corresponding reagents were used for plasma biochemistry tests. The laboratory parameters measured included blood urea nitrogen (BUN), creatinine, Na+, K+, AST, ALT, DBil, and TBil. Commercial enzyme-linked immunosorbent assay (ELISA) kits were used to determine the plasma concentrations of soluble ST2 (sST2, Presage®ST2 Assay, Critical Diagnostics, Boston, MA, USA), NT-proBNP (CEA485Pro, Cloud-clone, Wuhan, China), renin (H216, Nanjing Jiancheng, Nanjing, China), angiotensin II (H185, Nanjing Jiancheng, Nanjing, China), and aldosterone (H188, Nanjing Jiancheng, Nanjing, China) according to the manufacturer's instructions. The renal cortex was harvested, and the NE concentrations were detected using a commercial ELISA Kit (KA3836, Abnova, Taipei, China).

Histology Analysis

Histological analysis was performed after 1M-FU. Sample from LV non-ischemic area and renal arteries in both groups were collected and embedded in paraffin. Heart tissue sections were stained with Masson's staining for fibrosis. WGA, CD68, vWF were stained for cell size, inflammatory cells, and angiogenesis (all from Abcam Inc., Cambridge, MA, USA) under established protocol and quantified imageJ (National Institutes of Health, MD, USA). The intensity and algorithm were preset and maintained constant for analysis of all sections. Renal arteries were stained with Tyrosine hydroxylase (TH, Abcam Inc., Cambridge, MA, USA).

Western Blotting and Quantitative Real-Time Polymerase Chain Reaction

Samples from the non-ischemic area of the LV in both groups were collected. Protein extraction and western blotting were performed as previously described (24). Antibodies used for this experiment were as follows: GAPDH (1:1,000, Abcam Inc., Cambridge, MA, USA), collagen I (Col I, 1:1,000, Abcam Inc., Cambridge, MA, USA), collagen III (Col III, 1:1,000, Abcam Inc., Cambridge, MA, USA), αSMA (1:1,000, Abcam Inc., Cambridge, MA, USA), NF-κb (1:1,000, Abcam Inc., Cambridge, MA, USA), and TGFβ (1:1,000, Abcam Inc., Cambridge, MA, USA).

Total RNA was extracted from the tissues and reverse-transcribed into complementary deoxyribonucleic acid (DP419, TIANGEN, Beijing, China; RR037A, TAKARA, Iwate ken, Japan). Quantitative real-time polymerase chain reaction was performed to detect relative mRNA expression (Bio-Rad, Munich, Germany; RR420L, TAKARA, Iwate ken, Japan). The primer sequences used for the quantitative polymerase chain reaction are listed in **Supplementary Table 1**.

Statistical Analysis

Raw data of the groups were given as an input in GraphPad Prism 9.0 (GraphPad Software, San Diego, CA, USA) for statistical analysis. All data are expressed as mean ± standard error of the mean (SEM). Comparisons of the data between groups were performed using Student's *t*-test. Differences were considered statistically significant at $p < 0.05$.

RESULTS

Model Establishment and Immediate Evaluation

AMI was successfully induced in all of the 14 pigs (**Figures 1A,B**). The pigs were randomly assigned to undergo either renal angiography or immediate RDN after 1 h of hemodynamic monitoring. Blood pressure and heart rate were comparable between the two groups at baseline and 1 h post modeling (**Table 1**). No adverse vascular complications in the renal arteries (e.g., thrombosis, dissection, perforation, and fistulae) occurred immediately after RDN (**Figures 1C–H**).

Two pigs (one pig in the AMI+sham group and one pig in the AMI+RDN group) died of recurrent ventricular fibrillation in the first 24 h postoperatively during follow-up and were excluded from the statistical analysis. A total of 12 pigs completed the entire 1M-FU process (six pigs each in AMI+sham group and AMI+RDN group).

Immediate RDN Suppressed SNS and RAAS Overactivity in HF After AMI

TH is the rate-limiting enzyme in catecholamine synthesis and is often used to evaluate renal sympathetic nerve activity. At the end of the 1M-FU, renal artery tissues from both groups of pigs were harvested for TH staining and scored for intensity. As shown in **Figure 2A**, the TH staining intensity and score were significantly lower after immediate RDN in the AMI+RDN group than that in the AMI+sham group. Similar results were also obtained in the measurement of NE, as the NE concentration in the renal cortex of the AMI+RDN group was significantly reduced compared to that in the AMI+sham group (**Figure 2B**). These results suggest that immediate cryoablation effectively impairs renal sympathetic nerves and their functional activity.

The RAAS system remains continuously hyperactivated during the course of HF in addition to SNS overactivation, and the former plays a decisive role in myocardial remodeling. We found that immediate RDN suppressed the overactivation of RAAS to some extent by analyzing the peripheral blood of the two groups, as evidenced by a significant reduction in plasma renin, angiotensin, and aldosterone levels at the 1M-FU (**Figures 2C–E**).

Liver and renal function were also examined at the preoperative baseline and at the 1M-FU. The results showed a protective effect of immediate RDN on blood BUN and creatinine in the AMI+RDN group pigs, whereas the plasma potassium and sodium levels and liver function indices (AST, ALT, TBIL, and DBIL) did not differ between the two groups (**Table 1**).

Immediate RDN Improved Cardiac Function After AMI

Cardiac function was tested again using TTE at the 1M-FU (**Figure 3A**). The results indicated that immediate RDN exhibited remarkable improvement in several parameters of cardiac function, as evidenced by higher EF and fraction shortening of the left ventricle in the AMI+RDN group than that in the AMI+sham group (**Figures 3B,C**). Additionally, immediate RDN also significantly improved LV end-diastolic dimensions, LV end-systolic dimensions, end-systolic volume, and end-diastolic volume (**Figures 3D–G**).

We then examined cardiac function parameters in the circulation and found that NT-proBNP in the AMI+RDN group was significantly lower than that in the AMI+sham group, further suggesting a protective effect of immediate RDN on cardiac function (**Figure 3H**).

Immediate RDN Reduced Myocardial Remodeling in LV After AMI

Myocardial remodeling is the primary pathological basis of cardiac dysfunction. The results obtained from our study prompted us to explore the influence of immediate RDN on myocardial remodeling. As shown in **Figure 4A**, the collagen density was dramatically suppressed after immediate RDN at the 1M-FU with the progressive formation of fibrosis in the non-ischemic area. Moreover, cardiomyocytes in AMI+RDN group exhibited smaller sized compared to AMI+sham group (**Figure 4B**). We also assessed CD68 staining and found out that inflammatory infiltration during HF were inhibited after immediate RDN (**Figure 4C**). However, vWF staining showed no difference in angiogenesis between the two groups (**Supplementary Figure 1**).

Similar to the results obtained for the pathological analysis, the elevated mRNA and protein expression of fibrosis-related proteins such as Col I, Col III, and αSMA in remote area of the myocardial tissue after AMI were mitigated to some extent by immediate RDN (**Figures 4D,E**). These findings implicated a protective effect of immediate RDN in myocardial remodeling.

IL-33/ST2 Signaling Pathway May Be Involved in the Cardioprotective Effect of Immediate RDN

A protective role is played by sST2 in the circulation in myocardial remodeling, and it is now regarded as a prognostic biomarker for HF. Therefore, we wanted to determine whether the protective effects of immediate RDN on LV remodeling was through its effect on sST2. As expected, plasma sST2 levels were significantly lower in the AMI+RDN group than those in the AMI+sham group (**Figure 5A**). Additionally, sST2 expression in the non-ischemic areas of the LV was also reduced, but the expression level of its cardioprotective ligand IL-33 remained stable (**Figure 5B**).

NF-κB is important for inflammation and immunity in AMI and has also been reported to be activated by competitive binding of sST2 to IL-33, which promotes the synthesis of TGFβ. We verified downstream NF-κB activation and TGF-β expression to further validate the role of sST2 in the cardioprotective effects of immediate RDN and found significantly suppressed expression of these indicators in the AMI+RDN group (**Figure 5C** and **Supplementary Figure 2**). These results implied a protected activation of IL-33/ST2 signaling and the role of decreased sST2 in the anti-remodeling effects of immediate RDN.

DISCUSSION

In this study, we successfully established a porcine model of AMI and post-AMI RDN. Decreased cardiac function, determined by TTE, was observed postoperatively in pigs of both the AMI+sham and AMI+RDN groups. However, immediate RDN after AMI, which suppressed the SNS and RAAS hyperactivation, exhibited a protective effect on cardiac function and an overall improvement in plasma HF markers after 1 month. The cardioprotective effects of RDN were mainly a result of improved

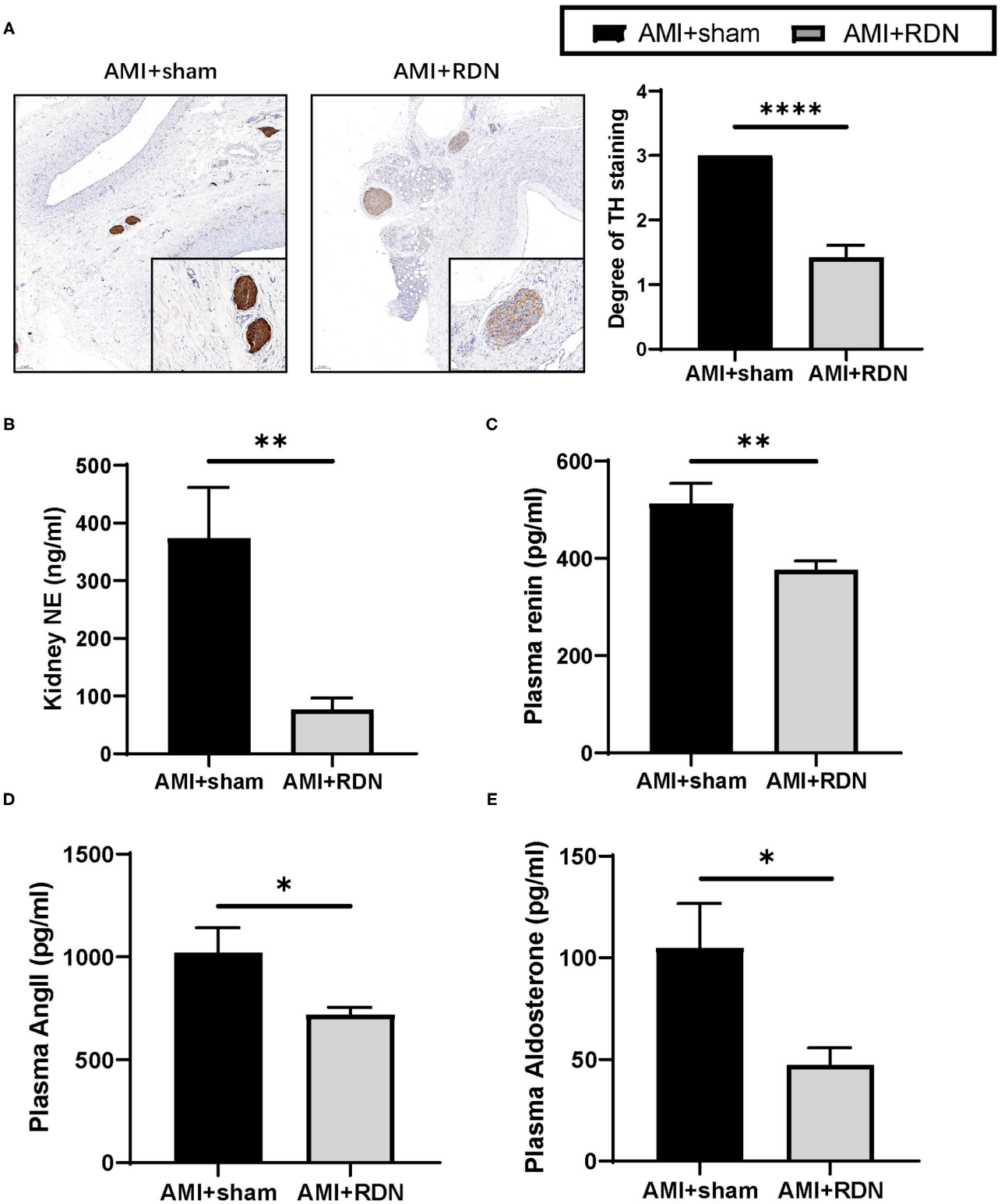

FIGURE 2 | Immediate RDN effectively reduces renal sympathetic activity and plasma RAAS indexes after AMI. **(A)** Representative TH-stained photomicrographs and degree of TH staining of nerves around the renal arteries of pigs from the AMI and AMI+RDN groups on a scale of 0–3: 0, no reaction; 1, patchy/very weak reaction; 2, weak to moderate reaction; 3, strong reaction. The minimum score that represents the most serious functional damage was adopted for each section. **(B)** Quantification of NE concentration per gram of renal cortex of pigs from the AMI and AMI+RDN groups. **(C–E)** Quantification of plasma renin, angiotensin II, and aldosterone levels at 1M-FU of pigs in the AMI and AMI+RDN groups by 1M-FU. Values are expressed as mean ± SEM ($n = 6$). One-way ANOVA was applied to determine the significance of the data. *$p < 0.05$, **$p < 0.01$, ****$p < 0.0001$. TH, tyrosine hydroxylase; NE, norepinephrine; SEM, standard error of the mean.

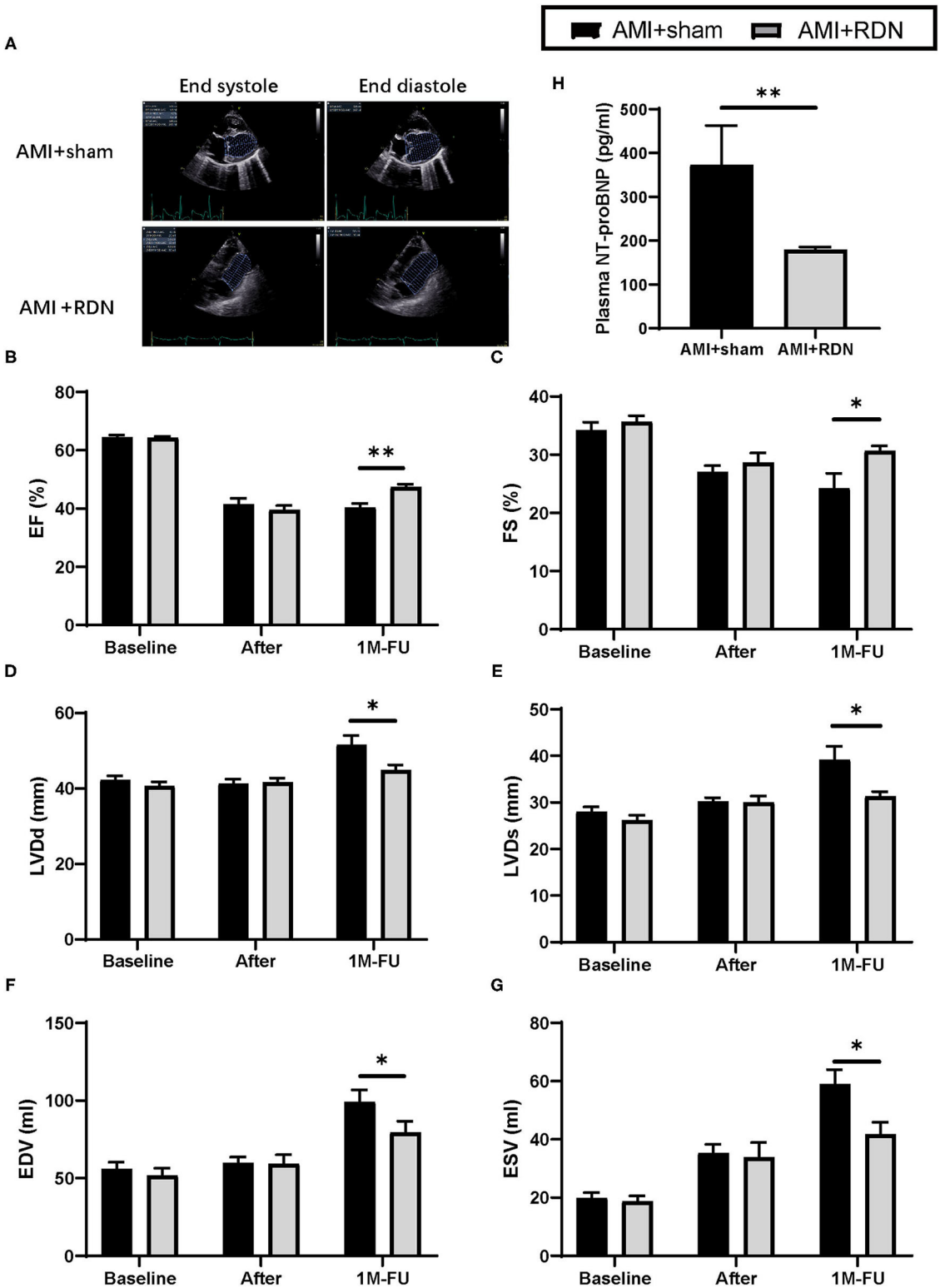

FIGURE 3 | Immediate RDN improves LV function and plasma NT-proBNP level in pigs after AMI. **(A)** Representative echocardiography images of pigs in the AMI+sham and AMI+RDN groups before, after gelatin embolism, and at 1M-FU. **(B–G)** Statistical analysis of EF, FE, LVDd, LVDs, EDV, EVS of pigs in AMI+sham and AMI+RDN groups before, after gelatin embolism, and at 1M-FU. **(H)** Quantification of plasma NT-proBNP level at 1M-FU in pigs in the AMI+sham and AMI+RDN groups. Values are expressed as mean ± SEM ($n = 6$). One-way ANOVA was applied to determine the significance of the data. *$p < 0.05$, **$p < 0.01$. EF, ejection fraction; FS, fractional shortening; LVDd, left ventricular end-diastolic dimension; LVDs, left ventricular end-systolic dimension; EDV, end-diastolic volume; ESV, end-systolic volume.

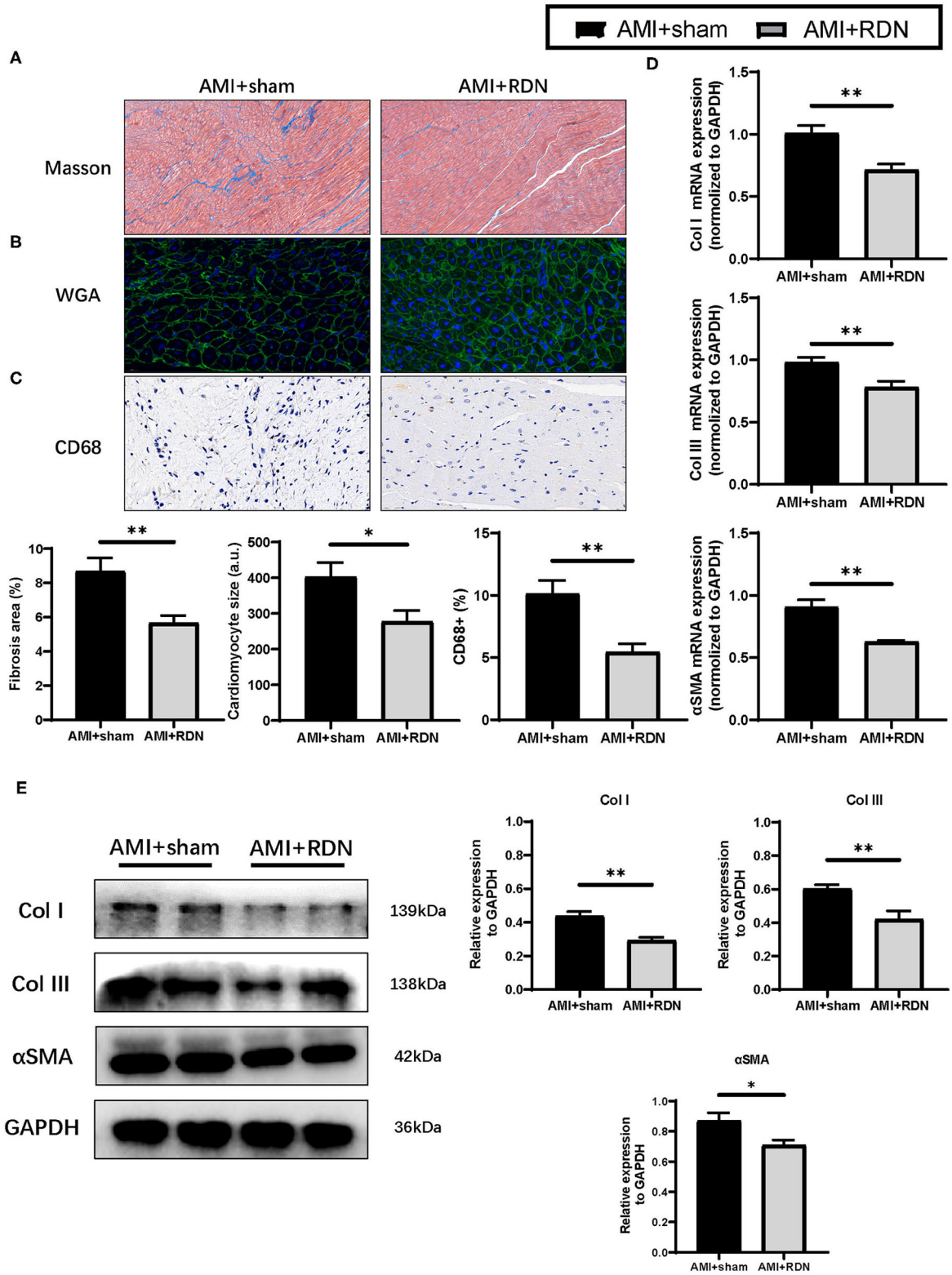

FIGURE 4 | Immediate RDN suppression LV remodeling after AMI. **(A–C)** Representative photomicrographs of Masson trichrome, WGA and CD68 staining and quantitative data of remote area in the extracted heart of pigs in AMI+sham and AMI+RDN groups by 1M-FU. **(D)** Relative mRNA expression of Col I, Col III, and αSMA in remote areas of pigs in AMI+sham and AMI+RDN groups at 1M-FU. **(E)** Representative images and relative protein expression of Col I, Col III, and αSMA in remote areas of pigs in AMI+sham and AMI+RDN groups by 1M-FU Western Blotting analyses. Values are expressed as mean ± SEM ($n = 6$). One-way ANOVA was applied to determine the significance of the data. *$p < 0.05$, **$p < 0.01$. a.u., astronomical unit.

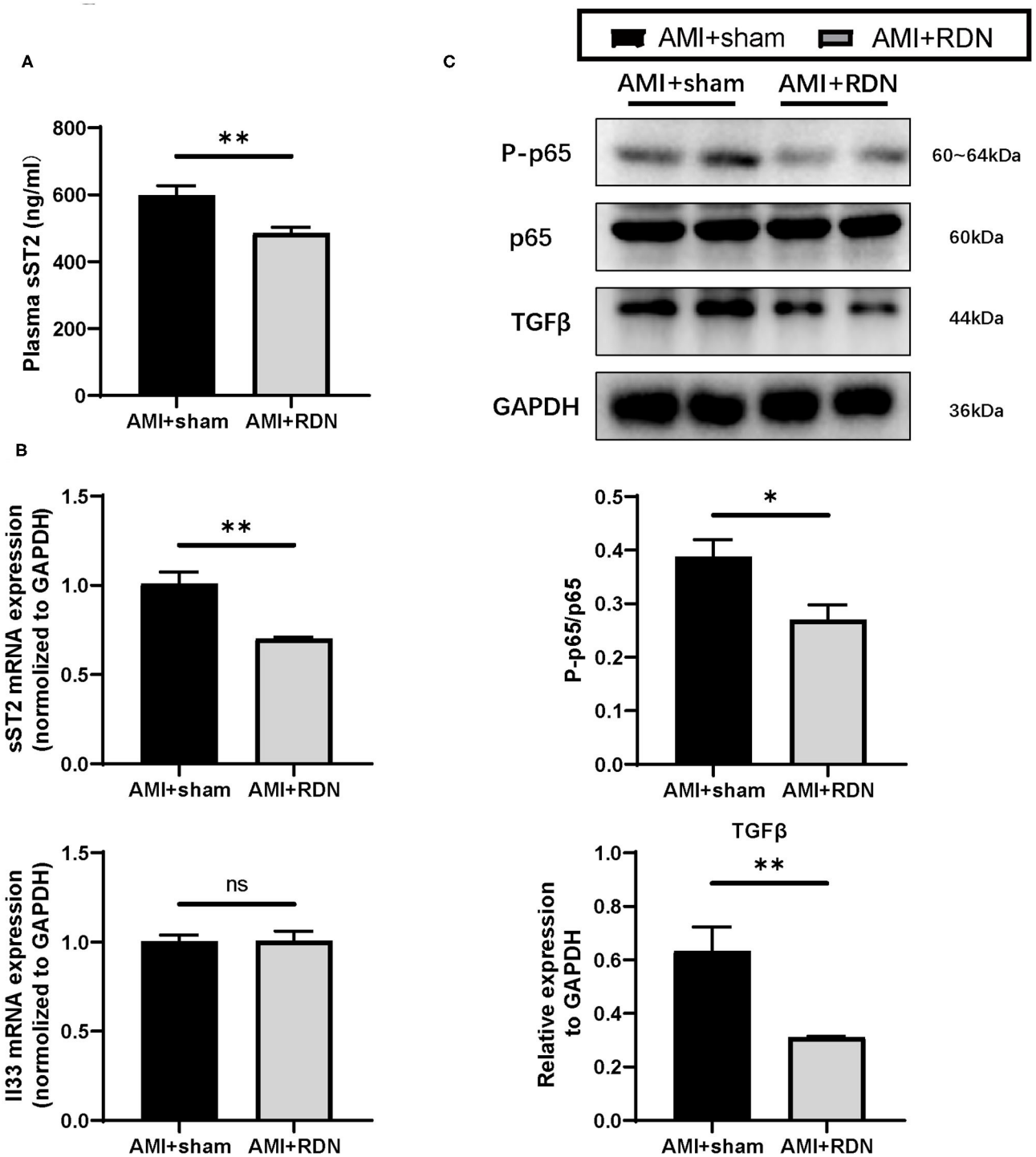

FIGURE 5 | IL-33/ST2 and downstream signaling after immediate RDN. **(A)** Quantification of the plasma sST2 level at 1M-FU of pigs in the AMI and AMI+RDN groups by 1M-FU. **(B)** Relative mRNA expression of sST2 and IL-33 in remote area of pigs in the AMI and AMI+RDN groups at 1M-FU. **(C)** Representative images and NF-κB activation (ratio of P-p65 to total p65) and relative protein expressions of TGFβ in remote area of pigs in AMI and AMI+RDN groups by 1M-FU Western Blotting analyses. Values are expressed as mean ± SEM ($n = 6$). One-way ANOVA was applied for determining the significance of data. *$p < 0.05$, **$p < 0.01$. sST2, soluble ST2.

LV remodeling, marked by a reduction in myocardial fibrosis, decreased cardiomyocytes hypertrophy and less inflammatory cell infiltration. Further analysis revealed attenuated expression of sST2 by immediate RDN, together with the involvement of IL-33/ST2 and downstream signaling in the reduction of myocardial remodeling.

In this study, the deterioration in cardiac function after AMI was significantly restrained by immediate RDN with improved TTE parameters and lower plasma NT-proBNP levels at the 1M-FU, suggesting a reduced need for compensatory mechanism. From a pathological perspective, myocardial remodeling persists in the course of HF, manifested mainly by myocardial fibrosis and hypertrophy (2, 20). Our study confirmed for the first time that immediate RDN after AMI significantly repressed fibrosis and cardiomyocytes hypertrophy in the non-ischemic myocardium. Previous studies have suggested that RDN has an antifibrotic role in many other pathological processes, such as delayed HF, renal fibrosis in chronic kidney dysfunction, and atrial fibrosis in arrhythmia (17, 21–24). The protective effect of RDN on myocardial hypertrophy has also been reported in hypertensive models (25). These all supported, to some extent, the results obtained from our findings at both the histological and molecular levels. Infiltration of inflammatory cells is another an important pathological process in remodeling (3). We also found that there were fewer CD68-positive cells in the LV of the AMI+RDN group than in the AMI+sham group. This is cohesive to our previous findings in an atherosclerotic $ApoE^{-/-}$ mice model where RDN mitigated the mobilization of inflammatory cells to plaques (14). Furthermore, we ensured a consistency of the infarct size to a large extent with the use of a permanent embolization model, eliminating the differences in cardiac function caused by this confounding factor, as it is reported that RDN can protect against cell death caused by reperfusion, thus reducing infarct size (26). Collectively, these results for the first time suggest that immediate RDN after AMI is cardioprotective and this effect is mainly exerted by counteracting myocardial remodeling from the onset of HF.

Additionally, we also reported for the first time that the expression of sST2, as a clinical biomarker, declined dramatically in the AMI+RDN group after immediate RDN compared with that in the AMI+sham group. Recently, sST2 has emerged as a prognostic biomarker for HF, and its peripheral level has been reported to reflect the degree of myocardial remodeling (27–29). sST2 is responsible for fibroblast activation, cardiomyocytes hypertrophy, and inflammatory responses in the progression of HF (30, 31). As a decoy receptor, it competitively weakens the binding of IL-33 to ST2L, which inhibits the activation of NF-κb, exerting a direct anti-inflammatory effect on one hand and suppressing the activation of TGFβ and its downstream profibrotic and pro-hypertrophic pathway on the other hand (32, 33). Likewise, the improvement in these phenotypes was also detected as the cardioprotective effect of immediate RDN. In our study, we observed reduced levels of sST2 after AMI by immediate RDN, together with changes in IL-33-related remodeling pathways, including reduced activation of NF-κb and expression of TGFβ. The inhibitory effect of RDN on NF-κb has been demonstrated previously, which further supports our findings that RDN exerts anti-remodeling effects by the reduction of sST2 and the subsequent modulation of the IL-33/ST2 pathway (34, 35).

With the use of a large animal model, this study may provide insights into the clinical application of RDN as it has several advantages. Inconsistence in results happened between large and small animal models (36). Swine models are closer to humans not only morphologically but also physiologically and are more suggestive in practice. The modeling of AMI in swine is also more similar to the pathological formation of AMI in human. Besides, to perform RDN, small animal are treated through open abdominal approaches, and there may be confounding of results due to traumatic strikes. Large animals, on the other hand, are underwent the same interventional approach as humans, and therefore can better simulate clinical treatment. Previously, improvement in exercise endurance and other surrogate endpoints have shown that RDN is protective in both HFrEF and HFpEF patients. In addition to the commonly used imaging or serological indicators in clinical application, our study also confirmed from a pathological perspective that immediate RDN can exert cardioprotective effects by directly restricting myocardial fibrosis and hypertrophy in non-ischemic areas and limiting inflammatory cell infiltration. More importantly, immediate RDN exhibited a significant protective effect on cardiac function while ensuring hemodynamic stability. Although RDN is antihypertensive, and the kidney is one of the most densely distributed sites of sympathetic nerves, RDN does not fully restore their excitability to normal levels, namely not from "too much" to "too little" (37). Moreover, in most of the previous studies, RDN was performed in the middle to late stages of HF, which may lead to a delay in the intervention that RDN would not display a full protective effect early in myocardial remodeling (38–40). From a clinical point of view, our study reaffirms the cardioprotective effects and clinical feasibility of immediate RDN. It suggested AMI as another potential indication for RDN and readmissions for interventions may not be necessary for AMI patients after their HF has progressed.

This study had several limitations. First, the follow-up period was relatively short. We found that immediate RDN exhibited inhibitory effects on myocardial remodeling of non-ischemic myocardial tissues in the first month after AMI, while these pathological progressions in HF last over years. Considering that nerve regeneration after RDN is barely visible and its antihypertensive effect persists for at least 3 years after operation, we presume to a certain extent that immediate RDN may also exert a sustained cardioprotective effect till the middle- and late-stage HF (41, 42). Second, in this study we discovered for the first time that RDN protected the failing heart via the modulation of IL-33/ST2 signaling, yet the detailed mechanism is still unclear. Existing studies have found that changes in IL-33/ST2 pathway are associated with the RAAS system (43, 44). Since RAAS is regulated by RDN, we speculate that RDN may exert a cardioprotective effect on IL-33/ST2 pathway through RAAS and further detailed mechanisms are under exploration. Third, although we confirmed the cardioprotective effects of immediate RDN after AMI, a pre-existing RDN operation is not protective against AMI. The optimal time window for RDN intervention, such as revascularization immediately after

RDN, in ischemic HF remains inconclusive. Therefore, relevant large animal experiments are underway to overcome this gap in knowledge.

CONCLUSIONS

Our study showed that immediate RDN after AMI inhibits early SNS and RAAS activation. It exhibited an improvement in cardiac function mainly by suppressing myocardial remodeling. For the first time, we found that these cardioprotective effects of immediate RDN was associated with a reduction in sST2 as well as the involvement of IL-33/ST2 and downstream signaling. This may provide another viable application of RDN beyond hypertension in emergency PCI.

DATA AVAILABILITY STATEMENT

The original contributions presented in the study are included in the article/**Supplementary Material**, further inquiries can be directed to either one of or both of our corresponding authors.

ETHICS STATEMENT

The animal study was reviewed and approved by Animal Care and Use Committee of Zhongshan Hospital, Fudan University.

AUTHOR CONTRIBUTIONS

JG supervised the study. LS supervised and critically revised the manuscript. HC performed the statistical analyses and drafted the manuscript. HC, RW, JY, ZG, FX, TZ, ZP, CL, and QL performed the experiments. All authors contributed to the manuscript and approved the submitted version.

FUNDING

This study was funded by Chinese Academy of Medical Sciences (2019-I2M-5-060 and 2020-JKCS-0154020) and Shanghai Shenkang Hospital Development Center (SHDC2020CR3023B100).

ACKNOWLEDGMENTS

The authors thank Kuiwen Zhao, Lingjuan Qiao, and Yuepeng Diao for kindly providing the cryoablation balloon catheters.

SUPPLEMENTARY MATERIAL

The Supplementary Material for this article can be found online at: https://www.frontiersin.org/articles/10.3389/fcvm.2021.746934/full#supplementary-material

REFERENCES

1. Lewis EF, Moye LA, Rouleau JL, Sacks FM, Arnold JMO, Warnica JW, et al. Predictors of late development of heart failure in stable survivors of myocardial infarction. *J Am Coll Cardiol.* (2003) 42:1446–53. doi: 10.1016/S0735-1097(03)01057-X
2. Cohn JN, Ferrari R, Sharpe N. Cardiac remodeling-concepts and clinical implications: a consensus paper from an international forum on cardiac remodeling. *J Am Coll Cardiol.* (2000) 35:569–82. doi: 10.1016/S0735-1097(99)00630-0
3. Westman PC, Lipinski MJ, Luger D, Waksman R, Bonow RO, Wu E, et al. Inflammation as a driver of adverse left ventricular remodeling after acute myocardial infarction. *J Am Coll Cardiol.* (2016) 67:2050–60. doi: 10.1016/j.jacc.2016.01.073
4. Kotter S, Kazmierowska M, Andresen C, Bottermann K, Grandoch M, Gorressen S, et al. Titin-based cardiac myocyte stiffening contributes to early adaptive ventricular remodeling after myocardial infarction. *Circ Res.* (2016) 119:1017–29. doi: 10.1161/CIRCRESAHA.116.309685
5. van den Borne SW, Diez J, Blankesteijn WM, Verjans J, Hofstra L, Narula J. Myocardial remodeling after infarction: the role of myofibroblasts. *Nat Rev Cardiol.* (2010) 7:30–7. doi: 10.1038/nrcardio.2009.199
6. Burrell LM, Risvanis J, Kubota E, Dean RG, MacDonald PS, Lu S, et al. Myocardial infarction increases ACE2 expression in rat and humans. *Eur Heart J.* (2005) 26:369–75; discussion: 22–4. doi: 10.1093/eurheartj/ehi114
7. Hartupee J, Mann DL. Neurohormonal activation in heart failure with reduced ejection fraction. *Nat Rev Cardiol.* (2017) 14:30–8. doi: 10.1038/nrcardio.2016.163
8. Vaseghi M, Barwad P, Malavassi Corrales FJ, Tandri H, Mathuria N, Shah R, et al. Cardiac sympathetic denervation for refractory ventricular arrhythmias. *J Am Coll Cardiol.* (2017) 69:3070–80. doi: 10.1016/j.jacc.2017.04.035
9. Albani S, Fabris E, Doimo S, Barbati G, Perkan A, Merlo M, et al. Early occurrence of drug intolerance as risk factor during follow-up in patients with acute coronary syndrome or coronary revascularization. *Eur Heart J Cardiovasc Pharmacother.* (2018) 4:195–201. doi: 10.1093/ehjcvp/pvy017
10. Khan R, Kaul P, Islam S, Savu A, Bagai A, van Diepen S, et al. Drug adherence and long-term outcomes in non-revascularized patients following acute myocardial infarction. *Am J Cardiol.* 152:49–56. doi: 10.1016/j.amjcard.2021.04.031
11. Krum H, Schlaich M, Whitbourn R, Sobotka PA, Sadowski J, Bartus K, et al. Catheter-based renal sympathetic denervation for resistant hypertension: a multicentre safety and proof-of-principle cohort study. *Lancet.* (2009) 373:1275–81. doi: 10.1016/S0140-6736(09)60566-3
12. Bohm M, Linz D, Urban D, Mahfoud F, Ukena C. Renal sympathetic denervation: applications in hypertension and beyond. *Nat Rev Cardiol.* (2013) 10:465–76. doi: 10.1038/nrcardio.2013.89
13. Linz D, van Hunnik A, Ukena C, Ewen S, Mahfoud F, Schirmer SH, et al. Renal denervation: effects on atrial electrophysiology and arrhythmias. *Clin Res Cardiol.* (2014) 103:765–74. doi: 10.1007/s00392-014-0695-1
14. Chen H, Wang R, Xu F, Zang TT, Ji M, Yin JS, et al. Renal denervation mitigates atherosclerosis in ApoE$^{-/-}$ mice via the suppression of inflammation. *Am J Transl Res.* (2020) 12:5362–80.
15. Rafiq K, Fujisawa Y, Sherajee SJ, Rahman A, Sufiun A, Kobori H, et al. Role of the renal sympathetic nerve in renal glucose metabolism during the development of type 2 diabetes in rats. *Diabetologia.* (2015) 58:2885–98. doi: 10.1007/s00125-015-3771-9
16. Agarwal A, Yancy CW, Huffman MD. Improving Care for heart failure with reduced ejection fraction-A potential polypill-based strategy. *JAMA.* (2020) 324:2259–60. doi: 10.1001/jama.2020.21395
17. Sharp TE, 3rd, Polhemus DJ, Li Z, Spaletra P, Jenkins JS, Reilly JP, et al. Renal denervation prevents heart failure progression via inhibition of the renin-angiotensin system. *J Am Coll Cardiol.* (2018) 72:2609–21. doi: 10.1016/j.jacc.2018.08.2186
18. Huo JY, Jiang WY, Geng J, Chen C, Zhu L, Chen R, et al. Renal denervation attenuates pressure overload-induced cardiac remodelling in rats with biphasic regulation of autophagy. *Acta Physiol.* (2019) 226:e13272. doi: 10.1111/apha.13272

19. Steinberg JS, Shabanov V, Ponomarev D, Losik D, Ivanickiy E, Kropotkin E, et al. Effect of renal denervation and catheter ablation vs. catheter ablation alone on atrial fibrillation recurrence among patients with paroxysmal atrial fibrillation and hypertension: the ERADICATE-AF randomized clinical trial. *JAMA*. (2020) 323:248–55. doi: 10.1001/jama.2019.21187
20. Abbate A, Biondi-Zoccai GG, Baldi A. Pathophysiologic role of myocardial apoptosis in post-infarction left ventricular remodeling. *J Cell Physiol*. (2002) 193:145–53. doi: 10.1002/jcp.10174
21. Cleutjens JP, Verluyten MJ, Smiths JF, Daemen MJ. Collagen remodeling after myocardial infarction in the rat heart. *Am J Pathol*. (1995) 147:325–38.
22. Yamada S, Fong MC, Hsiao YW, Chang SL, Tsai YN, Lo LW, et al. Impact of renal denervation on atrial arrhythmogenic substrate in ischemic model of heart failure. *J Am Heart Assoc*. (2018) 7:e007312. doi: 10.1161/JAHA.117.007312
23. Gong L, Jiang F, Zhang Z, Wang X, Li H, Kuang Y, et al. Catheter-based renal denervation attenuates kidney interstitial fibrosis in a canine model of high-fat diet-induced hypertension. *Kidney Blood Press Res*. (2019) 44:628–42. doi: 10.1159/000500918
24. Yamada S, Lo LW, Chou YH, Lin WL, Chang SL, Lin YJ, et al. Renal denervation ameliorates the risk of ventricular fibrillation in overweight and heart failure. *Europace*. (2020) 22:657–66. doi: 10.1093/europace/euz335
25. Jiang W, Tan L, Guo Y, Li X, Tang X, Yang K. Effect of renal denervation procedure on left ventricular hypertrophy of hypertensive rats and its mechanisms. *Acta Cir Bras*. (2012) 27:815–20. doi: 10.1590/S0102-86502012001100012
26. Pastormerlo LE, Burchielli S, Ciardetti M, Aquaro GD, Grigoratos C, Castiglione V, et al. Myocardial salvage is increased after sympathetic renal denervation in a pig model of acute infarction. *Clin Res Cardiol*. (2021) 110:711–24. doi: 10.1007/s00392-020-01685-y
27. O'Meara E, Prescott MF, Claggett B, Rouleau JL, Chiang LM, Solomon SD, et al. Independent prognostic value of serum soluble ST2 measurements in patients with heart failure and a reduced ejection fraction in the PARADIGM-HF trial (prospective comparison of ARNI with ACEI to determine impact on global mortality and morbidity in heart failure). *Circ Heart Fail*. (2018) 11:e004446. doi: 10.1161/CIRCHEARTFAILURE.117.004446
28. Emdin M, Aimo A, Vergaro G, Bayes-Genis A, Lupon J, Latini R, et al. sST2 Predicts outcome in chronic heart failure beyond NT-proBNP and high-sensitivity troponin T. *J Am Coll Cardiol*. (2018) 72:2309–20. doi: 10.1016/j.jacc.2018.08.2165
29. Aimo A, Januzzi JL Jr, Vergaro G, Richards AM, Lam CSP, Latini R, et al. Circulating levels and prognostic value of soluble ST2 in heart failure are less influenced by age than N-terminal pro-B-type natriuretic peptide and high-sensitivity troponin T. *Eur J Heart Fail*. (2020) 22:2078–88. doi: 10.1002/ejhf.1701
30. Matilla L, Arrieta V, Jover E, Garcia-Pena A, Martinez-Martinez E, Sadaba R, et al. Soluble St2 induces cardiac fibroblast activation and collagen synthesis via neuropilin-1. *Cells*. (2020) 9:1667. doi: 10.3390/cells9071667
31. Matilla L, Ibarrola J, Arrieta V, Garcia-Pena A, Martinez-Martinez E, Sadaba R, et al. Soluble ST2 promotes oxidative stress and inflammation in cardiac fibroblasts: an *in vitro* and *in vivo* study in aortic stenosis. *Clin Sci*. (2019) 133:1537–48. doi: 10.1042/CS20190475
32. Zheng G, Jiang C, Li Y, Yang D, Ma Y, Zhang B, et al. TMEM43-S358L mutation enhances NF-kappaB-TGFbeta signal cascade in arrhythmogenic right ventricular dysplasia/cardiomyopathy. *Protein Cell*. (2019) 10:104–19. doi: 10.1007/s13238-018-0563-2
33. Liu C, Chen X, Yang L, Kisseleva T, Brenner DA, Seki E. Transcriptional repression of the transforming growth factor beta (TGF-beta) Pseudoreceptor BMP and activin membrane-bound inhibitor (BAMBI) by Nuclear Factor kappaB (NF-kappaB) p50 enhances TGF-beta signaling in hepatic stellate cells. *J Biol Chem*. (2014) 289:7082–91. doi: 10.1074/jbc.M113.543769
34. Yao W, Wang N, Qian J, Bai L, Zheng X, Hou G, et al. Renal sympathetic denervation improves myocardial apoptosis in rats with isoproterenol-induced heart failure by downregulation of tumor necrosis factor-α and nuclear factor-κB. *Exp Ther Med*. (2017). 14:4104–10. doi: 10.3892/etm.2017.5066
35. Su E, Zhao L, Yang X, Zhu B, Liu Y, Zhao W, et al. Aggravated endothelial endocrine dysfunction and intimal thickening of renal artery in high-fat diet-induced obese pigs following renal denervation. *BMC Cardiovasc Disord*. (2020) 20:176. doi: 10.1186/s12872-020-01472-7
36. Timmers L, Sluijter JP, Verlaan CW, Steendijk P, Cramer MJ, Emons M, et al. Cyclooxygenase-2 inhibition increases mortality, enhances left ventricular remodeling, and impairs systolic function after myocardial infarction in the pig. *Circulation*. (2007) 115:326–32. doi: 10.1161/CIRCULATIONAHA.106.647230
37. Garcia-Touchard A, Maranillo E, Mompeo B, Sanudo JR. Microdissection of the human renal nervous system: implications for performing renal denervation procedures. *Hypertension*. (2020) 76:1240–6. doi: 10.1161/HYPERTENSIONAHA.120.15106
38. Gao JQ, Xie Y, Yang W, Zheng JP, Liu ZJ. Effects of percutaneous renal sympathetic denervation on cardiac function and exercise tolerance in patients with chronic heart failure. *Rev Port Cardiol*. (2017) 36:45–51. doi: 10.1016/j.repce.2016.12.006
39. Kresoja KP, Rommel KP, Fengler K, von Roeder M, Besler C, Lucke C, et al. Renal sympathetic denervation in patients with heart failure with preserved ejection fraction. *Circ Heart Fail*. (2021) 14:e007421. doi: 10.1161/CIRCHEARTFAILURE.120.007421
40. Fukuta H, Goto T, Wakami K, Kamiya T, Ohte N. Effects of catheter-based renal denervation on heart failure with reduced ejection fraction: a meta-analysis of randomized controlled trials. *Heart Fail Rev*. (2020). doi: 10.1007/s10741-020-09974-4. [Epub ahead of print].
41. Krum H, Schlaich MP, Sobotka PA, Böhm M, Mahfoud F, Rocha-Singh K, et al. Percutaneous renal denervation in patients with treatment-resistant hypertension: final 3-year report of the Symplicity HTN-1 study. *Lancet*. (2014) 383:622–9. doi: 10.1016/S0140-6736(13)62192-3
42. Esler MD, Bohm M, Sievert H, Rump CL, Schmieder RE, Krum H, et al. Catheter-based renal denervation for treatment of patients with treatment-resistant hypertension: 36 month results from the SYMPLICITY HTN-2 randomized clinical trial. *Eur Heart J*. (2014) 35:1752–9. doi: 10.1093/eurheartj/ehu209
43. Ambari AM, Setianto B, Santoso A, Radi B, Dwiputra B, Susilowati E, et al. Angiotensin converting enzyme inhibitors (ACEIs) decrease the progression of cardiac fibrosis in rheumatic heart disease through the inhibition of IL-33/sST2. *Front Cardiovasc Med*. (2020) 7:115. doi: 10.3389/fcvm.2020.00115
44. Weir RA, Miller AM, Murphy GE, Clements S, Steedman T, Connell JM, et al. Serum soluble ST2: a potential novel mediator in left ventricular and infarct remodeling after acute myocardial infarction. *J Am Coll Cardiol*. (2010) 55:243–50. doi: 10.1016/j.jacc.2009.08.047

Conflict of Interest: The authors declare that the research was conducted in the absence of any commercial or financial relationships that could be construed as a potential conflict of interest.

Publisher's Note: All claims expressed in this article are solely those of the authors and do not necessarily represent those of their affiliated organizations, or those of the publisher, the editors and the reviewers. Any product that may be evaluated in this article, or claim that may be made by its manufacturer, is not guaranteed or endorsed by the publisher.

Copyright © 2021 Chen, Wang, Li, Yin, Ge, Xu, Zang, Pei, Li, Shen and Ge. This is an open-access article distributed under the terms of the Creative Commons Attribution License (CC BY). The use, distribution or reproduction in other forums is permitted, provided the original author(s) and the copyright owner(s) are credited and that the original publication in this journal is cited, in accordance with accepted academic practice. No use, distribution or reproduction is permitted which does not comply with these terms.

frontiers in Cardiovascular Medicine

ORIGINAL RESEARCH
published: 28 October 2021
doi: 10.3389/fcvm.2021.762576

A Predictive Model Based on a New CI-AKI Definition to Predict Contrast Induced Nephropathy in Patients With Coronary Artery Disease With Relatively Normal Renal Function

Hanjun Mo[1†], Fang Ye[2†], Danxia Chen[1], Qizhe Wang[1], Ru Liu[1], Panpan Zhang[1], Yaxin Xu[1], Xuelin Cheng[1], Zhendong Mei[3], Yan Zheng[3,4,5], Yuxiang Dai[4], Sunfang Jiang[1,6]* and Junbo Ge[4]*

[1] Department of General Practice, Zhongshan Hospital, Fudan University, Shanghai, China, [2] Department of Radiology, Zhongshan Hospital, Fudan University, Shanghai, China, [3] State Key Laboratory of Genetic Engineering, School of Life Sciences, Human Phenome Institute, Fudan University, Shanghai, China, [4] Department of Cardiology, Zhongshan Hospital, National Clinical Research Center for Interventional Medicine, Shanghai Institute of Cardiovascular Disease, Shanghai, China, [5] Ministry of Education Key Laboratory of Public Health Safety, School of Public Health, Fudan University, Shanghai, China, [6] Health Management Center, Zhongshan Hospital, Fudan University, Shanghai, China

OPEN ACCESS

Edited by:
Hongmei Tan,
Sun Yat-sen University, China

Reviewed by:
Yafeng Li,
Shanxi Provincial People's Hospital, China
Zhiyong Lei,
University Medical Center Utrecht, Netherlands

***Correspondence:**
Sunfang Jiang
jiang.sunfang@zs-hospital.sh.cn
Yuxiang Dai
dai.yuxiang@zs-hospital.sh.cn

[†]These authors have contributed equally to this work

Specialty section:
This article was submitted to General Cardiovascular Medicine, a section of the journal Frontiers in Cardiovascular Medicine

Received: 22 August 2021
Accepted: 04 October 2021
Published: 28 October 2021

Citation:
Mo H, Ye F, Chen D, Wang Q, Liu R, Zhang P, Xu Y, Cheng X, Mei Z, Zheng Y, Dai Y, Jiang S and Ge J (2021) A Predictive Model Based on a New CI-AKI Definition to Predict Contrast Induced Nephropathy in Patients With Coronary Artery Disease With Relatively Normal Renal Function. Front. Cardiovasc. Med. 8:762576. doi: 10.3389/fcvm.2021.762576

Background: Contrast induced nephropathy (CIN) is a common complication in patients receiving intravascular contrast media. In 2020, the American College of Radiology and the National Kidney Foundation issued a new contrast induced acute kidney injury (CI-AKI) criteria. Therefore, we aimed to explore the potential risk factors for CIN under the new criteria, and develop a predictive model for patients with coronary artery disease (CAD) with relatively normal renal function (NRF).

Methods: Patients undergoing coronary angiography or percutaneous coronary intervention at Zhongshan Hospital, Fudan University between May 2019 and April 2020 were consecutively enrolled. Eligible candidates were selected for statistical analysis. Univariate and multivariate logistic regression analyses were used to identify the predictive factors. A stepwise method and a machine learning (ML) method were used to construct a model based on the Akaike information criterion. The performance of our model was evaluated using the area under the receiver operating characteristic curves (AUC) and calibration curves. The model was further simplified into a risk score.

Results: A total of 2,009 patients with complete information were included in the final statistical analysis. The results showed that the incidence of CIN was 3.2 and 1.2% under the old and new criteria, respectively. Three independent predictors were identified: baseline uric acid level, creatine kinase-MB level, and log (N-terminal pro-brain natriuretic peptide) level. Our stepwise model had an AUC of 0.816, which was higher than that of the ML model (AUC = 0.668, $P = 0.09$). The model also achieved accurate predictions regarding calibration. A risk score was then developed, and patients were divided into two risk groups: low risk (total score < 10) and high risk (total score ≥ 10).

Conclusions: In this study, we first identified important predictors of CIN in patients with CAD with NRF. We then developed the first CI-AKI model on the basis of the new criteria, which exhibited accurate predictive performance. The simplified risk score may be useful in clinical practice to identify high-risk patients.

Keywords: contrast induced nephropathy (CIN), coronary artery disease, contrast media (CM), incidence, risk factor, predictive model

INTRODUCTION

With the application of interventional therapy in cardiovascular diseases, coronary angiography (CAG) has become the gold standard for diagnosing coronary artery disease (CAD). Percutaneous coronary intervention (PCI) has also become one of the most important treatments for patients with CAD. Regardless of the above treatments, use of contrast media (CM) is essential. However, due to the nephrotoxicity of CM, patients exposed to them may develop contrast induced nephropathy (CIN), also known as contrast induced acute kidney injury (CI-AKI). CIN is the third leading cause of hospital-acquired acute kidney injury (1). This complication prolongs the patient's hospital stay and increases medical expenses, resulting in irreversible kidney injury, need for dialysis, or even death (2). Since CIN does not have effective therapies, early identification of high-risk patients and effective interventions are extremely important.

CIN is usually defined as an increase of ≥0.5 mg/dL or ≥25% in baseline serum creatinine (SCr), within 48–72 h after exposure to CM, excluding other causes of renal function impairment (3). In January 2020, the American College of Radiology and the National Kidney Foundation jointly issued a consensus (4) and recommended that the diagnostic criteria of CA-AKI/CI-AKI be referred to the one proposed by kidney disease improving global outcomes (KDIGO), that is, when within 48 h of CM administration, the SCr increased by ≥0.3 mg/dL (26.5 μmol/L) or ≥1.5 times the baseline value (5). To date, few studies have compared the incidence of CIN based on these two diagnostic criteria, and no model has been constructed on the basis of the new criteria.

Baseline renal insufficiency is the most important risk factor for CIN, and many other risk factors, such as advanced age and diabetes, have also been recognized (6). In clinical practice, patients with chronic kidney disease (CKD) undergo hydration before and after surgery (7, 8). However, for those with relatively normal renal function (NRF), it remains unknown whether there are new, unique indicators that can predict the occurrence of CIN. Therefore, we aimed to explore the potential risk factors for CIN among patients with CAD with NRF and establish a predictive model based on new criteria.

METHODS

Study Population

Consecutive patients undergoing CAG or PCI at Zhongshan Hospital, Fudan University, between May 2019 and April 2020, were retrospectively enrolled. Demographic data and baseline clinical characteristics were recorded, including age, sex, blood pressure, comorbidities, medical history, laboratory examinations, and procedure-associated factors. The endpoint was CIN occurrence. Inclusion criteria were patients diagnosed with CAD by CAG, with documented renal function (SCr level) at baseline and 48 h after the procedure. Exclusion criteria were patients receiving continuous dialysis for end-stage renal disease, exposure to CM within 1 week before surgery, use of nephrotoxic drugs, severe infections and liver insufficiency, combined with tumors, allergy to CM, and women during pregnancy and lactation. All included patients used low- or iso-osmolarity contrast agents and did not receive hydration therapy. The study was approved by the ethics committee of Zhongshan Hospital, Fudan University. A written informed consent was obtained from all patients upon admission, which allow for the analysis of clinical data for the purpose of scientific study.

Clinical Definitions

"Contrast induced nephropathy (CIN)" or "Contrast induced acute kidney injury (CI-AKI)" was defined as an increase of ≥50% or 0.3 mg/dL in pre-PCI serum creatinine at 48 h after surgery (4). "Coronary artery disease (CAD)" was defined as at least one major coronary artery (left main artery, left anterior descending artery, left circumflex artery, or right coronary artery) stenosis ≥50%, confirmed by CAG (9). "Hypertension" was defined as systolic blood pressure ≥140 mmHg and/or diastolic blood pressure ≥90 mmHg, or previous diagnosis of hypertension and taking antihypertensive medications (10, 11). "Diabetes mellitus" was defined on the basis of the American Diabetes Association criteria (12). "Moderate to severe congestive heart failure (CHF)" was defined as New York Heart Association (NYHA) functional class III–IV (13). "Anemia" was defined as a hematocrit value <39% for men and <36% for women (14). Hyperuricemia was defined as fasting serum uric acid level >7.0 mg/dL in men and >6.0 mg/dL in women (15). Perioperative myocardial infarction was defined on the basis of the fourth universal definition of MI (16).

Development of Stepwise Model and Risk Score

The data were preprocessed before the formal analysis, and missing values of eGFR were handled on the basis of the CKD-EPI formula (consistent with previously recorded data) (17). Values in the variables of "Hypertension" and "Diabetes Mellitus" were corrected on the basis of the definitions, in combination with actual blood pressure and blood glucose

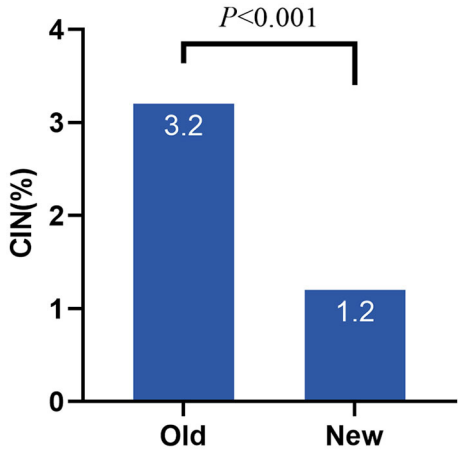

FIGURE 1 | Incidence of CIN under different criteria. CIN, contrast induced nephropathy; Old, old criteria; New, new criteria.

level (or glycosylated hemoglobin) of patients. Univariate and multivariate logistic regression analyses were used to identify the predictive factors. Variables with a $P < 0.1$ in the univariate analysis were available for further multivariate regression. A stepwise selection method was used to construct the best model on the basis of the Akaike information criterion (AIC). We also used the machine learning (ML) method (elastic net) to select statistically significant variables as a supplementary verification.

To evaluate the performance of our stepwise model, we used the area under the receiver operating characteristic curves (AUC) and calibration curves. Subsequently, to facilitate clinical use, we simplified the stepwise model and converted it into a risk score. Receiver operating characteristic (ROC) curves were used to identify the cut-off values of the continuous variables. Weighted scores were assigned to each risk factor on the basis of their new odds ratios (ORs). On the basis of their total scores, patients were further divided into different risk groups.

Statistical Analysis

All statistical analyses and plotting were performed using R 3.6.3 (Lucent Technologies, New Providence, the United States, https://www.r-project.org) and GraphPad Prism 8 (GraphPad Software, LaJolla, CA, USA, https://www.graphpad.com/scientific-software/prism). Some of the R packages "tidyverse," "MASS," "pROC," "RMS" were used. Continuous variables conforming to the normal distribution were represented as mean ± standard deviation (SD); otherwise, they are presented as median (interquartile range). Categorical variables were expressed as frequency (percentage) using the chi-square test or Fisher's exact test. All *P*-values were two-sided, and statistical significance was set at $P < 0.05$.

RESULTS

Patients and Clinical Characteristics

A total of 2,383 patients with CAD after the procedure were included consecutively in this study. Some patients were excluded

TABLE 1 | Basic characteristics of the CIN and non-CIN groups.

	Total (n = 2,009)	CIN (n = 24)	Non-CIN (n = 1,985)	*P*-value
Demographics and clinical characteristics				
Age, years	63.3 (±9.9)	62.9 (±11.0)	63.3 (±9.8)	0.82
Sex	1,588 (79.0%)	22 (91.7%)	1,566 (78.9%)	0.20
Male				
Female	421 (21.0%)	2 (8.3%)	419 (21.1%)	
BMI	25.1 (±3.0)	25.0 (±3.0)	25.1 (±3.0)	0.76
Missing	45 (2.2%)	1 (4.2%)	44 (2.2%)	
Systolic blood pressure, mmHg	133.7 (±19.2)	140.2 (±19.6)	133.6 (±19.1)	0.17
Missing	6 (0.3%)	0 (0%)	6 (0.3%)	
Diastolic blood pressure, mmHg	78.6 (±10.9)	84.9 (±13.1)	78.6 (±10.8)	**0.018**
Missing	6 (0.3%)	0 (0%)	6 (0.3%)	
Heart rate, per min	76.2 (±11.7)	82.5 (±19.3)	76.1 (±11.6)	0.063
Missing	3 (0.1%)	0 (0%)	3 (0.2%)	
Smoking	1,082 (53.9%)	10 (41.7%)	1,072 (54.0%)	**0.049**
Never				
Former	378 (18.8%)	2 (8.3%)	376 (18.9%)	
Current	547 (27.2%)	12 (50.0%)	535 (27.0%)	
Missing	2 (0.1%)	0 (0.0%)	2 (0.1%)	
CAD subtype	1,548 (77.1%)	11 (45.8%)	1,537 (77.4%)	**<0.001**
Stable CAD				
ACS	461 (22.9%)	13 (54.2%)	448 (22.6%)	
NYHA classification	1,818 (90.5%)	19 (79.2%)	1,799 (90.6%)	0.06
I				
II	160 (8.0%)	3 (12.5%)	157 (7.9%)	
III	29 (1.4%)	2 (8.3%)	27 (1.4%)	
IV	2 (0.1%)	0 (0.0%)	2 (0.1%)	
Comorbidities				
Hypertension	1,495 (74.4%)	16 (66.7%)	1,479 (74.5%)	0.36
Diabetes mellitus	822 (40.9%)	9 (37.5%)	813 (41.0%)	0.84
Dyslipidemia				
No	1,724 (85.8%)	21 (87.5%)	1,703 (85.8%)	0.93
Hypercholesterolemia	148 (7.4%)	2 (8.3%)	146 (7.4%)	
Hypertriglyceridemia	42 (2.1%)	0 (0.0%)	42 (2.1%)	
Combined	95 (4.7%)	1 (4.2%)	94 (4.7%)	
Previous AMI	216 (10.8%)	6 (25.0%)	210 (10.6%)	**0.037**
Previous PCI	676 (33.6%)	6 (25.0%)	670 (33.8%)	0.51
Previous CABG	31 (1.5%)	1 (4.2%)	30 (1.5%)	0.31
Family history of CAD	95 (4.7%)	0 (0.0%)	95 (4.8%)	0.63
Prior medication use				
Anti-platelet	1,718 (85.5%)	19 (79.2%)	1,699 (85.6%)	0.37
Aspirin	1,582 (78.7%)	18 (75.0%)	1,564 (78.8%)	0.62
Clopidogrel	799 (39.8%)	10 (41.7%)	789 (39.7%)	0.84
Missing	4 (0.2%)	0 (0.0%)	4 (0.2%)	
Statins	1,565 (77.9%)	18 (75.0%)	1,547 (77.9%)	0.63
Missing	9 (0.4%)	0 (0.0%)	9 (0.5%)	
ACEI/ARB	955 (47.5%)	10 (41.7%)	945 (47.6%)	0.68
Beta-blockers	952 (47.4%)	12 (50.0%)	940 (47.4%)	0.84
Calcium channel blockers	586 (29.2%)	6 (25.0%)	580 (29.2%)	0.82

(Continued)

TABLE 1 | Continued

	Total (n = 2,009)	CIN (n = 24)	Non-CIN (n = 1,985)	*P*-value
Nitrates	743 (37.0%)	9 (37.5%)	734 (37.0%)	1.0
Diuretics	161 (8.0%)	2 (8.3%)	159 (8.0%)	1.0
Laboratory data				
LVEF, %	61.9 (±7.6)	56.2 (±10.6)	62.0 (±7.6)	**0.003**
Missing	78 (3.9%)	0 (0%)	78 (3.9%)	
LVESD, mm	31.5 (±5.4)	35.4 (±9.7)	31.5 (±5.3)	**0.029**
Missing	78 (3.9%)	0 (0%)	78 (3.9%)	
LVEDD, mm	47.9 (±5.3)	49.2 (±7.0)	47.9 (±5.3)	0.75
Missing	78 (3.9%)	0 (0%)	78 (3.9%)	
RBC, $\times 10^{12}$ cells per L	4.4 (±0.5)	4.4 (±0.7)	4.4 (±0.5)	0.58
Hemoglobin, g/L	135.9 (±14.5)	137.0 (±20.1)	135.9 (±14.5)	0.60
Hematocrit, %	40.4 (±4.0)	40.3 (±5.4)	40.4 (±4.0)	0.86
WBC, $\times 10^{9}$ cells per L	6.7 (±1.9)	7.6 (±2.4)	6.7 (±1.9)	0.098
Neutrophils, %	61.2 (±9.4)	67.9 (±13.7)	61.1 (±9.3)	**0.002**
Lymphocytes, %	27.5 (±8.3)	21.5 (±11.1)	27.6 (±8.2)	**0.002**
NLR	2.7 (±2.3)	5.3 (±5.7)	2.7 (±2.2)	**0.002**
Eosinophils, %	2.6 (±2.2)	1.9 (±1.8)	2.6 (±2.2)	**0.041**
RDW, %	12.6 (±0.8)	12.8 (±1.0)	12.6 (±0.8)	0.29
PDW, %	13.1 (±2.6)	12.1 (±2.5)	13.1 (±2.6)	**0.036**
Missing	14 (0.7%)	0 (0%)	14 (0.7%)	
Albumin, g/L	42.3 (±3.8)	41.9 (±4.4)	42.3 (±3.8)	0.44
Missing	2 (0.1%)	1 (4.2%)	1 (0.1%)	
ALT, U/L	27.9 (±19.7)	32.7 (±17.8)	27.9 (±19.7)	0.086
Missing	2 (0.1%)	1 (4.2%)	1 (0.1%)	
AST, U/L	26.9 (±24.8)	57.7 (±77.5)	26.5 (±23.4)	**<0.001**
Missing	2 (0.1%)	1 (4.2%)	1 (0.1%)	
Baseline urea, mmol/L	5.8 (±1.6)	5.9 (±2.0)	5.8 (±1.6)	0.62
Baseline creatinine, μmol/L	78.9 (±14.9)	79.5 (±17.3)	78.9 (±14.9)	0.94
Baseline eGFR, mL/(min·1.73 m^2)	85.2 (±13.0)	85.8 (±14.0)	85.2 (±13.0)	0.68
Baseline UA, μmol/L	343.9 (±87.1)	380.2 (±112.2)	343.5 (±86.7)	0.20
FBG, mmol/L	7.2 (±3.3)	7.2 (±2.8)	7.2 (±3.3)	0.61
Missing	28 (1.4%)	1 (4.2%)	27 (1.4%)	
HbA1c, %	6.5 (±1.3)	6.2 (±0.9)	6.5 (±1.3)	0.49
Missing	91 (4.5%)	3 (12.5%)	88 (4.4%)	
TC, mmol/L	3.7 (±1.1)	4.1 (±1.0)	3.7 (±1.1)	0.055
Missing	6 (0.3%)	0 (0%)	6 (0.3%)	
TG, mmol/L	1.9 (±1.4)	1.6 (±0.7)	1.9 (±1.4)	0.29
Missing	6 (0.3%)	0 (0%)	6 (0.3%)	
LDL, mmol/L	1.9 (±1.0)	2.3 (±1.0)	1.9 (±1.0)	**0.015**
Missing	6 (0.3%)	0 (0%)	6 (0.3%)	
NHDL, mmol/L	2.7 (±1.1)	3.0 (±1.0)	2.7 (±1.1)	**0.041**
Missing	6 (0.3%)	0 (0%)	6 (0.3%)	
HDL, mmol/L	1.0 (±0.3)	1.0 (±0.3)	1.0 (±0.3)	0.84
Missing	6 (0.3%)	0 (0%)	6 (0.3%)	
Apo A-I, g/L	1.2 (±0.2)	1.2 (±0.2)	1.2 (±0.2)	0.90
Missing	7 (0.3%)	0 (0%)	7 (0.4%)	
Apo B, g/L	0.7 (±0.2)	0.8 (±0.2)	0.7 (±0.2)	**0.025**
Missing	7 (0.3%)	0 (0%)	7 (0.4%)	
Apo E, mg/L	38.8 (±16.7)	37.4 (±11.4)	38.8 (±16.7)	0.99
Missing	7 (0.3%)	0 (0%)	7 (0.4%)	
Lipoprotein, nmol/L	105.5 (±192.4)	116.4 (±257.8)	105.3 (±191.6)	0.47
Missing	7 (0.3%)	0 (0%)	7 (0.4%)	
CK-MB, U/L	18.5 (±28.0)	67.5 (±113.1)	17.9 (±24.7)	**0.025**
Missing	10 (0.5%)	0 (0%)	10 (0.5%)	
hs-CRP, mg/L	4.4 (±10.5)	6.9 (±9.9)	4.4 (±10.5)	**0.026**
Missing	19 (0.9%)	0 (0%)	19 (1.0%)	
cTnT, ng/mL	0.1 (±0.7)	0.9 (±2.1)	0.1 (±0.6)	**<0.001**
NT-proBNP, pg/mL	369.8 (±743.1)	1,372.1 (±1,690.6)	357.7 (±716.5)	**<0.001**
Missing	4 (0.2%)	0 (0%)	4 (0.2%)	
Procedural characteristics				
Contrast agent				
low-osmolarity	1,401 (69.7%)	20 (83.3%)	1,381 (69.6%)	0.18
iso-osmolarity	608 (30.3%)	4 (16.7%)	604 (30.4%)	
Contrast volume, mL	150.1 (±74.5)	167.1 (±84.0)	149.9 (±74.3)	0.42
Missing	24 (1.2%)	0 (0%)	24 (1.2%)	
Infarct-related artery, *N* (%)	214 (10.7%)	2 (8.3%)	212 (10.7%)	1.0
LM				
LAD	1,670 (83.1%)	19 (79.2%)	1,651 (83.2%)	0.58
LCX	1,224 (60.9%)	14 (58.3%)	1,210 (61.0%)	0.83
RCA	1,262 (62.8%)	15 (62.5%)	1,247 (62.8%)	1.0
No. of diseased vessel, *N* (%)	565 (28.1%)	8 (33.3%)	557 (28.1%)	0.93
1-vessel				
2-vessel	603 (30.0%)	6 (25.0%)	597 (30.1%)	
3-vessel	712 (35.4%)	9 (37.5%)	703 (35.4%)	
4-vessel	129 (6.4%)	1 (4.2%)	128 (6.4%)	
No. of stents used	1.4 (±1.0)	1.4 (±1.1)	1.4 (±1.0)	0.68
Total stent length, mm	40.7 (±30.5)	37.4 (±33.8)	40.8 (±30.5)	0.37
Missing	2 (0.1%)	0 (0%)	2 (0.1%)	

Continuous variables are shown as Mean (SD), and categorical variables are shown as frequency (percentage).

Boldface represents P <0.05.

BMI, body mass index; CAD, coronary artery disease; ACS, acute coronary syndrome; NYHA, New York Heart Association; AMI, acute myocardial infarction; PCI, percutaneous coronary intervention; CABG, coronary artery bypass grafting; ACEI, angiotensin converting enzyme inhibitor; ARB, angiotensin receptor blocker; LVEF, left ventricular ejection fraction; LVESD, left ventricular end-systolic dimension; LVEDD, left ventricular end-diastolic dimension; RBC, red blood cell; WBC, white blood cell; NLR, neutrophil to lymphocyte ratio; RDW, red cell distribution width; PDW, platelet distribution width; ALT, alanine transaminase; AST, aspartate aminotransferase; eGFR, estimated glomerular filtration rate calculated by the CKD-EPI equation; UA, uric acid; FBG, fasting blood glucose; HbA1c, glycosylated hemoglobin; TC, total cholesterol; TG, triglycerides; LDL, low-density lipoprotein cholesterol; NHDL, non-high-density lipoprotein cholesterol; HDL, high-density lipoprotein cholesterol; Apo A-I, apolipoprotein A1; Apo B, apolipoprotein B; Apo E, apolipoprotein E; CK-MB, creatine kinase-MB; hs-CRP, high-sensitivity C-reactive protein; cTnT, cardiac troponin T; NT-proBNP, N-terminal pro-brain natriuretic peptide; LM, left main coronary artery; LAD, left anterior descending; LCX, left circumflex artery; RCA, right coronary artery.

from the study: 41 cases without significant coronary artery lesions, 66 with a history of chronic kidney disease (CKD), 265 with eGFR<60 mL/min/1.73 m^2, and 2 with hepatic insufficiency. In all, 2,009 patients were included in the statistical analysis. Based on the old criteria, the incidence of CIN was 3.2%, whereas it declined to 1.2% under the new criteria (**Figure 1**).

The baseline demographic and clinicopathologic features are listed in **Table 1**. Overall, the mean age of all patients was 63.3 years, and 79.0% were male. Regarding CAD subtypes and comorbidities, 22.9% had ACS, 74.4% had hypertension, and 40.9% had diabetes mellitus. Patients who underwent low-osmolarity CM accounted for 69.7% of the patients, and the mean volume of contrast was 150.17 ± 4.5 mL. Patients who developed CIN (CINs) and those who did not (non-CINs) differed substantially with respect to the following variables: diastolic blood pressure, smoking status, CAD subtype, previous acute myocardial infarction (AMI) history, and laboratory examinations (left ventricular ejection fraction, left ventricular end-systolic dimension, neutrophils, lymphocytes, neutrophil to lymphocyte ratio, eosinophils, platelet distribution width, aspartate aminotransferase [AST], low density lipoprotein, non-high-density lipoprotein, apolipoprotein B, creatine kinase-MB [CK-MB], high-sensitivity C-reactive protein, cardiac troponin T [cTnT], and N-terminal pro-brain natriuretic peptide [NT-proBNP] levels).

Univariate and Multivariate Analysis

All the variables in **Table 1** were used in the subsequent univariate analysis, and some skewed variables (for example, alanine transaminase [ALT] and AST) were log-transformed. **Table 2** shows the factors with a $P < 0.1$. A total of 22 variables were significantly associated with the development of CIN, namely vital signs, medical history, comorbidities, cardiac ultrasound, and laboratory indexes. Afterward, considering the collinearity of some existing variables, we retained systolic blood pressure and LVEF instead of diastolic blood pressure and LVESD. A stepwise logistic regression was performed to construct the model. The final multivariate results are shown in **Table 3**. Baseline uric acid (UA), CK-MB, and log (NT-proBNP) levels were identified as independent predictors of CIN. The AIC of the model was 213.63 (**Table 3**).

Performance of the Stepwise Model

The performance of our stepwise model was evaluated using the AUC and the calibration curve (**Figure 2**). The AUC of the stepwise model was compared with that of the machine learning (ML) model, and the calibration was performed using internal validation. The AUC of the stepwise model was 0.816, which was higher than that of the ML model (AUC = 0.668, $P = 0.09$, **Figure 2A**). The calibration curve showed that the predictive incidence was significantly associated with the actual probability of CIN (**Figure 2B**).

Simplified Risk Score Development

To facilitate implementation in clinical practice, we simplified the stepwise model to a risk score. The cut-off values of the three variables were identified using ROC curves (**Supplementary Figure 1**). We chose baseline UA ≥450 μmol/L, CK-MB ≥48 U/L, and NT-proBNP ≥850 pg/mL as the cut-off values, and the new multivariate results are shown in **Supplementary Table 1**. A weighted score of 1 was assigned to each OR value, and the final risk score is shown in **Figure 3**. The total scores of the patients in our cohort were between 0 and 17 points. Based on the total scores, we divided patients into two risk groups (low risk and high risk, corresponding to a total score of <10 and ≥10, respectively). The CIN incidence of patients in the low-risk group was 1.0%, while the incidence increased to 14.8% when the total score was ≥10 (**Figure 4**).

TABLE 2 | Univariate analysis in our cohort.

Variables	OR	95% CI	*P*-value
Systolic blood pressure, / 10 mmHg	1.19	0.97–1.45	0.091
Diastolic blood pressure, / 10 mmHg	1.68	1.17–2.40	0.005
Heart rate, per min	1.04	1.01–1.07	0.007
Smoking (current smokers)	2.71	1.20–6.13	0.016
Previous AMI history	2.82	1.01–6.80	0.030
ACS	4.05	1.80–9.29	0.001
Congestive heart failure (NYHA III-IV)	6.13	0.95–22.18	0.017
LVEF, %	0.94	0.90–0.97	0.000
LVEF < 45 %	4.13	1.18–11.21	0.011
LVESD, mm	1.08	1.03–1.12	0.001
WBC, $\times 10^9$ cells per L	1.22	1.02–1.43	0.020
NLR	1.14	1.07–1.21	0.000
PDW, %	0.83	0.67–1.00	0.065
Log (AST), U/L	3.39	1.96–5.57	0.000
Baseline UA, μmol/L	1.00	1.00–1.01	0.040
TC, mmol/L	1.28	0.93–1.64	0.083
LDL, mmol/L	1.39	1.01–1.78	0.018
NHDL, mmol/L	1.29	0.93–1.67	0.085
Apo B, g/L	3.62	0.84–12.39	0.059
CK-MB, U/L	1.01	1.01–1.02	0.000
cTnT, ng/mL	1.49	1.19–1.80	0.000
Log (NT-proBNP), pg/mL	2.04	1.54–2.74	0.000

Variables with P < 0.1 are included in the table.
OR, odds ratio; CI, confidence interval; AMI, acute myocardial infarction; ACS, acute coronary syndrome; NYHA, New York Heart Association; LVEF, left ventricular ejection fraction; LVESD, left ventricular end-systolic dimension; WBC, white blood cell; NLR, neutrophil to lymphocyte ratio; PDW, platelet distribution width; AST, aspartate aminotransferase; UA, uric acid; TC, total cholesterol; LDL, low-density lipoprotein cholesterol; NHDL, non-high-density lipoprotein cholesterol; Apo B, apolipoprotein B; CK-MB, creatine kinase-MB; cTnT, cardiac troponin T; NT-proBNP, N-terminal pro-brain natriuretic peptide.

TABLE 3 | Multivariate analysis and the independent predictors in our cohort.

Variables	Model coefficient	OR	95% CI	*P*-value
Baseline UC	0.005	1.00	1.00–1.01	0.040
CK-MB, U/L	0.011	1.01	1.01–1.02	<0.001
Log (NT-proBNP), pg/mL	0.661	1.94	1.45–2.63	<0.001

AIC = 213.63.
OR, odds ratio; CI, confidence interval; UA, uric acid; CK-MB, creatine kinase MB; NT-proBNP, N-terminal pro-brain natriuretic peptide.

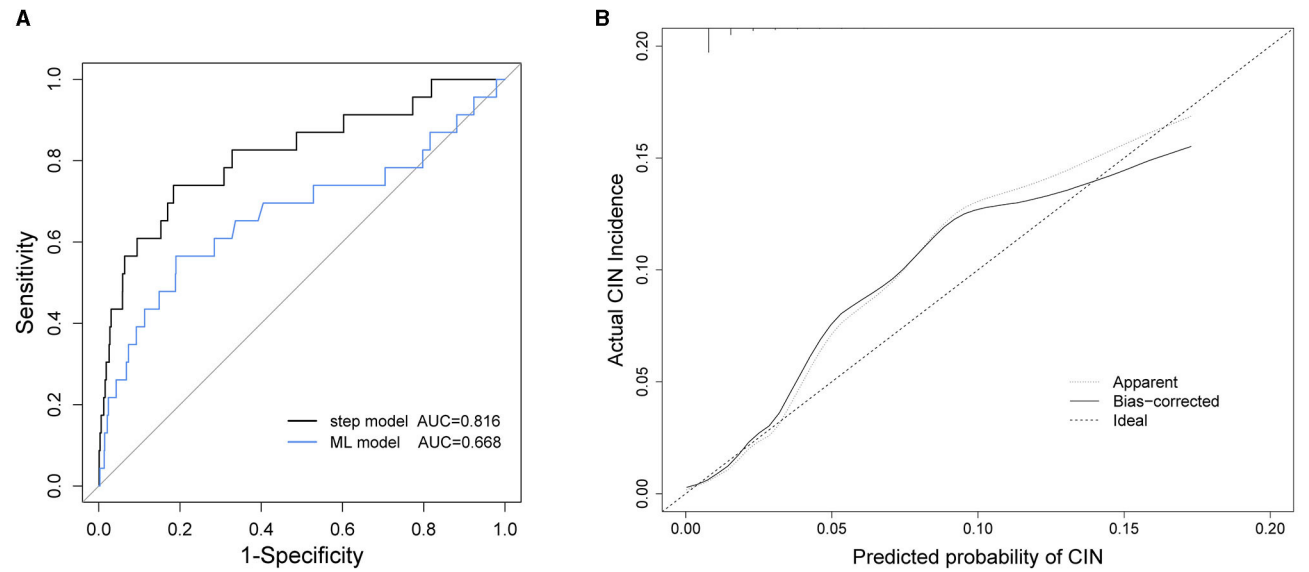

FIGURE 2 | (A) Receiver operating characteristic (ROC) curves of stepwise model and machine learning (ML) model. **(B)** Calibration curve of stepwise model. AUC, area under the receiver operating characteristic curves; CIN, contrast induced nephropathy.

Predictors	Scores	
Baseline UA>=450 μmol/L	3	
CK-MB>=48 U/L	8	
NT-proBNP>=850 pg/mL	6	
	Total Score	

FIGURE 3 | Simplified predictive score for CIN. UA, uric acid; CK-MB, creatine kinase MB; NT-proBNP, N-terminal pro-brain natriuretic peptide.

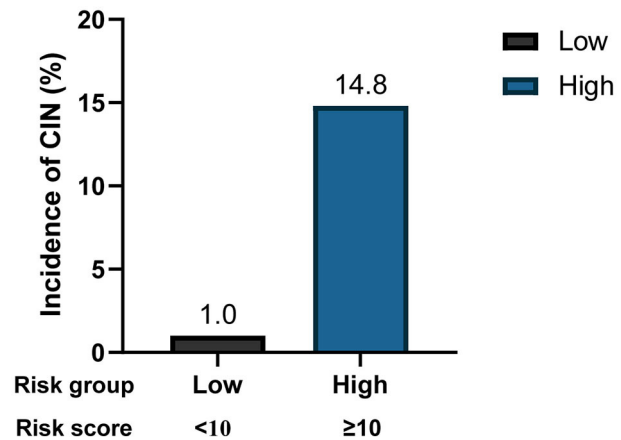

FIGURE 4 | CIN incidence based on different risk groups. CIN, contrast induced nephropathy.

DISCUSSION

In this study, we first compared the incidence of CIN using two different criteria. The incidence of CIN was generally low, with 3.4% under the old criteria and 1.6% under the new criteria. The incidence under the old criteria was very similar to the results of Rihal et al. (18). Therefore, based on the KDIGO criteria, the incidence of CIN decreased dramatically, indicating that the old definition of CIN, to some extent, may have exaggerated the development of CI-AKI. In addition, other factors such as the different study populations and the nature of the CAG procedure may also lead to the variance of incidence rate of CIN (19).

Next, we explored the risk factors for CIN development. The results showed that, except for traditional risk factors, there were other predictors of great importance for patients with relatively NRF. In the multivariate logistic regression analysis, we determined the predictive value of baseline UA, CK-MB, and log (NT-proBNP) levels. A stepwise model and a risk score were then constructed, and to the best of our knowledge, these two are the first CIN predictive models based on the new KDIGO criteria. Our model exhibited good predictive ability, with an AUC of 0.816. Furthermore, we simplified the model to a risk score, which facilitates its use by clinicians. Two risk groups were further defined: low-risk (<10 points) and high-risk (≥10 points). The incidence of CIN increased significantly as the score increased (**Figure 4**).

Hyperuricemia (or baseline UA level) has been widely confirmed to influence the occurrence of CIN (20). In the present study, baseline UA level was an independent risk factor (OR, 1.004; $P = 0.04$). Similarly, other studies have proved that hyperuricemia is significantly associated with a higher risk of

CI-AKI, regardless of renal function (15, 16). Nevertheless, it remains unknown whether UA lowering therapy can effectively reduce the incidence of CIN. A randomized controlled trial explored the role of allopurinol in preventing CIN after PCI and failed to show its efficacy (21). At any rate, it warned us that patients with high UA levels before PCI have the potential to develop CIN.

CK-MB is an early marker of myocardial injury with high specificity. Our analysis showed that CK-MB has an important value in predicting CIN (OR: 1.01, 95% CI: 1.01–1.02, $P < 0.001$). Previously, Zbierska-Rubinkiewicz et al. found that increased baseline CK-MB level was an independent risk factor for CIN among patients treated with PCI ($P = 0.001$) (22). The prediction model constructed by Gurm et al. also incorporated CK-MB as an important predictor (23). These findings are consistent with our results. Regarding the reason why cTnT was excluded from the model, we believe that this is due to the fact that the level of CK-MB is less affected by renal function; therefore, it can reflect patients' myocardial ischemia to a large extent. This makes CK-MB more favorable for predicting CIN.

Another finding in our study pertained to the level of NT-proBNP. In multivariate analysis, log (NT-proBNP) was statistically significant (OR, 1.94; 95%CI: 1.45–2.63, $P < 0.001$). BNP plays an important role in maintaining the circulating blood volume and osmotic pressure. In contrast, NT-proBNP, the precursor of BNP, is an important biomarker for the diagnosis of heart failure due to its long half-life and good *in vitro* stability (24). Nevertheless, since NT-proBNP is mainly filtered and cleared by the glomerulus, it is greatly affected by renal function. NT-proBNP has shown a predictive value for CIN in both STEMI and elective surgery patients (25–27). In 2015, Liu et al. found that preprocedural NT-proBNP levels could predict CIN as effectively as the Mehran risk score (13, 27). Our results are consistent with their work. When developing the simple risk score, we identified a cut-off value of NT-proBNP as $\geq$850 pg/mL and incorporated it into the model to achieve better prediction.

It is not clear why elevated NT-proBNP levels are associated with a higher risk of CIN. Some studies have proposed that BNP reduces the effects of catecholamines and potentiates the generation of nitric oxide, thereby potentially resulting in systemic vasodilation and renal hypoperfusion (27). Future research may further explore this potential mechanism.

Other recognized risk factors include advanced age, diabetes, CHF (NYHA III-IV), and anemia. In particular, Mehran et al. published a risk score that included eight variables: hypotension, IABP, CHF, CKD, diabetes, age >75 years, anemia, and volume of contrast (13). None of these variables showed statistical significance in our cohort, indicating that the three predictors (levels of UA, CK-MB, and NT-proBNP) were more significant. The type and amount of contrast medium are also associated with the development of CIN. It has been reported that the effect of the volume of contrast and CIN was dose dependent. In our study, the effect of contrast volume was not statistically significant (OR: 1.002, $P = 0.256$). We speculated that the amount of CM had little effect on patients with relatively NRF. Additionally, compared with studies conducted in Western countries, a smaller average amount of CM in our study (150.17 $\pm$ 4.5 mL) may also make the effect insignificant.

Our study is a well-designed research exploring the risk factors for predicting CIN in Chinese people, with a large sample size. The established stepwise model exhibited outstanding performance (AUC = 0.816) and could predict CIN precisely (**Figure 2**). The limitations of our work lie in the following aspects. First, the number of patients with CIN was relatively small. In other words, the incidence of CIN in our cohort was below average (new criteria: 1.2%). This may add some difficulty in determining the effects of the predictors. Moreover, the study was retrospective and could not control for all confounding factors. Finally, we used internal validation to evaluate the model in order to make full use of the data to construct the model. Therefore, additional external validation is required for further studies and model evaluation.

CONCLUSIONS

In the present study, we first identified three independent risk factors in patients with CAD with relatively NRF: baseline UA level, CK-MB level, and NT-proBNP level of CIN. Meanwhile, we developed the first stepwise model and risk score based on the new CI-AKI criteria, which exhibited accurate predictive ability. Two risk groups were defined on the basis of the total score of the patients. This simplified risk score may be helpful in clinical practice to identify high-risk patients in the future.

DATA AVAILABILITY STATEMENT

The raw data supporting the conclusions of this article will be made available by the authors, without undue reservation.

ETHICS STATEMENT

The studies involving human participants were reviewed and approved by the Ethics Committee of Zhongshan Hospital Fudan University (B2021-219). The patients/participants provided their written informed consent to participate in this study.

AUTHOR CONTRIBUTIONS

HM, FY, YD, SJ, and JG conceived and designed the study. HM, FY, ZM, YZ, and YD conducted the statistical analyses. HM and SJ drafted the manuscript. SJ and YD had full access to all the data and took responsibility for the integrity of the data and the accuracy of the data analysis. All authors participated in the interpretation of the results, revised the manuscript, read, and approved the final manuscript.

FUNDING

This study was supported by the National Key Research and Development Program of China (Grant No. 2016YFC1301200), the Program for Shanghai Outstanding Medical Academic Leader (Grant No. 2019LJ15), the Scientific Research Project

of Shanghai Science and Technology Commission (Grant No. 17ZR1404900), Clinical Research Plan of SHDC (Grant No. SHDC2020CR1007A), Animal Model Project of Shanghai Scientific Committee (Grant No. 19140900900), Natural Science Foundation of Shanghai (Grant No. 20ZR1439700), and Exploratory Clinical Research Projects of National Clinical Research Center for Interventional Medicine (Grant No. 2021-002). The funding agencies had no role in the design and conduct of the study, in the collection, management, analysis, interpretation of the data or in the preparation, review or approval of the manuscript, or decision to submit for publication.

SUPPLEMENTARY MATERIAL

The Supplementary Material for this article can be found online at: https://www.frontiersin.org/articles/10.3389/fcvm.2021.762576/full#supplementary-material

REFERENCES

1. Nash K, Hafeez A, Hou S. Hospital-acquired renal insufficiency. *Am J Kidney Dis.* (2002) 39:930–6. doi: 10.1053/ajkd.2002.32766
2. Almendarez M, Gurm HS, Mariani J. Jr., Montorfano M, Brilakis ES, Mehran R, et al. Procedural strategies to reduce the incidence of contrast-induced acute kidney injury during percutaneous coronary intervention. *JACC Cardiovasc Interv.* (2019) 12:1877–88. doi: 10.1016/j.jcin.2019.04.055
3. Khwaja A, KDIGO. Clinical practice guidelines for acute kidney injury. *Nephron Clinical Practice.* (2012) 120:C179–C84. doi: 10.1159/000339789
4. Davenport MS, Perazella MA, Yee J, Dillman JR, Fine D, McDonald RJ, et al. Use of intravenous iodinated contrast media in patients with kidney disease: consensus statements from the American college of radiology and the national kidney foundation. *Radiology.* (2020) 294:660–8. doi: 10.1148/radiol.2019192094
5. Palevsky PM, Liu KD, Brophy PD, Chawla LS, Parikh CR, Thakar CV, et al. KDOQI US commentary on the 2012 KDIGO clinical practice guideline for acute kidney injury. *Am J Kidney Dis.* (2013) 61:649–72. doi: 10.1053/j.ajkd.2013.02.349
6. Azzalini L, Spagnoli V, Ly HQ. Contrast-Induced Nephropathy: From Pathophysiology to Preventive Strategies. *Can J Cardiol.* (2016) 32:247–55. doi: 10.1016/j.cjca.2015.05.013
7. Liu Y, Tan N, Huo Y, Chen S, Liu J, Chen YD, et al. Hydration for prevention of kidney injury after primary coronary intervention for acute myocardial infarction: a randomised clinical trial. *Heart (British Cardiac Society).* (2021). doi: 10.1136/heartjnl-2021-319716. [Epub ahead of print].
8. Zhang F, Lu Z, Wang F. Advances in the pathogenesis and prevention of contrast-induced nephropathy. *Life Sci.* (2020) 259:118379. doi: 10.1016/j.lfs.2020.118379
9. Cassar A, Holmes DR. Jr., Rihal CS, Gersh BJ. *Chronic coronary artery disease: diagnosis and management. Mayo Clin Proc.* (2009) 84:1130–46. doi: 10.4065/mcp.2009.0391
10. Liu J. Highlights of the 2018 Chinese hypertension guidelines. *Clini Hypertens.* (2020) 26:8. doi: 10.1186/s40885-020-00141-3
11. Joint Committee for Guideline Revision. 2018 Chinese guidelines for prevention and treatment of hypertension-a report of the revision committee of chinese guidelines for prevention and treatment of hypertension. *J Geriatr Cardiol.* (2019) 16:182–241. doi: 10.11909/j.issn.1671-5411.2019.03.014
12. American Diabetes Association. Classification and diagnosis of diabetes: standards of medical care in diabetes-2019. *Diabetes Care.* (2019) 42:S13–s28. doi: 10.2337/dc19-S002
13. Mehran R, Aymong ED, Nikolsky E, Lasic Z, Iakovou I, Fahy M, et al. A simple risk score for prediction of contrast-induced nephropathy after percutaneous coronary intervention: development and initial validation. *J Am Coll Cardiol.* (2004) 44:1393–9. doi: 10.1016/S0735-1097(04)01445-7
14. Tziakas D, Chalikias G, Stakos D, Apostolakis S, Adina T, Kikas P, et al. Development of an easily applicable risk score model for contrast-induced nephropathy prediction after percutaneous coronary intervention: a novel approach tailored to current practice. *Int J Cardiol.* (2013) 163:46–55. doi: 10.1016/j.ijcard.2011.05.079
15. Bardin T, Richette P. Definition of hyperuricemia and gouty conditions. *Curr Opin Rheumatol.* (2014) 26:186–91. doi: 10.1097/BOR.0000000000000028
16. Thygesen K, Alpert JS, Jaffe AS, Chaitman BR, Bax JJ, Morrow DA, et al. Fourth Universal Definition of Myocardial Infarction (2018). *Circulation.* (2018) 138:e618–e51. doi: 10.1161/CIR.0000000000000617
17. Levey AS, Stevens LA, Schmid CH, Zhang YL, Castro AF. 3rd, Feldman HI, et al. A new equation to estimate glomerular filtration rate. *Ann Intern Med.* (2009) 150:604–12. doi: 10.7326/0003-4819-150-9-200905050-00006
18. Rihal CS, Textor SC, Grill DE, Berger PB, Ting HH, Best PJ, et al. Incidence and prognostic importance of acute renal failure after percutaneous coronary intervention. *Circulation.* (2002) 105:2259–64. doi: 10.1161/01.CIR.0000016043.87291.33
19. Hossain MA, Costanzo E, Cosentino J, Patel C, Qaisar H, Singh V, et al. Contrast-induced nephropathy: Pathophysiology, risk factors, and prevention. *Saudi J Kidney Dis Transpl.* (2018) 29:1–9. doi: 10.4103/1319-2442.225199
20. Barbieri L, Verdoia M, Schaffer A, Cassetti E, Marino P, Suryapranata H, et al. Uric acid levels and the risk of Contrast Induced Nephropathy in patients undergoing coronary angiography or PCI. *Nutr Metab Cardiovasc Dis.* (2015) 25:181–6. doi: 10.1016/j.numecd.2014.08.008
21. Ghelich Khan Z, Talasaz AH, Pourhosseini H, Hosseini K, Alemzadeh Ansari MJ, Jalali A. Potential role of allopurinol in preventing contrast-induced nephropathy in patients undergoing percutaneous coronary intervention: a randomized placebo-controlled trial. *Clin Drug Investig.* (2017) 37:853–60. doi: 10.1007/s40261-017-0542-z
22. Zbierska-Rubinkiewicz K, Trebacz O, Tomala M, Rubinkiewicz M, Chrzan I, Gackowski A. Creatine kinase-MB and red cell distribution width as predictors of contrast-induced nephropathy after percutaneous coronary intervention in acute myocardial infarction. *Folia Med Cracov.* (2017) 57:87–99.
23. Gurm HS, Seth M, Kooiman J, Share D, A. novel tool for reliable and accurate prediction of renal complications in patients undergoing percutaneous coronary intervention. *J Am Coll Cardiol.* (2013) 61:2242–8. doi: 10.1016/j.jacc.2013.03.026
24. Hall C. NT-ProBNP: the mechanism behind the marker. J Card Fail. (2005) 11:S81–3. doi: 10.1016/j.cardfail.2005.04.019
25. Goussot S, Mousson C, Guenancia C, Stamboul K, Brunel P, Brunet D, et al. N-terminal fragment of pro b-type natriuretic peptide as a marker of contrast-induced nephropathy after primary percutaneous coronary intervention for ST-segment elevation myocardial infarction. *Am J Cardiol.* (2015) 116:865–71. doi: 10.1016/j.amjcard.2015.06.007
26. Jarai R, Dangas G, Huber K, Xu K, Brodie BR, Witzenbichler B, et al. B-type natriuretic peptide and risk of contrast-induced acute

kidney injury in acute ST-segment-elevation myocardial infarction: a substudy from the HORIZONS-AMI trial. *Circ Cardiovasc Interv*. (2012) 5:813–20. doi: 10.1161/CIRCINTERVENTIONS.112.972356

27. Liu Y, He YT, Tan N, Chen JY, Liu YH, Yang DH, et al. Preprocedural N-terminal pro-brain natriuretic peptide (NT-proBNP) is similar to the Mehran contrast-induced nephropathy (CIN) score in predicting CIN following elective coronary angiography. *J Am Heart Assoc*. (2015) 4:e001410. doi: 10.1161/JAHA.114.001410

Conflict of Interest: The authors declare that the research was conducted in the absence of any commercial or financial relationships that could be construed as a potential conflict of interest.

Publisher's Note: All claims expressed in this article are solely those of the authors and do not necessarily represent those of their affiliated organizations, or those of the publisher, the editors and the reviewers. Any product that may be evaluated in this article, or claim that may be made by its manufacturer, is not guaranteed or endorsed by the publisher.

Copyright © 2021 Mo, Ye, Chen, Wang, Liu, Zhang, Xu, Cheng, Mei, Zheng, Dai, Jiang and Ge. This is an open-access article distributed under the terms of the Creative Commons Attribution License (CC BY). The use, distribution or reproduction in other forums is permitted, provided the original author(s) and the copyright owner(s) are credited and that the original publication in this journal is cited, in accordance with accepted academic practice. No use, distribution or reproduction is permitted which does not comply with these terms.

frontiers in Cardiovascular Medicine

SYSTEMATIC REVIEW
published: 03 November 2021
doi: 10.3389/fcvm.2021.761877

Research Progress of Electrical Stimulation in Ischemic Heart Disease

Ying Zhao[1], Pengyu Wang[1], Zhe Chen[2], Manman Li[1], Dengfeng Zhang[1], Liming Yang[3] and Hong Li[1]**

[1] Department of Pathophysiology, School of Basic Medical Sciences, Harbin Medical University, Harbin, China, [2] Department of Infectious Diseases, Beidahuang Group General Hospital, Harbin, China, [3] Department of Pathophysiology, Harbin Medical University-Daqing, Daqing, China

Ischemic heart disease (IHD) is a considerable health burden worldwide with high mortality and morbidity. Treatments for IHD are mainly focused on decreasing oxygen demand or increasing myocardial oxygen supply, including pharmacological, interventional, and surgical treatment, but there are also some limitations. Therefore, it is important to find a simple, effective, and economical treatment. As non-invasive and safe physiotherapy, electrical stimulation (ES) has a promising application in the treatment of IHD. Current studies suggest that ES can affect the occurrence and development of IHD by promoting angiogenesis, regulating autophagy and apoptosis, inhibiting the inflammatory response and oxidative stress. In this review, we focus predominantly on the mechanism of ES and the current progress of ES therapy in IHD, furthermore, give a brief introduction to the forms of ES in clinical application.

Keywords: electrical stimulation, ischemic heart disease, angiogenesis, apoptosis, autophagy, inflammation, oxidative stress

OPEN ACCESS

Edited by:
Hui Gong,
Fudan University, China

Reviewed by:
Ming-Jie Wang,
Fudan University, China
Bin He,
Shanghai Jiaotong University, China

****Correspondence:***
Liming Yang
limingyanghmu@163.com
Hong Li
drlihong1971@163.com

Specialty section:
This article was submitted to General Cardiovascular Medicine, a section of the journal Frontiers in Cardiovascular Medicine

Received: *20 August 2021*
Accepted: *08 October 2021*
Published: *03 November 2021*

Citation:
Zhao Y, Wang P, Chen Z, Li M, Zhang D, Yang L and Li H (2021) Research Progress of Electrical Stimulation in Ischemic Heart Disease. Front. Cardiovasc. Med. 8:761877. doi: 10.3389/fcvm.2021.761877

INTRODUCTION

Cardiovascular disease has been a serious threat to human life for a long time and its incidence is increasing (1). Coronary artery disease (CAD), also known as ischemic heart disease (IHD), is the main cause of heart failure, which seriously endangers the health of people and puts a huge burden on health care resources all over the world. In China, more than half of patients with heart failure developed from IHD (2). Therefore, it is a common problem for clinicians and researchers to explore the pathogenesis of IHD and carry out effective prevention and treatment. According to clinical studies, the onset of IHD is a long-term and complex process, which mainly involves pathophysiological changes such as coronary artery stenosis, coronary artery thrombosis and embolism, vasospasm, microcirculation disorder, inflammation, endothelial dysfunction, apoptosis, and autophagy cascading reactive activation, etc (3). It is mainly caused by the spread of severe coronary artery stenosis or complete blockage of chronic coronary arteries, resulting in an imbalance between the oxygen supply and oxygen demand of the myocardial cells, impaired myocardial energy metabolism leading to autophagy and ischemia-reperfusion injury, which then leads to a syndrome manifesting as heart enlargement, heart failure, arrhythmias, and other symptoms (4). In recent years, with the continuous development of molecular biology, people have a deeper knowledge and understanding of the occurrence and development of IHD. Furthermore, treatments for IHD are mainly focused on decreasing oxygen demand or increasing

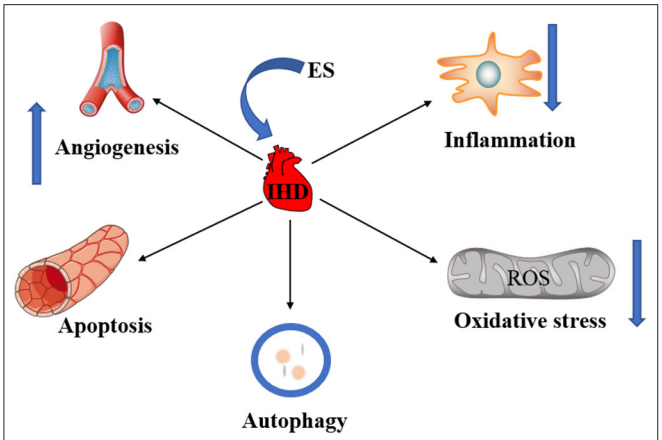

FIGURE 1 | The role of ES in IHD. ES can treat IHD by promoting angiogenesis. ES can treat IHD by regulating apoptosis and autophagy. The inhibition of inflammation and oxidative stress by ES is also critical to the treatment of IHD.

myocardial oxygen supply, including pharmacological, interventional, and surgical treatment, but there are also some limitations (5). Thus, it is important to find a simple, effective, and economical treatment.

The bioelectric phenomenon is one of the most basic life activities, almost every physiological process in the human body is related to bioelectricity, such as heart beating, muscle contraction, brain thinking. As early as the 19th century, scientists had discovered that exogenous ES of the human cortex led to behavioral changes (6). Since then, a large number of studies have demonstrated that electric fields can cause physiological changes in cells. ES therapy is a physical therapy method that uses electrical currents to cause changes in the morphology and function of cells or tissues through different pathways. In recent years, with the continuous development of control technology of ES and the deepening of research on different types of stimulation, the application of ES in IHD has received more and more attention. As non-invasive and safe physiotherapy, ES has been widely used in the rehabilitation of many diseases such as neuromuscular injuries (7). New advances in IHD are achieved through the application of different types of ES to influence cell proliferation and differentiation. Current studies suggest that ES can affect the occurrence and progress of IHD by promoting angiogenesis, regulating autophagy and apoptosis, inhibiting the inflammatory response and oxidative stress (**Figure 1**). Here, the role of ES in IHD was reviewed to further analyze the mechanism of ES and provide new ideas for the treatment of clinical IHD.

OVERVIEW OF ELECTRICAL STIMULATION

In more than 300 BC, Aristotle observed that electric rays paralyzed animals in the water by striking them with shock as they hunt. It was only after the 18th century, when the laws of electricity were discovered, that people gradually realized the nature of the biological discharge. With the invention of the electric motor and the battery, people began to figure out electricity. Then many scientists proved the existence of bioelectricity. With the invention of the galvanometer, people could measure bioelectricity directly. Subsequently, bioelectricity was studied, a membrane theory was developed and the transmembrane potential of cells was recorded. At this time, the research is not lotted to the phenomenon and the mechanism of occurrence. With the deepening of the research, people began to try to observe the biological electrical phenomenon of the body. Its principle was to use the electric excitability of nerve cells to stimulate the specific sensory nerve with electricity, and produce nerve impulses to produce the corresponding immune and humoral response in the area dominated by it, to play the role of regulating the body (8). ES can promote biomolecules to cross biofilms through ion osmosis, or interact with membrane proteins, cytoskeleton, and intracellular organelles (9, 10). ES therapy is a kind of physical therapy that uses electrical currents to cause changes in the morphology and function of cells or tissues through different pathways (11). Based on these remarkable advantages, it is now beginning to be widely used in the biomedical field (11). ES has become an active area of research in nerve, cardiac and skeletal muscle engineering. In tissue engineering and regenerative medicine, ES can directionally accelerate neuronal axon growth and embryonic stem cell differentiation into neuron (12). In addition, ES can stimulate the growth of nerve axons and increases cell alignment (13, 14). ES is already used in tissue engineering to improve the conduction and contractile properties of heart structure (15). Recent reports have shown that macrophages play a role in electrical conduction beyond the atrioventricular node, including atrial fibrillation and ischemic ventricular arrhythmias (16). IHD causes abnormalities in cardiac conduction. Stimulation of the carotid sinus has been shown to affect blood flow in areas of myocardial ischemia to relieve angina. Whether ES of the carotid sinus nerve improves conduction abnormalities in IHD *via* sinus node conduction needs to be further investigated. ES can promote the proliferation of osteoblasts, regulate the local endocrine environment, participate in osteogenic differentiation, and promote bone formation in bone tissue engineering (17). Ischemia-reperfusion injury is common pathological damage in the clinic of IHD. Currently, experts are trying to use ES to alleviate myocardial ischemia-reperfusion injury (18). Ninety percentage of IHD is caused by the narrowing of the coronary lumen caused by atherosclerosis, resulting in problems of myocardial ischemia and hypoxia. Our previous study found that ES could reduce macrophage inflammatory response, reduce lipid accumulation in foam cells, and reduce AS plaque area (19). As a new technique, ES has been widely used in the treatment of IHD. Although its specific mechanism remains unclear, it provides a new direction for the treatment of IHD.

Types of Electrical Stimulation

In recent years, with the continuous development of ES control technology, many different types of ES had been applied in biomedicine and achieved good efficacy. Depending on the output signal, ES can be in the form of a single-phase (DC)

or two-phase (AC), sinusoidal, sawtooth, or square-wave signal, pulse, pulse burst, or continuous pulse. Of these, the most basic is to apply a direct current voltage (20–25). ES can be divided into excitatory electrical stimulation and non-excitatory electrical stimulation according to whether the action potential is generated after ES. Current studies have shown that non-excitatory electrical stimulation on the left ventricular wall of rats can reduce cardiac ischemia-reperfusion injury by reducing the expression of calcitonin gene-related peptide (CGRP) (26). With the development of ES, so far, there have been many forms. First of all, studies have shown that percutaneous ES of the auricular branch of the vagus nerve has been applied to treat epilepsy and depression. Both animal experiments and clinical practice have proved their safety and effectiveness. Therefore, ES of the auricular branch of the vagus nerve would be a new non-invasive method to optimize cardiac autonomic tone in the treatment of ischemic heart failure (27–29). Another particular type of ES is electroacupuncture (EA). EA is a special form of ES, that is nervous electrical stimulation combined with acupuncture therapy and physical therapy, refers to the insertion of traditional Chinese medicine, based on pulse generator on the acupuncture needle passed close to the trace of human bioelectricity current wave, based on the original needle stimulates, attaches a certain amplitude of the continuous wave, discontinuous wave to stimulate acupuncture points, sustained, stable and accurate for the body, can be accused of stimulus, the electrophysiological effect of therapeutic effect (30). EA is easy to perform and avoids many of the adverse effects of drug pre-treatment. EA preconditioning, as an effective method of myocardial protection, can activate the endogenous protective mechanism of the body, mobilize the potential of the body, and improve the ability of the myocardium to adapt to the stress response. It has the advantage of adapting to a wide population and has a broad clinical application prospect. In recent years, animal experiments have shown that EA affects the whole process of autophagy flux by regulating the expression of the ULK1 complex, Beclin1, LC3, p62, and other autophagy-related markers. Further studies have shown that EA therapy may play a neuroprotective role in cerebral ischemia/reperfusion injury by regulating autophagy through the PI3K-Akt-mTOR signaling pathway (31). Current studies have shown that the locations of ES are also different, including the vagus nerve, spinal cord, cerebellar parietal nucleus, as well as the left cervicothoracic joint, sinoatrial node, and Neiguan acupoint (27, 28, 30). Scientists are trying to find areas where ES is most effective and least harmful to provide better theoretical and technical support for treating diseases with ES.

ROLES OF ES IN IHD

Angiogenesis

IHD is a condition in which the heart is affected by myocardial ischemia caused by narrowing or occlusion of the coronary arteries. The establishment of collateral coronary artery and its degree of development can reduce or prevent myocardial ischemia or necrosis and improve cardiac function. The body can promote the establishment of coronary collateral circulation through capillary angiogenesis. The role of angiogenesis in cardiovascular disease is still an important and unsolved problem, and there are different views on it in the medical community. Angiogenic cytokines have been widely considered to be useful in the treatment of IHD. As a new modulator, ES has been used in many ischemia models. ES can regulate angiogenesis by affecting cytokines and their receptors. However, the specific mechanism remains unclear and further studies are needed, but a large number of experiments have shown that ES has great potential in inducing angiogenesis and improving organ function.

Angiogenesis and IHD

IHD is a global public health problem with high morbidity and mortality. The main pathophysiological process of IHD is atherosclerosis. Coronary artery wall atherosclerosis causes stenosis of the vascular lumen, obstruction of coronary circulation, and insufficient blood supply to the myocardium, leading to myocardial ischemia, myocardial infarction, and other IHD (32). Importantly, restoring the blood supply is key to the successful treatment of IHD. Current treatments for IHD include drug therapy and surgical interventions that reduce the risk of cardiovascular events in IHD by dilating blood vessels to increase blood flow to damaged tissues. Angiogenesis is a novel therapeutic approach that can alleviate the symptoms of IHD (33). Angiogenesis is the development of new blood vessels from existing capillaries or post-capillary veins. Angiogenesis is an essential event involved in various physiological and pathological processes such as development, wound healing, and tumor growth (34). It involves the degradation of the vascular basement membrane, activation, proliferation, and migration of vascular endothelial cells during the activation phase; the reconstruction of blood vessels and vascular networks is a complex process involving multiple molecules and cells. Angiogenesis is a complex process of coordination between proangiogenic factors such as vascular endothelial growth factors (VEGF), fibroblast growth factors (FGF), and antiangiogenic factors such as thrombospondin-1, angiostatin, endostatin (35). VEGF (Vascular endothelial growth factor) is a subfamily of growth factors that stimulate the growth of new blood vessels and is an important signaling protein involved in angiogenesis and angiogenesis (36). Angiogenesis can promote the establishment of collateral circulation in ischemic peripheral tissues. The formation and opening of coronary collateral circulation can alleviate myocardial ischemia, prevent cell necrosis, prevent and delay the formation of ischemic cardiomyopathy, and improve the clinical symptoms and prognosis of patients. Studies have shown that neovascularization can effectively restore coronary blood perfusion and promote myocardial regeneration (37).

ES Can Promote Angiogenesis for IHD

Recently, subthreshold electrical stimulation is widely used in wound healing, fracture repair, and other clinical diseases due to its potential therapeutic ability. Given the experimental evidence that ES can promote wound healing by inducing the release of angiogenic factors and reducing the duration of the inflammatory period (38). The enhancement of angiogenesis by ES is considered to be a new chapter in the search for

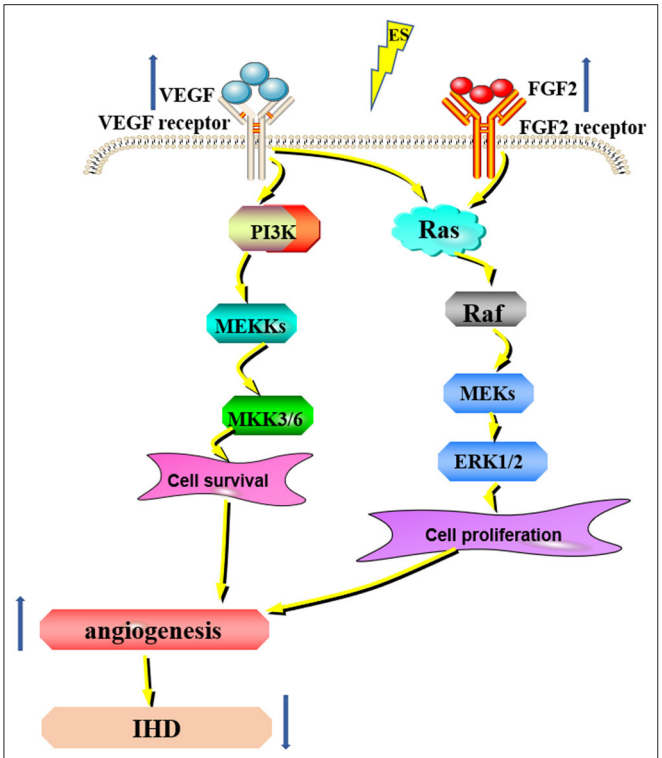

FIGURE 2 | ES can promote angiogenesis for IHD. ES can increase the expression of VEGF and FGF2 and promote angiogenesis through the MAPK/ERK signaling pathway, thus treating IHD.

new methods to treat ischemia (39). Additionally, studies have shown that ES facilitates the angiogenesis of human umbilical vein endothelial cells through MAPK/ERK signaling pathway by stimulating FGF2 secretion (40) (**Figure 2**). Moreover, it has been shown that the expression of the VEGF gene is upregulated in electrically stimulated rat skeletal muscle (41). ES directly induces the proangiogenic response of vascular endothelial cells through VEGF receptors (42, 43) (**Figure 2**). Twenty-five hertz and 50Hz low voltage ES can promote the expression of VEGF in the ischemic myocardium and lead to capillary angiogenesis (44, 45). The specific effects of ES on the downstream pathways of VEGF and FGF2 still need further study. Therefore, ES can promote angiogenesis in the ischemic myocardium, but the specific mechanism is still unclear and needs further study. Taken together, in the future, ES will be expected to be a simple and practical new method to promote angiogenesis in the ischemic myocardium.

Apoptosis

Coronary arteriosclerosis is the main cause of IHD. When the insufficient blood supply to the coronary artery of the heart fails to meet the energy needs of the myocardium, the myocardial tissue will accumulate toxic metabolites due to hypoxia and metabolic disorders, which will cause ischemic injury, and lead to myocardial death if it continues to develop. Apoptosis is an important mode of death of ischemic cardiomyocytes. ES is a new physical method to treat IHD by regulating apoptosis, the specific mechanism is not clear, there are some theories and hypotheses that need to be further confirmed, but the study of ES for the treatment of cardiovascular disease provides new thinking and method.

Apoptosis and IHD

Apoptosis is a form of programmed cell death that requires protein synthesis and a highly regulated process of cellular self-destruction by specific cellular signals and proteins (46). Apoptosis is a process strictly controlled by multiple genes. These genes are very conserved among species, such as the Bcl-2 family, caspase family, oncogene P53, etc. With the development of molecular biology techniques, there is considerable understanding of the process of apoptosis in a variety of cells, but the exact mechanism of apoptosis has not been fully understood up to now. And the disorder of the apoptotic process may have a direct or indirect relationship with the occurrence of many diseases. Such as tumors, autoimmune diseases, etc. Many factors can induce apoptosis, such as radiation, drugs, etc (47–50). IHD is a clinical syndrome that results in myocardial ischemia and hypoxia, apoptosis, and myocardial fibrosis caused by coronary atherosclerosis. Several recent studies have also confirmed the important role of apoptosis in IHD. Excessive apoptosis can promote myocardial cell death thus promoting myocardial ischemia, ischemia/reperfusion (I/R) injury, and post-ischemic cardiac remodeling in IHD (51, 52). In general, it is very important to find a new way to regulate apoptosis to contribute to the treatment of IHD and to provide a new therapeutic strategy.

ES Treats IHD by Regulating Apoptosis

Subthreshold electrical stimulation is a method used to manipulate cells to induce changes in various cellular processes, such as apoptosis and cell proliferation (53–55). Controversially, it has been shown that ES can both inhibit or induce apoptosis and promote cell proliferation. It has been shown that ES induces apoptosis by altering the permeability of the cell membrane and forming small pores in the cell membrane (electroporation) (56). In turn, it activates the apoptosis-related signal pathways and regulates apoptosis by altering the expression of p53 and Bcl-2 proteins (57) (**Figure 3**). ES can reduce apoptosis by altering intracellular protein expression and activating multiple signaling pathways (such as MAP kinase pathway) (58). ES to reduce apoptosis can also be used in the treatment of IHD. For instance, subthreshold electrical stimulation may reduce the apoptosis of rat ischemic cardiomyocytes by up-regulating the gene expression of Bcl-2 and down-regulating the gene expression of Bax, but the exact mechanism is unclear (59). In addition, other studies have shown that 25 Hz subthreshold electrical stimulation can reduce the apoptosis of ischemic cardiomyocytes in rats, and the mechanism may be related to the down-regulation of caspase-3 expression. Effective stimulation of Neiguan acupoints with EA pretreatment can reduce the production and level of TNF-α and intercellular adhesion factor-1 (ICAM-1) during myocardial ischemia-reperfusion injury, thereby reducing apoptosis of cardiomyocytes and tissue cells and suppressing the degree of

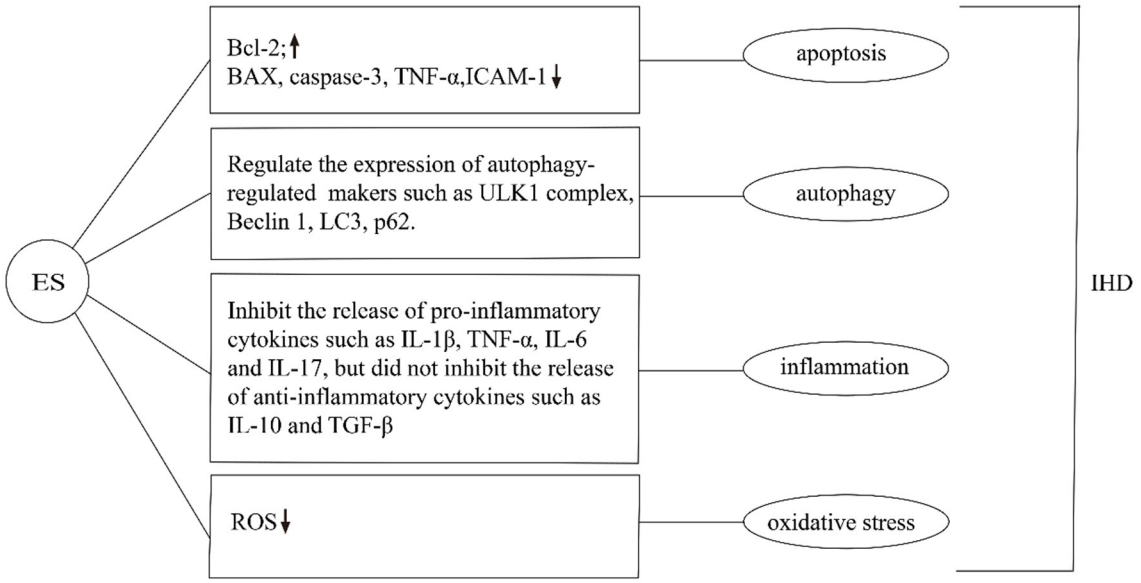

FIGURE 3 | Effects of ES on IHD in apoptosis, autophagy, inflammation, and oxidative stress. ES can regulate apoptosis by changing the expression of intracellular proteins. For example, Increase the expression of Bcl-2, inhibit the expression of Bax, Caspase-3, TNF-α, ICAM-1. ES can regulate the expression of autophagy-related markers such as ULK1 complex, Beclin1, LC3, and p62. Moreover, it can inhibit the release of pro-inflammatory cytokines such as IL-1β, TNF-α, IL-6, and IL-17, but did not inhibit the release of anti-inflammatory cytokines such as IL-10 and TGF-β. Additionally, ES can reduce ROS and inhibit oxidative stress in the treatment of IHD.

the inflammatory response to effectively regulate heart rate and increase cardiac blood output in patients after coronary artery bypass grafting for coronary artery disease, resulting in a decrease in cardiac troponin T concentration and contributing to the maintenance and improvement of cardiac function. Subthreshold electrical stimulation in both ischemic and non-ischemic areas can reduce apoptosis of ischemic cardiomyocytes in rats (60). The effect of EA on the expression of caspase genes and similar sequences in cardiac myocytes was significant, and it could protect myocytes in the ischemic area during ischemia-reperfusion by slowing down the apoptosis process of cardiac myocytes. The mechanism of the effect of EA stimulation on the prevention of myocardial hypertrophy in rats is related to the modulation of the ERK signaling pathway, and its effect on the prevention of myocardial hypertrophy may be through the inhibition of the neuroendocrine system angiotensin II and endothelin to regulate the ERK signaling pathway to exert anti-apoptotic effects on cardiomyocytes (61). However, it is noteworthy that the mechanism by which ES achieves this goal is unclear. Further studies by scientists are needed to provide a new direction for ES to regulate apoptosis.

Autophagy

Autophagy generally exists in the normal physiological and pathological processes of cells. Appropriate autophagy can be used to maintain homeostasis, but insufficient and excessive autophagy can lead to related diseases. IHD is involved in the complex regulation of autophagy in myocardial hypertrophy, myocardial fibrosis, and the efficacy after reperfusion therapy, both in the ischemic stage and in the later stage. At present, the role of autophagy in IHD has increasingly become the focus of research. The regulation of autophagy by ES has been studied in a variety of diseases, but the study in IHD is still in the preliminary stage, and the specific mechanism is not clear yet, which needs further study to confirm. Studies on the regulation of autophagy by ES will provide a new direction for the treatment of IHD.

Autophagy and IHD

Autophagy is a general term for intracellular lysosomal degradation substances that are considered essential for the maintenance of normal cardiac structure and function. It is also associated with several cardiac diseases, especially myocardial ischemia/reperfusion (I/R) injury (62). Autophagy plays an important role in maintaining normal cell homeostasis and energy metabolism balance and is a necessary condition for regulating cardiovascular function (63). There are three main forms of autophagy: microautophagy, autophagy with molecular chaperones, and macrophage, among which macrophage is the most common and the most thoroughly studied. There are several stages in the progression of macroautophagy, including autophagosome initiation, vesicle nucleation, autophagosome expansion and maturation, and autophagosome fusion and degradation (64). There is growing evidence for a regulatory role of autophagy in IHD. Recent studies have demonstrated its dual role in IHD. Moderate autophagy is thought to be cardioprotective, while excessive autophagy exacerbates cardiomyocyte death (65). During the myocardial ischemic phase, autophagy degrades nonfunctional cytoplasmic proteins to provide critical nutrients for key vital activities, thereby inhibiting apoptosis and necrosis. However, autophagy may

negatively affect the heart during the reperfusion phase. During the ischemic phase, mTOR acts through the AMPK/mTOR and phosphatidylinositol 3-kinase/Akt/mTOR pathways, whereas during the reperfusion phase, Beclin1 is upregulated (66). From what has been discussed above, the regulation of autophagy is helpful for the treatment of IHD.

ES Can Mitigate Cardiomyocyte Injury by Regulating Autophagy

Latterly, Studies have shown that subthreshold electrical stimulation plays an important role in the whole process of autophagy, including the initiation of autophagy, vesicle nucleation, expansion, and maturation of autophagic vesicles, and fusion and degradation of autophagic lysosomes (67–69). Currently, the results of animal experiments have shown that ES affects the whole process of autophagic flux by regulating the expression of autophagy-related markers such as ULK1 complex, Beclin1, LC3, and p62 (**Figure 3**). For instance, after ES was applied to skeletal muscle, the activities of autophagy autophagy-related proteins, were significantly increased, and the expression of the ubiquitin-ligase gene of proteasome and mRNA of autophagy-related genes were significantly up-regulated, suggesting that the level of autophagy in skeletal muscle was increased, and the mechanism was related to the regulation of adenylate activated protein kinase/ULK1-mediated signaling pathway (70). Another study suggests that ES treatment may regulate autophagy through the PI3K-AKT-mTOR signaling pathway, thus exerting neuroprotective effects in cerebral ischemia/reperfusion injury. The modulation of cerebral ischemia/reperfusion injury by autophagy depends on the duration of ischemia/reperfusion and parameters such as the selected acupuncture point, current intensity, waveform, and duration (31). EA may moderately regulate the autophagy level during MIRI by down-regulating the expression of LC3II and Beclin-1 proteins. EA pretreatment can effectively improve the pathological changes of the myocardium and reduce the damage of myocardium in rats with MIRI (71). ES can not only promote autophagy but also inhibit over-autophagy through different intensification of ES. The hippocampus of rats treated with ES can inhibit over-autophagy by activating the mammalian target pathway of rapamycin, thus exerting a brain-protective effect (72). The above findings indicate that ES is of potential significance in IHD treatment. However, the precise mechanisms involved remain obscure, and therefore more in-depth exploration and more adequate validation are needed to elucidate the clinical value of ES in IHD.

Inflammation

Inflammation is one of the research hotspots of the risk factors of IHD in recent years. When the body is in an inflammatory state, it can promote the occurrence of acute cardiac events of coronary heart disease, and affect the function and prognosis of the ischemic heart. Inflammation is crucial in the pathogenesis of IHD, but there is still a lack of a complete signaling network, and the role of inflammation in the pathogenesis remains unclear. As a new intervention means, ES has been shown in numerous studies to regulate inflammatory pathways and inhibit the secretion of inflammatory mediators. The regulation of ES on inflammation in IHD has also been studied, suggesting that ES can be used as a potential new method to inhibit inflammation in the treatment of IHD, but the specific mechanism remains to be further studied.

Inflammation and IHD

Inflammation plays an important role in atherosclerosis and cardiovascular disease. A large amount of research is currently being performed to demonstrate that inflammation is closely related to the development of atherosclerosis and coronary artery disease (73–75). Atherosclerosis is associated with activation of inflammatory processes and an increase in systemic pro-inflammatory molecules such as interleukin 1 beta (IL-1β), interleukin 6 (IL-6), tumor necrosis factor (TNF), and c-reactive protein (76). It has been shown that activation of NOD-like receptor family protein 3 (NLRP3) inflammasome leads to increased inflammation in ischemic myocardial tissue, which further worsens cardiac dysfunction and becomes a key component of the post-ischemic inflammatory response to myocardial ischemia as well as ischemic tissue repair (77). Modulating the activation of NLRP3 inflammatory vesicles can balance the inflammatory homeostasis of ischemic myocardial tissue and facilitate the repair and remodeling of ischemic myocardial tissue after injury. Numerous animal experiments have shown that NLRP3 expression is elevated in ischemic myocardial tissue and the inflammatory response is exacerbated. Conversely, the absence of NLRP3 inflammatory vesicle components attenuates the inflammatory response and promotes cardioprotective effects (78). In conclusion, it is easy for us to conceive that suppressing inflammation may represent a promising IHD treatment strategy.

ES Can Inhibit Inflammation to Treat IHD

Excitatory electrical stimulation can modulate the cholinergic anti-inflammatory pathway to inhibit the release of inflammatory mediators, thereby slowing the onset and progression of various inflammation-related diseases (79). The cholinergic anti-inflammatory pathway composed of the vagus nerve and its transmitter acetylcholine plays an important role in the regulation of inflammatory response. When the body is injured, the excitability of the vagus nerve increases, which promotes the release of acetylcholine from the peripheral nerve endings. It can inhibit the release of pro-inflammatory cytokines such as IL-1β, TNF-α, IL-6, and IL-17, but did not inhibit the release of anti-inflammatory cytokines such as IL-10 and TGF-β (80) (**Figure 3**). ES can also alter the function of inflammatory cells at the molecular level, thereby inhibiting the release of inflammatory mediators, without affecting the number of immune cells (81). The anti-inflammatory effect of electrical stimulation has been applied in the clinical treatment of various inflammation-related diseases. It has been shown that transcutaneous electrical stimulation of the vagus nerve can promote wound healing by suppressing the inflammatory response (82). ES can be used to treat ocular diseases by enhancing the neurotrophic potential of Muller cells and inhibiting the pro-inflammatory effect of microglial cells, thus improving the denaturing

FIGURE 4 | Pattern diagram of mouse acupuncture points. **(A)** Neiguan. Neiguan point was located in the medial side of the forelimb, between the ulnar and radial joints, saving 3 mm from the wrist pass; **(B)** Xinyu. Xinyu acupoint in the back, the fifth thoracic spinous process, besides 1.5 inches. That's about an inch and a half on each side of the fifth vertebra.

degree of photosensors (83, 84). ES has been widely used to regulate neuronal activity and restore some visual function (85). Additionally, diagenesis of the lumbar intervertebral disc is the main cause of lower back pain. Inflammatory factors were released near nerve roots, affected nerve roots, and caused pain. ES can reduce the activity of extracellular matrix modifier enzyme and matrix metalloproteinase-1, inhibit the secretion of inflammatory cytokines, and achieve the effect of pain relief (86). The stimulation of the apical splenic nerve by ES can reduce the inflammatory response and clinical symptoms in a mouse model of rheumatoid arthritis (87). Previous studies by our group have shown that ES downregulated the expression of the NLRP3 inflammasome, ASC and caspase-1, and inhibited the release of IL-1β and IL-18, suppressed the AS pyroptosis-mediated inflammation response (19). ES can inhibit the inflammatory response and experimental myocardial protective effect by reducing the level of inflammatory protein expression in myocardial tissue. EA at "Neiguan" and "Xinyu" points significantly reduced serum IL-1β content and NF-κB p65 protein expression level in rats with acute myocardial ischemia-reperfusion injury, and increased IL-10 content in myocardial tissues (88) (**Figure 4**). In conclusion, the above studies show that from bench to bedside, ES can inhibit inflammation to treat IHD. However, the specific mechanism is still unclear and needs further study.

Oxidative Stress

In the course of treatment, reperfusion may cause myocardial ischemia-reperfusion injury due to aggravation of oxidative stress state. Oxidative stress induced by ischemia acts on heart cells, and through different molecular mechanisms, can produce a series of pathological reactions, resulting in myocardial damage and impaired cardiac function. ES has the function of scavenging oxygen free radicals and inhibiting the damage of oxidative stress response to the central nervous system and heart. However, the specific mechanism remains to be further studied.

Oxidative Stress and IHD

It is well known that the occurrence, progression, metastasis, and other processes of IHD involve complex molecular mechanisms, and the current understanding of them is incomplete, which leads to a low cure rate of IHD. It is recognized that oxidative stress is closely related to coronary artery disease. In the pathological process, oxidative stress is induced, and its main characteristic is the elevated level of reactive oxygen species (ROS). As a major mediator, ROS not only deteriorates cell physiological functions and causes cell damage through its oxidative activity, but also participates in cell signal transduction and regulates disease progression, namely REDOX signal (89, 90). In IHD, excessive production of (ROS) leads to dysfunction of endothelial cells and smooth muscle, resulting in an imbalance between antioxidant capacity and oxidants (91). During myocardial ischemia, the production of free radicals and the activity of antioxidant enzymes is increased, which can lead to severe damage of myocardial cells to apoptosis. The activities of superoxide dismutase (SOD) and glutathione peroxidase (GSH-Px) in myocardial cells of the ischemic area were increased. Taken together, these findings suggest that reducing oxidative stress may serve as a novel treatment for IHD.

ES Can Reduce Oxidative Stress and Protect Cardiomyocytes

ES can be used to protect cells and tissues from damage caused by ROS (92). Intraoperative ES reduced oxidative stress and up-regulated the level of stimulating diaphragmatic autophagy (93). Studies have shown that electroacupuncture pretreatment and stimulation of Neiguan acupoint can significantly improve the enzyme activity of SOD, GSH-Px, and other endogenous oxidation free radical scavenging systems, inhibit the lipid peroxidation reaction of the myocardial cell membrane, reduce the content of serum MDA, and play a protective role in myocardium (94). Other studies have found that EA preconditioning has an obvious protective effect on the myocardium after reperfusion injury, can improve arrhythmia score, downregulate CK-MB level, regulate ROS production, and reduce the expression levels of CYT-C, Caspase-9, and Caspase-3 genes. Its myocardial protective effect may be based on the inhibition of ROS-mediated apoptosis of cardiomyocytes (95) (**Figure 3**). Our previous experiments have shown that ES can reduce VBP-induced oxidative stress in macrophages, thereby inhibiting caspase-1-dependent cell apoptosis. Meanwhile, ES can increase the expression of SIRT3 and improve VBP-induced autophagy of macrophages, thereby reducing oxidative stress (19). Overall, these researches suggest that the inhibition of oxidative stress by ES has the potential to be used as a new treatment for IHD.

Other Mechanisms

Current studies have shown that ES can also protect cardiomyocytes through other mechanisms to treat IHD. ES can inhibit intracellular calcium overload and maintain calcium homeostasis to protect the myocardium. EA stimulation of Neiguan acupoint can promote the gene expression of Ca^{2+}-ATPase mRNA in ischemia-reperfusion myocardial

cells, which can improve the effect of alleviating myocardial injury and protecting myocardial function (96). ES of the left cervicothoracic ganglion and the Neiguan acupoint-Jiangrong acupoint can down-regulate the expression of norepinephrine and catecholamine in the rat and rabbit myocardial ischemia models, respectively, and increase the blood flow in the infarction area, thus alleviating the myocardial ischemia-reperfusion injury (97, 98). ES of Neiguan acupoint can play a cardiac protective role by activating opioid receptors in the medulla oblongata and regulating the concentration of cAMP and cGMP in cardiomyocytes (99). Overall, ES is involved in the regulation of many cellular signaling pathways and plays a significant role in the occurrence, development, and clinical manifestations of IHD, indicating that ES is a potential way for IHD therapy.

CONCLUSION

At present, as a new intervention means, ES has the characteristics of non-invasive, safe, and fewer side effects, etc., and has been paid more and more attention in IHD. There is growing evidence that subthreshold electrical stimulation can promote angiogenesis, modulate autophagy and apoptosis, inhibit oxidative stress and excitatory electrical stimulation can inhibit inflammation via cholinergic anti-inflammatory pathways in IHD. However, the study of ES in the treatment of IHD should be in its infancy. Although ES has been used in the clinical treatment of nerve, bone, gynecology, and other diseases, some ES sites are special, and it is dangerous to directly use in clinical practice, which hinders its clinical application. Therefore, an in-depth understanding of the mechanism of ES in the treatment of IHD, as well as the search for appropriate parameters and appropriate implementation methods and locations that can effectively play a role, will help to provide better scientific data for clinical application and increase the feasibility of a clinical application. In conclusion, further in-depth mechanism research is the future research direction of ES. We believe that ES will certainly provide new ideas for treating IHD.

DATA AVAILABILITY STATEMENT

The original contributions presented in the study are included in the article/supplementary material, further inquiries can be directed to the corresponding authors.

AUTHOR CONTRIBUTIONS

YZ, HL, and LY designed and wrote the manuscript. YZ, PW, ZC, ML, DZ, LY, and HL edited the manuscript. All authors contributed to the article and approved the submitted version.

FUNDING

This review was funded by the National Natural Science Foundation of China (91939104, 82070465, 82170469); Heilongjiang Province Science Foundation for Distinguished Young Scholars (JQ2021H001); General project of Heilongjiang Provincial Health Commission (2020-075); Construction Project of Scientific Research and Innovation Team of Harbin Medical University-Daqing (HD-CXTD-202001); Key Discipline Construction Project of Harbin Medical University-Daqing (HD-ZDXK-202001).

REFERENCES

1. Levine GN, Bates ER, Bittl JA, Brindis RG, Fihn SD, Fleisher LA, et al. (2016). ACC/AHA Guideline Focused Update on Duration of Dual Antiplatelet Therapy in Patients With Coronary Artery Disease: A Report of the American College of Cardiology/American Heart Association Task Force on Clinical Practice Guidelines: An Update of the (2011). ACCF/AHA/SCAI Guideline for Percutaneous Coronary Intervention, (2011). ACCF/AHA Guideline for Coronary Artery Bypass Graft Surgery, (2012). ACC/AHA/ACP/AATS/PCNA/SCAI/STS Guideline for the Diagnosis and Management of Patients With Stable Ischemic Heart Disease, (2013). ACCF/AHA Guideline for the Management of ST-Elevation Myocardial Infarction, (2014). AHA/ACC Guideline for the Management of Patients With Non-ST-Elevation Acute Coronary Syndromes, and (2014). ACC/AHA Guideline on Perioperative Cardiovascular Evaluation and Management of Patients Undergoing Noncardiac Surgery. *Circulation*. (2016). 134: e123–55. doi: 10.1161/CIR.0000000000000452
2. Severino P, D'Amato A, Pucci M, Infusino F, Birtolo LI, Mariani MV, et al. Ischemic heart disease and heart failure: role of coronary ion channels. *Int J Mol Sci.* (2020) 21:3167. doi: 10.3390/ijms21093167
3. Pepine CJ, Nichols WW. The pathophysiology of chronic ischemic heart disease. *Clin Cardiol.* (2007) 30(2 Suppl 1):I4–9. doi: 10.1002/clc.20048
4. Thygesen K, Alpert JS, Jaffe AS, Simoons ML, Chaitman BR, White HD, et al. Third universal definition of myocardial infarction. *J Am Coll Cardiol.* (2012) 60:1581–98. doi: 10.1016/j.jacc.2012.08.001
5. Potz BA, Parulkar AB, Abid RM, Sodha NR, Sellke FW. Novel molecular targets for coronary angiogenesis and ischemic heart disease. *Coron Artery Dis.* (2017) 28:605–13. doi: 10.1097/MCA.0000000000000516
6. Zago S, Ferrucci R, Fregni F, Priori A. Bartholow, Sciamanna, Alberti: pioneers in the electrical stimulation of the exposed human cerebral cortex. *Neuroscientist.* (2008) 14:521–8. doi: 10.1177/1073858407311101
7. Ae C, Inoue T, Inglis MA, Viar KE, Huang L, Ye H, et al. C1 neurons mediate a stress-induced anti-inflammatory reflex in mice. *Nat Neurosci.* (2017) 20:700–7. doi: 10.1038/nn.4526
8. Hosomi K, Seymour B, Saitoh Y. Modulating the pain network–neurostimulation for central poststroke pain. *Nat Rev Neurol.* (2015) 11:290–9. doi: 10.1038/nrneurol.2015.58
9. Balint R, Cassidy NJ, Cartmell SH. Electrical stimulation: a novel tool for tissue engineering. *Tissue Eng Part B Rev.* (2013) 19:48–57. doi: 10.1089/ten.teb.2012.0183
10. Gratieri T, Santer V, Kalia YN. Basic principles and current status of transcorneal and transscleral iontophoresis. *Expert Opin Drug Deliv.* (2017) 14:1091–102. doi: 10.1080/17425247.2017.1266334
11. Zhao S, Mehta AS, Zhao M. Biomedical applications of electrical stimulation. *Cell Mol Life Sci.* (2020) 77:2681–99. doi: 10.1007/s00018-019-03446-1
12. Shapira Y, Sammons V, Forden J, Guo GF, Kipp A, Girgulis J, et al. Brief electrical stimulation promotes nerve regeneration following experimental in-continuity nerve injury. *Neurosurgery.* (2019) 85:156–63. doi: 10.1093/neuros/nyy221
13. Schmidt CE, Shastri VR, Vacanti JP, Langer R. Stimulation of neurite outgrowth using an electrically conducting polymer. *Proc Natl Acad Sci U S A.* (1997) 94:8948–53. doi: 10.1073/pnas.94.17.8948

14. Ghasemi-Mobarakeh L, Prabhakaran MP, Morshed M, Nasr-Esfahani MH, Baharvand H, Kiani S, et al. Application of conductive polymers, scaffolds and electrical stimulation for nerve tissue engineering. *J Tissue Eng Regen Med*. 5:e17–e35. doi: 10.1002/term.383
15. Radisic M, Park H, Shing H, Consi T, Schoen FJ, Langer R, et al. Functional assembly of engineered myocardium by electrical stimulation of cardiac myocytes cultured on scaffolds. *Proc Natl Acad Sci U S A*. (2004) 101:18129–34. doi: 10.1073/pnas.0407817101
16. Hulsmans M, Clauss S, Xiao L, Aguirre AD, King KR, Hanley A, et al. Macrophages facilitate electrical conduction in the heart. *Cell*. (2017) 169:510–22. doi: 10.1016/j.cell.2017.03.050
17. Kim IS, Song JK, Song YM, Cho TH, Lee TH, Lim SS, et al. Novel effect of biphasic electric current on *in vitro* osteogenesis and cytokine production in human mesenchymal stromal cells. *Tissue Eng Part A*. (2009) 15:2411–22. doi: 10.1089/ten.tea.2008.0554
18. Uitterdijk A, Yetgin T, Lintel Hekkert M, Sneep S, Krabbendam-Peters I, Beusekom HMMV, et al. Vagal nerve stimulation started just prior to reperfusion limits infarct size and no-reflow. *Basic Res Cardiol*. (2015) 110:508. doi: 10.1007/s00395-015-0508-3
19. Cong L, Gao Z, Zheng Y, Ye T, Wang Z, Wang P, et al. Electrical stimulation inhibits val-boroPro-induced pyroptosis in THP-1 macrophages *via* sirtuin3 activation to promote autophagy and inhibit ROS generation. *Aging*. (2020) 12:6415–35. doi: 10.18632/aging.103038
20. Mendonça AC, Barbieri CH, Mazzer N. Directly applied low intensity direct electric current enhances peripheral nerve regeneration in rats. *J Neurosci Methods*. (2003) 129:183–190. doi: 10.1016/S0165-0270(03)00207-3
21. Huh JE, Seo DM, Baek YH, Choi DY, Park DS, Lee JD. Biphasic positive effect of formononetin on metabolic activity of human normal and osteoarthritic subchondral osteoblasts. *Int Immunopharmacol*. (2010) 10:500–7. doi: 10.1016/j.intimp.2010.01.012
22. McLeod KJ, Rubin CT. The effect of low-frequency electrical fields on osteogenesis. *J Bone Joint Surg Am*. (1992) 74:920–9. doi: 10.2106/00004623-199274060-00014
23. Hartig M, Joos U, Wiesmann HP. Capacitively coupled electric fields accelerate proliferation of osteoblast-like primary cells and increase bone extracellular matrix formation *in vitro*. *Eur Biophys J*. (2000) 29:499–506. doi: 10.1007/s002490000100
24. Lohmann CH, Schwartz Z, Liu Y, Li Z, Simon BJ, Sylvia VL, et al. Pulsed electromagnetic fields affect phenotype and connexin 43 protein expression in MLO-Y4 osteocyte-like cells and ROS 17/2.8 osteoblast-like cells. *J Orthop Res*. (2003) 21:326–34. doi: 10.1016/S0736-0266(02)00137-7
25. Aaron RK, Wang S, Ciombor DM. Upregulation of basal TGFbeta1 levels by EMF coincident with chondrogenesis–implications for skeletal repair and tissue engineering. *J Orthop Res*. (2002) 20:233–40 doi: 10.1016/S0736-0266(01)00084-5
26. Guo ZJ, Guo Z. Non-excitatory electrical stimulation attenuates myocardial infarction *via* homeostasis of calcitonin gene-related peptide in myocardium. *Peptides*. (2015) 65:46–52. doi: 10.1016/j.peptides.2015.01.010
27. He W, Jing X, Wang X, Rong P, Li L, Shi H, et al. Transcutaneous auricular vagus nerve stimulation as a complementary therapy for pediatric epilepsy: a pilot trial. *Epilepsy Behav*. (2013) 28:343–6. doi: 10.1016/j.yebeh.2013.02.001
28. Wang Z, Yu L, Chen M, Wang S, Jiang H. Transcutaneous electrical stimulation of auricular branch of vagus nerve: a noninvasive therapeutic approach for post-ischemic heart failure. *Int J Cardiol*. (2014) 177:676–7. doi: 10.1016/j.ijcard.2014.09.165
29. Han JS. Acupuncture: neuropeptide release produced by electrical stimulation of different frequencies. *Trends Neurosci*. (2003) 26:17–22. doi: 10.1016/S0166-2236(02)00006-1
30. Liu PY, Tian Y, Xu SY. Mediated protective effect of electroacupuncture pretreatment by miR-214 on myocardial ischemia/reperfusion injury. *J Geriatr Cardiol*. (2014) 11:303–10. doi: 10.11909/j.issn.1671-5411.2014.04.005
31. Huang YG, Tao W, Yang SB, Wang JF, Mei ZG, Feng ZT. Autophagy: novel insights into therapeutic target of electroacupuncture against cerebral ischemia/reperfusion injury. *Neural Regen Res*. (2019) 14:954–61. doi: 10.4103/1673-5374.250569
32. Ahn A, Frishman WH, Gutwein A, Passeri J, Nelson M. Therapeutic angiogenesis: a new treatment approach for ischemic heart disease–part I. *Cardiol Rev*. (2008) 16:163–71. doi: 10.1097/CRD.0b013e3181620e3b
33. Johnson T, Zhao L, Manuel G, Taylor H, Liu D. Approaches to therapeutic angiogenesis for ischemic heart disease. *J Mol Med*. (2019) 97:141–51. doi: 10.1007/s00109-018-1729-3
34. Breier G, Damert A, Plate KH, Risau W. Angiogenesis in embryos and ischemic diseases. *Thromb Haemost*. (1997) 78:678–83. doi: 10.1055/s-0038-1657611
35. Ribatti D, Conconi MT, Nussdorfer GG. Nonclassic endogenous novel regulators of angiogenesis. *Pharmacol Rev*. 59:185–205. doi: 10.1124/pr.59.2.3
36. Carmeliet Peter. VEGF as a key mediator of angiogenesis in cancer. *Oncology*. (2005) 69 Suppl 3: 4–10. doi: 10.1159/000088478
37. Deveza L, Choi J, Yang F. Therapeutic angiogenesis for treating cardiovascular diseases. *Theranostics*. (2012) 2:801–14. doi: 10.7150/thno.4419
38. Asadi MR, Torkaman G, Hedayati M, Mofid M. Role of sensory and motor intensity of electrical stimulation on fibroblastic growth factor-2 expression, inflammation, vascularization, and mechanical strength of full-thickness wounds. *J Rehabil Res Dev*. (2013) 50:489–98. doi: 10.1682/JRRD.2012.04.0074
39. Kanno S, Oda N, Abe M, Saito S, Hori K, Handa Y, et al. Establishment of a simple and practical procedure applicable to therapeutic angiogenesis. *Circulation*. (1999) 99:2682–7. doi: 10.1161/01.CIR.99.20.2682
40. Geng K, Wang J, Liu P, Tian X, Liu H, Wang X, et al. Electrical stimulation facilitates the angiogenesis of human umbilical vein endothelial cells through MAPK/ERK signaling pathway by stimulating FGF2 secretion. *Am J Physiol Cell Physiol*. (2019) 317:C277–6. doi: 10.1152/ajpcell.00474.2018
41. Hang J, Kong L, Gu JW, Adair TH. VEGF gene expression is upregulated in electrically stimulated rat skeletal muscle. *Am J Physiol*. (1995). 269: H1827-31. doi: 10.1152/ajpheart.1995.269.5.H1827
42. Zhao M, Bai H, Wang E, Forrester JV, McCaig CD. Electrical stimulation directly induces pre-angiogenic responses in vascular endothelial cells by signaling through VEGF receptors. *J Cell Sci*. (2004) 117(Pt 3):397–405. doi: 10.1242/jcs.00868
43. Bai H, Forrester JV, Zhao M. DC electric stimulation upregulates angiogenic factors in endothelial cells through activation of VEGF receptors. *Cytokine*. (2011) 55:110–5. doi: 10.1016/j.cyto.2011.03.003
44. She Q. The study of angiogenesis induced by electrical stimulation below contraction threshold, in ischemic myocardium. *J China Med Univ*. (2003) 296–99. doi: 10.13406/j.cnki.cyxb.2003.03.012
45. Liu XD, Long YF, Wang YM, Shen Z. Effects of 50 Hz low voltage electric stimulation on angiogenesis and the expression of VEGF in the ischemic myocardium. *Chinese J Rehabilitation Med*. (2008) 30:378–80.
46. Kerr JF, Wyllie AH, Currie AR. Apoptosis: a basic biological phenomenon with wide-ranging implications in tissue kinetics. *Br J Cancer*. (1972) 26:239–57. doi: 10.1038/bjc.1972.33
47. Wyllie, AH. The genetic regulation of apoptosis. *Curr Opin Genetics Develop*. (1995) 5:97–104. doi: 10.1016/S0959-437X(95)90060-8
48. Vaux DL, Strasser A. The molecular biology of apoptosis. *Proc Natl Acad Sci USA*. (1996) 93:2239–44. doi: 10.1073/pnas.93.6.2239
49. Willis S, Day CL, Hinds MG, Huang DCS. The Bcl-2-regulated apoptotic pathway. *J Cell Sci*. (2003) 116(Pt 20):4053–6. doi: 10.1242/jcs.00754
50. Wang X, Simpson ER, Brown KA. p53: Protection against tumor growth beyond effects on cell cycle and apoptosis. *Cancer Res*. (2015) 75:5001–7. doi: 10.1158/0008-5472.CAN-15-0563
51. Dong Y, Chen H, Gao J, Liu Y, Li J, Wang J. Molecular machinery and interplay of apoptosis and autophagy in coronary heart disease. *J Mol Cell Cardiol*. (2019) 136:27–41. doi: 10.1016/j.yjmcc.2019.09.001
52. Wang X, Guo Z, Ding Z, Mehta JL. Inflammation, autophagy, and apoptosis after myocardial infarction. *J Am Heart Assoc*. (2018) 7:e008024. doi: 10.1161/JAHA.117.008024
53. Love MR, Palee S, Chattipakorn SC, Chattipakorn N. Effects of electrical stimulation on cell proliferation and apoptosis. *J Cell Physiol*. (2018) 233:1860–76. doi: 10.1002/jcp.25975
54. Baba T, Kameda M, Yasuhara T, Morimoto T, Kondo A, Shingo T, et al. Electrical stimulation of the cerebral cortex exerts antiapoptotic, angiogenic, and anti-inflammatory effects in ischemic stroke rats through phosphoinositide 3-kinase/Akt signaling pathway. *Stroke*. (2009) 40:e598–e605. doi: 10.1161/STROKEAHA.109.563627
55. Matsuki N, Takeda M, Ishikawa T, Kinjo A, Hayasaka T, Imai Y, et al. Activation of caspases and apoptosis in response to low-voltage electric pulses. *Oncol Rep*. (2010) 23:1425–33. doi: 10.3892/or_00000780

56. Oshima Y, Sakamoto T, Kawano Y, Hata Y, Yoshikawa H, Sonoda KH, et al. Synergistic effect of electric pulses and bleomycin on cultured rabbit subconjunctival fibroblasts. *Graefes Arch Clin Exp Ophthalmol.* (1998) 236:52–60. doi: 10.1007/s004170050042
57. Hernández-Bule ML, Trillo MÁ, Úbeda A. Molecular mechanisms underlying antiproliferative and differentiating responses of hepatocarcinoma cells to subthermal electric stimulation. *PLoS ONE.* (2014) 9:e84636. doi: 10.1371/journal.pone.0084636
58. Wang M, Li P, Liu M, Song W, Wu Q, Fan Y. Potential protective effect of biphasic electrical stimulation against growth factor-deprived apoptosis on olfactory bulb neural progenitor cells through the brain-derived neurotrophic factor-phosphatidylinositol 3'-kinase/Akt pathway. *Exp Biol Med.* (2013) 238:951–9. doi: 10.1177/1535370213494635
59. Yang F, Shen XC, He Y, Zhang B, Shen Z, Liu X. Effects of subthreshold electrical stimulation on cardiomyocyte apoptosis and gene expression of bcl-2 and bax in ischemic cardiomyocytes of rats. *J Nanjing Med Univ.* (2014) 39:494–7. doi: 10.19367/j.cnki.1000-2707.2014.04.013
60. Wei F, Liu X. The effects of subthreshold electrical stimulation on apoptosis and caspase-3 expression of ischemic cardiomyocyte. *Chin J Phys Med Rehab.* (2011) 33:808–11.
61. Lu Z, Yang H, Sutton MN, Yang M, Clarke CH, Liao WS, et al. ARHI (DIRAS3) induces autophagy in ovarian cancer cells by downregulating the epidermal growth factor receptor, inhibiting PI3K and Ras/MAP signaling and activating the FOXo3a-mediated induction of Rab7. *Cell Death Differ.* (2014) 21:1275–89. doi: 10.1038/cdd.2014.48
62. Duve CD. Lysosomes revisited. *Eur j biochem.* (1983) 137:391–7. doi: 10.1111/j.1432-1033.1983.tb07841.x
63. Jeanne MP, Vindis C. Autophagy in health and disease: focus on the cardiovascular system. *Essays in Biochemistry.* (2017) 61:721–732. doi: 10.1042/EBC20170022
64. Furlong K, Hwang S. Autophagy and noroviruses. *Viruses.* (2019) 11:1–8. doi: 10.3390/v11030244
65. Ma X, Liu H, Foyil SR, Godar RJ, Weinheimer CJ, Hill JA, et al. Impaired autophagosome clearance contributes to cardiomyocyte death in ischemia/reperfusion injury. *Circulation.* (2012) 125:3170–81. doi: 10.1161/CIRCULATIONAHA.111.041814
66. Shi B, Ma M, Zheng Y, Pan Y, Lin X. mTOR and Beclin1: two key autophagy-related molecules and their roles in myocardial ischemia/reperfusion injury. *J Cell Physiol.* (2019) 234:12562–8. doi: 10.1002/jcp.28125
67. He J, Huang ZY, Chen WB, Liu WL, Shang GH, Tao J, et al. Effects of protection of electroacupuncture against cerebral ischemic injury by inhibiting autophagy in rats. *Zhongguo Kangfu Yixue* Zazhi. 30:1203–7.
68. Li CM, Shu S, Qian XL, Li SS, Jin LJ, Yuan Y, et al. Effect of electroacupuncture at Shuigou point on the expression of autophagy-associated protein p62 in rats with cerebral ischemia reperfusion. *Liaoning Zhongyi Zazhi*. 43:2439–41. doi: 10.13192/j.issn.1000-1719.2016.11.070
69. Shu S, Li CM, You YL, Qian XL, Zhou S, Ling CQ, et al. Electroacupuncture ameliorates cerebral ischemia-reperfusion injury by regulation of autophagy and apoptosis. *Evid Based Complement Alternat Med*. (2016) 6:1–8. doi: 10.1155/2016/7297425
70. Yang Y J, Pessin J E, Wang L. High frequency electrical stimulation of sciatic nerve enhances skeletal muscle autophagy in mice. *Acta Physiologica Sinica.* (2017) 69:422–8.
71. Tan C, Wang C, Du L, Liu WW, Song J, Feng G, et al. Effect to electroacupuncture and Moxibustion pretreatment on Expression LC3 and Beclin1 in rats with myocardial ischemia reperfusion injury. *Acupunct Res.* (2018) 43:1–7. doi: 10.13702/j.1000-0607.170181
72. Zhou W, Chen H, Wang M, Ma F. Effect of electroacupuncture (EA) preconditioning on mTOR (mammalian target of rapamycin) in hippocampus following transient cerebral ischemia-reperfusion in mice. *Chin J Clin Oncol.* (2016) 10:1937–41.
73. Gaudino M, Crea F. Inflammation in coronary artery disease: Which biomarker and which treatment? *Eur J Prev Cardiol.* (2019) 26:869–71. doi: 10.1177/2047487319829307
74. Hansson GK. Inflammation, atherosclerosis, and coronary artery disease. *N Engl J Med.* (2005) 352:1685–95. doi: 10.1056/NEJMra043430
75. Azambuja MI. Inflammation as the cause of coronary heart disease. *Lancet Infect Dis.* (2010) 10:142–3. doi: 10.1016/S1473-3099(10)70029-3
76. Libby P. Inflammation in atherosclerosis. *Nature*. (2002) 420:868–74. doi: 10.1038/nature01323
77. Takahashi M. Role of NLRP3 inflammasome in cardiac inflammation and remodeling after myocardial infarction. *Biol Pharm Bull.* (2019) 42:518–23. doi: 10.1248/bpb.b18-00369
78. Toldo S, Marchetti C, Mauro AG, Chojnacki J, Mezzaroma E, Carbone S, et al. Inhibition of the NLRP3 inflammasome limits the inflammatory injury following myocardial ischemia-reperfusion in the mouse. *Int J Cardiol.* (2016) 209:215–20. doi: 10.1016/j.ijcard.2016.02.043
79. Song XM, Wu XJ, Li JG, Le LL, Liang H, Xu Y, et al. The effect of electroacupuncture at ST36 on severe thermal injury-induced remote acute lung injury in rats. *Burns.* (2015) 41:1449–58. doi: 10.1016/j.burns.2015.03.004
80. Sun X, Li M, Shen D, Hu L, Cai RL, Wu ZJ, et al. Effects of Acupuncture Neiguan (PC 6) and Xinshu (BL 15)on the expression of MMP-9 with coronary heart disease rats. *J Tradit Chin Med.* (2013) 036:5–9. doi: 10.19288/j.cnki.issn.1000-2723.2013.02.002
81. Kim MS, Lee SH, Kim JH, Kin OK, Yu AR, Baik HH. Anti-inflammatory effects of step electrical stimulation on complete freund's adjuvant (CFA) induced rheumatoid arthritis rats. *J Nanosci Nanotechnol.* (2019) 19:6546–53. doi: 10.1166/jnn.2019.17077
82. Gürgen SG, Sayin O, Cetin F, Yücel AT. Transcutaneous electrical nerve stimulation (TENS) accelerates cutaneous wound healing and inhibits pro-inflammatory cytokines. *Inflammation.* (2014) 37:775–84. doi: 10.1007/s10753-013-9796-7
83. Gekeler F, Zrenner E, Bartz-Schmidt KU. Ocular electrical stimulation: therapeutic application and active retinal implants for hereditary retinal degenerations. *Ophthalmologe.* (2015) 112:712–9. doi: 10.1007/s00347-015-0126-3
84. Zhou WT, Ni YQ, Jin ZB, Zhang M, Wu JH, Zhu Y, et al. Electrical stimulation ameliorates light-induced photoreceptor degeneration *in vitro via* suppressing the proinflammatory effect of microglia and enhancing the neurotrophic potential of Müller cells. *Exp Neurol.* (2012) 238:192–208. doi: 10.1016/j.expneurol.2012.08.029
85. Sun P, Li H, Lu Z, Su X, Ma Z, Chen J, et al. Comparison of cortical responses to the activation of retina by visual stimulation and transcorneal electrical stimulation. *Brain Stimul.* (2018) 11:667–75. doi: 10.1016/j.brs.2018.02.009
86. Shin J, Hwang M, Back S, Nam H, Yoo C, Park J, et al. Electrical impulse effects on degenerative human annulus fibrosus model to reduce disc pain using micro-electrical impulse-on-a-chip. *Sci Rep.* (2019) 9:5827. doi: 10.1038/s41598-019-42320-9
87. Mélanie Guyot, Thomas Simon, Clara Panzolini, Ceppo F, Daoudlarian D, Murris E, et al. Apical splenic nerve electrical stimulation discloses an anti-inflammatory pathway relying on adrenergic and nicotinic receptors in myeloid cells. *Brain Behav Immun.* (2019) 80:238–46. doi: 10.1016/j.bbi.2019.03.015
88. Cai R, Hu L, Yu Q, Liu L, Zhang T, Lei Y. Effects of electroacupuncture on serum interleukin-1β and interleukin-10 levels and myocardial NF-κB p65 protein expression in rats with acute myocardial ischemia-reperfusion injury. *J Tradit Chin Med.* (2014) 37:6–9. doi: 10.19288/j.cnki.issn.1000-2723.2014.02.002
89. Tullio F, Angotti C, Perrelli MG, Penna C, Pagliaro P. Redox balance and cardioprotection. *Basic Res Cardiol.* (2013) 108:392. doi: 10.1007/s00395-013-0392-7
90. Zhang C, Yu H, Shen Y, Ni X, Shen S, Das UN. Polyunsaturated fatty acids trigger apoptosis of colon cancer cells through a mitochondrial pathway. *Arch Med Sci.* (2015) 11:1081–94. doi: 10.5114/aoms.2015.54865
91. Yang X, He T, Han S, Zhang X, Yang S, Xing Y, et al. The role of traditional Chinese medicine in the regulation of oxidative stress in treating coronary heart disease. *Oxid Med Cell Longev.* (2019) 2019:3231424. doi: 10.1155/2019/3231424
92. Zhou T, Yan L, Xie C, Li P, Jiang L, Fang J, et al. A mussel-inspired persistent ROS-scavenging, electroactive, and osteoinductive scaffold based on electrochemical-driven *in situ* nanoassembly. *Small.* (2019) 15:e1805440. doi: 10.1002/smll.201805440
93. Mankowski RT, Ahmed S, Beaver T, Dirain M, Han C, Hess P, et al. Intraoperative hemidiaphragm electrical stimulation reduces oxidative stress and upregulates autophagy in surgery patients undergoing

mechanical ventilation: exploratory study. *J Transl Med.* (2016) 10:14. doi: 10.1186/s12967-016-1060-0

94. Sha F, Ye X, Zhao W, Xu CL, Wang L, Ding MH, et al. Effects of electroacupuncture on the levels of retinal gamma-aminobutyric acid and its receptors in a guinea pig model of lens-induced myopia. *Neuroscience.* (2015) 287:164–174. doi: 10.1016/j.neuroscience.2014.12.022
95. Zhang XL, Huang W, Yang QQ, Xiang LL, Jiang GD. Effect of electroacupuncture preconditioning on cell apoptosis mediated by mitochondrial reactive oxygen species in myocardial ischemia/reperfusion injury rats. *Zhen Ci Yan Jiu.* (2020) 45:961–7. doi: 10.13702/j.1000-0607.200053
96. Liu XL, Bai ZH, Ma TM, Ren L, Chen YG, Rong PJ, et al. Effects of electroacupuncture at Neiguan on gene expressions of β2 subunit of L-type voltage-gated $Ca2^{+}$ channels of rats with myocardial ischemia. *J Tradit Chin Med.* (2014) 2776–8.
97. Zhou W, Ko Y, Benharash P, Yamakawa K, Mahajan K. Cardioprotection of electroacupuncture against myocardial ischemia-reperfusion injury by modulation of cardiac norepinephrine release. *Am J Physiol Heart Circ Physiol.* (2012) 302:H1818–25. doi: 10.1152/ajpheart.00030.2012
98. Dart AM, Schömig A, Dietz R, Mayer E, Kübler W. Release of endogenous catecholamines in the ischemic myocardium of the rat. Part B: effect of sympathetic nerve stimulation. *Circ Res.* (1984) 55:702–6. doi: 10.1161/01.RES.55.5.702
99. Hu S, Zhao ZK, Liu R, Wang HB, Gu CY, Luo HM, et al. Electroacupuncture activates enteric glial cells and protects the gut barrier in hemorrhaged rats. *World J Gastroenterol.* (2015) 21:1468–78. doi: 10.3748/wjg.v21.i5.1468

Conflict of Interest: The authors declare that the research was conducted in the absence of any commercial or financial relationships that could be construed as a potential conflict of interest.

Publisher's Note: All claims expressed in this article are solely those of the authors and do not necessarily represent those of their affiliated organizations, or those of the publisher, the editors and the reviewers. Any product that may be evaluated in this article, or claim that may be made by its manufacturer, is not guaranteed or endorsed by the publisher.

Copyright © 2021 Zhao, Wang, Chen, Li, Zhang, Yang and Li. This is an open-access article distributed under the terms of the Creative Commons Attribution License (CC BY). The use, distribution or reproduction in other forums is permitted, provided the original author(s) and the copyright owner(s) are credited and that the original publication in this journal is cited, in accordance with accepted academic practice. No use, distribution or reproduction is permitted which does not comply with these terms.

frontiers in Cardiovascular Medicine

ORIGINAL RESEARCH
published: 30 November 2021
doi: 10.3389/fcvm.2021.736226

Plasma Exosomes at the Late Phase of Remote Ischemic Pre-conditioning Attenuate Myocardial Ischemia-Reperfusion Injury Through Transferring miR-126a-3p

*Danni Li†, Yang Zhao†, Chuyi Zhang, Fan Wang, Yan Zhou and Sanqing Jin**

Department of Anesthesia, The Sixth Affiliated Hospital, Sun Yat-sen University, Guangzhou, China

OPEN ACCESS

Edited by:
Hui Gong,
Fudan University, China

Reviewed by:
Pan Gao,
Fudan University, China
Xiyuan Lu,
Shanghai JiaoTong University, China

***Correspondence:**
Sanqing Jin
jinsq@mail.sysu.edu.cn

†These authors have contributed equally to this work and share first authorship

Specialty section:
This article was submitted to General Cardiovascular Medicine, a section of the journal Frontiers in Cardiovascular Medicine

Received: *04 July 2021*
Accepted: *02 November 2021*
Published: *30 November 2021*

Citation:
Li D, Zhao Y, Zhang C, Wang F, Zhou Y and Jin S (2021) Plasma Exosomes at the Late Phase of Remote Ischemic Pre-conditioning Attenuate Myocardial Ischemia-Reperfusion Injury Through Transferring miR-126a-3p. Front. Cardiovasc. Med. 8:736226. doi: 10.3389/fcvm.2021.736226

Background: Remote ischemic pre-conditioning (RIPC) alleviated the myocardial ischemia-reperfusion injury, yet the underlying mechanisms remain to be fully elucidated, especially at the late phase. Searching a key component as a transfer carrier may provide a novel insight into RIPC-mediated cardioprotection in the condition of myocardial ischemia-reperfusion.

Objective: To investigate the cardioprotective effect of plasma exosomes at the late phase of RIPC and its potential signaling pathways involved.

Methods and Results: Exosomes were isolated from the plasma of rats 48 h after the RIPC or control protocol. Although the total plasma exosomes level had no significant change at the late phase of RIPC (RIPC-exosome) compared with the control exosomes (Control-exosome), the RIPC-exosome afforded remarkable protection against myocardial ischemia-reperfusion (MI/R) injury in rats and hypoxia-reoxygenation (H/R) injury in cells. The miRNA array revealed significant enrichment of miR-126a-3p in RIPC-exosome. Importantly, both miR-126a-3p inhibitor and antagonist significantly blunted the cardioprotection of RIPC-exosome in H/R cells and MI/R rats, respectively, while miR-126a-3p mimic and agomir showed significant cardioprotection against H/R injury in cells and MI/R injury in rats. Mechanistically, RIPC-exosome, especially exosomal miR-126a-3p, activated the reperfusion injury salvage kinase (RISK) pathway by enhancing the phosphorylation of Akt and Erk1/2, and simultaneously inhibited Caspase-3 mediated apoptotic signaling.

Conclusions: Our findings reveal a novel myocardial protective mechanism that plasma exosomes at the late phase of RIPC attenuate myocardial ischemia-reperfusion injury via exosomal miR-126a-3p.

Keywords: remote ischemic pre-conditioning, exosomes, microRNA, miR-126a-3p, cardioprotection, myocardial ischemia-reperfusion, cardiomyocyte apoptosis

INTRODUCTION

It has been well-known that remote ischemic pre-conditioning (RIPC), a phenomenon where transient non-fatal ischemia of distant organs from the heart, protects the myocardium against myocardial ischemia-reperfusion (MI/R) injury (1). The protective effects of RIPC have early phase and late phase (2, 3). The early phase protection which occurs immediately after RIPC lasts for about 3 h. The late phase protection which appears 24–48 h after RIPC, lasts for 3–4 days and has lots of biology efficacies (4). The mechanisms underlying the cardioprotective effects of RIPC, especially at the late phase, remain elusive.

Many studies support that blood-borne mediators serve as signal transduction mechanisms (5, 6). Several studies have focused on exploring the nature of circulatory mediators in the blood that may carry pre-conditioning signals from remote organs to target organs, binds to respective receptors, and activates intracellular signaling pathways (7–13). Our previous studies show the cardioprotection of RIPC at the late phase can be transferred by plasma (14–17), but many questions about the mechanisms remain unanswered.

Exosomes are small (50–90 nm) endogenous membrane vesicles secreted by a variety of cells and are thought to be good mediators of intercellular communication and crosstalk through the transfer of various signaling molecules, including proteins, mRNAs, and non-coding RNAs such as miRNAs (18). In the last decade, the functions of exosomes in MI/R injury have been widely explored (19–23). It has been reported that long-term exercise-derived exosomes have cardioprotection against MI/R injury with exosomal miR-342-5p as a novel cardioprotective exerkine (24). Vincencio et al. proposed that exosomes induced by the RIPC at the early phase may act as carriers of the cardioprotective factors (25). Minghua et al. found that exosomal miR-24 at the early phase of RIPC in rats may play a central role in mediating the cardioprotective effects of RIPC (26). These findings suggest that exosomes may play a role in the cardiovascular benefits conferred by RIPC. Since small amounts of exosomes may have significant effects (27), it is crucial to explore the functional effects of exosomes, especially their cardioprotection in the late phase of RIPC.

In this study, we found that the cardioprotective effect could be transferred by plasma exosomes at the late phase of RIPC and exosomal miR-126a-3p might be a novel cardioprotective molecule against MI/R injury, which activated the RISK pathway and inhibited the activation of apoptotic protein Caspase-3.

MATERIALS AND METHODS

Animals

Male Sprague-Dawley rats (250–300 g, aged 7–8 weeks) were obtained from the Experimental Animal Center of Southern Medical University (China) and housed in separate cages in a temperature-controlled room (22–24°C) with free access to water and food. We used male rats in this study to avoid the possible interference of estrogen hormonal disturbances on the results because studies have shown that estrogen *per se* exerts cardiovascular protective effects. Rats were randomly assigned to either experimental or a control group, using a completely randomized design. This study was approved by the Animal Care Ethics Committees of the Sixth Affiliated Hospital, Sun Yat-sen University (IACUC-20190221-002 and IACUC-2020091101). Rats were anesthetized with an intraperitoneal injection of 3% sodium pentobarbital (60 mg/kg).

Animal Model of RIPC

RIPC was operated by binding elastic rubber bands around the proximal ends of both hind limbs with a 4-cycle procedure (5 min ischemia followed by 5 min reperfusion) after the rats were anesthetized. Cessation of blood flow to the hind limbs was confirmed using laser Doppler imaging to monitor microcirculatory blood flow in the hind limbs (Laser Doppler Blood Perfusion Imager, Perimed AB, Sweden). After 48 h, the rats in both groups were anesthetized, placed in a supine position, laparotomy performed, blood was drawn from the abdominal aorta using a $7^{\#}$ needle and rapidly removed into a vacutainer containing sodium citrate.

Isolation of Exosomes and Free-Exosomes Plasma

Exosomes were prepared by differential centrifugation at 4°C as follows. Whole blood samples were centrifuged at 1,600 × g for 20 min to obtain plasma, then centrifuged at 10,000 × g for 45 min to remove platelets and cells, and then twice at 100,000 × g for 70 min with a Type 100 Ti rotor (Beckman, Germany). After a series of differential centrifugation steps above, the final precipitation was considered as exosomes. Exosomes isolated from 1 ml of plasma were redissolved in 100 μl of PBS and filtered by a 0.22 μm pore filter and stored at −80°C for further experiments. *In vivo* study, 100 μL of the exosome suspension was further diluted to 1 ml before use. *In vitro* study, 100 μl of the exosome suspension was added to each well.

Free-exosome plasma was prepared by differential centrifugation at 4°C as follows. Whole blood samples were centrifuged at 1,600 xg for 20 min to obtain supernatant, then centrifuged at 2,000 × g for 45 min and 10,000 × g for 45 min to remove cells and platelets, and then at 110,000 × g for 70 min with a Type 100 Ti rotor. After that, the supernatant was considered as free-exosome plasma. Free-exosome plasma was also filtered using a 0.22 μm pore filter and stored at −80°C.

Transmission Electron Microscopy (TEM)

Transmission electron microscopy (FEI, Thermo Fisher, USA) was used to observe the exosomes. Exosomes purified from 1,000 μL of plasma were resuspended in 1,000 μl of PBS. Then, 10 μL of the exosome solution was loaded on a formvar/carbon-coated 200-mesh copper electron microscopy grid and incubated for 2 min at 25°C, and then was stained with 3% phosphotungstic acid for 2 min at 25°C. After that, the exosomes were visualized using a transmission electron microscope. Micrographs were used to quantify the diameter of exosomes.

Nanoparticle Tracking Analysis

Nanoparticle tracking analysis (NTA) was used to analyze the absolute size distribution of exosomes given that the Brownian movement of nanoparticles in a solution is related to their size (28). Exosomes isolated from 1 ml of plasma were resuspended in 1 ml of PBS,1:1000, dilutions were analyzed in NanoSight NS300 (Marvel, UK). The following settings were used: measurement temperature of 20 ± 1°C, 30 frames per second, and measurement time of 60 s. Each sample was tested thrice.

Cell Culture

The rat cardio-myoblast cell line (H9C2) was purchased from the Cell Bank of the Chinese Academy of Sciences. The H9C2 cells were cultured in a complete medium containing Dulbecco's modified Eagle's medium (DMEM) (Gibco, Thermo Fisher, USA), 10% fetal bovine serum (Gibco, Thermo Fisher, USA), and 1% penicillin-streptomycin (Sigma-Aldrich, USA).

Neonatal rat primary cardiomyocytes were isolated from 1or 2 days old Sprague Dawley rats. The ventricular parts of the hearts were minced into 1–2 mm^3 tissue blocks under sterile conditions. The tissues were repeatedly digested with freshly prepared compound digestive enzyme (collagenase II 1 mg/ml, 0.2 mg/ml in D-Hank's solution, sterile filtered, pH 7.2. Gibco, Thermo Fisher, USA) for 20 min in at 37°C until they were completely digested and then filtered through a 200 μm cell strainer. Filtered cardiac cells were cultured in a plate and incubated at 37°C for 1 h to remove fibroblasts. The suspensions were centrifuged at 1,000 rpm for 5 min at 4°C and then the cardiomyocytes were cultured in DMEM/F12 (Gibco, Thermo Fisher, USA) medium supplemented with 10% fetal bovine serum, 1% penicillin/streptomycin at 37°C in humid air with 5% CO_2 for 36 h before other treatments.

To study the functions of exosomes, exosomes purified from 1 ml of plasma and resuspended in 100 ul of PBS were cultured with cells in a 6-well-plate for 24 h before the induction of Hypoxia/Reoxygenation injury.

Exosome Labeling

To confirm exosome uptake by H9C2 cells, exosomes were labeled using a Dio green fluorescence kit (MCE, USA) according to the manufacturer's protocol. Lipophilic tracers Dio were prepared in stock solutions of dimethyl sulfoxide (DMSO) for the *in vitro* study. Exosomes were stained with 10 μM Dio for 10 min at 4°C and ultracentrifuged twice at 100,000 *g* for 40 min at 4°C to remove the excess dye. The isolated exosomes were resuspended in DMEM and used in the uptake experiments. Cells in the experimental group were incubated with Dio-stained exosomes and cells in the blank group were incubated only with Dio without exosomes. After a 2 h incubation, the cells were fixed with 4% paraformaldehyde (TCI, Japan) for 30 min and then visualized using a fluorescence microscope (IX73, Olympus, Japan) with 4′,6-diamidino-2-phenylindole, dihydrochloride (DAPI) stain. Dio emits green fluorescence under the excitation of light with a wavelength of 484 nm.

Cell Model of Hypoxia/Reoxygenation

The cells in serum-free and glucose-free DMEM were placed in a hypoxic chamber containing 95% N_2/5% CO_2 for 24 h. Subsequently, cells were subjected to reoxygenation in a standard incubator (95% air/5% CO_2) in a complete medium for 6 h.

Cell Viability Assay

Cell viability was observed using a Cell Counting kit-8 (CCK-8; Ape×bio, USA) according to the manufacturer's instructions. Cells were cultured into 96-well-plates at a density of 2,000 cells per well in a complete culture medium. Five replicates were set up for each group. The cells were treated according to the grouping. Subsequently, 10 μl CCK-8 was added to each well and incubated for 2 h. Optical density values were measured at 450 nm on a microplate reader (Multiskan FC, Thermo Fisher, USA).

Flow Cytometry

Fluorescein isothiocyanate (FITC)-conjugated Annexin V and propidium iodide (PI) (BD Biosciences, USA) were used to identify apoptotic cells. The left upper quadrant (FITC–/PI+) showed the dead cells; the right upper quadrant (FITC+/PI+) showed the late apoptotic cells; the left lower quadrant (FITC–/PI–) showed the intact cells, and the right lower quadrant (FITC+/PI–) showed the early apoptotic cells. Experiments were performed using a flow cytometer (Beckman, Germany), and the data obtained from the cell population were analyzed with Flow Jo_V10 (BD Biosciences, USA) software. The rate of total apoptotic cells was counted as the sum of early and late apoptotic rates.

Animal Model of Myocardial Ischemia/Reperfusion

Rats were anesthetized and intubated for mechanical ventilation in a supine position. The respiratory rate was 70 cycles/min, the tidal volume was 1 ml per 100 g body weight and the inspiration and expiration ratio was 1: 1 (Double channel Rodent Ventilator, ZH-DW-3000S, Zhenhua, China). A heating pad was used to keep rats' body temperature at around 37°C. Hemodynamic indices were recorded with a multi-channel physiological signal acquisition processing system (PowerLab, AD Instruments) that was connected to a pressure transducer. Then, the chest of a rat was opened via a lateral thoracotomy, and the heart was exposed through a pericardiotomy. A 6–0 nylon suture with a curved tapered needle was placed under the left anterior descending coronary artery (LAD) 3 mm below the left atrium. A small plastic tube was placed above the myocardium to reduce direct dissecting injury to the myocardium. The surgeon ligated the suture line with the small plastic tube for reversible LAD occlusion. Myocardial ischemia was confirmed by visual myocardium cyanosis and S-T segment elevation on electrocardiography. After 30 min LAD-ligation and the small plastic tube remove, reperfusion began and continued for 180 min. Finally, the rats were sacrificed after the reperfusion for histologic assessment. All procedures and analyses were performed by investigators blinded to the grouping. Rats that died from complications during anesthesia and surgery were excluded from the analysis. The sample size was chosen based

on our previous experience in the study of animal models of myocardial ischemia/reperfusion.

Tail Vein Injection of Exosomes or Free-Exosomes Plasma

Tail vein injection of exosomes or free-exosomes plasma was performed on rats 24 h before the induction of MI/R injury as described above. Briefly, male Sprague-Dawley rats (6 weeks old) were placed in a fixator. Exosomes purified from 1 ml of plasma and resuspended in 1 ml of PBS, or 1 ml of free-exosomes plasma were injected into the tail vein. The experiments were blindly operated by a researcher who did not know the grouping.

Echocardiography Measurements

Functional cardiac changes before the intervention and after the reperfusion were determined using echocardiography. The operator was blinded to the treatment. Transthoracic two-dimensional M-mode echocardiography was performed using the Vevo 2100 Imaging System (Visual Sonics, USA) equipped with an MS-250 probe (29–31). Left ventricular end-systolic and end-diastolic diameters (LVSD and LVDD, respectively), were measured after obtaining a 2-dimensional short-axis view of the left ventricle at the level of the papillary muscles. The mean value of the three measurements was determined for each sample. Left ventricular end-diastolic volume (EDV) and end-systolic volume (ESV) were calculated according to the Teichholz formula. The left ventricular ejection fraction (LVEF) was calculated as (EDV–ESV)/EDV × 100% (32). Changes in cardiac function were determined by the difference in the LVEF (ΔLVEF).

Measurement of Myocardial Infarct Size

Myocardial infarct size was determined by the Evans blue/triphenyl tetrazolium chloride (TTC) double staining method. After 180 min reperfusion, the LAD was ligated again. Two min later, the rat was injected with 2 ml of 3% Evans blue (Sigma-Aldrich, USA) via the femoral vein. The area of heart unstained by Evans blue was named the area at risk (AAR). After death from an overdose of sodium pentobarbital, the heart was immediately removed and washed off with 0.9% saline. Subsequently, the heart was frozen at −20°C for 60 min and then cut into 5 equal thickness transverse slices (2 mm each) from the apex to the base. These slices were placed in 1% TTC (TCI, Japan) for 10 min in the dark at 37°C, then fixed in 4% paraformaldehyde (TCI, Japan) for 24 h. After TTC staining, the white area was known as the infarct area (INF) and the red area was the viable myocardium in the AAR. Images were taken and quantified by planimetry with Image J software (version 1.52a, National Institutes of Health, USA) in a blinded manner. Myocardial infarct size was represented as the percentage of INF relative to the AAR (INF/AAR × 100%).

TUNEL Assay for Myocardial Apoptosis

Myocardial apoptosis was expressed by terminal deoxynucleotidyl transferase-mediated dUTP nick-end labeling (TUNEL) staining. An *In Situ* Cell Death Detection Kit (Roche, USA) was used according to the manufacturer's instructions. Briefly, the anterior wall of the left ventricular myocardium was cut into the freezing section. Apoptotic nuclei in the sections appeared green stained with the TUNEL, whereas all nuclei appeared blue by DAPI (4, 6-diamino-2-phenylindole; Beyotime, China). Each section was photographed at 400-magnification with a fluorescence microscope (IX73, Olympus, Japan). The apoptotic index was represented as the percentage of apoptotic myocytes relative to the total number of cardiomyocytes (green/blue) using Image J software (version 1.52a) in a blinded manner.

The miRNA Library Construction and Sequencing

Total RNAs from plasma exosomes isolated from the control rats and the RIPC rats were extracted using the Trizol reagent (Invitrogen, Carlsbad, CA, USA) according to the manufacturer's instructions ($n = 3$ per group). The miRNA library preparation and sequencing were conducted using an Illumina HiSeq 2500 platform (Ribobio, China). Both 3' and 5' adaptors were ligated with unique small RNA fractions to construct a small RNA sequencing library. Subsequently, the adaptor-ligated RNA fragments were reverse-transcribed and amplified using PCR and sequenced. Differential expression of miRNAs between the two groups was analyzed using cluster analysis.

Transfection of Cells

The miR-126a-3p mimics (50 nmol/L), inhibitors (100 nmol/L), and their negative control (50/100 nmol/L) RNAs (RiboBio, China) were transfected into cells with Lipofectamine 3000 (Life Technologies, USA) according to the manufacturer's instructions. Cells were incubated for 6 h with the transfection complex before it was discarded and replaced by fresh media. Experiments were performed 24 h after transfection.

Intracardiac Injection of miRNA Agomir or Antagomir

The miR-126a-3p agomir, antagomir, and their negative control (agomir-NC, antagomir-NC) (RiboBio, China) were used according to the manufacturer's instructions. Rats were intracardiac injected with 10 nmol miR-126a-3p antagomir, or 5 nmol miR-126a-3p agomir, or their negative control in 200 μl of the saline buffer. Briefly, anesthetized male Sprague-Dawley rats were placed in a supine position with respiratory support by a respiratory mask during the surgery, and the fourth intercostal space was exposed without thoracotomy or cutting the ribs. The 30-gauge needle was inserted at the place where the heart apical pulse was strongest. The needle tip was determined to be located in the heart cavity when pulsating blood return was sawn which was consistent with the heart pulse frequency. The chest wall was then closed following the injection. After 24 h, these rats were subjected to MI/R injury as described above in a blinded manner.

RNA Isolation and Quantitative Real Time-PCR

Exosome-RNAs were isolated from exosomes with Trizol (Invitrogen, Carlsbad, CA, USA) according to the standard

procedures and cel-miR-39 (RiboBio, China) was added to normalize the technical variation between samples. Tissue and cell RNAs were extracted with RNA-Quick Purification Kit for small RNA (ES Science, China) according to the protocols obtained from the manufacturers, and U6 (RiboBio, China) was used as the internal reference for miRNA. RNA concentrations were verified on the NanoDrop Spectrophotometer (Thermo Scientific, USA). Isolated RNA was reversely transcribed using miRNA primers (Bulge-LoopTM miRNA RT primer) and the riboSCRIPT Reverse Transcription Kit (RiboBio, China). qRT-PCR was performed on a Roche LightCycler 480°C System (Roche, Switzerland) using a TB Green Premix Ex Taq II Kit (Takara, Japan). Amplification was performed at 95°C for 30 s, followed by 40 cycles of 95°C for 5 s and 60°C for 20 s. All procedures were performed according to the protocols obtained from the manufacturers. Fold change in RNA species was calculated using formula $2^{(-\Delta\Delta}$Ct). $\Delta\Delta$Ct = (Ct target miRNA–Ct control). The sequences were as follows:

miR-126a-3p 5′-UCGUACCGUGAGUAAUAAUGCG-3′
let-7c-5p 5′-UGAGGUAGUAGGUUGUAUGGUU-3′
let-7f-5p 5′-UGAGGUAGUAGAUUGUAUAGUU-3′
miR-203a-3p 5′-GUGAAAUGUUUAGGACCACUAG-3′
miR-144-3p 5′-UACAGUAUAGAUGAUGUACU-3′
miR-98-5p 5′-UGAGGUAGUAAGUUGUAUUGUU-3′.

Western Blot

Tissues, cells, and purified exosomes were lysed with RIPA buffer (Beyotime, China). Protein concentration was determined using a BCA Protein Assay kit (Beyotime, China). Protein samples were separated using electrophoresis with SDS-PAGE (sodium dodecyl sulfate-polyacrylamide gel electrophoresis) and transferred onto a polyvinylidene difluoride (PVDF) membrane (Roche Diagnostics, USA). The membranes were blocked with 5% skimmed milk in TBS-T (Tris-buffered saline with 0.1% Tween 20) and incubated with the appropriate primary antibodies at 4°C for 12 h, followed by incubation with the corresponding secondary antibodies at 25°C for 1 h. The blots were detected by a Bio-Rad (California, USA) automatic chemiluminescence imaging analysis system using ECL supersensitive luminescent solution (Thermo Fisher, USA). TBS-T was used to wash the membranes. Primary antibodies against CD9 (ab92726), CD81 (ab109201) were purchased from Abcam (USA) and p-Akt (Ser473) (#4060), Akt (#2920), p-Erk1/2 (Thr202/Tyr204) (#4370), Erk1/2 (#4695), Caspase-3 (#14220), cleaved Caspase-3 (#9661), LY294002 (#9901), U0126 (#9903), and GAPDH (#97166) were purchased from Cell Signaling Technology (CST, USA). Secondary antibody goat anti-mouse IgG (ab205719) and goat anti-rabbit IgG (ab6721) were purchased from Abcam (USA). Antibodies against GAPDH were used as loading controls.

Statistical Analysis

All of the statistical tests and were performed with the SPSS 26.0 software (SPSS Inc., Chicago, IL, USA). Statistical significance was considered as $p < 0.05$. All values are presented as mean ± standard deviations of n independent experiments. Normality of data distribution was assessed using the Shapiro-Wilk normality test and the homogeneity of variance was tested by the Leven test. If the data of two groups conformed to normal distribution and homogeneity of variance, they were analyzed by two-tailed Student t-test, otherwise, they were analyzed by Mann-Whitney U-test. If other data conformed to normal distribution and homogeneity of variance, they were analyzed by ANOVA (three or more groups) followed by Bonferroni's correction, otherwise, they were analyzed by Kruskal-Wallis test.

RESULTS

Identification and Functional Verification of Plasma Exosomes at the Late Phase of RIPC *in vitro*

To better understand the function of plasma exosomes mediated cardioprotection induced by the late phase of RIPC, plasma exosomes were isolated from control rats (Control-exosome, C-exo) and RIPC-rats (RIPC-exosome, R-exo) 48 h after the RIPC protocol using the traditional differential ultracentrifugation (**Figures 1A,B**). Transmission electron microscopy revealed typical circular particles with diameters of 50–90 nm in separated sections (**Figure 1C**). Nanoparticle tracking analysis represented no significant differences in size distribution and concentration ($2.7 \times 10^9 \pm 0.3 \times 10^9$ ml^{-1} vs. $3.2 \times 10^9 \pm 0.6 \times 10^9$ ml^{-1}) between Control-exosome and RIPC-exosome (**Figures 1D–G**). Western blot analysis confirmed the presence and the similar levels of exosome marker proteins (CD81 and CD9) between RIPC-exosome and Control-exosome (**Figures 1H,I**). These results confirmed that exosomes had been successfully isolated and purified and the total plasma exosomes level had no significant change between RIPC-exosome and Control-exosome.

To confirm whether exosomes could be internalized by H9c2 cells, we incubated the H9C2 cells with Dio-labeled exosomes and observed that exosomes were taken up by H9C2 cells as indicated by confocal images (**Figure 1J**). Subsequently, to demonstrate the protective effects of RIPC-exosome, we performed functional experiments and the study design was shown in **Supplementary Figure 2A**. Importantly, pre-incubation with RIPC-exosome, but not Control-exosome, for 24 h attenuated cellular H/R injury as indicated by increased cell viability (**Figure 1K**) and reduced cell apoptosis (**Figure 1L**) when compared with the vehicle control. Collectively, these results showed that RIPC-exosome conferred protective effects against H/R injury in H9C2 cells.

Plasma Exosomes at the Late Phase of RIPC Exerted Cardioprotection Against MI/R Injury *in vivo*

To determine the cardioprotection of RIPC-exosome *in vivo*, exosomes or free-exosomes plasma were injected into rats 24 h before MI/R. This *in vivo* study design was shown in **Supplementary Figure 2B**. RIPC-exosome (R-exo) or Control-exosome (C-exo) purified from 1 ml of plasma were resuspended

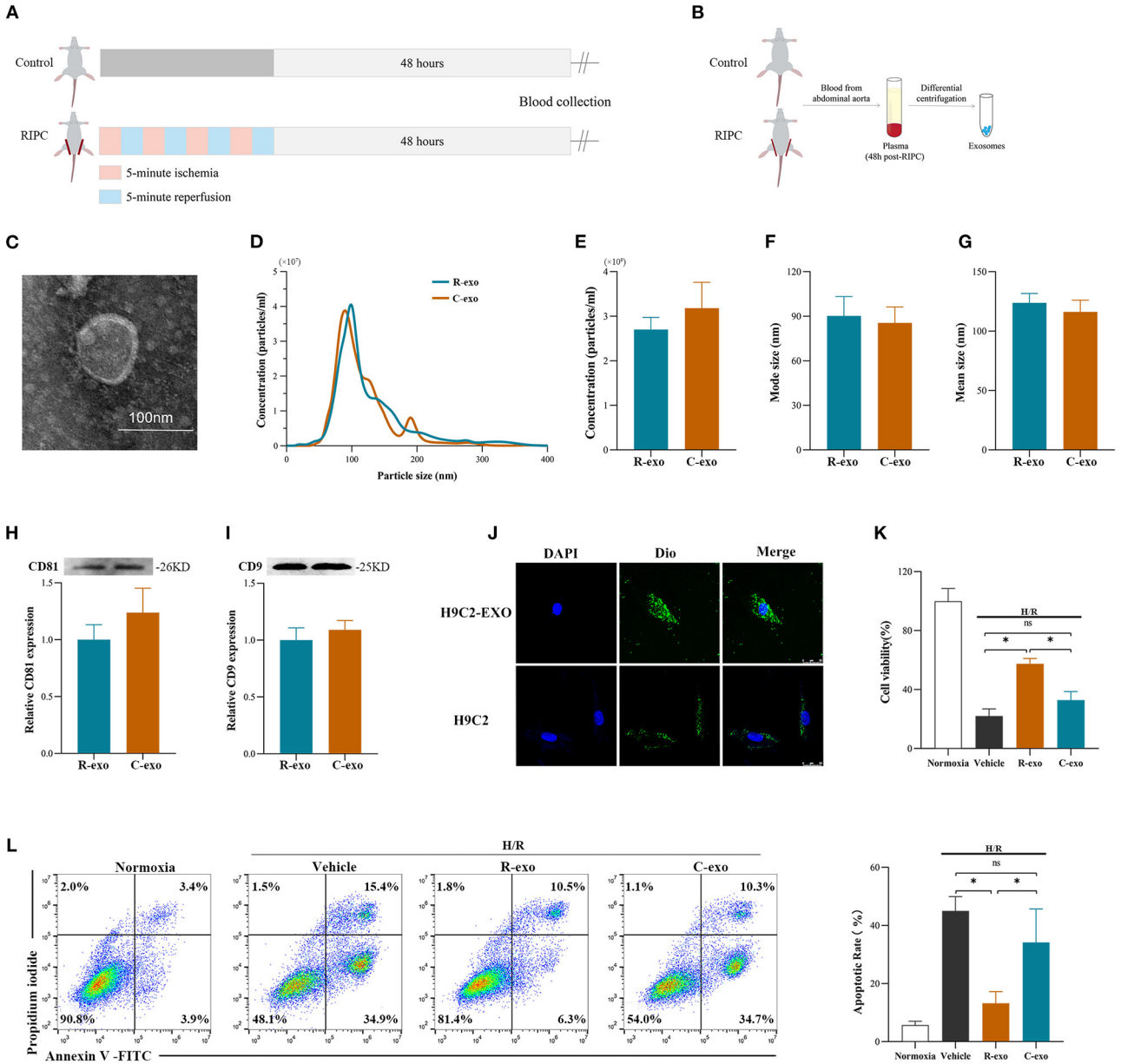

FIGURE 1 | Identification and functional verification of plasma exosomes at the late phase of RIPC *in vitro*. **(A)** Establishment of the late-phase RIPC model in rats. **(B)** The process to obtain the plasma exosomes from rats with or without the late-phase RIPC protocol. **(C)** Representative electron micrograph of isolated plasma exosomes. Scale bar: 100 nm. **(D)** Representative results of NTA (nanoparticle tracking analysis) demonstrating size distribution and concentration in Control-exosomes (C-exo) and RIPC-exosomes (R-exo). **(E)** The average concentration in Control-exosomes and RIPC-exosomes ($n = 4$). **(F)** Mode size in Control-exosomes and RIPC-exosomes ($n = 4$). **(G)** Mean size in Control-exosomes and RIPC-exosomes ($n = 4$). **(H)** Representative images of Western blot (top) and quantified data (bottom) in exosomal marker proteins CD81 in Control-exosomes and RIPC-exosomes ($n = 4$). **(I)** Representative images of Western blot (top) and quantified data (bottom) in exosomal marker proteins CD9 in Control-exosomes and RIPC-exosomes ($n = 4$). **(J)** Representative images of H9C2 cells that were incubated with the presence (H9C2-EXO) or absence (H9C2) of Dio-labeled exosomes (green). Cardiomyocyte nuclei were stained with DAPI (blue). Scale bar: 25 μm. **(K)** The data of cell viability showed that RIPC-exosomes improved cell viability with 24 h co-incubation and following H/R injury. **(L)** The data and representative images of cell apoptosis by flow cytometric analysis showed that RIPC-exosomes decreased cell apoptosis with 24 h co-incubation and following H/R injury ($n = 3$). RIPC, remote ischemic pre-conditioning; R-exo, exosomes isolated from the plasma of the late-phase RIPC rats; C-exo, exosomes isolated from the plasma of the control rats; H/R, Hypoxia/Reoxygenation (24/6 h). $^{*}p < 0.05$ and $^{ns}p > 0.05$.

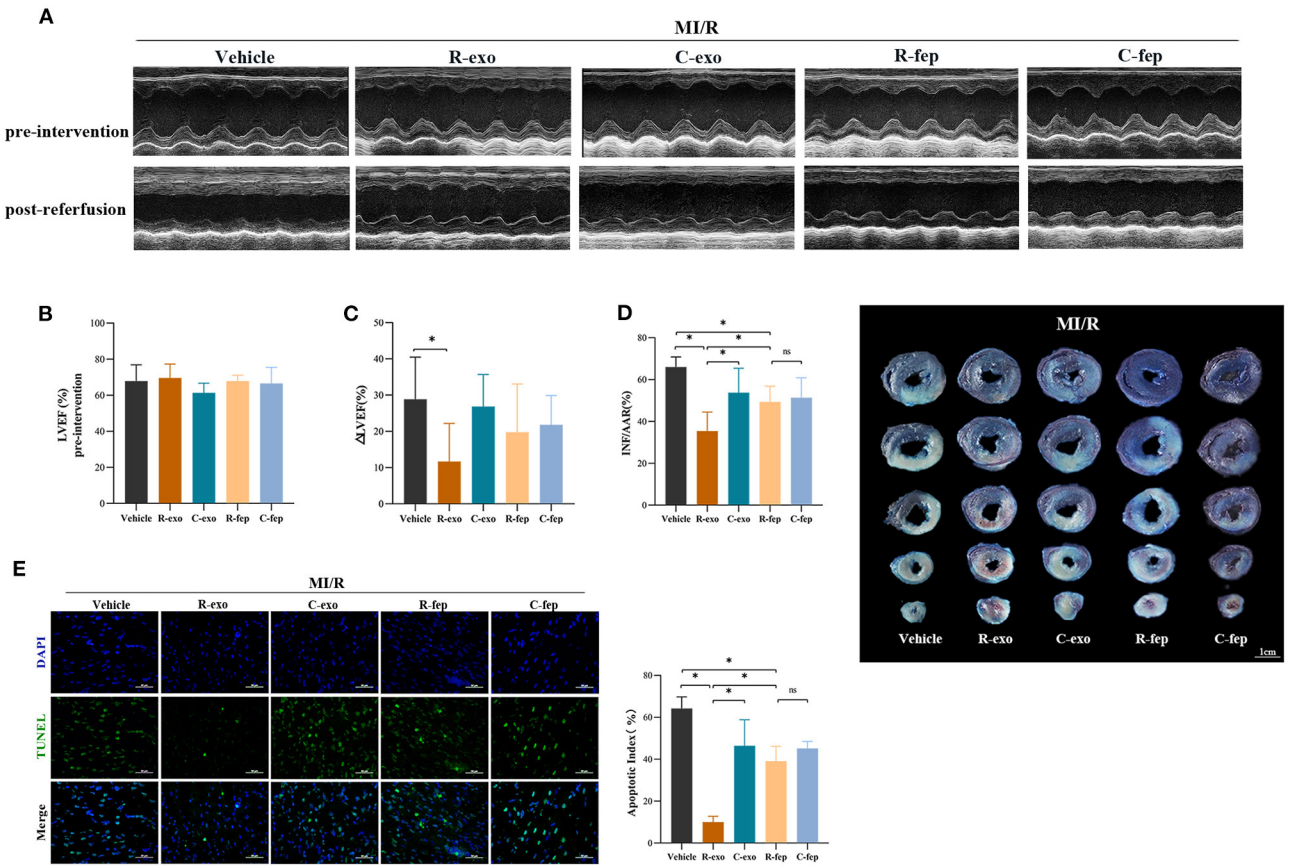

FIGURE 2 | Plasma exosomes at the late phase of RIPC exerted cardioprotection against MI/R injury *in vivo*. **(A)** Representative echocardiographic images of rats before the intervention (pre-intervention) and after the reperfusion (post-reperfusion) in each group of rats. **(B)** Left ventricular ejection fraction (LVEF) of rats in pre-intervention ($n = 8$). **(C)** ΔLVEF (the difference between the LVEF in pre-intervention and that in post-reperfusion) in each group. RIPC-exosome injected into rats for 24 h before MI/R improved cardiac function as evidence by significantly narrowed the ΔLVEF. **(D)** Quantified data and presentative photographs of heart sections. RIPC-exosome decreased infarct size in rats subjected to MI/R ($n = 8$). INF/AAR, infarct size as a percentage of myocardial area at risk. **(E)** Representative images and quantified data of TUNEL assay in each group showed that RIPC-exosome decreased myocardial apoptosis in rats subjected to MI/R. Myocardial apoptosis in rats determined by a percent of TUNEL-positive nuclei (green)/total nuclei (blue) ($n = 4$). Scale bar: 50 μm. MI/R, myocardial ischemia/reperfusion (30/180 min). R-exo, exosomes isolated from the plasma of the late-phase RIPC rats. C-exo, exosomes isolated from the plasma of the control rats. R-fep, the supernatant collected after the first ultracentrifugation from the plasma of the late-phase RIPC rats. C-fep, the supernatant collected after the first ultracentrifugation from the plasma of the control rats. $^{*}p < 0.05$, $^{ns}p > 0.05$.

in 1 ml of PBS (≈2.9 × 10^9 exosomes). The injection volume of free-exosomes plasma, isolated from the RIPC-rats (R-fep) or the control-rats (C-fep), was 1 ml. The cardiac function was assessed by the difference in LVEF before the intervention and after the reperfusion (ΔLVEF%). The cardiac function after MI/R injury had significant improvement in the R-exo group compared with that in the vehicle group as evidenced by narrowed the ΔLVEF (11.7 ± 10.5% vs. 28.8 ± 11.7%, $p < 0.05$, **Figures 2A–C**). Concomitantly, the infarct size relative to the area at risk (INF/AAR) was significantly smaller in the R-exo group compared with that in the vehicle group after MI/R injury (35.5 ± 9.1% vs. 66.0 ± 4.8%, $p < 0.05$, **Figure 2D**). Besides, reduced cell apoptosis was observed in the R-exo group compared with that in the vehicle group following MI/R (10.0 ± 2.7% vs. 64.2 ± 5.6%, $p < 0.05$; **Figure 2E**).

Taken together, these *in vivo* data suggested that transfer of RIPC-exosome improved cardiac function, reduced infarct size, and cell apoptosis in MI/R-induced rats.

miR-126a-3p Was Essential in the Cardioprotection Provided by Plasma Exosomes at the Late Phase of RIPC

It has been indicated that exosomal miRNAs may be an attractive candidate as a mediator of signal transmission in cardiovascular disease (18, 33, 34). To explore the cardioprotective effects of miRNAs induced by RIPC-exosome, we performed a miRNA profiling assay (763 rat miRNAs) comparing with RIPC-exosome (R-exo) and Control-exosome (C-exo) using Illumina HiSeq 2500 high-throughput sequencing. Overlapping miRNAs

accounted for 91.81% of the total, which indicates that there was a minor change in the RIPC-induced exosomal miRNAs (**Figure 3A**). Subsequently, a total of 57 differentially expressed miRNAs were detected (fold change >2.0; $p < 0.05$), and 23 of them were highly expressed in RIPC-exosome compared with those in Control-exosome (**Figures 3B,C**). Moreover, 6 miRNAs of the 23 ones, which were highly expressed and closely related to myocardial apoptosis and protective effects such as the promotion of myocardial angiogenesis, were further confirmed by qRT-PCR analysis. On comparing RIPC-exosome with Control-exosome, miR-126a-3p was upregulated most significantly in RIPC-exosome (**Figure 3D**). To better understand the level of exosomal miR-126a-3p in hearts after tail vein injection of plasma exosomes and MI/R injury, we assessed the level of miR-126a-3p in the heart by qRT-PCR. The miR-126a-3p level was elevated in hearts injected with RIPC-exosome following the treatments (**Supplementary Figure 3**).

To explore the *in vitro* function of exosomal miR-126a-3p using the model of H/R injury, the study design was shown in **Supplementary Figure 4A**. We first assessed levels of miR-126a-3p in H9C2 cells treated with RIPC-exosome. The miR-126a-3p level was significantly elevated in H9C2 cells incubated with RIPC-exosome and this change was significantly blunted with the transfection with miR-126a-3p inhibitor (**Figure 3E**), indicating that RIPC-exosome delivered miR-126a-3p to H9C2 cells. Subsequently, in both H9C2 cells and primary cardiomyocytes, the protective improvement in cell viability and cell apoptosis exerted by RIPC-exosome were markedly eliminated by inhibition of miR-126a-3p (**Figures 3F–I**).

Moreover, to further understand the *in vivo* function of exosomal miR-126a-3p induced by RIPC, we injected miR-126a-3p antagomir into rats and established the model of MI/R in rats. The study design was shown in **Supplementary Figure 4B**. Briefly, our results show that the miR-126a-3p antagomir injection markedly attenuated the cardioprotective effects of the RIPC-exosome. Firstly, improved cardiac function observed in rats treated with RIPC-exosome was significantly blunted by miR-126a-3p antagomir treatment as evidenced by increased the ΔLVEF (9.3 ± 5.1% vs. 24.2 ± 4.3%, $p < 0.05$, **Figures 3J–L**). Secondly, reduced myocardial infarct size in RIPC-exosome treated rats was eliminated by miR-126a-3p antagomir (31.8 ± 3.9% vs. 54.4 ± 9.7%, $p < 0.05$, **Figure 3M**). Third, reduced myocardial apoptosis in RIPC-exosome treatment was shown the same change (35.5 ± 5.1 vs. 51.3 ± 5.1%, $p < 0.05$, **Figure 3N**).

In sum, these results suggest that miR-126a-3p was an important component in cardioprotection induced by plasma exosomes at the late phase of RIPC.

miR-126a-3p Was an Important Molecule in Cardioprotection

To further explore the function of miR-126a-3p, miR-126a-3p mimic was transfected to increase miR-126a-3p expression in cells and then established the model of H/R (**Supplementary Figure 5A**). It showed that miR-126a-3p with increased expression level significantly improved cell viability and reduced cell apoptosis in both H/R induced H9C2 cells and primary cardiomyocytes (**Figures 4A–E**). Besides, *in vivo,* miR-126a-3p agomir was injected to detect the direct effect of miR-126a-3p against MI/R injury in rats (**Supplementary Figure 5B**). The cardiac function (9.1 ± 0.7% vs. 24.3 ± 5.7%, $p < 0.05$, **Figures 4F–H**), the myocardial infarct size (21.9 ± 2.9% vs. 52.2 ± 3.1%, $p < 0.05$, **Figure 4I**) and the myocardial apoptosis (21.0 ± 1.9% vs. 64.2 ± 4.2%, $p < 0.05$, **Figure 4J**) were significantly improved, compared with the miR-126a-3p agomir group and the agomir-NC group.

Meanwhile, to better understand the function of miR-126a-3p, we additionally performed experiments using miR-126a-3p inhibitors in H9C2 cells (**Supplementary Figure 5C**). Following H/R injury, decreased cell viability and increased cell apoptosis were showed in H9C2 cells transfected with miR-126a-3p inhibitor (**Figures 4K,L**).

Collectively, these results suggested that miR-126a-3p might be a possible and important molecule of some of the cardioprotection against MI/R injury.

The Signaling Pathways Involved in Plasma Exosomes at the Late Phase of RIPC Mediated Effects

Survival signals Akt and Erk1/2, which belong to the reperfusion injury salvage kinase (RISK) pathway, have been well-documented as key molecules in cardioprotection (35, 36). RIPC-exosome (R-exo) significantly increased the phosphorylation of Akt and Erk1/2 compared to Control-exosome or free-exosome plasma in rats subjected to MI/R injury (**Figure 5A**). The phosphorylation of Akt and Erk1/2 in the R-exo group was the most obvious and significantly different from that in the other groups, respectively. *In vitro,* similar results were observed in H9C2 cells subjected to H/R injury (**Figure 5B**). We also explored the Akt and Erk1/2 intervened by pathway inhibitors (LY294002 or U0126) in RIPC-exosome (**Supplementary Figures 6A,B**).

Moreover, we focused on Caspase-3 which is involved in both MI/R injury and the apoptosis pathway (**Figure 5A**). We found that RIPC-exosome significantly decreased the activation of Caspase-3 (cleaved Caspase-3/Caspase-3) compared to Control-exosome or free-exosome plasma in rats subjected to MI/R injury (**Figure 5A**). *In vitro,* similar results were observed in H9C2 cells subjected to H/R injury (**Figure 5B**).

Taken together, these results showed that RIPC-exosome exerted regulation over Akt and Erk1/2 activities and inhibited the activation of apoptotic protein Caspase-3.

The Signaling Pathways Involved in Plasma Exosomes at the Late Phase of RIPC via miR-126-3p Mediated Effects

In H9C2 cells subjected to H/R, the phosphorylation of Akt and Erk1/2 were significantly elevated with RIPC-exosome and this change was significantly blunted by the inhibition of miR-126a-3p (**Figure 6A**). Besides, the activation of Caspase-3 inhibited by RIPC-exosome was significantly reversed by the

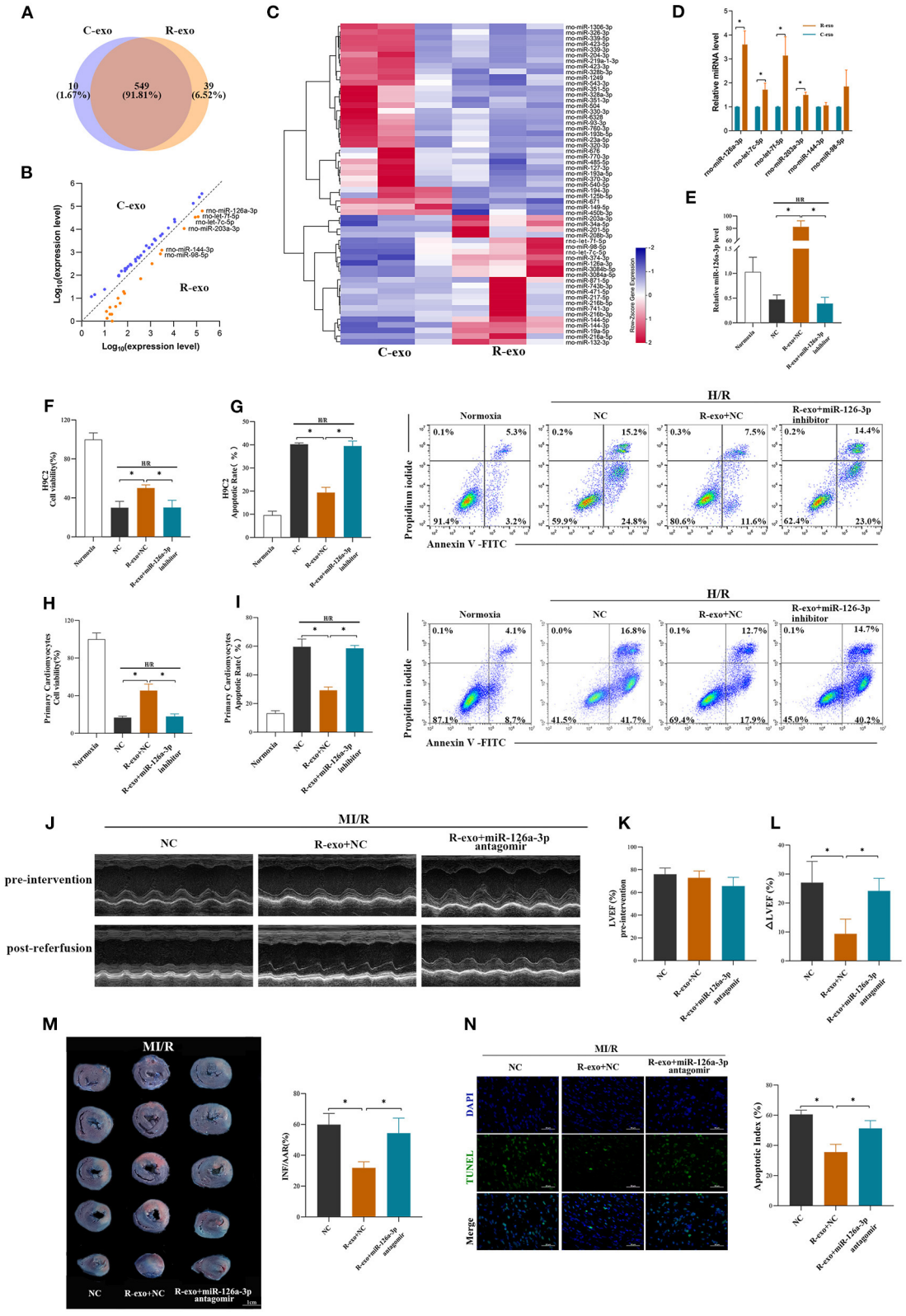

FIGURE 3 | miR-126a-3p was essential in the cardioprotection provided by plasma exosomes at the late phase of RIPC. **(A)** Venn diagram showing the numbers of overlapping and unique miRNAs detected in Control-exosome (C-exo) and RIPC-exosome (R-exo) (n =3). **(B)** The expression level of miRNAs in Control-exosome

(Continued)

FIGURE 3 | and RIPC-exosome. Yellow dots represented up-regulated miRNAs in RIPC-exosome and blue dots represented up-regulated miRNAs in Control-exosome (fold change >2 and $p < 0.05$, $n = 3$). **(C)** Heat map representing the miRNA profiling assays between Control-exosome and RIPC-exosome (fold change >2 and $p < 0.05$, $n = 3$). **(D)** qRT-PCR analysis of the six differentially expressed miRNAs in Control-exosome and RIPC-exosome. Data are normalized to cel-miR-39 ($n = 3$). **(E)** The qRT-PCR analysis of miR-126a-3p level in H9C2 cells treated with inhibitor negative control (NC), R-exo + NC, or R-exo + miR-126a-3p inhibitor followed by H/R. Data were presented as a fold change of the normoxia. U6 was used as an internal control ($n = 3$). **(F)** The data of cell viability showed that inhibition of miR-126a-3p attenuated the protective effects of RIPC-exosome in H9C2 cells subjected to H/R ($n = 3$). **(G)** The data and representative images of apoptosis of H9C2 cells subjected to H/R by flow cytometric analysis ($n = 3$). The protective effects of RIPC-exosome were eliminated by inhibition of miR-126a-3p. **(H)** The data of cell viability showed that the protective effects of RIPC-exosomal miR-126a-3p were reduced by a miR-126a-3p inhibitor in primary cardiomyocytes following H/R injury ($n = 3$). **(I)** The data and representative images of apoptosis of primary cardiomyocytes subjected to H/R by flow cytometric analysis ($n = 3$). The anti-apoptosis effects of RIPC-exosomal miR-126a-3p were eliminated by inhibition of miR-126a-3p ($n = 3$). **(J)** Representative echocardiographic images of rats in pre-intervention and post-reperfusion in each group of rats ($n = 5$). **(K)** Left ventricular ejection fraction (LVEF) of rats in pre-intervention. **(L)** ΔLVEF in each group showed that miR-126a-3p antagomir blunted the protective effects of RIPC-exosome in cardiac function. **(M)** Representative photographs of heart sections and quantified data demonstrated that miR-126a-3p antagomir observably attenuated the protective effects of RIPC-exosome in myocardial infarct size ($n = 5$). **(N)** Representative images and quantified data of TUNEL assay in each group demonstrated that miR-126a-3p antagomir observably blunted the protective effects of RIPC-exosome in myocardial apoptosis ($n = 4$). Scale bar: 50 μm. R-exo, exosomes isolated from the plasma of the late-phase RIPC rats. C-exo, exosomes isolated from the plasma of the control rats. H/R, Hypoxia/Reoxygenation (24/6 h). MI/R, myocardial ischemia/reperfusion (30/180 min). *$p < 0.05$.

inhibition of miR-126a-3p (**Figure 6A**). Similar anti-apoptotic effects of exosomal miR-126a-3p, namely the inhibition of Caspase-3 activation, also appeared in primary cardiomyocytes (**Supplementary Figure 7A**). These results showed that plasma exosomes at the late phase of RIPC activated the RISK pathway and inhibited the activation of apoptotic protein Caspase-3 through exosomal miR-126a-3p.

Moreover, in H9C2 cells subjected to H/R, the phosphorylation of Akt and Erk1/2 were elevated by a miR-126a-3p mimic (**Figure 6B**) and decreased by a miR-126a-3p inhibitor (**Figure 6C**). Simultaneously, the miR-126a-3p mimic significantly inhibited the activation of apoptotic protein Caspase-3 (**Figure 6B**), while the miR-126a-3p inhibitor promoted it (**Figure 6C**). Additionally, in primary cardiomyocytes, the activation of apoptotic protein Caspase-3 was also inhibited by a miR-126a-3p mimic (**Supplementary Figure 7B**), which might provide a better understanding of the anti-apoptotic effect of miR-126a-3p.

Collectively, the results indicated that exosomal miR-126a-3p exerted regulation over Akt and Erk1/2 activities and inhibited the activation of apoptotic protein Caspase-3. These effects were eliminated by transfection with miR-126a-3p inhibitor and augmented by transfection with miR-126a-3p mimic.

DISCUSSION

This study yielded three major findings. First, plasma exosomes obtained at the late phase of RIPC (RIPC-exosome) had protective effects against MI/R injury, suggesting that plasma exosomes were a carrier of protective substances induced by RIPC at the late phase. Second, exosomal miR-126a-3p played an important role in the cardioprotection induced by RIPC-exosome. Third, RIPC-exosome conferred cardioprotection through transferring miR-126a-3p by activating the RISK pathway and inhibiting the activation of apoptotic protein Caspase-3. These findings presented a novel mechanism for the endogenous cardioprotective effects conferred by RIPC-exosome through transferring miR-126a-3p (**Figure 7**, **Supplementary Figure 1**).

Our previous studies confirmed that the cardioprotective component is present in late-phase RIPC plasma (14–17), and no specific chemical inhibitors or knockout models exist to rigorously exclude exosomes in RIPC, so we separated the exosomes from the plasma and studied the differences between the plasma with or without exosomes. Results of this study further confirmed that exosomes isolated from the late-phase RIPC plasma were important in mediating the cardioprotective effects. The MI/R injury alleviated by the RIPC-exosome relied on improving cardiac function, reducing myocardial infarction and cell apoptosis. At the same time, the RIPC-exosome also exerted vital protection against H/R injury by improving cell viability and reducing cell apoptosis when they were internalized by cardiomyocytes. There are a few studies that have proposed that exosomes induced by the RIPC at the early phase may act as carriers of the cardioprotective factors (25, 26). Vincencio et al. determined that that endogenous plasma exosomes from rats and humans subjected to RIPC were powerfully cardioprotective in tested models of MI/R injury. Mechanically, they found the whole process of myocardial protection not only depended on toll-like receptor 4, further activation of Erk1/2, but also MAPK signaling pathways, following phosphorylation of the HSP27 (25). Similarly, Wen et al. verified rats subjected to RIPC produced a higher expression of miR-24 in plasma exosomes. More importantly, miR-24 contributed to improving cardiomyocyte apoptosis, infarct size, and cardiac function (26). Our results, which were concentrated in the late phase of RIPC, were consistent with the above findings. Importantly, our studies have indicated that the cardioprotection of RIPC at the late phase sustains long, which means that RIPC at the late phase may be a good preventive treatment strategy and convenient to translate into clinics. Our *in vivo* and *in vitro* results revealed that the cardioprotection produced by RIPC at the late phase may translate to others through exosomes as a certain carrier, which may provide a therapeutic strategy against MI/R injury in the future. Despite these scientific conclusions, further research needs to be conducted to explore the signaling and effector mechanism of exosomes.

Increasing evidence has shown that miRNAs are related to cardiac function, disease, and cardioprotection (37–40).

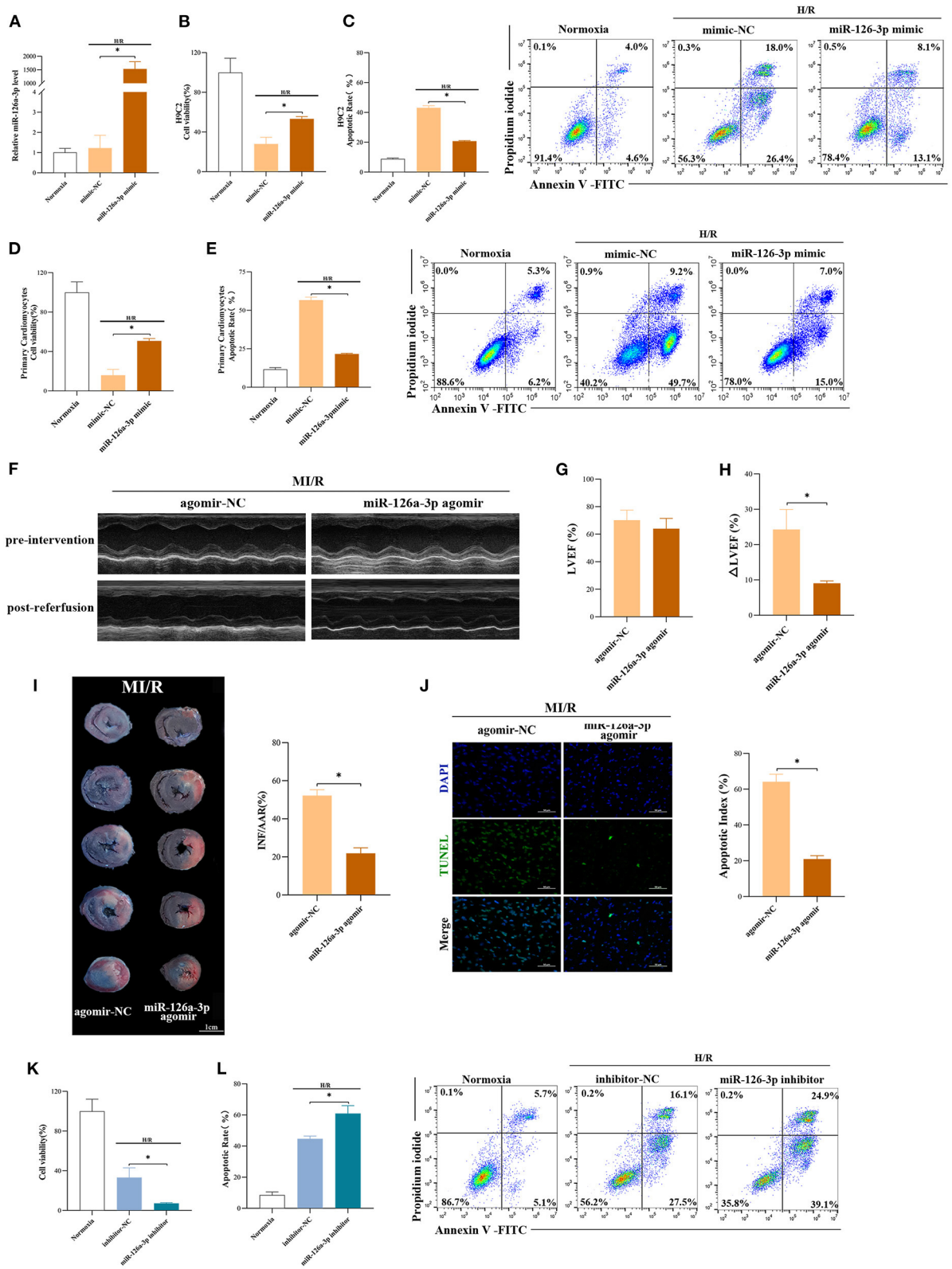

FIGURE 4 | miR-126a-3p was an important molecule in cardioprotection. **(A)** The qRT-PCR analysis of miR-126a-3p level in H9C2 cells transfected with miR-126a-3p mimic or negative control (mimic-NC) for 24 h followed by H/R. Data were presented as a fold change of the normoxia. U6 was used as an internal

(Continued)

FIGURE 4 | control ($n = 3$). **(B)** The increasing level of miR-126a-3p improved cell viability in H9C2 cells subjected to H/R ($n = 3$). **(C)** Flow cytometric data and representative images of apoptosis in H9C2 cells subjected to H/R ($n = 3$). The increasing level of miR-126a-3p decreased cell apoptosis in H9C2 cells subjected to H/R. **(D)** Cell viability in primary cardiomyocytes transfected with a miR-126a-3p mimic or mimic-NC followed by H/R injury (n =3). **(E)** Flow cytometric data and representative images of the anti-apoptosis effect of miR-126a-3p in primary cardiomyocytes treated with a miR-126a-3p mimic or mimic-NC followed by H/R injury (n =3). **(F)** Representative echocardiographic images of rats in pre-intervention and post-reperfusion in each group of rats ($n = 5$). **(G)** Left ventricular ejection fraction (LVEF) of rats in pre-intervention. **(H)** ΔLVEF in each group showed that miR-126a-3p agomir improved cardiac function. **(I)** Representative photographs of heart sections and quantified data demonstrated that miR-126a-3p agomir reduced myocardial infarct size ($n = 5$). **(J)** Representative images and quantified data of TUNEL assay in each group demonstrated that miR-126a-3p agomir reduced myocardial apoptosis ($n = 4$). Scale bar: 50 μm. **(K)** Cell viability in H9C2 cells treated with a miR-126a-3p inhibitor or inhibitor-NC followed by H/R ($n = 3$). **(L)** Flow cytometric data and representative images of apoptosis in H9C2 cells treated with a miR-126a-3p inhibitor or inhibitor-NC followed by H/R ($n = 3$). H/R, Hypoxia/Reoxygenation (24/6 h). MI/R, myocardial ischemia/reperfusion (30/180 min). *$p < 0.05$.

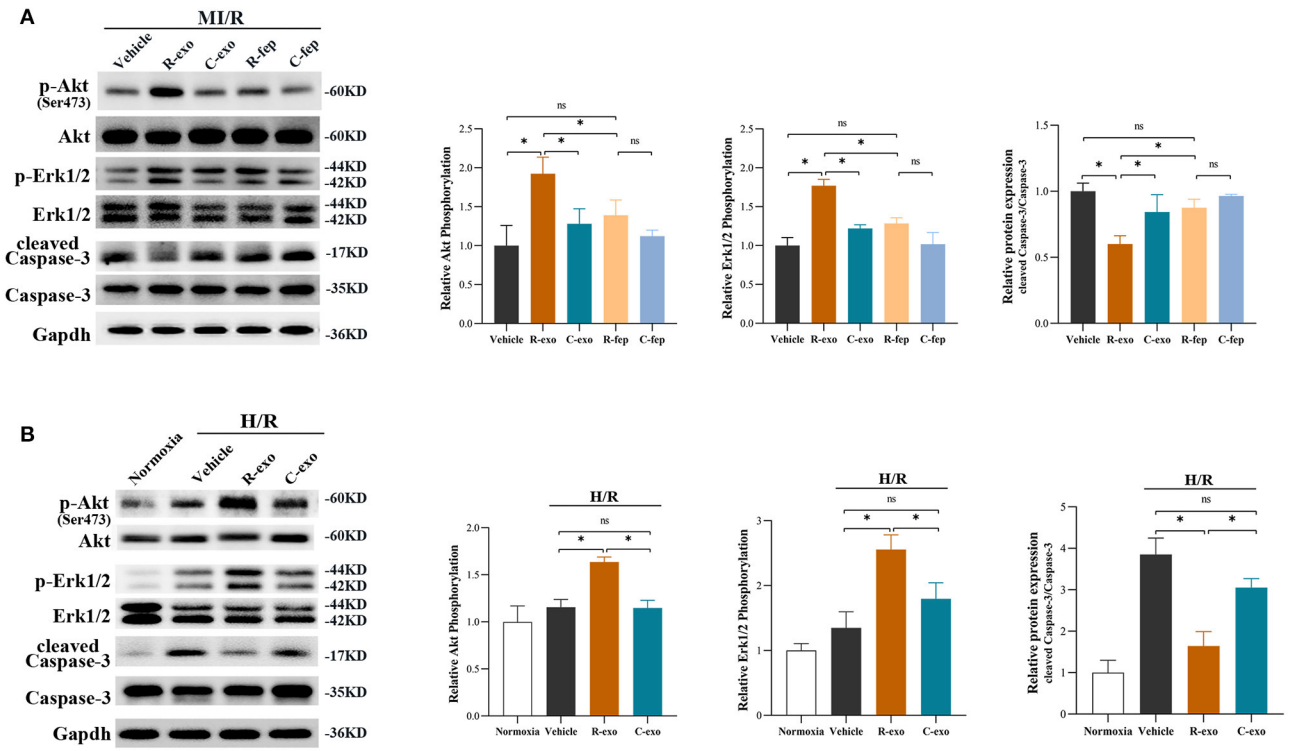

FIGURE 5 | The signaling pathways involved in plasma exosomes at the late phase of RIPC mediated effects. **(A)** Representative images of Western blot and quantified data in rats received R-exo, C-exo, R-fep, C-fep, or vehicle for 24 h followed by MI/R. ($n = 3$). **(B)** Representative images of Western blot and quantified data in H9C2 cells preincubated with R-exo, C-exo, or vehicle for 24 h followed by H/R ($n = 3$). GAPDH was used as a loading control. Quantified data showed phosphorylation level of Akt, expressed as the ratio of p-Akt to Akt; phosphorylation level of Erk1/2, expressed as the ratio of p-Erk1/2 to Erk1/2; the activation of Caspase-3 expressed as the ratio of cleaved Caspase-3 to Caspase-3. MI/R, myocardial ischemia/reperfusion (30/180 min). H/R, Hypoxia/Reoxygenation (24/6 h). R-exo, exosomes isolated from the plasma of the late-phase RIPC rats; C-exo, exosomes isolated from the plasma of the control rats; R-fep, the supernatant collected after the first ultracentrifugation from the plasma of the late-phase RIPC rats; C-fep, the supernatant collected after the first ultracentrifugation from the plasma of the control rats. *$p < 0.05$, $^{ns}p > 0.05$.

Regarding cardioprotection, the expression of several miRNAs, such as miR-1, miR-21, and miRNA-125b, have been identified to be significantly changed due to ischemic pre- or post-conditioning (41–44). Similarly, Li et al. suggested that miR-144 may be a circulating mediator of RIPC and a potential biomarker for the successful application of pre-conditioning (45). However, to date, the expression profiles of miRNAs in RIPC-exosome and their potential roles in RIPC-related cardioprotection against MI/R injury are still unknown. In this study, we thus determined the expression profile of miRNAs in RIPC-exosome. We found 23 miRNAs with higher expression in RIPC-exosome, of which miR-126a-3p has the highest expression. Recent studies have revealed that miR-126a-3p plays an important role in prohibiting apoptosis and promoting the survival of endothelial cells, promoting angiogenesis and secretion of angiogenic factors (46–50). The reduced miR-126 expression has also been identified as a novel mechanism that limits cardiac functional improvement (51, 52). Circulating miR-126 has been found to play a role in cardiac repair during cardiovascular injury (21, 22). Therefore, we were focused on miR-126a-3p in this study and tested its potential involvement in cardioprotection induced by RIPC-exosome. However, other

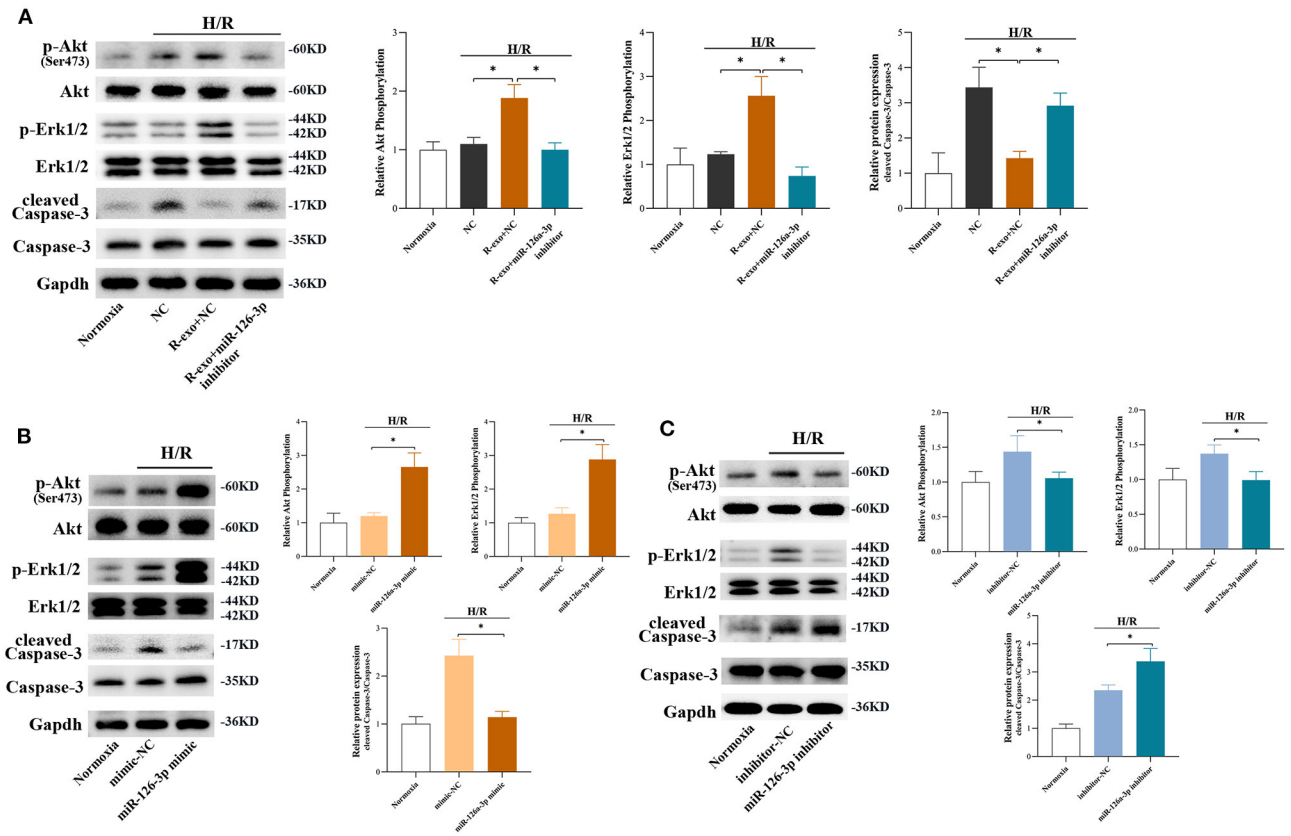

FIGURE 6 | The signaling pathways involved in plasma exosomes at the late phase of RIPC via miR-126-3p mediated effects. **(A)** Representative images of Western blot and quantified data in H9C2 cells treated with inhibitor-NC, R-exo + NC, or R-exo + miR-126a-3p inhibitor followed by H/R ($n = 3$). **(B)** Representative images of Western blot and quantified data in H9C2 cells transfected with miR-126a-3p mimics or mimic-NC for 24 h followed by H/R ($n = 3$). **(C)** Representative images of Western blot and quantified data in H9C2 cells transfected with miR-126a-3p inhibitors or negative control (inhibitor-NC) for 24 h followed by H/R ($n = 3$). GAPDH was used as a loading control. Quantified data showed phosphorylation level of Akt, expressed as the ratio of p-Akt to Akt; phosphorylation level of Erk1/2, expressed as the ratio of p-Erk1/2 to Erk1/2; the activation of Caspase-3 expressed as the ratio of cleaved Caspase-3 to Caspase-3. H/R, Hypoxia/Reoxygenation (24/6 h). R-exo, exosomes isolated from the plasma of the late-phase RIPC rats. *$p < 0.05$.

miRNAs which were aberrantly expressed in RIPC-exosome, are also significant enough for investigation in future studies.

We hypothesized that miR-126a-3p might be a critical participant in cardioprotection induced by RIPC-exosome. To test it, we first determined the function of exosomal miR-126a-3p. The result demonstrated that the cardioprotective effect of RIPC-exosome was significantly eliminated by miR-126a-3p inhibitor transfection *in vitro* and miR-126a-3p antagomir treatment *in vivo*. To further test our hypothesis, miR-126a-3p mimic was applied in cultured H9C2 cells before they were damaged by H/R injury. We found that H/R-induced injuries on H9C2 cells were attenuated via miR-126a-3p overexpression. In addition, the opposite results were showed in H9C2 cells transfected with miR-126a-3p inhibitor. The study by Wang et al. demonstrated that miR-126 may play a protective role in MI/R injury through regulating ERRFI1 (53). Wang et al. differed from us in that they focused on the role of miR-126 in MI/R injury, but did not study the role of exosomes. Our data supplied the first glimpse of the role of plasma exosomes at the late phase of RIPC against MI/R injury, and attempted to condense the protective effect of RIPC into exosomes and exosomal miR-126a-3p, so that RIPC might play a protective role in a more convenient, efficient, and lasting form, providing new ideas for the prevention and treatment of MI/R injury.

Recently, exosomes and miRNAs have been considered as potential biomarkers of heart injury and potential therapeutic tools for cardiovascular disease (54–56). Exosomes have been proposed to be involved in the range of cardiovascular processes and show great potential for discovery and application of new therapeutic strategies, as well as for diagnosis. Exosomes have several advantages over existing methods. They are biocompatible, stable, non-immunogenic, non-tumorigenic, and freeze-thaw resistant. Also, they can circulate throughout the body and cross the blood-brain barrier (57, 58). According to the existing research results, researchers believe that miRNAs have a good prospect for clinical transformation, and some miRNAs are currently being studied for clinical transformation. For example, miR-92a, miR-208, and miR-15 in the treatment

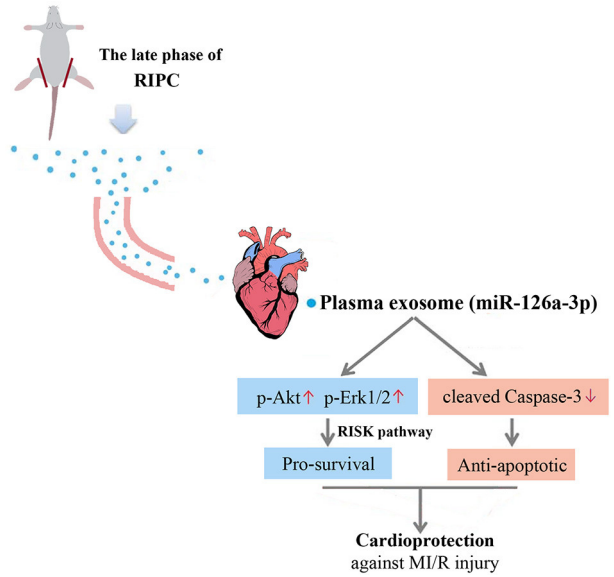

FIGURE 7 | Proposed mechanisms by which plasma exosomes at the late phase of RIPC protect the heart against MI/R injury through transferring miR-126a-3p. Plasma exosomes could be used as a carrier to transfer the myocardial protective effect of RIPC at the late phase against MI/R injury, activate the RISK pathway by increasing the phosphorylation level of Akt, and Erk1/2, and inhibit the activation of apoptotic protein Caspase-3 by reducing the expression level of cleaved Caspase-3.

of heart failure, hypertensive cardiomyopathy, and myocardial infarction are undergoing preclinical studies (59); and miR-29b mimic (MRG201-30-001) in the treatment of pathological fibrosis is entering phase I clinical study; miR-122 antagonist (SPC3649) for hepatitis C has entered phase II clinical study (60). Current exosome purification and identification techniques limit the use of exosomes as biomarkers for cardiovascular disease. Although some researchers have proposed to use exosomes as drug delivery carriers, the safety, quality control and pharmacokinetics of exosomes need to be comprehensively evaluated before implementation (61, 62). In our study, the myocardial protective effect of exosomal miR-126a-3p was confirmed by the models of MI/R injury *in vivo* and H/R injury *in vitro*, providing a new idea for the treatment methods and therapeutic targets for the cardioprotection against myocardial ischemia/reperfusion injury.

The reperfusion injury salvage kinase (RISK) pathway which consists of several survival protein kinases including Akt and Erk1/2, has been considered to confer powerful myocardial protection induced by ischemic pre-conditioning (63–66). Previous studies have shown that the activation of survival signaling Akt and Erk1/2 pathways and apoptosis-signaling pathway inactivation may represent an important mechanism in the cardioprotection conferred by RIPC (67–69). And our previous studies suggested that the RISK pathway might be involved in the cardioprotection of preconditioned plasma at the late phase of RIPC (17). Therefore, our study continued to explore the phosphorylation levels of Akt and Erk to verify whether the RISK pathway was involved in myocardial protection induced by the plasma exosomes at the late phase of RIPC through miR-126a-3p. Our present *in vivo* and *in vitro* studies both showed that, under the intervention of RIPC-exosome, the phosphorylation of Akt, Erk1/2 were significantly increased, but cleaved Caspase-3 was significantly decreased. Further study showed that these differential expressions induced by RIPC-exosome were inhibited by the miR-126a-3p inhibitor. It also showed that the phosphorylation of Akt, Erk1/2 increased and cleaved Caspase-3 decreased in cardiomyocytes preincubated with the miR-126a-3p mimic. The opposite results were showed in cardiomyocytes preincubated with the miR-126a-3p inhibitor. These further confirm the cardioprotective effects of the RIPC plasma exosomal miR-126a-3p, affected by enhancing Akt and Erk1/2 signaling and exerting anti-apoptotic effects by targeting Caspase-3 in cardiomyocytes.

Previous studies have shown that early-phase RIPC leads to an increased number of plasma exosomes (25, 26). However, this study showed that late-phase RIPC did not significantly increase the number of exosomes in plasma, but significantly altered the contents especially the level of the miRNA in exosomes. This result was interesting and may suggest a different mechanism between early- and late-phase RIPC. The exact reasons are not clear. It may be that the increase in the number of exosomes released at the early phase of RIPC is transient, and it will be adjusted by itself after some time.

This study has some limitations. First, there is currently a lack of animal models or specific inhibitors for blocking exosome production *in vivo*, which precludes *in vivo* loss-of-function studies with RIPC-induced exosomes concerning cardioprotection. Second, although the results demonstrated the protective role of plasma exosomes at the late phase of RIPC, the free-exosome plasma at the late phase of RIPC also had the potential for cardioprotection. This result suggested that there may be also other protective materials in pre-conditioned plasma, although exosomes were more representative and applicable. Third, the protective mechanism of plasma exosomes at the early phase and the late phase may be different. Further study was needed to explore the reason for the differences between plasma exosomes at the early phase and the late phase. Fourth, we focused more on the cardioprotective effect of plasma exosomes at the late phase of RIPC and only made a preliminary exploration on the mechanism.

CONCLUSION

In conclusion, the late-phase RIPC derived plasma exosomes may be a carrier to transfer the cardioprotection against myocardial ischemia-reperfusion injury and exosomal miR-126a-3p was identified as an important cardioprotective molecule, which activated the RISK pathway and inhibited the activation of apoptotic protein Caspase-3. These findings present a novel mechanism underlying the exosomes at the late phase RIPC transferred cardioprotection against MI/R injury through miR-126a-3p. Exosomal miR-126a-3p might be a novel

cardioprotective molecule in the prevention and rehabilitation of MI/R injury.

DATA AVAILABILITY STATEMENT

The original contributions presented in the study are publicly available. This data can be found here: GEO accession number: GSE182675.

ETHICS STATEMENT

The animal study was reviewed and approved by Animal Care Ethics Committees of the Sixth Affiliated Hospital, Sun Yat-sen University.

AUTHOR CONTRIBUTIONS

SJ supervised the study and revised the manuscript. DL performed the experiments, analyzed data, and drafted the manuscript. YZha designed the study and revised the manuscript. CZ and FW performed the experiments. YZho analyzed the data. All authors contributed to the article and approved the submitted version.

FUNDING

This research was supported by grants from the National Natural Science Foundation of China (Grant No. 81600396).

ACKNOWLEDGMENTS

The authors thank Professor Zhi-Yi Zuo at the Sun Yat-sen Memorial Hospital, Sun Yat-sen University, and Deputy Director Jian-wen Chen at the School of Pharmaceutical Sciences, Sun Yat-sen University (Guangzhou, China) for providing laboratory.

SUPPLEMENTARY MATERIAL

The Supplementary Material for this article can be found online at: https://www.frontiersin.org/articles/10.3389/fcvm.2021.736226/full#supplementary-material

Supplementary Figure 1 | Schematic diagram of the experimental design. Plasma exosomes, isolated from the plasma of the rats subjected to the late phase of RIPC, exert cardioprotection against MI/R injury. By miRNA sequencing and subsequent functional validation, the late-phase RIPC-induced exosomal miR-126a-3p was identified as an important cardioprotective molecule. Exosomes and miR-126a-3p exerted cardioprotective effects against MI/R injury through enhancing the survival signaling (p-Akt and p-Erk1/2) in the RISK pathway and inhibiting the activation of apoptotic protein Caspase-3 in the apoptotic pathway. RIPC, remote ischemic pre-conditioning; MI/R, myocardial ischemia/reperfusion; H/R, hypoxia/ reoxygenation.

Supplementary Figure 2 | Flowchart of study design for the effect of exosomes. **(A)** *In vitro* Study design. H9C2 cells were assigned to 4 groups ($n = 3$). The normoxia group included cells in a normal culture without H/R injury. The vehicle group included cells subjected to H/R. The R-exo group included cells pre-incubated with RIPC-exosome 24 h before H/R injury. The C-exo group included cells pre-incubated with Control-exosome 24 h before H/R injury. **(B)** *In vivo* study design. Forty rats were randomized into 5 groups including the vehicle group, R-exo group, C-exo group, R-fep group, and C-fep group ($n = 8$). The rats in the vehicle group were injected with 1 ml of PBS. The rats in the R-exo group were injected with RIPC exosomes isolated from equal volumes (1 ml) of plasma. The rats in the C-exo group were injected with control exosomes isolated from equal volumes (1 ml) of plasma. The rats in the R-fep group were injected with 1 ml of free-exosome plasma from the RIPC rats. The rats in the C-fep group were injected with 1 ml of free-exosome plasma from the control rats. The fluid in each group was injected from the tail vein 24 h before the MI/R injury procedure. The experiments were performed by an investigator blinded to group allocation. Four rats in total died during the procedure. In the vehicle group, one died due to surgery. In the C-exo group, one died due to an anesthesia accident. In the C-fep group, two died of pneumothorax and surgery. H/R, Hypoxia/Reoxygenation (24/6 h). MI/R, myocardial ischemia/reperfusion (30/180 min). R-exo, exosomes isolated from the plasma of the late-phase RIPC rats; C-exo, exosomes isolated from the plasma of the control rats; R-fep, the supernatant collected after the first ultracentrifugation from the plasma of the late-phase RIPC rats; C-fep, the supernatant collected after the first ultracentrifugation from the plasma of the control rats.

Supplementary Figure 3 | qRT-PCR analysis of miR-126a-3p expression in rats' myocardium via tail-vein injection in MI/R-injury. Twenty-four hours after the tail vein injection of R-exo, C-exo, or PBS, rats were subjected to MI/R, then myocardial RNAs were extracted and detected by qRT-PCR ($n = 4$). R-exo, exosomes isolated from the plasma of the late-phase RIPC rats; C-exo, exosomes isolated from the plasma of the control rats. MI/R, myocardial ischemia/reperfusion (30/180 min). Data are normalized to U6. $^*p < 0.05$.

Supplementary Figure 4 | Flowchart of study design for the effect of miR-126a-3p in plasma exosomes at the late phase of RIPC. **(A)** The *in vitro* study design for evaluating the effects of exosomal miR-126a-3p in cells. Cells were assigned to 4 groups. Cells were assigned to be transfected with miR-126a-3p inhibitors or negative control (inhibitor-NC) for 24 h and then pre-incubated with RIPC-exosome for 24 h followed by H/R. The normoxia group included cells in a normal culture without H/R injury. The NC+H/R group included cells transfected with inhibitor-NC at 100 nmol/L and then subjected to H/R injury. The R-exo + NC + H/R group included cells pre-incubated with RIPC exosomes and transfected with inhibitor-NC at 100 nmol/L and then subjected to H/R injury. The R-exo + miR-126a-3p inhibitor + H/R group included cells pre-incubated with RIPC exosomes and transfected with miR-126a-3p inhibitor at 100 nmol/L and then subjected to H/R injury. **(B)** The *in vivo* study design for evaluating the effects of exosomal miR-126a-3p in rats. Fifteen rats were randomly assigned to 3 groups and were intracardiac injected 24 h before the MI/R ($n = 5$). The rats in the NC group were intramyocardially injected with 10 nmol/L antagomir-NC. The rats in the R-exo + NC group were intramyocardially injected with 10 nmol/L antagomir-NC and RIPC-exosome isolated from 1 ml RIPC-plasma. The rats in the R-exo + miR-126a-3p antagomir group were intramyocardially injected with 10 nmol/L miR-126a-3p antagomir and RIPC-exosome isolated from 1 ml RIPC-plasma. In the miR-126-3p antagomir group, a rat died in an anesthesia accident. MI/R, myocardial ischemia/reperfusion (30/180 min). R-exo, exosomes isolated from the plasma of the late-phase RIPC rats; C-exo, exosomes isolated from the plasma of the control rats.

Supplementary Figure 5 | Flowchart of study design for the effect of miR-126a-3p. **(A)** The *in vitro* study design for evaluating the direct effects of the miR-126a-3p in cells. Cells were assigned to 3 groups ($n = 3$). Cells were assigned to be transfected with miR-126a-3p mimics or negative control (mimic-NC) for 24 h followed by H/R. The miR-126a-3p mimic and mimic-NC were used at a concentration of 50 nmol/L. The normoxia group included cells in a normal culture without H/R injury. The mimic-NC+H/R group included cells transfected with mimic-NC and then subjected to H/R injury. The miR-126a-3p mimi + H/R group included cells transfected with miR-126a-3p mimic and then subjected to H/R injury. **(B)** The *in vivo* study design for evaluating the direct effects of the miR-126a-3p in rats. Ten rats were randomly assigned to 2 groups and intracardiac injected miR-126a-3p agomir or agomir-NC 24 h before the MI/R, including the agomir-NC group and miR-126a-3p agomir group ($n = 5$). The rats in the agomir-NC group were injected with 5 nmol/L agomir-NC. The rats in the miR-126a-3p agomir group were intramyocardially injected with 5 nmol/L miR-126a-3p agomir. In the miR-126-3p agomir group, a rat died in the surgery. **(C)** The *in vitro* study design for evaluating the effects when miR-126a-3p were inhibited in H9C2 cells. H9C2 cells were assigned to 3 groups ($n = 3$). H9C2 cells

were assigned to be transfected with miR-126a-3p inhibitors or negative control (inhibitor-NC) for 24 h followed by H/R. The miR-126a-3p inhibitor and inhibitor-NC were used at a concentration of 100 nmol/L. The normoxia group included cells in a normal culture without H/R injury. The inhibitor -NC+H/R group included cells transfected with inhibitor-NC and then subjected to H/R injury. The miR-126a-3p inhibitor + H/R group included cells transfected with miR-126a-3p inhibitor and then subjected to H/R injury. H/R, Hypoxia/Reoxygenation (24/6 h). MI/R, myocardial ischemia/reperfusion (30/180 min).

Supplementary Figure 6 | The intervention by pathway inhibitors in plasma exosomes at the late phase of RIPC. Representative images of Western blot. H9C2 cells were pretreated with LY294002 (10 μM) for 1 h and then treated with RIPC-exosome or Control-exosome for 24 h before the H/R injury ($n = 3$). The increased phosphorylation of Akt in the RIPC-exosomes group was eliminated by LY294002. **(B)** Representative images of Western blot. H9C2 cells were pre-treated with U0126 (10 μM) for 1 h and then treated with RIPC-exosome or Control-exosome for 24 h before the H/R injury ($n = 3$). The increased phosphorylation of Erk1/2 in the RIPC-exosomes group was eliminated by U0126. GAPDH was used as a loading control. Quantified data showed phosphorylation level of Akt, expressed as the ratio of p-Akt to Akt; phosphorylation level of Erk1/2, expressed as the ratio of p-Erk1/2 to Erk1/2. H/R, Hypoxia/Reoxygenation (24/6 h). R-exo, exosomes isolated from the plasma of the late-phase RIPC rats; C-exo, exosomes isolated from the plasma of the control rats.

Supplementary Figure 7 | The activation of apoptotic protein Caspase-3 via RIPC-exosomal miR-126-3p mediated effects in primary cardiomyocytes. **(A)** Representative images of Western blot showing activation of apoptotic protein Caspase-3 in primary cardiomyocytes treated with inhibitor-NC, R-exo ± NC, or R-exo ± miR-126a-3p inhibitor followed by H/R ($n = 3$). **(B)** Representative images of Western blot showing activation of apoptotic protein Caspase-3 in primary cardiomyocytes transfected with miR-126a-3p mimics or mimic-NC for 24 h followed by H/R ($n = 3$). GAPDH was used as a loading control. H/R, Hypoxia/Reoxygenation (24/6 h). R-exo, exosomes isolated from the plasma of the late-phase RIPC rats.

REFERENCES

1. Birnbaum Y, Hale SL, Kloner RA. Ischemic preconditioning at a distance: reduction of myocardial infarct size by partial reduction of blood supply combined with rapid stimulation of the gastrocnemius muscle in the rabbit. *Circulation.* (1997) 96:1641–6. doi: 10.1161/01.CIR.96.5.1641
2. Murry CE, Jennings RB, Reimer KA. Preconditioning with ischemia: a delay of lethal cell injury in ischemic myocardium. *Circulation.* (1986) 74:1124–36. doi: 10.1161/01.CIR.74.5.1124
3. Mauser M, Hoffmeister HM, Nienaber C, Schaper W. Influence of ribose, adenosine, and "AICAR" on the rate of myocardial adenosine triphosphate synthesis during reperfusion after coronary artery occlusion in the dog. *Circ Res.* (1985) 56:220–30. doi: 10.1161/01.RES.56.2.220
4. Loukogeorgakis SP, Panagiotidou AT, Broadhead MW, Donald A, Deanfield JE, MacAllister RJ. Remote ischemic preconditioning provides early and late protection against endothelial ischemia-reperfusion injury in humans: role of the autonomic nervous system. *J Am Coll Cardiol.* (2005) 46:450–6. doi: 10.1016/j.jacc.2005.04.044
5. Gho BC, Schoemaker RG, van den Doel MA, Duncker DJ, Verdouw PD. Myocardial protection by brief ischemia in noncardiac tissue. *Circulation.* (1996) 94:2193–200. doi: 10.1161/01.CIR.94.9.2193
6. Weinbrenner C, Nelles M, Herzog N, Sarvary L, Strasser RH. Remote preconditioning by infrarenal occlusion of the aorta protects the heart from infarction: a newly identified non-neuronal but PKC-dependent pathway. *Cardiovasc Res.* (2002) 55:590–601. doi: 10.1016/S0008-6363(02)00446-7
7. Konstantinov IE, Li J, Cheung MM, Shimizu M, Stokoe J, Kharbanda RK, et al. Remote ischemic preconditioning of the recipient reduces myocardial ischemia-reperfusion injury of the denervated donor heart via a Katp channel-dependent mechanism. *Transplantation.* (2005) 79:1691–5. doi: 10.1097/01.TP.0000159137.76400.5D
8. Dickson EW, Blehar DJ, Carraway RE, Heard SO, Steinberg G, Przyklenk K. Naloxone blocks transferred preconditioning in isolated rabbit hearts. *J Mol Cell Cardiol.* (2001) 33:1751–6. doi: 10.1006/jmcc.2001.1436
9. Dickson EW, Porcaro WA, Fenton RA, Heard SO, Reindhardt CP, Renzi FP, et al. "Preconditioning at a distance" in the isolated rabbit heart. *Acad Emerg Med.* (2000) 7:311–7. doi: 10.1111/j.1553-2712.2000.tb02228.x
10. Dickson EW, Reinhardt CP, Renzi FP, Becker RC, Porcaro WA, Heard SO. Ischemic preconditioning may be transferable via whole blood transfusion: preliminary evidence. *J Thromb Thrombolysis.* (1999) 8:123–9. doi: 10.1023/A:1008911101951
11. Shimizu M, Tropak M, Diaz RJ, Suto F, Surendra H, Kuzmin E, et al. Transient limb ischaemia remotely preconditions through a humoral mechanism acting directly on the myocardium: evidence suggesting cross-species protection. *Clin Sci.* (2009) 117:191–200. doi: 10.1042/CS20080523
12. Serejo FC, Rodrigues LF Jr, da Silva Tavares KC, de Carvalho AC, Nascimento JH. Cardioprotective properties of humoral factors released from rat hearts subject to ischemic preconditioning. *J Cardiovasc Pharmacol.* (2007) 49:214–20. doi: 10.1097/FJC.0b013e3180325ad9
13. Lang SC, Elsasser A, Scheler C, Vetter S, Tiefenbacher CP, Kubler W, et al. Myocardial preconditioning and remote renal preconditioning–identifying a protective factor using proteomic methods? *Basic Res Cardiol.* (2006) 101:149–58. doi: 10.1007/s00395-005-0565-0
14. Zhao Y, Zheng ZN, Cheung CW, Zuo ZY, Jin SQ. Transfusion of plasma collected at late phase after preconditioning reduces myocardial infarct size induced by ischemia-reperfusion in rats *in vivo*. *Chin Med J.* (2017) 130:303–8. doi: 10.4103/0366-6999.198933
15. Zhao Y, Zheng ZN, Jin SQ, Liang HM. Effects of plasma collected 48 hours after transient limb ischemia on blood pressure recovery in homogenic rats after myocardial ischemia reperfusion *in vivo*. *Chin Med J.* (2013) 126:2894–9. doi: 10.3760/cma.j.issn.0366-6999.20131018
16. Zhao Y, Zheng ZN, Liu X, Dai G, Jin SQ. Effects of preconditioned plasma collected during the late phase of remote ischaemic preconditioning on ventricular arrhythmias caused by myocardial ischaemia reperfusion in rats. *J Int Med Res.* (2018) 46:1370–9. doi: 10.1177/0300060518755268
17. Zhao Y, Zheng ZN, Pi YN, Liang X, Jin SQ. Cardioprotective effects of transfusion of late-phase preconditioned plasma may be induced by activating the reperfusion injury salvage kinase pathway but not the survivor activating factor enhancement pathway in rats. *Oxid Med Cell Longev.* (2017) 2017:8526561. doi: 10.1155/2017/8526561
18. Valadi H, Ekstrom K, Bossios A, Sjostrand M, Lee JJ, Lotvall JO. Exosome-mediated transfer of mRNAs and microRNAs is a novel mechanism of genetic exchange between cells. *Nat Cell Biol.* (2007) 9:654–9. doi: 10.1038/ncb1596
19. Sharma S, Mishra R, Bigham GE, Wehman B, Khan MM, Xu H, et al. A deep proteome analysis identifies the complete secretome as the functional unit of human cardiac progenitor cells. *Circ Res.* (2017) 120:816–34. doi: 10.1161/CIRCRESAHA.116.309782
20. De Rosa S, Fichtlscherer S, Lehmann R, Assmus B, Dimmeler S, Zeiher AM. Transcoronary concentration gradients of circulating microRNAs. *Circulation.* (2011) 124:1936–44. doi: 10.1161/CIRCULATIONAHA.111.037572
21. Sahoo S, Losordo DW. Exosomes and cardiac repair after myocardial infarction. *Circ Res.* (2014) 114:333–44. doi: 10.1161/CIRCRESAHA.114.300639
22. Zampetaki A, Willeit P, Tilling L, Drozdov I, Prokopi M, Renard JM, et al. Prospective study on circulating MicroRNAs and risk of myocardial infarction. *J Am Coll Cardiol.* (2012) 60:290–9. doi: 10.1016/j.jacc.2012.03.056
23. Charles CJ, Li RR, Yeung T, Mazlan SMI, Lai RC, de Kleijn DPV, et al. Systemic mesenchymal stem cell-derived exosomes reduce myocardial infarct size: characterization with MRI in a porcine model. *Front Cardiovasc Med.* (2020) 7:601990. doi: 10.3389/fcvm.2020.601990
24. Hou Z, Qin X, Hu Y, Zhang X, Li G, Wu J, et al. Longterm exercise-derived exosomal miR-342-5p: a novel exerkine for cardioprotection. *Circ Res.* (2019) 124:1386–400. doi: 10.1161/CIRCRESAHA.118.314635
25. Vicencio JM, Yellon DM, Sivaraman V, Das D, Boi-Doku C, Arjun S, et al. Plasma exosomes protect the myocardium from ischemia-reperfusion injury. *J Am Coll Cardiol.* (2015) 65:1525–36. doi: 10.1016/j.jacc.2015.02.026

26. Minghua W, Zhijian G, Chahua H, Qiang L, Minxuan X, Luqiao W, et al. Plasma exosomes induced by remote ischaemic preconditioning attenuate myocardial ischaemia/reperfusion injury by transferring miR-24. *Cell Death Dis.* (2018) 9:320. doi: 10.1038/s41419-018-0274-x
27. Caby MP, Lankar D, Vincendeau-Scherrer C, Raposo G, Bonnerot C. Exosomal-like vesicles are present in human blood plasma. *Int Immunol.* (2005) 17:879–87. doi: 10.1093/intimm/dxh267
28. Dragovic RA, Gardiner C, Brooks AS, Tannetta DS, Ferguson DJ, Hole P, et al. Sizing and phenotyping of cellular vesicles using nanoparticle tracking analysis. *Nanomedicine.* (2011) 7:780–8. doi: 10.1016/j.nano.2011.04.003
29. Aronsen JM, Espe EKS, Skardal K, Hasic A, Zhang L, Sjaastad I. Noninvasive stratification of postinfarction rats based on the degree of cardiac dysfunction using magnetic resonance imaging and echocardiography. *Am J Physiol Heart Circ Physiol.* (2017) 312:H932–42. doi: 10.1152/ajpheart.00668.2016
30. Yamazaki T, Izumi Y, Nakamura Y, Hanatani A, Shimada K, Muro T, et al. Novel device that produces carbon dioxide mist for myocardial infarction treatment in rats. *Circ J.* (2012) 76:1203–12. doi: 10.1253/circj.CJ-11-1116
31. Yamazaki T, Izumi Y, Nakamura Y, Yamashita N, Fujiki H, Osada-Oka M, et al. Tolvaptan improves left ventricular dysfunction after myocardial infarction in rats. *Circ Heart Fail.* (2012) 5:794–802. doi: 10.1161/CIRCHEARTFAILURE.112.968750
32. Teichholz LE, Kreulen T, Herman MV, Gorlin R. Problems in echocardiographic volume determinations: echocardiographic-angiographic correlations in the presence of absence of asynergy. *Am J Cardiol.* (1976) 37:7–11. doi: 10.1016/0002-9149(76)90491-4
33. Creemers EE, Tijsen AJ, Pinto YM. Circulating microRNAs: novel biomarkers and extracellular communicators in cardiovascular disease? *Circ Res.* (2012) 110:483–95. doi: 10.1161/CIRCRESAHA.111.247452
34. Skog J, Wurdinger T, van Rijn S, Meijer DH, Gainche L, Sena-Esteves M, et al. Glioblastoma microvesicles transport RNA and proteins that promote tumour growth and provide diagnostic biomarkers. *Nat Cell Biol.* (2008) 10:1470–6. doi: 10.1038/ncb1800
35. Hausenloy DJ, Yellon DM. Myocardial ischemia-reperfusion injury: a neglected therapeutic target. *J Clin Invest.* (2013) 123:92–100. doi: 10.1172/JCI62874
36. Hausenloy DJ, Yellon DM. Reperfusion injury salvage kinase signalling: taking a RISK for cardioprotection. *Heart Fail Rev.* (2007) 12:217–34. doi: 10.1007/s10741-007-9026-1
37. Chen AQ, Gao XF, Wang ZM, Wang F, Luo S, Gu Y, et al. Therapeutic exosomes in prognosis and developments of coronary artery disease. *Front Cardiovasc Med.* (2021) 8:691548. doi: 10.3389/fcvm.2021.691548
38. Ranjan P, Kumari R, Goswami SK, Li J, Pal H, Suleiman Z, et al. Myofibroblast-derived exosome induce cardiac endothelial cell dysfunction. *Front Cardiovasc Med.* (2021) 8:676267. doi: 10.3389/fcvm.2021.676267
39. Wang W, Zheng H. Myocardial infarction: the protective role of MiRNAs in myocardium pathology. *Front Cardiovasc Med.* (2021) 8:631817. doi: 10.3389/fcvm.2021.631817
40. Xue R, Tan W, Wu Y, Dong B, Xie Z, Huang P, et al. Role of exosomal miRNAs in heart failure. *Front Cardiovasc Med.* (2020) 7:592412. doi: 10.3389/fcvm.2020.592412
41. Cheng Y, Zhu P, Yang J, Liu X, Dong S, Wang X, et al. Ischaemic preconditioning-regulated miR-21 protects heart against ischaemia/reperfusion injury via anti-apoptosis through its target PDCD4. *Cardiovasc Res.* (2010) 87:431–9. doi: 10.1093/cvr/cvq082
42. Duan X, Ji B, Wang X, Liu J, Zheng Z, Long C, et al. Expression of microRNA-1 and microRNA-21 in different protocols of ischemic conditioning in an isolated rat heart model. *Cardiology.* (2012) 122:36–43. doi: 10.1159/000338149
43. Perrino C, Barabasi AL, Condorelli G, Davidson SM, De Windt L, Dimmeler S, et al. Epigenomic and transcriptomic approaches in the post-genomic era: path to novel targets for diagnosis and therapy of the ischaemic heart? Position paper of the European society of cardiology working group on cellular biology of the heart. *Cardiovasc Res.* (2017) 113:725–36. doi: 10.1093/cvr/cvx070
44. Varga ZV, Zvara A, Farago N, Kocsis GF, Pipicz M, Gaspar R, et al. MicroRNAs associated with ischemia-reperfusion injury and cardioprotection by ischemic pre- and postconditioning: protectomiRs. *Am J Physiol Heart Circ Physiol.* (2014) 307:H216–27. doi: 10.1152/ajpheart.00812.2013
45. Li J, Rohailla S, Gelber N, Rutka J, Sabah N, Gladstone RA, et al. MicroRNA-144 is a circulating effector of remote ischemic preconditioning. *Basic Res Cardiol.* (2014) 109:423. doi: 10.1007/s00395-014-0423-z
46. Schober A, Nazari-Jahantigh M, Wei Y, Bidzhekov K, Gremse F, Grommes J, et al. MicroRNA-126-5p promotes endothelial proliferation and limits atherosclerosis by suppressing Dlk1. *Nat Med.* (2014) 20:368–76. doi: 10.1038/nm.3487
47. Meng S, Cao JT, Zhang B, Zhou Q, Shen CX, Wang CQ. Downregulation of microRNA-126 in endothelial progenitor cells from diabetes patients, impairs their functional properties, via target gene Spred-1. *J Mol Cell Cardiol.* (2012) 53:64–72. doi: 10.1016/j.yjmcc.2012.04.003
48. Harris TA, Yamakuchi M, Ferlito M, Mendell JT, Lowenstein CJ. MicroRNA-126 regulates endothelial expression of vascular cell adhesion molecule 1. *Proc Natl Acad Sci USA.* (2008) 105:1516–21. doi: 10.1073/pnas.0707493105
49. Wang S, Aurora AB, Johnson BA, Qi X, McAnally J, Hill JA, et al. The endothelial-specific microRNA miR-126 governs vascular integrity and angiogenesis. *Dev Cell.* (2008) 15:261–71. doi: 10.1016/j.devcel.2008.07.002
50. Jansen F, Yang X, Hoelscher M, Cattelan A, Schmitz T, Proebsting S, et al. Endothelial microparticle-mediated transfer of MicroRNA-126 promotes vascular endothelial cell repair via SPRED1 and is abrogated in glucose-damaged endothelial microparticles. *Circulation.* (2013) 128:2026–38. doi: 10.1161/CIRCULATIONAHA.113.001720
51. Nicoli S, Standley C, Walker P, Hurlstone A, Fogarty KE, Lawson ND. MicroRNA-mediated integration of haemodynamics and Vegf signalling during angiogenesis. *Nature.* (2010) 464:1196-200. doi: 10.1038/nature08889
52. Wang X, Lian Y, Wen X, Guo J, Wang Z, Jiang S, et al. Expression of miR-126 and its potential function in coronary artery disease. *Afr Health Sci.* (2017) 17:474-80. doi: 10.4314/ahs.v17i2.22
53. Wang W, Zheng Y, Wang M, Yan M, Jiang J, Li Z. Exosomes derived miR-126 attenuates oxidative stress and apoptosis from ischemia and reperfusion injury by targeting ERRFI1. *Gene.* (2019) 690:75–80. doi: 10.1016/j.gene.2018.12.044
54. Dickhout A, Koenen RR. Extracellular vesicles as biomarkers in cardiovascular disease; chances and risks. *Front Cardiovasc Med.* (2018) 5:113. doi: 10.3389/fcvm.2018.00113
55. Zamani P, Fereydouni N, Butler AE, Navashenaq JG, Sahebkar A. The therapeutic and diagnostic role of exosomes in cardiovascular diseases. *Trends Cardiovasc Med.* (2019) 29:313–3. doi: 10.1016/j.tcm.2018.10.010
56. Sluijter JPG, Davidson SM, Boulanger CM, Buzas EI, de Kleijn DPV, Engel FB, et al. Extracellular vesicles in diagnostics and therapy of the ischaemic heart: position paper from the working group on cellular biology of the heart of the european society of cardiology. *Cardiovasc Res.* (2018) 114:19–34. doi: 10.1093/cvr/cvx211
57. Ha D, Yang N, Nadithe V. Exosomes as therapeutic drug carriers and delivery vehicles across biological membranes: current perspectives and future challenges. *Acta Pharm Sin B.* (2016) 6:287–96. doi: 10.1016/j.apsb.2016.02.001
58. Zhang Y, Bi J, Huang J, Tang Y, Du S, Li P. Exosome: a review of its classification, isolation techniques, storage, diagnostic and targeted therapy applications. *Int J Nanomedicine.* (2020) 15:6917–34. doi: 10.2147/IJN.S264498
59. Lew JK, Pearson JT, Schwenke DO, Katare R. Exercise mediated protection of diabetic heart through modulation of microRNA mediated molecular pathways. *Cardiovasc Diabetol.* (2017) 16:10. doi: 10.1186/s12933-016-0484-4
60. Janssen HL, Reesink HW, Lawitz EJ, Zeuzem S, Rodriguez-Torres M, Patel K, et al. Treatment of HCV infection by targeting microRNA. *N Engl J Med.* (2013) 368:1685–94. doi: 10.1056/NEJMoa1209026
61. Lener T, Gimona M, Aigner L, Borger V, Buzas E, Camussi G, et al. Applying extracellular vesicles based therapeutics in clinical trials - an ISEV position paper. *J Extracell Vesicles.* (2015) 4:30087. doi: 10.3402/jev.v4.30087
62. Morishita M, Takahashi Y, Nishikawa M, Takakura Y. Pharmacokinetics of exosomes-an important factor for elucidating the biological roles of exosomes and for the development of exosome-based therapeutics. *J Pharm Sci.* (2017) 106:2265–9. doi: 10.1016/j.xphs.2017.02.030
63. Hausenloy DJ, Mocanu MM, Yellon DM. Cross-talk between the survival kinases during early reperfusion: its contribution to ischemic preconditioning. *Cardiovasc Res.* (2004) 63:305–12. doi: 10.1016/j.cardiores.2004.04.011

64. Hausenloy DJ, Tsang A, Mocanu MM, Yellon DM. Ischemic preconditioning protects by activating prosurvival kinases at reperfusion. *Am J Physiol Heart Circ Physiol.* (2005) 288:H971–6. doi: 10.1152/ajpheart.00374.2004
65. Breivik L, Helgeland E, Aarnes EK, Mrdalj J, Jonassen AK. Remote postconditioning by humoral factors in effluent from ischemic preconditioned rat hearts is mediated via PI3K/Akt-dependent cell-survival signaling at reperfusion. *Basic Res Cardiol.* (2011) 106:135–45. doi: 10.1007/s00395-010-0133-0
66. Skyschally A, Gent S, Amanakis G, Schulte C, Kleinbongard P, Heusch G. Across-species transfer of protection by remote ischemic preconditioning with species-specific myocardial signal transduction by reperfusion injury salvage kinase and survival activating factor enhancement pathways. *Circ Res.* (2015) 117:279–88. doi: 10.1161/CIRCRESAHA.117.306878
67. Lai CC, Tang CY, Chiang SC, Tseng KW, Huang CH. Ischemic preconditioning activates prosurvival kinases and reduces myocardial apoptosis. *J Chin Med Assoc.* (2015) 78:460–8. doi: 10.1016/j.jcma.2015.04.006
68. Heusch G, Botker HE, Przyklenk K, Redington A, Yellon D. Remote ischemic conditioning. *J Am Coll Cardiol.* (2015) 65:177–95. doi: 10.1016/j.jacc.2014.10.031
69. Sivaraman V, Pickard JM, Hausenloy DJ. Remote ischaemic conditioning: cardiac protection from afar. *Anaesthesia.* (2015) 70:732–48. doi: 10.1111/anae.12973

Conflict of Interest: The authors declare that the research was conducted in the absence of any commercial or financial relationships that could be construed as a potential conflict of interest.

Publisher's Note: All claims expressed in this article are solely those of the authors and do not necessarily represent those of their affiliated organizations, or those of the publisher, the editors and the reviewers. Any product that may be evaluated in this article, or claim that may be made by its manufacturer, is not guaranteed or endorsed by the publisher.

Copyright © 2021 Li, Zhao, Zhang, Wang, Zhou and Jin. This is an open-access article distributed under the terms of the Creative Commons Attribution License (CC BY). The use, distribution or reproduction in other forums is permitted, provided the original author(s) and the copyright owner(s) are credited and that the original publication in this journal is cited, in accordance with accepted academic practice. No use, distribution or reproduction is permitted which does not comply with these terms.

frontiers in Cardiovascular Medicine

ORIGINAL RESEARCH
published: 20 December 2021
doi: 10.3389/fcvm.2021.814402

Expression Profiles of Circular RNA in Aortic Vascular Tissues of Spontaneously Hypertensive Rats

Ying Liu[1,2,3†], Ying Dong[1,2†], Zhaojie Dong[1,2†], Jiawei Song[1,2,3], Zhenzhou Zhang[1,2], Lirong Liang[1,3], Xiaoyan Liu[1,2], Lanlan Sun[4], Xueting Li[1,2], Miwen Zhang[1,2], Yihang Chen[1,2], Ran Miao[1,3] and Jiuchang Zhong[1,2,3*]*

[1] Heart Center and Beijing Key Laboratory of Hypertension, Beijing Chaoyang Hospital, Capital Medical University, Beijing, China, [2] Department of Cardiology, Beijing Chaoyang Hospital, Capital Medical University, Beijing, China, [3] Department of Respiratory and Critical Care Medicine, Beijing Institute of Respiratory Medicine and Beijing Chaoyang Hospital, Capital Medical University, Beijing, China, [4] Department of Echocardiography, Beijing Chaoyang Hospital, Capital Medical University, Beijing, China

OPEN ACCESS

Edited by:
Hui Gong,
Fudan University, China

Reviewed by:
Dan Meng,
Fudan University, China
Liming Yang,
Harbin Medical University, China

***Correspondence:**
Jiuchang Zhong
jczhong@sina.com
orcid.org/0000-0002-2315-3515
Ran Miao
mr1019@163.com

[†]These authors have contributed equally to this work

Specialty section:
This article was submitted to General Cardiovascular Medicine, a section of the journal Frontiers in Cardiovascular Medicine

Received: *13 November 2021*
Accepted: *01 December 2021*
Published: *20 December 2021*

Citation:
Liu Y, Dong Y, Dong Z, Song J, Zhang Z, Liang L, Liu X, Sun L, Li X, Zhang M, Chen Y, Miao R and Zhong J (2021) Expression Profiles of Circular RNA in Aortic Vascular Tissues of Spontaneously Hypertensive Rats. Front. Cardiovasc. Med. 8:814402. doi: 10.3389/fcvm.2021.814402

Background: Circular RNAs (circRNAs), as a kind of endogenous non-coding RNA, have been implicated in ischemic heart diseases and vascular diseases. Based on theirs high stability with a closed loop structure, circRNAs function as a sponge and bind specific miRNAs to exert inhibitory effects in heart and vasculature, thereby regulating their target gene and protein expression, *via* competitive endogenous RNA (ceRNA) mechanism. However, the exact roles and underlying mechanisms of circRNAs in hypertension and related cardiovascular diseases remain largely unknown.

Methods and Results: High-throughput RNA sequencing (RNA-seq) was used to analyze the differentially expressed (DE) circRNAs in aortic vascular tissues of spontaneously hypertensive rats (SHR). Compared with the Wistar-Kyoto (WKY) rats, there were marked increases in the levels of systolic blood pressure, diastolic blood pressure and mean blood pressure in SHR under awake conditions *via* the tail-cuff methodology. Totally, compared with WKY rats, 485 DE circRNAs were found in aortic vascular tissues of SHR with 279 up-regulated circRNAs and 206 down-regulated circRNAs. Furthermore, circRNA-target microRNAs (miRNAs) and the target messenger RNAs (mRNAs) of miRNAs were predicted by the miRanda and Targetscan softwares, respectively. Additionally, real-time RT-PCR analysis verified that downregulation of rno_circRNA_0009197, and upregulation of rno_circRNA_0005818, rno_circRNA_0005304, rno_circRNA_0005506, and rno_circRNA_0009301 were observed in aorta of SHR when compared with that of WKY rats. Then, the potential ceRNA regulatory mechanism was constructed *via* integrating 5 validated circRNAs, 31 predicted miRNAs, and 266 target mRNAs. More importantly, three hub genes (NOTCH1, FOXO3, and STAT3) were recognized according to PPI network and three promising circRNA-miRNA-mRNA regulatory axes were found in hypertensive rat aorta, including rno_circRNA_0005818/miR-615/NOTCH1, rno_circRNA_0009197/miR-509-5p/FOXO3, and rno_circRNA_0005818/miR-10b-5p/STAT3, respectively.

Conclusions: Our results demonstrated for the first time that circRNAs are expressed aberrantly in aortic vascular tissues of hypertensive rats and may serve as a sponge linking with relevant miRNAs participating in pathogenesis of hypertension and related ischemic heart diseases *via* the circRNA-miRNA-mRNA ceRNAnetwork mechanism.

Keywords: competing endogenous RNAs network, microRNA, circular RNA, hypertensive vascular injury, ischemia heart disease

INTRODUCTION

Hypertension is a leading risk factor of ischemic heart diseases and hypertensive heart diseases that mainly leads to the high morbidity and mortality (1, 2). It is estimated that ∼1.56 billion adults worldwide expected to be influenced by hypertension by 2025 (3). To our knowledge, cardiovascular damage is an essential pathological characteristic of hypertension. Especially, impaired vascular remodeling and endothelial dysfunction result in the evolution of coronary artery abnormalities (4), eventually causing ischemia heart disease. A variety of mechanisms lead to the generation of myocardial ischemia during hypertension (5). However, current studies on the effective biomarkers of hypertensive vascular injury are still limited.

Non-coding RNAs (ncRNAs) play critical roles in hypertension and hypertensive vascular disorders, including ribosomal RNAs, transfer RNAs, small nuclear RNAs, microRNAs (miRNAs), and long non-coding RNAs (lncRNAs) (6). Recently, circRNA is a kind of bioactive RNA molecules with a closed loop structure (7). The majority of circRNAs are widely available in cardiovascular system and have multiple critical specific functions in vascular physiology and homeostasis at the posttranscriptional level (8). Based on the high stability, circRNAs function as a sponge and bind specific miRNAs to exert inhibitory effects on regulating the gene and protein expression, *via* ceRNA mechanism (9). Several circRNAs have been involved in vascular injury in pulmonary arterial hypertension (9, 10). However, the regulatory roles and underlying mechanisms of circRNAs in hypertension and hypertensive vascular diseases remain largely unclear.

In current study, the differentially expressed (DE) circRNAs were detected in aortic vascular tissues of the spontaneously hypertensive rat (SHR) and the Wistar-Kyoto (WKY) rats by high-throughput RNA sequencing (RNA-Seq) analysis and the real-time polymerase chain reaction (RT-PCR) validation, respectively. More importantly, three promising circRNA-miRNA-mRNA regulatory axes network were highlighted in hypertensive rat aorta, providing potential therapeutic targets for hypertension and hypertensive vascular disorders.

MATERIALS AND METHODS

Experimental Animals, Blood Pressure Measurement, and Tissue Preparation

A total of five male 13-week-old SHR and five age- and weight-matched WKY rats regarded as control groups were purchased from Beijing Vital River Laboratory Animal Technology Co., Ltd. All the experiments were conformed to the guidelines of animal experiments reported at Capital Medical University. Rats were maintained in a temperature and humidity-controlled animal room with 12:12 h day:night cycle, meanwhile different cages were used for each group. All of the animals were accessed to tap water and laboratory feed. Systolic blood pressure (SBP), diastolic blood pressure (DBP), and mean blood pressure (MBP) were non-invasively measured under awake conditions *via* tail-cuff methodology (Softron, BP-98A, Japan). The thoracic aorta was extracted, removed fat and connective tissues and frozen in liquid nitrogen immediately. Samples were shipped to the laboratory and stored at −80°C until analysis. All experiments were approved and performed in accordance with the National Institutes of Health guide for the care and use of Laboratory animals (NIH Publications No. 8023), Animal Research Ethics Committee of Beijing Chaoyang Hospital affiliated to Capital Medical University.

The Elastica Van Gieson Staining

The EVG staining was intended for use in the histological demonstration of elastin in tissues and collagen fiber. The demonstration of elastic in tissue was useful in vascular diseases. The deparaffinize sections were hydrated in distilled water. Put the slides in Elastic stain solution for 15 min and washed the slide by use of running tap water. Then, the slides were kept in Sodium Thiosulfate Solution for 1 min and in Van Gieson's Solution for 2–5 min, and then rinse in two changes of 95% alcohol and dehydrate in absolute alcohol (Abcam, Cambridge, MA).

Total RNA Isolation and Library Preparation for circRNA Sequencing

Total RNAs were isolated from thoracic aorta from SHR and WKY rats, a total amount of 5 μg RNA per sample was used as input material for the RNA sample preparations using TRIzol reagent (Invitrogen, USA). Furthermore, RNA purity was checked using the NanoPhotometer®spectrophotometer (IMPLEN, CA, USA) and RNA integrity was evaluated using the RNA Nano 6000 Assay Kit of the Bioanalyzer 2100 system (Aglient Technologies, CA, USA). Additionally, ribosomal RNA was depleted from total RNA using the Epicenter Ribozero™ rRNA Removal Kit (Epicenter, USA), and rRNA free residue was cleaned up by ethanol precipitation. Subsequently, the linear RNA was digested with 3U of RNase R (Epicenter, USA) per μg of RNA. The sequencing libraries were generated by NEBNext®Ultra™ Directional RNA Library Prep Kit for Illumina® (NEB, USA) following manufacturer's recommendations by Shanghai Genechem Co.,

Ltd., Shanghai, China. The clustering of the index-coded samples was performed on a cBot Cluster Generation System using TruSeq PE Cluster Kit v3-cBot-HS (Illumina) according to the manufacturer's instructions. After cluster generation, the libraries were sequenced on an Illumina platform and 150 bp paired-end reads were generated.

Quality Control and circRNA Identification

The raw data of quality control was firstly processed through in-house perlscripts. After removing reads containing adapter, poly-N or low-quality reads, clean reads were left. Meanwhile, Q20, Q30, and GC content of the clean reads were calculated (**Supplementary Table 1**). Importantly, clean reads with high quality were applied among all the downstream analyses. Index of the reference genome was built using bowtie2 v2.2.8 and paired-end clean reads were aligned to the reference genome using Bowtie software (11).

Differential Expression Analysis of circRNAs

Differential expression analysis between the two groups was assessed using the DESeq R package (1.10.1). DESeq provided statistical routines for determining differential expression in digital gene expression data using a model based on the negative binomial distribution. The resulting *P*-values were corrected using the Benjamini and Hochberg's approach for controlling the false discovery rate, shown as q values. Genes with an adjusted *P*-value or *q*-value < 0.05 were regarded as statistical significance.

GO and KEGG Pathway of circRNAs and mRNAs in the Network

Gene Ontology (GO) (http://www.geneontology.org) and Kyoto Encyclopedia of Genes and Genomes (KEGG) signal pathway enrichment analysis (http://www.genome.jp/kegg) were conducted to explore the biological function of targeted genes. Gene function was categorized into three separate subgroups: biological processes (BPs), cellular components (CCs), and molecular functions (MFs), respectively.

Validation of RNA Sequencing With Real Time Reverse Transcription-Polymerase Chain Reaction Analysis

Five pairs of SHR and WKY rats were employed to confirm the expression levels of DE circRNAs by RT-PCR analysis. In brief, total RNAs were reversed transcribed into cDNA using PrimeScript^{TM} reverse transcription reagent kit (Takara Bio, Inc., Otsu, Japan) according to the manufacturer's protocol. Then, cDNAs were used for RT-PCR analysis to examine the expression of circRNA by the ABI Prism 7500 sequence detection system (Applied, Biosystems, CA). GADPH was served as a normalizing standard for all target circRNAs. The primers for each circRNAs were summarized in **Supplementary Table 2**. All samples were run in triplicate. The relative expression of selected circRNAs were calculated using the $2^{-\Delta\Delta CT}$ method.

Prediction of circRNA-miRNA-mRNA Interaction Network and Identification of Hub Genes

We next predicted the sequence identity of the circRNA in human and rat by using Basic Local Alignment Search Tool (https://blast.ncbi.nlm.nih.gov/Blast.cgi) and the circAtlas 2.0 software (http://circatlas.biols.ac.cn/). Moreover, the altered circRNAs in hypertensive rat aorta with corresponding miRNAs and the potential target mRNAs were used to establish a circRNA-miRNA-mRNA interaction network. The miRNA-mRNA interactions were firstly predicted using Targetscan (www.targetscan.org/). The circRNA-miRNA-mRNA network to further visualize the interactions using Cytoscape 3.8.2 software. Moreover, the STRING database (http://string-db.org/) was used to establish the protein-protein interaction (PPI) of the predicted mRNA, and then visualized by using Cytoscape version 3.8.2 software. Subsequently, hub genes were also determined using cytoHubba app of Cytoscape.

Statistical Analysis

The data analyses were conducted using SPSS software version 21.0 (IBM SPSS, Chicago, IL, USA). GraphPad Prism version 7.0 (GraphPad software, Inc., LaJolla, CA, USA) and Cytoscape version 3.8.2 were applied to generate the figures. All the data were presented as means ± standard deviations (SDs) and compared using the Student's *t*-test, and a *P*-value or *q*-value $<$ 0.05 was regarded as significant. All experiments were carried out three times.

RESULTS

Expression Profiling of Aortic circRNAs Between SHR and WKY Rats

Vascular circRNAs expressions between SHR and WKY rats were measured using RNA sequencing analysis. Firstly, compared with WKY rats, the levels of SBP, DBP and MBP were significantly elevated in SHR (**Figure 1A**). Furthermore, information of circRNAs was exhibited, including the raw reads, read counts, raw bases, GC content (%), and Q30% etc (**Supplementary Table 1**). The basic information and classifications of sequencing quality for circRNAs were revealed in aortic vascular tissues of SHR and WKY rats (**Supplementary Figure 1**). Box plots showing the circRNA profiles revealed the similar distributions of all datasets in the detected samples (**Figure 1B**). The circRNA transcripts were mostly 300 bp in length (**Figure 1C**). In addition, clustered heatmap was conducted to aortic circRNA according to their expression levels among rats (**Figure 1D**), indicating that the circRNA profiles were different between SHR and WKY rats. To determine these different circRNAs expressions in hypertension, the variation between each group was analyzed by the volcano plot. Significantly DE circRNAs were identified as $q < 0.05$ and $|\log2(\text{fold changes})| > 1$. Totally, 485 DE circRNAs were detected in SHR (279 up-regulated and 206 down-regulated circRNAs) compared with WKY rats (**Figure 1E**). We further classified the distributions of DE circRNAs according to the chromosomes

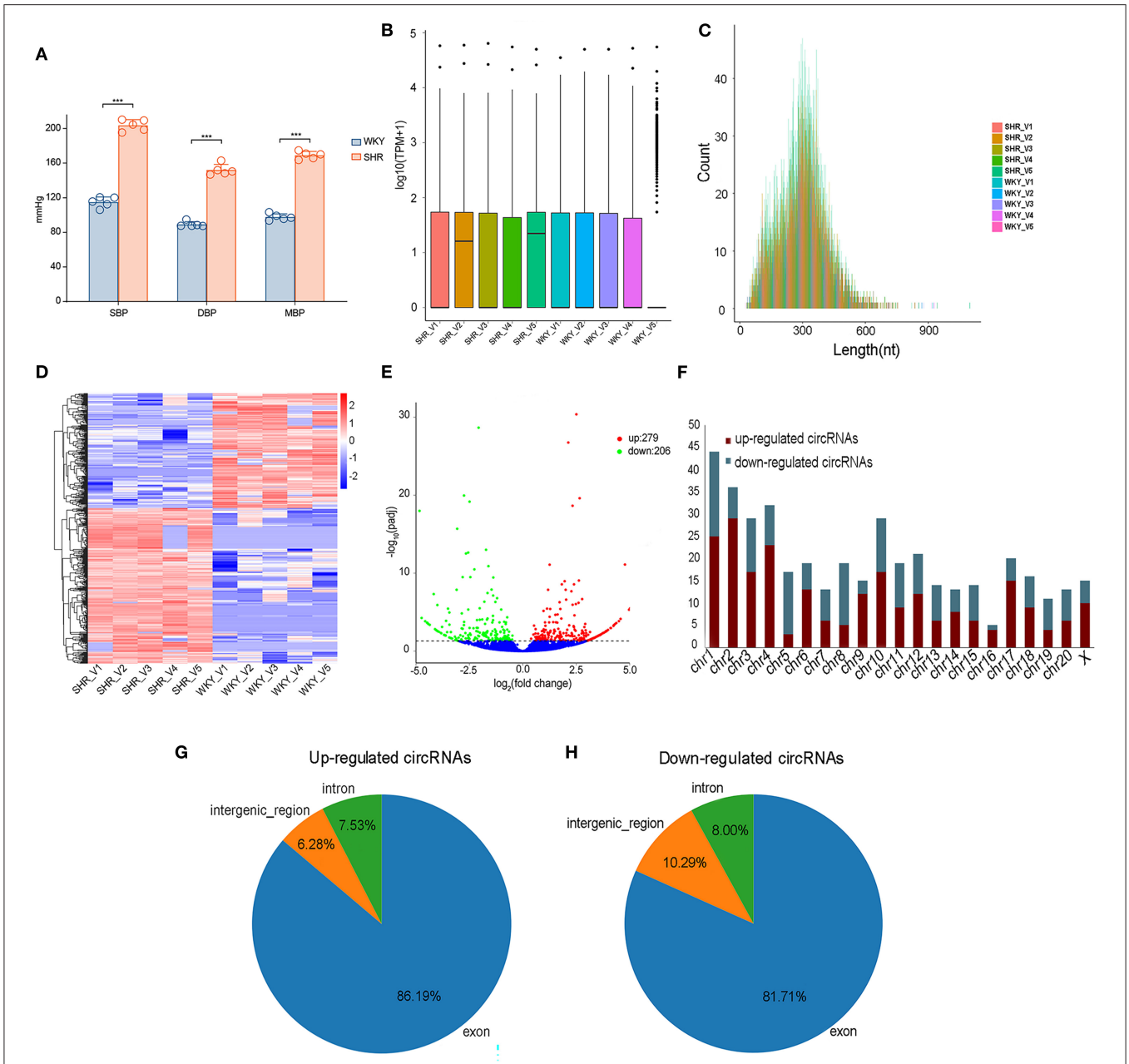

FIGURE 1 | The expression profiling of vascular circRNAs was screened and analyzed by RNA-seq of aortic vascular tissues between SHR and WKY rats. **(A)** Compared with WKY controls, SBP levels, DBP levels and MBP levels were significantly elevated in SHR rats. **(B)** The data standardization of the total expression of the circRNAs. **(C)** The length of circRNA profiles. **(D)** The hierarchical cluster analysis was performed with the significantly different circRNA expression profiles in SHR and WKY aorta (Fold Change > 2 and $P < 0.05$); Red and blue denoted high and low relative expression, respectively, each circRNA was expressed by a single row of colored boxes and each sample was represented by a single column. **(E)** Volcano plot showed that the differential expression analysis of circRNAs (red, up-regulated; green, down-regulated). **(F)** The distribution of chromosomes of upregulated and downregulated circRNAs, respectively. **(G,H)** The identification of exon, intron and intergenic region of upregulated and downregulated circRNAs. RNA-seq, high-throughput RNA sequencing; WKY, Wistar-Kyoto; SHR spontaneously hypertensive rat; SBP, systolic blood pressure; DBP, diastolic blood pressure; MBP, mean blood pressure; circRNAs, circular RNAs.

transcribed from, which demonstrated that among these DE circRNAs, most up-regulated circRNAs mainly came from chromosomes (chr) 1 (chr1), chr2, chr3, chr4, and chr10, whereas the down-regulated circRNAs came from chr1, chr3, chr5, chr8, and chr10 (**Figure 1F**). Moreover, among these DE circRNAs, abundant RNAs were generated most commonly from exons of protein-coding genes (86.19 and 81.71% from up-regulated and down-regulated circRNAs, respectively) (**Figures 1G,H**).

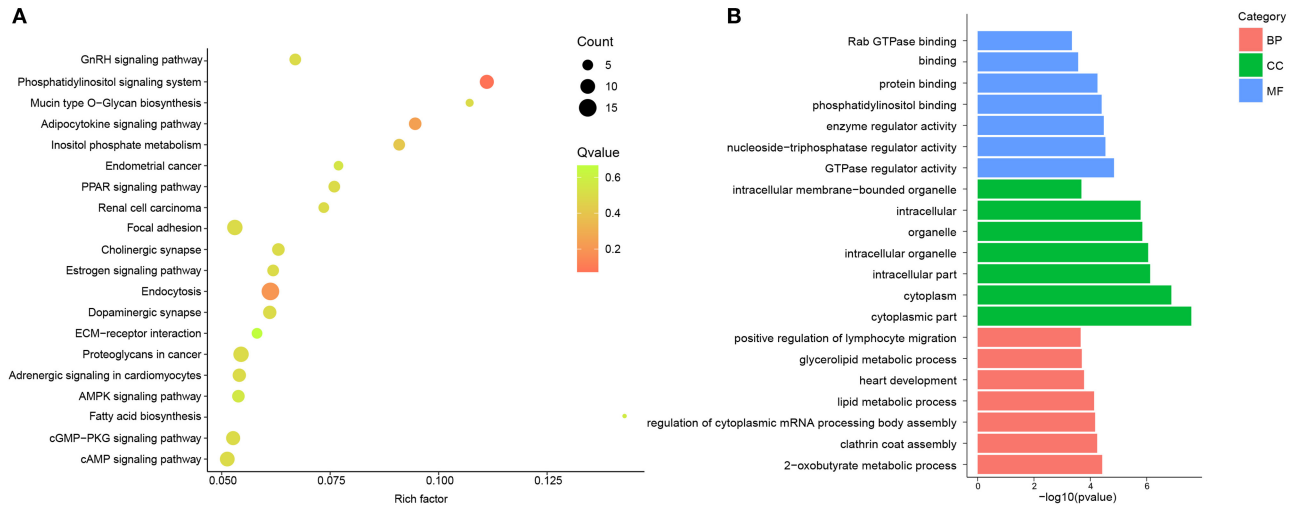

FIGURE 2 | GO and KEGG pathway analysis of DE circRNAs between and SHR and WKY rat aorta. **(A)** Top 20 KEGG pathways for DE circRNAs were identified in SHR and WKY rat aorta. **(B)** Top 7 GO enriched terms were analyzed for biological process (BP), cellular component (CC), and molecular function (MF), respectively. GO, gene ontology; KEGG, Kyoto encyclopedia of genes and genomes; DE, differentially expressed; circRNAs, circular RNAs; WKY, Wistar-Kyoto; SHR spontaneously hypertensive rat.

GO and KEGG Pathway of DE circRNAs in Hypertensive Rat Aorta

To describe and synthesize potential mechanisms of confirmed circRNAs, the GO and KEGG pathways were analyzed in hypertensive rat aorta. The enriched pathways analyzed by KEGG were Endocytosis, Focal adhesion, cyclic adenosine monophosphate (cAMP) signaling pathway, AMP-activated protein kinase (AMPK), phosphatidylinositol (PI) signaling pathway and extracellular matrix (ECM)-receptor interaction (**Figure 2A**; **Supplementary Table 3**). In addition, GO enrichment analysis reflected the top 30 enriched GO term of the DE circRNAs (**Supplementary Table 4**). In the term of MF, the DE circRNAs were mainly enriched in Guanosine-Triphosphate hydrolase (GTPase) regulator activity. In the CC, the main term of GO analysis was cytoplasmic part. Besides, in the term of BP, the central term of was 2-oxobutyrate metabolic process (**Figure 2B**). Thus, the cAMP, AMPK, PI, and GTPase signaling pathways may be partially responsible for circRNAs- mediated vascular pathophysiology and homeostasis of hypertension.

Confirmation of DE circRNAs Candidates by RT-PCR Between SHR and WKY Rats

Subsequently, the top 20 significantly up-regulated and down-regulated circRNAs ($q < 0.05$ and $|\log2(\text{foldchange})| > 4$) were listed in **Table 1**. Of which, seven DE circRNAs were chosen for further confirmation by RT-PCR analysis. The RT-PCR validation demonstrated the similar trends with RNA-seq, suggesting the reliability of our circRNAs expression profiles. Particularly, five significant circRNAs including rno_circRNA_0005818, rno_circRNA_0005304, rno_circRNA_0005506, rno_circRNA_0009301, and rno_circRNA_0009197 were validated by RT-PCR analysis (**Figure 3A**). The results indicated that the expressions of rno_circRNA_0005818, rno_circRNA_0005304, rno_circRNA_0005506, and rno_circ RNA_0009301 were significantly increased in SHR aorta (7.92-fold, $P < 0.001$; 3.42-fold, $P < 0.001$; 5.09-fold, $P < 0.001$; and 7.29-fold, $P < 0.001$, respectively). In addition, rno_circRNA_ 0009197 was significantly decreased in SHR aorta (2.26-fold, $P < 0.001$). More importantly, we found that there were highly similar homologous sequences in rno_circRNA_0009197 and rno_circRNA_0005506 with human circRNA, according to the criterion of evalue and identity by using Basic Local Alignment Search Tool and the circAtlas 2.0 software, respectively. Generally, the higher the similarity between sequences of human and rat circRNAs, the higher the possibility that they are homologous sequences. In addition, when the evalue is close to zero or zero, it is exactly a match sequences of human and rat circRNAs. Notably, rno_circ_0009197 and rno_circ_0005506 were identified highly homologous with hsa_circ_0018685| chr10:73337670-73559386 (identity 0.907; evalue 1.87E-18) and hsa_circ_0112669| chr1:237865277-237921076 (identity0.874; evalue 1.66E-105), respectively. Moreover, EVG staining showed aggravated elastin and collagen fiber of thoracic aorta in SHR compared with the WKY rats, characterized with thickened collagen fibers and augmented ECM deposition (**Figure 3B**), indicating that upregulations of rno_circRNA_0005818, rno_circRNA_0005304, rno_circRNA_0005506, and rno_circ_RNA_0009301 and downregulation of rno_circRNA_0009197 may play potential roles in aortic hypertrophy and remodeling of hypertensive rats.

Prediction of circRNA-miRNA Interactions

The top 3 target miRNAs of confirmed circRNAs were predicted by using the miRanda software. Notably, rno-miR-615, rno-miR-223-3p, and rno-miR-29a-3p

TABLE 1 | Top 20 significantly up-regulated and down-regulated circRNAs in SHR rat (|log2FoldChange| > 4, *Q*-value < 0.05).

CircRNA	*Q*-value	log2FoldChange	Regulation	chrom	strand	CircRNA_type	GeneSymbol
rno_circRNA_0009301	1.51E-17	7.3709	Up	chr20	+	Exonic	–
rno_circRNA_0005304	2.28E-12	6.4932	Up	chr17	+	Intergenic	–
rno_circRNA_0008384	3.59E-09	5.9610	Up	chr1	–	Intergenic	–
rno_circRNA_0001706	8.23E-09	5.7243	Up	chr11	–	Exonic	Adcy5
rno_circRNA_0000407	3.37E-06	5.0298	Up	chr10	–	Exonic	Snx29
rno_circRNA_0010188	3.18E-06	5.0262	Up	chr2	+	Exonic	Frrs1
rno_circRNA_0000489	3.56E-06	5.0107	Up	chr10	+	Exonic	Sap30l
rno_circRNA_0012471	4.90E-06	4.9696	Up	chr4	+	Exonic	RGD1565355
rno_circRNA_0010453	7.82E-12	4.7779	Up	chr2	+	Exonic	Ddah1
rno_circRNA_0012704	7.38E-05	4.5727	Up	chr4	–	Intergenic	–
rno_circRNA_0002616	1.42E-04	4.4966	Up	chr12	–	Exonic	Fry
rno_circRNA_0005818	2.48E-04	4.3747	Up	chr17	–	Exonic	Dnajc1
rno_circRNA_0009971	3.39E-04	4.3142	Up	chr2	+	Exonic	Arnt
rno_circRNA_0018260	4.52E-04	4.2612	Up	chr9	–	Exonic	Smap1
rno_circRNA_0004376	5.72E-04	4.2419	Up	chr15	+	Exonic	Scara5
rno_circRNA_0005506	1.10E-03	4.1191	Up	chr17	–	Exonic	Ryr2
rno_circRNA_0011085	1.09E-03	4.1051	Up	chr3	–	Exonic	Fbn1
rno_circRNA_0011717	1.89E-03	3.9862	Up	chr3	–	Exonic	Golga1
rno_circRNA_0018702	2.53E-03	3.9256	Up	chr9	–	Exonic	Bard1
rno_circRNA_0004164	2.48E-03	3.921	Up	chr15	+	Exonic	Samd4a
rno_circRNA_0018394	1.70E-15	7.0728	Down	chr9	+	Exonic	Bivm
rno_circRNA_0018389	1.91E-10	6.1736	Down	chr9	–	Exonic	Kdelc1
rno_circRNA_0002969	4.17E-08	5.633	Down	chr13	–	Exonic	Cfh
rno_circRNA_0006911	1.80E-07	5.4753	Down	chr19	+	Exonic	Spg7
rno_circRNA_0006284	3.86E-07	5.3752	Down	chr18	+	Exonic	Wdr7
rno_circRNA_0001637	5.32E-07	5.3332	Down	chr11	–	Intronic	Ccdc80
rno_circRNA_0010322	1.05E-06	5.2562	Down	chr2	–	Exonic	Npnt
rno_circRNA_0014612	2.86E-06	5.1309	Down	chr5	+	Exonic	Rgs3
rno_circRNA_0012056	5.79E-10	5.064	Down	chr3	+	Intergenic	–
rno_circRNA_0015320	4.61E-06	5.0522	Down	chr6	–	Exonic	Hadhb
rno_circRNA_0019038	1.02E-18	4.8343	Down	chrX	+	Intergenic	–
rno_circRNA_0001500	5.59E-05	4.7371	Down	chr11	+	Intronic	Ttc3
rno_circRNA_0019050	0.000147	4.5686	Down	chrX	–	Intergenic	–
rno_circRNA_0000840	0.000236	4.481	Down	chr10	–	Exonic	Rph3al
rno_circRNA_0009286	0.000223	4.4693	Down	chr20	–	Exonic	Psmb9
rno_circRNA_0008598	0.000325	4.4257	Down	chr1	–	Exonic	AABR07007032.1
rno_circRNA_0007580	0.000423	4.3558	Down	chr1	+	Exonic	Pde3b
rno_circRNA_0009197	4.79E-08	4.1701	Down	chr20	–	Exonic	Cdh23
rno_circRNA_0011093	0.001512	4.1075	Down	chr3	+	Exonic	Slc27a2
rno_circRNA_0017128	0.001937	4.0647	Down	chr8	+	Exonic	Snrk

circRNAs, circular RNAs; SHR, spontaneously hypertensive rats; Chrom, chromosome; Adcy5, adenylate cyclase 5; Fbn1, fibrillin-1; Cfh, complement factor H.

were predicted to construct ceRNA relationships with rno_circRNA_0005818 (**Figure 4A**). Rno-miR-194-5p, rno-miR-93-3p, and rno-miR-320-5p were predicted to construct ceRNA relationships with rno_circRNA_0005304 (**Figure 4B**). Moreover, rno-miR-628, rno-miR-676, and rno-miR-873-5p were predicted to construct ceRNA relationships with rno_circRNA_0009301 (**Figure 4C**). Rno-miR-122-3p, rno-miR-298-5p, and rno-miR-509-3p were predicted to build ceRNA relationships with rno_circRNA_0005506 (**Figure 4D**). Additionally, rno-miR-383-3p, rno-miR-34a-3p, and rno-miR-509-5p were predicted to construct ceRNA relationships with rno_circRNA_0009197 (**Figure 4E**). Collectively, circRNAs serve as a miRNA sponge associating with relevant miRNAs, which may further construct the circRNA-miRNA axis participating in pathogenesis of hypertension.

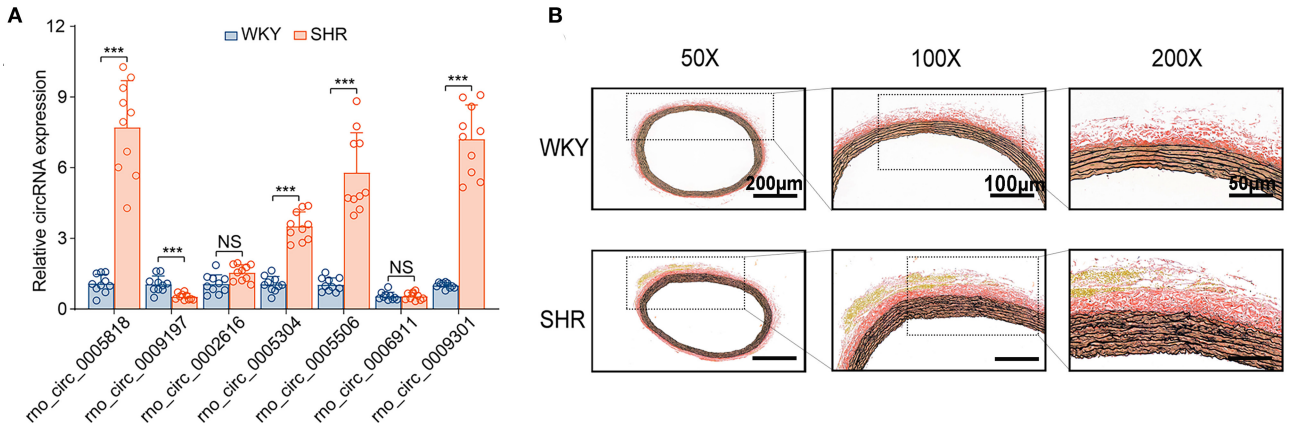

FIGURE 3 | DE circRNAs candidates were validated by RT-PCR between SHR and WKY rat aorta. **(A)** The seven DE circRNAs were detected by the RT-PCR between SHR and WKY rat aorta. Five significant aortic circRNAs were confirmed in hypertensive rats, including rno_circRNA_0005818, rno_circRNA_0005304, rno_circRNA_0005506, rno_circRNA_0009301, and rno_circRNA_0009197. **(B)** The EVG staining illustrated that the regulation of circRNAs were associated with thin elastic fiber and thick collagen fiber. Black color represents elastic fiber, red color represents collagen fiber. $n = 10$ for each group, $^{***}P < 0.001$. DE, differentially expressed; circRNAs, circular RNAs; RT-PCR, real-time polymerase chain reaction; WKY, Wistar-Kyoto; SHR spontaneously hypertensive rat.

Establishment of Validated circRNA-Related ceRNA Network in Aortic Vascular Tissues of Hypertensive Rats

To further explore the underlying mechanisms, the five validated circRNAs with related miRNAs as well as the downstream mRNAs were used to construct circRNA-miRNA-mRNA network using Cytoscape 3.8.2 software. The network was established with 31 predicted miRNAs and 266 mRNAs, which suggesting that circRNAs could modulate target miRNA indirectly by competing for miRNA-binding through common miRNA binding sites. Moreover, NOTCH1, a target of miR-615, was predicted to possess a ceRNA network with rno_circRNA_0005818. Forkhead box class O3 (FOXO3), a target of miR-509-5p, was predicted to possess a ceRNA network with rno_circRNA_0009197. Additionally, STAT3, a target of miR-10b-5p, was predicted to possess a ceRNA relationship with rno_circRNA_0005818 (**Figure 5**).

Construction of PPI Network and Identification of Hub Genes in Rat Aorta

The hub genes were selected by the cytoHubba app in Cytoscape 3.8.2 software. Top 30 hub genes were identified in rat aorta, including signal transducer and activator of transcription 3 (STAT3), NOTCH1, FOXO3 (**Figure 6A**). Then, according to the STRING database, a PPI network (involving 30 nodes and 344 edges) was constructed (**Figure 6B**). The enriched GO terms of top 30 hub genes were conducted. Moreover, the top enriched GO-BP terms, included regulation of cell population proliferation and cell differentiation. There were several enriched terms related to GO-MF, such as protein binding, signaling receptor binding, molecular function regulator. In addition, GO-CC terms included cytoplasm, membrane and nucleus (**Figure 7A**). Furthermore, the top 20 GO and KEGG pathway of 30 hub genes were estimated by Metascape (**Figure 7B**), including epidermal growth factor receptor tyrosine kinase inhibitor resistance, vasculature development, regulation of cell migration and positive regulation of mitogen-activated protein kinases cascade.

DISCUSSION

CircRNAs form covalently closed continuous loops with high tissue specific expression, which are critical contributors to vascular pathophysiology and homeostasis (8, 9). CircRNAs are highly abundant in cardiovascular tissues, the regulation of circRNAs could mediate importantly physiological and pathological processes in the development of hypertension and related vascular diseases (9). In the present study, 485 DE circRNAs were found in aortic vascular tissues of hypertensive rats with 279 up-regulated circRNAs and 206 down-regulated circRNAs. Moreover, among these DE circRNAs, abundant RNAs were generated most commonly from exons of protein-coding genes (86.19 and 81.71% from up-regulated circRNAs and down-regulated circRNAs, respectively). Up till now, the understanding of circRNAs predicted functions in hypertensive rats remains largely unknown. To fully understand the functions of the confirmed circRNAs, clustering of GO terms performed that these circRNAs were enriched in the cytoplasmic part and GTPase regulator activity in molecular function. Besides, these circRNAs involved in the process of Endocytosis, Focal adhesion, cAMP signaling pathway, AMPK signaling pathway and ECM-receptor interaction by KEGG analysis. Therefore, based on bioinformatic analysis, we deduced that the significant confirmed circRNAs could link with hypertension and hypertensive vascular injury by modulating these signaling pathways.

Intriguingly, we further verified that downregulation of rno_circRNA_0009197, and upregulation of rno_circRNA_0005818, rno_circRNA_0005304,

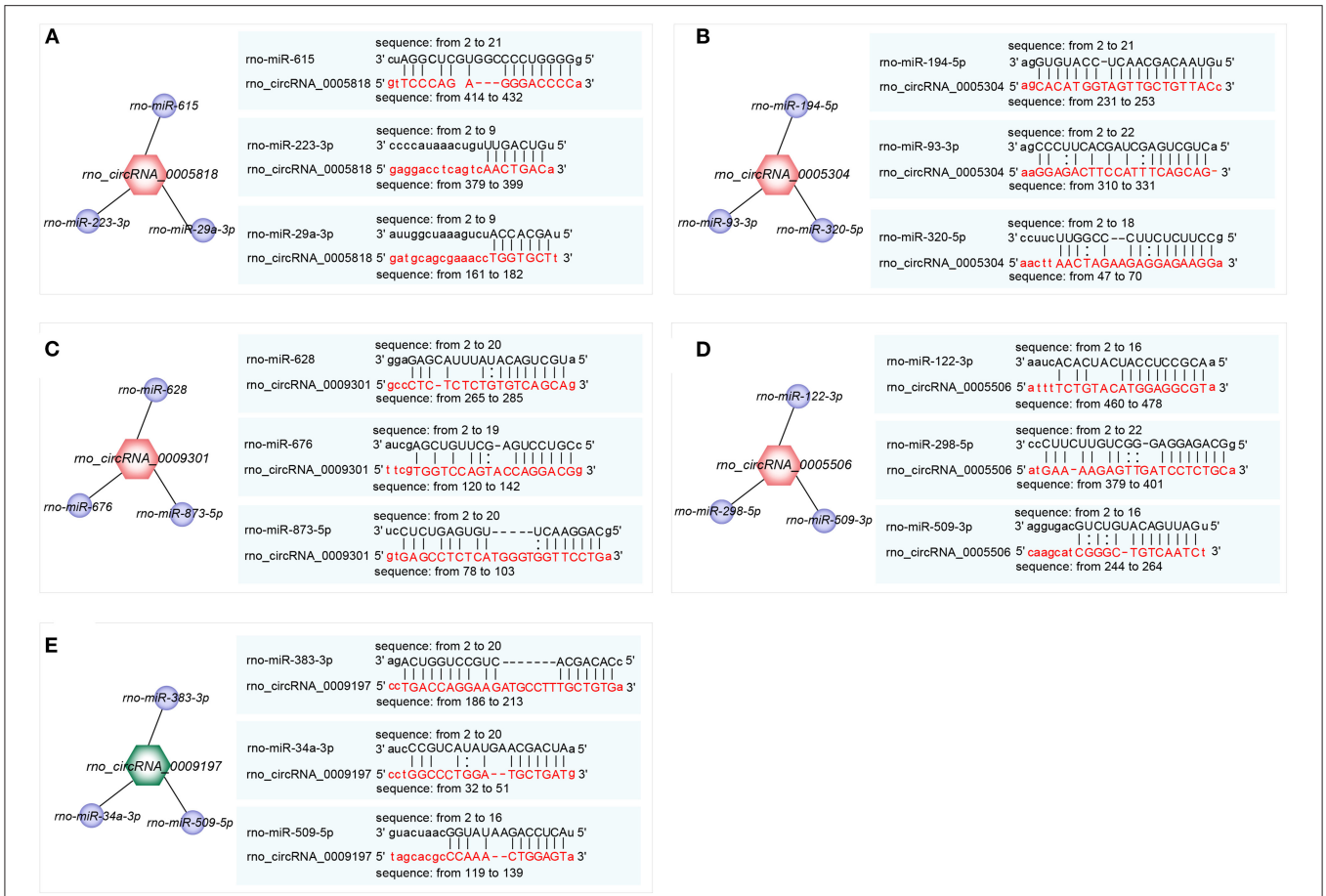

FIGURE 4 | Prediction of the binding sites of circRNA-miRNA. **(A–E)** The top 3 miRNAs associated with each selected circRNA and the predicted binding sites. **(A)** rno_ circRNA_0005818 target pairs: rno_circRNA_0005818→ rno-miR-615; rno_circRNA_0005818→ rno-miR-223-3p; rno_circRNA_0005818→ rno-miR-29a-3p; **(B)** rno_circRNA_0005304 target pairs: rno_circRNA_0005304→ rno-miR-194-5p; rno_circRNA_0005304→ rno-miR-93-3p; rno_circRNA_0005304→ rno-miR-320-5p; **(C)** rno_circRNA_0009301 target pairs: rno_circRNA_0009301→ rno-miR-628; rno_circRNA_0009301→ rno-miR-676; rno_circRNA_0009301→ rno-miR-873-5p; **(D)** rno_circRNA_0005506 target pairs: rno_circRNA_0005506→ rno-miR-122-3p; rno_circRNA_0005506→ rno-miR-298-5p; rno_circRNA_0005506→ rno-miR-509-3p; **(E)** rno_circRNA_0009197 target pairs: rno_circRNA_0009197→ rno-miR-383-3p; rno_circRNA_0009197→ rno-miR-34a-3p; rno_circRNA_0009197→ rno-miR-509-5p. Target miRNAs of confirmed circRNAs were predicted using the miRanda software (http://www.miranda.org). circRNA, circular RNA; miRNA, microRNA.

rno_circRNA_0005506, and rno_circRNA_0009301 were shown in aorta of SHR when compared with that of WKY rats by real-time RT-PCR analysis. These changes were associated with aggravated elastin and collagen fiber of thoracic aorta of hypertensive rats, implying that abnormal expression of aortic circRNAs may play potential roles in hypertensive vascular remodeling and dysfunction.

According to the circRNA-miRNA interactions, the circRNAs had been proven to combine with miRNAs binding sites and modulate the expression of mRNA through integrating with miRNA binding (9, 12). In the light of miRNA-mRNA interactions, a growing body of evidence indicated that the effects of miRNA were exerted by the target mRNAs (12, 13). In this work, circRNA-target miRNAs and the target mRNAs of miRNAs were predicted by the miRanda and Targetscan softwares, respectively. Then, the circRNA-miRNA-mRNA network was constructed, which provided a novel insight into the potential regulatory actions in the hypertension and hypertensive vascular injury. In accordance with previous reports, multiple miRNAs had been showed to modulate major genes participated in the development of hypertensive vascular injury. Subsequently, bioinformatics databases were used to predict the miRNAs that contained concrete and highly conserved binding sites of these significant confirmed circRNAs. We next to investigate the potential mainly regulator of miRNAs in vascular damage. To the best of our knowledge, fibrosis, oxidative stress, and ischemia have a close association with hypertension and ischemic heart diseases, which are the major pathways to cardiovascular remodeling (14). In response to the downstream miRNAs of the confirmed circRNAs, we revealed that miR-509-5p may be a promising target by inhibiting proliferation, migration and apoptosis in vasculature (15, 16). Vascular dysfunction is

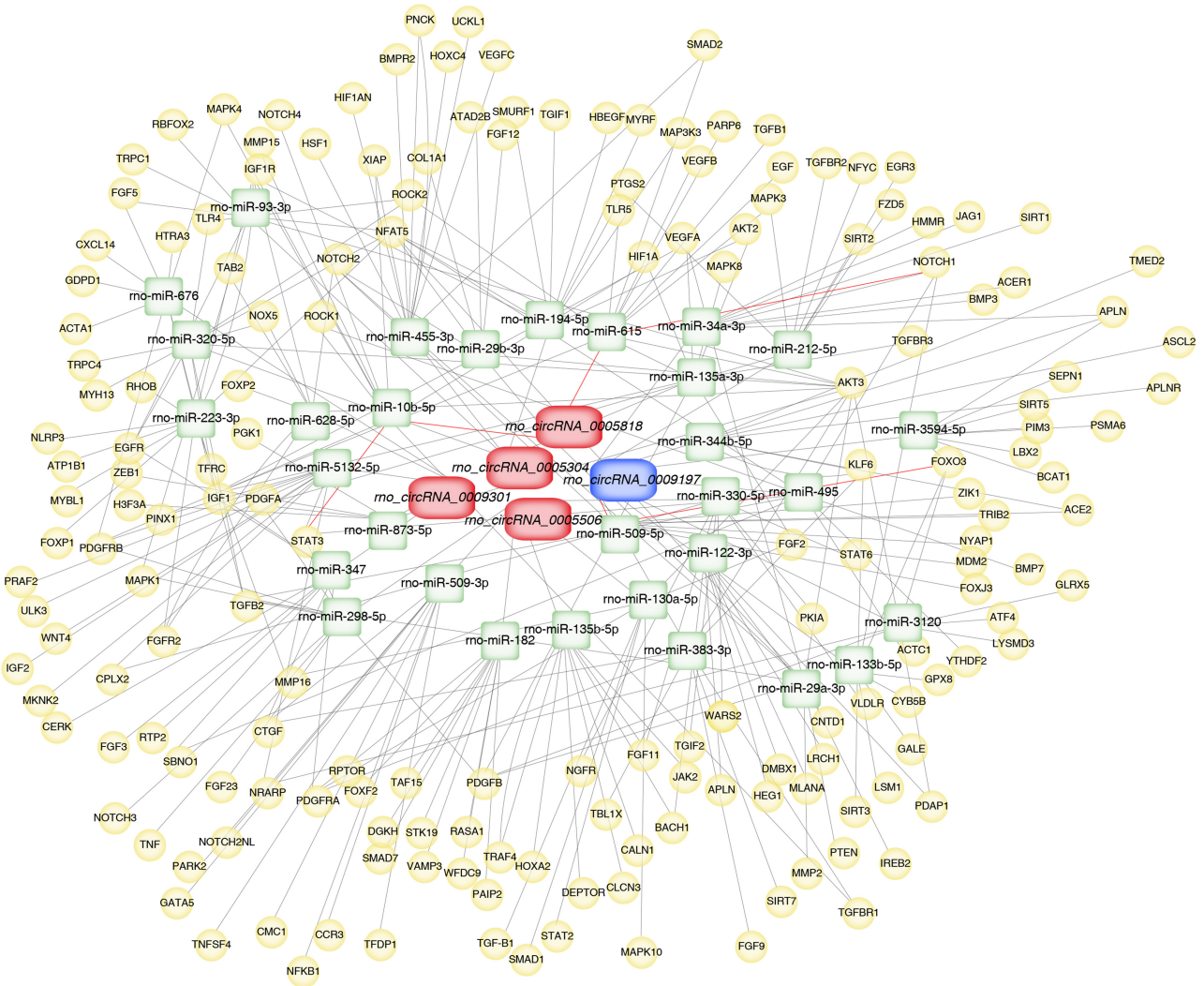

FIGURE 5 | Construction of circRNA-miRNA-mRNA network in aortic vascular tissues of rats. The red color and blue color represent upregulated and downregulated significant DE circRNAs, respectively. Green color represents miRNAs, yellow color represents mRNAs. Red bold lines represent three promising circRNA-miRNA-mRNA regulatory axes were selected in hypertensive rat aorta, including rno_circRNA_0005818/miR-615/NOTCH1, rno_circRNA_0009197/miR-509-5p/FOXO3 and rno_circRNA_0005818/miR-10b-5p/STAT3, respectively. circRNAs, circular RNAs; miRNA, microRNA; mRNA, messenger RNAs; DE, differentially expressed.

closely linked with endothelial cell (EC) dysfunction through abnormal gene modulation. The recent studies suggest that abnormal expression of miR-615 significantly repressed EC proliferation, migration, network tube formation in matrigel, the release of nitric oxide (17). Overexpression of miR-615 could reduce oxidative stress, apoptosis and ischemia involving in regulation of EC dysfunction and endothelial nitric oxide synthase (17, 18). Further, miR-10b-5p has vital actions on vascular remodeling (19), and has markedly less microscopic and macroscopic calcification nodules (20). At the same time, miR-10b-5p represses the myocardial fibrosis and ameliorated cardiomyocyte apoptosis and cardiac function after ischemia (21). However, different target genes of miRNAs have important biological functions in regulating target genes. Therefore, it is central to pay close attention on the underlying mechanisms of mRNAs in vascular pathophysiology in hypertension.

Combined with the PPI network, we found that three key hub genes played important roles in the PPI network. The three hub genes, STAT3, NOTCH1, and FOXO3, which are crucial essential factors to regulate the vascular diseases, and closely associated with modulation of proliferation, migration, differentiation and ischemia in a wide range of vascular diseases (22–24). STAT3, as a critical inducer and proangiogenic key regulator, is involved in EC proliferation, migration, and degradation of the ECM (25). STAT3 has been demonstrated to influence the expression of angiogenic and angiostatic mediators, such as basic fibroblast growth factor, vascular endothelial growth factor (VEGF) (26, 27). Additionally, STAT3

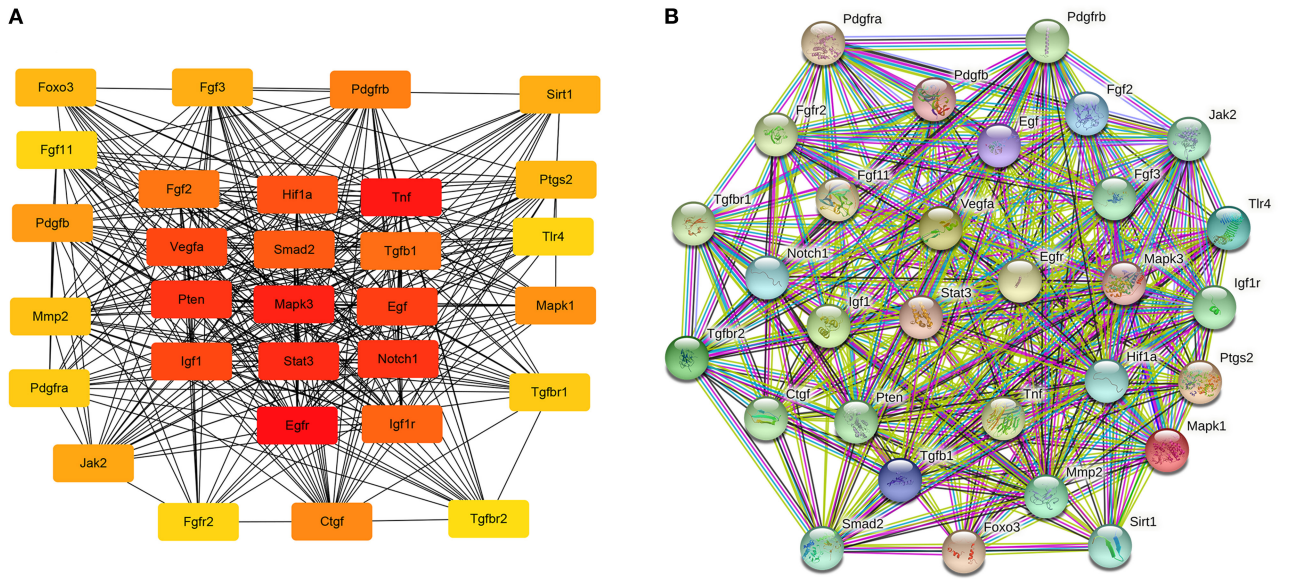

FIGURE 6 | The potential interactions of hub genes in the PPI network in aortic vascular tissues of rats. **(A)** The top 30 hub genes were selected by the cytoHubba app in Cytoscape 3.8.2 software; The node color changes gradually from yellow to red in ascending order according to the score of hub genes. **(B)** The protein and protein interaction of top 30 hub genes by the online database STRING (involving 30 nodes and 344 edges). PPI, protein and protein interaction.

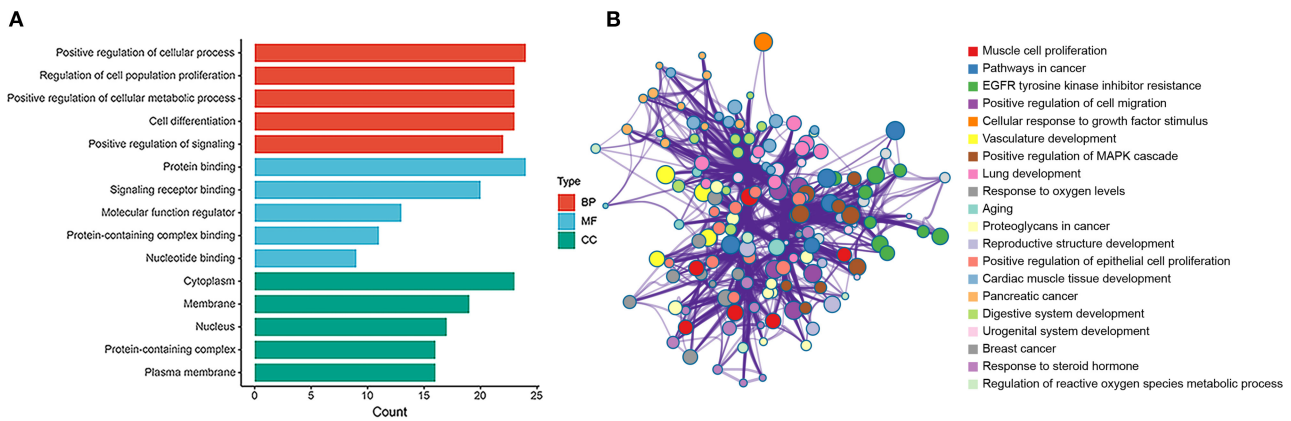

FIGURE 7 | GO and enrichment network of top 30 hub genes between SHR and WKY rat aorta. **(A)** Top 5 GO enriched terms were analyzed in rat aorta for biological process (BP), cellular component (CC), and molecular function (MF), respectively. **(B)** The enrichment network of top 30 hub genes was identified in rat aorta. Nodes represent functions enriched for an annotated ontology term and node size indicates the number of genes that fall into that term. GO, gene ontology; WKY, Wistar-Kyoto; SHR spontaneously hypertensive rat; EGFR, epidermal growth factor receptor; MAPK, mitogen-activated protein kinase.

signaling might activate as a promising approach to inhibit the progression of vascular narrowing (28). The alternative splice variant of VEGF (VEGFxxxb) $VEGF_{165}b$, modulates endothelial VEGF receptor 1-STAT3 signaling pathway in ischemia and peripheral arterial disease (29). NOTCH activation is a major pathogenic mechanism participated in the progression of pulmonary vascular remodeling (30). Repression of NOTCH1 could alleviate vascular lesion, including endothelial function-related factors, oxidative stress-related factors, and reduce apoptosis of aortic EC of hypertensive rats (31, 32). Interesting, NOTCH1 is necessary for VEGF-induced migration, proliferation and survival of EC (33). Activated Notch signaling and inhibited TGF-β1/Smad3 signaling could repress myocardial fibrosis after myocardial infarction (MI) (29). FOXO3, as a transcriptional factor and important mediator, has been shown to contribute to the protective effects of cardiovascular fibrosis and ischemia-reperfusion (I/R) injury (34). miR-629 promoted cell proliferation, migration and apoptosis by targeting FOXO3 in vascular remodeling (35). The functions of miR-124 on hypertensive pulmonary fibroblast proliferation were mediated through FOXO3/cdk inhibitor cdkn1a signaling (36). These results indicate that hub-genes

play critical roles in proliferation,cell differentiation, ischemia, and cardiovascular fibrosis. In the present work, we selected three promising circRNA-miRNA-mRNA regulatory axes in hypertensive rat aorta, including rno_circRNA_0005818/miR-615/NOTCH1, rno_circRNA_0009197/miR-509-5p/FOXO3, rno_circRNA_0005818/miR-10b-5p/STAT3, which may have further exploration for the pathological process of hypertensive vascular injury and dysfunction.

In summary, we demonstrated, for the first time, new insight into the 485 DE circRNAs in SHR aorta compared with WKY rat aorta through RNA-seq array and real-time RT-PCR validation. Of these, 5 DE circRNAs were verified in hypertensive rat aorta. Particularly, rno_circRNA_0009197 was down-regulated in aortic vascular tissues of hypertensive rats with up-regulated levels of rno_circRNA_0005818, rno_circRNA_0005304, rno_circRNA_ 0005506, and rno_circRNA_0009301. More importantly, we found that there were highly similar homologous sequences in rno_circRNA_0009197 and rno_circRNA_0005506 with hsa_circ_0018685|chr10:73337670-73559386 and hsa_circ_0112669|chr1: 237865277-237921076, respectively. Moreover, three hub genes (NOTCH1, FOXO3, and STAT3) according to PPI network were found. Furthermore, based on the ceRNA regulatory mechanism, the circRNA-miRNA-mRNA network was constructed for three promising circRNA-miRNA-mRNA regulatory axes, including rno_circRNA_0005818/miR-615/NOTCH1, rno_circRNA_0009197/miR-509-5p/FOXO3, and rno_circRNA_0005818/miR-10b-5p/STAT3, respectively. Therefore, our findings exhibited that aortic circRNAs play potential roles in regulating hypertensive vascular remodeling and dysfunction and aortic circRNAs are the vital therapeutic targets for hypertension-related vascular diseases.

DATA AVAILABILITY STATEMENT

The datasets presented in this study can be found in online repositories. The names of the repository/repositories and accession number(s) can be found at: NCBI SRA; PRJNA785011.

ETHICS STATEMENT

The animal study was reviewed and approved by National Institutes of Health guide for the care and use of Laboratory animals (NIH Publications No. 8023). Animal Research Ethics Committee of Beijing Chaoyang Hospital affiliated to Capital Medical University.

AUTHOR CONTRIBUTIONS

YL, YD, and ZD: writing-original draft, methodology, supervision, writing-review and editing, read, and approved the final manuscript. JS, ZZ, LL, and XL: collected and recorded the samples, read, and approved the final manuscript. LS, XL, MZ, and YC: formal analysis, read, and approved the final manuscript. JZ and RM: methodology, supervision, writing—review and editing, read, and approved the final manuscript. All authors contributed to the article and approved the submitted version.

FUNDING

This study was supported by the General Program and the National Major Research Plan Training Program of the National Natural Science Foundation of China (Nos. 81770253, 91849111, 81370362, 82170302, and 81300044), Shanghai Sailing Program (20YF1444100), Beijing Natural Science Foundation (7162069), Beijing Hospitals Authority Youth Programme (QML20200305), Open Foundation from Beijing Key Laboratory of Hypertension Research (2019GXY-KFKT-02), Talent Project of Beijing Chaoyang Hospital Affiliated to Capital Medical University.

SUPPLEMENTARY MATERIAL

The Supplementary Material for this article can be found online at: https://www.frontiersin.org/articles/10.3389/fcvm.2021.814402/full#supplementary-material

REFERENCES

1. Navaneethabalakrishnan S, Goodlett BL, Lopez AH, Rutkowski JM, Mitchell BM. Hypertension and reproductive dysfunction: a possible role of inflammation and inflammation-associated lymphangiogenesis in gonads. *Clin Sci.* (2020) 134:3237–57. doi: 10.1042/CS20201023
2. Stanton T, Dunn FG. Hypertension, left ventricular hypertrophy, and myocardial ischemia. *Med Clin North Am.* (2017) 101:29–41. doi: 10.1016/j.mcna.2016.08.003
3. Xu J, White AJ, Niehoff NM, O'Brien KM, Sandler DP. Airborne metals exposure and risk of hypertension in the Sister Study. *Environ Res.* (2020) 191:110144. doi: 10.1016/j.envres.2020.110144
4. Zhang CJ, Shi YN, Liao DF, Du K, Qin L. Molecular mechanism of vascular remodeling in hypertension and Chinese medicine intervention. *Sheng Li Xue Bao.* (2019) 71:235–47. doi: 10.13294/j.aps.2019.0014
5. Kumrah R, Vignesh P, Rawat A, Singh S. Immunogenetics of Kawasaki disease. *Clin Rev Allergy Immunol.* (2020) 59:122–39. doi: 10.1007/s12016-020-08783-9
6. Siasos G, Sara JD, Zaromytidou M, Park KH, Coskun AU, Lerman LO, et al. Local low shear stress and endothelial dysfunction in patients with nonobstructive coronary atherosclerosis. *J Am Coll Cardiol.* (2018) 71:2092–102. doi: 10.1016/j.jacc.2018.02.073
7. Kumar S, Gonzalez EA, Rameshwar P, Etchegaray JP. Non-coding RNAs as mediators of epigenetic changes in malignancies. *Cancers.* (2020) 12:1–32. doi: 10.3390/cancers12123657
8. Saaoud F, Drummer IVC, Shao Y, Sun Y, Lu Y, Xu K, et al. Circular RNAs are a novel type of non-coding RNAs in ROS regulation, cardiovascular metabolic inflammations and cancers. *Pharmacol Ther.* (2021) 220:107715. doi: 10.1016/j.pharmthera.2020.107715
9. Zhang J, Li Y, Qi J, Yu X, Ren H, Zhao X, et al. Circ-calm4 Serves as an miR-337-3p sponge to regulate Myo10 (Myosin 10) and promote pulmonary artery smooth muscle proliferation. *Hypertension.* (2020) 75:668–79. doi: 10.1161/HYPERTENSIONAHA.119.13715
10. Wen G, Zhou T, Gu W. The potential of using blood circular RNA as liquid biopsy biomarker for human diseases. *Protein Cell.* (2020) 12:1–36. doi: 10.1007/s13238-020-00799-3

11. Langmead B, Salzberg SL. Fast gapped-read alignment with Bowtie 2. *Nat Methods*. (2012) 9:357–9. doi: 10.1038/nmeth.1923
12. Cheng X, Zhang L, Zhang K, Zhang G, Hu Y, Sun X, et al. Circular RNA VMA21 protects against intervertebral disc degeneration through targeting miR-200c and X linked inhibitor-of-apoptosis protein. *Ann Rheum Dis*. (2018) 77:770–9. doi: 10.1136/annrheumdis-2017-212056
13. Zhao Y, Xu L, Wang X, Niu S, Chen H, Li C. A novel prognostic mRNA/miRNA signature for esophageal cancer and its immune landscape in cancer progression. *Mol Oncol*. (2021) 15:1088–109. doi: 10.1002/1878-0261.12902
14. Shenasa M, Shenasa H. Hypertension, left ventricular hypertrophy, and sudden cardiac death. *Int J Cardiol*. (2017) 237:60–3. doi: 10.1016/j.ijcard.2017.03.002
15. Li X, Li Y, Wan L, Chen R, Chen F. miR-509-5p inhibits cellular proliferation and migration via targeting MDM2 in pancreatic cancer cells. *Onco Targets Ther*. (2017) 10:4455–64. doi: 10.2147/OTT.S130378
16. Sun J, Niu L, Gao S, Yi X, Chen J. miR-509-5p downregulation is associated with male infertility and acts as a suppressor in testicular germ cell tumor cells through targeting MDM2. *Onco Targets Ther*. (2019) 12:10515–22. doi: 10.2147/OTT.S215998
17. Icli B, Wu W, Ozdemir D, Li H, Cheng HS, Haemmig S, et al. MicroRNA-615-5p regulates angiogenesis and tissue repair by targeting AKT/eNOS (protein kinase B/endothelial nitric oxide synthase) signaling in endothelial cells. *Arterioscler Thromb Vasc Biol*. (2019) 39:1458–74. doi: 10.1161/ATVBAHA.119.312726
18. Liu C, Yao MD, Li CP, Shan K, Yang H, Wang JJ, et al. Silencing of circular RNA-ZNF609 ameliorates vascular endothelial dysfunction. *Theranostics*. (2017) 7:2863–77. doi: 10.7150/thno.19353
19. Henn D, Abu-Halima M, Wermke D, Falkner F, Thomas B, Köpple C, et al. MicroRNA-regulated pathways of flow-stimulated angiogenesis and vascular remodeling *in vivo*. *J Transl Med*. (2019) 17:22. doi: 10.1186/s12967-019-1767-9
20. Chao CT, Yeh HY, Tsai YT, Chiang CK, Chen HW. A combined microRNA and target protein-based panel for predicting the probability and severity of uraemic vascular calcification: a translational study. *Cardiovasc Res*. (2021) 117:1958–73. doi: 10.1093/cvr/cvaa255
21. Wu L, Chen Y, Chen Y, Yang W, Han Y, Lu L, et al. Effect of HIF-1α/miR-10b-5p/PTEN on hypoxia-induced cardiomyocyte apoptosis. *J Am Heart Assoc*. (2019) 8:e011948. doi: 10.1161/JAHA.119.011948
22. Li X, Zou F, Lu Y, Fan X, Wu Y, Feng X, et al. Notch1 contributes to TNF-α-induced proliferation and migration of airway smooth muscle cells through regulation of the Hes1/PTEN axis. *Int Immunopharmacol*. (2020) 88:106911. doi: 10.1016/j.intimp.2020.106911
23. Yan P, Li Q, Wang L, Lu P, Suzuki K, Liu Z, et al. FOXO3-Engineered human ESC-derived vascular cells promote vascular protection and regeneration. *Cell Stem Cell*. (2019) 24:447–61.e8. doi: 10.1016/j.stem.2018.12.002
24. Pitulescu ME, Schmidt I, Giaimo BD, Antoine T, Berkenfeld F, Ferrante F, et al. Dll4 and Notch signalling couples sprouting angiogenesis and artery formation. *Nat Cell Biol*. (2017) 19:915–27. doi: 10.1038/ncb3555
25. Loperena R, Van Beusecum JP, Itani HA, Engel N, Laroumanie F, Xiao L, et al. Hypertension and increased endothelial mechanical stretch promote monocyte differentiation and activation: roles of STAT3, interleukin 6 and hydrogen peroxide. *Cardiovasc Res*. (2018) 114:1547–63. doi: 10.1093/cvr/cvy112
26. Li H, Zhang HM, Fan LJ, Li HH, Peng ZT, Li JP, et al. STAT3/miR-15a-5p/CX3CL1 loop regulates proliferation and migration of vascular endothelial cells in atherosclerosis. *Int J Med Sci*. (2021) 18:964–74. doi: 10.7150/ijms.49460
27. Ouyang S, Li Y, Wu X, Wang Y, Liu F, Zhang J, et al. GPR4 signaling is essential for the promotion of acid-mediated angiogenic capacity of endothelial progenitor cells by activating STAT3/VEGFA pathway in patients with coronary artery disease. *Stem Cell Res Ther*. (2021) 12:149. doi: 10.1186/s13287-021-02221-z
28. Wu QY, Cheng Z, Zhou YZ, Zhao Y, Li JM, Zhou XM, et al. A novel STAT3 inhibitor attenuates angiotensin II-induced abdominal aortic aneurysm progression in mice through modulating vascular inflammation and autophagy. *Cell Death Dis*. (2020) 11:131. doi: 10.1038/s41419-020-2326-2
29. Ganta VC, Choi M, Kutateladze A, Annex BH. VEGF165b modulates endothelial VEGFR1-STAT3 signaling pathway and angiogenesis in human and experimental peripheral arterial disease. *Circ Res*. (2017) 120:282–95. doi: 10.1161/CIRCRESAHA.116.309516
30. Babicheva A, Yuan JX. Endothelial Notch1 in pulmonary hypertension. *Circ Res*. (2019) 124:176–9. doi: 10.1161/CIRCRESAHA.118.314496
31. Xue YZ, Li ZJ, Liu WT, Shan JJ, Wang L, Su Q. Down-regulation of lncRNA MALAT1 alleviates vascular lesion and vascular remodeling of rats with hypertension. *Aging*. (2019) 11:5192–205. doi: 10.18632/aging.102113
32. Sahoo S, Li Y, de Jesus D, Sembrat J, Rojas MM, Goncharova E, et al. Notch2 suppression mimicking changes in human pulmonary hypertension modulates Notch1 and promotes endothelial cell proliferation. *Am J Physiol Heart Circ Physiol*. (2021) 321:H542–57. doi: 10.1152/ajpheart.00125.2021
33. Hernandez-Gonzalez I, Tenorio-Castano J, Ochoa-Parra N, Gallego N, Pérez-Olivares C, Lago-Docampo M, et al. Novel genetic and molecular pathways in pulmonary arterial hypertension associated with connective tissue disease. *Cells*. (2021) 10:1–10. doi: 10.3390/cells10061488
34. Su Y, Zhu C, Wang B, Zheng H, McAlister V, Lacefield JC, et al. Circular RNA Foxo3 in cardiac ischemia-reperfusion injury in heart transplantation: a new regulator and target. *Am J Transplant*. (2021) 21:2992–3004. doi: 10.1111/ajt.16475
35. Zhao M, Chen N, Li X, Lin L. MiR-629 regulates hypoxic pulmonary vascular remodelling by targeting FOXO3 PERP. *J Cell Mol Med*. (2019) 23:5165–75. doi: 10.1111/jcmm.14385
36. Wang D, Zhang H, Li M, Frid MG, Flockton AR, McKeon BA, et al. MicroRNA-124 controls the proliferative, migratory, and inflammatory phenotype of pulmonary vascular fibroblasts. *Circ Res*. (2014) 114:67–78. doi: 10.1161/CIRCRESAHA.114.301633

Conflict of Interest: The authors declare that the research was conducted in the absence of any commercial or financial relationships that could be construed as a potential conflict of interest.

Publisher's Note: All claims expressed in this article are solely those of the authors and do not necessarily represent those of their affiliated organizations, or those of the publisher, the editors and the reviewers. Any product that may be evaluated in this article, or claim that may be made by its manufacturer, is not guaranteed or endorsed by the publisher.

Copyright © 2021 Liu, Dong, Dong, Song, Zhang, Liang, Liu, Sun, Li, Zhang, Chen, Miao and Zhong. This is an open-access article distributed under the terms of the Creative Commons Attribution License (CC BY). The use, distribution or reproduction in other forums is permitted, provided the original author(s) and the copyright owner(s) are credited and that the original publication in this journal is cited, in accordance with accepted academic practice. No use, distribution or reproduction is permitted which does not comply with these terms.

frontiers in Cardiovascular Medicine

ORIGINAL RESEARCH
published: 22 December 2021
doi: 10.3389/fcvm.2021.761537

Serum Free Fatty Acids Independently Predict Adverse Outcomes in Acute Heart Failure Patients

Yi Yu, Chunna Jin, Chengchen Zhao, Shiyu Zhu, Simin Meng, Hong Ma, Jian'an Wang and Meixiang Xiang**

Department of Cardiology, The Second Affiliated Hospital, Zhejiang University School of Medicine, Hangzhou, China

Background: Perturbation of energy metabolism exacerbates cardiac dysfunction, serving as a potential therapeutic target in congestive heart failure. Although circulating free fatty acids (FFAs) are linked to insulin resistance and risk of coronary heart disease, it still remains unclear whether circulating FFAs are associated with the prognosis of patients with acute heart failure (AHF).

Methods: This single-center, observational cohort study enrolled 183 AHF patients (*de novo* heart failure or decompensated chronic heart failure) in the Second Affiliated Hospital, Zhejiang University School of Medicine. All-cause mortality and heart failure (HF) rehospitalization within 1 year after discharge were investigated. Serum FFAs were modeled as quartiles as well as a continuous variable (per SD of FFAs). The restricted cubic splines and cox proportional hazards models were applied to evaluate the association between the serum FFAs level and all-cause mortality or HF rehospitalization.

Results: During a 1-year follow-up, a total of 71 (38.8%) patients had all-cause mortality or HF rehospitalization. The levels of serum FFAs positively contributed to the risk of death or HF rehospitalization, which was not associated with the status of insulin resistance. When modeled with restricted cubic splines, the serum FFAs increased linearly for the incidence of death or HF rehospitalization. In a multivariable analysis adjusting for sex, age, body-mass index, coronary artery disease, diabetes mellitus, hypertension, left ventricular ejection fraction and N-terminal pro-brain natriuretic peptid, each SD (303.07 μmol/L) higher FFAs were associated with 26% higher risk of death or HF rehospitalization (95% confidence interval, 2–55%). Each increasing quartile of FFAs was associated with differentially elevated hazard ratios for death or HF rehospitalization of 1 (reference), 1.71 (95% confidence interval, [0.81, 3.62]), 1.41 (95% confidence interval, [0.64, 3.09]), and 3.18 (95% confidence interval, [1.53, 6.63]), respectively.

Conclusion: Serum FFA levels at admission among patients with AHF were associated with an increased risk of adverse outcomes. Additional studies are needed to determine the causal-effect relationship between FFAs and acute cardiac dysfunction and whether FFAs could be a potential target for AHF management.

Keywords: acute heart failure, free fatty acids, Lipolysis, Mortality, rehospitalization

OPEN ACCESS

Edited by:
Hongmei Tan,
Sun Yat-sen University, China

Reviewed by:
Xiaodong Zhuang,
The First Affiliated Hospital of Sun Yat-sen University, China
Aijuan Qu,
Capital Medical University, China

****Correspondence:***
Meixiang Xiang
xiangmx@zju.edu.cn
Jian'an Wang
wangjianan111@zju.edu.cn

Specialty section:
This article was submitted to General Cardiovascular Medicine, a section of the journal Frontiers in Cardiovascular Medicine

Received: *20 August 2021*
Accepted: *15 November 2021*
Published: *22 December 2021*

Citation:
Yu Y, Jin C, Zhao C, Zhu S, Meng S, Ma H, Wang J and Xiang M (2021) Serum Free Fatty Acids Independently Predict Adverse Outcomes in Acute Heart Failure Patients. Front. Cardiovasc. Med. 8:761537. doi: 10.3389/fcvm.2021.761537

INTRODUCTION

Heart failure (HF) has become a major and growing public health challenge with a worldwide prevalence of 64.3 million cases (1). Over the last 30 years, despite tremendous advances in the management of chronic HF, the central treatment of AHF remains symptomatic but less satisfactory due to the high heterogeneity of underlying etiology, resulting in a remarkably high risk of mortality and rehospitalization (2, 3).

The normal heart function predominantly relies on fatty acid (FA) oxidation, responsible for 60–90% of ATP production (4). Since the *de novo* synthesis of FAs is inactive in the heart, FA oxidation largely depends on the uptake of circulating free fatty acids (FFAs), the byproducts of lipolysis (5). Although FFAs serve as the major energy substrate for the heart, high circulating FFA levels may exert deleterious effects on the heart. FA metabolism requires more oxygen than other substrates like glucose or ketone bodies, which potentially exacerbates the hypoxia injury under some pathological conditions (6). Moreover, elevated FFAs lead to the augmented myocardial FFAs uptake as well as excessive FA storage in cardiomyocytes, which drives cardiac lipotoxicity and causes myocardial damage (4). Thus, circulating FFAs may serve as a risk factor, hallmark, or potential target for diverse conditions.

Indeed, previous studies have shown that FFAs serve as a risk factor for obesity (7), diabetes (8), and coronary heart diseases (9, 10). Elevated FFAs are independently associated with compensatory HF (11, 12) and linked to higher 3-month mortality (13). A surge in catecholamines, inflammatory cytokines such as tumor necrosis factor (TNF)-alpha, and natriuretic peptides may, in part, explain the increased level of FFAs (9), which are all lipolytic inducers (14). In return, elevated FFAs can induce insulin resistance in cardiomyocytes and impair cardiac function as revealed by animal studies (15).

Considering FFAs are closely tied to fatty acid oxidation under exercise and stress (16), it is reasonable to propose that serum FFAs levels may provide important prognostic information for patients with AHF. It would be valuable for risk stratification and tailoring of therapy to optimize the management of AHF. However, more direct evidence for the prognostic value of FFAs in AHF is still lacking. We aim to determine whether higher levels of FFAs predict adverse outcomes among Chinese patients admitted with AHF.

METHODS

Study Population

This is a single-center, observational cohort study. Patients admitted for AHF in Department of Cardiology, the Second Affiliated Hospital, Zhejiang University School of Medicine between January 2019 and December 2019 were enrolled. Ethics Committee approvals were obtained from the Institutional Review Board for Human Studies of Second Affiliated Hospital of Zhejiang University School of Medicine (<city>Hangzhou</city>, China), and verbal informed consent was obtained from the patients during telephone follow-up.

The diagnosis of AHF was based on the ESC Guidelines and required elevated N-terminal pro-B-type natriuretic peptide (NT-proBNP) concentrations $\geq$1,000 ng/L and only those whose duration from onset of AHF or symptom exacerbation $\leq$1 month were recruited. Those with severe renal failure (eGFR<30 mL/min·1.73 m^2), renal replacement therapy, severe liver dysfunction (serum aminotransferase concentration more than 10 times above upper limit of normal range), serious infection, severe pulmonary diseases, systemic autoimmune disorder, malignancies, valvular disease, pregnancy, missing FFAs measurement or younger than 18 years were excluded in the study. Only those who survived to hospital discharge with complete full 1-year follow-up data ($n = 183$) were included in the analysis (**Supplementary Figure 1**).

Definition of Events

The study endpoint was the composite of all-cause death and HF rehospitalization through the 1-year follow-up after discharge. The endpoint events were ascertained based on rehospitalization records and telephone contacts.

Data Collection

Clinical data were extracted from electronic medical records. The laboratory parameters were measured at admission. For patients who received a laboratory test multiple times during this time period, only the first test results were included. Serum FFAs, low-density lipoprotein cholesterol (LDL-C), high-density lipoprotein cholesterol (HDL-C), total cholesterol (TC), triglycerides (TG), fasting glucose (FBG) and glycated hemoglobin A1c (HbA1c) were measured in an overnight fasting state, generally within 24 h after admission, while fasting status was unknown for the evaluation of the other laboratory parameters including N-terminal pro-brain natriuretic peptide (NT-proBNP), alanine aminotransferase (ALT), aspartate aminotransferase (AST), urea nitrogen (BUN) and creatinine. The measurements of serum FFAs, LDL-C, HDL-C, TG, TC, FBG, ALT, AST, BUN, and creatinine were performed on a Beckman Coulter instrument AU5800 (Beckman Coulter, Brea, California, USA). Serum levels of FFAs were analyzed using an enzymatic reagent (ACS-ACOD method) from LEADMAN (Beijing, China). The level of HbA1c was determined by a TOSOH HLC-723G8 automatic glycohemoglobin analyzer (Tosoh Corporation, Yamaguchi 746-0042, Japan). NT-proBNP was measured by electrochemiluminescence on an Cobas e801 (Roche Diagnostics, Rotkreuz, Switzerland). Echocardiography was used to measure left ventricular ejection fraction (LVEF), which was obtained during the hospital stay. Estimated glomerular filtration rate (eGFR) was estimated by the Chronic Kidney Disease Epidemiology Collaboration (CKD-EPI) formula. The triglyceride-glucose (TyG) index was calculated as the ln[fasting glucose level (mg/dL)×triglyceride level (mg/dL)/2].

Statistical Analysis

Baseline characteristics were compared among quartiles of FFAs using ANOVA or Kruskal-Wallis test for continuous variables, depending on the data distribution, and $\chi 2$ for categorical

TABLE 1 | Characteristics of patients with acute heart failure at baseline by quartiles of serum free fatty acids.

	All patients ***n*** **= 183**	**Q1 (≤385.60)** ***n*** **= 46**	**Q2 (385.60–596.20)** ***n*** **= 46**	**Q3 (596.20–797.30)** ***n*** **= 46**	**Q4 (>797.30)** ***n*** **= 45**	***P*-value**
Age, years	73 (63, 79)	72 (65, 78)	76 (63, 82)	77 (69, 83)	66 (57, 73)	**<0.001**
Male sex, *n* (%)	117 (63.9)	28 (60.9)	31 (67.4)	30 (65.2)	28 (62.2)	0.915
Body-mass index, kg/m²	23.8 (20.8, 26.0)	22.2 (20.2, 25.4)	24.1 (22.0,26.3)	24.2 (20.8, 26.9)	24.2 (20.8, 25.3)	0.224
MAP, mmHg	90.7 (82.0, 100.7)	91.0 (82.8, 99.3)	89.3 (81.7, 94.8)	91.0 (79.0, 106.4)	91.7 (85.7, 104.0)	0.783
LVEF, %	35.3 (28.2, 48.5)	39.0 (30.2, 54.7)	34.3 (27.6, 55.3)	37.3 (28.5, 45.1)	32.0 (26.5,43.4)	0.197
NYHA functional class						0.078
II, *n* (%)	33 (18.0)	11 (23.9)	10 (21.7)	6 (13.0)	6 (13.3)	
III, *n* (%)	81 (44.3)	25 (54.3)	18 (39.1)	23 (50.0)	15 (33.3)	
IV, *n* (%)	69 (37.7)	10 (21.7)	18 (39.1)	17 (37.0)	24 (53.3)	
De novo HF, *n* (%)	47 (25.7)	13 (28.3)	12 (26.1)	10 (21.7)	12 (26.7)	0.905
Co-morbidities, *n* (%)						
Coronary artery disease	71 (38.8)	21 (45.7)	14 (30.4)	21 (45.7)	15 (33.3)	0.291
Diabetes mellitus	51 (27.9)	9 (19.6)	16 (34.8)	11 (23.9)	15 (33.3)	0.296
Hypertension	98 (53.6)	27 (58.7)	26 (56.5)	25 (54.3)	20 (44.4)	0.539
Atrial fibrillation/atrial flutter	87 (47.5)	18 (39.1)	21 (45.7)	25 (54.3)	23 (51.1)	0.483
Smoking	67 (36.6)	15 (32.6)	22 (47.8)	17 (37.0)	13 (28.9)	0.265
Medications during hospitalization, *n* (%)						
Intravenous Diuretics	128 (69.9)	26 (56.5)	33 (71.7)	32 (69.6)	37 (82.2)	0.065
Intravenous vasodilator	15 (8.2)	4 (8.7)	3 (6.5)	6 (13.0)	2 (4.4)	0.482
Intravenous vasopressor	6 (3.3)	0 (0)	1 (2.2)	2 (4.3)	3 (6.7)	0.317
Intravenous inotropic agent	54 (29.5)	12 (26.1)	14 (30.4)	11 (23.9)	17 (37.8)	0.484
ACEI/ARB	127 (69.4)	31 (67.4)	34 (73.9)	32 (69.6)	30 (66.7)	0.876
Beta-blockers	131 (71.6)	30 (65.2)	38 (82.6)	34 (73.9)	29 (64.4)	0.178
ARNI	43 (23.5)	8 (17.4)	14 (30.4)	10 (21.7)	11 (24.4)	0.515
Amiodarone	29 (15.8)	9 (19.6)	7 (15.2)	5 (10.9)	8 (17.8)	0.689
Digoxin	59 (32.2)	11 (23.9)	13 (28.3)	15 (32.6)	20 (44.4)	0.182
Antiplatelet agents	101 (55.2)	29 (63.0)	26 (56.5)	24 (52.2)	22 (48.9)	0.558
Anticoagulants	79 (43.2)	16 (34.8)	18 (39.1)	24 (52.2)	21 (46.7)	0.338
Statins	111 (60.7)	33 (71.1)	29 (63.0)	21 (45.7)	28 (62.2)	0.076
Insulin	15 (8.2)	3 (6.5)	5 (10.9)	4 (8.7)	3 (6.7)	0.858
Oral hypoglycemic agents	39 (21.3)	8 (17.4)	12 (26.1)	7 (15.2)	12 (26.7)	0.418
Trimetazidine	37 (20.2)	7 (15.2)	10 (21.7)	11 (23.9)	9 (20.0)	0.760
Calcium antagonists	32 (17.5)	8 (17.4)	11 (23.9)	7 (15.2)	6 (13.3)	0.568
Laboratory test						
NT-proBNP, pg/mL	4264.0 (2449.0, 8054.0)	3025.5 (1590.6, 5529.8)	3525.0 (2156.8, 5250.3)	5989.1 (2719.8, 9570.3)	5167.3 (3191.5, 9483.0)	**0.001**
ALT, U/L	28.0 (17.0, 43.0)	22.0 (15.0, 34.3)	26.0 (15.0, 35.0)	31.0 (17.5, 45.0)	36.0 (21.5,57.5)	**0.022**
AST, U/L	39.0 (29.0, 59.0)	32.5 (25.0, 49.3)	38.5 (31.0, 58.0)	39.0 (29.8, 52.0)	46.0 (29.5, 69.5)	0.051
BUN, mmol/L	8.4 (7.2, 9.6)	8.3 (7.2, 9.5)	8.8 (7.4, 9.7)	8.8 (7.4, 9.7)	7.7 (6.5, 9.0)	0.135
Creatinine, μmol/L	91.0 (81.0, 98.0)	92.0 (80.5, 99.0)	90.5 (83.0, 100.0)	92.0 (81.8, 98.0)	88.0 (79.5, 96.5)	0.669
eGFR, mL/min·1.73 m^2	66.9 ± 18.4	65.3 ± 20.2	65.4 ± 18.0	64.7 ± 17.5	72.3 ± 17.4	0.157
Total cholesterol, mmol/L	3.8 ± 1.0	4.1 ± 1.0	3.5 ± 1.0	3.8 ± 0.8	3.8 ± 1.0	**0.032**
LDL-C, mmol/L	2.0 ± 0.7	2.1 ± 0.7	1.7 ± 0.6	2.0 ± 0.5	2.0 ± 0.7	**0.038**
HDL-C, mmol/L	1.1 (0.9, 1.3)	1.2 (1.0, 1.3)	1.0 (0.9, 1.3)	1.0 (0.9, 1.3)	1.1 (0.8, 1.2)	0.072
Triglycerides, mmol/L	1.0 (0.7, 1.3)	1.0 (0.7, 1.5)	1.0 (0.7, 1.3)	0.9 (0.7, 1.2)	1.0 (0.8, 1.5)	0.622
Fasting glucose, mmol/L	5.2(4.7, 6.5)	5.2(4.5, 5.8)	5.4(4.7, 8.3)	5.2(5.0, 5.9)	5.2(4.7, 7.9)	0.684

(Continued)

TABLE 1 | Continued

	All patients $n = 183$	Q1 (≤385.60) $n = 46$	Q2 (385.60–596.20) $n = 46$	Q3 (596.20–797.30) $n = 46$	Q4 (>797.30) $n = 45$	*P*-value
TyG index	8.4(8.1, 8.7)	8.4(8.1, 9.0)	8.5(8.0, 8.8)	8.4(8.1, 8.6)	8.5(8.1, 8.8)	0.669
HbA1c, %	6.2 (5.8, 7.1)	6.1 (5.8, 6.9)	6.3 (5.7, 7.4)	6.2 (5.7, 6.8)	6.2 (5.9, 7.1)	0.708
Incidence of all-cause death or HF rehospitalization through the 1- year follow-up	71 (38.8)	12 (26.1)	18 (39.1)	17 (37.0)	24 (53.3)	0.066

Continuous variables are presented as median (interquartile range) or mean (standard deviation), Categorical variables are expressed as number (percentages). MAP, mean arterial pressure; LVEF, left ventricular ejection fraction; NYHA, New York Heart Association; ACEI/ARB, angiotensin-converting enzyme inhibitor/angiotensin receptor blocker; ARNI, angiotensin receptor-neprilysin inhibitor; NT-proBNP, N-terminal pro brain natriuretic peptide; ALT, alanine aminotransferase; AST, aspartate amino transferase; BUN, urea nitrogen; eGFR, estimated glomerular filtration rate; LDL-C, low-density lipoprotein cholesterol; HDL-C, high-density lipoprotein cholesterol; TyG index, Triglyceride-glucose index; HbA1c, glycated hemoglobin A1c. Bold font indicates statistical significance.

variables. Continuous variables were presented as mean ± standard deviation (SD) or median [inter-quartile range (IQR)] if skewed. Categorical variables were presented as N (%). Correlation between two variables was examined by the Pearson or Spearman analysis. Cubic splines were utilized to evaluate the linearity of the relationship between FFAs and the incidence of study endpoints. Cox proportional hazards regression models were used to analyze the association between FFAs levels and time to event (only the first endpoint event was accounted in our analysis). FFAs were modeled as quartiles as well as a continuous variable (per SD increase of FFAs). Subgroup analysis of patients and outcomes and the receiver-operating curve (ROC) analysis were performed (presented in **Supplementary Material**). A two-tailed $P < 0.05$ was considered statistically significant. Statistical analyses were performed with SPSS statistical software (version 23.0) and R statistical software (version 4.1.0).

RESULTS

Descriptive Analysis

A total of 183 patients with AHF were included in the study, with a median age of the study participants was 73 years (IQR: 63∼79). The baseline demography was compared according to FFAs quartiles as shown in **Table 1**. After 1 year follow-up, 71 (38.8%) participants suffered from all cause of death ($n = 13$), or HF rehospitalization ($n = 61$). Participants who developed adverse events were with higher FFAs levels, consistent with higher NT-proBNP although the difference was not statistically significant (**Supplementary Table 1**). Interestingly, the total serum lipids were not significantly different among participants with different quartiles of FFAs.

Correlation of FFAs With Baseline Characteristics

As illustrated in **Table 2**, the serum levels of FFAs showed significant positive correlations with NT-proBNP, NYHA. A negative correlation between FFAs levels and LVEF was also implicated. Besides, the FFAs levels were correlated with age, eGFR, ALT, and AST but did not show any significant correlation with BMI and MAP. Although the total serum lipid levels did not show any correlation with FFAs, HDL-cholesterol was negatively associated with FFAs instead of any other components of serum lipids. Notably, we saw no significant association between FFAs and TyG index, the reliable surrogate marker of insulin resistance (IR) (17).

TABLE 2 | Correlation analyses of free fatty acids with clinical and laboratory parameters.

	FFAs	
	r	*P*-value
Age, years	**−0.175**	**0.018**
BMI, Kg/m^2	0.114	0.126
MAP, mmHg	0.085	0.252
NYHA	**0.207**	**0.005**
NT-pro BNP, pg/mL	**0.287**	**<0.001**
LVEF, %	**−0.193**	**0.009**
ALT, U/L	**0.241**	**0.001**
AST, U/L	**0.203**	**0.006**
eGFR, mL/min·1.73 m^2	**0.160**	**0.030**
Total cholesterol, mmol/L	−0.050	0.498
LDL-C, mmol/L	0.032	0.670
HDL-C, mmol/L	**−0.173**	**0.019**
Triglycerides, mmol/L	−0.018	0.810
Fasting glucose, mmol/L	0.037	0.615
HbA1c	0.087	0.262
TyG index	0.001	0.989

BMI, body-mass index; MAP, mean arterial pressure; LVEF, left ventricular ejection fraction; NYHA, New York Heart Association; NT-proBNP, N-terminal pro brain natriuretic peptide; ALT, alanine aminotransferase; AST, aspartate amino transferase; eGFR, estimated glomerular filtration rate; LDL-C, low-density lipoprotein cholesterol; HDL-C, high-density lipoprotein cholesterol; TyG index, Triglyceride-glucose index; HbA1c, glycated hemoglobin A1c. Bold font indicates statistical significance.

Association of FFAs With Adverse Events

During the 1-year flow-up after discharge, 71 out of a total of 183 AHF patients (38.8%) experienced an adverse event (all-cause death or HF rehospitalization). After adjusting for variables that may influence the prognosis in HF and the incidence of all-cause death or HF rehospitalization analyzed by the univariate analysis in the present study (**Supplementary Table 2**) (18–21), there was a positive association between FFAs levels and the risk

TABLE 3 | Univariate and multivariate Cox regression model for all-cause death or HF rehospitalization according to quartiles/standard deviation of serum free fatty acids.

FFAs range	Free Fatty Acids Quartiles				Continuous
	Q1 (≤385.60)	Q2 (385.60–596.20)	Q3 (596.20–797.30)	Q4 (>797.30)	Per standard deviation (303.07) greater
Events/N at risk	12/46	18/46	17/46	24/45	71/183
Unadjusted HR (95%CI)	1.00(Ref.)	1.60 (0.77, 3.32)	1.51 (0.72, 3.17)	2.71 (1.36, 5.43)	1.24(1.02, 1.51)
Adjusted Model * HR (95%CI)	1.00(Ref.)	1.71 (0.81, 3.62)	1.41 (0.64, 3.09)	3.18 (1.53, 6.63)	1.26 (1.02, 1.55)

**Adjusted for age, sex, BMI, CAD, DM, hypertension, LVEF, NT-proBNP. BMI, body-mass index; CAD, coronary artery disease; DM, diabetes mellitus; LVEF, left ventricular ejection fraction; NT-proBNP, N-terminal pro brain natriuretic peptide.*

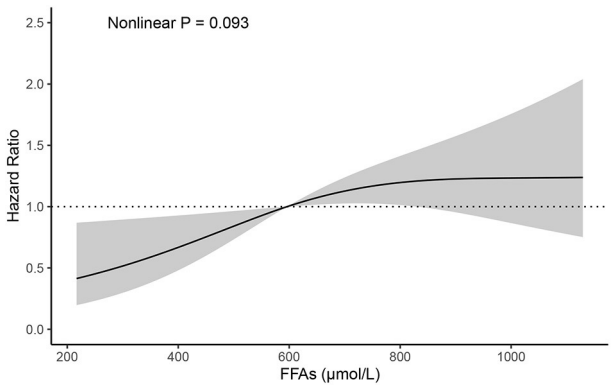

FIGURE 1 | Cubic spline depicting the association of FFAs with the incidence of all-cause mortality or HF rehospitalization, P non-liner = 0.093 (adjusted for age, sex, BMI, CAD, DM, hypertension, LVEF, NT-proBNP). BMI, body-mass index; CAD, coronary artery disease; DM, diabetes mellitus; LVEF, left ventricular ejection fraction; NT-proBNP, N-terminal pro brain natriuretic peptide.

of death or HF rehospitalization (**Table 3**). In a multivariable analysis adjusting for sex, age, body-mass index, coronary artery disease, diabetes mellitus, hypertension, LVEF, NT-proBNP, each SD (303.07 μmol/L) higher FFAs were associated with 26% higher risk of death or HF rehospitalization (95% confidence interval, 2–55%). Each increasing quartile of FFAs was associated with differentially elevated hazard ratios for death or HF rehospitalization of 1 (reference), 1.71 (95% confidence interval, [0.81, 3.62]), 1.41 (95% confidence interval, [0.64, 3.09]), and 3.18 (95% confidence interval, [1.53, 6.63]), respectively. Assessment of cubic splines also supports a linear relationship between the serum levels of FFAs and the incidence of death or HF rehospitalization (P non-liner = 0.093) (**Figure 1**).

DISCUSSION

Our study shows that serum FFAs concentration is an independent risk factor for all-cause death or HF rehospitalization after discharge of patients with AHF, indicating that FFAs may predict adverse outcomes in AHF patients.

Øie et al. conducted a cross-sectional study, which showed that 183 patients with stable HF had higher FFAs levels than that in healthy control subjects (11). Previous studies have reported that circulating FFAs were associated with various risks factors for HF including coronary heart disease (9, 10), hypertension (22), diabetes mellitus (8), atrial fibrillation (23). This would lead to a higher risk of HF (12) and higher 3-month mortality of HF (13). Accumulating evidence showed that Asian/Chinese population may have a different fatty acid metabolism pattern (24). Our study not only provided direct evidence with the positive correlation between serum FFAs and acute heart failure, but also for the first time showed that FFAs may have good prognostic value in predicting adverse events in Chinese population. Moreover, this prognostic value may last longer than we expected, which may be more than 1 years. All these studies, with our findings together, call for a future study whether diet management, energetic therapy, or metabolic modulation may have therapeutic potential.

FFAs are primarily derived from lipolysis of adipose tissue (25). Some hormones, such as catecholamines and inflammatory cytokines, which can exert strong lipolytic signals on hormone-sensitive lipase, were found markedly elevating in HF patients, contributing to the enhanced concentration of FFAs in circulation (14). Since the rate of fatty acids (FAs) uptake by the heart is mainly dependent upon the concentration of FFAs in the circulation, FAs delivery to cardiomyocytes are also increased along with the growing concentration of FFAs (26). Of note, an increased FAs uptake is not accompanied by a concomitant augmented FA oxidation. Indeed, evidence is mounting that deteriorated cardiac function comes with a decline in FA oxidation rates (27, 28). The imbalance between FA uptake and oxidation results in intracellular storage of lipids, which are in part stored as triglycerides (TAGs), but can also be transported into non-oxidative pathways, leading to the production of toxic lipid species like diacylglycerol and ceramide, which drives the cardiac lipotoxicity (4). The cardiac lipotoxicity, inefficient FA metabolism, together with the negative impact of high FFAs on cardiovascular system including insulin resistance, oxidative stress, inflammation and endothelial dysfunction (29, 30), indicates that elevated FFAs play an important role in HF pathophysiology and might contribute to the development and progression of HF. Notably, Studies in humans and animal models have revealed that heart failure is associated with generalized insulin resistance (31). And evidence showed that excess of circulating FFAs are the major cause of

IR by inhibiting insulin signaling (32, 33). Unexpectedly, we found no significant association between FFAs and TyG index, the reliable surrogate of IR, to some extent suggesting that the relationship of FFAs and insulin resistance is more complex in HF patients, at least in the acute phase, which deserves further investigation. Our data suggests a positive correlations of serum levels of FFAs with NYHA and NT-proBNP, in accord with the results of a previous study (34), verifying again the relationship between serum FFAs levels and HF severity.

Given the facts listed above, and the highly significant association between FFAs levels and the adverse clinical outcomes among AHF patients, as presented in our study and a previous study (13), it seems reasonable to suppose that modulation of FFAs utilization by application of medicines might improve the cardiac function and outcomes in HF patients. Perhexiline, reducing FAO through inhibiting carnitine palmitoyltransferase-1 and 2 (CPT-1/2), the transport proteins responsible for mitochondrial FAs uptake from the cytoplasm (35), was found that could improve symptoms, the peak exercise oxygen consumption (VO2 max) and LVEF in patients with chronic HF (36–39). Trimetazidine, acting as a inhibitor of long-chain mitochondrial 3-ketoacyl coenzyme A thiolase enzyme, leading to the reduced myocardial FA oxidation (40), improved left ventricular (LV) function and functional class, reduced rehospitalization rates (41–43) and all-cause mortality (43–45) in HF patients. However, different results also have been reported. Use of acipimox, a nicotinic acid analog, did not result in the same favorable effect on myocardial function among HF patient, which can reduce the availability of circulating FFAs through inhibition of adipose tissue lipolysis. Four-week administration of acipimox in non-diabetic patients with chronic HF did not change cardiac function or exercise capacity (46). What's more, Tuunanen H et al. showed that acute serum FFAs depletion contributed to the deteriorated myocardial efficiency in idiopathic dilated cardiomyopathy patients (47). It's worth noting that these studies did not include AHF patients. AHF patients may have had experienced a more deranged change of myocardial metabolism when compared to stable HF patient, which may respond differently to the limitation of FFAs disposal. Therefore, it is necessary to further explore the mechanism of FFAs in contributing to the development and progression of both stable HF and AHF patients.

Study Limitations

Our study was an observational study, while its relatively small sample size and single-center in design might introduce selective bias and therefore limit its clinical application. Besides that, the small study sample size precluded us from adequately powered subgroup analysis (presented in **Supplementary Material**). Moreover, a single measurement of serum FFAs failed to provide information about the longitudinal changes in FFAs levels over time and how the changes affect the clinical outcomes of AHF patients. A caveat of our study was that we were unable to detect the composition of serum FFAs but the total class for all the non-esterized fatty acids. Previous data suggested that FFAs composition may influence myocardial function and associated with total mortality in chronic heart failure population (11) and linked to the incidence of HF in meddle-aged adults (48). However, evidence for an association between the composition of FFAs and AHF is still limited, which warrant further investigation. A more precise evaluation about the specific components of FFAs may give a deeper insight of cardiac energetics and help to seek more specific therapeutic targets. In future, basic researches are in great need to clarify the role of FFAs in the development and progression of HF.

CONCLUSION

In conclusion, our data demonstrated an increased risk of adverse clinical outcomes with higher FFAs concentration among AHF patients. FFAs levels, which can be easily measured in clinical setting at relatively lower costs, may have a great prognostic potential for risk stratification in AHF patients.

DATA AVAILABILITY STATEMENT

The original contributions presented in the study are included in the article/**Supplementary Materials**, further inquiries can be directed to the corresponding authors.

ETHICS STATEMENT

The studies involving human participants were reviewed and approved by the Institutional Review Board for Human Studies of Second Affiliated Hospital of Zhejiang University School of Medicine (Hangzhou, China). Written informed consent for participation was not required for this study in accordance with the national legislation and the institutional requirements.

AUTHOR CONTRIBUTIONS

YY performed data collection, patient follow-up, statistical analysis and manuscript writing. CJ participated in statistical analysis. CZ participated in data collection. SZ and SM participated in data collection and analysis. HM conceived the study and revised the manuscript. MX and JW provided funding and overall supervision. All authors contributed to the article and approved the submitted version.

FUNDING

This article was supported by Provincial and Ministry Joint Major Projects of National Health Commission of China (WKJ-ZJ-1703 to MX), the Key Research and Development Project of Department of Science and Technology of Zhejiang Province (2020C03118 to MX), National Natural Science Foundation of China (82070251 and 81870203 to MX, 82070252 to HM) and grants from and Zhejiang Provincial Natural Science Foundation (LR21H020001 to HM).

SUPPLEMENTARY MATERIAL

The Supplementary Material for this article can be found online at: https://www.frontiersin.org/articles/10.3389/fcvm.2021.761537/full#supplementary-material

REFERENCES

1. Groenewegen A, Rutten FH, Mosterd A, Hoes AW, Degoricija V, Trbua i M, et al. Epidemiology of heart failure. *Eur J Heart Fail.* (2020) 22:1342–56. doi: 10.1002/ejhf.1858
2. Ponikowski P, Voors AA, Anker SD, Bueno H, Cleland J, Coats A, et al. 2016 ESC Guidelines for the diagnosis and treatment of acute and chronic heart failure: the task force for the diagnosis and treatment of acute and chronic heart failure of the European Society of Cardiology (ESC) developed with the special contribution of the Heart Failure Association (HFA) of the ESC. *Eur Heart J.* (2016) 37:2129–200. doi: 10.1093/eurheartj/ehw128
3. Voors AA, van Veldhuisen DJ. Why do drugs for acute heart failure fail? *Eur J Heart Fail.* (2012) 14:955–6. doi: 10.1093/eurjhf/hfs122
4. Bertero E, Maack C. Metabolic remodelling in heart failure. *Nat Rev Cardiol.* (2018) 15:457–70. doi: 10.1038/s41569-018-0044-6
5. Schulze PC, Drosatos K, Goldberg IJ. Lipid use and misuse by the heart. *Circ Res.* (2016) 118:1736–51. doi: 10.1161/CIRCRESAHA.116.306842
6. Lopaschuk GD, Ussher JR, Folmes CD, Jaswal JS, Stanley WC. Myocardial fatty acid metabolism in health and disease. *Physiol Rev.* (2010) 90:207–58. doi: 10.1152/physrev.00015.2009
7. Boden G. Obesity and free fatty acids. *Endocrinol Metab Clin North Am.* (2008) 37:635-46, viii-ix. doi: 10.1016/j.ecl.2008.06.007
8. Djoussé L, Khawaja O, Bartz TM, Biggs ML, Ix JH, Zieman SJ, et al. Plasma fatty acid-binding protein 4, nonesterified fatty acids, and incident diabetes in older adults. *Diabetes Care.* (2012) 35:1701–7. doi: 10.2337/dc11-1690
9. Carlsson M, Wessman Y, Almgren P, Groop L. High levels of nonesterified fatty acids are associated with increased familial risk of cardiovascular disease. *Arterioscler Thromb Vasc Biol.* (2000) 20:1588–94. doi: 10.1161/01.ATV.20.6.1588
10. Westphal S, Gekeler GH, Dierkes J, Wieland H, Luley C, A. free fatty acid tolerance test identifies patients with coronary artery disease among individuals with a low conventional coronary risk profile. *Heart Vessels.* (2002) 16:79–85. doi: 10.1007/s003800200000
11. Øie E, Ueland T, Dahl CP, Bohov P, Berge C, Yndestad A, et al. Fatty acid composition in chronic heart failure: low circulating levels of eicosatetraenoic acid and high levels of vaccenic acid are associated with disease severity and mortality. *J Intern Med.* (2011) 270:263–72. doi: 10.1111/j.1365-2796.2011.02384.x
12. Djoussé L, Benkeser D, Arnold A, Kizer JR, Zieman SJ, Lemaitre RN, et al. Plasma free fatty acids and risk of heart failure: the Cardiovascular Health Study. *Circ Heart Fail.* (2013) 6:964–9. doi: 10.1161/CIRCHEARTFAILURE.113.000521
13. Degoricija V, Trbušić M, Potočnjak I, Radulović B, Pregartner G, Berghold A, et al. Serum concentrations of free fatty acids are associated with 3-month mortality in acute heart failure patients. *Clin Chem Lab Med.* (2019) 57:1799–804. doi: 10.1515/cclm-2019-0037
14. Doehner W, Frenneaux M, Anker SD. Metabolic impairment in heart failure: the myocardial and systemic perspective. *J Am Coll Cardiol.* (2014) 64:1388–400. doi: 10.1016/j.jacc.2014.04.083
15. Han L, Liu J, Zhu L, Tan F, Qin Y, Huang H, et al. Free fatty acid can induce cardiac dysfunction and alter insulin signaling pathways in the heart. *Lipids Health Dis.* (2018) 17:185. doi: 10.1186/s12944-018-0834-1
16. Frandsen J, Vest SD, Ritz C, Larsen S, Dela F, Helge JW. Plasma free fatty acid concentration is closely tied to whole body peak fat oxidation rate during repeated exercise. *J Appl Physiol*. (1985). (2019) 126:1563–71. doi: 10.1152/japplphysiol.00995.2018
17. Du T, Yuan G, Zhang M, Zhou X, Sun X, Yu X. Clinical usefulness of lipid ratios, visceral adiposity indicators, and the triglycerides and glucose index as risk markers of insulin resistance. *Cardiovasc Diabetol*. (2014) 13:146. doi: 10.1186/s12933-014-0146-3
18. Sciomer S, Moscucci F, Salvioni E, Marchese G, Bussotti M, Corrà U, et al. Role of gender, age and BMI in prognosis of heart failure. *Eur J Prev Cardiol.* (2020) 27(2_suppl):46–51. doi: 10.1177/2047487320961980
19. Lehrke M, Marx N. Diabetes mellitus and heart failure. *Am J Med*. (2017) 130(6S):S40–S50. doi: 10.1016/j.amjmed.2017.04.010
20. Pfeffer MA. Heart failure and hypertension: importance of prevention. *Med Clin North Am.* (2017) 101:19–28. doi: 10.1016/j.mcna.2016.08.012
21. Pagliaro BR, Cannata F, Stefanini GG, Bolognese L. Myocardial ischemia and coronary disease in heart failure. *Heart Fail Rev.* (2020) 25:53–65. doi: 10.1007/s10741-019-09831-z
22. Fagot-Campagna A, Balkau B, Simon D, Warnet JM, Claude JR, Ducimetière P, et al. High free fatty acid concentration: an independent risk factor for hypertension in the Paris Prospective Study. *Int J Epidemiol.* (1998) 27:808–13. doi: 10.1093/ije/27.5.808
23. Khawaja O, Bartz TM, Ix JH, Heckbert SR, Kizer JR, Zieman SJ, et al. Plasma free fatty acids and risk of atrial fibrillation (from the Cardiovascular Health Study). *Am J Cardiol.* (2012) 110:212–6. doi: 10.1016/j.amjcard.2012.03.010
24. Sun L, Zong G, Li H, Lin X. Fatty acids and cardiometabolic health: a review of studies in Chinese populations. *Eur J Clin Nutr.* (2021) 75:253–66. doi: 10.1038/s41430-020-00709-0
25. Wang S, Soni KG, Semache M, Casavant S, Fortier M, Pan L, et al. Lipolysis and the integrated physiology of lipid energy metabolism. *Mol Genet Metab.* (2008) 95:117–26. doi: 10.1016/j.ymgme.2008.06.012
26. Stanley WC, Recchia FA, Lopaschuk GD. Myocardial substrate metabolism in the normal and failing heart. *Physiol Rev.* (2005) 85:1093–129. doi: 10.1152/physrev.00006.2004
27. Doenst T, Nguyen TD, Abel ED. Cardiac metabolism in heart failure: implications beyond ATP production. *Circ Res.* (2013) 113:709–24. doi: 10.1161/CIRCRESAHA.113.300376
28. Kolwicz SJ, Purohit S, Tian R. Cardiac metabolism and its interactions with contraction, growth, and survival of cardiomyocytes. *Circ Res.* (2013) 113:603–16. doi: 10.1161/CIRCRESAHA.113.302095
29. Ghosh A, Gao L, Thakur A, Siu PM, Lai C. Role of free fatty acids in endothelial dysfunction. *J Biomed Sci.* (2017) 24:50. doi: 10.1186/s12929-017-0357-5
30. Pilz S, März W. Free fatty acids as a cardiovascular risk factor. *Clin Chem Lab Med.* (2008) 46:429–34. doi: 10.1515/CCLM.2008.118
31. Riehle C, Abel ED. Insulin Signaling and Heart Failure. *Circ Res.* (2016) 118:1151–69. doi: 10.1161/CIRCRESAHA.116.306206
32. Capurso C, Capurso A. From excess adiposity to insulin resistance: the role of free fatty acids. *Vascul Pharmacol.* (2012) 57:91–7. doi: 10.1016/j.vph.2012.05.003
33. Delarue J, Magnan C. Free fatty acids and insulin resistance. *Curr Opin Clin Nutr Metab Care.* (2007) 10:142–8. doi: 10.1097/MCO.0b013e328042ba90
34. Zhu N, Jiang W, Wang Y, Wu Y, Chen H, Zhao X. Plasma levels of free fatty acid differ in patients with left ventricular preserved, mid-range, and reduced ejection fraction. *BMC Cardiovasc Disord.* (2018) 18:104. doi: 10.1186/s12872-018-0850-0
35. Ashrafian H, Horowitz JD, Frenneaux MP. Perhexiline. *Cardiovasc Drug Rev.* (2007) 25:76–97. doi: 10.1111/j.1527-3466.2007.00006.x
36. Lee L, Campbell R, Scheuermann-Freestone M, Taylor R, Gunaruwan P, Williams L, et al. Metabolic modulation with perhexiline in chronic heart failure: a randomized, controlled trial of short-term use of a novel treatment. *Circulation.* (2005) 112:3280–8. doi: 10.1161/CIRCULATIONAHA.105.551457
37. Beadle RM, Williams LK, Kuehl M, Bowater S, Abozguia K, Leyva F, et al. Improvement in cardiac energetics by perhexiline in heart failure due to dilated cardiomyopathy. *JACC Heart Fail.* (2015) 3:202–11. doi: 10.1016/j.jchf.2014.09.009
38. Abozguia K, Elliott P, McKenna W, Phan TT, Nallur-Shivu G, Ahmed I, et al. Metabolic modulator perhexiline corrects energy deficiency and improves exercise capacity in symptomatic hypertrophic cardiomyopathy. *Circulation.* (2010) 122:1562–9. doi: 10.1161/CIRCULATIONAHA.109.934059
39. Phan TT, Shivu GN, Choudhury A, Abozguia K, Davies C, Naidoo U, et al. Multi-centre experience on the use of perhexiline in chronic heart failure and refractory angina: old drug, new hope. *Eur J Heart Fail.* (2009) 11:881–6. doi: 10.1093/eurjhf/hfp106
40. Lopatin YM, Rosano GM, Fragasso G, Lopaschuk GD, Seferovic PM, Gowdak LH, et al. Rationale and benefits of trimetazidine by acting on cardiac metabolism in heart failure. *Int J Cardiol.* (2016) 203:909–15. doi: 10.1016/j.ijcard.2015.11.060
41. Zhang L, Lu Y, Jiang H, Zhang L, Sun A, Zou Y, et al. Additional use of trimetazidine in patients with chronic heart failure: a meta-analysis. *J Am Coll Cardiol.* (2012) 59:913–22. doi: 10.1016/j.jacc.2011.11.027

42. Zhou X, Chen J. Is treatment with trimetazidine beneficial in patients with chronic heart failure? *PLoS ONE.* (2014) 9:e94660. doi: 10.1371/journal.pone.0094660
43. Gao D, Ning N, Niu X, Hao G, Meng Z. Trimetazidine: a meta-analysis of randomised controlled trials in heart failure. *Heart.* (2011) 97:278–86. doi: 10.1136/hrt.2010.208751
44. Grajek S, Michalak M. The effect of trimetazidine added to pharmacological treatment on all-cause mortality in patients with systolic heart failure. *Cardiology.* (2015) 131:22–9. doi: 10.1159/000375288
45. Fragasso G, Rosano G, Baek SH, Sisakian H, Di Napoli P, Alberti L, et al. Effect of partial fatty acid oxidation inhibition with trimetazidine on mortality and morbidity in heart failure: results from an international multicentre retrospective cohort study. *Int J Cardiol.* (2013) 163:320–5. doi: 10.1016/j.ijcard.2012.09.123
46. Halbirk M, Nørrelund H, Møller N, Schmitz O, Gøtzsche L, Nielsen R, et al. Suppression of circulating free fatty acids with acipimox in chronic heart failure patients changes whole body metabolism but does not affect cardiac function. *Am J Physiol Heart Circ Physiol.* (2010) 299:H1220–5. doi: 10.1152/ajpheart.00475.2010
47. Tuunanen H, Engblom E, Naum A, Någren K, Hesse B, Airaksinen KE, et al. Free fatty acid depletion acutely decreases cardiac work and efficiency in cardiomyopathic heart failure. *Circulation.* (2006) 114:2130–7. doi: 10.1161/CIRCULATIONAHA.106.645184
48. Yamagishi K, Nettleton JA, Folsom AR. Plasma fatty acid composition and incident heart failure in middle-aged adults: the Atherosclerosis Risk in Communities (ARIC) Study. *Am Heart J.* (2008) 156:965–74. doi: 10.1016/j.ahj.2008.06.017

Conflict of Interest: The authors declare that the research was conducted in the absence of any commercial or financial relationships that could be construed as a potential conflict of interest.

Publisher's Note: All claims expressed in this article are solely those of the authors and do not necessarily represent those of their affiliated organizations, or those of the publisher, the editors and the reviewers. Any product that may be evaluated in this article, or claim that may be made by its manufacturer, is not guaranteed or endorsed by the publisher.

Copyright © 2021 Yu, Jin, Zhao, Zhu, Meng, Ma, Wang and Xiang. This is an open-access article distributed under the terms of the Creative Commons Attribution License (CC BY). The use, distribution or reproduction in other forums is permitted, provided the original author(s) and the copyright owner(s) are credited and that the original publication in this journal is cited, in accordance with accepted academic practice. No use, distribution or reproduction is permitted which does not comply with these terms.

frontiers in Cardiovascular Medicine

ORIGINAL RESEARCH
published: 03 February 2022
doi: 10.3389/fcvm.2022.803036

Elevation of Hemoglobin A1c Increases the Atherosclerotic Plaque Vulnerability and the Visit-to-Visit Variability of Lipid Profiles in Patients Who Underwent Elective Percutaneous Coronary Intervention

Duanbin Li[1,2†], Ya Li[1,2†], Cao Wang[1,2,3†], Hangpan Jiang[4], Liding Zhao[5], Xulin Hong[1,2], Maoning Lin[1,2], Yi Luan[1,2], Xiaohua Shen[1,2], Zhaoyang Chen[6*] and Wenbin Zhang[1,2*]*

[1] Department of Cardiology, Sir Run Run Shaw Hospital, College of Medicine, Zhejiang University, Hangzhou, China, [2] Key Laboratory of Cardiovascular Intervention and Regenerative Medicine of Zhejiang Province, Hangzhou, China, [3] Department of Cardiology, Haiyan People's Hospital, Jiaxing, China, [4] Department of Cardiology, The Fourth Affiliated Hospital, College of Medicine, Zhejiang University, Yiwu, China, [5] Department of Cardiology, The First Affiliated Hospital, College of Medicine, Zhejiang University, Hangzhou, China, [6] Department of Cardiology, Union Hospital, Fujian Medical University, Fuzhou, China

Background: Increased plaque vulnerability and higher lipid variability are causes of adverse cardiovascular events. Despite a close association between glucose and lipid metabolisms, the influence of elevated glycated hemoglobin A1c (HbA1c) on plaque vulnerability and lipid variability remains unclear.

Methods: Among subjects undergoing percutaneous coronary intervention (PCI) from 2009 through 2019, 366 patients received intravascular optical coherence tomography (OCT) assessment and 4,445 patients underwent the scheduled follow-ups within 1 year after PCI. Vulnerability features of culprit vessels were analyzed by OCT examination, including the assessment of lipid, macrophage, calcium, and minimal fibrous cap thickness (FCT). Visit-to-visit lipid variability was determined by different definitions including standard deviation (SD), coefficient of variation (CV), and variability independent of the mean (VIM). Multivariable linear regression analysis was used to verify the influence of HbA1c on plaque vulnerability features and lipid variability. Exploratory analyses were also performed in non-diabetic patients.

Results: Among enrolled subjects, the pre-procedure HbA1c was 5.90 ± 1.31%, and the average follow-up HbA1c was 5.98 ± 1.16%. By OCT assessment, multivariable linear regression analyses demonstrated that patients with elevated HbA1c had a thinner minimal FCT ($\beta = -6.985$, $P = 0.048$), greater lipid index (LI) ($\beta = 226.299$, $P = 0.005$), and higher macrophage index ($\beta = 54.526$, $P = 0.045$). Even in non-diabetic patients, elevated HbA1c also linearly decreased minimal FCT ($\beta = -14.011$, $P = 0.036$), increased LI ($\beta = 290.048$, $P = 0.041$) and macrophage index ($\beta = 120.029$, $P = 0.048$). Subsequently, scheduled follow-ups were performed during 1-year following PCI. Multivariable linear regression analyses proved that elevated average follow-up HbA1c levels increased the VIM of lipid profiles, including low-density lipoprotein cholesterol

OPEN ACCESS

Edited by:
Yaoliang Tang,
Augusta University, United States

Reviewed by:
Triantafyllos Didangelos,
Aristotle University of Thessaloniki, Greece
Hong Ma,
Zhejiang University, China

***Correspondence:**
Wenbin Zhang
3313011@zju.edu.cn
Zhaoyang Chen
chenzhaoyang888@126.com
Xiaohua Shen
clare0117@sina.com

[†] These authors have contributed equally to this work

Specialty section:
This article was submitted to General Cardiovascular Medicine, a section of the journal Frontiers in Cardiovascular Medicine

Received: 27 October 2021
Accepted: 11 January 2022
Published: 03 February 2022

Citation:
Li D, Li Y, Wang C, Jiang H, Zhao L, Hong X, Lin M, Luan Y, Shen X, Chen Z and Zhang W (2022) Elevation of Hemoglobin A1c Increases the Atherosclerotic Plaque Vulnerability and the Visit-to-Visit Variability of Lipid Profiles in Patients Who Underwent Elective Percutaneous Coronary Intervention. Front. Cardiovasc. Med. 9:803036. doi: 10.3389/fcvm.2022.803036

($\beta = 2.594$, $P < 0.001$), high-density lipoprotein cholesterol ($\beta = 0.461$, $P = 0.044$), non-high-density lipoprotein cholesterol ($\beta = 1.473$, $P < 0.001$), total cholesterol ($\beta = 0.947$, $P < 0.001$), and triglyceride ($\beta = 4.217$, $P < 0.001$). The result was consistent in non-diabetic patients and was verified when SD and CV were used to estimate variability.

Conclusion: In patients undergoing elective PCI, elevated HbA1c increases the atherosclerotic plaque vulnerability and the visit-to-visit variability of lipid profiles, which is consistent in non-diabetic patients.

Keywords: hemoglobin A1c, optical coherence tomography, lipid variability, plaque vulnerability, percutaneous coronary intervention

BACKGROUND

Coronary artery disease (CAD) has contributed to the cardiovascular disease being the leading cause of death around the world (1). Meanwhile, as a traditional risk factor, diabetes mellitus (DM) doubles or even triples the incidence of CAD (2).

DM is a disease of abnormal metabolism and characterized by chronic hyperglycemia. Of all the glycemia indicators, glycated hemoglobin A1c (HbA1c) has been a well-established one for the assessment of long-term glycemic levels (3). The American Diabetes Association (ADA) and the World Health Organization (WHO) recommend HbA1c $\geq$6.5% and 5.7–6.4% as the diagnostic cut-off points for diabetes and pre-diabetes, respectively (4). In diabetic patients, elevated HbA1c level has been confirmed to increase the risk of cardiac death, cardiovascular diseases, and strokes (5). Even in non-diabetic CAD patients, elevated HbA1c levels were also related to a raised risk of long-term mortality and myocardial infarction (MI) (6, 7). However, the mechanism by which HbA1c levels affect the prognosis of CAD patients remains unclear.

The increased plaque vulnerability is associated with dyslipidemia and has been identified as the leading cause of adverse cardiovascular events (8). Due to the high resolution (10–15 μm), optical coherence tomography (OCT) allows the quantitative assessment of vulnerability features in the coronary artery (9, 10). Thinner fibrous cap thickness (FCT), larger lipid cores, and more macrophage infiltration all indicate a greater vulnerability feature and an underlying poor prognosis (11). The visit-to-visit lipid variability has been verified as another strong predictor of adverse cardiovascular events for CAD patients (12, 13). Even in the general population, elevated lipid variability has also been shown to raise the incidence of all-cause death, myocardial infarction (MI), and strokes (14). The variability of several lipids has been identified to be associated with adverse cardiovascular events, including low-density lipoprotein cholesterol (LDL-C), high-density lipoprotein cholesterol (HDL-C), non-high-density lipoprotein cholesterol (non-HDL), total cholesterol (TC), and triglyceride (TG) (15–18). Some genetic-level evidence has indicated that glucose dysregulation may be associated with increased lipid variability (19, 20).

Due to the strong association between glucose and lipid metabolisms, elevated HbA1c may contribute to adverse cardiovascular events by increasing plaque vulnerability and the visit-to-visit lipid variability. However, these potential relationships remain unclear. Therefore, we conducted the current study to explore the influence of HbA1c on plaque vulnerability features and lipid variability.

Abbreviations: CAD, coronary artery disease; DM, diabetes mellitus; HbA1c, hemoglobin A1c; ADA, the American Diabetes Association; WHO, the World Health Organization; MI, myocardial infarction; PCI, percutaneous coronary intervention; OCT, optical coherence tomography; FCT, fibrous cap thickness; LDL-C, low-density lipoprotein cholesterol; HDL-C, high-density lipoprotein cholesterol; non-HDL-C, non-high-density lipoprotein cholesterol; TC, total cholesterol; TG, triglyceride; TIMI, Thrombolysis in Myocardial Infarction; ICC, intraclass correlation coefficient; SD, standard deviation; CV, coefficient of variation; VIM, variability independent of the mean; eGFR, estimated glomerular filtration rate; LOWESS, locally weighted scatterplot smoothing; ACS, acute coronary syndromes; SAP, stable angina pectoris.

METHODS

Study Subjects

In this retrospective cross-sectional study, patients who underwent elective PCI were eligible for screening from January 2009 through April 2019. The flow chart of the current study is shown in **Figure 1**. Patients were included if they received elective PCI and/or OCT examination. In the vulnerability feature analysis, subjects were excluded according to (i) culprit vessels with Thrombolysis in Myocardial Infarction (TIMI) flow $\leq$2; (ii) in-stent restenosis; (iii) bypass graft vessel; (iv) chronic total occlusion vessel; (v) insufficient OCT image quality; and (vi) antidiabetic therapy change before PCI. If the patient had multiple vessels examined by OCT, only the culprit vessel will be included. Besides, in lipid variability analyses, subjects were excluded if patients had severe renal or hepatic dysfunction, hematology disorder, malignant tumor, and severe infectious diseases. Patients who did not achieve scheduled laboratory tests (at least 3 times lipid assessments and 2 times HbA1c assessments during 1-year follow-up) were considered dropping out. Eventually, a total of 366 culprit vessels from 366 independent subjects were enrolled in the vulnerability feature analyses, and 4,445 patients were enrolled in the visit-to-visit lipid variability analyses. The ethical approval was obtained from the Medical Ethical

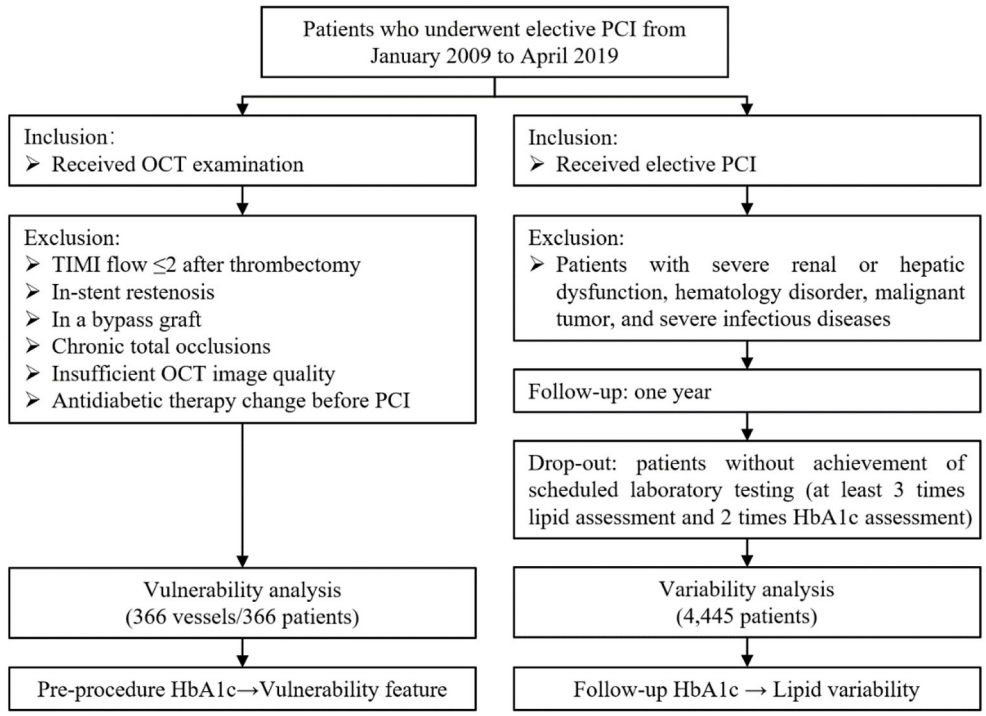

FIGURE 1 | Flow chart of the current study.

Review Committee of Sir Run Run Shaw Hospital (NO. 20201217-36).

The Assessment of HbA1c Levels

Pre-procedure and follow-up HbA1c levels were measured and recorded for analysis. According to the criteria of ADA and WHO, subjects were divided into 3 groups based on HbA1c levels of normal status (Tertile1: HbA1c <5.7%), pre-diabetes status (Tertile2: HbA1c 5.7-6.4%), and diabetes status (Tertile3: HbA1c ≥6.5%) (4). Pre-procedure HbA1c levels were used for vulnerability analysis, and average follow-up HbA1c levels were used for lipid variability analysis. In this study, all patients were recommended the regular HbA1c testing at 3rd, 6th, 9th, and 12th months after the PCI procedure. Enrolled patients should receive at least 2 times HbA1c assessments (interval at least 3 months) during 1-year follow-ups.

The Acquisition of OCT Images

OCT examinations were conducted after intracoronary use of approximately 150 μg nitroglycerin. The current study employed the frequency domain OCT (C7-XR system, Saint Jude Medical, Westford, MA, USA). By using the non-occlusive flushing technique, the OCT imaging catheter was automatically pulled back and scanned for the morphology of culprit vessels at a speed of 20 mm/s. The obtained image was stored digitally. Off-line OCT image analysis was performed using proprietary OCT Review Software.

The Vulnerability Assessment by OCT Examination

Vulnerable morphology features of culprit vessels were defined using previously established criteria (11). Representative OCT images of plaque features were shown in **Figure 2**. The minimal FCT was measured for three times, and a mean value was recorded. The lipid accumulation was a strong signal attenuation region with a signal-rich fibrous cap overlying. The macrophage infiltration was 1 or more signal-rich regions with sharp trailing attenuation that changed frame-by-frame. The calcium depositions were characterized by having poor signals and sharp borders. The angles of lipid accumulation, macrophage infiltration, and calcium deposition were analyzed every 1 mm with the mass center of lumens being angle points, and mean angles were calculated. The length of lipid accumulation, macrophage infiltration, and calcium deposition was computed as the total frame number of each finding multiplied by the distance between adjacent frames. To integrate the angle and length of vulnerability features, a volume index was calculated by mean angle × total length.

The vulnerability feature of culprit vessels was reviewed by 2 experienced interventional cardiologists who were blinded to the angiography and clinical presentation. Repeated measurements of 30 random OCT pullbacks were performed to determine intra-observer reproducibility of the same reader after 4 weeks

following the initial measurement. An analysis of the consistency (inter- and intra-observer) was estimated by the intra-class correlation coefficient (ICC). A good reproducibility of inter- and intra-observer was verified on lipid arcs (ICC = 0.902, 0.917) and macrophage arcs (ICC = 0.875, 0.903), calcium arcs (ICC = 0.892, 0.912), and minimal FCT (ICC = 0.914, 0.927).

The Assessment of Visit-to-Visit Lipid Variability

All subjects were recommended the lipid assessment scheduled at 1st, 3rd, 6th, 9th, and 12th months after the PCI procedure. Enrolled patients should receive at least 3 times lipid assessments during follow-ups. The blood sample was collected after fasting for more than 8 h. For a more comprehensive assessment of lipid variability, three different indices were employed: (i) the standard deviation (SD); (ii) the coefficient of variation (CV, calculated as SD/mean × 100%); (iii) variability independent of the mean (VIM, calculated as SD/mean$^{\alpha}$ × 100%) with α being regression coefficient based on the natural logarithm of SD and the natural logarithm of the mean (21).

Definition

The definition of intensive statin treatment was atorvastatin 40 mg or rosuvastatin 20 mg per day. Subjects were categorized into current smoker or non-current smoker. Current smoker was defined as smoking on admission/quitting smoking for <3 months on admission/any cigarette use during follow-ups. The rest are defined as non-current smokers.

Statistical Analyses

Normally distributed continuous variable was shown as the mean ± SD and compared by one-way analysis of variance (ANOVA). Non-normally distributed continuous variable was shown as median (interquartile range) and compared by the Kruskal-Wallis test. The categorical variable was represented as counts (proportions) and compared using the Chi-square test or Fisher's exact test (if the expected cell value was <5). *P*-value for trend (*P* trend) was calculated with a Wilcoxon type test for continuous variables or a linear-by-linear association for categorical variables across ordered HbA1c categories. The smooth curves visualized the association of HbA1c levels with vulnerability features using the locally weighted scatterplot smoothing (LOWESS) algorithm. The multivariable linear regression model was used to estimate the influence of HbA1c on the vulnerability features and lipid variability after adjusting various covariates involving demographic data, laboratory testing, and medications. Exploratory analyses were conducted in subgroups according to diabetes (yes or no), HbA1c categories (<5.7%, 5.7–6.4%, ≥6.5%), clinical presentation [acute coronary syndrome (ACS) or stable angina pectoris (SAP)], types of statins (atorvastatin or rosuvastatin), and lipid-lowering regimen (regular statins/intensive statins/statins plus ezetimibe).

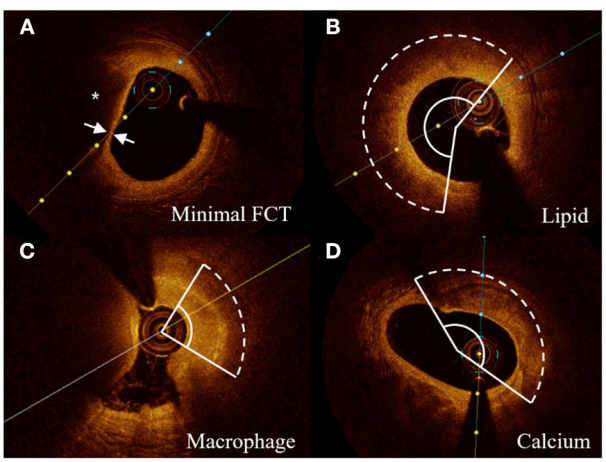

FIGURE 2 | Representative cross-sectional OCT images. **(A)** Lipid core (*) and minimal FCT were detected. **(B–D)** The arcs of lipid accumulation, macrophage infiltration, and calcium deposition were measured in representative cross-sectional OCT images, respectively. FCT indicates fibrous cap thickness.

TABLE 1 | Patient characteristics.

	Vulnerability analysis (*n* = 366)	Variability analysis (*n* = 4,445)
Patient characteristics		
Age, years	61.4 ± 11.1	63.8 ± 10.3
Male, *n* (%)	303 (82.8)	3,187 (71.7)
Current smoker, *n* (%)	144 (39.3)	1,001 (22.5)
Hypertension, *n* (%)	253 (69.1)	2,845 (64.0)
Diabetes mellitus, *n* (%)	115 (31.4)	1,139 (25.6)
Dyslipidemia, *n* (%)	192 (52.5)	2,148 (48.3)
Prior MI, *n* (%)	60 (16.4)	166 (3.7)
Prior PCI, *n* (%)	79 (21.6)	345 (7.7)
Prior CABG, *n* (%)	5 (1.4)	26 (0.6)
Ejection fraction, %	59.7 ± 9.6	64.8 ± 10.1
Clinical presentation, *n* (%)		
Acute coronary syndromes	213 (58.2)	1,028 (23.1)
Stable angina pectoris	153 (41.8)	3,417 (76.9)
Target imaging vessel, *n* (%)		
LAD	176 (48.1)	2,275 (49.4)
LCX	60 (16.4)	738 (16.0)
RCA	130 (35.5)	1,595 (34.6)
Laboratory testing		
HbA1c, %	5.90 ± 1.31	5.98 ± 1.16
LDL-C, mmol/L	2.98 ± 0.94	2.38 ± 0.97
HDL-C, mmol/L	1.17 ± 0.29	1.04 ± 0.28
Triglyceride, mmol/L	1.43 ± 0.84	1.77 ± 1.38
Total cholesterol, mmol/L	4.81 ± 1.06	4.35 ± 1.24
eGFR, ml/min/1.73 m^2	70.6 ± 23.7	85.0 ± 19.7

Values are mean ± SD or n (%). Dyslipidemia is defined LDL-C <1.8 mmol/L. OCT, optical coherence tomography; MI, myocardial infarction; PCI, percutaneous coronary intervention; CABG, coronary artery bypass grafting; LAD, left anterior descending artery; LCX, left circumflex artery; LDL-C, low-density lipoprotein cholesterol; HDL-C, high-density lipoprotein cholesterol; RCA, right coronary artery; eGFR, estimated glomerular filtration rate.

TABLE 2 | Vulnerability features of the culprit vessel by OCT assessment according to HbA1c levels.

	HbA1c <5.7%	HbA1c 5.7–6.4%	HbA1c ≥6.5%	*P* value	*P* trend	Pairwise comparison		
	(*n* = 191)	(*n* = 92)	(*n* = 83)			P_1	P_2	P_3
Minimum lumen area, mm^2	1.16 ± 0.92	1.15 ± 0.83	0.98 ± 0.61	0.378	0.150	–	0.118	–
Mean reference lumen area, mm^2	7.8 ± 4.1	7.0 ± 2.3	6.3 ± 2.1	0.102	0.033*	–	0.038*	–
Percent area stenosis, %	81.7 ± 10.7	80.4 ± 12.6	82.5 ± 9.6	0.733	0.916	–	0.032*	–
Lesion length, mm	23.1 ± 8.0	23.2 ± 9.3	25.1 ± 8.6	0.190	0.113	–	0.082*	0.136
Plaque rupture, *n* (%)	79 (41.3)	27 (29.3)	30 (36.1)	0.143	0.239	0.033*	–	–
Thrombus, *n* (%)	90 (47.1)	30 (32.6)	47 (56.6)	0.005*	0.419	0.014*	0.094	0.001*
Thrombus with plaque rupture, *n* (%)	55 (28.8)	17 (18.5)	25 (30.1)	0.128	0.841	0.062	–	0.072
Thrombus without plaque rupture, *n* (%)	35 (18.3)	13 (14.1)	22 (26.5)	0.106	0.212	–	0.087	0.032*
Calcified nodule, *n* (%)	3 (2.2)	2 (2.9)	3 (4.6)	0.637	0.353	–	–	–
Microchannel, *n* (%)	71 (37.0)	36 (39.1)	37 (44.6)	0.513	0.265	–	0.154	–
Cholesterol crystal, *n* (%)	48 (25.1)	24 (26.1)	29 (34.9)	0.232	0.121	–	0.066	0.134*
Thin–cap fibroatheroma, *n* (%)	80 (41.8)	26 (28.2)	42 (50.6)	0.009*	0.458	0.018*	0.115	0.002*
Minimal fibrous cap thickness, μm	105.0 ± 53.4	101.1 ± 43.0	87.7 ± 44.2	0.008*	0.003*	–	0.003*	0.032*
Lipid characteristics								
Lipid index, degree × mm	1476.8 [847.7, 2213.7]	1521.8 [900.3, 2200.7]	1863.1 [1093.6, 2832.5]	0.004*	0.002*	–	0.003*	0.046*
Lipid length, mm	10.0 [7.0, 15.0]	11.0 [7.0, 14.0]	12.0 [8.0, 18.0]	0.020*	0.009*	–	0.017*	–
Max lipid angle, degree	238.8 [175.1, 305.8]	237.2 [183.4, 289.7]	249.5 [205.4, 309.5]	0.269	0.120	–	0.106	–
Macrophage characteristics								
Macrophage index, degree × mm	385.9 [194.8, 617.5]	412.9 [237.7, 727.3]	437.7 [291.1, 781.1]	0.067	0.049*	–	0.037*	–
Macrophage length, mm	7.0 [4.0, 11.0]	8.0 [4.0, 12.0]	9.0 [6.0, 13.0]	0.075	0.039*	–	0.041*	–
Max macrophage angle, degree	89.0 [66.6, 130.2]	97.5 [65.8, 134.7]	103.6 [69.7, 132.8]	0.412	0.186	–	–	–
Calcium characteristics								
Calcium index, degree × mm	301.4 [129.2, 778.2]	390.2 [182.3, 1114.0]	418.7 [100.6, 986.0]	0.051	0.017*	–	0.023*	–
Calcium length, mm	5.0 [2.0, 10.0]	6.0 [2.0, 12.0]	6.0 [2.0, 13.0]	0.274	0.110	–	–	–
Max calcium angle, degree	93.2 [63.9, 135.5]	119.8 [65.1, 190.0]	107.5 [65.8, 171.7]	0.115	0.128	–	–	–

*Values are mean ± SD or median [interquartile range] for continuous variables and n (%) for categorical variables. P-value < 0.2 for pairwise comparison was presented. Pairwise comparison P_1 indicates P-value for HbA1c < 5.7% vs. HbA1c 5.7–6.4%; P_2, P value for HbA1c < 5.7% vs. HbA1c ≥ 6.5%; P_3, P value for HbA1c 5.7–6.4% vs. HbA1c ≥ 6.5%. *P <0.05.*

A two-tailed *P*-value <0.05 was considered significant. Statistical analysis was performed using SPSS software version 18.0 (SPSS Inc., Chicago, IL, USA) and R version 3.5.1 (The R Foundation for Statistical Computing, Vienna, Austria).

RESULT

Patient Characteristics

Among the subjects who underwent elective PCI, 366 patients (58.2% ACS) were enrolled in the vulnerability feature analysis, and 4,445 patients (23.1% ACS) were enrolled in the lipid variability analysis. Patient characteristics have been summarized in **Table 1** and **Supplementary Tables S1**, **S2**. Patients who received OCT examination were 61.4 ± 11.1 years, with 31.4% diabetes, 69.1% hypertension, and 52.5% dyslipidemia. The pre-procedure HbA1c level was 5.9 ± 1.3%. Among them, 60 (16.4%) subjects had a history of MI, and 79 (21.6%) subjects had a history of PCI. Pre-procedure pharmacologic therapies indicated that 34.4% of patients had statins more than 8 weeks, 35.2% had aspirin, and 27.3% had $P2Y_{12}$ inhibitors. For patients who underwent scheduled follow-ups in lipid variability analysis, the average age was 63.8 ± 10.3 years, of which 64.0% had hypertension and 25.6% had diabetes. The average follow-up HbA1c level was 6.0 ± 1.2%.

Vulnerability Features of Culprit Vessels

OCT findings were summarized in **Table 2** according to pre-procedure HbA1c levels (Tertile1: HbA1c <5.7%, Tertile2: HbA1c 5.7–6.4%, Tertile3: HbA1c ≥6.5%). The vulnerability features were estimated by the minimal FCT, lipid index, macrophage index, and calcium index of the entire culprit vessel. Three-group comparisons identified a significant difference for minimal FCT ($P = 0.008$) and the pairwise comparisons indicated that HbA1c ≥6.5% group had a thinner minimal FCT than HbA1c 5.7–6.4% group (87.7 ± 44.2 vs. 101.1 ± 43.0 μm, $P = 0.032$) and HbA1c <5.7% group (87.7 ± 44.2 vs. 105.0 ± 53.4 μm, $P = 0.003$). Trend analysis showed a decreasing trend in minimum FCT with increasing HbA1c (P trend = 0.003). Besides, there was a significant difference in lipid index between three groups ($P = 0.004$). HbA1c ≥6.5% group showed a greater lipid index than HbA1c 5.7–6.4% group [1863.1 (1093.6, 2832.5) vs. 1521.8 (900.3, 2200.7) mm°, $P = 0.046$] and HbA1c <5.7% group [1863.1 (1093.6, 2832.5) vs. 1476.8 (847.7, 2213.7) mm°, $P = 0.003$], respectively. Trend analysis showed an increasing

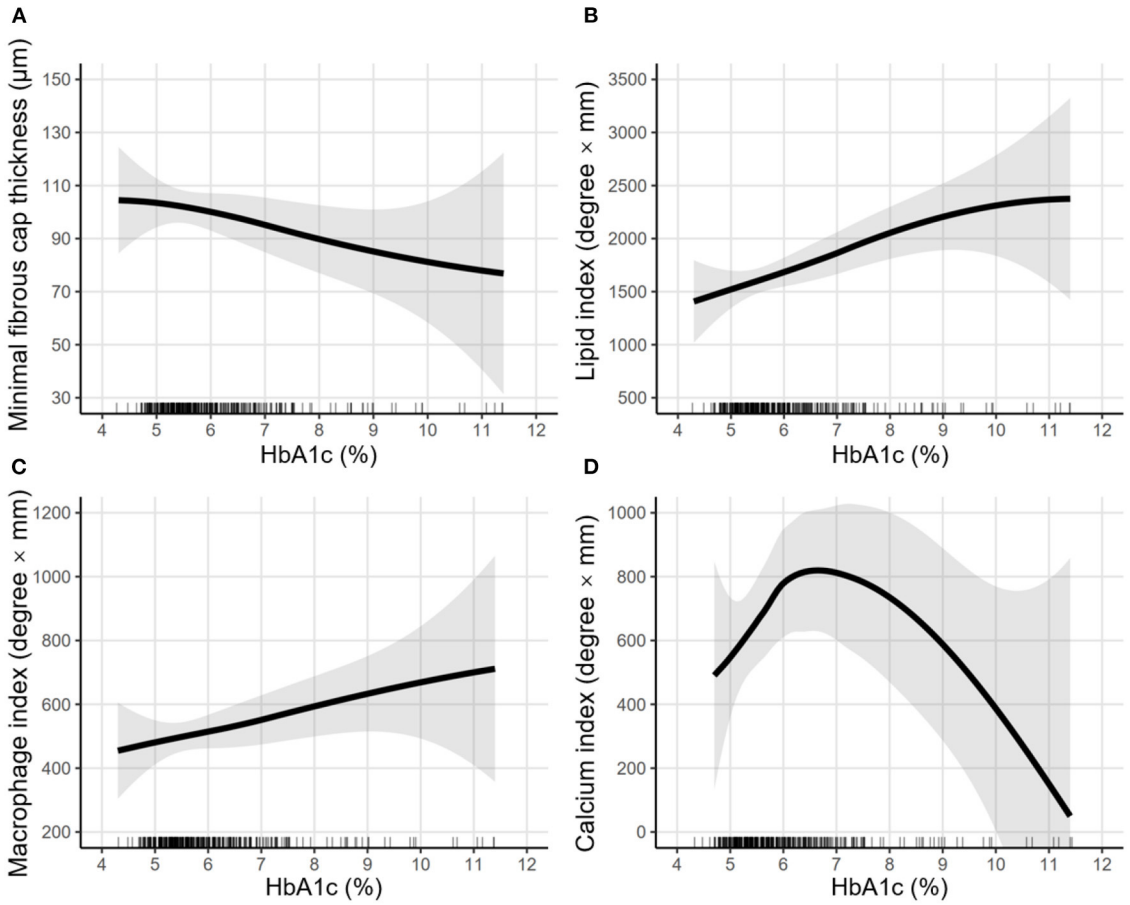

FIGURE 3 | LOWESS curves of the association between pre-procedural HbA1c levels and vulnerability features. Locally weighted scatterplot smoothing (LOWESS) curves were used to visualize the rough association between pre-procedural HbA1c levels and vulnerability features, including **(A)** minimal fibrous cap thickness, **(B)** lipid index, **(C)** macrophage index, and **(D)** calcium index. The semi-transparent ribbon around the solid line indicates the 95% confidence interval. Rug plots show the distribution of pre-procedural HbA1c levels.

trend of lipid index with increasing HbA1c (P trend = 0.002). For macrophage and calcium feature assessment, HbA1c ≥6.5% group had a higher macrophage index [437.7 (291.1, 781.1) vs. 385.9 (194.8, 617.5) mm°, P = 0.037] and a greater calcium index [418.7 (100.6, 986.0) vs. 301.4 (129.2, 778.2) mm°, P = 0.023] than HbA1c <5.7% group. Trend analyses suggested that elevated HbA1c increased macrophage index (P trend = 0.049) and calcium index (P trend = 0.017). Compared to HbA1c <6.5 group, HbA1c ≥6.5 group had greater lesion length [24.00 (18.85, 29.50) vs. 22.20 (17.70, 27.35) mm, P = 0.019], higher prevalence of thrombus (56.6 vs. 42.4%, P = 0.024) and TCFA (50.6 vs. 37.5%, P = 0.041) (**Supplementary Figure S3**).

Effects of Pre-procedure HbA1c Levels on Vulnerability Features

In **Figure 3**, LOWESS curves visualized the rough association of pre-procedural HbA1c levels with minimal FCT (downtrend), lipid index (uptrend), macrophage index (uptrend), and calcium index (reverse U-shaped). Linear regression models with multiple adjustments were subsequently performed and proved that elevated HbA1c was an independent risk factor for thinner minimal FCT [β = −6.985, 95% CI (−13.902 to −0.068), P = 0.048], higher lipid index [β = 226.299, 95% CI (67.977–384.621), P = 0.005], and greater macrophage index [β = 54.526, 95% CI (1.268–107.785), P = 0.045] (**Table 3**). Consistently, in non-diabetic CAD patients, elevated pre-procedure HbA1c still linearly decrease minimal FCT [β = −14.011, 95% CI (−27.393 to −1.221), P = 0.036], increase lipid index [β = 290.048, 95% CI (25.041–582.264), P = 0.041], and increase macrophage index [β = 120.029, 95% CI (2.031–240.362), P = 0.048] (**Figure 4**).

The Visit-to-Visit Variability of Lipid Profile During Follow-Ups

Patient characteristics of variability analysis were summarized in **Supplementary Table S2** according to the average follow-up HbA1c categories (Tertile1: HbA1c <5.7%, Tertile2: HbA1c 5.7–6.4%, Tertile3: HbA1c ≥6.5%). Three-group comparisons indicated that elevated follow-up average HbA1c levels were associated with greater VIM of lipid profiles, including LDL-C (Tertile1: 74.8 ± 44.2; Tertile2: 76.0 ± 47.5; Tertile3: 80.0 ±

TABLE 3 | Linear regression analyses of pre-procedure HbA1c levels on vulnerability features.

	Model 1		Model 2		Model 3	
	Unadjusted-β [95% CI]	***P*-value**	**Adjusted-β [95% CI]**	***P*-value**	**Adjusted-β [95% CI]**	***P*-value**
Minimal FCT	−4.528 [−9.308 to 0.252]	0.063	−6.735 [−13.589 to 0.119]	0.054	−6.985 [−13.902 to −0.068]	0.048*
Lipid index	240.686 [133.924 to 347.448]	<0.001*	226.835 [71.11 to 382.561]	0.004*	226.299 [67.977 to 384.621]	0.005*
Macrophage index	38.248 [2.206 to 74.29]	0.038*	57.451 [5.227 to 109.675]	0.031*	54.526 [1.268 to 107.785]	0.045*
Calcium index	31.816 [−75.623 to 139.255]	0.560	−100.204 [−255.258 to 54.849]	0.204	−81.223 [−239.805 to 77.358]	0.314

Model 1 adjusted for none.

Model 2 adjusted for age, male, diabetes, hypertension, prior myocardial infarction, prior percutaneous coronary intervention, current smoker, low-density lipoprotein cholesterol, ejection fraction, estimated glomerular filtration rate.

Model 3 additionally adjusted for covariates of pre-procedure medications, including statin, aspirin, $P2Y_{12}$ inhibitor, insulin treatment.

*FCT indicates fibrous cap thickness; CI, confidence interval. *P < 0.05.*

46.9/1,000, $P = 0.029$), HDL-C (Tertile1: 30.5 ± 12.6; Tertile2: 30.7 ± 13.9; Tertile3: 32.9 ± 15.4/1,000, $P < 0.001$), non-HDL-C (Tertile1: 20.0 ± 14.9; Tertile2: 20.9 ± 17.1; Tertile3: 22.8 ±1 8.0/1,000, $P = 0.001$), TC (Tertile1: 7.7 ± 6.5; Tertile2: 8.4 ± 7.3; Tertile3: 9.7 ± 8.3/1,000, $P < 0.001$), and TG (Tertile1: 27.6 ± 27.9; Tertile2: 27.3 ± 25.5; Tertile3: 35.4 ± 40.7/1,000, $P < 0.001$) (**Supplementary Table S2**). The consistent results were confirmed when SD or CV was used to estimate variability (**Supplementary Table S2**).

Effects of Follow-Up HbA1c Levels on Lipid Variability

Multivariable linear regression analyses were performed and found that elevated follow-up HbA1c led to greater VIM of lipid profiles, including LDL-C [$\beta = 2.594$, 95% CI (1.175–4.013), $P < 0.001$], HDL-C [$\beta = 0.461$, 95% CI (0.012–0.911), $P = 0.044$], Non-HDL-C [$\beta = 1.473$, 95% CI (0.926–2.021), $P < 0.001$], TC [$\beta = 0.947$, 95% CI (0.721–1.174), $P < 0.001$], and TG [$\beta = 4.217$, 95% CI (3.186–5.249), $P < 0.001$] (**Table 4**). Consistently, the findings remained when SD or CV was employed (**Supplementary Tables S4**, **S5**).

Consistently, in non-diabetic patients, elevated follow-up HbA1c levels still increased the VIM of lipid profiles, including LDL-C [$\beta = 3.457$, 95% CI (1.001–5.914), $P = 0.006$], Non-HDL-C [$\beta = 2.193$, 95% CI (1.277–3.110), $P < 0.001$], TC ($\beta = 1.415$, 95% CI (1.036–1.794), $P < 0.001$], and TG [$\beta = 6.172$, 95% CI (4.622–7.721), $P < 0.001$] (**Figure 5**). Consistently, the findings remained when SD or CV was employed (**Supplementary Figures S1**, **S2**).

DISCUSSION

This retrospective observational study enrolled the patient who underwent elective PCI. By using OCT assessment, elevated pre-procedure HbA1c level was verified to increase the plaque vulnerability of culprit vessels, including thinner minimal FCT, higher lipid index, and greater macrophage index. Besides, elevated average follow-up HbA1c level was identified as an independent risk factor for higher visit-to-visit variability of lipids, including LDL-C, HDL-C, non-HDL-C, TC, and TG. Exploratory analyses also confirmed that the above findings were consistent in non-diabetic patients.

Due to the high resolution (10–15 μm), OCT provides a detailed depiction of the vulnerable features in atherosclerotic lesions, which has been recognized as the gold standard for coronary morphology evaluation (22). Numerous studies have shown that abnormal glucose metabolism is associated with increased plaque vulnerability, which thus leads to the incidence of adverse cardiovascular events (2). By using OCT assessment, Milzi et al. found that the presence of type 2 DM was associated with a thinner FCT in CAD patients (23). Suzuki et al. found that patients with impaired glucose tolerance had larger lipid cores and thinner FCT compared to patients with normal glucose tolerance (24). Kato et al. proved that macrophage infiltration was more frequent in patients with HbA1c ≥8% (25). By using magnetic resonance imaging, Sun et al. found that elevated HbA1c was correlated with greater carotid plaque vulnerability (26). Consistently, by using OCT assessment in 366 independent CAD patients, the current study demonstrated that elevated HbA1c increased the atherosclerotic plaque vulnerability, including thinner minimal FCT, greater lipid index, and higher macrophage index.

Some underlying mechanisms may be involved in the vulnerable features. For features of lipid and FCT, the elevation of HbA1c may contribute to lipid accumulation in culprit vessels by directly raising serum atherogenic lipid levels. In previous studies, increased glucose levels have been verified to up-regulated atherogenic lipid levels throughout the entire range of blood glucose (27, 28). Elevated atherogenic lipids can lead to lipid accumulation in the coronary artery, which thus promotes the progression of atherosclerosis and makes FCT thinner (29).

For the macrophage features, elevated HbA1c may increase macrophage infiltration by up-regulating the level of chronic inflammation. Chronic exposure to hyperglycemia and insulin resistance has been found to up-regulate inflammation levels through endoplasmic reticulum stress and mitochondrial superoxide overproduction, thereby promoting macrophage

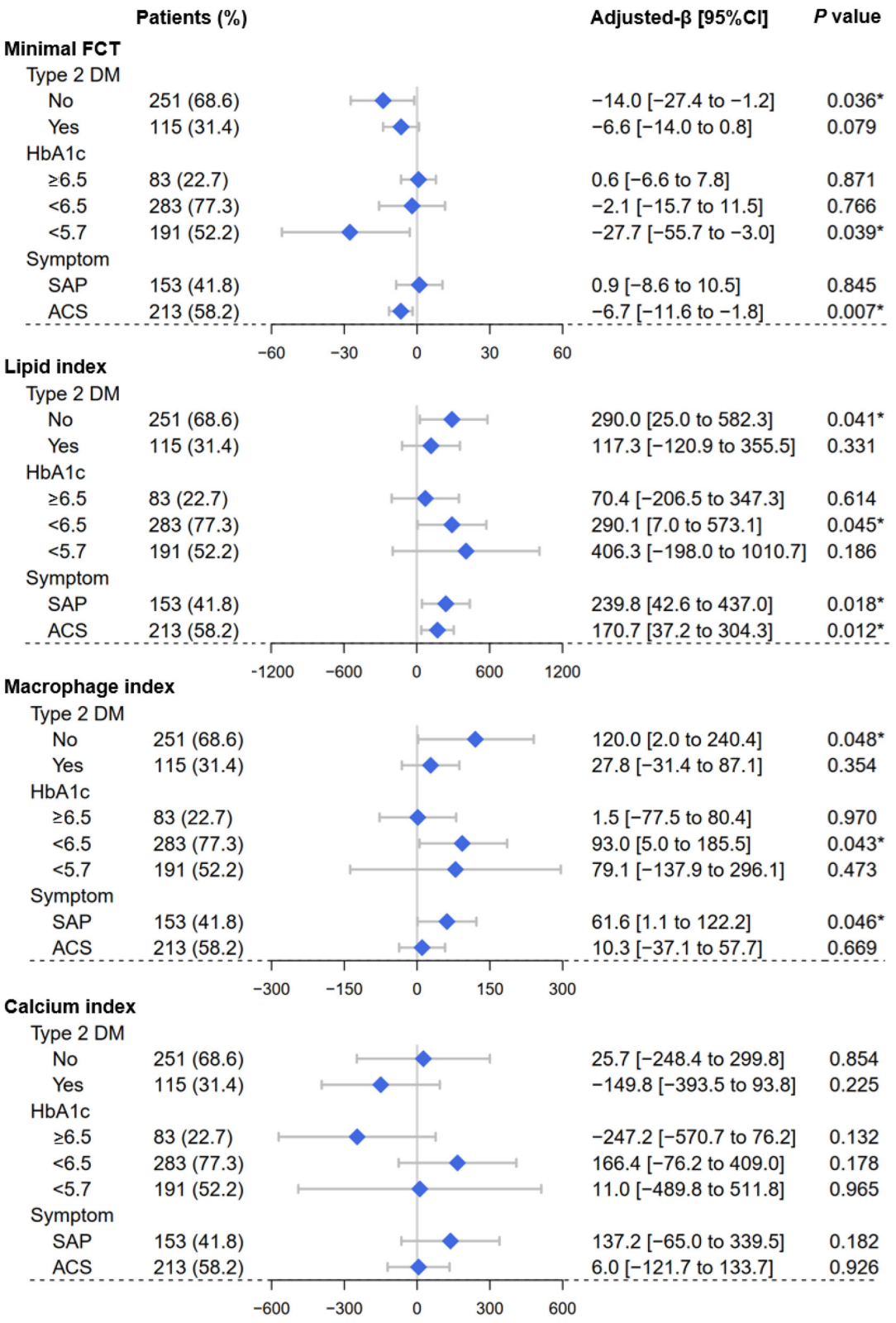

FIGURE 4 | Forest plots of the vulnerability feature analyses. By using OCT assessment, forest plots depicted the effect of pre-procedure HbA1c levels on the vulnerability feature of culprit vessels, including minimal fibrous cap thickness, lipid index, macrophage index, and calcium index. Subgroups were determined according to Type 2 DM (yes or no), HbA1c categories (<5.7%, 5.7–6.4%, ≥6.5%), clinical symptom (SAP or ACS). OCT, optical coherence tomography; SAP, stable angina pectoris; ACS, acute coronary syndrome; FCT, fibrous cap thickness; DM, diabetes mellitus. *$P < 0.05$.

TABLE 4 | Linear regression analyses of average follow-up HbA1c levels on the visit-to-visit variability of lipid profiles.

The VIM of lipid profiles	Model 1		Model 2		Model 3	
	Unadjusted-β [95% CI]	*P*-value	Adjusted-β [95% CI]	*P*-value	Adjusted-β [95% CI]	*P*-value
LDL-C	2.802 [1.600–4.005]	<0.001	3.465 [1.953–4.978]	<0.001	2.594 [1.175–4.013]	<0.001
HDL-C	0.634 [0.271–0.996]	0.001	0.544 [0.090–0.998]	0.019	0.461 [0.012–0.911]	0.044
Non-HDL-C	1.221 [0.777–1.666]	<0.001	1.653 [1.094–2.213]	<0.001	1.473 [0.926–2.021]	<0.001
TC	0.849 [0.659–1.039]	<0.001	1.069 [0.831–1.308]	<0.001	0.947 [0.721–1.174]	<0.001
TG	3.710 [2.895–4.526]	<0.001	4.345 [3.321–5.370]	<0.001	4.217 [3.186–5.249]	<0.001

Model 1 adjusted for none.

Model 2 adjusted for age, male, diabetes, hypertension, prior myocardial infarction, prior percutaneous coronary intervention, current smoker, ejection fraction, estimated glomerular filtration rate.

Model 3 additionally adjusted for covariates of medications during follow-up, including the type of statin (atorvastatin/rosuvastatin/others), the intensive statin treatment (vs. regular), statin combined with ezetimibe treatment (vs. without), insulin treatment (vs. without).

Lipid variability was represented by VIM. VIM, variability independent of the mean; LDL-C, low-density lipoprotein cholesterol; HDL-C, high-density lipoprotein cholesterol; TC, total cholesterol; TG, triglyceride; CI, confidence interval.

adhesion to the vascular wall and the development of atherosclerosis (30, 31). Indeed, the up-regulation of inflammation levels has been detected as early as pre-diabetes status (32).

For calcium features, it is still a controversial issue regarding the association between abnormal glucose metabolism and coronary calcium deposits. Some studies have shown that the presence of type 2 DM increases the calcium burden in the coronary artery (33, 34). While by using OCT assessment, Milzi et al. proved that the presence of type 2 DM was not related to calcium deposits in culprit lesions (23). In the current study, the pairwise comparison indicated that HbA1c ≥6.5% group had a greater calcium index than HbA1c <5.7% group [418.7 (100.6, 986.0) vs. 301.4 (129.2, 778.2) mm°, $P = 0.023$]. However, no significant linear correlation was found between HbA1c and calcium index. This may be due to the fact that calcium index is less affected by HbA1c levels, compared to other vulnerable features.

The visit-to-visit variability of lipid profiles has been identified as an independent risk factor for adverse cardiovascular events (17). By intravascular ultrasound examination, the association between higher lipid variability and greater plaque vulnerability has been revealed (12). Furthermore, the current study verified the close relationship between the elevated follow-up HbA1c levels and the visit-to-visit variability of lipid profiles, which was also confirmed in non-diabetic patients.

Although the mechanism is not entirely clear, several possible explanations are worth considering. On the one hand, genome-wide association analysis has indicated an underlying association between glucose dysregulation of lipid variability. For instance, DKK3 (Dickkopf-3) gene expression is positively correlated to the visit-to-visit variability of HDL-C (19). Meanwhile, DKK3 was aberrantly expressed in β-cells of patients with type 2 diabetes, which can inhibit the Wnt signaling pathway, thereby depressing the survival and proliferation of β cells (20). The suppression of β cells could lead to an increased HbA1c level. On the other hand, medication non-compliance is also one of the potential explanations. Medication non-compliance has been shown to not only increase the visit-to-visit lipid variability but is also related to poor glycemic control in diabetic patients (35, 36). Therefore, the positive correlation between HbA1c levels and lipid variability may partly result from medication non-compliance.

Some new insights in the current study are worth noting. On the one hand, the current study confirmed that even in non-diabetic patients, elevated HbA1c increases not only plaque vulnerability but also the visit-to-visit lipid variability. These results provide a novel idea for preventive medicine that preventive glucose management may benefit non-diabetic CAD patients. On the other hand, the current study verified the association of elevated HbA1c with higher lipid index and greater macrophage index in patients with SAP, who had a relatively fewer plaques rupture event. This indicates that elevated HbA1c levels have already exerted an influence on the plaque vulnerability before plaque rupture.

The current study still has several limitations. First, the inherent bias cannot be eliminated due to the retrospective design. Second, HbA1c levels can be affected by antidiabetic therapy. The regression analysis has adjusted for the covariate of insulin therapy. However, detailed antidiabetic therapy was not further adjusted and may introduce potential bias. Third, some patients did not strictly comply with the follow-up procedures scheduled at 1st, 3rd, 6th, 9th, and 12th months following PCI, which may affect the assessment of lipid variability. Finally, the current study did not address the long-term clinical outcome, which was expected in further studies.

CONCLUSION

In patients undergoing elective PCI, elevated HbA1c increases the atherosclerotic plaque vulnerability and the visit-to-visit variability of lipid profiles, which is consistent in non-diabetic patients.

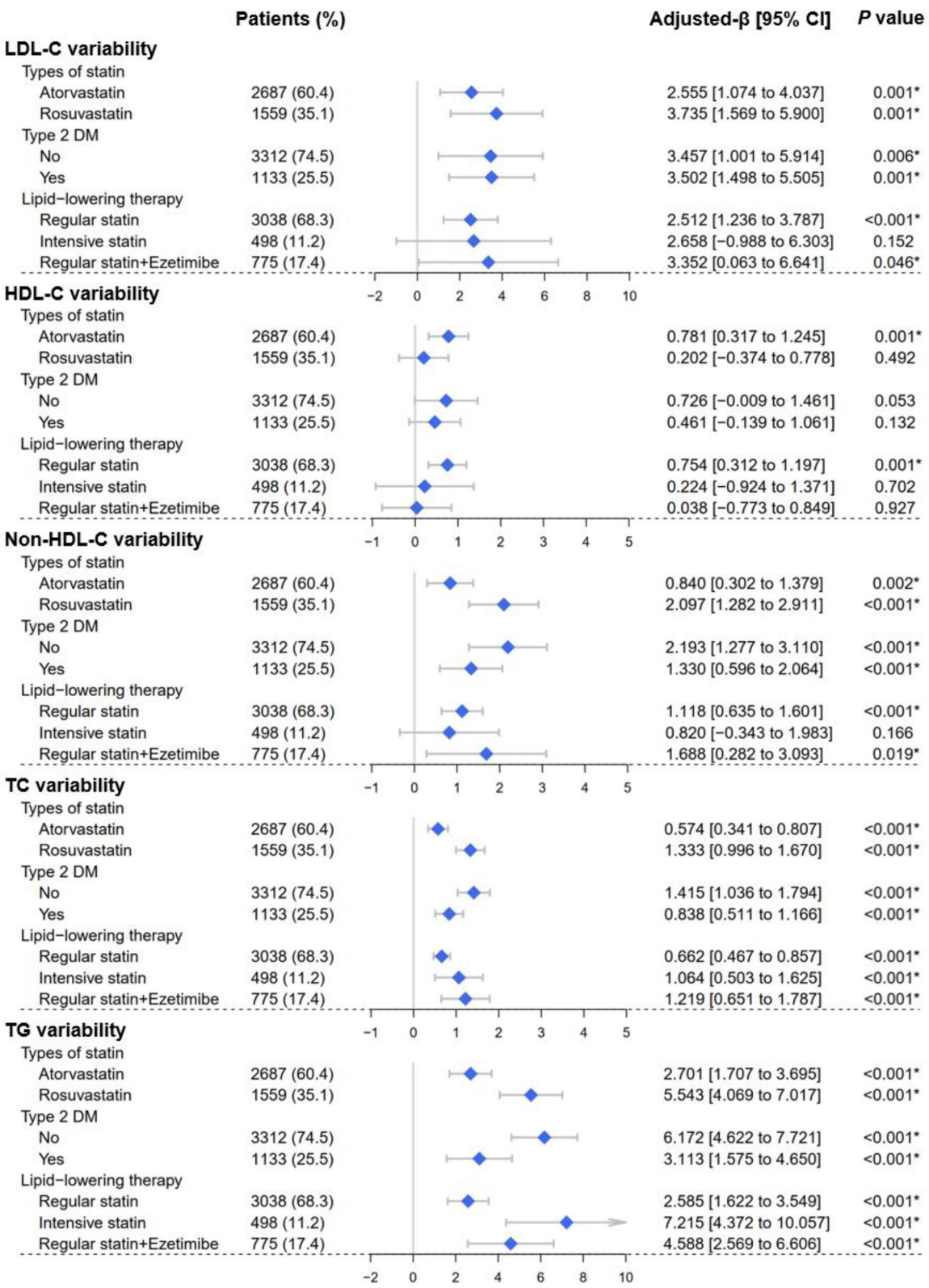

FIGURE 5 | Forest plots of the lipid variability analyses. Forest plots depicted the effect of average follow-up HbA1c levels on visit-to-visit variability of lipid profiles, including LDL-C, HDL-C, Non-HDL-C, TC, and TG. Lipid variability was represented by the variability independent of the mean (VIM). Subgroups were determined according to Type 2 DM (yes or no), types of statins (atorvastatin or rosuvastatin), and lipid-lowering therapy strategy (regular statins/intensive statins/statins plus ezetimibe). LDL-C, low-density lipoprotein cholesterol; HDL-C, high-density lipoprotein cholesterol; Non-HDL-C, non-high-density lipoprotein cholesterol; TC, total cholesterol; TG, triglyceride; DM, diabetes mellitus. *$P < 0.05$.

DATA AVAILABILITY STATEMENT

The raw data supporting the conclusions of this article will be made available by the authors, without undue reservation.

ETHICS STATEMENT

The studies involving human participants were reviewed and approved by the Ethics Committee of Sir Run Run Shaw Hospital of Zhejiang University. Written informed consent for participation was not required for this study in accordance with the national legislation and the institutional requirements.

AUTHOR CONTRIBUTIONS

WZ, ZC, and XS conceived and designed the study. DL organized these data and drafted the manuscript with the help of YLi, CW, and HJ. DL analyzed the data. LZ drew the pictures. XH, ML, and YLu detected any errors in the whole process. All authors have read and approved the manuscript for submission.

FUNDING

This work was supported by grants from the National Natural Science Foundation of China (82070408), the Medical Health Science and Technology Project of Zhejiang Provincial Health Commission (2021RC014), the Traditional Chinese Medicine Science and Technology Project of Zhejiang Province (2021ZB172), and the Joint Funds for the Innovation of Science and Technology, Fujian province (2018Y9094).

SUPPLEMENTARY MATERIAL

The Supplementary Material for this article can be found online at: https://www.frontiersin.org/articles/10.3389/fcvm.2022.803036/full#supplementary-material

REFERENCES

1. Joseph P, Leong D, McKee M, Anand SS, Schwalm J-D, Teo K, et al. Reducing the global burden of cardiovascular disease, part 1: the epidemiology and risk factors. *Circ Res.* (2017) 121:677–94. doi: 10.1161/CIRCRESAHA.117.308903
2. Eckel RH, Wassef M, Chait A, Sobel B, Barrett E, King G, et al. Prevention conference VI: diabetes and cardiovascular disease: writing group II: pathogenesis of atherosclerosis in diabetes. *Circulation.* (2002) 105:e138–43. doi: 10.1161/01.CIR.0000013954.65303.C5
3. American Diabetes Association. Glycemic targets: standards of medical care in diabetes-2020. *Diabetes Care.* (2020) 43:S66–76. doi: 10.2337/dc20-S006
4. American Diabetes Association. Diagnosis and classification of diabetes mellitus. *Diabetes Care.* (2014) 37(Suppl. 1):S81–90. doi: 10.2337/dc14-S081
5. Xu L, Chan WM, Hui YF, Lam TH. Association between HbA1c and cardiovascular disease mortality in older Hong Kong Chinese with diabetes. *Diabet Med.* (2012) 29:393–8. doi: 10.1111/j.1464-5491.2011.03456.x
6. Geng J, Zhang Y, Wang B, Xie J, Xu B, Li J. Glycosylated hemoglobin levels and clinical outcomes in nondiabetic patients with coronary artery disease: a meta-analysis. *Medicine.* (2017) 96:e6784. doi: 10.1097/MD.0000000000006784
7. Liu Y, Yang YM, Zhu J, Tan HQ, Liang Y, Li JD. Prognostic significance of hemoglobin A1c level in patients hospitalized with coronary artery disease. A systematic review and meta-analysis. *Cardiovasc Diabetol.* (2011) 10:98. doi: 10.1186/1475-2840-10-98
8. Zhang D, He L, Yu B. Advances in the identification and treatment of coronary vulnerable plaques by intravascular imaging. *Chin J Interv Cardiol.* (2021) 9:520–2. doi: 10.3969/j.issn.1004-8812.2021.008
9. Fan L, Chen Q, Han Z, Zhuo Y, Hu J, Zeng H, et al. Layered plaque assessed by optical coherence tomography is related to coronary artery plaque vulnerability. *Chin J Interv Cardiol.* (2021) 9:484–9. doi: 10.3969/j.issn.1004-8812.2021.002
10. Aguirre AD, Arbab-Zadeh A, Soeda T, Fuster V, Jang IK. Optical coherence tomography of plaque vulnerability and rupture: JACC focus seminar part 1/3. *J Am Coll Cardiol.* (2021) 78:1257–65. doi: 10.1016/j.jacc.2021.06.050
11. Tearney GJ, Regar E, Akasaka T, Adriaenssens T, Barlis P, Bezerra HG, et al. Consensus standards for acquisition, measurement, and reporting of intravascular optical coherence tomography studies: a report from the International Working Group for Intravascular Optical Coherence Tomography Standardization and Validation. *J Am Coll Cardiol.* (2012) 59:1058–72. doi: 10.1016/j.jacc.2011.09.079
12. Clark D III, Nicholls SJ, St John J, Elshazly MB, Kapadia SR, Tuzcu EM, et al. Visit-to-visit cholesterol variability correlates with coronary atheroma progression and clinical outcomes. *Eur Heart J.* (2018) 39:2551–8. doi: 10.1093/eurheartj/ehy209
13. Zhao L, Xu T, Li Y, Luan Y, Lv Q, Fu G, et al. Variability in blood lipids affects the neutrophil to lymphocyte ratio in patients undergoing elective percutaneous coronary intervention: a retrospective study. *Lipids Health Dis.* (2020) 19:124. doi: 10.1186/s12944-020-01304-9
14. Han BH, Han K, Yoon KH, Kim MK, Lee SH. Impact of mean and variability of high-density lipoprotein-cholesterol on the risk of myocardial infarction, stroke, and mortality in the general population. *J Am Heart Assoc.* (2020) 9:e015493. doi: 10.1161/JAHA.119.015493
15. Boey E, Gay GM, Poh KK, Yeo TC, Tan HC, Lee CH. Visit-to-visit variability in LDL- and HDL-cholesterol is associated with adverse events after ST-segment elevation myocardial infarction: a 5-year follow-up study. *Atherosclerosis.* (2016) 244:86–92. doi: 10.1016/j.atherosclerosis.2015.10.110
16. Wan EYF, Yu EYT, Chin WY, Barrett JK, Mok AHY, Lau CST, et al. Greater variability in lipid measurements associated with cardiovascular disease and mortality: a 10-year diabetes cohort study. *Diabetes Obes Metab.* (2020) 22:1777–88. doi: 10.1111/dom.14093
17. Lee EY, Yang Y, Kim HS, Cho JH, Yoon KH, Chung WS, et al. Effect of visit-to-visit LDL-, HDL-, and non-HDL-cholesterol variability on mortality and cardiovascular outcomes after percutaneous coronary intervention. *Atherosclerosis.* (2018) 279:1–9. doi: 10.1016/j.atherosclerosis.2018.10.012
18. Kim MK, Han K, Kim HS, Park YM, Kwon HS, Yoon KH, et al. Cholesterol variability and the risk of mortality, myocardial infarction, and stroke: a nationwide population-based study. *Eur Heart J.* (2017) 38:3560–6. doi: 10.1093/eurheartj/ehx585
19. Smit RAJ, Jukema JW, Postmus I, Ford I, Slagboom PE, Heijmans BT, et al. Visit-to-visit lipid variability: clinical significance, effects of lipid-lowering treatment, and (pharmaco) genetics. *J Clin Lipidol.* (2018) 12:266–76.e63. doi: 10.1016/j.jacl.2018.01.001
20. Kuljanin M, Bell GI, Sherman SE, Lajoie GA, Hess DA. Proteomic characterisation reveals active Wnt-signalling by human multipotent stromal cells as a key regulator of beta cell survival and proliferation. *Diabetologia.* (2017) 60:1987–98. doi: 10.1007/s00125-017-4355-7
21. Rothwell PM, Howard SC, Dolan E, O'Brien E, Dobson JE, Dahlöf B, et al. Prognostic significance of visit-to-visit variability, maximum systolic blood pressure, and episodic hypertension. *Lancet.* (2010) 375:895–905. doi: 10.1016/S0140-6736(10)60308-X
22. Reith S, Battermann S, Hoffmann R, Marx N, Burgmaier M. Optical coherence tomography derived differences of plaque characteristics in coronary culprit lesions between type 2 diabetic patients with and without acute coronary syndrome. *Catheter Cardiovasc Interv.* (2014) 84:700–7. doi: 10.1002/ccd.25267
23. Milzi A, Burgmaier M, Burgmaier K, Hellmich M, Marx N, Reith S. Type 2 diabetes mellitus is associated with a lower fibrous cap thickness

but has no impact on calcification morphology: an intracoronary optical coherence tomography study. *Cardiovasc Diabetol.* (2017) 16:152. doi: 10.1186/s12933-017-0635-2
24. Suzuki K, Takano H, Kubota Y, Inui K, Nakamura S, Tokita Y, et al. Plaque characteristics in coronary artery disease patients with impaired glucose tolerance. *PLoS ONE.* (2016) 11:e0167645. doi: 10.1371/journal.pone.0167645
25. Kato K, Yonetsu T, Kim SJ, Xing L, Lee H, McNulty I, et al. Comparison of nonculprit coronary plaque characteristics between patients with and without diabetes A 3-vessel optical coherence tomography study. *JACC Cardiovasc Interv.* (2012) 5:1150–8. doi: 10.1016/j.jcin.2012.06.019
26. Sun B, Zhao H, Liu X, Lu Q, Zhao X, Pu J, et al. Elevated hemoglobin A1c is associated with carotid plaque vulnerability: novel findings from magnetic resonance imaging study in hypertensive stroke patients. *Sci Rep.* (2016) 6:33246. doi: 10.1038/srep33246
27. Zhang L, Qiao Q, Tuomilehto J, Hammar N, Alberti KG, Eliasson M, et al. Blood lipid levels in relation to glucose status in European men and women without a prior history of diabetes: the DECODE Study. *Diabetes Res Clin Pract.* (2008) 82:364–77. doi: 10.1016/j.diabres.2008.08.022
28. Zhang L, Qiao Q, Tuomilehto J, Hammar N, Janus ED, Soderberg S, et al. Blood lipid levels in relation to glucose status in seven populations of Asian origin without a prior history of diabetes: the DECODA study. *Diabetes Metab Res Rev.* (2009) 25:549–57. doi: 10.1002/dmrr.994
29. Li Fan ZX, Qizhi C, Yang Z, Changqian W. Relationship between characteristics of coronary artery lesions and plaque prolapse after stent guided by optical coherence tomography. *Chin J Interv Cardiol.* (2020) 182:506–10. doi: 10.3969/j.issn.1004-8812.2020.09.006
30. Ramji DP, Davies TS. Cytokines in atherosclerosis: key players in all stages of disease and promising therapeutic targets. *Cytokine Growth Factor Rev.* (2015) 26:673–85. doi: 10.1016/j.cytogfr.2015.04.003
31. Giacco F, Brownlee M. Oxidative stress and diabetic complications. *Circ Res.* (2010) 107:1058–70. doi: 10.1161/CIRCRESAHA.110.223545
32. Al-Daghri NM, Al-Ajlan AS, Alfawaz H, Yakout SM, Aljohani N, Kumar S, et al. Serum cytokine, chemokine and hormone levels in Saudi adults with pre-diabetes: a one-year prospective study. *Int J Clin Exp Pathol.* (2015) 8:11587–93.
33. Nicoll R, Zhao Y, Ibrahimi P, Olivecrona G, Henein M. Diabetes and hypertension consistently predict the presence and extent of coronary artery calcification in symptomatic patients: a systematic review and meta-analysis. *Int J Mol Sci.* (2016) 17:1481. doi: 10.3390/ijms17091481
34. Wong ND, Nelson JC, Granston T, Bertoni AG, Blumenthal RS, Carr JJ, et al. Metabolic syndrome, diabetes, and incidence and progression of coronary calcium: the Multiethnic Study of Atherosclerosis study. *JACC Cardiovasc Imaging.* (2012) 5:358–66. doi: 10.1016/j.jcmg.2011.12.015
35. Mann DM, Glazer NL, Winter M, Paasche-Orlow MK, Muntner P, Shimbo D, et al. A pilot study identifying statin nonadherence with visit-to-visit variability of low-density lipoprotein cholesterol. *Am J Cardiol.* (2013) 111:1437–42. doi: 10.1016/j.amjcard.2013.01.297
36. Raum E, Kramer HU, Ruter G, Rothenbacher D, Rosemann T, Szecsenyi J, et al. Medication non-adherence and poor glycaemic control in patients with type 2 diabetes mellitus. *Diabetes Res Clin Pract.* (2012) 97:377–84. doi: 10.1016/j.diabres.2012.05.026

Conflict of Interest: The authors declare that the research was conducted in the absence of any commercial or financial relationships that could be construed as a potential conflict of interest.

The reviewer HM declared a shared affiliation, though no other collaboration, with several of the authors, HJ and LZ, to the handling editor.

Publisher's Note: All claims expressed in this article are solely those of the authors and do not necessarily represent those of their affiliated organizations, or those of the publisher, the editors and the reviewers. Any product that may be evaluated in this article, or claim that may be made by its manufacturer, is not guaranteed or endorsed by the publisher.

Copyright © 2022 Li, Li, Wang, Jiang, Zhao, Hong, Lin, Luan, Shen, Chen and Zhang. This is an open-access article distributed under the terms of the Creative Commons Attribution License (CC BY). The use, distribution or reproduction in other forums is permitted, provided the original author(s) and the copyright owner(s) are credited and that the original publication in this journal is cited, in accordance with accepted academic practice. No use, distribution or reproduction is permitted which does not comply with these terms.

frontiers in Cardiovascular Medicine

ORIGINAL RESEARCH
published: 08 March 2022
doi: 10.3389/fcvm.2022.774193

Exosome-Derived From Sepsis Patients' Blood Promoted Pyroptosis of Cardiomyocytes by Regulating miR-885-5p/HMBOX1

Guo-wei Tu[1†], Jie-fei Ma[1,2†], Jia-kun Li[1], Ying Su[1], Jing-chao Luo[1], Guang-wei Hao[1], Ming-hao Luo[3], Yi-rui Cao[4], Yi Zhang[4,5] and Zhe Luo[1,2,6*]*

[1] Department of Critical Care Medicine, Zhongshan Hospital, Fudan University, Shanghai, China, [2] Department of Critical Care Medicine, Xiamen Branch, Zhongshan Hospital, Fudan University, Xiamen, China, [3] Shanghai Medical College, Fudan University, Shanghai, China, [4] Shanghai Key Laboratory of Organ Transplantation, Shanghai, China, [5] Biomedical Research Center, Institute for Clinical Sciences, Zhongshan Hospital, Fudan University, Shanghai, China, [6] Shanghai Key Laboratory of Lung Inflammation and Injury, Shanghai, China

OPEN ACCESS

Edited by:
Hongmei Tan,
Sun Yat-sen University, China

Reviewed by:
Zhiyan Wang,
Shanghai Jiao Tong University, China
Hao Wang,
Shandong University, China

***Correspondence:**
Zhe Luo
luo.zhe@zs-hospital.sh.cn
Yi Zhang
yzhang_med@fudan.edu.cn

[†] These authors have contributed equally to this work

Specialty section:
This article was submitted to General Cardiovascular Medicine, a section of the journal Frontiers in Cardiovascular Medicine

Received: 11 September 2021
Accepted: 24 January 2022
Published: 08 March 2022

Citation:
Tu G-w, Ma J-f, Li J-k, Su Y, Luo J-c, Hao G-w, Luo M-h, Cao Y-r, Zhang Y and Luo Z (2022) Exosome-Derived From Sepsis Patients' Blood Promoted Pyroptosis of Cardiomyocytes by Regulating miR-885-5p/HMBOX1. Front. Cardiovasc. Med. 9:774193. doi: 10.3389/fcvm.2022.774193

Background: Septic myocardial depression has been associated with increased morbidity and mortality. miR-885-5p has been shown to regulate cell growth, senescence, and/or apoptosis. Published studies demonstrated that Homeobox-containing protein 1 (HMBOX1) inhibits inflammatory response, regulates cell autophagy, and apoptosis. However, the role of miR-885-5p/HMBOX1 in sepsis and septic myocardial depression and the underlying mechanism is not fully understood.

Materials and Methods: Exosomes (exos) derived from sepsis patients (sepsis-exos) were isolated using ultracentrifugation. Rats were subjected to cecal ligation and puncture surgery and treated with sepsis-exos. HMBOX1 was knocked down or overexpressed in AC16 cells using lentiviral plasmids carrying short interfering RNAs targeting human HMBOX1 or carrying HMBOX1 cDNA. Cell pyroptosis was measured by flow cytometry. The secretion of IL-1β and IL-18 was examined by ELISA kits. Quantitative polymerase chain reaction (PCR) or western blot was used for gene expression.

Results: Sepsis-exos increased the level of miR-885-5p, decreased HMBOX1, elevated IL-1β and IL-18, and promoted pyroptosis in AC16 cells. Septic rats treated with sepsis-exos increased the serum inflammatory cytokines is associated with increased pyroptosis-related proteins of hearts. MiR-885-5p bound to the three prime untranslated regions of HMBOX1 to negatively regulate its expression. Overexpressing HMBOX1 reversed miR-885-5p-induced elevation of inflammatory cytokines and upregulation of NLRP3, caspase-1, and GSDMD-N in AC16 cells. The mechanistic study indicated that the effect of HMBOX1 was NF-κB dependent.

Conclusion: Sepsis-exos promoted the pyroptosis of AC16 cells through miR-885-5p *via* HMBOX1. The results show the significance of the miR-885-5p/HMBOX1 axis in myocardial cell pyroptosis and provide new directions for the treatment of septic myocardial depression.

Keywords: sepsis, exosomes, pyroptosis, cardiomyocytes, microRNA

INTRODUCTION

Sepsis is a serious inflammatory disease caused by the systemic immune response to infections (1). About 15% of sepsis patients undergo septic shock, leading to 10% admissions to intensive care units and a 50% death rate (2). It has been estimated that 15% of sepsis-related mortality is secondary to myocardial depression (3). The best treatment for myocardial dysfunction is sepsis management. Although myocardial depression in sepsis has been the focus of many investigations, its etiology and molecular mechanism remain unclear.

Exosomes (exos) play an important role in intercellular communication (4). Exos can deliver various bioactive substances to target cells to regulate different biological processes (5). Wang et al. indicated that miR-223 in exos derived from mesenchymal stem cells inhibited macrophage inflammation in sepsis (6). Upregulated levels of serum exosomal miR-885-5p were found in hepatitis C virus-infected blood donors and pre-eclampsia women (7, 8). Besides, miR-885-5p was reported to be a tumor-suppressive factor in inhibiting cell cycle progression and cell survival (9). Therefore, further clarifying the function of serum exosomal miRNAs especially miR-885-5p in patients with sepsis will help in the understanding of the pathogenesis of sepsis affecting myocardial function.

Cardiomyocytes involve in the contractile function of the heart (10). Sepsis is characterized by overwhelming inflammation followed by immunosuppression (11). Pyroptosis, first reported in 1992, is a form of necrotic and inflammatory programmed cell death mediated by masterminds and inflammatory caspases (12). Pyroptosis could be activated *via* the canonical caspase-1 inflammasome pathway (13). The activated caspase-1 not only elevates inflammatory cytokines but also cleaves gasdermin D (GSDMD) to form membrane pores, leading to pyroptosis (14, 15). Numerous studies have proved the correlation between inflammation and pyroptosis. For example, Zeng et al. have shown that pyroptosis tightly controls the release of inflammatory cytokines, and inflammation (16). It has also been demonstrated that inflammation and subsequent myocardial dysfunction, were dramatically increased in caspase-$1^{-/-}$ mice (17). Therefore, the pyroptosis of myocardial cells may be one of the reasons for myocardial dysfunction caused by sepsis. It has been reported that homeobox-containing protein 1 (HMBOX1) is a key immunosuppressive factor that protects hepatocytes from inflammatory responses by inhibiting the infiltration and activation of macrophages (18). In addition, HMBOX1 is also involved in regulating autophagy and apoptosis of vascular endothelial cells (19). Importantly, data collected from the Targetscan database (http://www.targetscan.org/) indicated that HMBOX1 is a potential target for miR-885-5p. However, the detailed relationship between HMBOX1 and miR-885-5p is still unclear in cardiomyocytes.

Although many studies have been carried out, the function of miR-885-5p and HMBOX1 in cardiomyocytes and the role of sepsis in affecting myocardial function are still not fully understood. Therefore, in this study, using AC16 cells, we elaborated the roles of miR-885-5p/HMBOX1 in cardiomyocyte pyroptosis.

MATERIALS AND METHODS

Blood Samples

Blood samples of sepsis patients and corresponding healthy individuals ($n = 15$) were recruited from the Zhongshan Hospital, Fudan University from June 2017 to October 2019, including 22 males and 8 females, age range 37–67 years old, mean age 52.1 ± 6.0 years old). Septic shock was defined as persisting hypotension requiring vasopressors to maintain mean arterial pressure (MAP) ≥ 65 mmHg and a serum lactate level > 2 mmol/L (18 mg/dl) despite adequate volume resuscitation (20). We excluded patients under 18 years old; those with pregnancy, severe anemia, active bleeding, platelet disorders, or chemotherapy; or those using full-dose heparin or any other medications that interfere with platelet function. The enrolled patients had 30 ml blood samples collected from a central venous catheter. Healthy volunteers provided blood samples that served as controls. All the patients were given informed consent. The study has the approval from the ethics committee of Zhongshan Hospital (B2021-390R), Fudan University.

Cell Culture and Transfection

Human myocardial cells (AC16) were from ATCC. Cells were cultured using DMEM with 10% FBS under a 5% CO_2 atmosphere at 37°C. Oligonucleotides including miR-885-5p mimic and the miR-885-5p inhibitor anti-miR-885-5p were used (Thermo Scientific, Lafayette, CO, USA) for overexpression or inhibition of miR-885-5p, respectively. For cell transfection assays, the synthetic oligonucleotides were transfected into cells using a Lipofectamine RNAiMAX Kit (Invitrogen, Carlsbad, CA, USA) at about 50% confluence. The media were changed 24 h post transfection and the indicated cells were used for further investigations. In some experiments, the Nuclear factor kappa B (NF-κB) inhibitor PDTC (10 μM; S1809, Beyotime Biotechnology, China) was dissolved in DMSO (Sigma-Aldrich, St. Louis, USA) and used to treat cells.

Exosome Collection

Exosomes from sepsis patients (sepsis-exos) or controls (control-exos) were collected as described previously (21). In brief, blood serum was centrifuged at 2,000 g for 20 min to separate cellular debris, and the supernatant was further centrifuged twice at 1,000 g for 30 min twice using a 100-kDa MWCO hollow fiber membrane (Millipore, Bedford, MA, USA). Then, the supernatant was diluted, underlaid on 30% sucrose/D_2O cushion (density 1.210 g/cm^3), and ultracentrifugated at 100,000 g for 1.5 h at 4°C. Exosome-enriched fractions were centrifuged thrice at 1,000 g for 30 min, and filtered. In some experiments, AC16 cells were seeded (50,000 cells/well) and provided with PKH67-labeled exos for 4 h. Cells were observed using a fluorescence microscope.

Transmission Electron Microscopic (TEM) Analysis

The exosome pellets were suspended in PBS and then fixed in paraformaldehyde (4%) and glutaraldehyde (4%) in PBS (0.1 M, pH 7.4) at 4°C for 5 min. After adding a drop of the

exosomal sample, the carbon-coated copper grid was immersed in a phosphotungstic acid solution (2%, pH 7.0) for 30 s. The morphology and size of exos were observed using TEM analysis (JEM-1200EX; Jeol Ltd., Akishima, Japan).

Exosome Endocytosis Assay

AC16 cells were seeded into 24-well plates. A total of 250 μg sepsis-exos or control-exos were labeled using PKH Lipophilic Membrane Dyes (cat. no. PKH67GL; Sigma-Aldrich, Merck KGaA) according to the manufacturer's instructions. PKH67-labeled exos were centrifuged (40,000 × g; 4°C; 70 min) and suspended in PBS (50 μl). Cells were incubated with normal medium (Thermo Fisher Scientific, Inc., Bremen, Germany) or medium containing PKH-67-labeled exos (20 μg/ml) at 37°C for 4 h. Subsequently, DAPI was used to stain the nucleus. Cells were observed under a fluorescent microscope (Olympus IX71; Olympus, Tokyo, Japan).

Cecal Ligation and Puncture (CLP) Surgery Model

Cecal ligation and puncture-induced sepsis model was established as previously described. In brief, rats (200–250 g) were anesthetized with 1% pentobarbital, and a 2–3 cm incision was made to expose the caecum, which was punctured once with an 18-gauge needle. A small amount of feces was extruded from the hole to ensure patency. The abdominal incision was closed by applying sample running sutures. Rats underwent the same procedure except CLP was used as the sham group. All the rats were kept in warm water immediately after surgery. In some experiments, sepsis-exos (100 μg/kg) were i.v. injected into rats after surgery. Serum and heart tissues were harvested for study 72 h after surgery.

Quantitative PCR (QPCR)

Total RNA was extracted from AC6 cells using TRIzol® reagent (Thermo Fisher Scientific, Bremen, Germany). Total RNA (0.5 μg) in 10 μl volume was reverse transcribed into cDNA using the RevertAid^{TM} First Strand cDNA Synthesis kit (Thermo Fisher Scientific, Bremen, Germany) according to the manufacturer's protocol. RNAs were extracted, reverse transcribed into cDNA for qPCR with the following conditions: 95°C, 10 min followed by 40 × (95°C, 15 s; 60°C, 45 s). Fold changes were calculated by $2^{-\Delta\Delta Ct}$. The primers were listed as follows: (5′ −3′): HMBOX1, GCA CAG GTA ACA GGT ATC AG, and CAT TCA GGG TCC TCT ATT GG; GAPDH, AAT CTC ATC AGC ATC TAC and AGT CTG TAG TCA TGC TCC; hsa-miR-885-5p, GCG CGT CCA TTA CAC TAC CCT and AGT GTA GCG TCG GAG GTG TT; U6, CTC GGT TAG GCC GCT CA and AAG GCT ACA CYA ATG TGG GT.

Western Blot

Cells were lysed and total protein was quantified using a bicinchoninic acid assay (Beyotime Biotechnology, China). Proteins (20 μg) were separated *via* 12% SDS-PAGE and

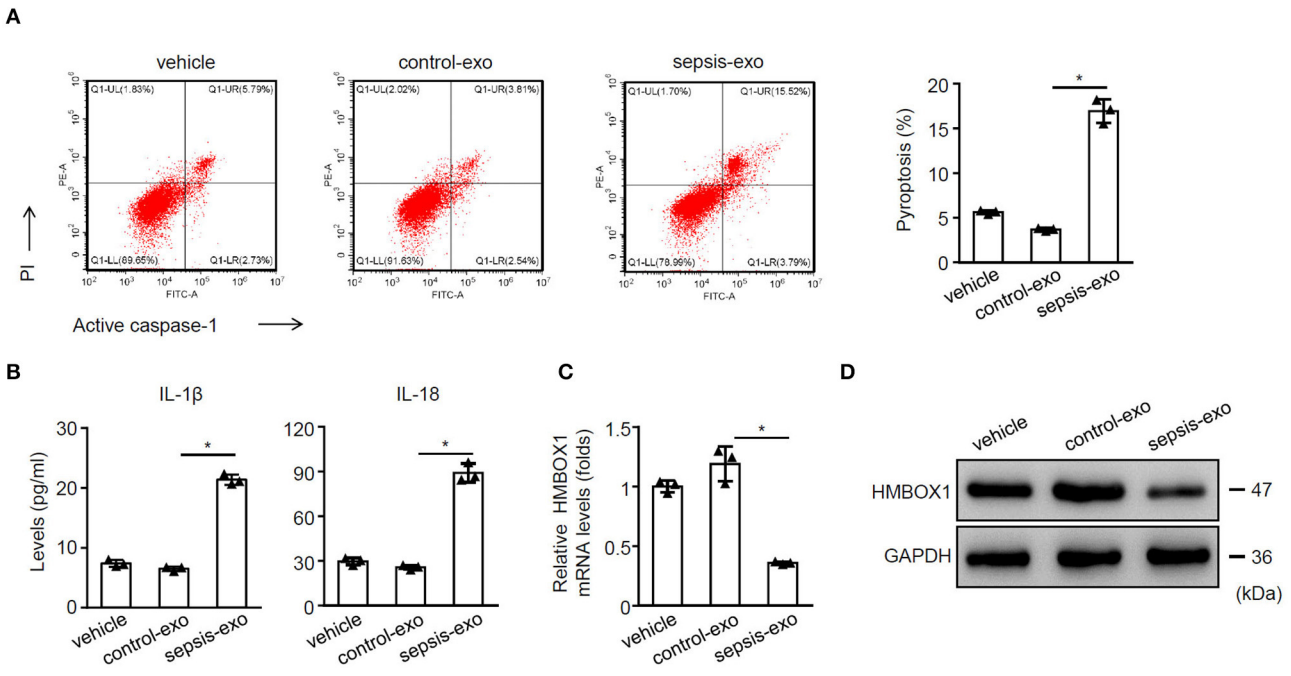

FIGURE 1 | Sepsis-exos promoted the pyroptosis of human myocardial cells. Human myocardial cells AC16 were treated with 50 μg/ml exosomes isolated from sepsis patients (sepsis-exos) or corresponding healthy donors (control-exos) for 24 h. **(A)** PI^+caspase-1^+ pyroptosis was measured by flow cytometry. Representative images were shown on the left and summarized results are on the right. **(B)** Supernatant levels of IL-1β and IL-18 were measured by ELISA. **(C)** mRNA expression of HMBOX1 in cells was measured by qPCR. Data are normalized to expression levels of vehicle. **(D)** The protein level of HMBOX1 in cells were measured by western blot. **(A–C)** Data are mean ± SD from three independent experiments ($n = 3$ per group). *$p < 0.05$.

transferred onto polyvinylidene difluoride membranes at 300 mA for 120 min. The membranes were blocked with 5% BSA (Beyotime Biotechnology, China) for 1 h at room temperature. Subsequently, the membranes were incubated overnight at 4°C with the following primary antibodies diluted 1,000-fold that recognized HMBOX1 (16123-1-AP, Proteintech, USA), NLRP3 (Ab214185 and ab263899, Abcam, UK), pro-caspase-1 (ab179515, Abcam, USA), active caspase-1 (sc-398715, Santa), GSDMD-N (Ab215203 and ab219800, Abcam), NF-κB (#8242, CST, USA), H3 (#4499, CST). CD9 (1:1000, Ab92726, Abcam), CD63 (Ab271286, Abcam, UK), CD81 (1:700, Ab109201, Abcam), and GAPDH (1:5000, 60004-1-1G, Proteintech). Following primary incubation, the membranes were washed with TBS-Tween-20 (1%) and incubated with a horseradish peroxidase-conjugated goat antirabbit secondary antibody (1:10,000) at room temperature for 1 h. Protein bands were visualized using an enhanced chemiluminescence system (Thermo Fisher Scientific, Bremen, Germany).

Enzyme-Linked Immunosorbent Assay (ELISA)

The levels of IL-1β and IL-18 in supernatants of AC16 cell and rat serum were assessed with ELISA kits (R&D Systems, Minneapolis, MN, USA) according to the manufacturer's instructions.

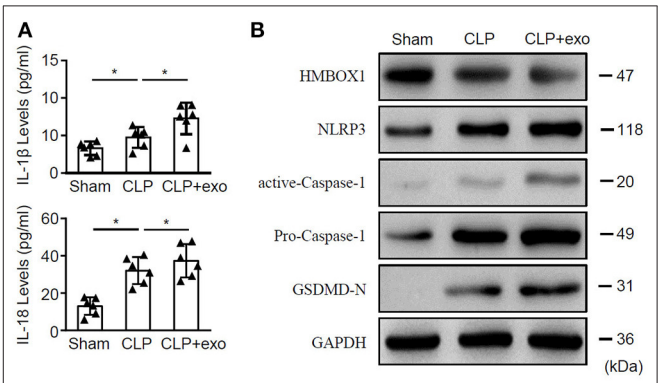

FIGURE 3 | Sepsis-exos promote sepsis *in vivo*. Septic rats underwent CLP surgery were i.v. injected with sepsis-exos (100 μg/kg). Serum and heart tissues from sham, CLP, or sepsis-exo-treated mice were sampled 72 h after surgery. **(A)** Serum levels of IL-1β and IL-18 were measured by ELISA. Data are mean ± SD from three independent experiments ($n = 6$ mice per group). **(B)** Protein levels of HMBOX1, NLRP3, caspase-1, and GSDMD-N in hearts were measured by western blot. * $p < 0.05$.

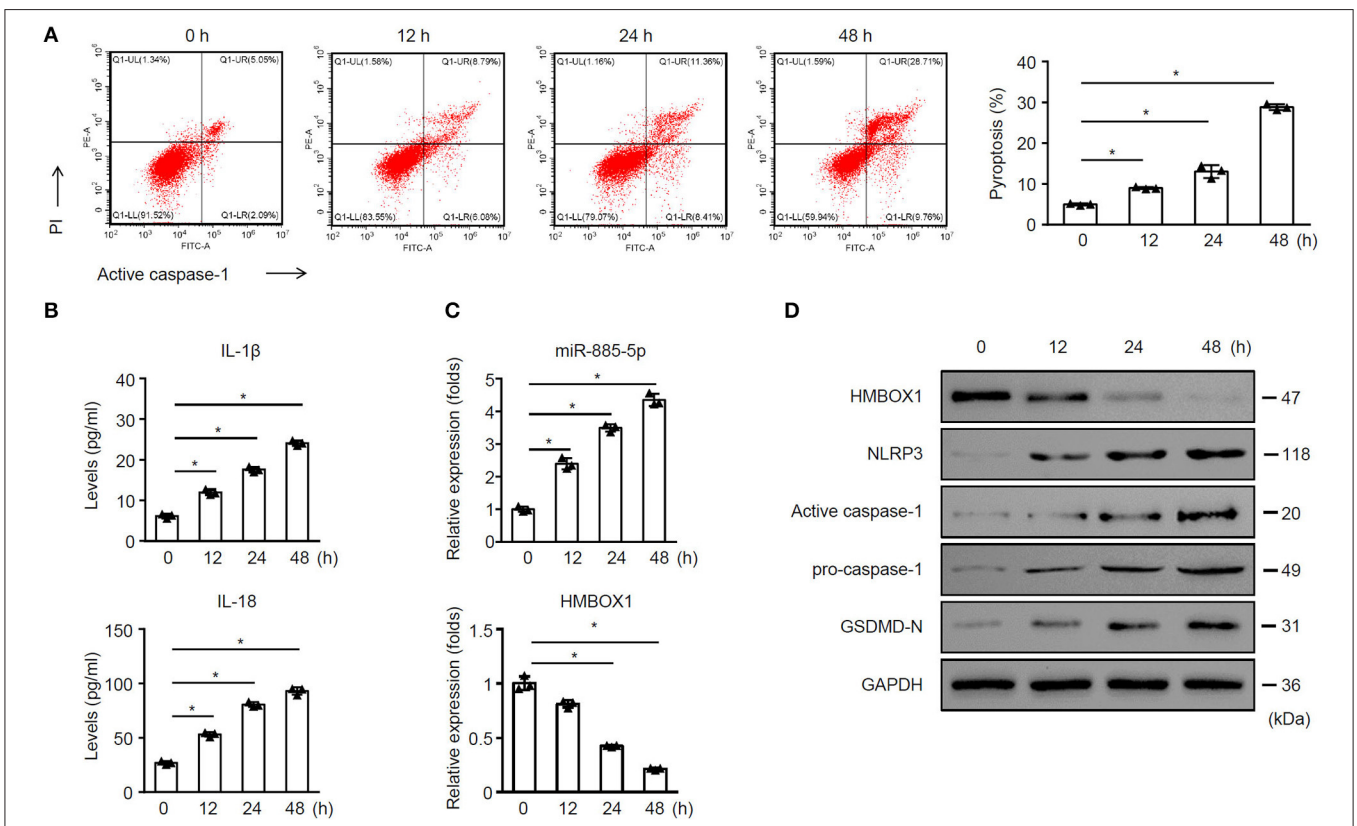

FIGURE 2 | Sepsis-exos time-dependently promoted AC16 pyroptosis. AC16 cells were treated with sepsis-exos (50 μg/ml) for 0, 12, 24 and 48 h. **(A)** $PI^+caspase\text{-}1^+$ pyroptosis was measured by flow cytometry. Representative images were shown on the left and summarized results are on the right. **(B)** Supernatant levels of IL-1β and IL-18 were measured by ELISA. **(C)** Levels of miR-885-5p and HMBOX1 in cells was measured by qPCR. Data are normalized to expression levels of 0 h data. **(D)** Protein levels of HMBOX1, NLRP3, caspase-1, and GSDMD-N were measured by western blot. **(A–C)** Data are mean ± SD from three independent experiments ($n = 3$ per group). * $p < 0.05$.

Knockdown and Overexpression of HMBOX1

Short interfering RNAs targeting human HMBOX1 (siHMBOX1-1: 5′- GCA UUG GAA UGG UAG AUA ATT-3′, position: 337-355; siHMBOX1-2, 5′-GCA UCU UCC UCU ACA GCU ATT-3′, position: 641-659; and siHMBOX1-3 5′-CCU AGA UGU AGA UGA UAA ATT-3′, position: 865-883), along with a scrambled control siRNA (siNC, 5′-UUC UUC GCA CGU CUC ACG UAT-3′), were ligated into lentiviral vector pLKO.1. pLVX-puro having HMBOX1 or mock plasmids were transfected using Lipofectamine 2000 reagent (Thermo Fisher scientific).

Flow Cytometry

To assess pyroptosis, active caspase-1 was labeled with caspase-1 antibody/FITC (active caspase-1, EL900443-100, Eterlife, USA) according to manufactures instructions and propidium iodide (PI) to mark cells with membrane pores (Life technology, Carlsbad, CA, USA). Cells that underwent pyroptosis were based on the detection of active caspase-1 and PI-positive (Caspase-1^+PI^+) populations.

Luciferase Reporter Assay

The wild type (WT) human HMBOX1 3′UTR sequence was amplified *via* PCR and cloned into the Dual-Luciferase Reporter Assay System (psiCHECK-2 vector; Promega, Madison, WI, USA). To construct the mutant (mut) plasmid, the complementary sequences for miR-885-5p in the 3′UTR of HMBOX1 were mutated. AC16 cells were co-transfected with HMBOX1-WT or HMBOX1-mut and miR-885-5p mimic or miR-control. At 36 h after transfection, luciferase activities were detected using the dual-luciferase reporter assay system.

Data Analysis

Data (mean ± SD) were analyzed by Prism 7.0 (GraphPad Software, San Diego, CA, USA). For comparative analyses of

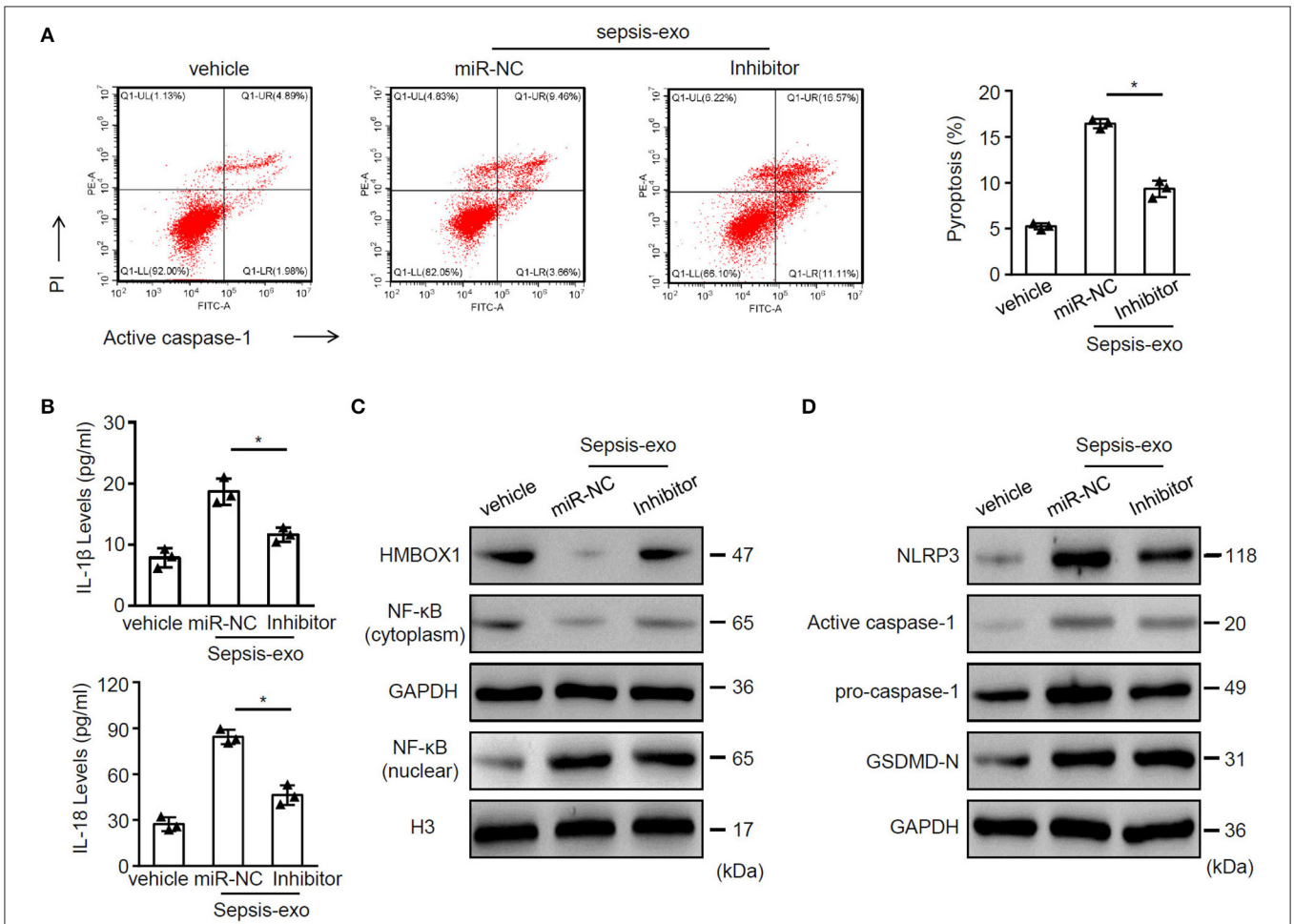

FIGURE 4 | Inhibition of miR-885-5p suppressed sepsis-exo-induced cell pyroptosis. AC16 cells transfected with anti-miR-885-5p (Inhibitor) or anti-miR-control (miR-NC) were treated with sepsis-exos (50 μg/ml). **(A)** PI^+caspase-1^+ pyroptosis was measured by flow cytometry. Representative images were shown on the left and summarized results are on the right. **(B)** Supernatant levels of IL-1β and IL-18 were measured by ELISA. The protein levels of HMBOX1, NF-κB (cytoplasm), NF-κB (nuclear) **(C)** and NLRP3, caspase-1, GSDMD-N **(D)** were measured by western blot. **(A,B)** Data are mean ± SD from three independent experiments ($n = 3$ per group). * $p < 0.05$.

normally distributed variables, Student's *t*-tests and ANOVA were used. The nonparametric Mann-Whitney test was used when the distribution was not normal. $P < 0.05$ was defined as statistically significant.

RESULTS

Sepsis-Exos Promoted the Pyroptosis of Human Myocardial Cells

To study the effect of spesis-exos on pyroptosis, sepsis-exos, and control-exos were successfully isolated. The exos morphology was observed using TEM (**Supplementary Figure 1A**) and confirmed by exosomal markers CD9, CD63, and CD81 (**Supplementary Figure 1B**). Results also suggested that exos could be uptaken by AC16 cells (**Supplementary Figure 1C**). Sepsis-exos dramatically increased pyroptosis of AC16 cells compared with control-exos (**Figure 1A**). Sepsis-exos also enhanced the secretion of IL-1β and IL-18 (**Figure 1B**) and decreased HMBOX1 expression in mRNA (**Figure 1C**) and protein levels (**Figure 1D**). The data suggest that sepsis-exo treatment increased the pyroptosis, elevated inflammatory cytokines, but inhibited HMBOX1 in human myocardial cells.

Sepsis-Exos Time-Dependently Promoted AC16 Pyroptosis

The further time-course study indicated that sepsis-exos time-dependently promoted AC16 pytoptosis (**Figure 2A**). Sepsis-exos time-dependently elevated IL-1β and IL-18 (**Figure 2B**), increased miR-885-5p but decreased HMBOX1 expression (**Figure 2C**). Sepsis-exos also decreased the expression of HMBOX1 but increased the levels of NLRP3, active caspase-1, pro-caspase-1, and GSDMD-N (**Figure 2D**). The results indicated sepsis-exos time-dependently enhanced AC16 pyroptosis.

Sepsis-Exos Promote the Severity of Sepsis in Rats

To further elucidate the impact of sepsis-exos *in vivo*, septic rats underwent CLP surgery were treated with sepsis-exos. Sham rats served as control. Treatment of sepsis-exos significantly increased the serum levels of IL-1β and IL-18 72 h after surgery (**Figure 3A**). Moreover, levels of HMBOX1 in heart tissues were dramatically decreased, while expression of pyroptosis-related proteins NLRP3, caspase-1, and GSDMD-N were all upregulated after treatment of sepsis-exos (**Figure 3B**). These

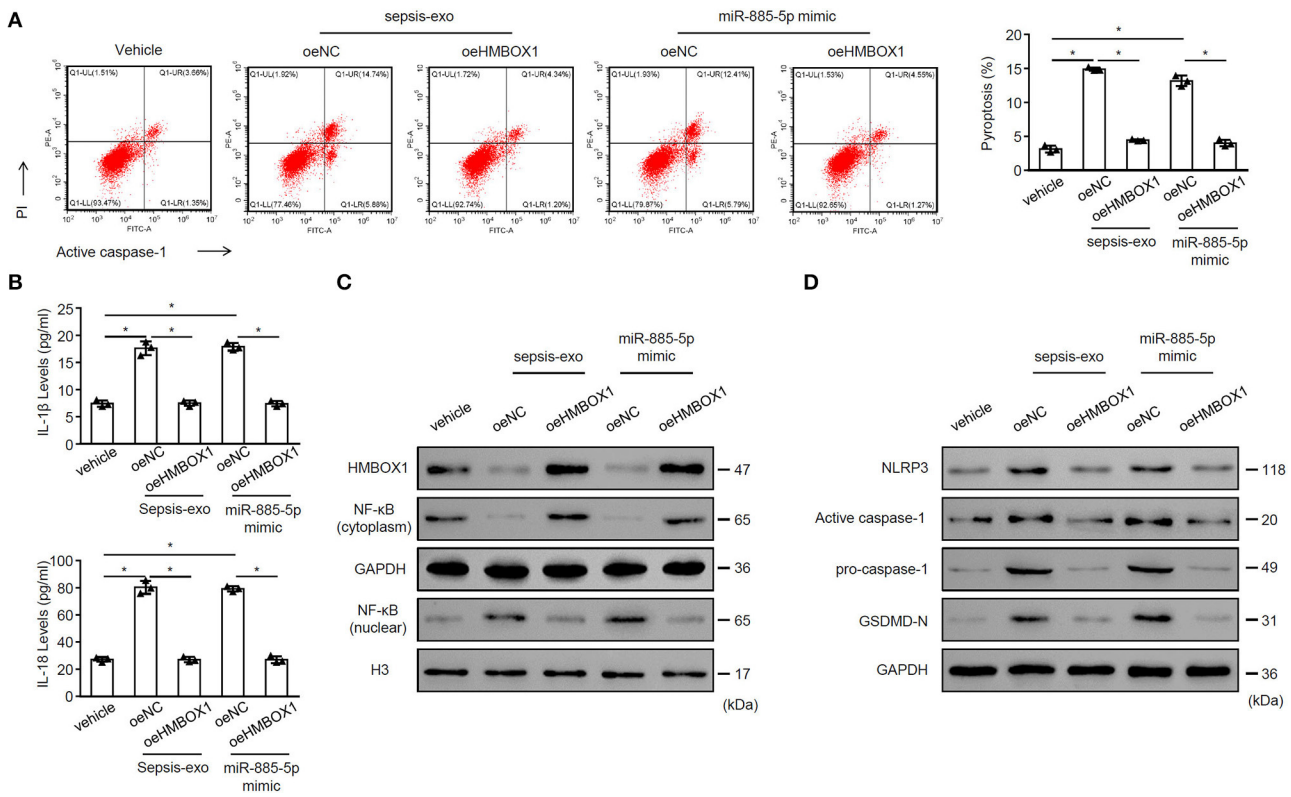

FIGURE 5 | MiR-885-5p mimics and sepsis-exos showed similar effects. AC16 cells with HMBOX1 overexpression (oeHMBOX1) or not (oeNC) were treated with sepsis-exos (50 μg/mL) or miR-885-5p mimic for 24 h. **(A)** PI^+caspase-1^+ pyroptosis was measured by flow cytometry. Representative images were shown on the left and summarized results are on the right. **(B)** Supernatant levels of IL-1β and IL-18 were measured by ELISA. The protein levels of HMBOX1, NF-κB (cytoplasm), NF-κB (nuclear) **(C)** and NLRP3, caspase-1, GSDMD-N **(D)** were measured by western blot. **(A,B)** Data are mean ± SD from three independent experiments ($n = 3$ per group). *$p < 0.05$.

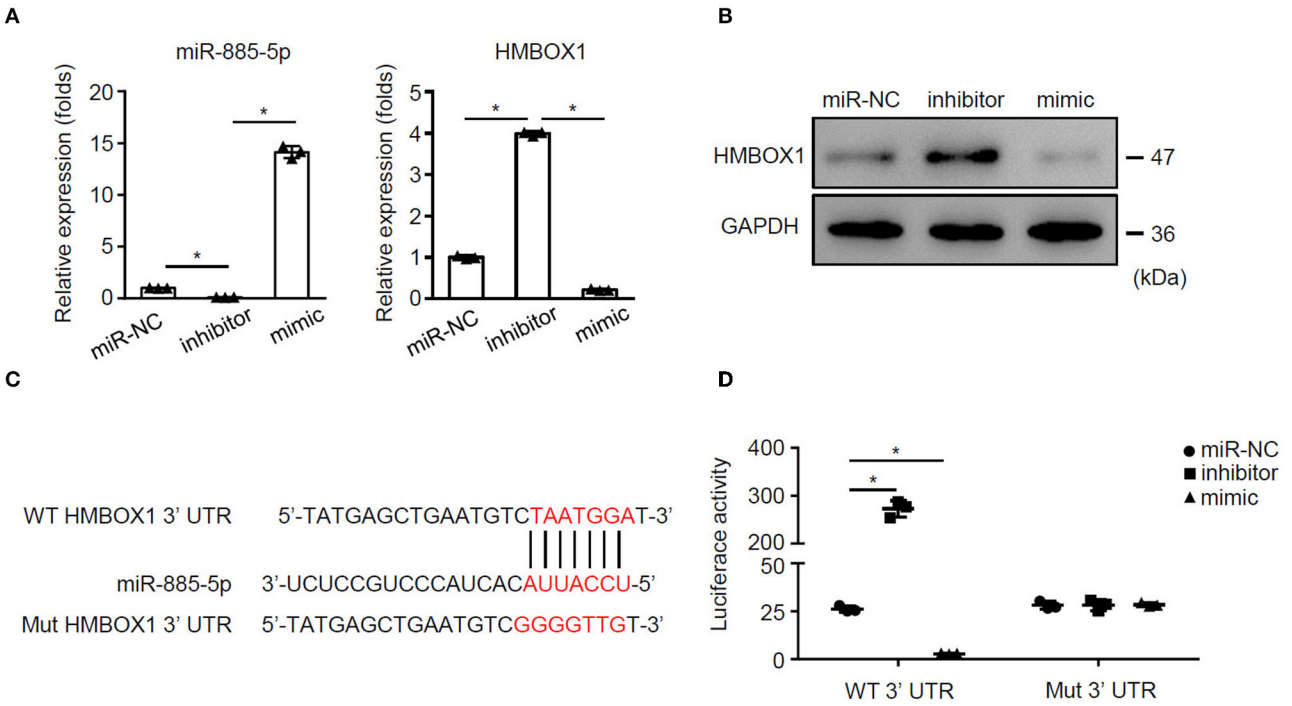

FIGURE 6 | miR-885-5p inhibited HMBOX1 through binding on its 3′UTR. AC16 cells were treated with anti-miR-control (miR-NC), inhibitor or mimic of miR-885-5p. **(A)** Levels of miR-885-5p and HMBOX1 in cells was measured by qPCR. Data are normalized to expression levels of miR-control. **(B)** Protein levels of HMBOX1 were measured by western blot. **(C)** Wild type (WT) or mutant (mut) miR-885-5p binding sites. **(D)** Luciferase activity was determined 36 h after transfection. (A,D) Data are mean ± SD from three independent experiments ($n = 3$ per group). * $p < 0.05$.

data demonstrated that sepsis-exos increased the inflammatory cytokines is associated with increased pyroptosis-related proteins of hearts in septic rats.

miR-885-5p Modulated Pyroptosis of AC16 Cells

Given that miR-885-5p was aberrantly expressed in sepsis-exos, we hypothesized that miR-885-5p may regulate AC16 cell pyroptosis. To test our hypothesis, sepsis-exos were used to treat AC16 cells, with or without miR-885-5p inhibitor. We found that inhibition of miR-885-5p significantly suppressed AC16 pyroptosis (**Figure 4A**) and the secretion of IL-1β and IL-18 (**Figure 4B**). Besides, treatment of miR-885-5p inhibitor upregulated the expression of HMBOX1 and NF-κB (cytoplasm), but decreased nuclear NF-κB, NLRP3, caspase-1, and GSDMD-N (**Figures 4C,D**).

To evaluate whether overexpressing HMBOX1 might reverse the effect of miR-885-5p, sepsis-exos or miR-885-5p mimic was used to treat AC16 cells, with or without HMBOX1 overexpression. We found that both sepsis-exos and miR-885-5p mimic promoted AC16 pyroptosis, which was abolished by overexpressing HMBOX1 (**Figure 5A**). The elevated secretion of IL-1β and IL-18, and expression pattern of HMBOX1, NF-κB (cytoplasm), nuclear NF-κB, NLRP3, caspase-1, and GSDMD-N were all reversed by overexpression of HMBOX1 (**Figures 5B–D**), showing that sepsis-exos and miR-885-5p mimic had similar effects on AC16 cells. These data demonstrated that miR-885-5p modulated AC16 pyroptosis is associated with HMBOX1.

miR-885-5p Suppressed HMBOX1 *via* Binding to 3′UTR

To investigate the mechanism of miR-885-5p's regulation on HMBOX1 expression, miR-885-5p was silenced/overexpressed. Silencing miR-885-5p increased HMBOX1 while overexpressing miR-885-5p decreased HMBOX1 (**Figures 6A,B**). Bioinformatic analysis showed a binding site of miR-885-5p in 3′UTR of HMBOX1 (**Figure 6C**). Next, HMBOX1 HMBOX1 3′UTR-WT/3′UTR-Mut and miR-885-5p inhibitor/mimics were transfected. Inhibiting enhanced HMBOX1 promoter activity, which was suppressed by miR-885-5p overexpression. Mutating HMBOX1's miR-885-5p binding site abolished miR-885-5p's effect (**Figure 6D**). The data suggested that miR-885-5p is bound to 3′UTR to inhibit HMBOX1.

Nuclear Factor Kappa B Inhibitor PDTC Rescued the Function of HMBOX1 in AC16 Cells

To understand the role of NF-κB in pyroptosis, NF-κB inhibitor PDTC was introduced in this study. Silencing of HMBOX1 caused significant increase of pyroptosis in AC16 cells, which was blocked by the administration of NF-κB inhibitor PDTC (**Figure 7A**). Silencing of HMBOX1 also resulted in the elevated secretion of IL-1β and IL-18, which was diminished by PDTC

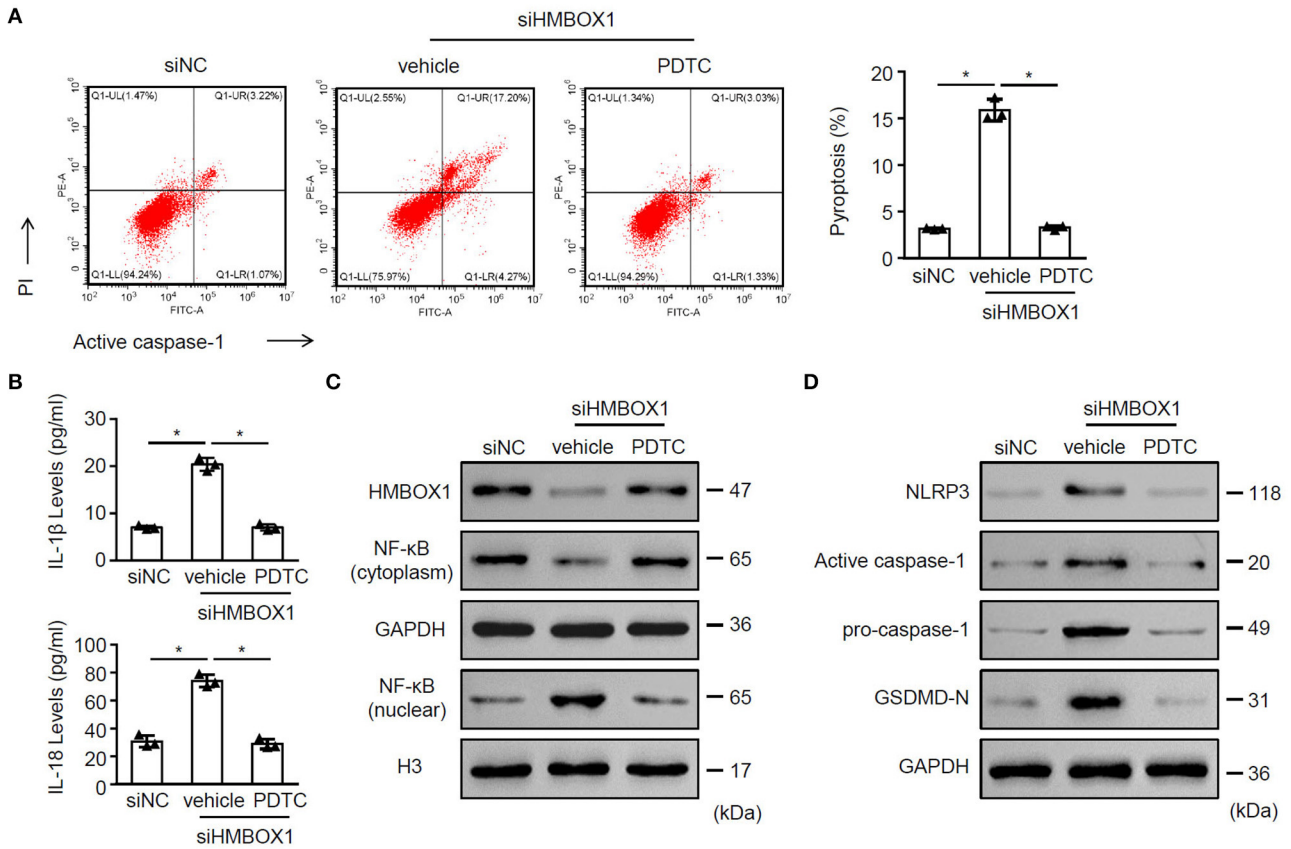

FIGURE 7 | The NF-κB inhibitor PDTC rescued the function of HMBOX1 in AC16 cells. AC16 cells with HMBOX1 silencing (siHMBOX1) or not (siNC) were treated with NF-κB inhibitor PDTC (10 μM) for 24 h. **(A)** PI^+caspase-1^+ pyroptosis was measured by flow cytometry. Representative images were shown on the left and summarized results are on the right. **(B)** Supernatant levels of IL-1β and IL-18 were measured by ELISA. The protein levels of HMBOX1, NF-κB (cytoplasm), NF-κB (nuclear) **(C)** and NLRP3, caspase-1, GSDMD-N **(D)** were measured by western blot. **(A,B)** Data are mean ± SD from three independent experiments ($n = 3$ per group). * $p < 0.05$.

treatment (**Figure 7B**). Administration of NF-κB inhibitor PDTC also blocked HMBOX1 silencing-caused downregulation of HMBOX1 and NF-κB (cytoplasm), and upregulation of NF-κB (nuclear), NLRP3, caspase-1, and GSDMD-N in AC16 cells (**Figures 7C,D**). These findings demonstrated that the administration of NF-κB inhibitor PDTC rescued the effect of HMBOX1 silencing on AC16 cells.

DISCUSSION

We showed that sepsis-exo treatment elevated IL-1β and IL-18, decreased HMBOX1, and promoted pyroptosis in AC16 cells. The mechanistic study indicated that miR-885-5p negatively regulates HMBOX1. Overexpression of HMBOX1 significantly reduced the cardiomyocyte pyroptosis caused by sepsis-exos or miR-885-5p mimic.

MicroRNAs (miRNAs) function by negatively regulating their target genes. Different miR-885-5p targets have been shown over the years. Afanasyeva et al. demonstrated that miR-885-5p suppresses neuroblastoma *via* inhibiting cyclin-dependent kinase (9). Yu et al. indicated that overexpressing miR-885-5p enhanced proliferation of MG-63 cells by targeting cell division cycle protein 73 homolog (22). Xu et al. have demonstrated that miR-885-5p overexpression suppressed hepatocellular carcinoma cell proliferation through regulating its target hexokinase 2 (23). HMBOX1 is characterized by containing homeobox domain (24). Studies revealed that HMBOX1 promotes the proliferation of gastric cancer cells (25). Loss of HMBOX1 has been demonstrated to promote LPS-induced apoptosis of vascular endothelial cells (26). Our data indicated that miR-885-5p negatively regulated HMBOX1. Overexpressing HMBOX1 reversed miR-885-5p-induced elevation of inflammatory factors, and upregulation of nuclear NF-κB, NLRP3, caspase-1, and GSDMD-N, and promotion of AC16 pyroptosis. The results increase our knowledge of miR-885-5p/HMBOX1 in the injury of cardiomyocytes and broaden our understanding of septic myocardial depression.

Pyroptosis involves different diseases. For example, dysregulation of pyroptosis led to tissues damage (27). Pyroptosis has also been related to type II diabetic mellitus through activated caspase-1 and elevated IL-1β/IL-18 (28). In gastric cancer cells, increased GSDMD inhibits tumor development through cell cycle arrest (29). An *in vivo* study by Lei et al. demonstrated that pyroptosis contributes to cardiomyocyte injury in myocardial

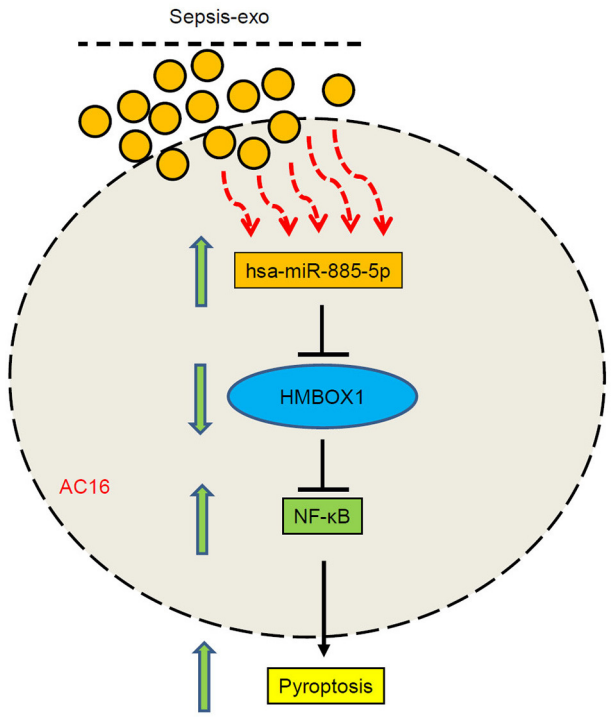

FIGURE 8 | A schematic diagram showing that sepsis-exos induced cardiomyocytes pyroptosis by regulating miR-885-5p/HMBOX1 *via* NF-κB signaling.

infarction (30). We showed that sepsis-exo or miR-885-5p mimic not only elevated IL-1β and IL-18, but also increased NLRP3, caspase-1, and GSDMD-N, leading to promotion of pyroptosis. These results demonstrated the significance of pyroptosis in regulating miR-885-5p/HMBOX1-mediated cardiomyocyte injury. We also further showed that miR-885-5p/HMBOX1-mediated cardiomyocyte injury is NF-κB-dependent. It has been confirmed that activation of the NF-κB-dependent pathway induces NLRP3-mediated pyroptosis (31). In this study, our results indicated that overexpression of HMBOX1 inhibited the translocation of NF-κB from the cytoplasm to nuclear in sepsis-exo-treated AC16 cells. Importantly, the NF-κB inhibitor PDTC rescued the function of HMBOX1 in siHMBOX1 transfecting cells. Hence, these findings demonstrated that HMBOX1 is involved in the network of NF-κB-dependent pathways and suppressed the translocation of NF-κB from the cytoplasm to nuclear. Moreover, these findings indicate the functional role of miR-885-5p/HMBOX1 in cardiomyocyte injury, and therefore, improve our knowledge of septic myocardial depression. Although future studies based on animals or clinical specimens can provide more relevant and pervasive data, we show a novel mechanism underlying septic myocardial depression. However, although our present data showed that exsomal miR-885-5p plays a critical role in human myocardial cell pyroptosis, we still cannot exclude that miR-885-5p might work in cell apoptosis. The cellular and molecular mechanisms of exsomal miR-885-5p in other forms of cell death need further investigation.

In short, this study revealed a new function of miR-885-5p/HMBOX1 signaling, showing that sepsis-exos-induced cardiomyocytes damage *via* miR-885-5p and HMBOX1 (**Figure 8**). These findings identified an important role of the miR-885-5p/HMBOX1 axis which is relevant to cardiomyocytes pyroptosis, and might contribute to septic myocardial depression treatment.

DATA AVAILABILITY STATEMENT

The raw data supporting the conclusions of this article will be made available by the authors, without undue reservation.

ETHICS STATEMENT

The studies involving human participants were reviewed and approved by Ethics Committee of Zhongshan Hospital, Fudan University. The patients/participants provided their written informed consent to participate in this study.

AUTHOR CONTRIBUTIONS

YZ and ZL conceived the project, designed the project, and approved the final manuscript. G-wT drafted the manuscript. G-wT, J-fM, and J-kL conducted the experiments. YS, J-cL, G-wH, and Y-rC analyzed data and contributed to experiments. All authors contributed to the article and approved the submitted version.

FUNDING

This article was supported by grants from the Natural Science Foundation of Shanghai (20ZR1411100 to ZL, 21ZR1412900 to YS), Science and Technology Commission of Shanghai Municipality (20DZ2261200 to ZL), Program of Shanghai Academic/Technology Research Leader (20XD1421000 to G-wT), National Natural Science Foundation of China (82070085 to G-wT), Construction program of key but weak disciplines of shanghai health commission (2019ZB0105 to ZL), Clinical Research Project of Zhongshan Hospital (2020ZSLC38 to G-wT, 2020ZSLC27 to ZL), Smart Medical Care of Zhongshan Hospital (2020ZHZS01 to ZL), and Project for elite backbone of Zhongshan Hospital (2021ZSGG06 to G-wT).

SUPPLEMENTARY MATERIAL

The Supplementary Material for this article can be found online at: https://www.frontiersin.org/articles/10.3389/fcvm.2022.774193/full#supplementary-material

Supplementary Figure 1 | Characterization of exosomes. **(A)** Sepsis-exos and control-exos were subjected to TEM observation. Scale bar, 1 μm. **(B)** The protein levels exosome markers CD9, CD63, and CD81 were measured by western blot. **(C)** The exosome endocytosis assay was observed by a fluorescent microscope. Scale bar, 25 μm. **(A–C)** Data are from three independent experiments. * $p < 0.05$.

Supplementary Figure 2 | Overexpression and knockdown of HMBOX1 in AC cells. **(A,B)** HMBOX1 was overexpressed in AC16 cells. **(A)** mRNA expression of HMBOX1 in cells was measured by qPCR. Data are normalized to expression

levels of control. **(B)** The protein level of HMBOX1 in cells were measured by western blot. **(C,D)** HMBOX1 was silenced in AC cells with 3 siRNAs, respectively. **(C)** mRNA expression of HMBOX1 in cells was measured by qPCR. Data are normalized to expression levels of control. **(D)** The protein level of HMBOX1 in cells were measured by western blot. **(A–C)** Data are mean ± SD from three independent experiments ($n = 3$ per group). * $p < 0.05$.

REFERENCES

1. Gyawali B, Ramakrishna K, Dhamoon AS. Sepsis: The evolution in definition, pathophysiology, and management. *SAGE Open Med.* (2019) 7:2050312119835043. doi: 10.1177/2050312119835043
2. Dugar S, Choudhary C, Duggal A. Sepsis and septic shock: Guideline-based management. *Cleve Clin J Med.* (2020) 87:53–64. doi: 10.3949/ccjm.87a.18143
3. Antonucci E, Fiaccadori E, Donadello K, Taccone FS, Franchi F, Scolletta S. Myocardial depression in sepsis: from pathogenesis to clinical manifestations and treatment. *J Crit Care.* (2014) 29:500–11. doi: 10.1016/j.jcrc.2014.03.028
4. Zhang Y, Bi J, Huang J, Tang Y, Du S, Li P. Exosome: A review of its classification, isolation techniques, storage, diagnostic and targeted therapy applications. *Int J Nanomedicine.* (2020) 15:6917–34. doi: 10.2147/IJN.S264498
5. Farooqi AA, Desai NN, Qureshi MZ, Librelotto DRN, Gasparri ML, Bishayee A, et al. Exosome biogenesis, bioactivities and functions as new delivery systems of natural compounds. *Biotechnol Adv.* (2018) 36:328–34. doi: 10.1016/j.biotechadv.2017.12.010
6. Wang X, Gu H, Qin D, Yang L, Huang W, Essandoh K, et al. Exosomal miR-223 Contributes to mesenchymal stem cell-elicited cardioprotection in polymicrobial sepsis. *Sci Rep.* (2015) 5:13721. doi: 10.1038/srep13721
7. McGowan K, Simpson KJ, Petrik J. Expression profiles of exosomal MicroRNAs from HEV- and HCV-infected blood donors and patients: A pilot study. *Viruses.* (2020) 12. doi: 10.3390/v12080833
8. Sandrim VC, Luizon MR, Palei AC, Tanus-Santos JE, Cavalli RC. Circulating microRNA expression profiles in pre-eclampsia: evidence of increased miR-885-5p levels. *BJOG.* (2016) 123:2120–8. doi: 10.1111/1471-0528.13903
9. Afanasyeva EA, Mestdagh P, Kumps C, Vandesompele J, Ehemann V, Theissen J, et al. MicroRNA miR-885-5p targets CDK2 and MCM5, activates p53 and inhibits proliferation and survival. *Cell Death Differ.* (2011) 18:974–84. doi: 10.1038/cdd.2010.164
10. Ryan MJ. Have a heart: failure to increase GLP-1 caused by heart failure increases the risk of diabetes. *Clin Sci (Lond).* (2020) 134:3119–21. doi: 10.1042/CS20201029
11. Nedeva C, Menassa J, Puthalakath H. Sepsis: inflammation is a necessary evil. *Front Cell Dev Biol.* (2019) 7:108. doi: 10.3389/fcell.2019.00108
12. Zychlinsky A, Prevost MC, Sansonetti PJ. Shigella flexneri induces apoptosis in infected macrophages. *Nature.* (1992) 358:167–9. doi: 10.1038/358167a0
13. Liu X, Lieberman J. A mechanistic understanding of pyroptosis: the fiery death triggered by invasive infection. *Adv Immunol.* (2017) 135:81–117. doi: 10.1016/bs.ai.2017.02.002
14. Liu X, Zhang Z, Ruan J, Pan Y, Magupalli VG, Wu H, et al. Inflammasome-activated gasdermin D causes pyroptosis by forming membrane pores. *Nature.* (2016) 535:153–8. doi: 10.1038/nature18629
15. Wang YY, Liu XL, Zhao R. Induction of pyroptosis and its implications in cancer management. *Front Oncol.* (2019) 9:971. doi: 10.3389/fonc.2019.00971
16. Zeng C, Wang R, Tan H. Role of pyroptosis in cardiovascular diseases and its therapeutic implications. *Int J Biol Sci.* (2019) 15:1345–57. doi: 10.7150/ijbs.33568
17. Kawaguchi M, Takahashi M, Hata T, Kashima Y, Usui F, Morimoto H, et al. Inflammasome activation of cardiac fibroblasts is essential for myocardial ischemia/reperfusion injury. *Circulation.* (2011) 123:594–604. doi: 10.1161/CIRCULATIONAHA.110.982777
18. Zhao H, Han Q, Lu N, Xu D, Tian Z, Zhang J. HMBOX1 in hepatocytes attenuates LPS/D-GalN-induced liver injury by inhibiting macrophage infiltration and activation. *Mol Immunol.* (2018) 101:303–11. doi: 10.1016/j.molimm.2018.07.021
19. Ma H, Su L, Yue H, Yin X, Zhao J, Zhang S, et al. HMBOX1 interacts with MT2A to regulate autophagy and apoptosis in vascular endothelial cells. *Sci Rep.* (2015) 5:15121. doi: 10.1038/srep15121
20. Singer M, Deutschman CS, Seymour CW, Shankar-Hari M, Annane D, Bauer M, et al. The third international consensus definitions for sepsis and septic shock (Sepsis-3). *JAMA.* (2016) 315:801–10. doi: 10.1001/jama.2016.0287
21. Zhu W, Huang L, Li Y, Zhang X, Gu J, Yan Y, et al. Exosomes derived from human bone marrow mesenchymal stem cells promote tumor growth in vivo. *Cancer Lett.* (2012) 315:28–37. doi: 10.1016/j.canlet.2011.10.002
22. Yu FQ, Wang Z, Wang XW, Wang SL, Li XD, Huang QS, et al. MicroRNA-885-5p promotes osteosarcoma proliferation and migration by downregulation of cell division cycle protein 73 homolog expression. *Oncol Lett.* (2019) 17:1565–72. doi: 10.3892/ol.2018.9802
23. Xu F, Yan JJ, Gan Y, Chang Y, Wang HL, He XX, et al. miR-885-5p Negatively regulates warburg effect by silencing hexokinase 2 in liver cancer. *Mol Ther Nucleic Acids.* (2019) 18:308–19. doi: 10.1016/j.omtn.2019.09.002
24. Dai J, Wu L, Zhang C, Zheng X, Tian Z, Zhang J. Recombinant expression of a novel human transcriptional repressor HMBOX1 and preparation of anti-HMBOX1 monoclonal antibody. *Cell Mol Immunol.* (2009) 6:261–8. doi: 10.1038/cmi.2009.35
25. Diao N, Li Y, Yang J, Jin C, Meng X, Jiao W, et al. High expression of HMBOX1 contributes to poor prognosis of gastric cancer by promoting cell proliferation and migration. *Biomed Pharmacother.* (2019) 115:108867. doi: 10.1016/j.biopha.2019.108867
26. Ma H, Su L, He X, Miao J. Loss of HMBOX1 promotes LPS-induced apoptosis and inhibits LPS-induced autophagy of vascular endothelial cells in mouse. *Apoptosis.* (2019) 24:946–57. doi: 10.1007/s10495-019-01572-6
27. Bergsbaken T, Fink SL, Cookson BT. Pyroptosis: host cell death and inflammation. *Nat Rev Microbiol.* (2009) 7:99–109. doi: 10.1038/nrmicro2070
28. Vandanmagsar B, Youm YH, Ravussin A, Galgani JE, Stadler K, Mynatt RL, et al. The NLRP3 inflammasome instigates obesity-induced inflammation and insulin resistance. *Nat Med.* (2011) 17:179–88. doi: 10.1038/nm.2279
29. Fang Y, Tian S, Pan Y, Li W, Wang Q, Tang Y, et al. Pyroptosis: A new frontier in cancer. *Biomed Pharmacother.* (2020) 121:109595. doi: 10.1016/j.biopha.2019.109595
30. Lei Q, Yi T, Chen C. NF-kappaB-Gasdermin D (GSDMD) axis couples oxidative stress and NACHT, LRR and PYD domains-containing protein 3 (NLRP3) inflammasome-mediated cardiomyocyte pyroptosis following myocardial infarction. *Med Sci Monit.* (2018) 24:6044–52. doi: 10.12659/MSM.908529
31. Xu S, Chen H, Ni H, Dai Q. Targeting HDAC6 attenuates nicotine-induced macrophage pyroptosis via NF-kappaB/NLRP3 pathway. *Atherosclerosis.* (2021) 317:1–9. doi: 10.1016/j.atherosclerosis.2020.11.021

Conflict of Interest: The authors declare that the research was conducted in the absence of any commercial or financial relationships that could be construed as a potential conflict of interest.

Publisher's Note: All claims expressed in this article are solely those of the authors and do not necessarily represent those of their affiliated organizations, or those of the publisher, the editors and the reviewers. Any product that may be evaluated in this article, or claim that may be made by its manufacturer, is not guaranteed or endorsed by the publisher.

Copyright © 2022 Tu, Ma, Li, Su, Luo, Hao, Luo, Cao, Zhang and Luo. This is an open-access article distributed under the terms of the Creative Commons Attribution License (CC BY). The use, distribution or reproduction in other forums is permitted, provided the original author(s) and the copyright owner(s) are credited and that the original publication in this journal is cited, in accordance with accepted academic practice. No use, distribution or reproduction is permitted which does not comply with these terms.

Advantages of publishing in Frontiers

OPEN ACCESS
Articles are free to read for greatest visibility and readership

FAST PUBLICATION
Around 90 days from submission to decision

HIGH QUALITY PEER-REVIEW
Rigorous, collaborative, and constructive peer-review

TRANSPARENT PEER-REVIEW
Editors and reviewers acknowledged by name on published articles

Frontiers
Avenue du Tribunal-Fédéral 34
1005 Lausanne | Switzerland

Visit us: www.frontiersin.org
Contact us: frontiersin.org/about/contact

REPRODUCIBILITY OF RESEARCH
Support open data and methods to enhance research reproducibility

DIGITAL PUBLISHING
Articles designed for optimal readership across devices

FOLLOW US
@frontiersin

IMPACT METRICS
Advanced article metrics track visibility across digital media

EXTENSIVE PROMOTION
Marketing and promotion of impactful research

LOOP RESEARCH NETWORK
Our network increases your article's readership